A Study of Factors Governing the Performance of Systems using Pulse-length Modulation

P. J. W. Rayner

University of Aston in Birmingham
Department of Electrical Engineering

Ph.D. Thesis September, 1968.

THE
OF
B
LIBRARY
20FEB1969
Thesis 116362
621.376
RAY

Summary

Since many semiconductor devices may be operated as very efficient switches it is desirable to make use of these switching properties as a means of obtaining high efficiency linear power amplification. One method of achieving this is to vary the length of the pulses of a wavetrain in accordance with the signal to be amplified. The modulated wavetrain may be demodulated by simply passing the wavetrain through a low-pass filter. The majority of the published work on this technique is concerned with ideal systems. It is the objective of this research work to establish some of the more important design criteria for pulse-length modulation systems. The analytical work is divided into three distinct sections.

The first of these sections deals with distortion arising in the modulation process. The effects of system parameters on the system linearity are analysed on a static basis, where the system input is d.c., and in the frequency domain. In general the static analysis is required before the analysis in the frequency domain can be made. In addition to examining, in detail, the effect of a number of particular system parameters a generalised spectrum analysis has been made for non-linear pulse-length modulation.

The second section considers the efficiency of switching output stages operating in conjunction with the low-pass filter necessary for demodulation. The power dissipation in the elements of the output stage is analysed in terms of the d.c. characteristics of the active elements. As a result of the complexity of the problem a quasi-dynamic approach has been used. Expressions are obtained relating the power dissipation

to the pulse length. The pulse length is then modulated in a sinusoidal manner and the power dissipation integrated over one cycle of the modulating frequency.

It was shown in the first section that non-linearities in the modulation process give rise to systems with non-linear transfer functions. The final section of the thesis introduces the possibility of producing systems with prescribed non-linear transfer functions by means of pulse-length modulation.

Index

List of Symbols

All symbols are defined in the text and only the principal symbols are given in the following list.

A_k = Coefficient in the generalised spectrum analysis of non-linear pulse length modulation.

a_n = Coefficient in the power series representation of the positions of the pulse-edges in a system with a bandwidth-limited integrator amplifier.

B_k = Coefficient in the generalised spectrum analysis of non-linear pulse-length modulation.

b_n = Coefficient in the power series representation of the positions of the pulse-edges in a system with a bandwidth-limited integrator amplifier.

C_k = Coefficient in the generalised spectrum analysis of non-linear pulse-length modulation.

C = Integrator time constant capacitance.

D_k = Coefficient in the generalised spectrum analysis of non-linear pulse-length modulation.

DF_n = n^{th} harmonic distortion factor.

E_n = Coefficient in the generalised spectrum analysis of non-linear pulse-length modulation.

E_1 , E_2 = Static error in the amplitude of the demodulated system output.

F_n = Coefficient in the generalised spectrum analysis of non-linear pulse-length modulation.

$F(t)$ = Spectrum of a pulse-length modulated wavetrain.

G_n = Coefficient in the generalised spectrum analysis of non-linear pulse-length modulation.

$G(\omega)$ = Transfer function of low-pass filter.

H_n = Coefficient in the generalised spectrum analysis of non-linear pulse-length modulation.

h = Amplitude of the pulse-train in the non-linear function generation system.

I = Maximum current through the amplifier load resistance R_L $(=\frac{V_L}{R_L})$

I_{ES1} , I_{ES2} = Emitter saturation current of transistors VT1 and VT2 in the output stage.

I_{s1} , I_{s2} , I_{s3} , I_{s4} = Saturation current of diodes D1, D2, D3, and D4 in the output stage.

$i(t)$ = Current as a time function.

$J_n(x)$ = Bessel function of the first kind and of order n.

K_n = Coefficient in the generalised spectrum analysis of non-linear pulse-length modulation.

k = Boltzmann's constant ($1.3805.10^{-23}$ joules/degree)

L = Low-pass filter inductance.

M = Modulation index.

M(max) = Maximum value of modulation index for which certain sections of the analytical work are valid.

$\overline{P}_{VT1}, \overline{P}_{VT2}, \overline{P}_{D1}, \overline{P}_{D2}, \overline{P}_{D3}, \overline{P}_{D4}$ = Average power dissipation, for d.c. modulation, in the output stage elements VT1, VT2, D1, D2, D3 and D4 respectively.

$P_{VT1}, P_{VT2}, P_{D1}, P_{D2}, P_{D3}, P_{D4}$ = Average power dissipation, over one cycle of the modulation frequency, in the output stage elements VT1, VT2, D1, D2, D3 and D4 respectively.

q = The electronic charge ($1.602.10^{-19}$ Coulombs)

$R_{D1}, R_{D2}, R_{D3}, R_{D4}$ = Effective series resistance of diodes D1, D2, D3 and D4 of the output stage.

R_{E1}, R_{E2} = Effective series emitter resistance of transistors VT1 and VT2 of the output stage.

R_L = Amplifier load resistance.

R = Integrator time constant resistance.

R_o = Output resistance of integrator amplifier.

R_i = Input resistance of integrator amplifier.

T_N = Normalised time constant.

T_m = Period of modulation frequency (ω_m).

T_e = Modified integrator time constant.

T_c = Period of pulse repetition frequency.

T_a = Time constant of integrator amplifier.

T = Absolute temperature.

T_o = Unmodulated pulse-length.

T_1 = Modulated pulse-length.

t_{dl} , t_{dt} = Time deviation of the pulse leading and trailing edges respectively.

t_1 , t_2 = Positions of the pulse leading and trailing edges respectively (except in Chapter III).

$\overset{\circ}{t}_1$, $\overset{\circ}{t}_2$ = Unmodulated positions of the pulse leading and trailing edges respectively.

t = time variable

$\left(\frac{u}{n}\right)$ = Binomial coefficient = $\frac{u(u-1)(u-2)\text{----}(u-n+1)}{n!}$

V_t = Level-detector threshold voltage.

V_{in} = d.c. modulating input to the system.

$\hat{V}_{in+}$, $\hat{V}_{in-}$ = Positive and negative values of system input voltage required for full modulation.

$V_{EB1}(t)$, $V_{EB2}(t)$ = Emitter-base voltages of transistors VT1 and VT2 in the output stage.

$V_{D1}(t)$, $V_{D2}(t)$, $V_{D3}(t)$, $V_{D4}(t)$ = Forward voltages of diodes D1, D2, D3 and D4 in the output stage.

$V_{CE1}(t)$, $V_{CE2}(t)$ = Collector-emitter voltages of transistors VT1 and VT2 in the output stage.

V_{CB1} , V_{CB2} = Collector-base voltages of transistors VT1 and VT2 in the output stage.

V_{av} = Amplitude of demodulated wavetrain for d.c. modulation.

V_o = Amplitude of demodulated output of non-linear function generation system.

$V_{2p\cdot p}$ = Peak to peak value of sections of the integrator output waveform (The particular section is defined in the text).

$v(t)$= Voltage as a time function.

$\hat{v}(t)$= Peak value of voltage time function

α = Integrator amplifier voltage gain.

α_n, β_n= Coefficients in the generalised power series for the positions of the leading and trailing pulse-edges respectively.

γ_n, δ_n= Coefficients in the generalised spectrum analysis of non-linear pulse-length modulation.

δ = Hysteresis of the level-detector.

Δ = Half of the peak to peak excursion of the triangular approximation to the low-pass filter input current.

θ = Phase angle of low-pass filter transfer function.

λ = Low-pass filter constant.

ϕ_n = Phase angle in the generalised spectrum analysis of non-linear pulse-length modulation.

ϕ = Modulation index modifying function.

γ = A design parameter for systems with bandwidth-limited integrator amplifier $\left(= \frac{CR}{T_a}\left[\frac{T_a}{CR} + 1 + \alpha\right]^2 \right)$

ω_m = Angular frequency of the modulating signal.

ω_c = Angular pulse repetition frequency.

ω_o = 3dB. frequency of the low-pass filter.

CHAPTER I

General Introduction to Pulse-length Modulation Systems

1. Basic principles of pulse-length modulation amplifiers

In conventional power amplifier systems the control devices (i.e. thermionic-valves or transistors) are operated in the linear or quasi-linear region which is an inherently inefficient mode of operation due to the relatively large power dissipation in the control device. Thus high-power amplifier systems must be designed around devices capable of dissipating a considerable amount of power. Provision usually has to made to remove the heat generated in order to maintain the control devices at a reasonable temperature. However a number of modern semiconductor devices, transistors in particular, are capable of operating as very efficient switches. In the "on" condition the voltage drop across the device may be less than a volt, whilst in the "off" condition the current through the device may only be a few microamps. Thus a method of linear amplification which could make use of the efficient switching properties of transistors would present an attractive alternative to the conventional Class A and Class B modes of operation normally used. Pulse-length modulation affords a means of achieving this objective.

Pulse-length modulation is a process whereby the length of the pulses in a pulse-train are varied in accordance with some modulating function. Fig. 1.1. shows the manner in which the length-modulated pulses are utilised. The two switches are operated at a constant frequency and in such a manner that when one switch is open so the other is closed. The period T_1 for which SW1 is closed (and SW2 is open) is varied in accordance with the modulating signal V_{in}. The waveforms associated with the circuit show that the average value of the voltage appearing across the load resistance is:

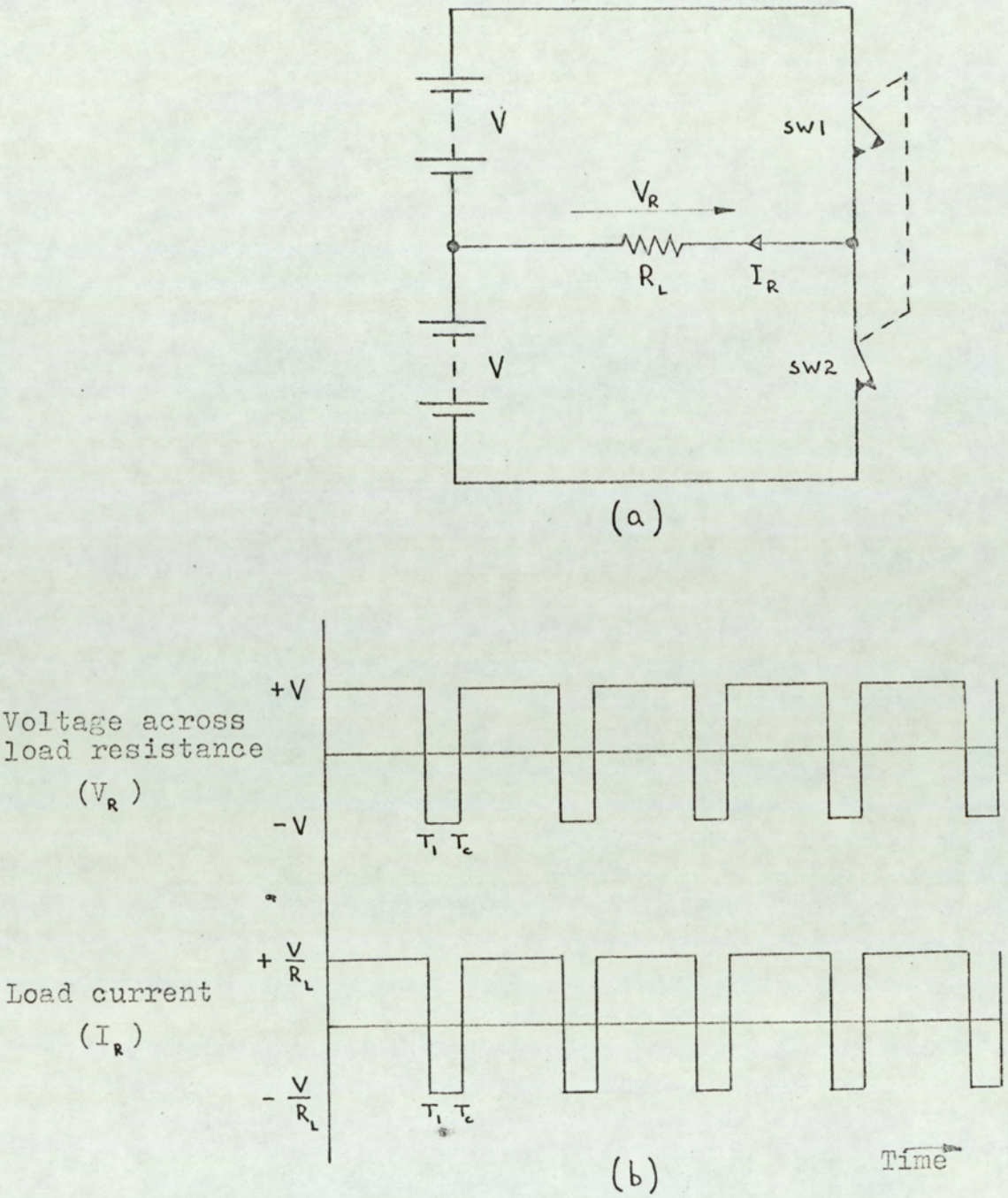

Fig.1.1. Basic pulse-length modulation amplifier

(a) Schematic circuit

(b) Circuit waveforms

$$V_{av} = \frac{V}{T_c}\left(2T_1 - T_c\right) \qquad .. \qquad (1.1)$$

If the period T_1 is equal to $\frac{Tc}{2}$ when no modulating signal is present, then the period T_1 may be written as:

$$T_1 = \frac{T_c}{2} + k_o T_c V_{in} \qquad .. \qquad (1.2)$$

where $k.T_c$ relates the variation of T_1 to the modulating signal V_{in}. Substituting eqn. (1.2) in (1.1) gives:

$$V_{av} = 2 k_o V_{in} \qquad .. \qquad (1.3)$$

Thus the average voltage appearing across the load is directly proportional to the modulating signal. Now the average value of the switching waveform is, by definition, the d.c. component of the waveform. Therefore an inductance may be connected in series with the load resistor to filter the high frequency components of the waveform as shown in fig. 1.2. If the inductance is sufficiently large then the voltage across the load resistance will have a value directly proportional to the modulating signal V_{in} and linear amplification is achieved by means of switches. If the switches are replaced by transistors then high efficiency should be obtained since the transistors are operated in either the "on" or "off" condition where the device dissipation is low.

Fig. 1.3 shows the block diagram of a system for producing length-modulated wavetrains, and fig. 1.4 shows the waveforms associated with the system. The output of the square-wave generator is integrated to produce a triangular sampling waveform as shown in fig. 1.4(b).

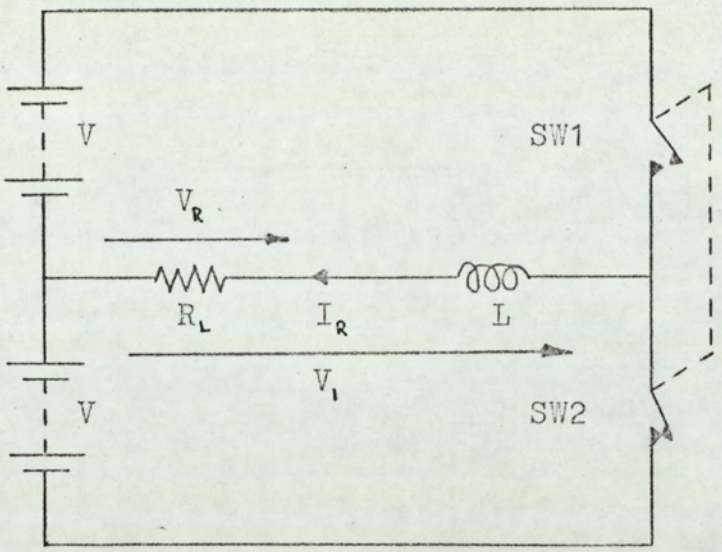

(a)

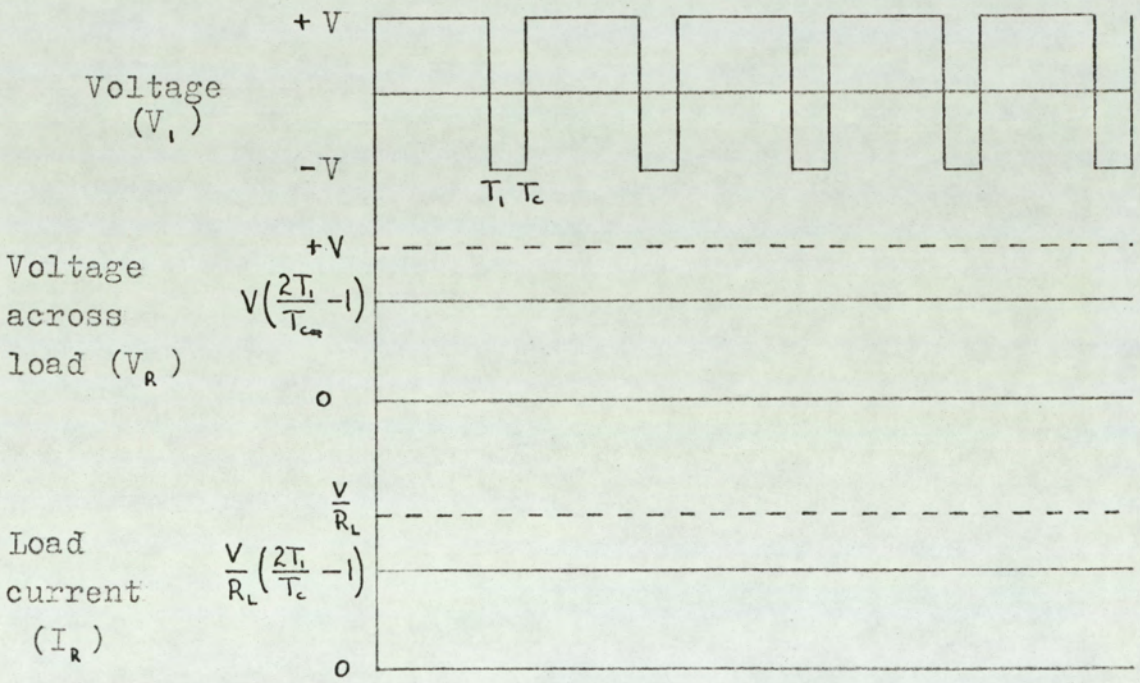

(b)

Fig.1.2 Basic pulse-length modulation amplifier with series inductance for low-pass filtering.

(a) Schematic circuit

(b) Circuit waveforms

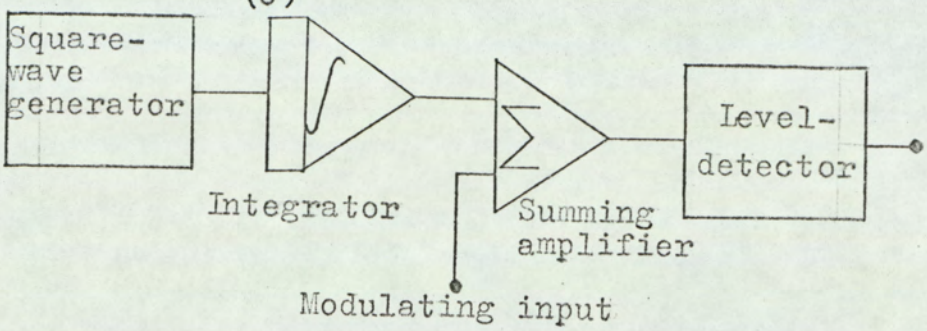

Fig.1.3. Pulse-length modulation system

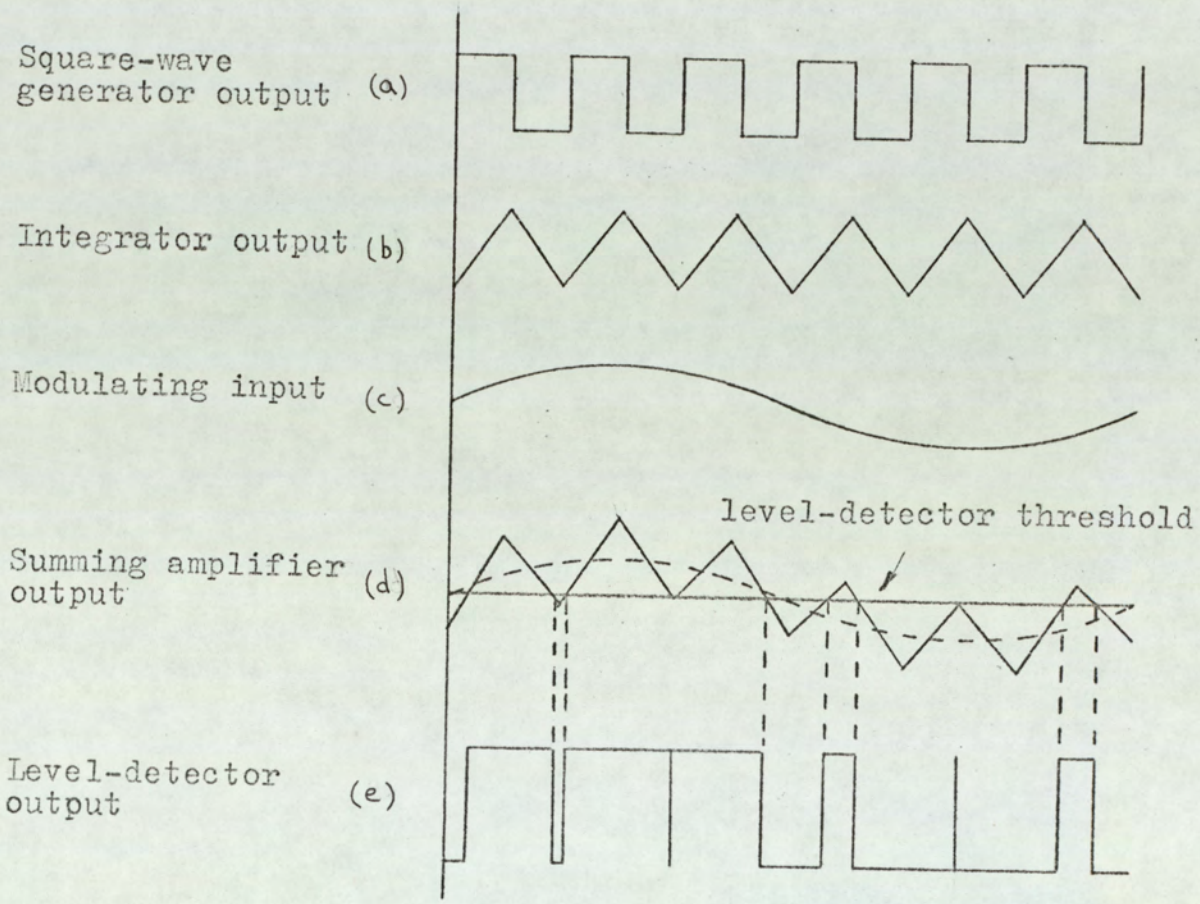

Fig.1.4. Waveforms for pulse-length modulation system

This triangular waveform is added to the modulating input voltage V_{in} and the sum applied to the input of the level-detector. Now the operation of the level-detector is such that the output changes state whenever the voltage applied to its input crosses the threshold level as shown in fig. 1.4(d) and (e). From fig. 1.4(e) it can be seen that the level-detector output waveform is a length-modulated wavetrain which can be used to switch the devices in a high power output stage.

The principle of pulse-length modulation as a means of achieving continuous control predates the introduction of transistors by at least fifty years as will be seen in the following section which is a survey of previous work.

2. Previous work

One of the earliest applications of pulse-length modulation techniques was to the temperature control of an oven, described by Gouy[1] in 1897. The system consists of an oven heated by a resistive heating element, a mercury thermometer and an electrical contact mounted on a motor-driven eccentric. The motor-driven eccentric periodically immerses the electrical contact in the mercury of the thermometer thus closing a circuit and causing current to flow in the coil of a relay. The relay is connected in series with the heater coil of the oven in such a manner that heater current flows when the relay is not energised (i.e. when the switch contact is not immersed in the mercury). Thus the current supplied to the heater coil is a periodic pulse-train. The motor driven contact is so arranged that as the oven temperature rises, the mercury level rises and the contact remains immersed in the mercury for a longer period, hence decreasing the period of the current pulses supplied to the heater coil. Since the pulse period is reduced, the average power dissipated in the heater coil is reduced and the oven temperature falls. Thus closed-loop control of the oven temperature is achieved. The first publication dealing with pulse-length modulation in electronic systems appears to be a patent, taken out by Bedford[2] in 1931, which describes a low frequency amplifier using thyratrons as the switching elements. The next application of pulse-length modulation was in television systems when a number of workers[3,4,5] considered the possibility of using the line synchronising period to transmit the sound channel as length modulated pulses. However the technique found very little application until the advent of World

War II, when the need for high power communication equipment stimulated an interest in pulse modulation. A number of papers[8-12] appeared in the immediate post-war years dealing with theoretical and practical aspects of pulse-length modulation which had arisen from the war effort. Further papers[13-17] published at this time discuss the spectrum analysis of pulse-length modulated wavetrains. Although these early papers do not deal with pulse-length modulation as a technique for achieving audio amplification they do provide the theoretical foundations of the modulation process. Up to this point in time (i.e. the late 1940's) the only devices capable of switching at the required pulse repetition frequency were thermionic valves which are not very efficient as high-power switches. However the development of the junction transistor led to a resurgence of interest in pulse-length modulation as a means of achieving high efficiency amplification.

One of the first references to the use of transistors in this manner is a paper by Bright[18] which describes the switching properties of junction transistors and briefly describes a hypothetical system for controlling the field current of a d.c. motor. The first paper dealing specifically with pulse-length modulation amplifiers is by Milnes[19] who describes various systems which are analogous to the well known phase-controlled thyratron systems for controlling the average current into a load from an a.c. supply. After this publication a number of papers appeared [20-32] describing various pulse-length modulation amplifiers and regulator systems. None of these papers attempt to establish any analytical basis for the systems apart from calculations of losses occuring in transistor switching output stages. In general the analyses are of a very much simplified nature with a few exceptions[23,24,25] where

the authors have considered the output stage efficiency from a more realistic point of view. It is interesting to note that in spite of the fairly considerable amount of work published on the spectrum analysis of pulse-length modulated wavetrains none of these papers on pulse-length modulation amplifiers makes more than a passing comment on the required pulse repetition frequency.

The first published work which gives serious consideration to the theoretical aspects of pulse-length modulation amplifiers is by Miller[33]. He makes use of the spectrum analyses developed by workers in the radio-communication field to establish the required pulse-repetition frequency for an amplifier system. He also gives some consideration to the problems involved in operating switching output stages into the low-pass filter necessary to demodulate the wavetrain. Turnbull and Townsend[35] present complete designs for two pulse-length modulation amplifiers which can deliver an output power of 2 watts into a 15Ω load. The first of these two amplifiers is described as an "open-loop" system since the basic square-wave, which produces the sampling waveform, is derived from a separate oscillator in the same manner as the system shown in fig. 1.3. The second system dispenses with the square-wave generator by connecting the system output back to the integrator input in such a manner that the feedback is positive and the system oscillates. Although this overall feedback is positive the system can be designed so that the feedback for the modulation frequency components is negative thus giving some improvement in performance. This type of amplifier is called a "closed-loop" system. With this system not only is the pulse-length varied but also the frequency. The "closed-loop" system is well known in control system theory[36] and is often referred to as a

relay amplifier. Previous authors[37-41] have also suggested a "closed-loop" system as an alternative to the normal "open-loop" systems as a means of designing high efficiency amplifiers. The article by Turnbull and Townsend[35] raised a certain amount of controversy [42,43], particularly with regard to the claims the authors make for the efficiency of the amplifiers. The controversy arises from aspects of operating switching output stages into an inductive load (i.e. a filter) which gives entirely different operating conditions to a reistive load. These problems are discussed in considerably more detail by Turnbull and Townsend[44,45] in two later articles. Johnson[46,47,48] has published a critique of pulse-length modulation amplifiers in which he examines the performance of various types of system from the point of view of distortion and efficiency. The majority of the discussion is based on intuitive reasoning rather than on mathematical analysis. However these papers do show the need for a considerable amount of analytical investigation into the performance of practical pulse-length modulation amplifier systems.

3. Classification of pulse-length modulation processes.

As discussed in the survey of previous work there are two types of pulse-length modulation amplifier: namely "open-loop" systems and "closed-loop" systems. The "open-loop" system is basically more simple and is the fundamental pulse-length modulation process, since the pulse-repetition frequency also varies in the "closed-loop" system. For this reason it is considered that design principles should be established for the "open-loop" system. However, many of the principles can probably be applied to the "closed-loop" system.

There are two fundamental methods of producing pulse-length modulation and these are normally called natural sampling and periodic sampling. With periodic sampling the length of the pulses are made proportional to the instantaneous value of the modulating input at strictly periodic intervals. Natural sampling is rather more complex since the position of the pulse-edge is determined by the instantaneous amplitude of the modulating input at the time of occurence of the pulse-edge. The two types of modulation are shown in figs. 3.1 and 3.2. A further classification of the modulation processes is to define which of the pulse-edges is being modulated. Thus both natural and periodic sampling can be sub-divided into the following classes. Leading-edge modulation where the trailing edges of the pulses occur at periodic intervals and the leading pulse-edges are modulated according to the particular type of modulation being considered (i.e. Natural sampling or periodic sampling). Double-edge modulation where the positions of both the leading and trailing pulse-edges are modulated.

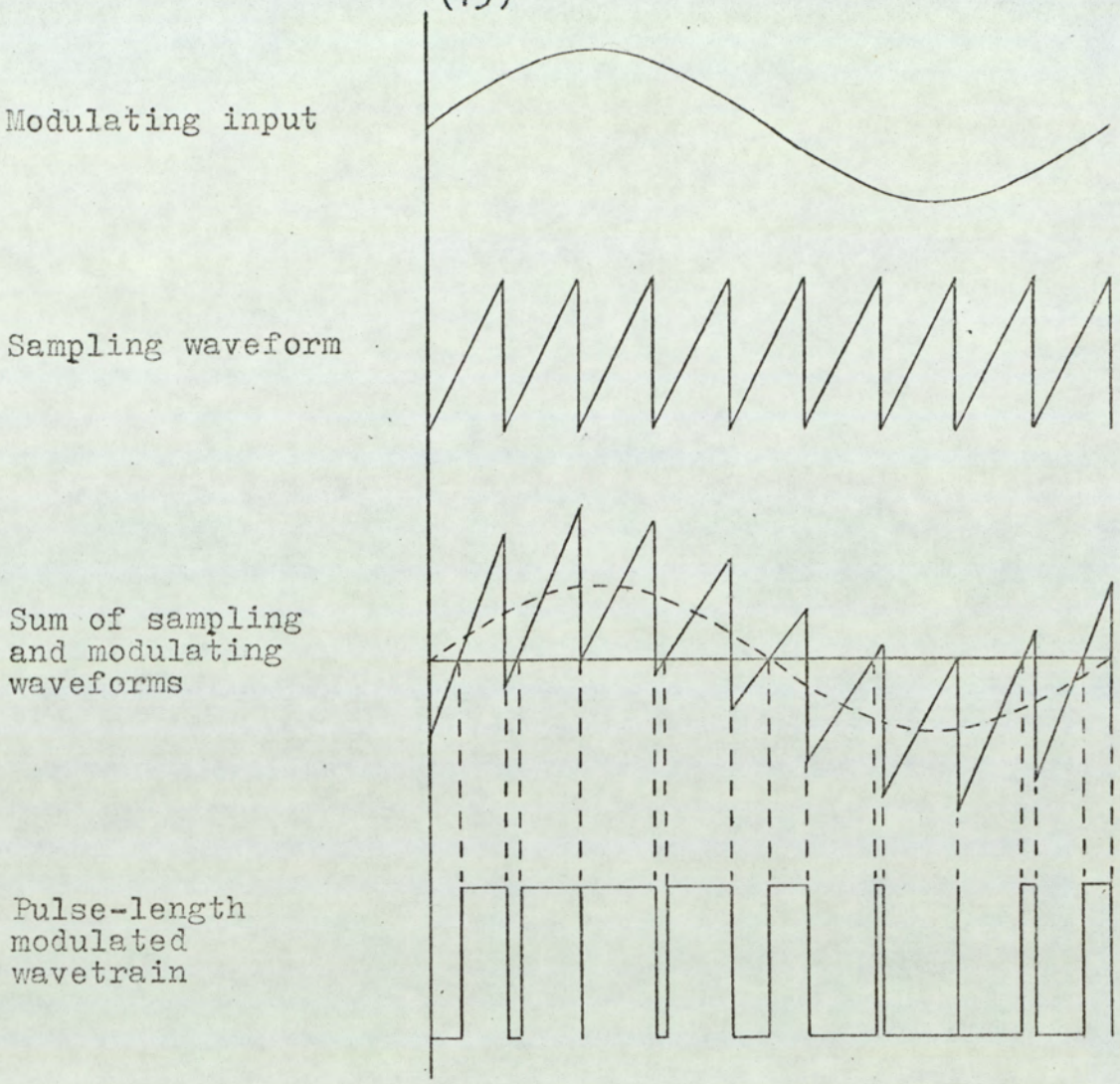

Fig.3.1. Pulse-length modulated wavetrain produced by natural sampling.

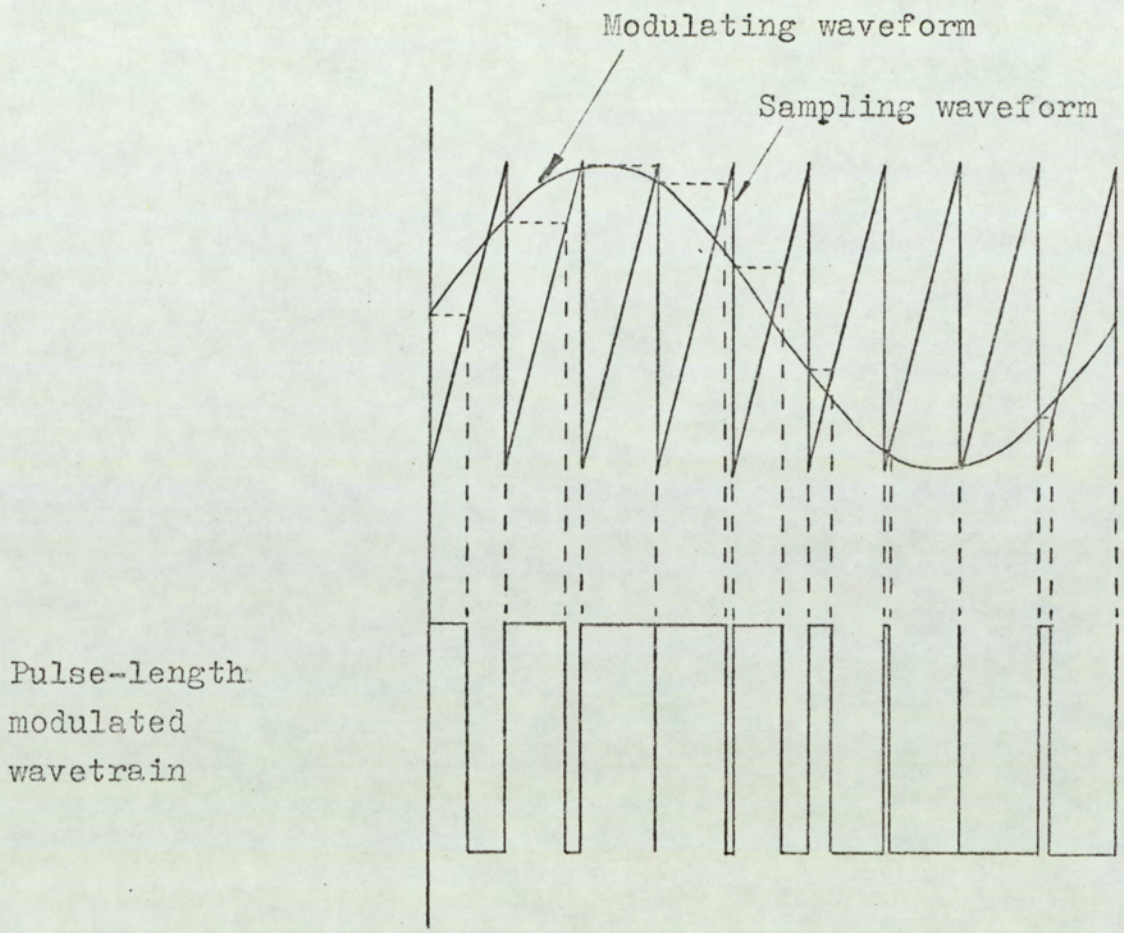

Fig.3.2. Pulse-length modulated wavetrain produced by periodic sampling.

Finally there is trailing-edge modulation where the leading pulse-edges occur at periodic intervals and the positions of the trailing pulse-edges are modulated. Pulse-length modulated wavetrains produced according to these various classifications have rather different characteristics which are discussed in the following chapter.

CHAPTER II

Distortion in the Pulse-length Modulation Process

1. General

Distortion in the pulse-length modulation process is of two types, namely sideband distortion and harmonic distortion. Sideband distortion results from lower order sidebands, of the sampling and modulation frequencies, falling within the pass-band of the system. This type of distortion is inherent in all methods of pulse-length modulation. Distortion in the form of harmonics of the modulation frequency is not inherent in the pulse-length modulation process but can arise as a result of imperfections in the system. Much attention has been given in the literature to the problem of sideband distortion, and the major contributions will now be reviewed.

Lawson, Lord and Kharbanda [6] present a limited analysis of pulse-length modulation with natural sampling, the analysis being based on a quasi-dynamic method. The quasi-dynamic method entails setting up the Fourier series for a train of pulses of constant length, and then replacing the pulse length with a time-dependent function. This method of analysis lacks mathematical rigour since the pulse length is not a function of the instantaneous amplitude of the modulating signal at periodic intervals. Thus, the resulting modulated wavetrain is non-periodic and application of Fourier series analysis requires, in the words of the authors, "some mathematical courage". A further fault in the analysis is that the spectrum is derived for double-edge length-modulated wavetrains, and the results applied to a single-edge length modulation system. Roberts and Simmonds [13] also make use of the quasi-dynamic method for analysis of pulse-length modulation

with natural sampling. Fredendall, Schlesinger and Schroeder[7] analyse in some detail a system where the length of a pulse is proportional to the amplitude of the modulating wave at the instant corresponding to the centre line of the pulse. This is a form of periodic sampling; however, it is obviously impossible to achieve, since the positions of the pulse edges are determined by the value of the modulating wave at some time after the leading pulse edge has occurred. The authors apply this analysis for periodic sampling to a system having single-edge modulation with natural sampling. This lack of rigorous definition of the type of modulation process being analysed is a common feature of the early papers on the subject. A number of workers have published analyses of pulse-length modulation which do not rely on the rather dubious quasi-dynamic method. Fitch[11] approaches the problem by synthesising $2N + 1$ cycles of a rectangular wavetrain with $2N + 1$ positive step functions and $2N + 1$ negative step functions. The Fourier transform for each of the positive step functions is written with the appropriate time shift, and a series formed by summing the Fourier transforms. A similar process is carried out for the negative step functions and the two series added. N is then allowed to increase indefinitely and the limit of the series obtained. The resulting expression enables the individual effects of the leading and trailing edges of the pulses to be readily identified; the pulse length can then be modulated as required. Even this method is not completely rigorous, since the limiting process really only produces a Fourier series from the sum of the Fourier transforms. A similar method is outlined by Levy[12] for pulse-length modulation with natural sampling. However, he defines the pulse-length incorrectly so that the mathematical analysis is actually for a system with periodic sampling. Stuart[49] develops a method

similar to that of Fitch[11], except that the modulation is applied to the appropriate parameter of the pulse before the limit is taken of the sum of the Fourier transforms of the individual pulses. Bennett[50] developed a method of analysing rectified waves by means of a double Fourier series in two variables. He also extends the method to analysing pulse-length modulated wavetrains, but did not publish the work. Black[51], however, has published an analysis based on Bennett's unpublished work. The method is rigorous but requires rather more routine mathematical work than the Fourier integral method[11,49]. A further method of analysing pulse-length modulated wavetrains was introduced independently by Krauss and Ordung[16] and Bloch[52]. The method is to synthesise a rectangular wavetrain from two triangular wavetrains displaced in time, and to maintain the amplitude of the pulse train constant by introducing an amplitude-correction factor. The phase of either, or both, of the triangular wavetrains is modulated to produce a pulse-length modulated wavetrain. The derivation of the amplitude correction term is dealt with in some detail by Krauss and Ordung[16] but is not treated rigorously. Kretzmer[14] utilises the quasi-dynamic method of analysis but takes some care in correctly defining the switching instants for pulse-length modulation with natural sampling. Moss[17] presents an extensive treatment of pulse modulation of various types, including periodically and naturally sampled pulse-length modulation. The analysis is developed in a general way for pulses of arbitrary shape modulated in amplitude and time. Introduction of a spectral shape-factor for each type

of pulse enables the development to be concentrated on the essential features of each type of modulation. Time modulation is achieved by deforming the time variable. The analyses are developed in abstract terms so that careful consideration is required in order to follow the argument.

At this point it is convenient to introduce the results of the rigorous spectrum analyses.[17,51] For single-edge pulse length modulation with periodic sampling, the frequency spectrum is given by equation 1.1.

$$F(t) = k_o - \sum_{n=1}^{\infty} \frac{J_n\left(\frac{n\pi M\omega_m}{\omega_c}\right)}{n\pi\,\frac{\omega_m}{\omega_c}} \sin\left(n\omega_m t - \frac{2n\pi k_o\omega_m}{\omega_c} - \frac{n\pi}{2}\right) + \sum_{p=1}^{\infty} \frac{1 - J_o(p\pi M)}{p\pi} \sin(p\omega_c t)$$

$$- \sum_{p=1}^{\infty} \sum_{n=\pm 1}^{\pm\infty} \frac{J_n\left[(p\omega_c + n\omega_m)\frac{\pi M}{\omega_c}\right]}{(p\omega_c + n\omega_m)\frac{\pi}{\omega_c}} \sin\left[(p\omega_c + n\omega_m)\left(t - \frac{2\pi k_o}{\omega_c}\right) - \frac{n\pi}{2}\right] \quad .. \quad (1.1)$$

where k_o = ratio of unmodulated pulse length to the period of the unmodulated wavetrain

ω_c = angular frequency of the wavetrain

ω_m = angular modulation frequency

M = modulation index

modulation function = $M.\cos(\omega_m t)$

It will be noted from equation 1.1. that the amplitude of the component at the fundamental of the modulating frequency is not linearly related to the modulation index M . Furthermore, distortion is present in the form of harmonics of the modulating frequency. Sideband components $p\omega_c - n\omega_m$, which extend

down to the system pass-band, also produce distortion. Thus, harmonic and sideband distortion exists if the periodically-sampled, length-modulated wavetrain is demodulated by passing the modulated wavetrain through a low-pass filter. It may be shown [8,51] that distortionless demodulation may be achieved by first converting the periodically length-modulated wavetrain into a pulse-amplitude modulated wavetrain having pulse amplitudes directly proportional to the length of the corresponding pulses of the length-modulated wavetrain. Demodulation of the pulse amplitude modulated wavetrain may then be achieved by low-pass filtering. However, the conversion of pulse-length into a proportional pulse amplitdue is likely to be a very inefficient process at high power levels. This technique is therefore not suitable as a means of producing high power amplification.

The frequency spectrum for pulse-length modulated waves, with natural sampling, is given in equation 1.2. for single-edge modulation, and in equation 1.3. for double-edge modulation [11,17,33,34,51].

For single-edge modulation:

$$F(t) = k_o\left[1 + M\cos(\omega_m t)\right] +$$

$$\sum_{p=1}^{\infty} \frac{\sin(p\omega_c t)}{p\pi} - \sum_{p=1}^{\infty} \frac{J_o(2p\pi k_o M)}{p\pi} \sin(p\omega_c t - 2k_o p\pi) -$$

$$\sum_{p=1}^{\infty} \sum_{n=\pm 1}^{\pm\infty} \frac{J_n(2p\pi k_o M)}{p\pi} \sin\left[(p\omega_c + n\omega_m)t - 2p\pi k_o - \frac{n\pi}{2}\right] \quad .. \quad (1.2)$$

For double-edge modulation:

$$F(t) = k_o\left[1+M.\cos(\omega_m t)\right] + \sum_{p=1}^{\infty} \frac{2\,J_o(p\pi k_o M)}{p\pi} \sin(p\pi k_o).\cos(p\omega_c t) +$$

$$\sum_{p=1}^{\infty} \sum_{n=\pm 1}^{\pm\infty} \frac{2J_n(p\pi k_o M)}{p\pi} \sin\left(p\pi k_o + \frac{n\pi}{2}\right).\cos\left[(p\omega_c + n\omega_m)t\right] \quad . . (1.3)$$

where the symbols have the same significance as in equation 1.1.

Equation 1.2. gives the frequency spectrum for trailing-edge modulation. To obtain the spectrum for leading-edge modulation, it is merely necessary to reverse the sign of the time variable throughout equation 1.2. The frequency spectra for single-edge and double-edge modulation contain a constant term k and an undistorted modulating-frequency component $k_o M \cos \omega_m t$. They also contain components at all the harmonics $p\omega_c$ of the carrier frequency and sidebands $(p\omega_c \pm n\omega_m)$ of each harmonic of the modulating frequency. It should be noted that no harmonics of the modulating frequency occur and that the amplitude of the component at the fundamental of the modulating frequency is directly proportional to the modulation index . Demodulation can therefore be achieved by simply passing the modulated wavetrain through a low-pass filter. Thus pulse-length modulation with natural sampling is an inherently better technique for high power amplification than pulse-length modulation with periodic sampling. Some of the lower sideband frequencies $(p\omega_c - n\omega_m)$, in particular $(\omega_c - n\omega_m)$, fall within the system pass-band and cause sideband distortion.

Before continuing the discussion of sideband distortion, some further observations will be made from equations 1.2. and 1.3. The modulation frequency term $k_o M \cos \omega_m t$ has the maximum value of $k_o \cos \omega_m t$ when $M = 1$, and there is full modulation of the pulse from zero to $2k_o$. If k_o (the ratio of the unmodulated pulse length to the period of the unmodulated wavetrain) has the value 0.5, then the pulse length can be modulated from zero to $\frac{2\pi}{\omega_c}$. For the double-edge modulation spectrum, equation 1.3. shows that, with $k_o = 0.5$, the sidebands $(p\omega_c \pm n\omega_m)$ are eliminated when n is odd and $p = 1$. This is not the case with single-edge modulation. Also, although not immediately apparent from equations 1.2 and 1.3., the lower sidebands $(\omega_c - n.\omega_m)$ for double-edge modulation are smaller in amplitude than the corresponding sidebands for single-edge modulation. An intuitive explanation of this fact is that, for a given value of modulation index, the time deviation of each pulse edge with double-edge modulation is only half the time deviation of the pulse edge for single-edge modulation. Figs. 1.1a. and 1.1b. show how the amplitude of the various sideband components vary with the modulation index M for single-edge and double-edge modulation respectively. In fig. 1.1., the value of k_o is 0.5, since this allows full modulation of the pulse length from zero to $\frac{2\pi}{\omega_c}$. From fig. 1.1. it can be seen that, if the sideband components falling within the system pass-band are to be attenuated by at least 60 dB, with respect to $k_o \cos \omega_m t$, then the pulse-repetition rate ω_c must be greater than $9\ \omega_m$

Fig.1.1(a). Sideband amplitude for single-edge modulation

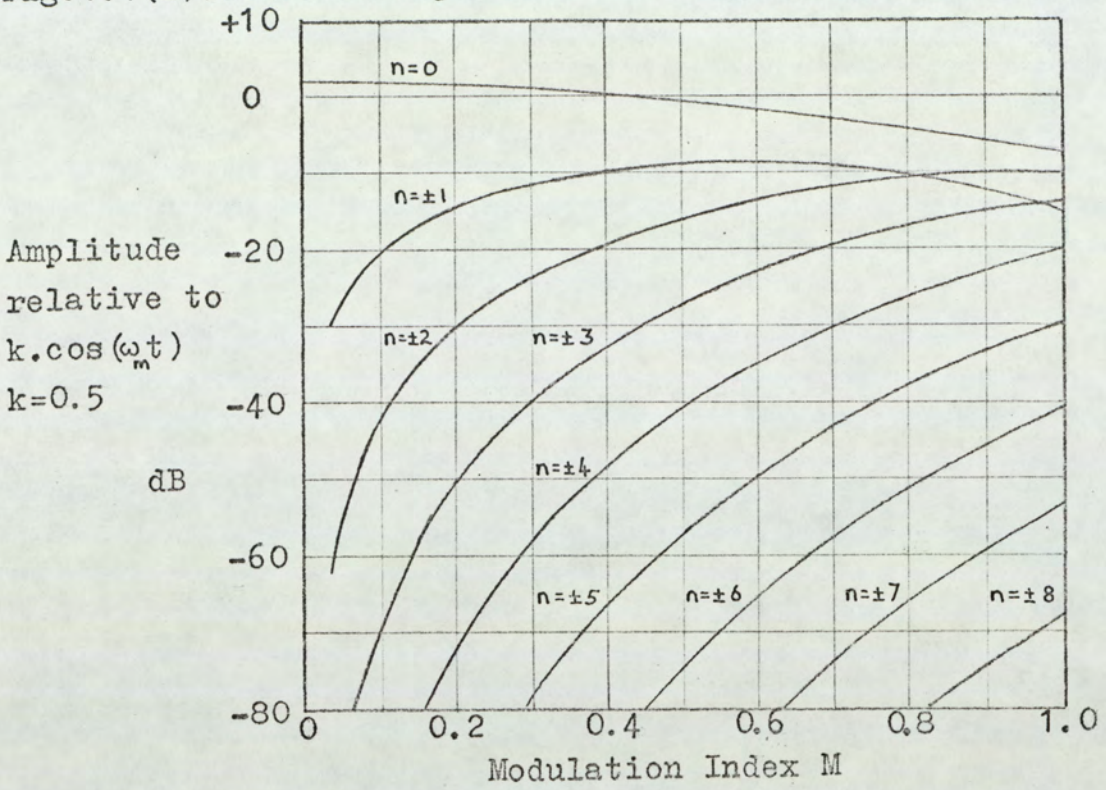

Fig.1.1(b). Sideband amplitude for double-edge modulation

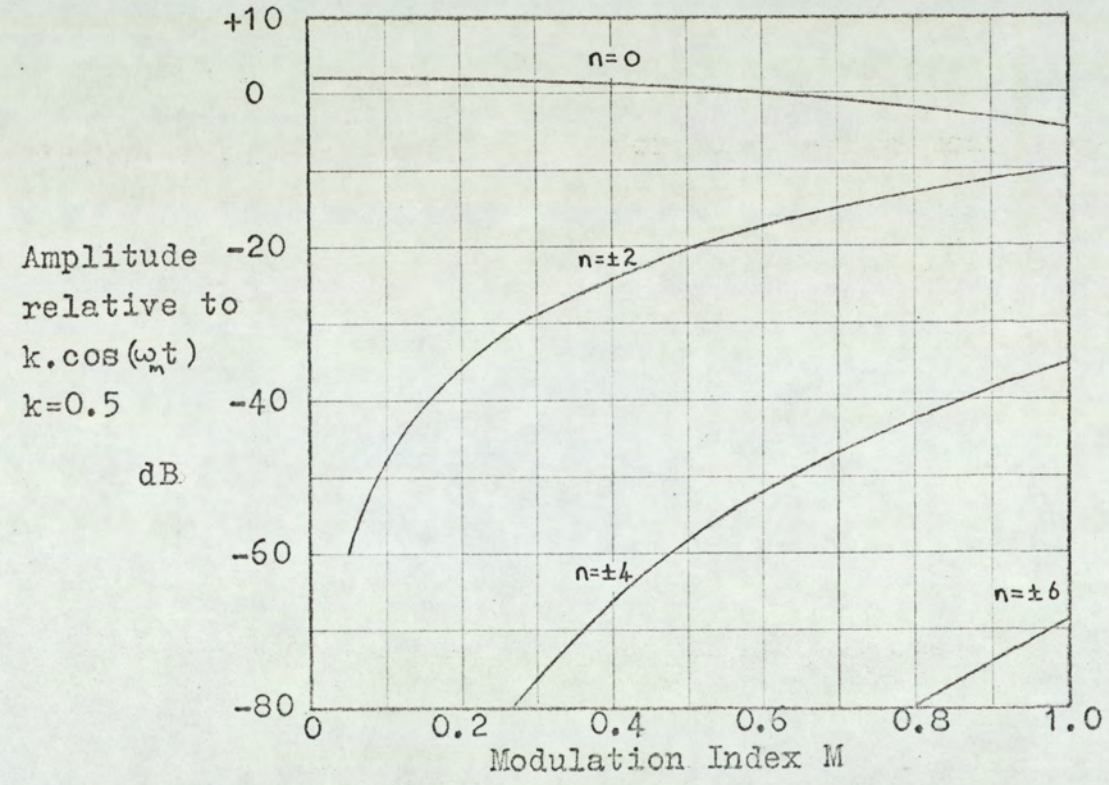

for single-edge modulation. In order to meet the same specification with double-edge modulation, it is only necessary that the pulse-repetition rate is greater than $7\omega_m$, where ω_m is the upper limit of the required system pass-band. Thus, there is a considerable theoretical advantage in using double-edge modulation because a lower pulse repetition rate can be used for a given level of sideband distortion.

All the literature reviewed on distortion in pulse-length modulation systems assumes that the modulation process is ideal in that the pulse length is linearly related to the modulating input to the system. Very little information has been published dealing with distortion that can arise in a practical pulse-length modulation system. Narayana Rao[53] develops expressions for the harmonic distortion resulting from non-linearity in a particular type of thermonic-valve modulator. Although not stated, the type of modulation is single-edge modulation with natural sampling. The expressions developed give the pulse length as a function of the modulating signal and its harmonics. No account is taken of sideband distortion and the work is of very limited application. Further discussion of distortion in the pulse-length modulation process have been published[32,35]. However, these papers are not primarily concerned with the distortion aspect of pulse-length modulation so that they do not present any work which has not been covered in the previous references. Johnson[48] discusses the general problem of sideband distortion but does not introduce any analytical work.

Thus, the need exists for analytical expressions relating

harmonic and sideband distortions to modulator parameters in order that the design of pulse-length modulation systems can be carried out on an analytical basis rather than empirically.

Since it has been shown that there are sound theoretical reasons for utilising naturally-sampled pulse-length modulation, as opposed to periodic sampling, all further work will be with reference to natural sampling.

2. Discussion of Generalised Pulse-Length Modulation Systems

Fig. 2.1(a). shows a generalised system for producing double-edge length-modulated wavetrains with natural sampling. The waveforms associated with the system of fig. 2.1(a). are shown in fig. 2.1(b). The block diagram of a generalised system for producing single-edge modulation with natural sampling is shown in fig. 2.2(a). The switches associated with the operational integrator operate in synchronism every $k.T_c$ seconds, where k is an integer and T_c $(= \frac{2\pi}{\omega_c})$ is the pulse repetition period. It is assumed that the switches are closed for an infinitesimally short time so that the system waveforms are as shown in fig. 2.2(b). The output waveforms of the summing amplifiers, in figs. 2.1(b). and 2.2(b)., are idealised to some extent, since the sloping edges are shown as straight lines. This is not a true representation, since the modulating input is time varying during the scan of the triangular wave. Although many circuits can be envisaged for producing pulse-length modulation, the majority of systems perform the functions shown in figs. 2.1. and 2.2. Moreoever, with the advent of integrated circuits, the designer must work in terms of the type of standard circuit blocks shown in figs. 2.1. and 2.2. rather than design a discrete-component circuit for each specific application.

It was shown in section 1 that for a sideband distotion level of - 60 dB, the pulse-repetition rate must be greater than $7\omega_m$ for double-edge modulation, and greater than $9\omega_m$ for single-edge modulation. Thus, if a system is to have a pass-band extending

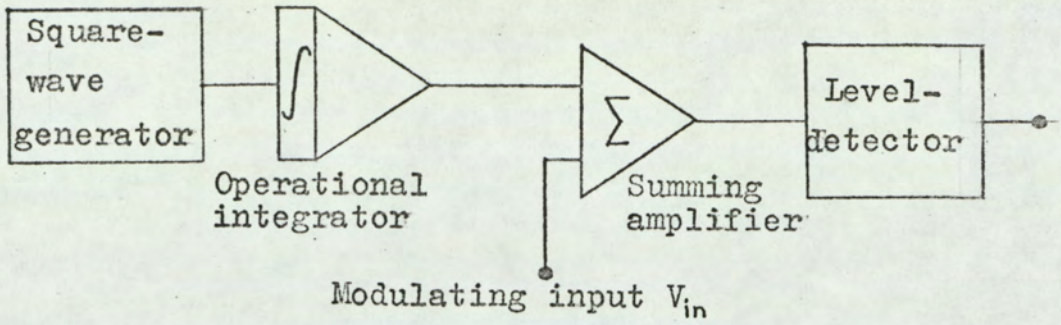

Fig.2.1(a). Double-edge modulation system.

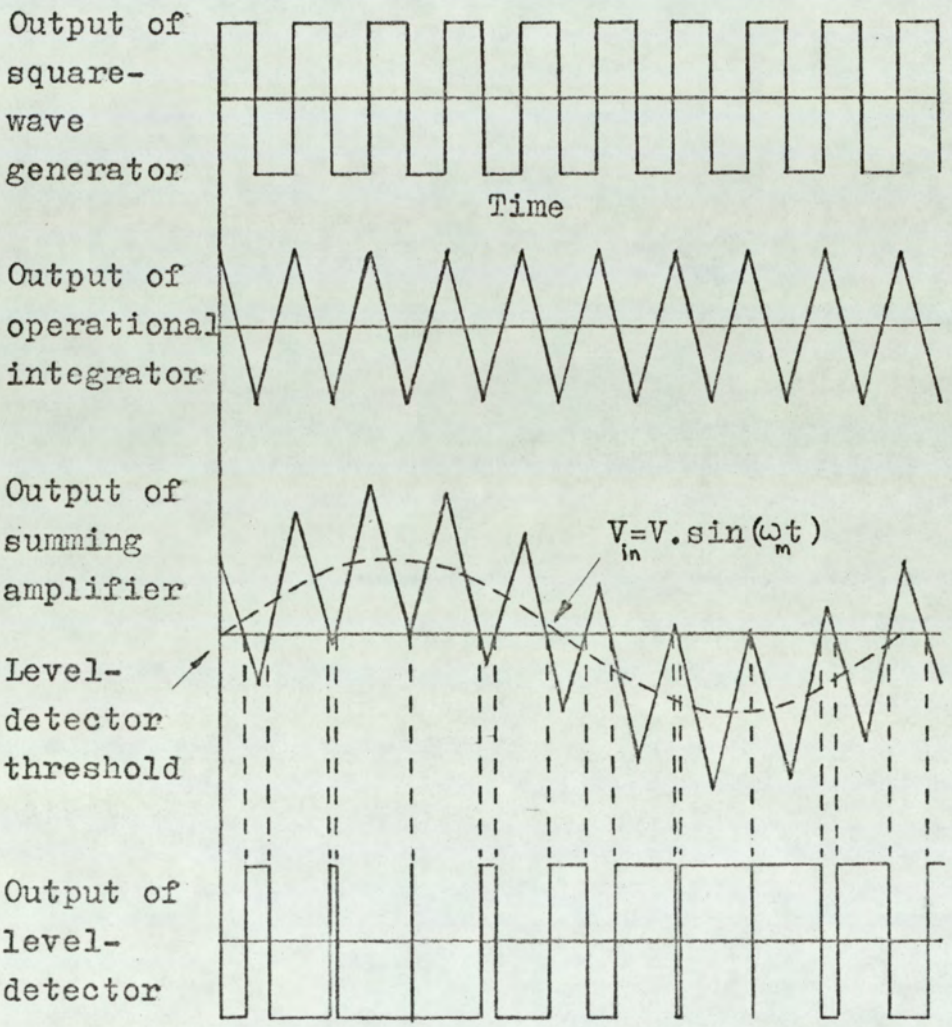

Fig.2.1(b). Waveforms for double-edge pulse-length modulation system.

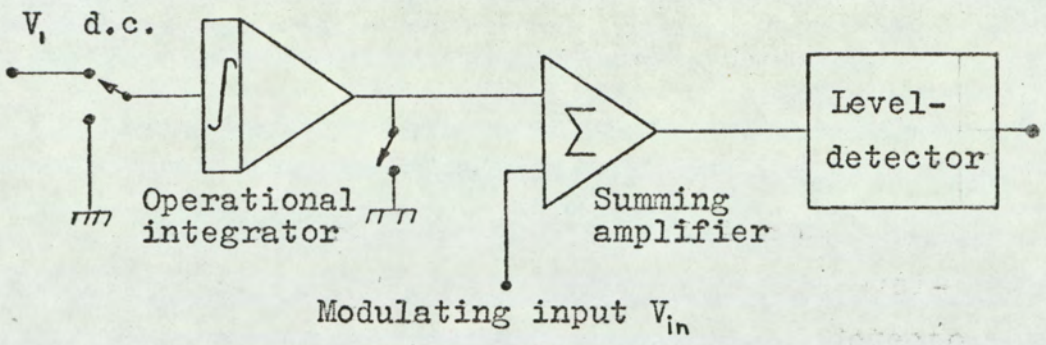

Fig.2.2(a). Single-edge modulation system.

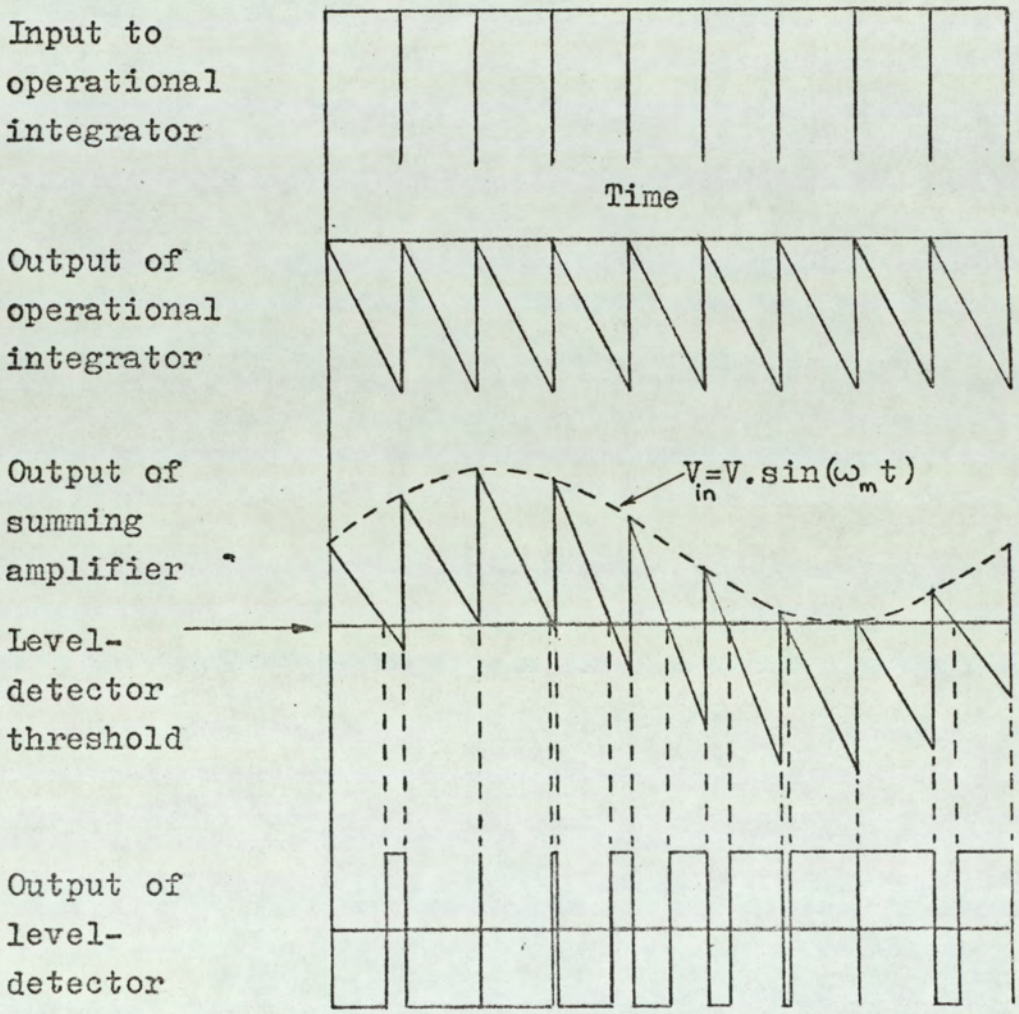

Fig.2.2(b). Waveforms for single-edge pulse-length modulation system.

to 17 kHz, the pulse-repetition rate must be of the order of 120 kHz for double-edge modulation and 160 kHz for single-edge modulation. This is only a very limited consideration of the problem, but it enables some useful conclusions to be drawn regarding the specification for the functional blocks of these systems. For the double-edge modulation system of fig. 2. 1(a)., it is necessary to generate a square-wave having rise and fall times much less than the period. With a repetition rate of the order of 120 kHz, the period is approximately 8 μsec. so that a square-wave having rise and fall times much less than the period may be generated by well established techniques [54].

The problem of maintaining unity mark-space ratio, in order to maintain a symmetrical triangular wave, may be overcome by using a rectangular wave generator, of arbitrary mark-space ratio, operating at twice the required pulse repetition rate. The correct repetition rate, and a well-defined mark-space ratio of unity, may then be obtained by dividing the output of the rectangular wave generator by a single binary divider circuit. With the single-edge modulation system of fig. 2. 2(a). the square wave generator is not necessary. However, the integrator must be reset periodically and in a time much shorter than this period so the problem is much the same as for double-edge modulation. Since the rise and fall time of the square wave generator for double-edge modulation, and the integrator reset time for single-edge modulation, can both be accomplished in a time very much less than the period, this part of the system will be considered ideal.

The operational integrator section of the two systems presents the major design problem. There are several parameters to be considered, the major ones being: gain, input resistance, output resistance and open-loop bandwidth. Unfortunately, it is not possible to make each of these parameters approach the idealised values without introducing considerable complexity into the design. In fact, with a practical operational integrator, these parameters are very often inter-dependent. For instance, increasing the gain of an operational integrator usually requires additional amplifier stages with a resulting decrease in bandwidth. A further problem with high-gain amplifiers is that there are a number of time-constants, and high-frequency instability can occur when the amplifier is used as an operational integrator.

The bandwidth of the summing amplifier has to be sufficient to pass the summation of the sampling waveform and the modulating input waveform without distortion. Since the bandwidth of the sampling waveform is much greater than that of the modulating waveform, the requirement is essentially that the summing amplifier bandwidth be sufficient to pass the sampling waveform without distortion. Now, the sampling waveform for single-edge modulation is a sawtooth which has a jump discontinuity. It can be shown[55] that the Fourier series coefficients of a waveform with a jump discontinuity decrease as $^1/_n$, where n is the order of the harmonic. For double-edge modulation, the sampling waveform is triangular and the Fourier coefficients decrease as $^1/_{n^2}$. Thus

the bandwidth requirements of the summing amplifier are rather more severe for single-edge modulation. In many practical systems, the summation is carried out by means of a resistance network, so bandwidth limitation is not a problem. For summation, only a low gain is required and relatively large bandwidths are easily achieved. Therefore, the summing amplifier need not be further discussed. It is shown in section 6.1. that this part of the modulator can usually be eliminated as a separate circuit element.

The output of the level detector of figs. 2.1(a). and 2.2(a) changes state whenever its input signal crosses the threshold level. A large class of level detectors exhibit a hysteresis effect; the threshold voltage for positive-going input voltages differs from that for negative-going input voltages. The transfer function of a typical level detector is shown in fig. 2.3. In the

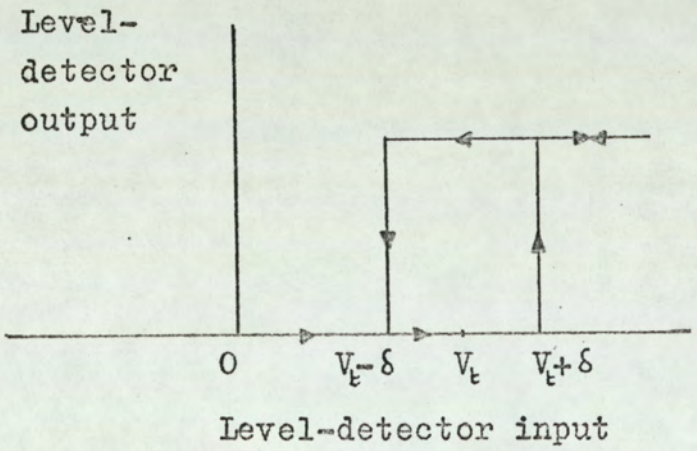

Fig.2.3. Transfer function of hysteretic level-detector.

design of a pulse-length modulation system, it is therefore necessary to know what effect the level detector hysteresis has on system performance.

In view of the points raised above, the analysis of distortion in practical modulation systems has been concentrated on the operational integrator and level detector functions. Development of expressions relating system distortion to system parameters has been carried out in two stages. First, a static analysis is made, section 3, in which the switching instants of the level detector are related to system parameters for a d.c. modulating input. From these expressions, the static error in the averaged value of the level detector output can be deduced. The second stage, section 4, is to analyse the frequency spectrum of the modulated waveform when the system input is sinusoidal. In order to do this, it is necessary to make use of the expressions for the level-detector switching instants which are obtained in the static analysis.

3. Static Analysis

3.1. Static Error due to Finite Operational Integrator Gain

Fig. 3.1.1. shows an operational integrator consisting of an operational amplifier (having a finite voltage gain, $-\alpha$) and a resistance-capacitance network to produce the integrating action. It is assumed that, apart from the finite gain, the amplifier is ideal in that the input resistance and bandwidth are infinite, and the output resistance is zero.

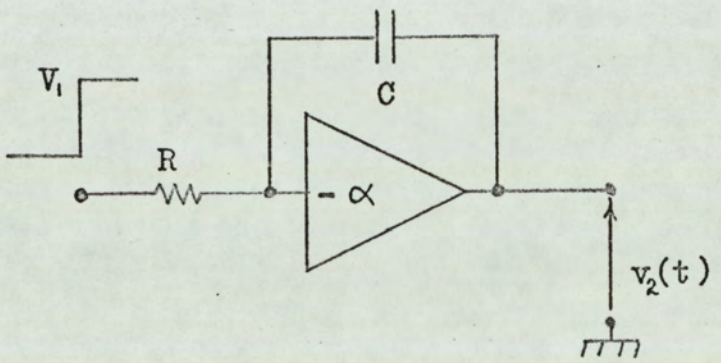

Fig.3.1.1. Operational integrator.

The output voltage of the operational integrator of Fig. 3.1.1. in response to a positive step input of V_1, is:

$$v_2(t) = -\alpha V_1 \left[1 - \exp\left(\frac{-t}{(1+\alpha)CR}\right)\right] \qquad .. \quad (3.1.1)$$

The above expression is the basis for the following analyses of static error in pulse-length modulation systems with finite integrator gain.

3.1.1. Single-edge Modulation

Consider the single-edge modulation system of fig. 2.2(a). using the operation amplifier of fig. 3.1.1. to produce the sampling waveform. The sampling waveform is added to the system modulating input V_{in} and the sum is applied to the input of the level detector. The output of the level detector changes state whenever the voltage applied to its input crosses the threshold. If it is assumed that the level detector does not exhibit hysteresis, the waveforms will be as shown in fig. 3.1.2. It can be seen that the trailing edge of the level detector output pulse occurs at periodic intervals of T_c. The switching instant, t_1, of the leading edge is obtained by solving the equation:

$$v_2(t_1) + V_{in} = V_t \qquad .. \qquad (3.1.2)$$

where V_t is the level-detector threshold voltage.

Consideration must now be given to choosing the level detector threshold V_t. Demodulation of the pulse-length modulated wavetrain at the output of the level detector may be achieved by passing the modulated wavetrain through a low-pass filter. If the attenutation of the a.c. components of the waveform is sufficient, then filtering is equivalent to taking the average value of the modulated wavetrain. Fig. 3.1.2. shows that the average value of the level-detector output waveform is:

$$V_{av} = 1 - 2 \cdot \frac{t_1}{T_c} \qquad .. \qquad (3.1.3)$$

The level detector threshold voltage can be set to give two distinct conditions. The first of these conditions is that

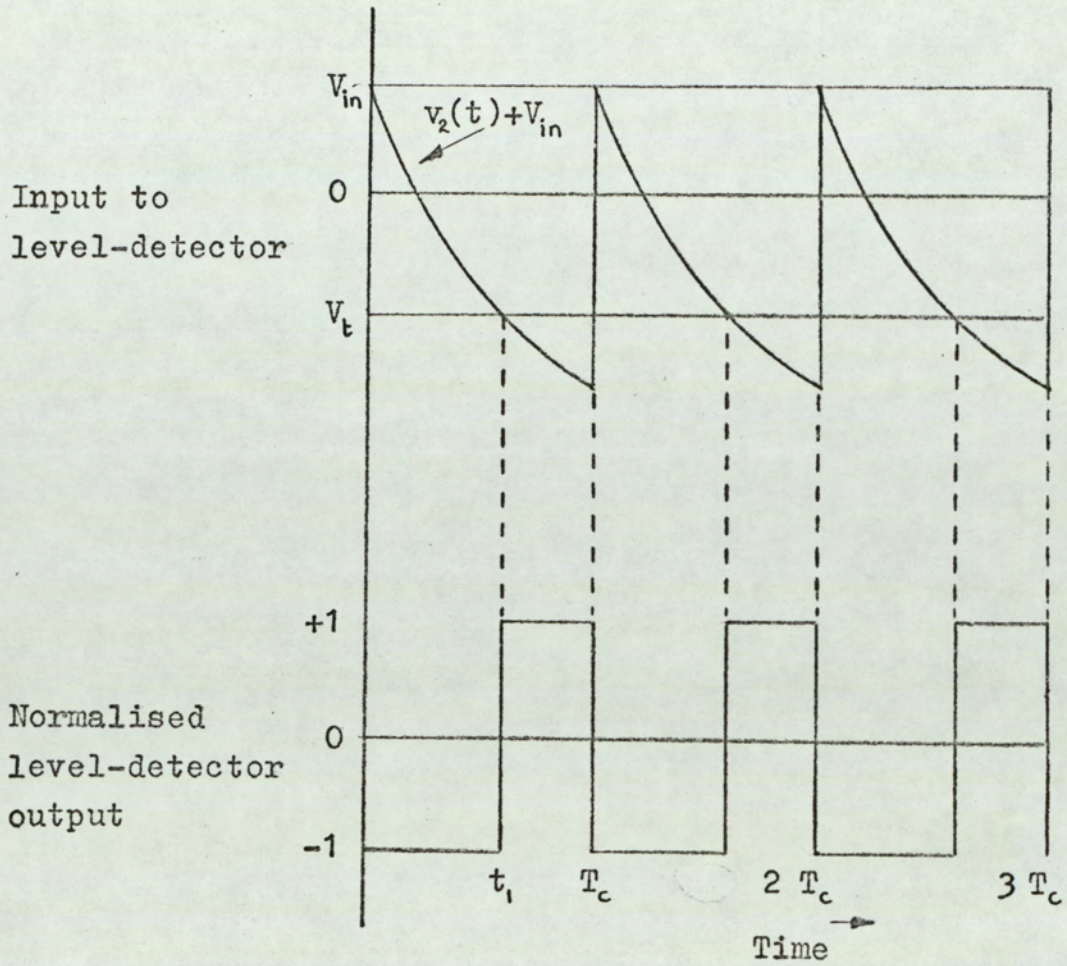

Fig.3.1.2. Waveforms for single-edge modulation system with finite integrator gain.

the average value of the level-detector output is zero for zero input modulating voltage. The value of t_1 necessary to satisfy this condition is given by equation 3.1.3., (i.e., $t_1 = \frac{T_c}{2}$ for $V_{av} = 0$ when $V_{in} = 0$.) It is evident from fig. 3.1.2. that the threshold voltage must be set at the value of the sampling waveform at time $T_c/2$ if the unmodulated pulse length is to equal $T_c/2$. Equation 3.1.1. expresses the sampling waveform as a function of time, and substituting $T_c/2$ for t gives the value for the threshold voltage as:

$$V_t = -\alpha V_1 \left[1 - \exp\left(\frac{-T_c}{2(1+\alpha)CR}\right)\right] \quad .. \quad (3.1.4)$$

Substituting equations 3.1.4. and 3.1.1. into equation 3.1.2. gives:

$$-\alpha V_1\left[1-\exp\left(\frac{-t_1}{(1+\alpha)CR}\right)\right] + V_{in} = -\alpha V_1\left[1-\exp\left(\frac{-T_c}{2(1+\alpha)CR}\right)\right] \quad (3.1.5)$$

from which the switching instant t_1 can be calculated.

It is of interest to calculate the positive and negative values of V_{in} required for full modulation. Now, full modulation for positive values of V_{in} is given by the condition that $t_1 = T_c$. Full modulation for negative values of V_{in} is given by $t_1 = 0$. From equation 3.1.5. with $t_1 = 0$ and $t_1 = T_c$:

$$\hat{V}_{in-} = -\alpha V_1\left[1 - \exp\left(\frac{-T_c}{2(1+\alpha)CR}\right)\right] \quad .. \quad (3.1.6)$$

$$\hat{V}_{in+} = -\alpha V_1\left[1-\exp\left(\frac{-T_c}{2(1+\alpha)CR}\right)\right] + \alpha V_1\left[1-\exp\left(\frac{-T_c}{(1+\alpha)CR}\right)\right] \quad .. \quad (3.1.7)$$

where $\hat{V}_{in+}$ and $\hat{V}_{in-}$ are respectively the positive and negative values of V_{in} necessary to achieve full modulation. These results could also have been obtained by considering fig. 3.1.2. It will be noted that for finite values of integrator gain α, the absolute magnitude of the peak negative input $\hat{V}_{in-}$ is greater than the absolute magnitude of the peak positive input $\hat{V}_{in+}$. This leads to the second condition for which the threshold level of the level-detector may be set; namely that the positive and negative values of modulating input voltage V_{in}, necessary for full modulation, have equal absolute values, i.e., $\hat{V}_{in+} = -\hat{V}_{in-}$. As stated previously, the peak positive input is given by the condition that $t_1 = T_c$. Similarly, the peak negative input is given by the condition $t_1 = 0$. Substituting equation 3.1.1., for the sampling waveform, into equation 3.1.2 gives:

$$-\alpha V_1\left[1 - \exp\left(\frac{-t_1}{(1+\alpha)CR}\right)\right] + V_{in} = V_t \quad .. \quad (3.1.8)$$

The value of the threshold voltage V_t, necessary to satisfy the condition $\hat{V}_{in+} = -\hat{V}_{in-}$, may be calculated from equation 3.1.8. by substituting $t_1 = 0$ and $t_1 = T_c$. Solution of the simultaneous equations so formed gives:

$$V_t = -\frac{\alpha V_1}{2}\left[1 - \exp\left(\frac{-T_c}{(1+\alpha)CR}\right)\right] \quad .. \quad (3.1.9)$$

$$\hat{V}_{in+} = -V_t = \frac{\alpha V_1}{2}\left[1 - \exp\left(\frac{-T_c}{(1+\alpha)CR}\right)\right] \quad .. \quad (3.1.10)$$

Thus, the threshold voltage is equal to half the peak value of the sampling waveform. The positive input $\hat{V}_{in+}$ necessary for full modulation is equal and opposite to the threshold voltage. These conclusions could also be deduced by considering fig. 3.1.2. With the threshold voltage set at the value given by equation 3.1.9., the unmodulated mark-to-space is not unity, so the averaged value of the level-detector output is not zero when the modulating input V_{in} is zero.

As the integrator gain is increased, the sampling waveform approaches an ideal triangular waveform and the two values obtained for the threshold level tend to the same value. With the aid of theory to be developed, a system should be designed as that the difference between the two conditions is negligible. However, for high-power amplifiers, the second condition (i.e. $\hat{V}_{in+} = -\hat{V}_{in-}$) is likely to be more useful; attention will therefore be concentrated on this condition. The switching point t_1 may be calculated by substituting the threshold voltage expression (equation 3.1.9.) into equation 3.1.8, which gives:

$$-\alpha V_1\left[1 - \exp\left(\frac{-t_1}{(1+\alpha)CR}\right)\right] + V_{in} = -\frac{\alpha V_1}{2}\left[1 - \exp\left(\frac{-T_c}{(1+\alpha)CR}\right)\right] \quad (3.1.11)$$

The modulation index, M, may be defined as $V_{in}/\hat{V}_{in+}$.

The limit values of the modulation index are ± 1. Dividing equation 3.1.11. by the peak value of V_{in} (from equation 3.1.10.) leads to the following expression for the switching instant t_1:

$$\frac{t_1}{T_c} = -\frac{(1+\alpha)CR}{T_c}\left\{\log\left[1-\exp\left(\frac{-T_c}{(1+\alpha)CR}\right)\right] - \log\left[1-M.K\right]\right\} \qquad (3.1.12)$$

where

$$K = \frac{1-\exp\left[\frac{-T_c}{(1+\alpha)CR}\right]}{1+\exp\left[\frac{-T_c}{(1+\alpha)CR}\right]}$$

The manner in which t_1/T_c varies with the modulation index M may be more clearly seen if the second of the logarithmic terms in equation 3.1.12. is expanded as the following Maclaurin series (the expression is valid since $|M.K| < 1$).

$$\frac{t_1}{T_c} = -\frac{(1+\alpha)CR}{T_c}\left\{\log\frac{1}{2}\left[1+\exp\left(\frac{-T_c}{(1+\alpha)CR}\right)\right] - \sum_{n=1}^{\infty}\frac{1}{n}\left(M.K\right)^n\right\} \qquad (3.1.13)$$

The normalised average value of the level-detector output, V_{av}, (given by equation 3.1.3.) is:

$$V_{av} = 1 - 2\frac{t_1}{T_c}$$

Therefore, from equations 3.1.12. and 3.1.13., the average value of the normalised level-detector output may be expressed as:

$$V_{av} = 1 + \frac{2(1+\alpha)CR}{T_c}\left\{\log\frac{1}{2}\left[1+\exp\left(\frac{-T_c}{(1+\alpha)CR}\right)\right] - \log\left[1-M.K\right]\right\} \qquad (3.1.14)$$

or $$V_{av} = 1 - \frac{2(1+\alpha)CR}{T_c}\left\{\log\frac{1}{2}\left[1+\exp\left(\frac{-T_c}{(1+\alpha)CR}\right)\right] - \sum_{n=1}^{\infty}\frac{1}{n}(M.K)^n\right\} \qquad (3.1.15)$$

where $$K = \frac{1-\exp\left[\frac{-T_c}{(1+\alpha)CR}\right]}{1+\exp\left[\frac{-T_c}{(1+\alpha)CR}\right]}$$

Fig. 3.1.3. shows the transfer function of a single-edge pulse-length modulation system for selected values of integrator gain α and time constant $\frac{T_c}{CR}$. It will be noted that the linearity of the system improves with increasing gain, and that the transfer function is not symmetrical about the origin. From equations 3.1.14. and 3.1.15., the demodulated wavetrain consists of a constant term (arising from the manner in which the level-detector threshold was specified) and a power series in terms of the modulation index M.

There are two ways in which the error in the system output may be defined. The first is to define the error E_1 as the departure of the system transfer function from that of a system having an ideal sawtooth sampling waveform (i.e., a system having infinite integrator gain). Thus the system error E_1 is:

$$E_1 = V_{av} - V_{av}\Big|_{\alpha=\infty} \qquad (3.1.16)$$

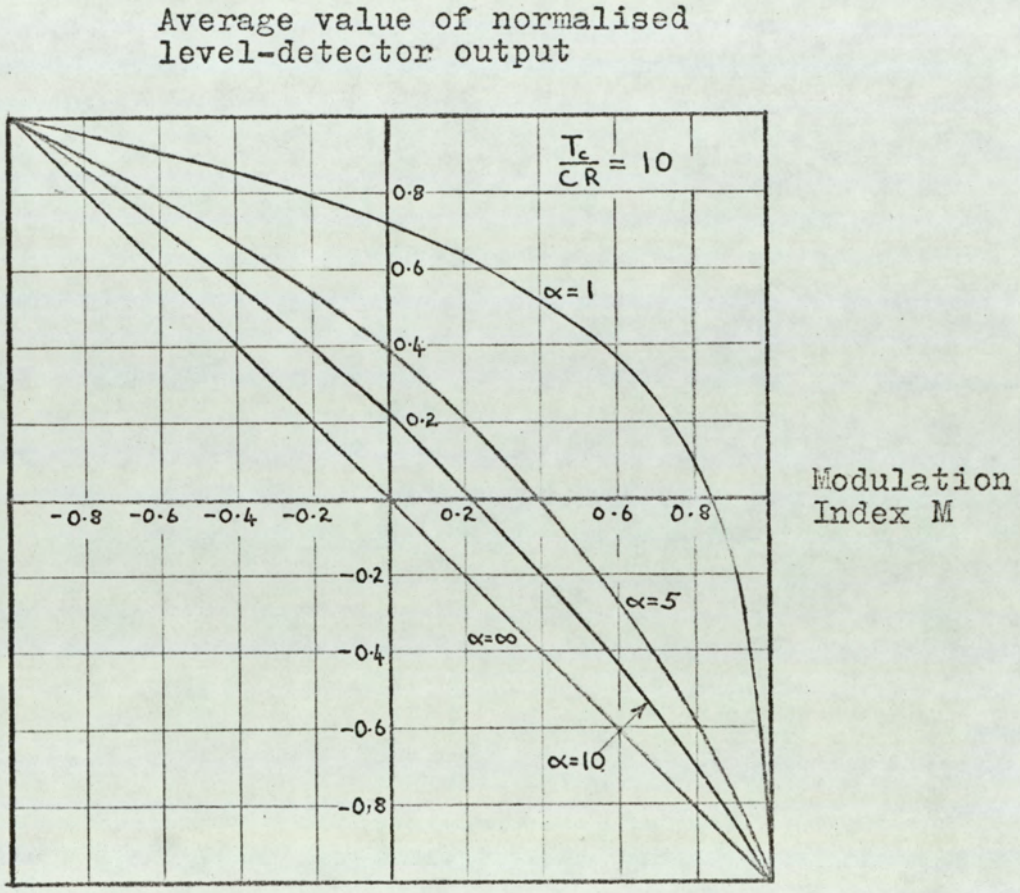

Fig.3.1.3. Transfer function of single-edge modulation system with finite integrator gain.

Since the normalised level-detector output waveform has been defined in such a manner that the transfer function has a phase inversion, the error may be written as:

$$E_1 = V_{av} + M \qquad .. \qquad (3.1.17)$$

Fig. 3.1.4. shows the system error, E_1, as a function of the normalised time constant $\frac{T_c}{(1+\alpha)CR}$ and the modulation index M. A disadvantage of defining the error by equation 3.1.16. is that the general form of the error curves are not consistent with those obtained from an analysis with a sinusoidal modulating input. This may be deduced readily from equation 3.1.15, which expresses the system output as a power series in terms of the modulation index. If the modulation index varies sinusoidally, then the error (defined as harmonic distortion) is greatest when $M = 1$. This result contradicts the results of fig. 3.1.4. which shows the error to be zero for $M = 1$. For this reason, an alternative definition of the static error in the system output may be preferred.

In equation 3.1.15, the term directly proportional to the modulating input is $\frac{-2(1+\alpha)CR}{T_c}$ (M.K.). Thus, the static error, E_2, in the amplitude demodulated wavetrain may be defined as:

$$E_2 = V_{av} - \left[\frac{2(1+\alpha)CR}{T_c} \cdot M.K\right]$$

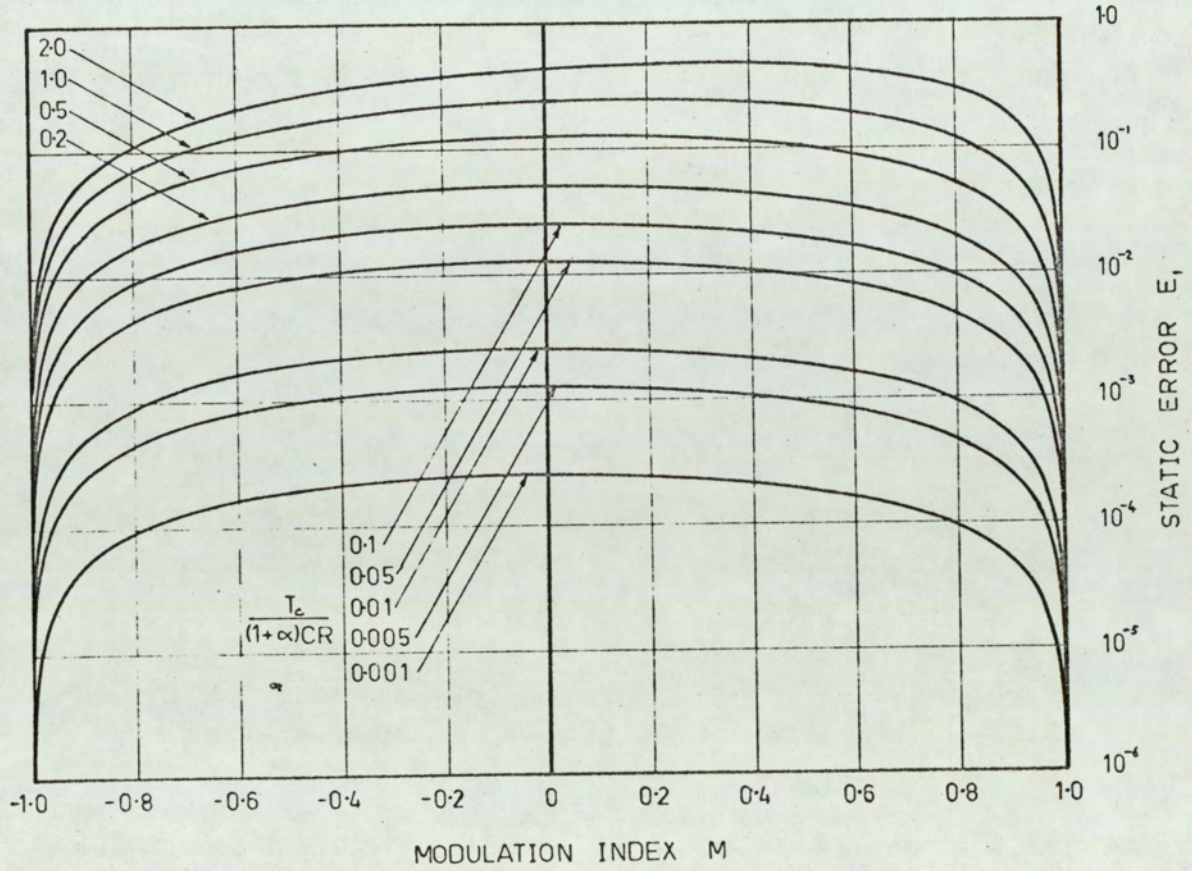

Fig.3.1.4. Static error E_1 for single-edge modulation system with finite integrator gain.

$$\therefore \quad E_2 = 1 + \frac{2(1+\alpha)CR}{T_c}\left\{\log\frac{1}{2}\left[1+\exp\left(\frac{-T_c}{(1+\alpha)CR}\right)\right]+\log\left[1-M.K\right]+M.K\right\} \qquad (3.1.18)$$

$$\text{or} \quad E_2 = 1 + \frac{2(1+\alpha)CR}{T_c}\left\{\log\frac{1}{2}\left[1+\exp\left(\frac{-T_c}{(1+\alpha)CR}\right)\right]-\sum_{n=2}^{\infty}\frac{1}{n}\left(M.K\right)^n\right\} \qquad (3.1.19)$$

Fig. 3.1.5. shows the system error, E_2, as a function of the normalised time constant $\frac{T_c}{(1+\alpha)CR}$ and the modulation index M.

Which of the two alternative error definitions is more useful in the design of a pulse-length modulation system largely depends on how the system is to be used. If the input to the system is d.c., then the first error definition is probably of more use. If, however, the input is a.c., then the second definition of error gives a better indication of system performance. It should be noted that the static-error expression gives only an indication of how the system behaves with a.c. inputs; a detailed analysis is given in a later section.

Considerable care is required when calculating, from equations 3.1.17., 3.1.18. and 3.1.19, the system error for small values of normalised time constant. This is particularly so when evaluating the constant term which tends to zero as the integrator gain tends to infinity. The numerical methods used for calculating the error are discussed in Appendix 1. An Algol programme was written in accordance with the flow chart

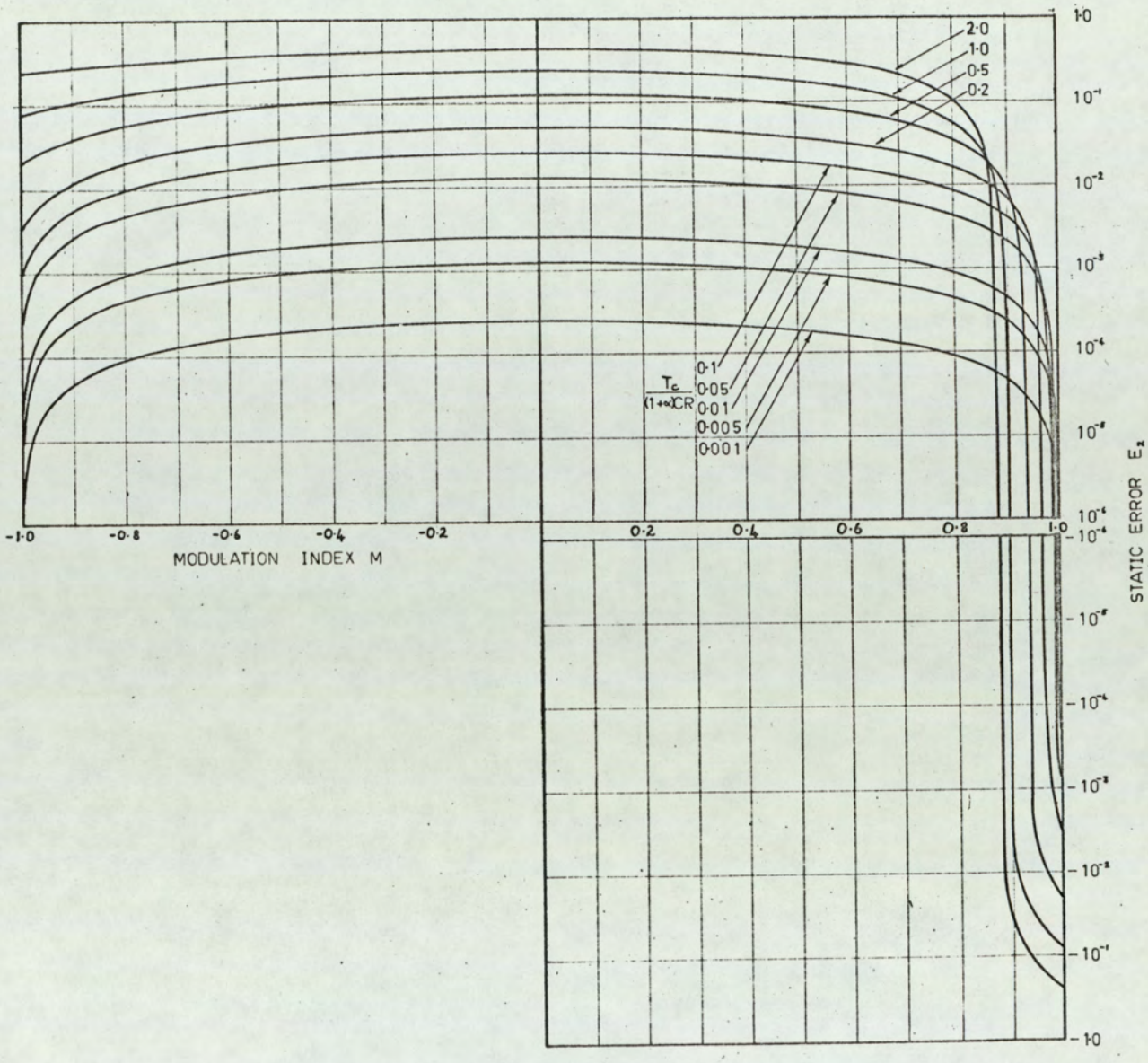

Fig.3.1.5. Static error E_2 for single-edge modulation system with finite integrator gain.

shown in Appendix 1 and the error equations evaluated on an Elliott 803 digital computer.

From figs. 3.1.4. and 3.1.5. the static error in the system decreases with decreasing values of normalised time constant $\frac{T_c}{(1+\alpha)CR}$. If the value of the time constant CR is increased, the peak value of the integrator output waveform (i.e., the sampling waveform) decreases and the specification for the accuracy of the threshold level of the level-detector becomes more stringent. Thus, under circumstances where only a limited gain is available, the choice of the integrator time constant is a compromise between making the normalised time constant $\frac{T_c}{(1+\alpha)CR}$ small enough to give an acceptable value of static error, and large enough to give a reasonable value for the peak value of the integrator output waveform. The peak value of the integrator output, obtained by setting $t = T_c$ in equation 2.1.1., is given by:

$$\hat{v}_2(t) = v_2(T_c) = -\alpha V_1\left[1 - \exp\left(\frac{-T_c}{(1+\alpha)CR}\right)\right] \qquad (3.1.20)$$

As was discussed earlier, if the positive and negative values of input voltage necessary for full modulation are to have equal amplitudes, then the threshold level of the level-detector must be set at a value equal to half the peak value of the sampling waveform. Therefore, a useful parameter in the design of a system is the ratio:

$$\frac{1}{2} \times \frac{\text{peak integrator output}}{\text{integrator input}}$$

From equation 3.1.20., this is:

$$\frac{1}{2}\,\frac{\hat{v}_2(t)}{V_1} = -\frac{\alpha}{2}\left[1-\exp\left(\frac{-T_c}{(1+\alpha)CR}\right)\right] \qquad (3.1.21)$$

Fig. 3.1.6. shows this ratio plotted as a function of normalised time constant $\frac{T_c}{CR}$ and integrator gain α.

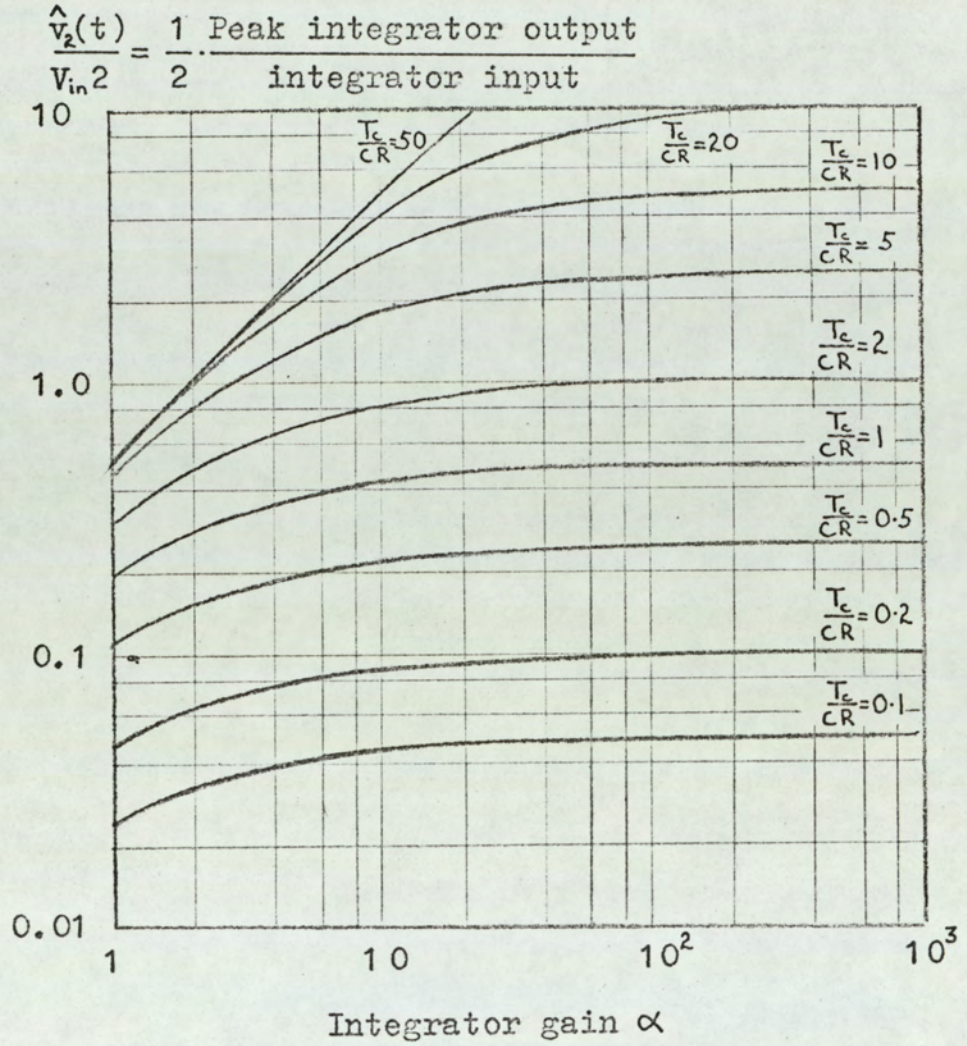

Fig.3.1.6. Normalised peak integrator output as a function of gain and time-constant.

3.1.2. Double-Edge Modulation

Consider the double-edge pulse-length modulation system shown in fig. 2.1(a)., the operational amplifier of fig. 3.1.1. being used to produce the sampling waveform. As a first step in the analysis for the static error of the system, it is necessary to derive an expression for the output of an operational amplifier when a square wave is applied to the input. The square wave of fig. 3.1.7. may be synthesised from a series of positive and negative step functions with appropriate time delays.

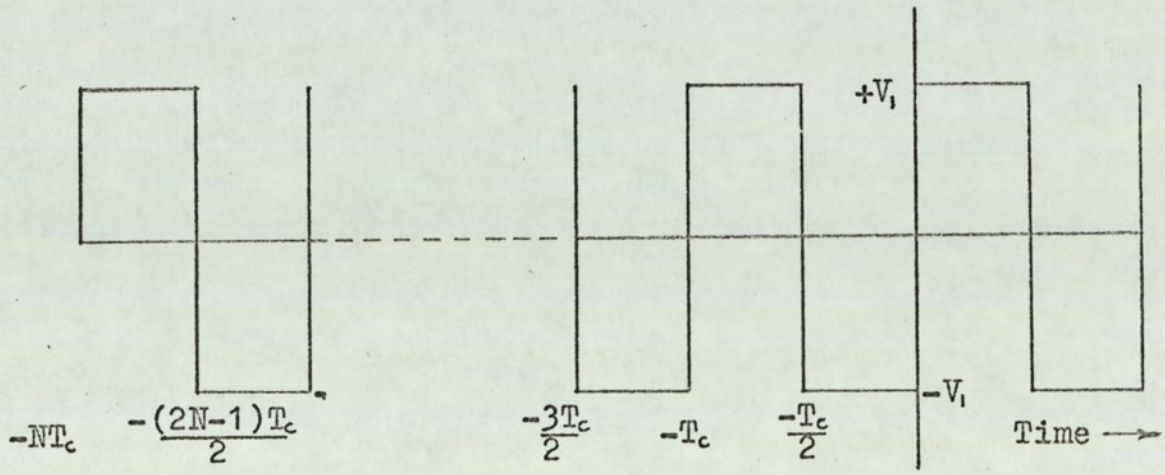

Fig.3.1.7. Square wave input to operational integrator.

The output of an operational integrator in response to a step-function input is given by equation 3.1.1. The output for a

square wave input, obtained by summing the outputs resulting from the sequence of time-delayed step functions comprising the square wave, is:

$$v_2(t) = \lim_{N\to\infty}\left\{-\alpha V_1\left[1-\exp\left(\frac{-(t+NT_c)}{(1+\alpha)CR}\right)\right] - 2\alpha V_1\sum_{n=0}^{N-1}\left[1-\exp\left(\frac{-(t+n.T_c}{(1+\alpha)CR}\right)\right] + 2\alpha V_1\sum_{n=0}^{N-1}\left[1-\exp\left(\frac{-(t+nT_c+\frac{1}{2}T_c)}{(1+\alpha)CR}\right)\right]\right\}$$

$$= -\alpha V_1 . \lim_{N\to\infty}\left\{1-\exp\left(\frac{-(t+NT_c)}{(1+\alpha)CR}\right) - 2\exp\left(\frac{-t}{(1+\alpha)CR}\right)\times \left[1-\exp\left(\frac{-T_c}{2(1+\alpha)CR}\right)\right]\sum_{n=0}^{N-1}\exp\left(\frac{-nT_c}{(1+\alpha)CR}\right)\right\} \quad \text{for } 0\leq t\leq\frac{T_c}{2} \qquad (3.1.22)$$

The summation term in equation 3.1.22. is a geometric progression, so the sum can be written in closed form:

$$v_2(t) = -\alpha V_1 . \lim_{N\to\infty}\left\{1-\exp\left(\frac{-(t+NT_c)}{(1+\alpha)CR}\right) - 2.\exp\left(\frac{-t}{(1+\alpha)CR}\right)\times \left[1-\exp\left(\frac{-T_c}{2(1+\alpha)CR}\right)\right]\frac{\left[1-\exp\left(\frac{-NT_c}{(1+\alpha)CR}\right)\right]}{\left[1-\exp\left(\frac{-T_c}{(1+\alpha)CR}\right)\right]}\right\}$$

If N is now allowed to tend to infinity, the response of the integrator to an infinite train of square waves is given by:

$$v_2(t) = -\alpha V_1 \left\{ 1 - \frac{2.\exp\left(\frac{-t}{(1+\alpha)CR}\right)}{1+\exp\left(\frac{-T_c}{2(1+\alpha)CR}\right)} \right\} \qquad (3.1.23)$$

for $0 \leqslant t \leqslant \frac{T_c}{2}$

An expression for the integrator output during the period $\frac{T_c}{2}$ to T_c may be obtained by adding, to equation 3.1.23., a term corresponding to the integrator output for a negative step input at time $t = \frac{T_c}{2}$. This procedure leads to the following expression:

$$v_2(t) = -\alpha V_1 \left\{ -1 + \frac{2\exp\left(\frac{-(t-\frac{T_c}{2})}{(1+\alpha)CR}\right)}{1+\exp\left(\frac{-T_c}{2(1+\alpha)CR}\right)} \right\} \qquad (3.1.24)$$

for $\frac{T_c}{2} \leqslant t \leqslant T_c$

The input to the level-detector is the sum of the sampling waveform (given by equations 3.1.23. and 3.1.24.) and the modulating input voltage V_{in} (see figs. 2.1(a). and (b).) The output of the level detector changes state whenever the input to the level-detector crosses the threshold, i.e., when:

$$v_2(t_1) + V_{in} = V_t \qquad 0 \leqslant t_1 \leqslant \frac{T_c}{2} \qquad (3.1.25)$$

$$v_2(t_2) + V_{in} = V_t \qquad \frac{T_c}{2} \leqslant t_2 \leqslant T_c \qquad (3.1.26)$$

where V_t is the level-detector threshold voltage.

The waveforms defining the switching instants t_1 and t_2 are shown in fig. 3.1.8. The peak positive output of the integrator $\hat{v}_2(t)$ is given by equation 3.1.23. with t set to zero, and the peak negative output by equation 3.1.24. with $t = \frac{T_c}{2}$. It will be noted that the peak positive and negative outputs have equal amplitudes.

$$\hat{v}_2(t) = -\alpha V_1 \left[1 - \frac{2}{1 + \exp\left(\frac{-T_c}{2(1+\alpha)CR}\right)} \right] \qquad (3.1.27)$$

From fig. 3.1.8., full modulation for positive input (V_{in+}) is achieved when the pulse length is zero (i.e. $t_1 = t_2 = \frac{T_c}{2}$) and full modulation for negative input (V_{in-}) is achieved when the pulse length is T_c (i.e. $t_1 = 0$, $t_2 = T_c$). If the positive and negative input voltages necessary for full modulation are to be of equal amplitude, then fig. 3.1.8. shows that the level-detector threshold voltage must be half the peak-to-peak value of the integrator output waveform. Since the positive and negative values of the peak integrator output are equal in amplitude the threshold voltage must be zero. Thus the positive modulating input voltage $\hat{V}_{in+}$, necessary to produce full modulation is equal to the peak positive value of

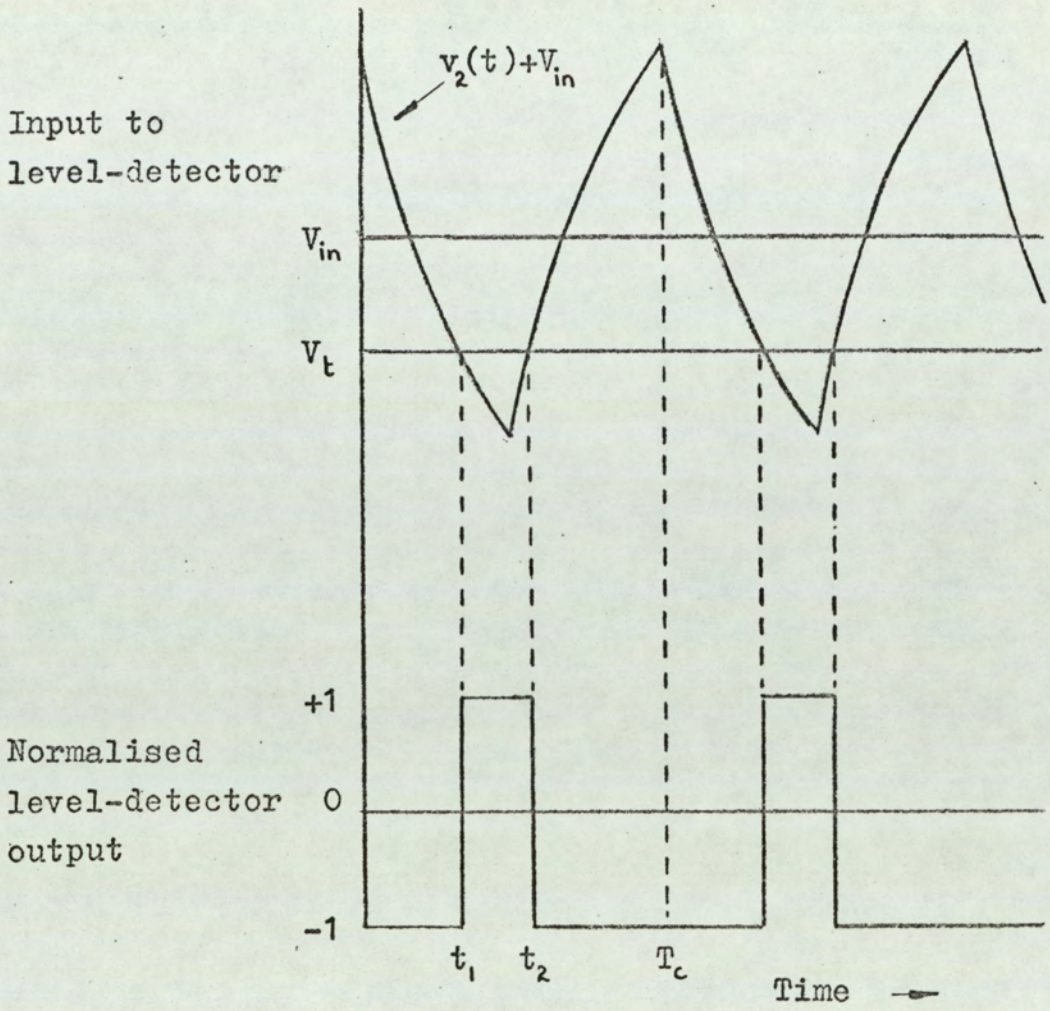

Fig.3.1.8. Waveforms for double-edge modulation system with finite integrator gain.

the integrator waveform (given by equation 3.1.27.), i.e.:

$$\hat{V}_{in+} = \hat{v}_2(t) \qquad (3.1.28)$$

These deductions could equally well have been made by substituting, in equations 3.1.25. and 3.1.26., the conditions corresponding to full modulation, and solving the resulting simultaneous equations.

Setting $V_t = 0$ in equations 3.1.25. and 3.1.26., and dividing through by the peak modulating input voltage $\hat{V}_{in+}$ gives:

$$\frac{v_2(t_1)}{\hat{V}_{in+}} = -M \qquad 0 \leqslant t_1 \leqslant \frac{T_c}{2} \qquad (3.1.29)$$

$$\frac{v_2(t_2)}{\hat{V}_{in+}} = -M \qquad \frac{T_c}{2} \leqslant t_2 \leqslant T_c \qquad (3.1.30)$$

where M is the modulation index $V_{in}/\hat{V}_{in+}$.
Substituting equations 3.1.23., 3.1.24, 3.1.27. and 3.1.28. into equations 3.1.29. and 3.1.30., and solving the resulting equations for the switching instants t_1 and t_2:

$$\frac{t_1}{T_c} = -\frac{(1+\alpha)CR}{T_c}\left\{\log\frac{1}{2}\left[1+\exp\left(\frac{-T_c}{2(1+\alpha)CR}\right)\right]+\log\left[1-M.K\right]\right\} \qquad (3.1.31)$$

$$\frac{t_2}{T_c} = \frac{1}{2} - \frac{(1+\alpha)CR}{T_c}\left\{\log\frac{1}{2}\left[1+\exp\left(\frac{-T_c}{2(1+\alpha)CR}\right)\right]+\log\left[1+MK\right]\right\} \qquad (3.1.32)$$

where $$K = \frac{1 - \exp\left(\frac{-T_c}{2(1+\alpha)CR}\right)}{1 + \exp\left(\frac{-T_c}{2(1+\alpha)CR}\right)}$$

The variation of the switching instants, t_1 and t_2, with modulation index may be more clearly seen if the logarithmic terms containing the modulation index are expanded as follows:

$$\frac{t_1}{T_c} = -\frac{(1+\alpha)CR}{T_c}\left\{\log\frac{1}{2}\left[1 - \exp\left(\frac{-T_c}{2(1+\alpha)CR}\right)\right] - \sum_{n=1}^{\infty}\frac{1}{n}(M.K)^n\right\} \qquad (3.1.33)$$

$$\frac{t_2}{T_c} = \frac{1}{2} - \frac{(1+\alpha)CR}{T_c}\left\{\log\frac{1}{2}\left[1 - \exp\left(\frac{-T_c}{2(1+\alpha)CR}\right)\right] - \sum_{n=1}^{\infty}\frac{1}{n}(-M.K)^n\right\} \qquad (3.1.34)$$

The effect of passing the pulse-length modulated wave-train through a low-pass filter is equivalent to taking the average value of the waveform, since the modulating input is a d.c. voltage V_{in}. The average value V_{av} of the modulated waveform over one cycle (from fig. 3.1.8.) is:

$$V_{av} = 2\left(\frac{t_2}{T_c} - \frac{1}{2} - \frac{t_1}{T_c}\right) \qquad (3.1.35)$$

Substituting equations 3.1.31., 3.1.32., 3.1.33. and 3.1.34.

in equation 3.1.35. leads to the following expressions for the amplitude of the demodulated wavetrain:

$$V_{av} = -\frac{2(1+\alpha)CR}{T_c} \log\left(\frac{1+M.K}{1-M.K}\right) \qquad (3.1.36)$$

or

$$V_{av} = -\frac{4(1+\alpha)CR}{T_c} \sum_{n=1}^{\infty} \frac{1}{(2n-1)} (M.K)^{2n-1} \qquad (3.1.37)$$

Two interesting observations may be made from equations 3.1.36. and 3.1.37. Firstly, no constant term exists, so the amplitude of the demodulated wavetrain is zero when the modulation index is zero. Secondly, only terms involving odd powers of the modulation index occur in the series representation of V_{av}, so the system transfer function is symmetrical about the origin. Fig. 3.1.9. shows the system transfer function for selected values of integrator gain and normalised time constant.

The static error in the demodulated wavetrain will be defined in the same manner as for single edge modulation (Section 3.1.1.). The first definition of error, E_1, is the departure of the system transfer function from that of a system having an ideal triangular sampling waveform (i.e. a system having infinite integrator gain).

$$E_1 = V_{av} - V_{av}\Big|_{\alpha=\infty}$$

$$= V_{av} + M \qquad \text{(see eqn 3.1.16)}$$

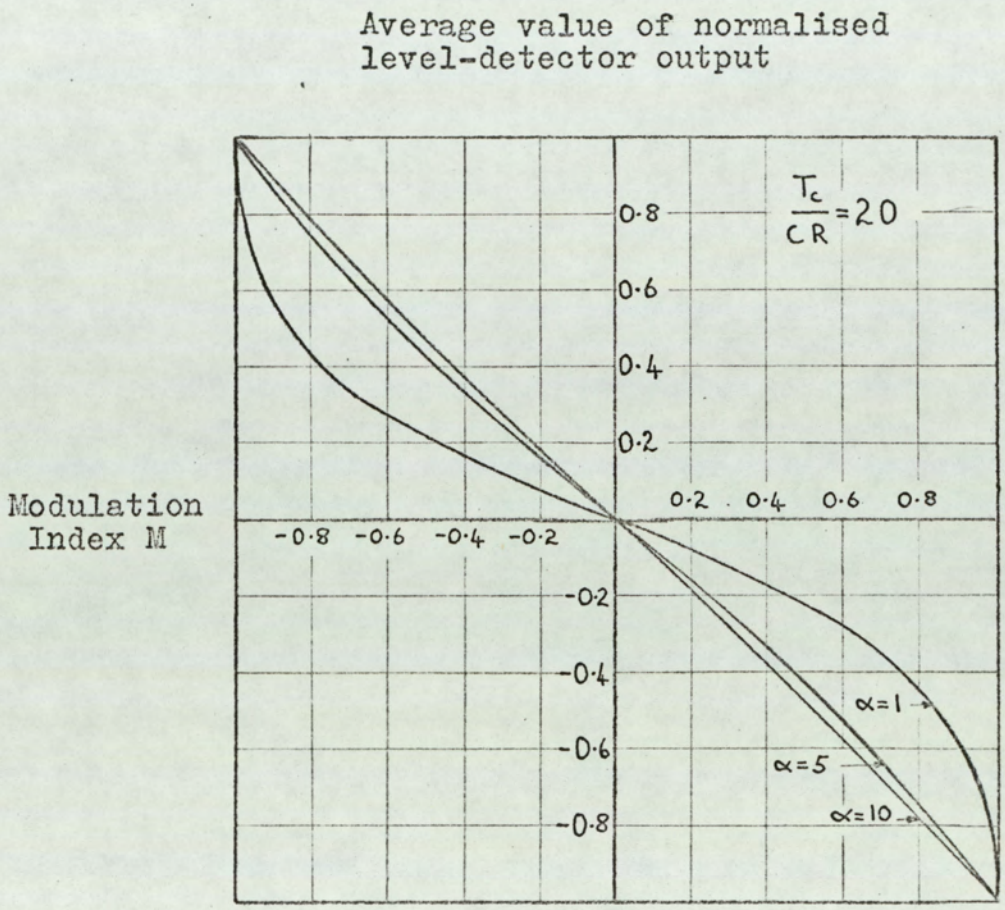

Fig.3.1.9. Transfer function of double-edge modulation system.

Fig. 3.1.10. shows the system error, E_1, as a function of the normalised time constant $\frac{T_c}{(1+\alpha)CR}$ and the modulation index M. For the reasons discussed in section 3.1.1., an alternative definition of error is more consistent with the results to be expected from an analysis of system error with a sinusoidal modulating input voltage. From equation 3.1.37., the component of the demodulated wavetrain which is directly proportional to the modulation index is $\frac{-4(1+\alpha)CR}{T_c}$ M.K. The system static error may therefore be defined as:

$$E_2 = V_{av} + \frac{4(1+\alpha)CR}{T_c} \cdot M.K \qquad (3.1.38)$$

Substituting equations 3.1.36., 3.1.37. in 3.1.38. gives:

$$E_2 = -\frac{2(1+\alpha)CR}{T_c}\left\{\log\left(\frac{1+M.K}{1-M.K}\right) - 2M.K\right\} \qquad (3.1.39)$$

$$E_2 = -\frac{4(1+\alpha)CR}{T_c}\sum_{n=2}^{\infty}\frac{1}{(2n-1)}(M.K)^{2n-1} \qquad (3.1.40)$$

Fig. 3.1.11. shows the system static error, E_2, as a function of the normalised time constant $\frac{T_c}{(1+\alpha)CR}$ and the modulation index M. As was explained in section 3.1.1., which error definition is more useful in the design of a pulse-length modulation system largely depends upon how the system is to be used.

Numerical evaluation of the error expressions presents

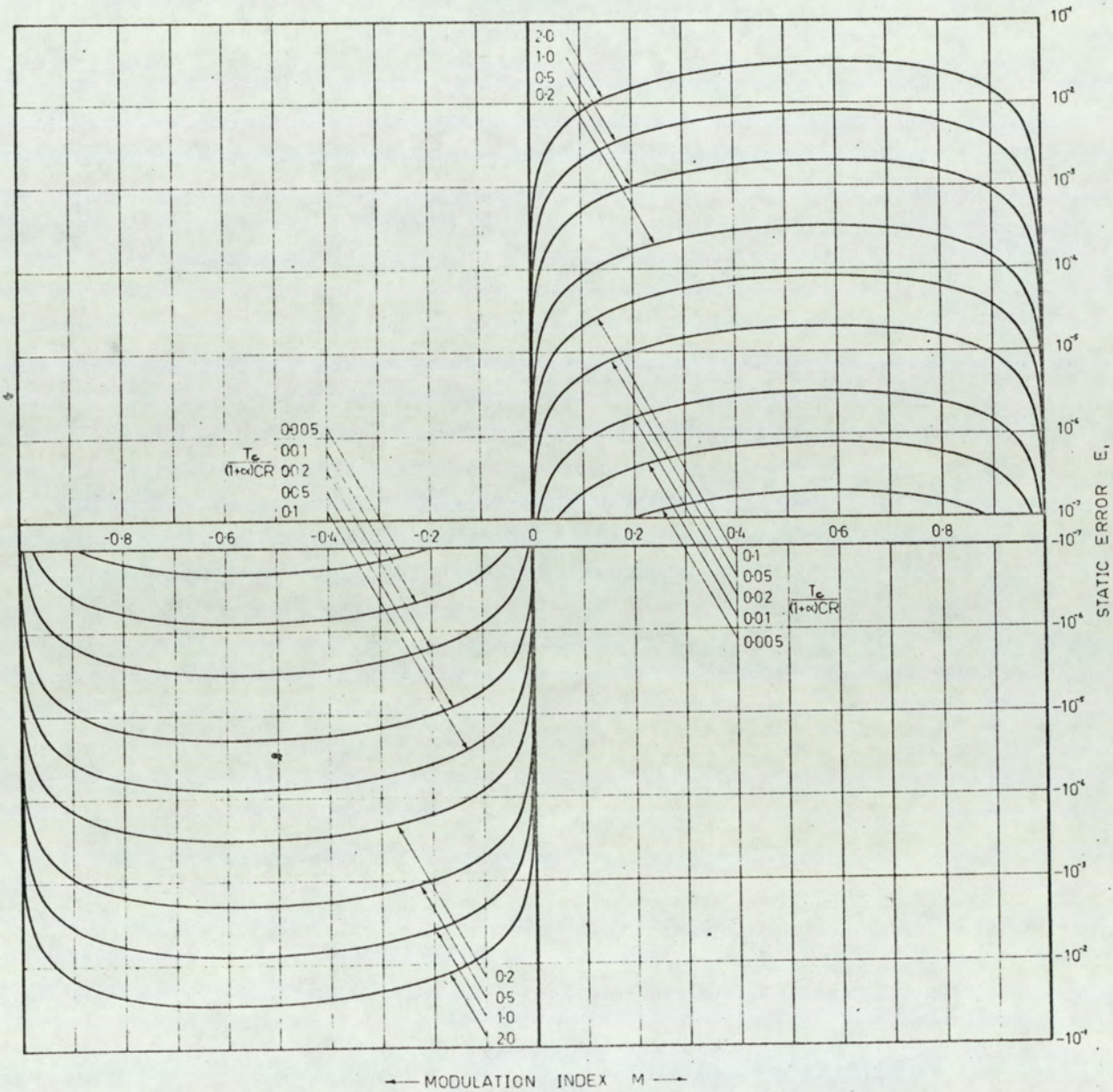

Fig.3.1.10. Static error E_1 for double-edge modulation system with finite integrator gain.

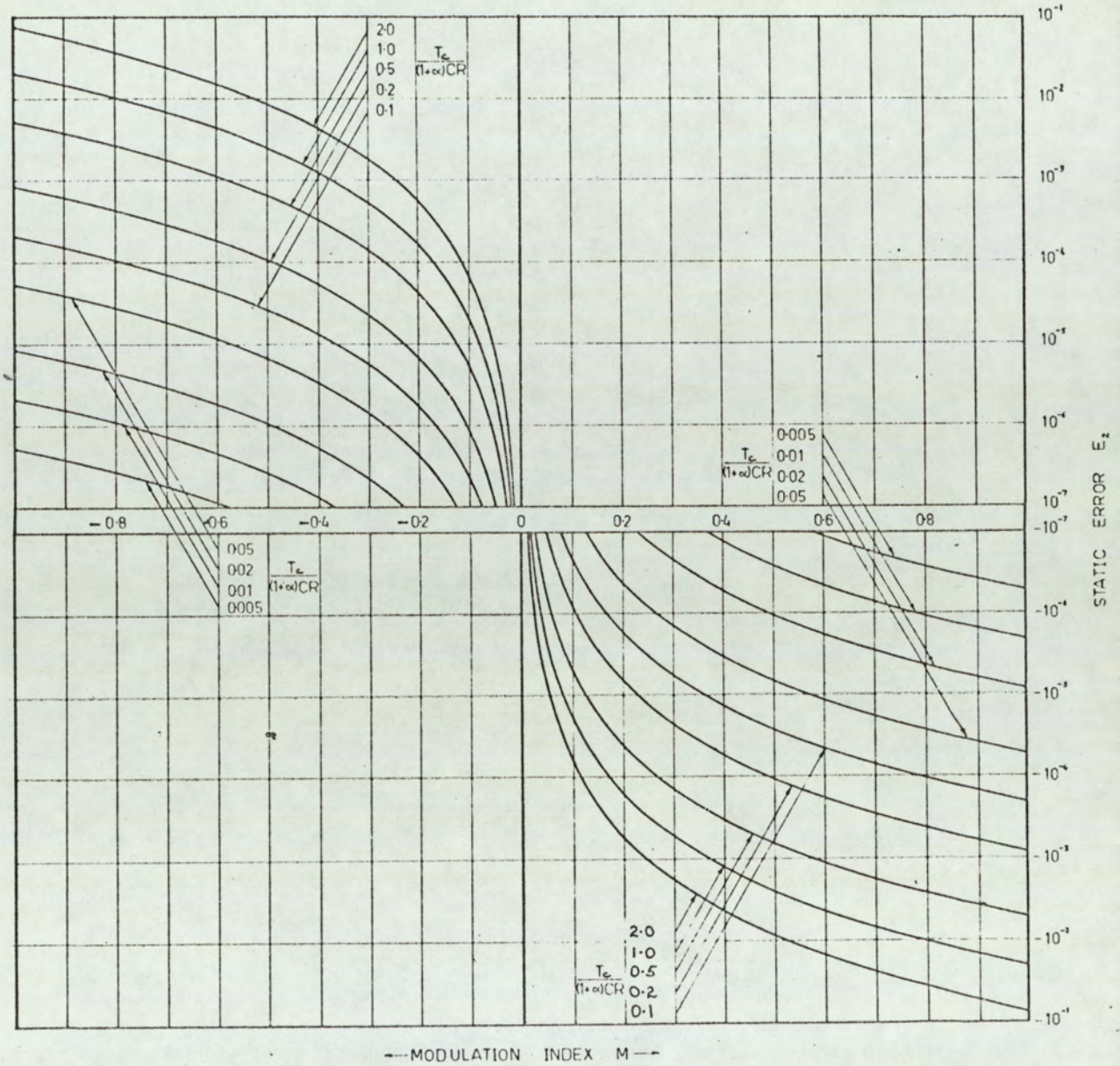

Fig.3.1.11. Static error E_2 for double-edge modulation system with finite integrator gain.

rather fewer problems than the corresponding expressions for single-edge modulation, since the constant term is not present. Evaluation of the constant K is similar to the procedure for evaluating K for single-edge modulation (see Appendix 1), the only difference being that, with double-edge modulation, the effective time constant $(1 + \alpha)CR$, is multiplied by a factor of two.

A parameter which must be taken into account in the design of a system is the peak amplitude of the sampling waveform, since the accuracy required for the level-detector threshold depends on the amplitude of the sampling waveform. As the amplitude of the sampling waveform is decreased, so the threshold level has to be defined more accurately. The ratio of the peak integrator output to the amplitude of the integrator step function input, from equation 3.1.27., is:

$$\frac{\hat{v}_2(t)}{V_1} = \mp \alpha \left\{ 1 - \frac{2}{1 + \exp\left(\frac{-T_c}{2(1+\alpha)CR}\right)} \right\} \qquad (3.1.41)$$

Fig. 3.1.12. shows this ratio plotted as a function of the integrator gain α and the normalised time constant $\frac{T_c}{CR}$.

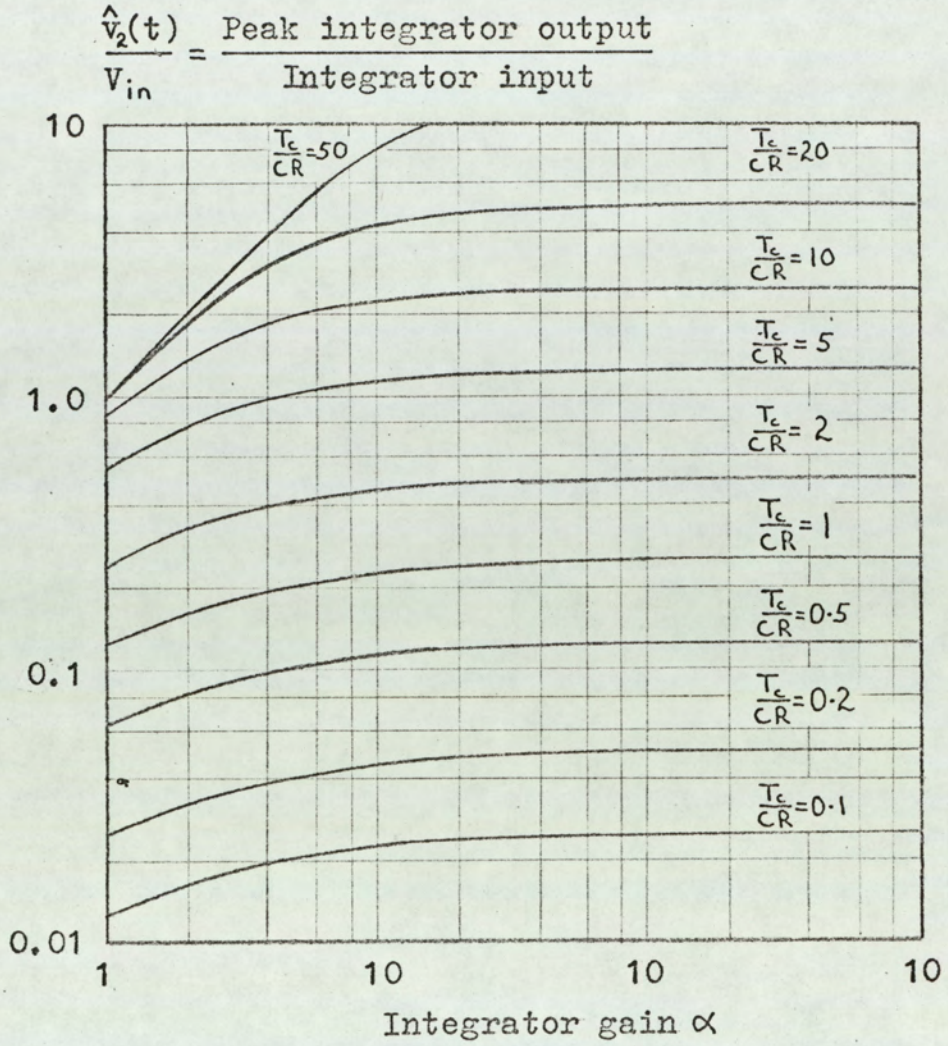

Fig.3.1.12. Normalised peak integrator output as a function of gain and time-constant.

3.1.3. Conclusions

The static error in the outputs of pulse-length modulation systems, operating with finite integrator gain, has been related to the system parameters. The most striking feature of the analytical results is the large improvement in system performance obtained with double-edge modulation. The reasons for this improvement are discussed in a later section (section 3.5.). A second feature of the results is that, with double-edge modulation, a surprisingly large value of normalised time constant $\frac{T_c}{(1+\alpha)CR}$ can be tolerated without introducing significant error. For instance, if the static errors (E_1 and E_2) are to be less than 10^{-3}, then figs. 3.1.10. and 3.1.11. show that the normalised time constant must be less than 0.2. Obviously this fact is of importance in the design of a system since the sampling waveform can be obtained from an integrator with a relatively low gain.

3.2 Static error due to finite input and output resistance of the integrator

Fig. 3.2.1 shows an integrator utilising an operational amplifier with finite voltage gain α, input resistance R_1 and output resistance R_o.

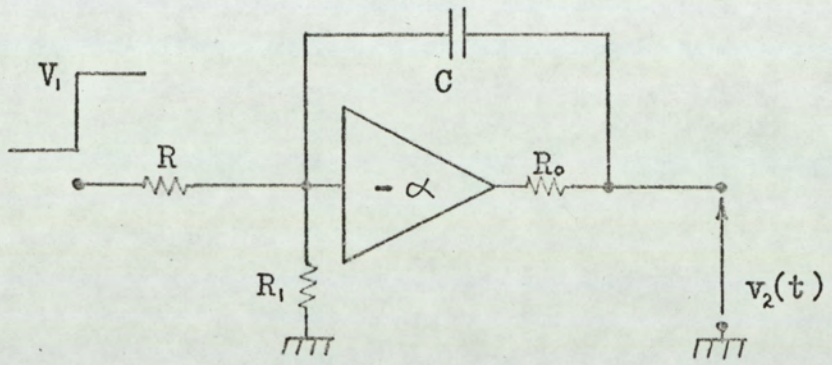

Fig.3.2.1. Operational integrator.

The output voltage $v_2(t)$ of the operational integrator, in response to a positive step input voltage V_1 is:

$$v_2(t) = -\frac{\alpha V_1}{\left(1 + R/R_1\right)}\left[1 - \left(1 + \frac{CR_o}{\alpha T_e}\right)\exp\left(\frac{-t}{T_e}\right)\right] \qquad (3.2.1(a))$$

where $$T_e = \frac{(1+\alpha)CR}{1 + R/R_1} + CR_o \qquad (3.2.1(b))$$

The input resistance of the amplifier R_1 and the time-constant resistance R form a potential divider which reduces the effective value of the time constant. The effect of the amplifier output resistance R_o is to increase the effective time constant. The integrator step-function response, given by equation 3.2.1, is the basis for the following analyses of system static error.

3.2.1 Single-edge modulation

Consider the single-edge pulse-length modulation system of fig. 2.2a with the operational integrator of fig. 3.2.1 being used to produce the sampling waveform. Fig. 3.2.2 shows the integrator output waveform for the system, evaluated from equation 3.2.1 and normalised to the value of the output at time $t = T_c$. It will be noted that the effect of the constant term, $(1 + \frac{CR_o}{\alpha T_c})$, is such that the amplitude of the output waveform is not zero at time $t = 0_+$. The integrator output waveform is added to the modulating input voltage V_{in} and the resulting sum applied to the input of the level detector. The output of the level detector changes state whenever the voltage applied to its input crosses the threshold level. The waveforms associated with the level detector are shown in fig. 3.2.3. The trailing edges of the level-detector output-pulse train occur at periodic intervals of nT_c, whilst the leading edges of the pulse train are position modulated in accordance with some function of the input voltage V_{in}. The position, t_1, of the leading edge is defined by the expression:

$$v_2(t_1) + V_{in} = V_t$$

where V_t is the level-detector threshold voltage.

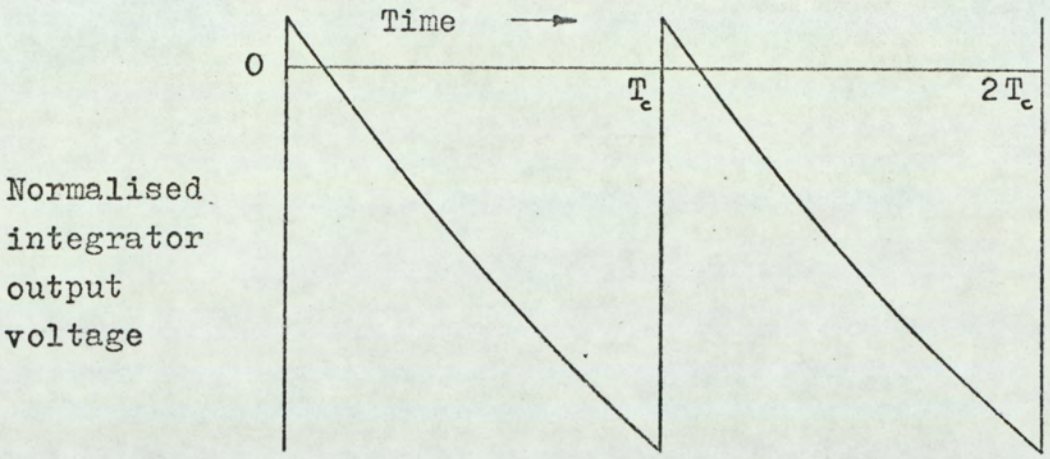

Fig.3.2.2. Normalised integrator output waveform with finite input and output resistance.

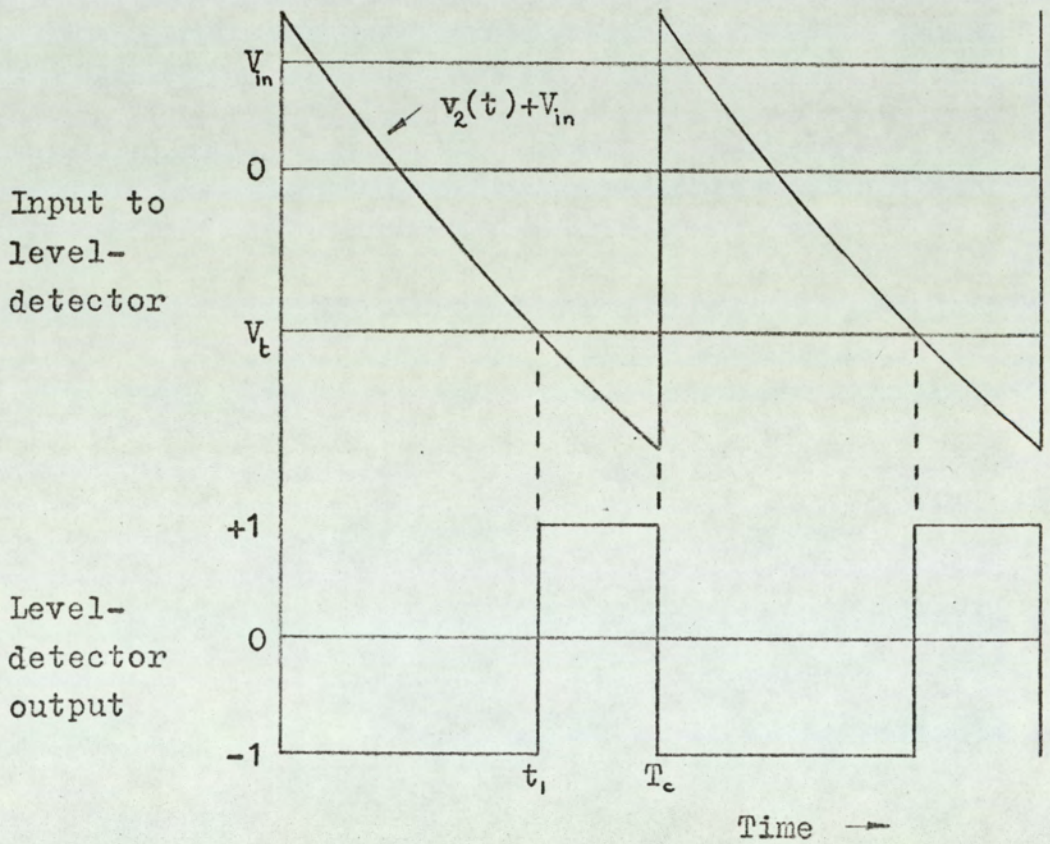

Fig.3.2.3. Waveforms for single-edge modulation system with finite gain, input resistance and output resistance.

Therefore, from equation 3.2.1:

$$-\frac{\alpha V_1}{1+R/R_1}\left[1-\left(1-\frac{CR_o}{\alpha T}\right)\exp\left(\frac{-t_1}{T}\right)\right]+V_{in}=V_t \qquad (3.2.2)$$

The factors to be considered when setting a value for the threshold V_t are discussed in some detail in section 3.1.1. Briefly, the threshold level can be set to satisfy two conditions:

1) The average value of the level-detector output waveform (i.e. the modulated wavetrain) is zero when the modulating input voltage V_{in} is zero.
2) The positive and negative input voltages, $\hat{V}_{in+}$ and $\hat{V}_{in-}$ respectively, required to produce the two states of full modulation are equal in amplitude.

It was shown in section 3.1.1 that, in order to satisfy the first of the two conditions, the level-detector threshold voltage must be equal to the value of the sampling waveform at time $t=\frac{T_c}{2}$. Therefore, from equation 3.2.1:

$$V_t=-\frac{\alpha V_1}{1+R/R_1}\left[1-\left(1-\frac{CR_o}{\alpha T_e}\right)\exp\left(\frac{-T_c}{2T_e}\right)\right] \qquad (3.2.3)$$

Substituting equation 3.2.3 in equation 3.2.2 enables the switching instant t_1, of the leading pulse edge, to be calculated from:

$$-\frac{\alpha V_1}{1+R/R_1}\left[1-\left(1-\frac{CR_o}{\alpha T_e}\right)\exp\left(\frac{-t_1}{T_e}\right)\right]+V_{in}$$

$$=-\frac{\alpha V_1}{1+R/R_1}\left[1-\left(1+\frac{CR_o}{\alpha T_e}\right)\exp\left(\frac{-T_c}{2T_e}\right)\right] \qquad (3.2.4)$$

From fig. 3.2.3, full modulation for positive values of V_{in} corresponds to the condition $t_1=T_c$. Full modulation for

negative values of V_{in} corresponds to the condition $t_1 = 0$. Substituting these conditions in equation 3.2.4 leads to the following expressions for the positive and negative input voltages required to produce full modulation.

$$\hat{V}_{in+} = \frac{\alpha V_1}{1+R/R_1}\left[1-\frac{CR_o}{\alpha T_e}\right]\left[1-\exp\left(\frac{-T_c}{2T_e}\right)\right]\exp\left(\frac{-T_c}{2T_e}\right) \qquad (3.2.5)$$

$$\hat{V}_{in-} = -\frac{\alpha V_1}{1+R/R_1}\left[1-\frac{CR_o}{\alpha T_e}\right]\left[1-\exp\left(\frac{-T_c}{2T_e}\right)\right] \qquad (3.2.6)$$

From equations 3.2.5 and 3.2.6 it can be seen that the input voltages, $\hat{V}_{in+}$ and $\hat{V}_{in-}$, required for full modulation are not of equal amplitude. This observation leads to the second of the two conditions for which the level detector threshold may be set, namely: $\hat{V}_{in+} = -\hat{V}_{in-}$.

If the two sets of conditions defining full modulation (i.e. $t_1 = T_c$ when $V_{in} = \hat{V}_{in+}$, $t_1 = 0$ when $V_{in} = \hat{V}_{in-}$) are substituted in equation 3.2.2, together with the added condition that $\hat{V}_{in+} = -\hat{V}_{in-}$, then the two simultaneous equations formed may be solved for V_t and $\hat{V}_{in+}$.

$$V_t = -\frac{1}{2}\,\frac{\alpha V_1}{1+R/R_1}\left\{2-\left[1-\frac{CR_o}{\alpha T_e}\right]\left[1-\exp\left(\frac{-T_c}{T_e}\right)\right]\right\} \qquad (3.2.7)$$

$$\hat{V}_{in+} = -\hat{V}_{in-} = \frac{1}{2}\cdot\frac{\alpha V_1}{1+R/R_1}\left[1-\frac{CR_o}{\alpha T_e}\right]\left[1-\exp\left(\frac{-T_c}{T_e}\right)\right] \qquad (3.2.8)$$

Substituting the above expression for the threshold voltage in equation 3.2.2 and dividing through by $\hat{V}_{in+}$ enables an expression to be deduced for the switching point t_1 of the leading edges of the pulse-length modulated wavetrain.

$$\frac{t_1}{T_c} = -\frac{T_e}{T_c}\left\{\log\frac{1}{2}\left[1-\exp\left(\frac{-T_c}{T_e}\right)\right]-\log\left[1-M.K\right]\right\} \qquad (3.2.9)$$

where: $M = \frac{V_{in}}{\hat{V}_{in+}}$, the modulation index.

$$T_e = \frac{(1+\alpha)CR}{1+\frac{R}{R_1}} + CR_o$$

$$K = \frac{1-\exp\left(\frac{-T_c}{T_e}\right)}{1+\exp\left(\frac{T_c}{T_e}\right)}$$

The logarithmic term containing the modulation index M may be expanded as a Maclaurin series in order to gain a clearer insight into the manner in which switching instant t_1 varies with the modulation index. Such an expansion is valid since $|M.K.| < 1$.

$$\frac{t_1}{T_c} = -\frac{T_e}{T_c}\left\{\log\frac{1}{2}\left[1-\exp\left(\frac{-T_c}{T_e}\right)\right] - \sum_{n=1}^{\infty}\frac{1}{n}(M.K)^n\right\} \qquad (3.2.10)$$

Comparing equations 3.2.9 and 3.2.10 with the corresponding expressions for the switching instant of the pulse leading edge in a system utilising an integrator with ideal values of amplifier resistances (equations 3.1.12 and 3.1.13 of section 3.1.1), it will be seen that the expressions are identical in form. The effect of the finite input and output resistances is simply to modify the effective time constant from $(1+\alpha)CR$ to $\frac{(1+\alpha)CR}{1+\frac{R}{R_1}} + CR_o$. Thus the expressions for the amplitude of the demodulated wavetrain V_{av} and the static error in the demodulated wavetrain may be written down by inspection of the corresponding equations relating to the system with ideal amplifier resistances.

(Equations 3.1.14, 3.1.15, 3.1.17, 3.1.18 and 3.1.9; Section 3.1.1). Therefore:

$$V_{av} = 1 - \frac{2T_e}{T_c}\left\{\log\frac{1}{2}\left[1-\exp\left(\frac{-T_c}{T_e}\right)\right] - \log\left[1-M.K\right]\right\} \qquad (3.2.11)$$

$$V_{av} = 1 + \frac{2T_e}{T_c}\left\{\log\frac{1}{2}\left[1-\exp\left(\frac{-T_c}{T_e}\right)\right] - \sum_{n=1}^{\infty}\frac{1}{n}\left(M.K\right)^n\right\} \qquad (3.2.12)$$

$$E_1 = V_{av} + M \qquad (3.2.13)$$

$$E_2 = 1 + \frac{2T_e}{T_c}\left\{\log\frac{1}{2}\left[1-\exp\left(\frac{-T_c}{T_e}\right)\right] - \log\left[1-M.K\right] + M.K\right\} \qquad (3.2.14)$$

$$E_2 = 1 - \frac{2T_e}{T_c}\left\{\log\frac{1}{2}\left[1-\exp\left(\frac{-T_c}{T_e}\right)\right] - \sum_{n=2}^{\infty}\frac{1}{n}\left(M.K\right)^n\right\} \qquad (3.2.15)$$

The manner in which the error, E_1 and E_2, are defined is discussed in section 3.1.1. Since the error expressions for the system with finite amplifier input and output resistance are identical in form to the corresponding expressions for the system with ideal amplifier resistances it is not necessary to plot further graphs of static error. In order to determine the error for a system with finite amplifier resistances, the graphs of error for the system with ideal amplifier resistances may be used by simply replacing $\frac{T_c}{(1+\alpha)\,CR}$, in figs. 3.1.4 and 3.1.5, with $\frac{T_c}{T_e}$. These figures show that the system static error decreases with increasing values of effective integrator time constant. Thus the effect of the finite amplifier input resistance is to increase the error, as may be seen from equation 3.2.1(b) for the effective integrator time constant T_e. The amplifier output resistance increases the effective time

constant and, hence, reduces the error. However, the output resistance cannot be increased indefinitely, since increasing values of R_o reduce the time-varying component of integrator output in the manner shown in fig. 3.2.4. The peak negative value of the integrator output occurs at time $t = T_c$ for small values of R_o. However, as R_o is increased, the time-varying part of the output waveform is effectively superimposed on a positive d.c. term so that, for large enough values of R_o, the output waveform is never negative. For this reason, knowledge of the integrator output at only time $t = T_c$ is of little use when designing a system. The additional information required is the peak-to-peak value of the time-varying component of the integrator output waveform $V_{2p.p.}$ as shown in fig. 3.2.5.

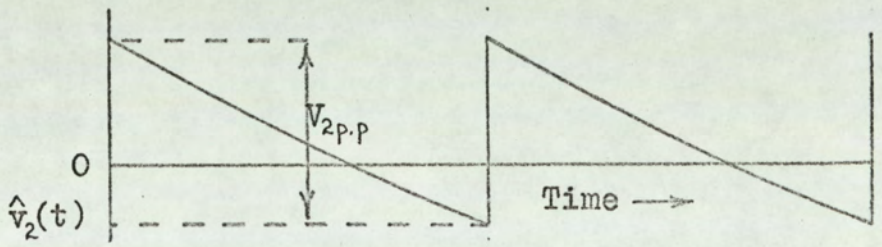

Fig.3.2.5.

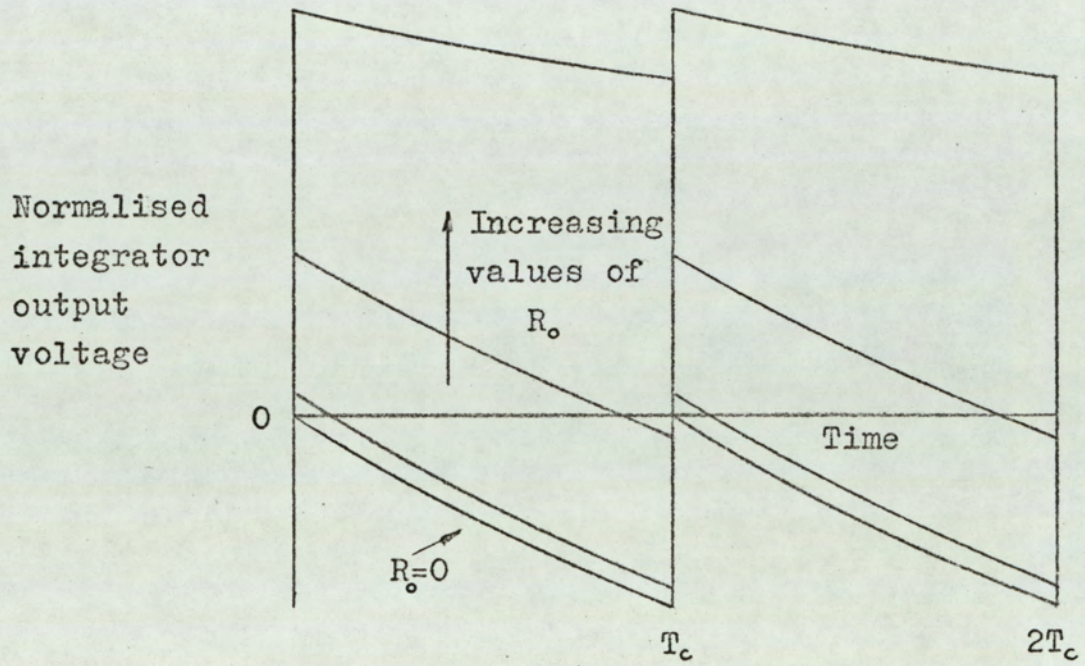

Fig.3.2.4. Normalised integrator output waveform showing the effect of increasing the integrator output resistance R_o.

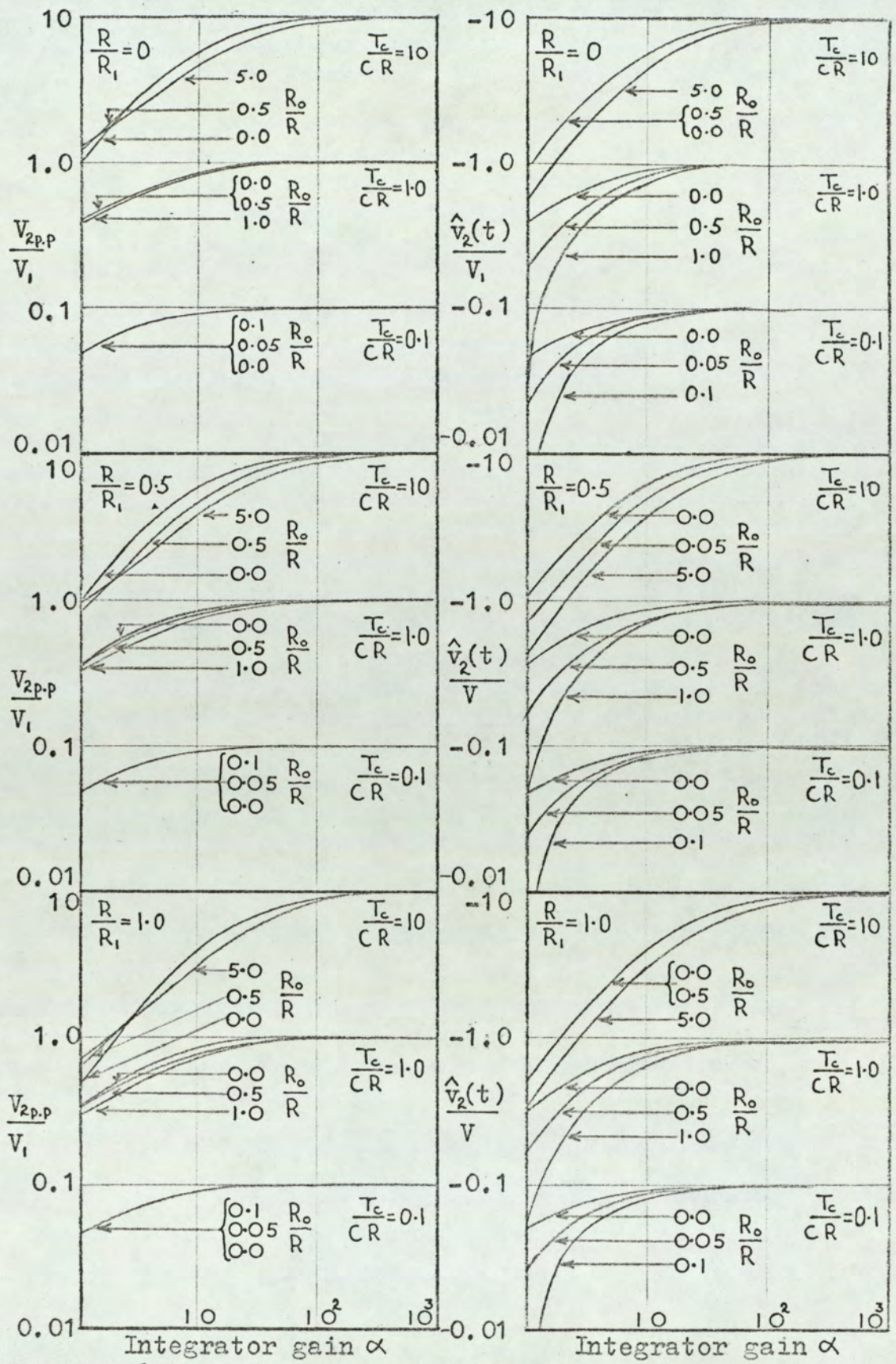

Fig.3.2.6. Peak integrator output voltages for single-edge modulation system.

$$V_{2_{p\cdot p}} = v_2(0) - v_2(T_c) \qquad (3.2.16)$$

∴ From equation 3.2.1

$$V_{2_{p\cdot p}} = \frac{\alpha V_1}{1 + R/R_1}\left[1 - \frac{C R_o}{\alpha T_e}\right]\left[1 - \exp\left(\frac{-T_c}{T_e}\right)\right] \qquad (3.2.17)$$

$$\hat{v}_2(t) = v_2(T_c) = -\frac{\alpha V_1}{1 + R/R_1}\left[1 - \left(1 - \frac{C R_o}{\alpha T_e}\right)\exp\left(\frac{-T_c}{T_e}\right)\right] \qquad (3.2.18)$$

Fig. 3.2.6 shows $\frac{V_{2p.p}}{V_1}$ and $\frac{\hat{v}_2(t)}{V_1}$ plotted as a function of the integrator gain α for a range of values of the normalised amplifier output resistance $\frac{R_o}{R}$ and of the reciprocal of the normalised amplifier input resistance $\frac{R_1}{R}$. Unfortunately fig. 3.2.6 does not indicate very clearly the manner in which the peak-to-peak integrator output $V_{2p.p}$ varies with amplifier output resistance R_o. However it does give a reasonable indication of the variation of the peak-to-peak output. Two points of interest arise from fig. 3.2.6. Firstly, neither the peak-to-peak output $V_{2p.p}$ nor the peak output $\hat{v}_2(t)$ are very strongly dependent on the amplifier input resistance R_1. Secondly, the peak output $\hat{v}_2(t)$ varies quite rapidly with varying amplifier output resistance, whereas the peak-to-peak output is only slightly affected by the output resistance.

3.2.2 Double-edge modulation

Consider the double-edge pulse-length modulation system, shown in fig. 2.1(a), with the operational integrator of fig. 3.2.1 being used to produce the sampling waveform. It is necessary to

derive an expression for the output waveform of the integrator when a square wavetrain is applied to the input. In section 3.1.2 a procedure was developed which enabled the square-wave response of an operational amplifier with finite gain, to be derived from the step response. Now, the step response of an operational integrator with an amplifier having finite values of voltage gain, input resistance and output resistance is given by equation 3.2.1. Since the procedure for obtaining the square-wave response from equation 3.2.1 is identical to that used in section 3.1.2, only the results will be given here.

$$V_2(t) = -\frac{\alpha V_1}{1+R/R_1}\left\{1-\frac{2\left(1+\frac{CR_o}{\alpha T_e}\right)}{1+\exp\left(\frac{-T_c}{2T_e}\right)}\cdot\exp\left(\frac{-t}{T_e}\right)\right\} \qquad 0 \leqslant t \leqslant \frac{T_c}{2} \qquad (3.2.19)$$

$$V_2(t) = -\frac{\alpha V_1}{1+R/R_1}\left\{-1+\frac{2\left(1+\frac{CR_o}{\alpha T_e}\right)}{1+\exp\left(\frac{-T_c}{2T_e}\right)}\exp\left(\frac{-(t-\frac{T_c}{2})}{T_e}\right)\right\} \qquad \frac{T_c}{2} \leqslant t \leqslant T_c \qquad (3.2.20)$$

$$T_e = \frac{(1+\alpha)CR}{1+R/R_1} + CR_o = CR\left[\frac{1+\alpha}{1+R/R_1} + \frac{R_o}{R}\right]$$

The term $\left(1 + \frac{CR_O}{\alpha T_e}\right)$, in equations 3.2.19 and 3.2.20, produces a step discontinuity in the waveform at multiples of $\frac{Tc}{2}$ as can be seen in fig. 3.2.7, which shows the integrator output waveform for selected values of the parameters. The second effect of the finite values of amplifier input and output resistance is to modify the effective integrator time constant from
$(1+\alpha)\,CR$ to $\frac{(1+\alpha)\,CR}{1+\frac{R}{R_1}} + CR_o$.

In the block diagram of the system, fig. 2.2(a), the integrator output waveform is added to the modulating input voltage V_{in}, and the resulting voltage applied to the input of the level detector. The output of the level detector changes

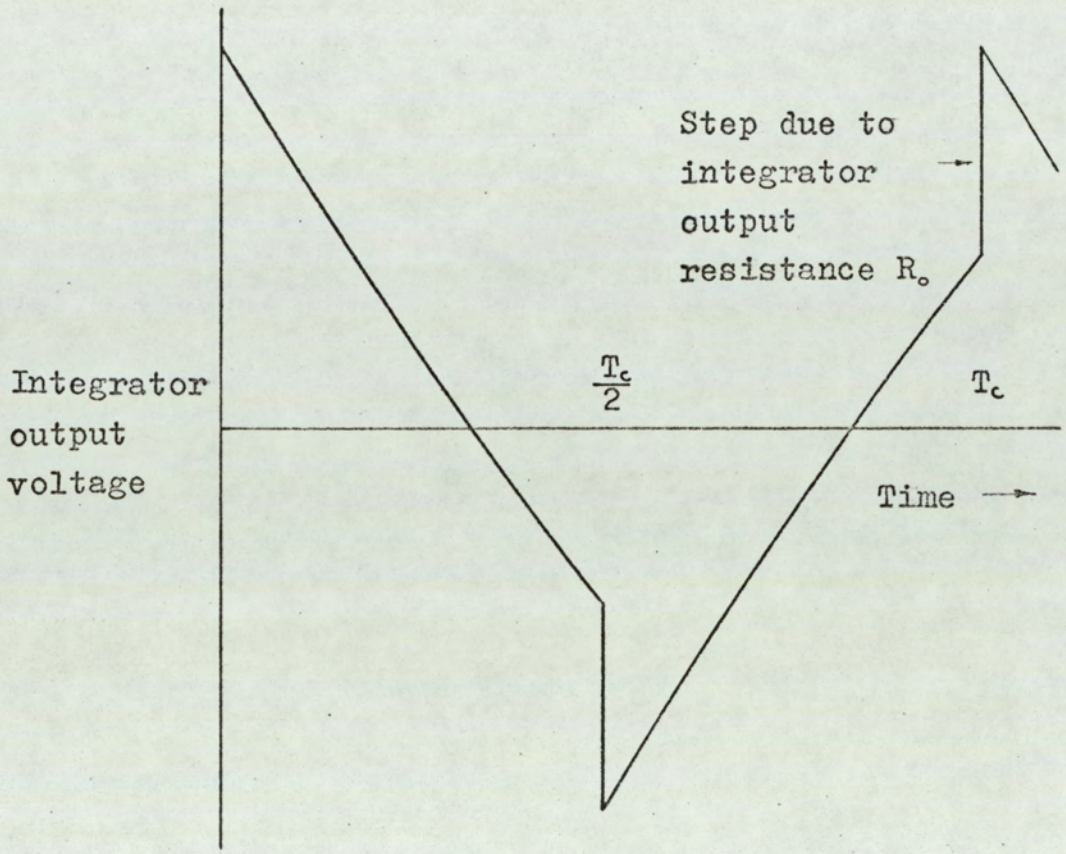

Fig.3.2.7. Effect of finite values of amplifier input and output resistance on the integrator output waveform.

state at times t_1 and t_2, as defined by the following expressions.

$$v_2(t_1) + V_{in} = V_t \qquad 0 \leq t_1 \leq \frac{T_c}{2} \qquad (3.2.21)$$

$$v_2(t_2) + V_{in} = V_t \qquad \frac{T_c}{2} \leq t_2 \leq T_c \qquad (3.2.22)$$

where V_t is the level-detector threshold voltage.

Fig. 3.2.8 shows the waveforms associated with the level detector. In section 3.1.2 it was shown that if the peak positive and negative values of the integrator output waveform are equal in amplitude, then the following conditions ensure that the positive and negative values of the modulating input voltage required for full modulation, $\hat{V}_{in+}$ and $\hat{V}_{in-}$ respectively, are equal in amplitude.

$$V_t = 0 \qquad (3.2.23)$$

$$\hat{v}_2(t) = \hat{V}_{in+} \qquad (3.2.24)$$

where $\hat{v}_2(t)$ is the peak positive value of the integrator output waveform. Now, the peak value of the integrator waveform occurs at time $t = 0+$. Therefore, from equation 3.2.19:

$$\hat{v}_2(t) = -\frac{\alpha V_1}{1 + R/R_1}\left\{1 - \frac{2\left(1 + \frac{CR_o}{\alpha T_e}\right)}{1 + \exp\left(\frac{-T_c}{2T_e}\right)}\right\} \qquad (3.2.25)$$

Substituting equations 3.2.23, 3.2.24 and 3.2.25 in equations 3.2.21 and 3.2.22, and dividing through by the peak input $\hat{V}_{in+}$, gives:

$$1 - \frac{2\left(1 + \frac{CR_o}{\alpha T_e}\right)}{1 + \exp\left(\frac{-T_c}{2T_e}\right)} \exp\left(\frac{-t_1}{T_e}\right) = -M\left[1 - \frac{2\left(1 + \frac{CR_o}{\alpha T_e}\right)}{1 + \exp\left(\frac{-T_c}{2T_e}\right)}\right] \qquad (3.2.26)$$

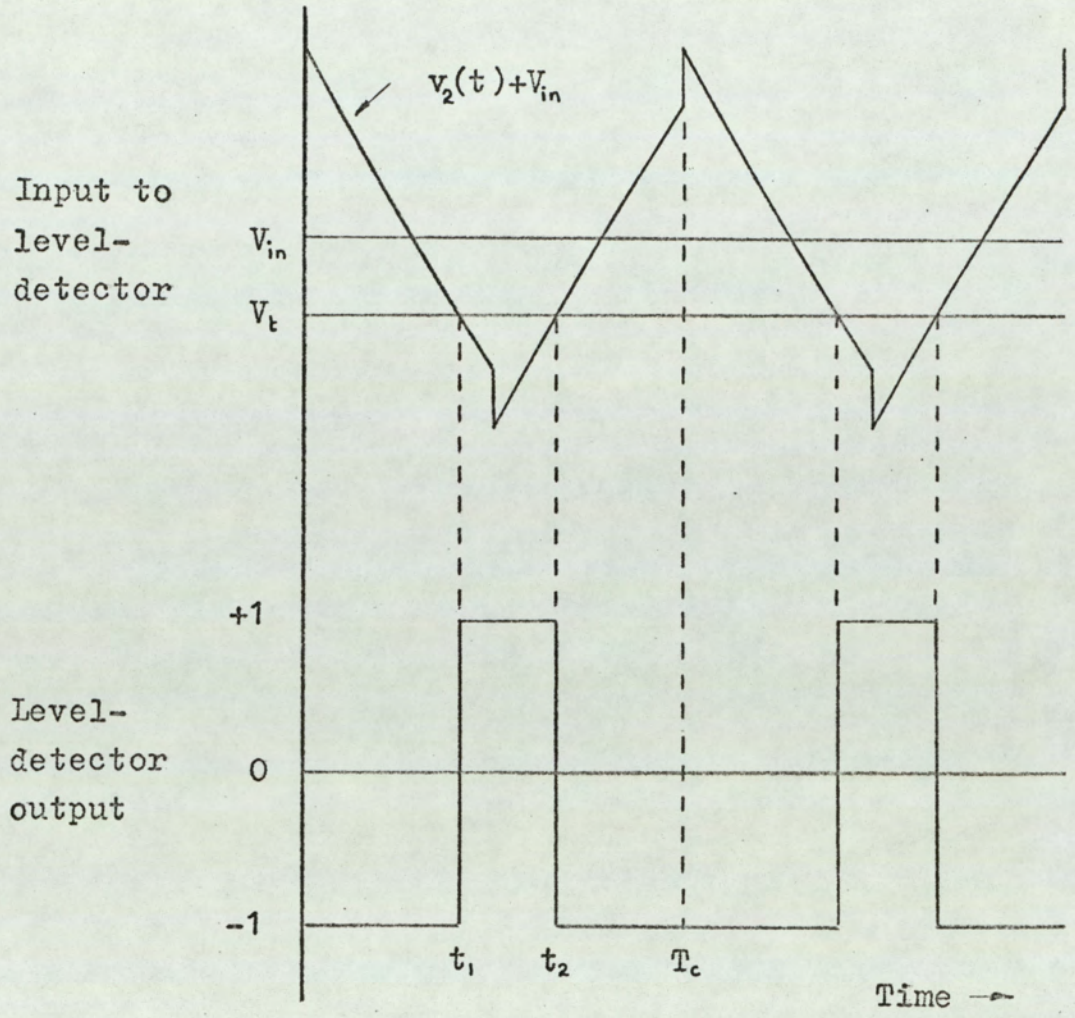

Fig.3.2.8. Waveforms for double-edge modulation system with finite values of integrator gain, input resistance and output resistance.

$$-1+\frac{2\left(1+\frac{CR_o}{\alpha T_e}\right)}{1+\exp\left(\frac{-T_c}{2T_e}\right)}\exp\left(\frac{-\left(t_2-\frac{T_c}{2}\right)}{T_e}\right)=-M\left[1-\frac{2\left(1+\frac{CR_o}{\alpha T_e}\right)}{1+\exp\left(\frac{-T_c}{2T_e}\right)}\right] \qquad (3.2.27)$$

where $M = \frac{V_{in}}{\hat{V}_{in+}}$ is the modulation index.

From equations 3.2.26 and 3.2.27 expressions may be obtained for t_1 and t_2, the time positions of the leading and trailing edges of the pulse-length modulated wavetrain at the output of the level detector.

$$\frac{t_1}{T_c}=-\frac{T_e}{T_c}\left\{\log\frac{1+\exp\left(\frac{-T_c}{2T_e}\right)}{2\left(1+\frac{CR_o}{\alpha T_e}\right)}+\log\left[1+M\left(1-\frac{2\left(1+\frac{CR_o}{\alpha T_e}\right)}{1+\exp\left(\frac{-T_c}{2T_e}\right)}\right)\right]\right\} \qquad (3.2.28)$$

$$\frac{t_2}{T_c}=\frac{1}{2}-\frac{T_e}{T_c}\left\{\log\frac{1+\exp\left(\frac{-T_c}{2T_e}\right)}{2\left(1+\frac{CR_o}{\alpha T_e}\right)}+\log\left[1-M\left(1-\frac{2\left(1+\frac{CR_o}{\alpha T_e}\right)}{1+\exp\left(\frac{-T_c}{2T_e}\right)}\right)\right]\right\} \qquad (3.2.29)$$

Comparing the above expressions with the corresponding ones for the system with ideal amplifier resistances (equations 3.1.31 and 3.1.32) shows that there is a close similarity in general form. This similarity is more marked if equations 3.2.28 and 3.2.29 are rewritten as:

$$\frac{t_1}{T_c}=-\frac{T_e}{T_c}\left\{\log\frac{1+\exp\left(\frac{-T_c}{2T_e}\right)}{2\left(1+\frac{CR_o}{\alpha T_e}\right)}+\log\left(1-M\phi K\right)\right\} \qquad (3.2.30)$$

$$\frac{t_2}{T_c}=\frac{1}{2}-\frac{T_e}{T_c}\left\{\log\frac{1+\exp\left(\frac{-T_c}{2T_e}\right)}{2\left(1+\frac{CR_o}{\alpha T_e}\right)}+\log\left(1+M\phi K\right)\right\} \qquad (3.2.31)$$

where:
$$\phi = \frac{1 - \frac{2\left(1+\frac{CR_o}{\alpha T_e}\right)}{1+\exp\left(\frac{-T_c}{2T_e}\right)}}{1 - \frac{2}{1+\exp\left(\frac{-T_c}{2T_e}\right)}} \qquad (3.2.32(a))$$

$$K = \frac{1-\exp\left(\frac{-T_c}{2T_e}\right)}{1+\exp\left(\frac{T_c}{2T_e}\right)} \qquad (3.2.32(b))$$

Apart from the constant term, equations 3.2.30 and 3.2.31 are identical to those for a system with infinite amplifier input resistance and zero output resistance, but with an effective integrator time constant of T_e and an effective modulation index of $M\phi$.

Demodulation of the wavetrain at the level-detector output is equivalent to taking the average value of the modulated wavetrain. Therefore, the expression for the amplitude of the demodulated wavetrain is:

$$V_{av} = 2\left(\frac{t_2}{T_c} - \frac{1}{2} - \frac{t_1}{T_c}\right)$$

Substituting equations 3.2.30 and 3.2.31 in the above expression gives:

$$V_{av} = -\frac{2T_e}{T_c}\log\left(\frac{1+M\phi K}{1-M\phi K}\right) \qquad (3.2.33)$$

The logarithmic term in the above expression may be expanded as an infinite series:

$$V_{av} = -\frac{4T_e}{T_c}\sum_{n=1}^{\infty}\frac{1}{(2n-1)}\left(M\phi K\right)^{2n-1} \qquad (3.2.34)$$

Since the constant terms in equations 3.2.30 and 3.2.31 have

cancelled out, the amplitude of the demodulated wavetrain is zero when the modulation index is zero. Equations 3.2.33 and 3.2.34 are identical in form to the corresponding expressions for a system with infinite amplifier input resistance and zero output resistance (equations 3.1.36 and 3.1.37). Therefore expressions for the error in the amplitude of the demodulated wavetrain for a system with finite amplifier input and output resistance may be written down by inspection of equations 3.1.16, 3.1.38, 3.1.39 and 3.1.40.

$$E_1 = V_{av} + M \qquad (3.2.35)$$

$$E_2 = -\frac{2T_e}{T_c}\left\{\log\left(\frac{1+M\phi K}{1-M\phi K}\right) - 2M\phi K\right\} \qquad (3.2.36)$$

$$E_2 = -\frac{4T_e}{T_c}\sum_{n=2}^{\infty}\frac{1}{(2n-1)}(M\phi K)^{2n-1} \qquad (3.2.37)$$

The considerations underlying the choice of definition of the error expressions are discussed in sections 3.1.1 and 3.1.2. Equation 3.2.35 may be rewritten as:

$$E_1 = V_{av} + M\phi + M(1-\phi) \qquad (3.2.38)$$

Now the term $V_{av} + M\phi$, in equation 3.2.38, is identical to the static error E_1 for a double-edge modulation system with infinite amplifier input resistance and zero output resistance, operating with a modulation index $M\phi$ and an effective integrator time constant of T_e. Thus, the graph of error E_1 for a system with non-finite amplifier input and output resistance (Fig. 3.1.9) may be used to evaluate the term

$V_{av} + M\phi$ by replacing the system parameters $\frac{T_c}{(1+\alpha)CR}$ and M by $\frac{T_c}{T_e}$ and $M\phi$ respectively. Graphical presentation of the factor $(1-\phi)$, as a function of the individual variables R_o, R_1, α and $\frac{T_c}{CR}$, is not practicable. It is possible, however, to plot $(1-\phi)$ as a function of the variables $\frac{CR_o}{\alpha T_e}$ and $\frac{T_c}{T_e}$, as shown in fig. 3.2.9. Interpretation of this diagram is facilitated if the functions $\frac{CR_o}{\alpha T_e}$ and $\frac{T_c}{T_e}$ are rewritten as:

$$\frac{CR_o}{\alpha T_e} = \frac{1}{\alpha\left[\frac{(1+\alpha)R/R_o}{1+R/R_1} + 1\right]} \qquad (3.2.39)$$

$$\frac{T_c}{T_e} = \frac{T_c}{CR}\left[\frac{1}{\frac{(1+\alpha)}{1+R/R_1} + \frac{R_o}{R}}\right] \qquad (3.2.40)$$

The additional error term $M(1-\phi)$, in equation 3.2.38 for E_1, can now be evaluated with the aid of fig. 3.2.9.

Equations 3.2.36 and 3.2.37 for the system static error E_2 are identical in form to the corresponding error expressions for the double-edge modulation system with ideal amplifier input and output resistances (equations 3.1.39 and 3.1.40). Thus, fig. 3.1.10 can be used to determine the error of the system with finite values of amplifier input and output resistance by simply replacing the system parameters M and $\frac{T_c}{(1+\alpha)CR}$, in fig. 3.1.10, with $M\phi$ and $\frac{T_c}{T_e}$ respectively; the value of ϕ is then obtained from fig. 3.2.9.

The finite values of amplifier input and output resistance affect the system error in a number of ways, and these cancel out

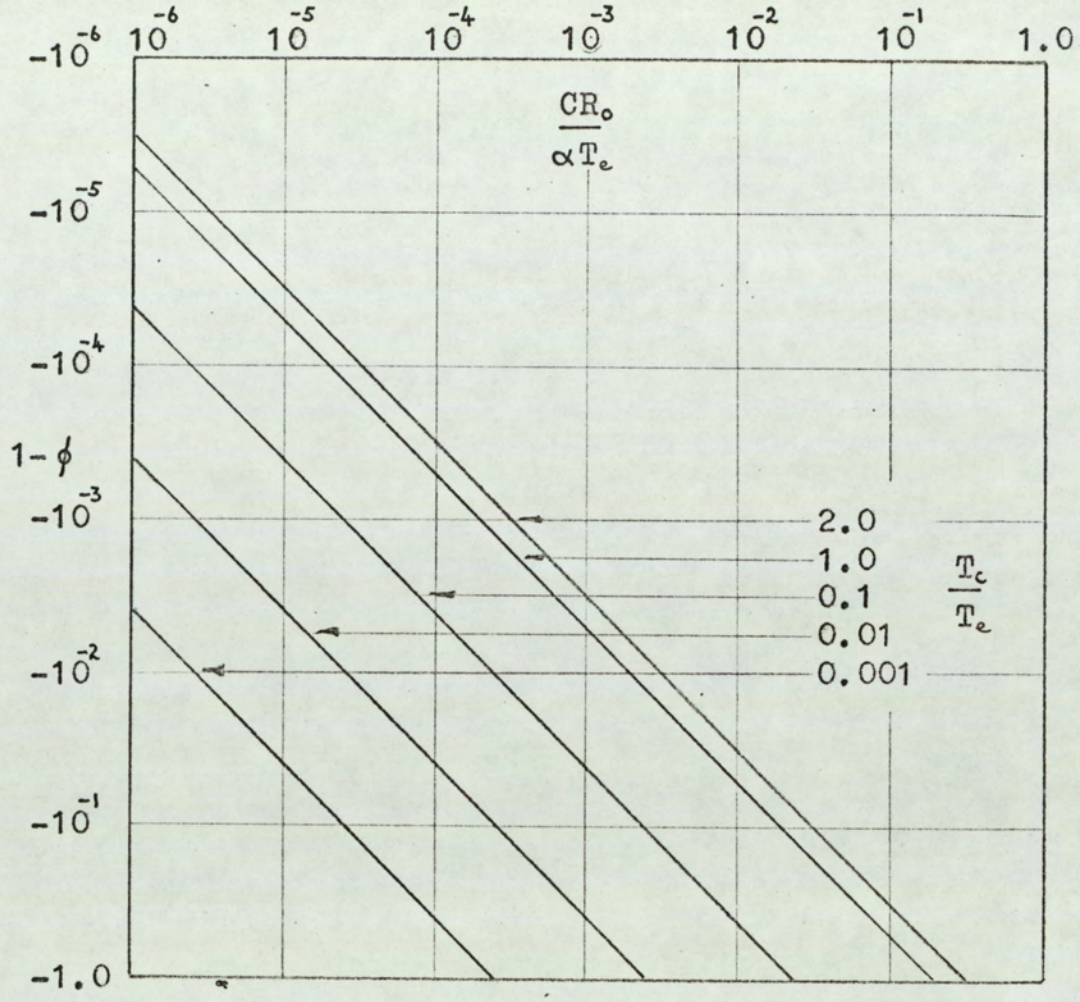

Fig.3.2.9. Modulation index modifying function ϕ for double-edge modulation system with finite values of amplifier input resistance and output resistance.

to some extent. The output resistance causes an increase in the effective integrator time constant, hence decreasing the system error, whilst the amplifier input resistance decreases the effective time constant and increases the system error. The function ϕ modifying the modulation index is due to the output resistance, but it is also a function of the input resistance. It is not possible, in general, to state whether the finite values of amplifier input and output resistance cause an increase or a decrease in system static error, since this depends on the particular values of the system parameters. It is clear, however, from fig. 3.2.9 and equations 3.2.39 and 3.2.40, that a remarkably large value of output resistance can be tolerated without producing a significant increase in system error.

It has been implicitly assumed that the preceding analysis of system error is valid for all values of modulation index M. That this assumption is not valid may be seen from fig. 3.2.8. As the modulating input voltage V_{in} is increased in the positive direction, the position t_1 of the leading edge approaches $\frac{T_c}{2}$. When the input voltage is equal and opposite to the smaller of the amplitudes of the sampling waveform at time $\frac{T_c}{2}$, then the leading edge of the pulse occurs at time $t_1 = \frac{T_c}{2}$. Any further increase in the input voltage will only affect the position of the trailing edge of the pulse. However, this condition is not given by the analytical expressions. The position t_1 of the leading edge was derived from equations 3.2.19 and 3.2.21. If, in equation 3.2.21, the input voltage V_{in} is greater than the integrator output $v_2(t)$ at time $\frac{T_c}{2}$,

then the value for t_1 will be greater than $\frac{T_c}{2}$. This is not a valid condition, since equation 3.2.19 for the integrator output waveform is only valid for $0 \leqslant t \leqslant \frac{T_c}{2}$. This condition is illustrated by fig. 3.2.10. Since the integrator output waveform is symmetrical, a similar argument holds for negative values of modulating input voltage. The maximum positive input voltage $V_{in}(max)$, for which the analytical work is valid, is equal and opposite to the smaller of the two values of the integrator waveform at time $\frac{T_c}{2}$. Therefore, from equation 3.2.19

$$V_{in}(max) = \frac{\alpha V_1}{1 + R/R_1}\left\{1 - \frac{2\left(1 + \frac{CR_o}{\alpha T_e}\right)}{1 + \exp\left(\frac{-T_c}{2T_e}\right)} \exp\left(\frac{-T_c}{2T_e}\right)\right\} \qquad (3.2.41)$$

The maximum input voltage $V_{in}(max)$ may be expressed as a modulation index:

$$M(max) = \frac{V_{in}(max)}{\hat{V}_{in}} \qquad (3.2.42)$$

From equations 3.2.23 and 3.2.25:

$$M(max) = \frac{\left(1 + \frac{2CR_o}{\alpha T_e}\right)\exp\left(\frac{-T_c}{2T_e}\right) - 1}{\exp\left(\frac{-T_c}{2T_e}\right) - \left(1 - \frac{2CR_o}{\alpha T_e}\right)} \qquad (3.2.43)$$

Fig. 3.2.11 shows M (max) plotted as a function of $\frac{CR_o}{\alpha T_e}$ and $\frac{T_c}{T_e}$. The number of variables and the form of equation 2.2.42 is such that direct graphical presentation of M (max) as a function of the system parameters R_o, R_1, $\frac{T_c}{CR}$ and α is not practicable.

Analytical expressions for the system error will not be developed for values of modulation index greater than M (max).

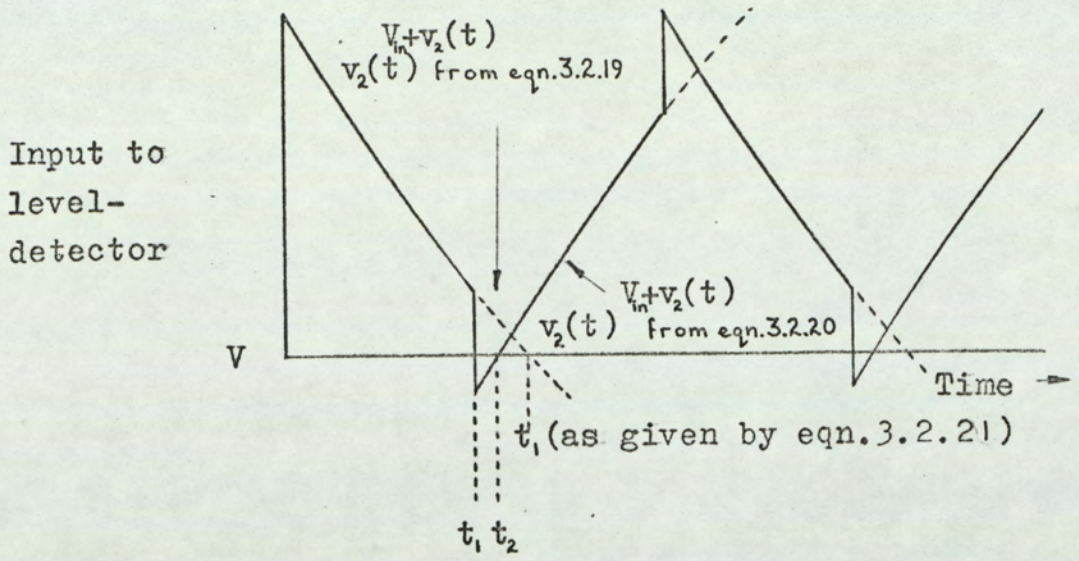

Fig.3.2.10. Level-detector input waveform.

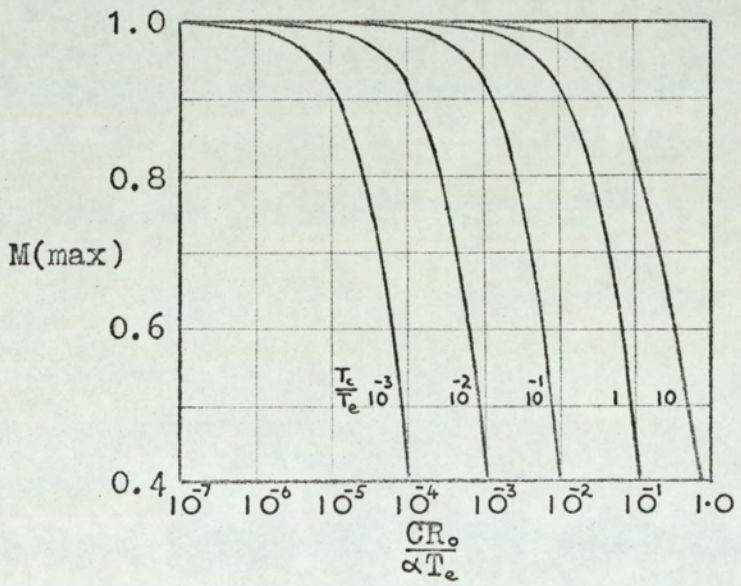

Fig.3.2.11. Maximum value of the modulation index for which the analytical expressions are valid.

When a system is designed, the values of the system parameters will normally be chosen so that M (max) is insignificantly different from unity. Substitution of typical values in fig. 3.2.11 show that this condition is easily met.

As discussed in sections 3.1.1 and 3.1.2, a parameter of importance in the design of a pulse-length modulation system is the peak amplitude of the sampling waveform, as given by equation 3.2.25. It is also of interest to know the amplitude of the lower of the two values of the integrator output waveform at the step discontinuity introduced by finite amplifier resistances. Fig. 3.2.12 shows that, as the amplifier output resistance is increased, so the lower of the two values of the integrator waveform at the discontinuity changes polarity. On account of this polarity change, graphical representation of this value of the integrator output waveform on a logarithmic scale will yield rather confusing results. For this reason , it is better to plot the peak - to - peak value of the continuously varying component $V_{2p.p}$ of the integrator output waveform as a function of the system parameters. Fig. 3.2.13 shows the manner in which $V_{2p.p}$ is defined.

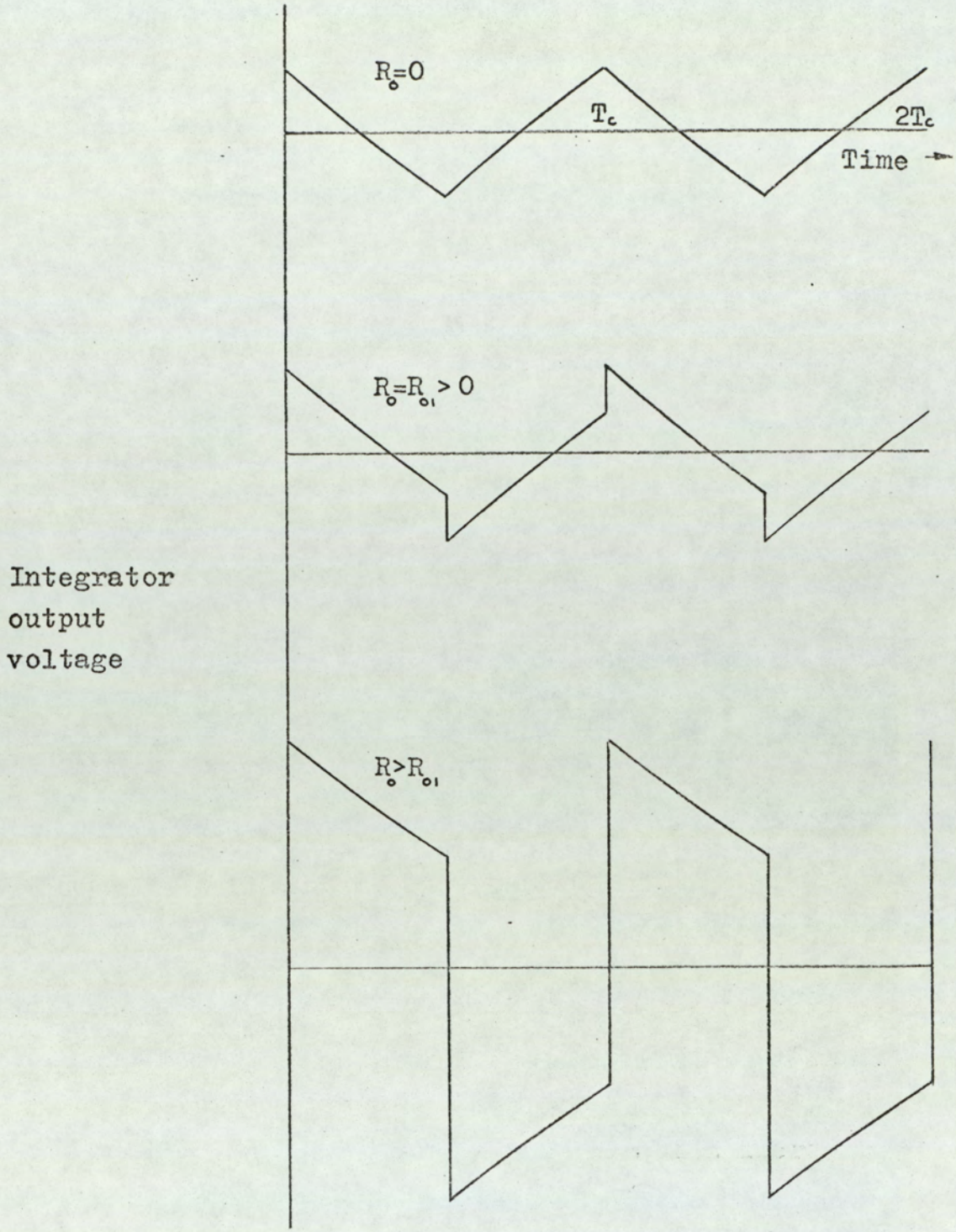

Fig.3.2.12. Integrator output waveform with increasing values of output resistance R_o.

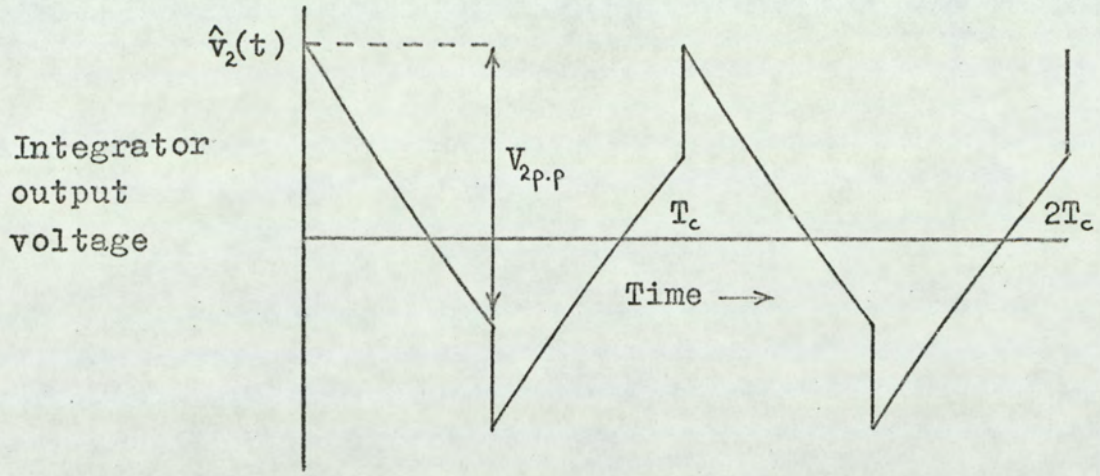

Fig.3.2.13.

Now $V_{2p.p} = v_2(0) - v_2(\frac{T_c}{2})$

Therefore, from equation 3.2.19,

$$V_{2p.p} = \frac{\alpha V_1}{1 + R/R_1} \left\{ 2\left(1 - \frac{CR_o}{\alpha T_e}\right) \frac{1 - \exp\left(\frac{-T_c}{2T_e}\right)}{1 - \exp\left(\frac{-T_c}{2T_e}\right)} \right\} \qquad (3.2.44)$$

Fig. 3.2.14 shows $\frac{V_{2p.p}}{V_1}$ and $\frac{\hat{v}_2(t)}{V_1}$ (from equations 3.2.25 and 3.2.44 respectively) plotted as a function of the integrator gain α for a range of values of normalised amplifier output resistance $\frac{R_o}{R}$ and of the reciprocal of the normalised amplifier input resistance $\frac{R_1}{R}$. As with the single-edge modulation case, it is rather unfortunate that the form of the equations which define $V_{2p.p}$ and $\hat{v}_2(t)$ lead to graphical results which are rather complicated. However, fig. 3.2.14 does give a reasonable indication of the manner in which $\frac{V_{2p.p}}{V_1}$ and $\frac{\hat{v}_2(t)}{V_1}$ vary with the system parameters. If accurate results are required, it is a simple matter to calculate the values from equations 3.2.25 and 3.2.44.

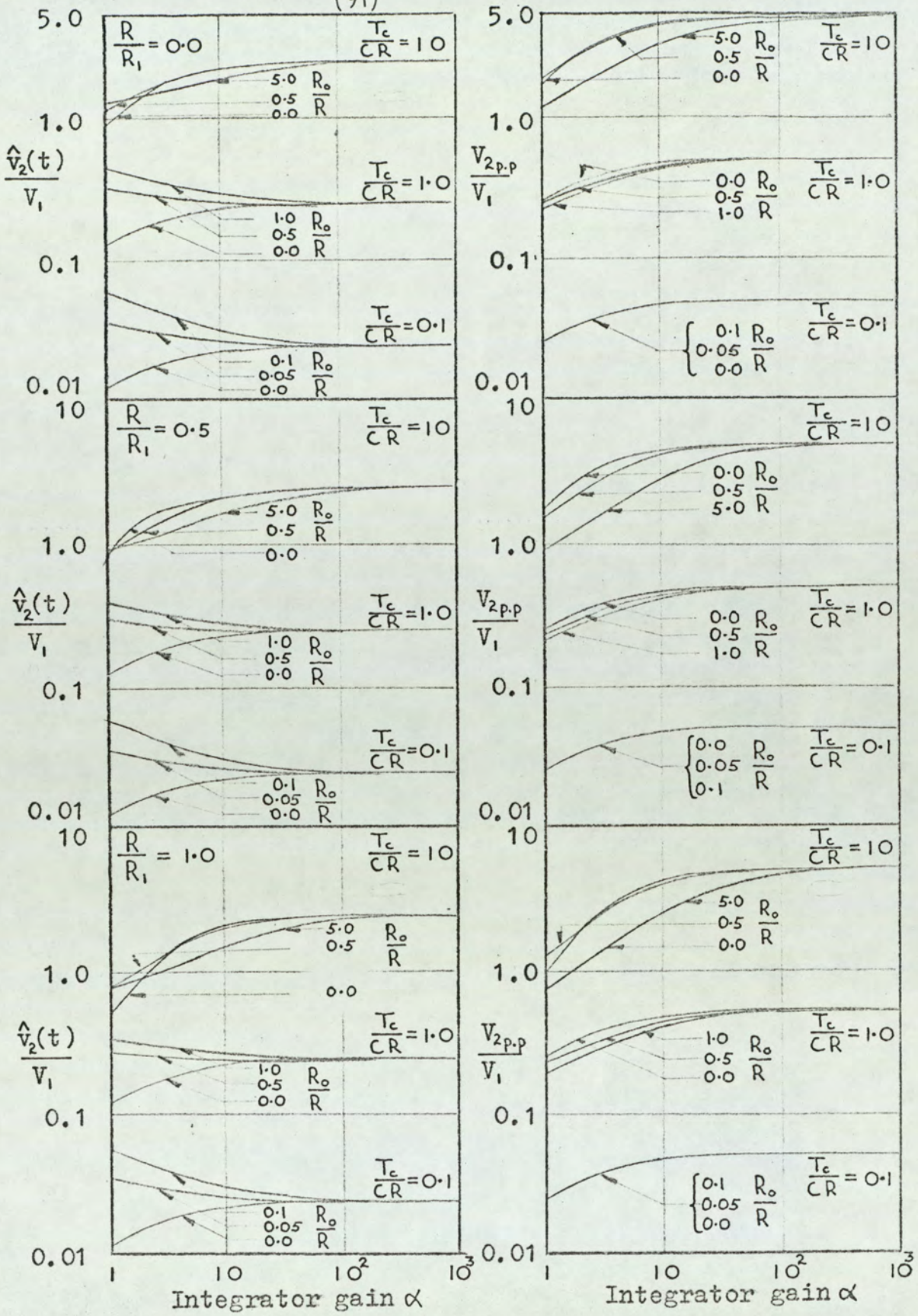

Fig.3.2.14. Peak integrator output voltages for double-edge modulation system.

3.2.3 Conclusions

Expressions have been derived for the static error in the demodulated output of pulse-length modulation systems utilising operational integrators with finite values of amplifier input and output resistance. The error of the system has been expressed in terms of the error of an equivalent system having infinite amplifier input resistance and zero output resistance.

For the single-edge modulation system, a finite value of input resistance increases the static error, whilst finite output resistance decreases the error. The overall effect of the finite values of resistance is more complex for the double - edge modulation system. It is not possible to state in general terms what is the effect of the finite resistances, since the nature of the effect depends on the actual values of the system parameters.

The most striking feature of the results is that a relatively large value of output resistance can be tolerated without producing any significant change in system performance. This may be seen from equation 3.2.40 for the normalised time constant $\frac{T_c}{T_e}$. The output resistance R_o must be comparable with $(1 + \alpha) R$ before it has any significant effect on the normalised time constant. The value of output resistance that can be tolerated without significantly affecting the factor ϕ is best demonstrated by considering a practical example. (See section 5).

3.3 Static error due to finite bandwidth of the integrator amplifier

When specifying an amplifier for use as an operational integrator in a pulse-length modulation system one important parameter is the bandwidth of the amplifier. Since the cost of an amplifier increases with bandwidth, it is obviously desirable to use the minimum bandwidth consistent with the required system performance. It is the objective of this section to relate the system static error to the bandwidth of the amplifier used in the operational integrator. It will be assumed that the upper turnover frequency of the amplifier is defined by a single time constant T_a so that the amplifier transfer function $\alpha(s)$ has the form:

$$\alpha(s) = \frac{-\alpha}{1 + sT_a} \qquad (3.3.1)$$

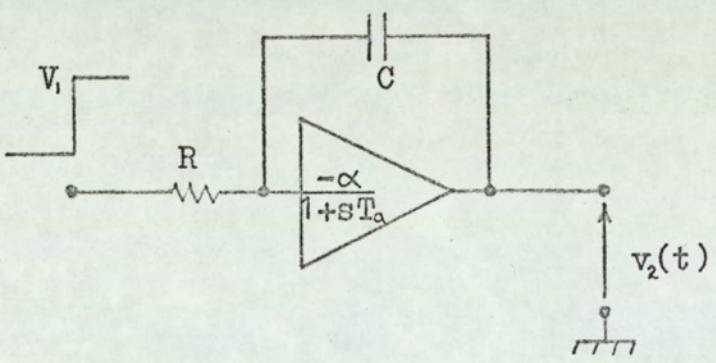

Fig.3.3.1. Operational integrator with bandwidth-limited amplifier.

The response of the operational integrator of fig. 3.3.1 to a positive step-function input voltage V_1 is:

$$v_2(t) = -\alpha V_1 \left\{ 1 - \frac{1}{1 - k_1/k_2} \exp(-k_1 t) - \frac{1}{1 - k_2/k_1} \exp(-k_2 t) \right\} \qquad (3.3.2)$$

$$k_1 = \frac{1}{2} \left\{ \frac{T_a + (1+\alpha)CR}{T_a . CR} + \sqrt{\left[\left(\frac{T_a + (1+\alpha)CR}{T_a . CR} \right)^2 - \frac{4}{T_a . CR} \right]} \right\} \qquad (3.3.3(a))$$

$$k_2 = \frac{1}{2} \left\{ \frac{T_a + (1+\alpha)CR}{T_a . CR} - \sqrt{\left[\left(\frac{T_a + (1+\alpha)CR}{T_a . CR} \right)^2 - \frac{4}{T_a . CR} \right]} \right\} \qquad (3.3.3(b))$$

The integrator step response given by equation 3.3.2 is the basis for the following analyses of system static error.

3.3.1 Single-edge modulation

Consider the single-edge pulse-length modulation system of fig. 2.2(a) using the operational amplifier of fig. 3.3.1 to produce the sampling waveform. Fig. 3.3.2 shows the effect of finite amplifier bandwidth on the integrator output waveform, the amplitude of the waveform being normalised to the amplitude at time $t = T_c$. In general, the waveform shown in fig. 3.3.2(a) is somewhat unrealistic, since it is assumed that the finite bandwidth does not affect the reset time of the integrator. However, since the reset time rather depends on the particular method used, the analysis of static error will be carried out for a system with zero reset time. The sampling waveform is added to the modulating input voltage, V_{in}, and the sum applied to the input of the

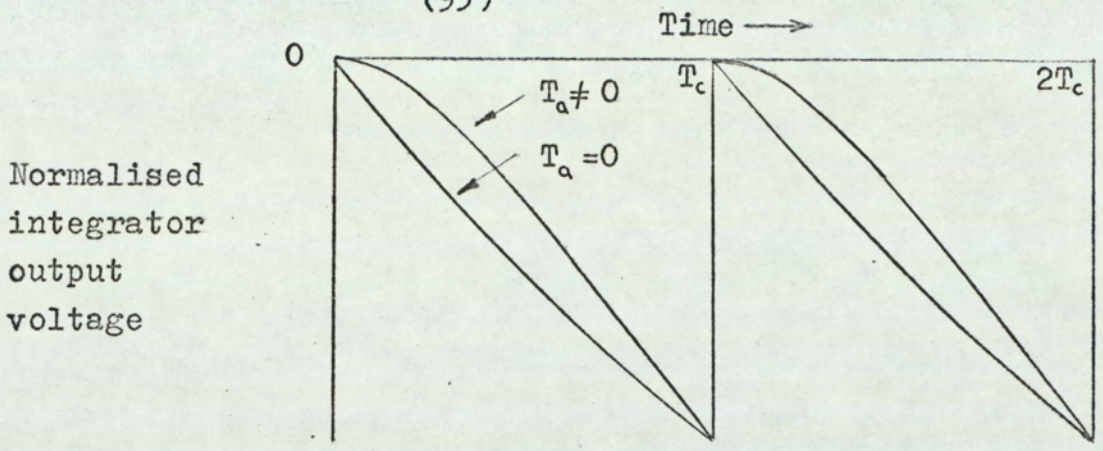

Fig.3.3.2(a) Effect of finite amplifier bandwidth on the normalised integrator output waveform.

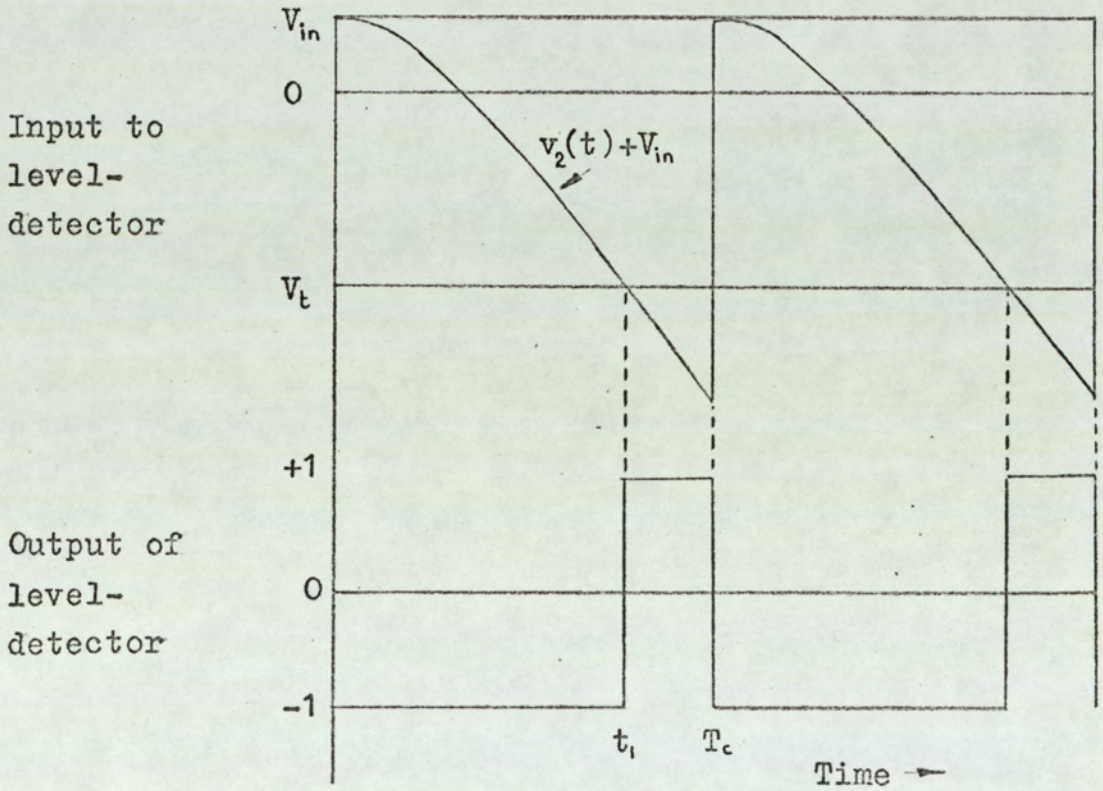

Fig.3.3.2(b) Waveforms for single-edge modulation system with bandwidth-limited integrator amplifier.

level-detector. The output of the level-detector changes state whenever the voltage applied to its input crosses the threshold level. The waveforms associated with the level-detector are shown in fig. 3.3.2(b) The trailing edges of the level-detector output pulses occur at periodic intervals of n T_c. The position of the leading edge is modulated in accordance with some function of the modulating input voltage V_{in}. The switching instant t_1 of the leading pulse edge is defined by the expression:

$$v_2(t_1) + V_{in} = V_t \qquad (3.3.4)$$

where V_t is the level-detector threshold voltage.

As discussed in section 3.1.1, the level-detector threshold voltage may be set to give two different conditions. The first of these conditions is that the amplitude V_{av} of the demodulated wavetrain is zero when the modulating input voltage is zero. It was shown in section 3.1.1 that, in order to satisfy this condition, the threshold voltage must be set at the value of the integrator output waveform at time $t = \frac{T_c}{2}$. Substituting $t = \frac{T_c}{2}$ in equation 3.3.2 gives:

$$V_t = v_2\left(\frac{T_c}{2}\right) = -\alpha V_1\left\{1 - \frac{1}{1 - k_1/k_2}\exp\left(\frac{-k_1 T_c}{2}\right) - \frac{1}{1 - k_2/k_1}\exp\left(\frac{-k_2 T_c}{2}\right)\right\} \qquad (3.3.5)$$

Now, from fig. 3.3.3, full modulation, for positive values of input voltage V_{in}, corresponds to the condition $t_1 = T_c$; full modulation for negative values of input voltage corresponds to $t_1 = 0$. Substituting these conditions into equations 3.3.4 leads to the following expressions for the positive and negative input voltages, $\hat{V}_{in+}$ and $\hat{V}_{in-}$ respectively, necessary to produce full modulation.

$$\hat{V}_{in+} = V_t - v_2(T_c) \qquad (3.3.6)$$

$$= \alpha V_1 \left\{ \frac{1}{1 - k_1/k_2} \exp\left(\frac{-k_1 T_c}{2}\right)\left[1 - \exp\left(\frac{-k_1 T_c}{2}\right)\right] + \frac{1}{1 - k_2/k_1} \exp\left(\frac{-k_2 T_c}{2}\right)\left[1 - \exp\left(\frac{-k_2 T_c}{2}\right)\right] \right\} \qquad (3.3.7)$$

$$\hat{V}_{in-} = V_t - v_2(0) \qquad (3.3.8)$$

$$= -\alpha V_1 \left\{ \frac{1}{1 - k_1/k_2}\left[1 - \exp\left(\frac{-k_1 T_c}{2}\right)\right] + \frac{1}{1 - k_2/k_1}\left[1 - \exp\left(\frac{-k_2 T_c}{2}\right)\right] \right\} \qquad (3.3.9)$$

In general, $\hat{V}_{in+}$ and $\hat{V}_{in-}$ are not equal and opposite. However, under certain conditions they can be made equal in magnitude. If $\hat{V}_{in+} = -\hat{V}_{in-}$, then from equations 3.3.6 and 3.3.8:

$$V_t = \frac{1}{2} v_2(T_c) \qquad (3.3.10)$$

Substituting from equation 3.3.5 in equation 3.3.10 gives:

$$v_2\left(\frac{T_c}{2}\right) = \frac{1}{2} v_2(T_c) \qquad (3.3.11)$$

Thus, if the positive and negative input voltages for full modulation are to be equal in magnitude, then the integrator output voltage at time $t = \frac{T_c}{2}$ must be equal to half the integrator output voltage at time $t = T_c$. Fig. 3.3.2 shows that this condition could be satisfied by suitable choice of amplifier bandwidth. The relationship between this particular value of bandwidth and the other system parameters will not be derived at this point. Equation 3.3.11 may be considered as a special case of the second of the two conditions

for which the level detector threshold may be set, i.e., that the positive and negative input voltages for full modulation are equal and opposite.

The value of the threshold voltage required to satisfy the condition $\hat{V}_{in+} = -\hat{V}_{in-}$ may be derived from equation 3.3.4 by setting t_1 to 0 and T_c (i.e. the values of the switching instant t_1 corresponding to full modulation).

$$v_2(0) + \left(-\hat{V}_{in+}\right) = V_t \qquad (3.3.12)$$

$$v_2(T_c) + \hat{V}_{in+} = V_t \qquad (3.3.13)$$

Substituting equation 3.3.2 in the above, and solving the simultaneous equations, gives the following expressions for the positive value of the modulating input voltage $\hat{V}_{in+}$ required for full modulation, and for the level detector threshold voltage V_t.

$$V_t = \frac{1}{2} v_2(T_c) = -\frac{\alpha V_1}{2}\left\{1 - \frac{1}{1-k_1/k_2}\exp(-k_1 T_c) - \frac{1}{1-k_2/k_1}\exp(-k_2 T_c)\right\} \qquad (3.3.14)$$

$$\hat{V}_{in+} = -V_t \qquad (3.3.15)$$

Substituting equations 3.3.14 and 3.3.15 in equation 3.3.4, and dividing through by $\hat{V}_{in+}$ gives:

$$\left\{1 - \frac{1}{1-k_1/k_2}\exp(-k_1 t_1) - \frac{1}{1-k_2/k_1}\exp(-k_2 t_1)\right\} =$$

$$\frac{1}{2}(1+M)\left\{1 - \frac{1}{1-k_1/k_2}\exp(-k_1 T_c) - \frac{1}{1-k_2/k_1}\exp(-k_2 T_c)\right\} \qquad (3.3.16)$$

where $M = \dfrac{V_{in}}{\hat{V}_{in+}}$ is the modulation index.

Equation 2.3.16 defines the position t_1 of the leading edge of the pulse occuring at the output of the level detector. Unfortunately, equation 2.3.16 is not amenable to direct solution. Consequently, either numerical methods or infinite-series methods must be used to evaluate t_1. Since the results of the static analysis need to be used when the dynamic analysis is made, a numerical analysis will be of little use. For this reason, a formula will be derived which expresses the switching point t_1 as a power series in terms of the modulation index M.

$$\frac{t_1}{T_c} = \sum_{n=0}^{\infty} a_n . M^n \qquad 3.3.17$$

The method of deriving expressions for the coefficients a_n is covered in detail in Appendix 2, and only the results will be given here.

$$a_0 = \frac{\overset{\circ}{t}_1}{T_c} \qquad (3.3.18(a))$$

$$a_1 = \frac{1}{T_N}\left[D\left(\frac{1}{A_2} - \frac{1}{A_1}\right)\right]\left[\frac{1}{F_0}\right] \qquad (3.3.18(b))$$

$$a_2 = \frac{1}{T_N 2!}\left[D\left(\frac{1}{A_2} - \frac{1}{A_1}\right)\right]^2\left[\frac{F_1}{F_0^3}\right] \qquad (3.3.18(c))$$

$$a_3 = \frac{1}{T_N 3!}\left[D\left(\frac{1}{A_2} - \frac{1}{A_1}\right)\right]^3\left[\frac{3F_1^2 - F_0F_2}{F_0^5}\right] \qquad (3.3.18(d))$$

$$a_4 = \frac{1}{T_N 4!}\left[D\left(\frac{1}{A_2} - \frac{1}{A_1}\right)\right]^4\left[\frac{-10F_0F_1F_2 + F_0^2F_3 + 15F_1^3}{F_0^7}\right] \qquad (3.3.18(e))$$

$$a_5 = \frac{1}{T_N 5!}\left[D\left(\frac{1}{A_2} - \frac{1}{A_1}\right)\right]^5\left[\frac{15F_0^2F_1F_3 + 10F_0^2F_2^2 + 105F_1^4 - F_0^3F_4 - 105F_0F_1^2F_3}{F_0^9}\right] \qquad (3.3.18(f))$$

$$a_6 = \frac{1}{T_N\, 6!}\left[D\left(\frac{1}{A_2} - \frac{1}{A_1}\right)\right]^6 \left[\frac{21F_o^3F_1F_4 + 35F_o^3F_2F_3 + 1260F_oF_1^3F_2 - F_o^4F_5 - 280F_o^2F_1F_2^2 - 945F_1^5 - 210F_o^2F_1^2F_3}{F_o^{11}}\right] \qquad (3.3.18(g))$$

$$a_7 = \frac{1}{T_N\, 7!}\left[D\left(\frac{1}{A_2} - \frac{1}{A_1}\right)\right]^7 \left[\frac{28F_o^4F_1F_5 + 56F_o^4F_2F_4 + 35F_o^4F_3^2 + 3150F_o^2F_1^3F_3 + 6300F_o^2F_1^2F_2^2 + 10395F_1^6 - F_o^5F_6 - 378F_o^3F_1^2F_4 - 1260F_o^3F_1F_2F_3 - 280F_o^3F_2^3 - 17325F_oF_1^4F_2}{F_o^{13}}\right] \qquad (3.3.18(h))$$

where:

$$T_N = \frac{T_c}{(1+\alpha)CR}\left[\frac{1}{1 + \frac{T_a}{(1+\alpha)CR}}\right] \qquad (3.3.19(a))$$

$$A_2 = 1 + \frac{2.1}{2!}\left(\frac{1}{\Psi}\right) + \frac{2^2.1.3}{3!}\left(\frac{1}{\Psi}\right)^2 + \frac{2^3.1.3.5}{4!}\left(\frac{1}{\Psi}\right)^3 + \text{- - - -} \qquad (3.3.19(b))$$

$$\Psi = \frac{CR}{T_a}\left[\frac{T_a}{CR} + (1+\alpha)\right]^2 \qquad (3.3.19(c))$$

$$A_1 = \Psi - A_2 \,. \qquad (3.3.19(d))$$

$$D = \frac{1}{2}\left\{1 - \frac{A_2}{A_2 - A_1}\exp\left(-A_1T_N\right) - \frac{A_1}{A_1 - A_2}\exp\left(-A_2T_N\right)\right\} \qquad (3.3.19(e))$$

$$E_n = A_2^n \exp\left(-A_2T_N\,\frac{\overset{\circ}{t}_1}{T_c}\right) - A_1^n \exp\left(-A_1T_N\,\frac{\overset{\circ}{t}_1}{T_c}\right) \qquad (3.3.20)$$

$\overset{\circ}{t}_1$ is the unmodulated position of the leading-edge of the pulse, i.e. $\overset{\circ}{t}_1 = t_1 /_{M=0}$.

Figs.3.3.3 (a), (b), (c) and (d) show the coefficients a_n plotted as functions of the normalised time constant $T_n = \frac{T_c}{(1+\alpha)\,CR}\left[\frac{1}{1+\frac{T_a}{(1+\alpha)\,CR}}\right]$ and the parameter γ. The reasons for choosing these two particular parameters are discussed in Appendix 2. A number of interesting observations may be made from these curves. The constant term, $a_o = \frac{t_1^\circ}{T_c}$, passes through the value 0.5 as the parameter γ decreases. It is therefore possible, by suitable choice of the amplifier bandwidth, to make the unmodulated mark-space ratio unity. This would, at first sight, seem to be a desirable state of affairs. However, as the parameter γ is reduced, so a_1 (the coefficient of M in equation 3.3.17) decreases. Coefficients a_2 and a_7 change very abruptly once a particular value of the parameter γ has been reached. This critical value of γ depends on the particular coefficient under consideration and on the value of the normalised time constant T_N. The reason for this rapid change in the values of the coefficents is evident from equation 3.3.20 for the factor F_n in the expressions for the coefficients. For large values of γ the term $A_2^n \exp(-A_2 \cdot T_N \cdot \frac{t_1^\circ}{T_c})$ dominates the expressions for F_n, whilst for lower values of γ the term $A_1^n \exp(-A_1 \cdot T_N \cdot \frac{t_1^\circ}{T_c})$ becomes the dominant factor. Considerable care is required in interpreting figs. 3.3.3 (a), (b), (c) and (d), since γ has a minimum value which is a function of the integrator gain α. This minimum value occurs when:

$$\frac{T_a}{CR} = 1 + \alpha \qquad (3.3.21(a))$$

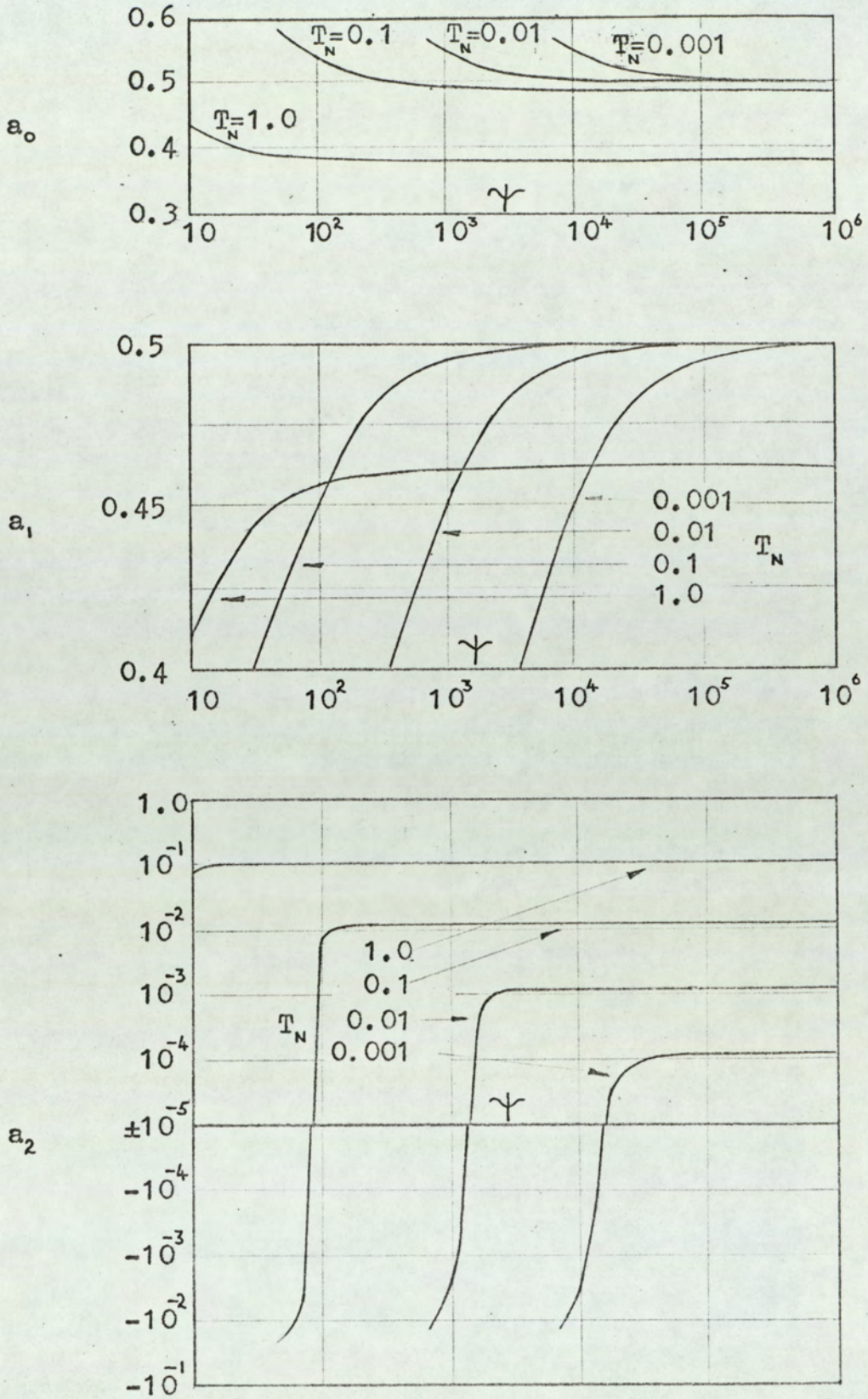

Fig.3.3.3(a). Coefficients a_o, a_1 and a_2 for single-edge modulation system with bandwidth-limited integrator amplifier.

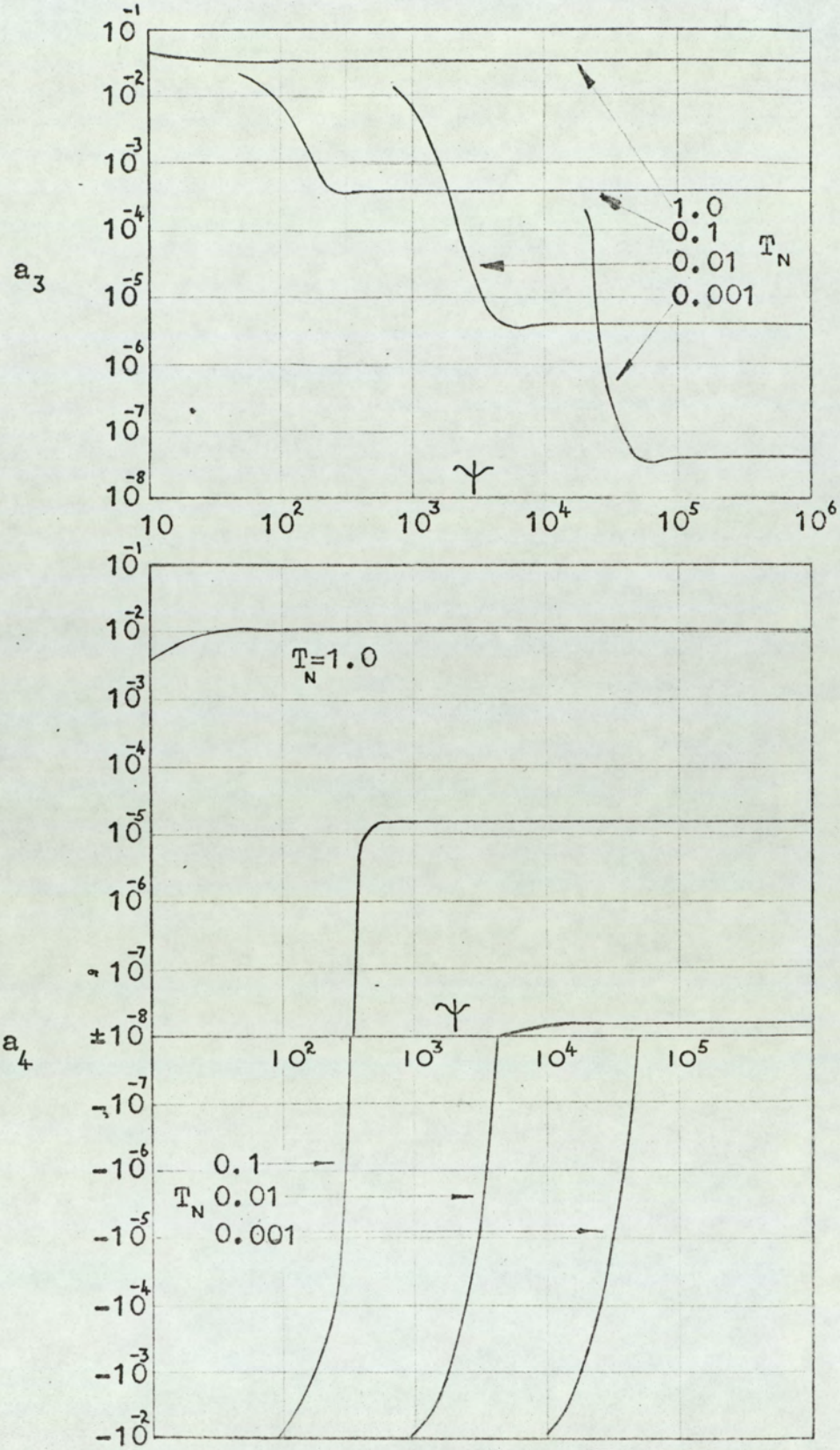

Fig.3.3.3(b). Coefficients a_3 and a_4 for single-edge modulation system with bandwidth-limited integrator amplifier.

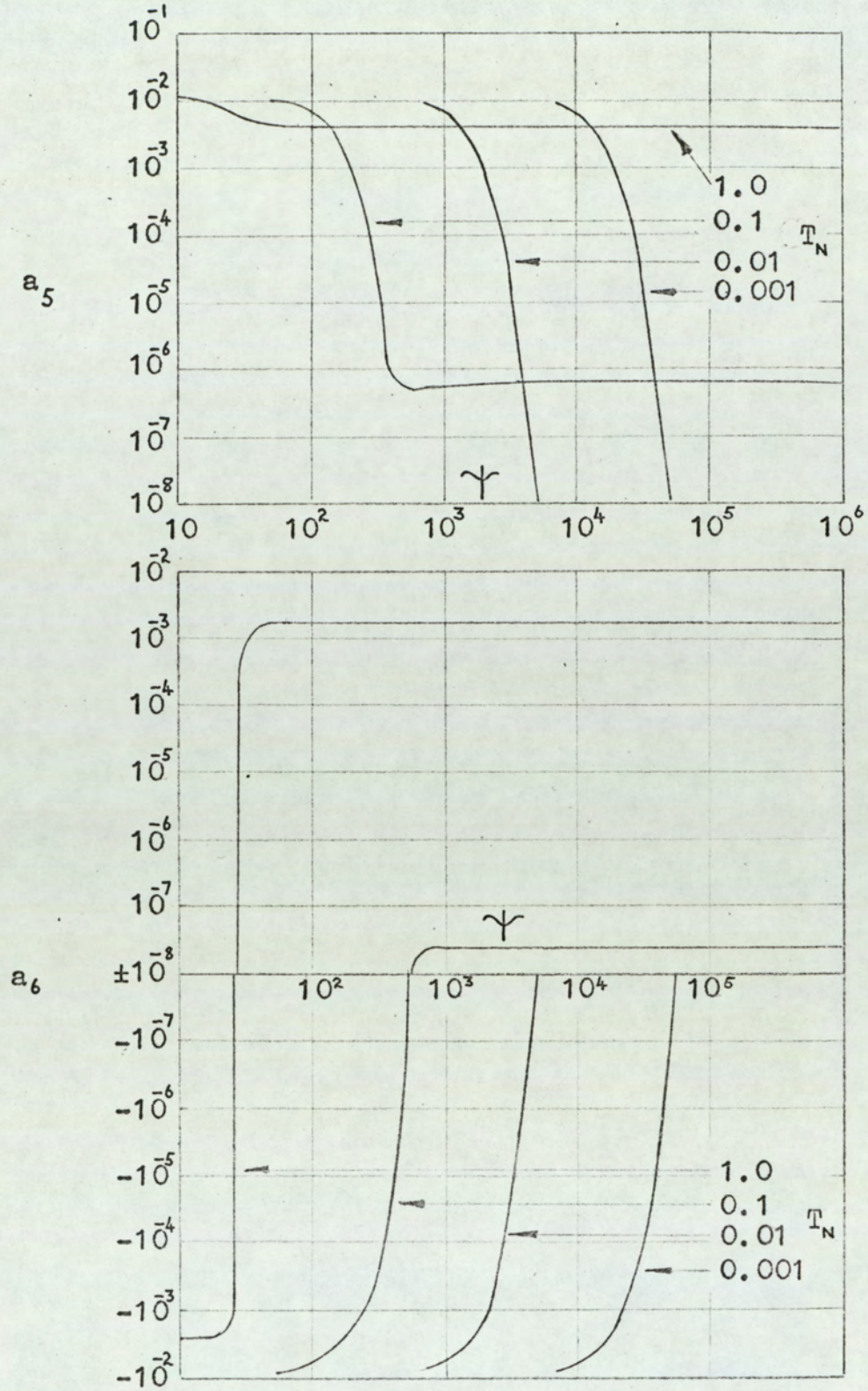

Fig.3.3.3(c). Coefficients a_5 and a_6 for single-edge modulation system with bandwidth-limited integrator amplifier.

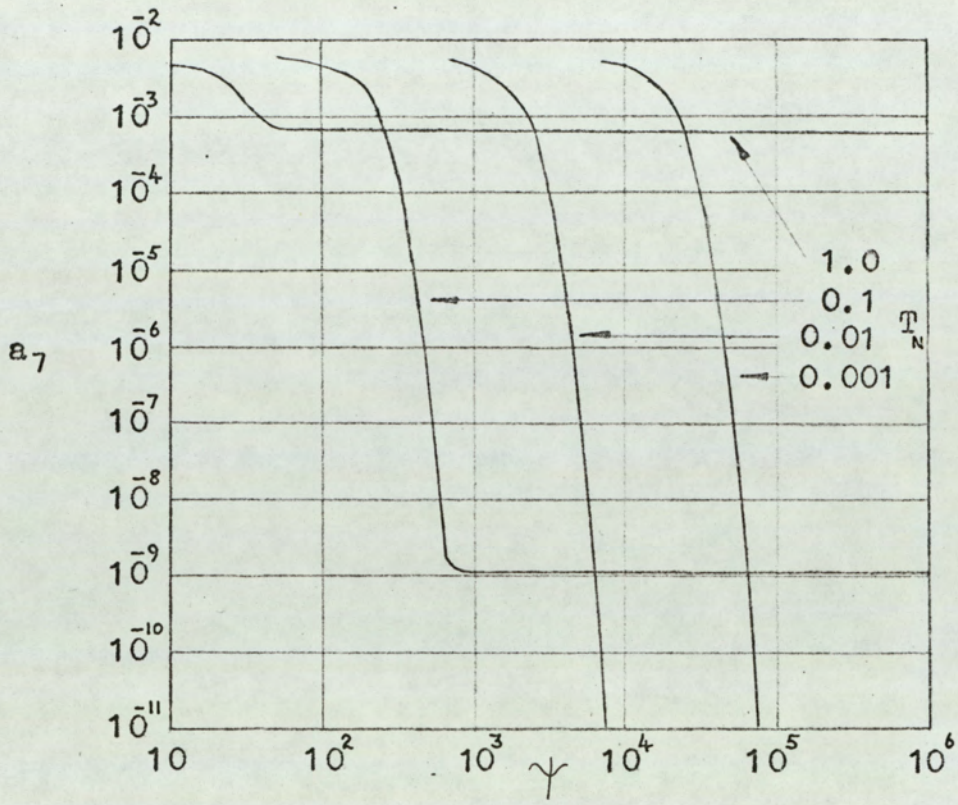

Fig.3.3.3(d). Coefficient a_7 for single-edge modulation system with bandwidth-limited integrator.

and the magnitude of the term Ψ is given by:

$$\Psi_{min} = 4(1+\alpha) \qquad (3.3.21(b))$$

Thus, for a particular value of α, as the term $\frac{T_a}{CR}$ increases, so the term Ψ decreases to the minimum value and then increases again.

Now, as discussed in section 3.1.1, demodulation of the pulse-length modulated wavetrain is equivalent to taking the average value of the waveform over one cycle of the repetition frequency. From fig. 3.3.2(b), the average value over one cycle is:

$$V_{av} = 1 - \frac{2t_1}{T_c} \qquad (3.3.22)$$

Substituting equation 3.3.17 in equation 3.3.22 gives the following expression for the amplitude of the demodulated wavetrain:

$$V_{av} = 1 - 2\sum_{n=0}^{\infty} a_n M^n \qquad (3.3.23)$$

In section 3.1.1 the static error E_1 in the system output was defined as:

$$E_1 = V_{av} + M \qquad (3.3.24)$$

$$E_1 = (1+M) - 2\sum_{n=0}^{\infty} a_n M^n \qquad (3.3.25)$$

Because of the number of variables involved, it is not practicable to present graphs of E_1 as a function of the system parameters and of all values of modulation index M. By definition, the value of E_1 is zero for the two conditions of full modulation (i.e. $M=\pm 1$).

Thus, a knowledge of the static error E_1 for $M = -0.5$, 0.0 and $+0.5$ will give a reasonable indication of the manner in which the error varies as a function of the modulation index. Figs. 3.3.4 (a) and (b) show the static error as a function of the normalised time constant T_N and the parameter γ for these three values of modulation index. From these diagrams it can be seen that, for particular values of γ, the error E_1 is zero. Unfortunately, the particular value of γ is a function of the modulation index; zero error cannot, therefore, be obtained for all values of M. It may be possible to choose the bandwidth in order to minimise the mean-square error, but this has not been attempted. That the static error E_1 is zero for particular values of the system parameters may be seen by considering the normalised integrator output waveform for various values of the amplifier time constant, as shown in fig. 3.3.5. The dotted line in this figure represents the ideal sampling waveform, for which the system static error is zero for all values of modulation index M. Since the integrator waveform crosses this ideal waveform, there is a value of modulating input voltage, V_{in}, such that the level-detector output changes state at the point where the ideal and actual waveforms are coincident. Under these conditions the static error E_1 is zero.

For reasons discussed in section 2.1.1, the static error in the demodulated wavetrain may also be expressed as the difference between the actual output V_{av} and the component of V_{av} that is directly proportional to the modulation index M.

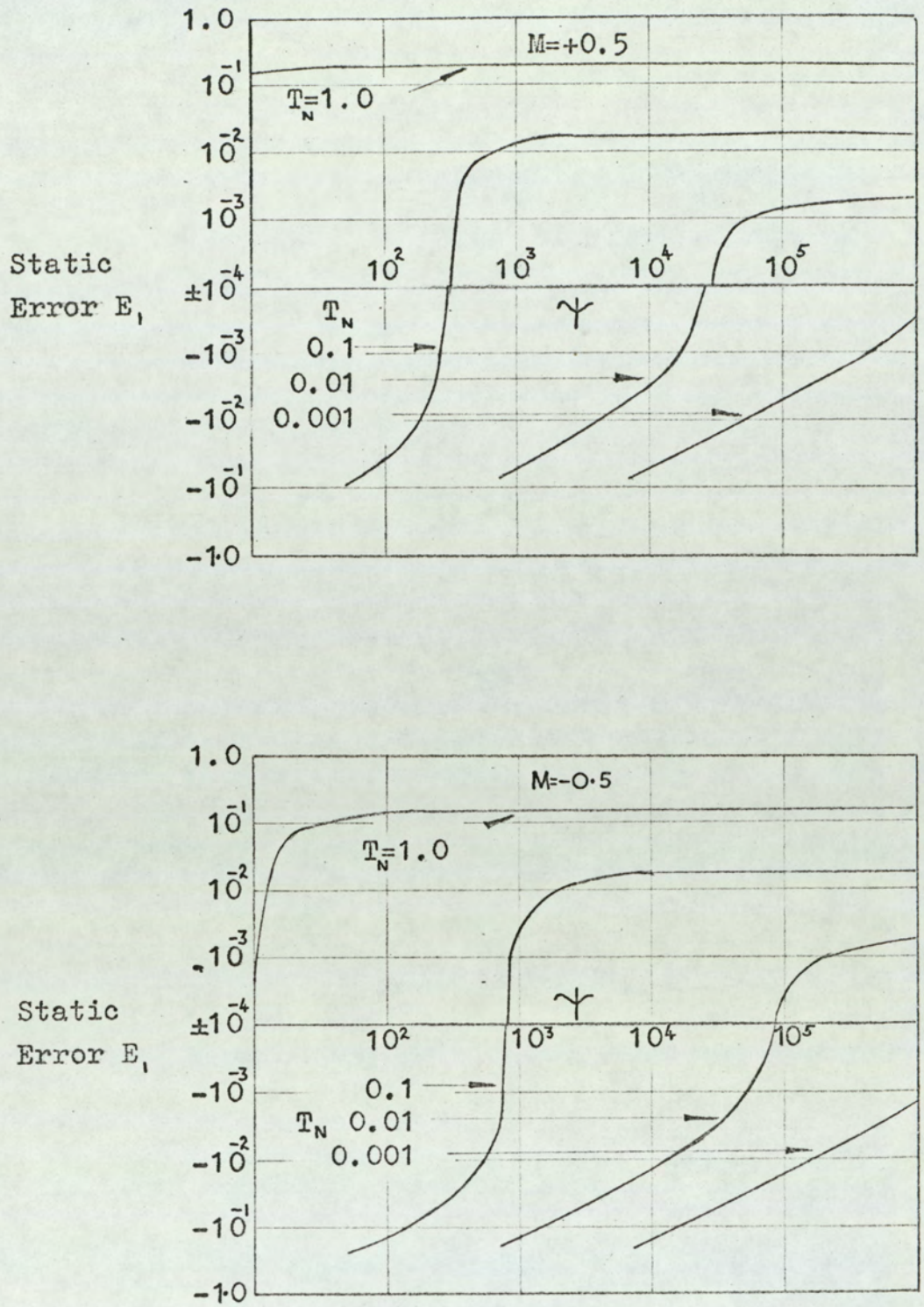

Fig.3.3.4(a). Static error E_1 for single-edge modulation system with bandwidth-limited integrator amplifier.

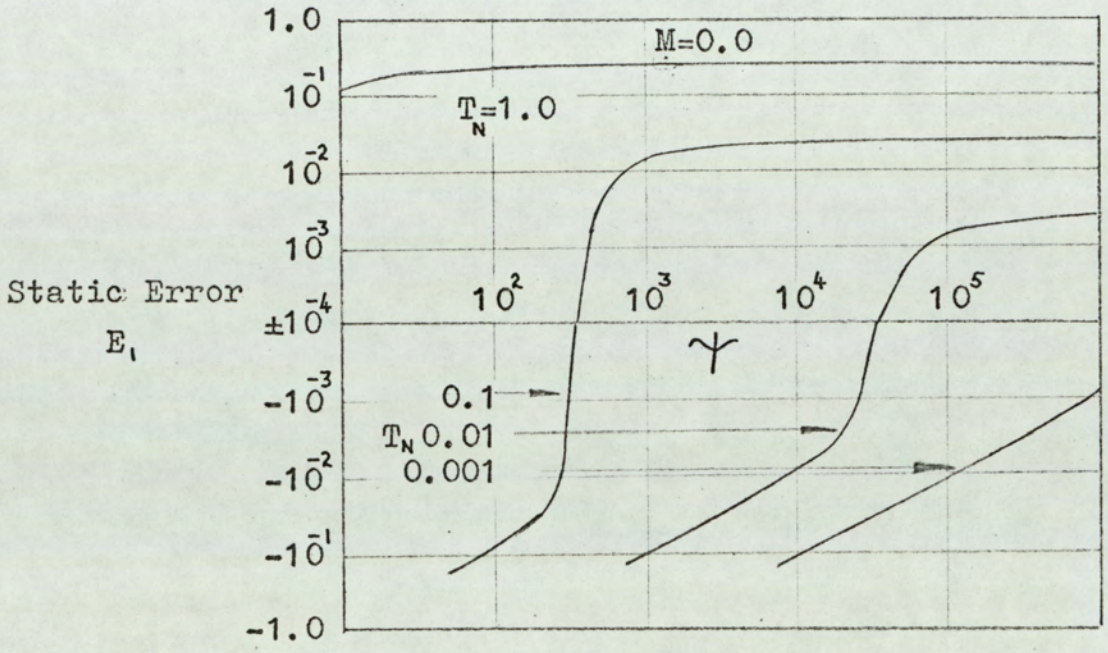

Fig. 3.3.4(b). Static error E_1 for single-edge modulation system with bandwidth-limited integrator amplifier.

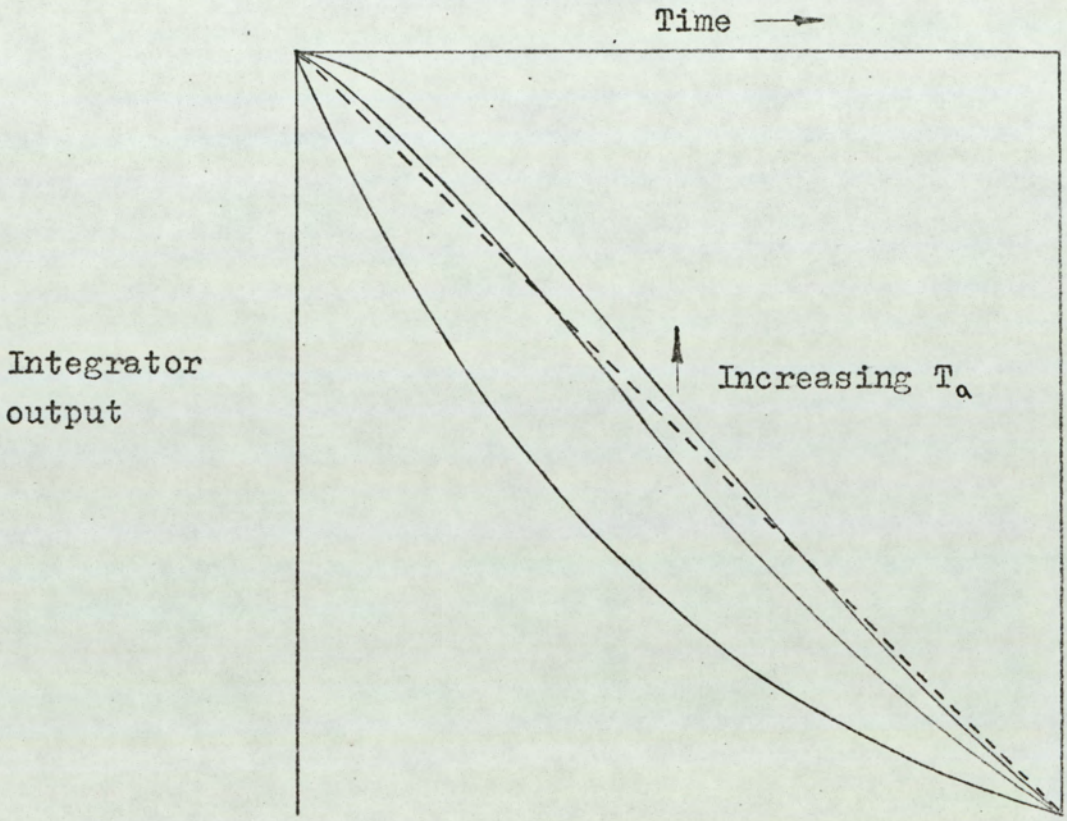

Fig.3.3.5. Integrator output waveform for single-edge modulation system with bandwidth-limited integrator amplifier.

Therefore, from equation 3.3.22:

$$E_2 = 1 - 2a_0 - 2\sum_{n=2}^{\infty} a_n . M^n \qquad (3.3.26)$$

As with the static error E_1, it is not practicable to present the error E_2 in graphical form for all values of the variables. From consideration of fig. 3.1.5 (section 3.1.1) for the static error E_2 of a single-edge pulse-length modulation system with finite integrator gain and infinite bandwidth, the values of modulation index which give the best indication of system performance are +1.0, 0.0 and -1.0. However, the analytical results for double-edge modulation (which are derived in section 3.3.2) are not valid for full modulation. When comparing the performance of the two systems it is convenient for the graphs of static error to be presented for the same value of modulation index. A value of $M = \pm 0.5$ ensures that the analytical results for the double-edge modulation system are valid over the required range of system parameters. Fig. 3.3.6 shows the static error E_2 for the single-edge modulation system for values of M of +0.5 and -0.5. The value of E_2 for $M = 0$ is, from equation 3.3.26:

$$E_2\Big|_{M=0} = 1 - 2a_0 \qquad (3.3.27)$$

Equation 3.3.27 is identical to equation 3.3.24 for E_1 with $M = 0$. It is not necessary to plot a graph of E_2 with $M=0$ since $E_1 / _{M=0}$ is already shown in fig. 3.3.4 (b). Fig. 3.3.6 shows that the static error E_2 decreases to zero as γ decreases. Further decrease of γ causes the static

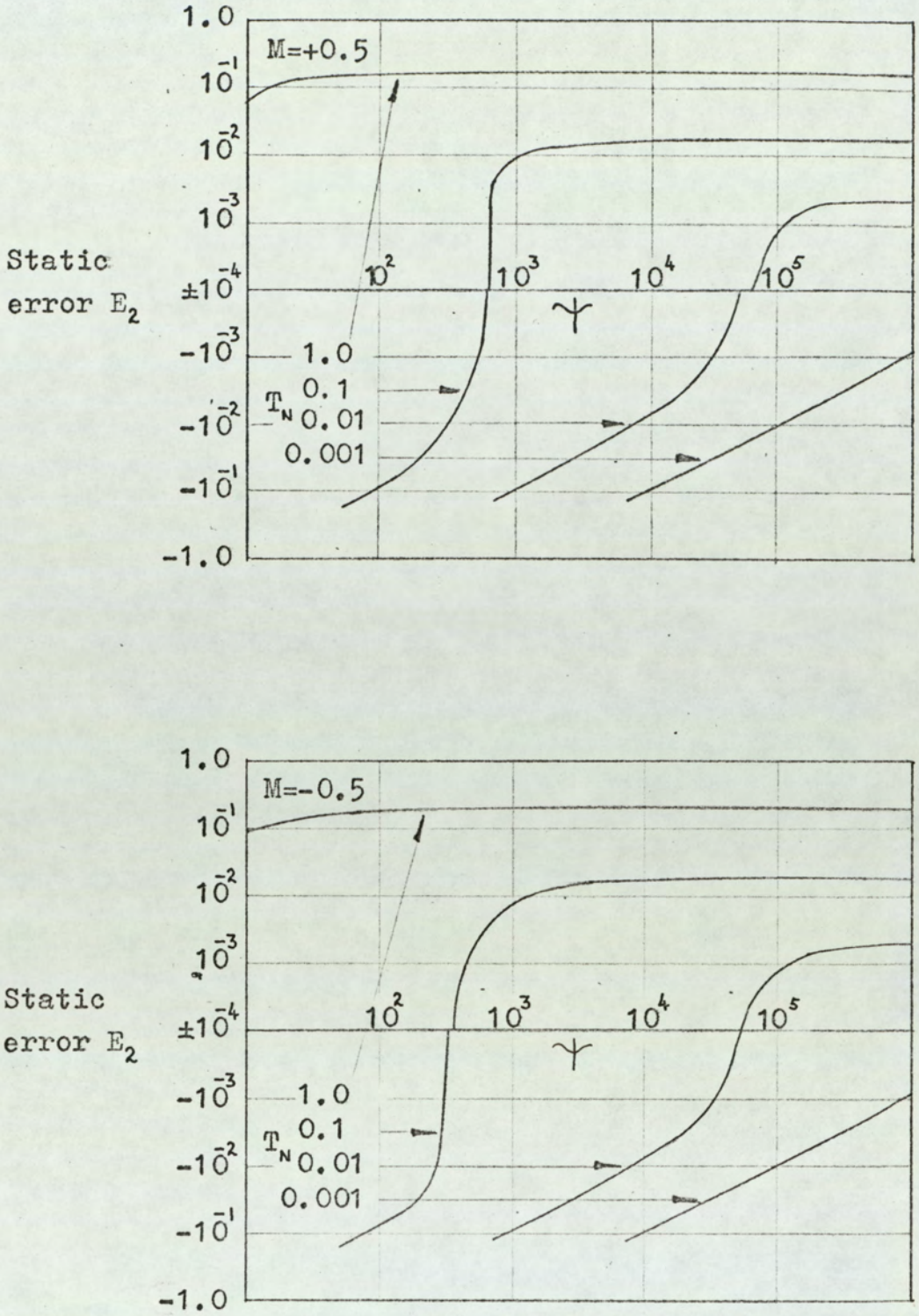

Fig.3.3.6. Static error E_2 for single-edge modulation system with bandwidth-limited integrator amplifier.

error to increase in the negative direction. As was discussed in relation to figs. 3.3.3 (a), (b), (c) and (d) (see equations 3.3.21 (a) and (b)), care must be taken in interpreting the factor Υ .

Since the specification for the accuracy of the threshold level of the level detector depends on the peak amplitude of the sampling waveform, it is of interest to examine the manner in which the peak output of the integrator varies as a function of the system parameters. The peak integrator output occurs at time $t = T_c$. Therefore, from equation 2.3.2:

$$\frac{\hat{v}_2(t)}{V_1} = -\alpha\left\{1 - \frac{1}{1-k_1/k_2}\exp\left(-k_1T_c\right) - \frac{1}{1-k_2/k_1}\exp\left(-k_2T_c\right)\right\} \qquad (3.3.28)$$

where the terms k_1 and k_2 are given by equations 3.3.2 and 3.3.3.

Fig. 3.3.7 shows $\frac{\hat{v}_2(t)}{V_1}$ plotted as a function of the system parameters. It will be noted that decreasing the amplifier bandwidth decreases the peak integrator output.

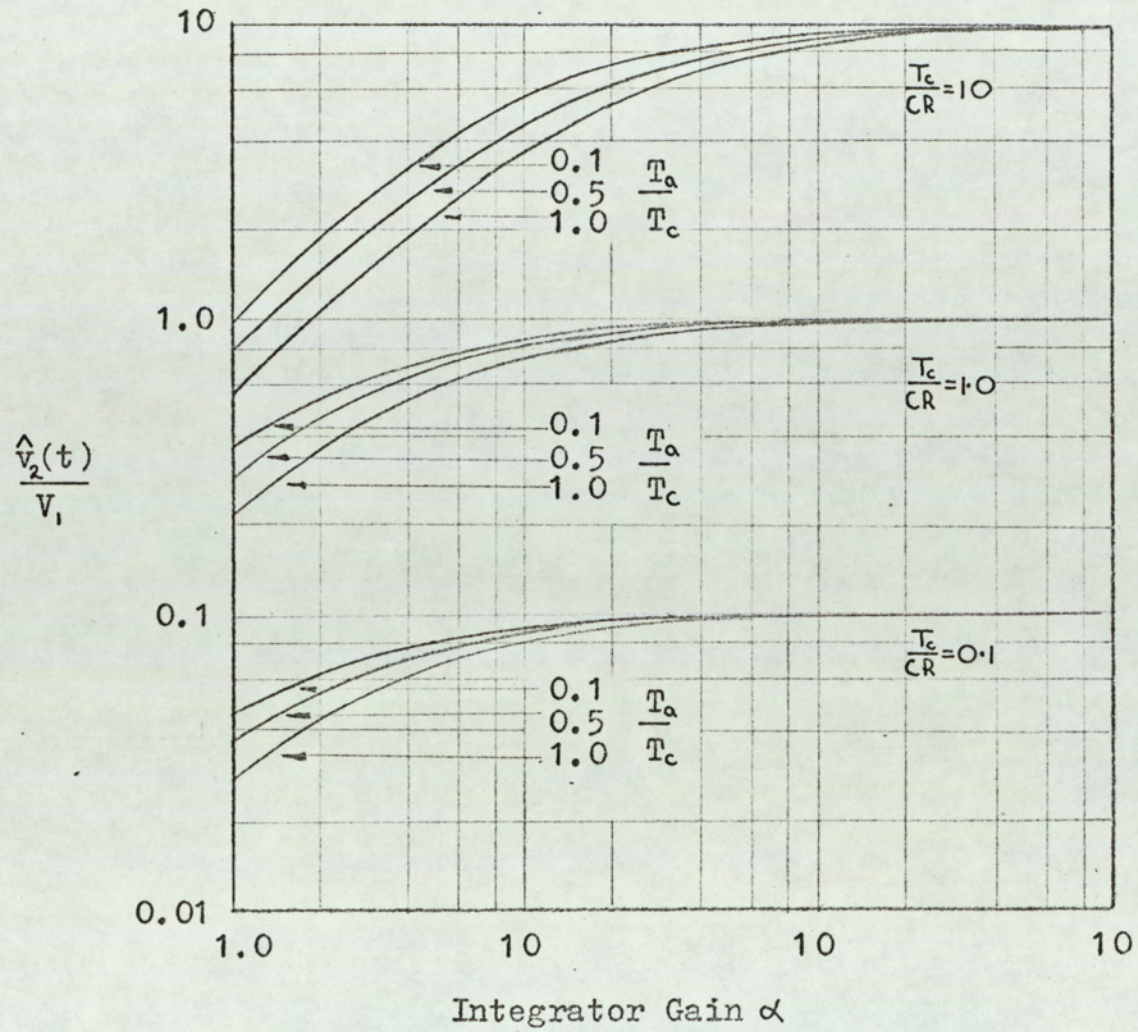

Fig.3.3.7. Peak integrator output for a single-edge modulation system with bandwidth-limited integrator amplifier.

3.3.2 Double-edge modulation

In order to investigate the performance of the double-edge modulation system shown in fig. 2.4.(a), when the operational integrator has a finite open-loop bandwidth, it is necessary to derive an expression for the output of the integrator in response to a square wavetrain input. A procedure was developed in section 3.1.2 for deriving the square-wavetrain response of a finite-gain integrator, having infinite open-loop bandwidth, from the step response. The step response of the integrator with finite amplifier bandwidth is given by equation 3.3.2. Since the procedure for obtaining the square wavetrain response from equation 3.3.2 is identical to that used in section 3.1.2, only the results will be quoted here:

$$V_2(t) = -\alpha V_1 \left\{ 1 - \frac{2\left(\frac{k_2}{k_2 - k_1}\right)}{1+\exp\left(\frac{-k_1 T_c}{2}\right)} \exp(-k_1 t) - \frac{2\left(\frac{k_1}{k_1 - k_2}\right)}{1+\exp\left(\frac{-k_2 T_c}{2}\right)} \exp(-k_2 t) \right\} \qquad 0 \leq t \leq \frac{T_c}{2} \qquad (3.3.29)$$

$$V_2(t) = -\alpha V_1 \left\{ -1 + \frac{2\left(\frac{k_2}{k_2 - k_1}\right)}{1+\exp\left(\frac{-k_1 T_c}{2}\right)} \exp\left[-k_1\left(t - \frac{T_c}{2}\right)\right] + \frac{2\left(\frac{k_1}{k_1 - k_2}\right)}{1+\exp\left(\frac{-k_2 T_c}{2}\right)} \exp\left[-k_2\left(t - \frac{T_c}{2}\right)\right] \right\} \qquad \frac{T_c}{2} \leq t \leq T_c \qquad (3.3.30)$$

where k_1 and k_2 are given by equation 3.3.3.

Fig. 3.3.8 shows the integrator output waveform for selected values of the system parameters. It will be noted that the peak output does not occur at time $t = 0$. However, the positive and negative values of the peak output are equal in magnitude.

In the block diagram of the system, fig. 2.4.(a), the integrator output voltage is added to the modulating input voltage V_{in}, and the sum is applied to the input of the level detector. The output of the level detector changes state whenever the sum of the

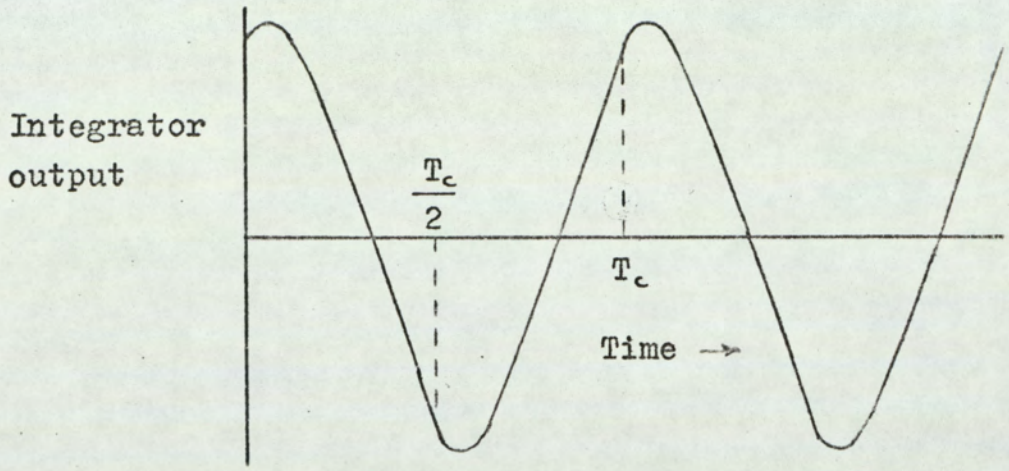

Fig.3.3.8. Output waveform for integrator with bandwidth-limited amplifier.

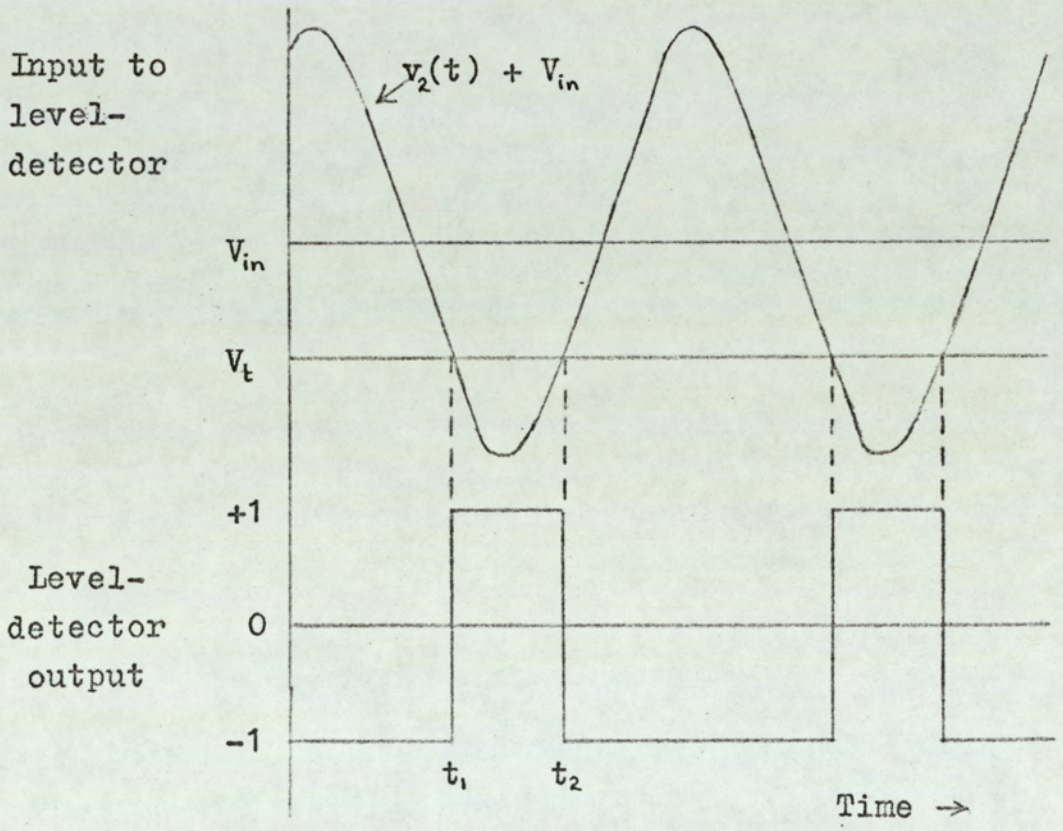

Fig.3.3.9. Waveforms for double-edge modulation system with bandwidth-limited integrator amplifier.

modulating input voltage and the integrator output voltage crosses the threshold voltage of the level detector, as shown in fig. 3.3.9. Thus, the switching points of the leading and trailing edges of the level detector output pulse, t_1 and t_2 respectively, are defined by:

$$v_2(t_1) + V_{in} = V_t \qquad \text{for} \quad 0 \leq t_1 \leq \frac{T_c}{2} \tag{3.3.31}$$

$$v_2(t_2) + V_{in} = V_t \qquad \text{for} \quad \frac{T_c}{2} \leq t_2 \leq T_c \tag{3.3.32}$$

where V_t is the level-detector threshold voltage.

It was shown in section 3.1.2 that, if the positive and negative values of the modulating input voltage required for full modulation are to be of equal amplitude and the peak positive and negative values of the integrator waveform are equal and opposite, the threshold level V_t must be set to zero. Under these conditions, the value of input $\hat{V}_{in+}$ for full modulation is equal to the peak positive value of the integrator. output $\hat{v}_2(t)$.

$$V_t = 0 \tag{3.3.33}$$

$$\hat{V}_{in+} = \hat{v}_2(t) \tag{3.3.34}$$

Substituting equations 3.3.33 and 3.3.34 into the expressions defining the switching points t_1 and t_2 (equations 3.3.31 and 3.3.32) gives:

$$\frac{v_2(t_1)}{\hat{v}_2(t)} = -M \tag{3.3.35}$$

$$\frac{v_2(t_2)}{\hat{v}_2(t)} = -M \tag{3.3.36}$$

where $M = \dfrac{V_{in}}{\hat{V}_{in+}}$, the modulation index.

The time $\hat{t}$ at which the peak value $\hat{v}_2(t)$ of the integrator output occurs may be obtained by differentiating equation 3.3.29 with respect to time and equating the differential to zero.

$$\frac{\exp(-k_1\hat{t})}{1+\exp\left(\frac{-k_1T_c}{2}\right)} = \frac{\exp(-k_2\hat{t})}{1+\exp\left(\frac{-k_2T_c}{2}\right)}$$

Therefore

$$\exp(-k_2\hat{t}) = \left[\frac{1+\exp\left(\frac{-k_1T_c}{2}\right)}{1+\exp\left(\frac{-k_2T_c}{2}\right)}\right]^{\frac{k_2}{k_1-k_2}} \qquad (3.3.37)$$

$$\exp(-k_1\hat{t}) = \left[\frac{1+\exp\left(\frac{-k_1T_c}{2}\right)}{1+\exp\left(\frac{-k_2T_c}{2}\right)}\right]^{\frac{k_1}{k_1-k_2}} \qquad (3.3.38)$$

Substituting equations 3.3.37 and 3.3.38 in equation 3.3.29 gives the following expressions for the peak positive output of the integrator.

$$\hat{v}_2(t) = -\alpha V_1\left\{1-2\left[1+\exp\left(\frac{-k_1T_c}{2}\right)\right]^{\frac{k_2}{k_1-k_2}}\left[1+\exp\left(\frac{-k_2T_c}{2}\right)\right]^{\frac{-k_1}{k_1-k_2}}\right\} \qquad (3.3.39)$$

From equations 3.3.29, 3.3.30, 3.3.35, 3.3.36 and 3.3.39, the positions of the leading and trailing edges of the level detector output pulse are defined by:

$$\left\{1-\frac{2\left(\frac{k_2}{k_2-k_1}\right)}{1+\exp\left(\frac{-k_1T_c}{2}\right)}\exp(-k_1t_1)-\frac{2\left(\frac{k_1}{k_1-k_2}\right)}{1+\exp\left(\frac{-k_2T_c}{2}\right)}\exp(-k_2t_1)\right\}$$

$$=-M\left\{1-2\left[1+\exp\left(\frac{-k_1T_c}{2}\right)\right]^{\frac{k_2}{k_1-k_2}}\left[1+\exp\left(\frac{-k_2T_c}{2}\right)\right]^{\frac{-k_1}{k_1-k_2}}\right\} \qquad (3.3.40)$$

$$\left\{-1+\frac{2\left(\frac{k_2}{k_2-k_1}\right)}{1+\exp\left(\frac{-k_1T_c}{2}\right)}\exp\left[-k_1\left(t_2-\frac{T_c}{2}\right)\right]+\frac{2\left(\frac{k_1}{k_1-k_2}\right)}{1+\exp\left(\frac{-k_2T_c}{2}\right)}\exp\left[-k_2\left(t_2-\frac{T_c}{2}\right)\right]\right\}$$

$$=-M\left\{1-2\left[1+\exp\left(\frac{-k_1T_c}{2}\right)\right]^{\frac{k_2}{k_1-k_2}}\left[1+\exp\left(\frac{-k_2T_c}{2}\right)\right]^{\frac{-k_1}{k_1-k_2}}\right\} \qquad (3.3.41)$$

Unfortunately, it is not possible to obtain direct solutions to t_1 and t_2 from equations 3.3.40 and 3.3.41; numerical methods or series methods must therefore be used. From the point of view of the static analysis, numerical solution of equations 3.3.40 and 3.3.41, for a range of values of the parameters, would be adequate. However, the results of the static analysis are to be used for the spectrum analysis, and a list of values of t_1 and t_2 would be of little use. For this reason, the switching of the pulse leading and trailing edges will be expressed as power series in terms of the modulation index M.

$$\frac{t_1}{T_c}=\sum_{n=0}^{\infty}a_nM^n \qquad (3.3.42)$$

$$\frac{t_2}{T_c}-\frac{1}{2}=\sum_{n=0}^{\infty}b_nM^n \qquad (3.3.43)$$

The expressions for the coefficients a_n and b_n are derived in Appendix 3, and only the results will be quoted here. The reason for obtaining a power series for $(\frac{t_2}{T_c}-\frac{1}{2})$ instead of $\frac{t_2}{T_c}$ is apparent in the appendix.

$$a_0 = \frac{\overset{\circ}{t}_1}{T_c} \qquad (3.3.44(a))$$

$$a_1 = \frac{1}{T_N}\left[\frac{-D}{2}\left(\frac{1}{A_2}-\frac{1}{A_1}\right)\right]\left[\frac{1}{F_0}\right] \qquad (3.3.44(b))$$

$$a_2 = \frac{1}{T_N 2!}\left[\frac{-D}{2}\left(\frac{1}{A_2}-\frac{1}{A_1}\right)\right]^2\left[\frac{F_1}{F_0^3}\right] \qquad (3.3.44(c))$$

$$a_3 = \frac{1}{T_N 3!}\left[\frac{-D}{2}\left(\frac{1}{A_2}-\frac{1}{A_1}\right)\right]^3\left[\frac{3F_1^2 - F_0F_2}{F_0^5}\right] \qquad (3.3.44(d))$$

$$a_4 = \frac{1}{T_N 4!}\left[\frac{-D}{2}\left(\frac{1}{A_2}-\frac{1}{A_1}\right)\right]^4\left[\frac{-10F_0F_1F_2 + F_0^2F_3 + 15F_1^3}{F_0^7}\right] \qquad (3.3.44(e))$$

$$a_5 = \frac{1}{T_N 5!}\left[\frac{-D}{2}\left(\frac{1}{A_2}-\frac{1}{A_1}\right)\right]^5\left[\frac{15F_0^2F_1F_3 + 10F_0^2F_2^2 + 105F_1^4 - F_0^3F_4 - 105F_0F_1^2F_3}{F_0^9}\right] \qquad (3.3.44(f))$$

$$a_6 = \frac{1}{T_N 6!}\left[\frac{-D}{2}\left(\frac{1}{A_2}-\frac{1}{A_1}\right)\right]^6\left[\frac{21F_0^3F_1F_4 + 35F_0^3F_2F_3 + 1260F_0F_1^3F_2 - F_0^4F_5 - 280F_0^2F_1F_2^2 - 945F_1^5 - 210F_0^2F_1^2F_3}{F_0^{11}}\right] \qquad (3.3.44(g))$$

$$a_7 = \frac{1}{T_N 7!}\left[\frac{-D}{2}\left(\frac{1}{A_2}-\frac{1}{A_1}\right)\right]^7\left[\frac{28F_0^4F_1F_5 + 56F_0^4F_2F_4 + 35F_0^4F_3^2 + 3150F_0^2F_1^3F_3 + 6300F_0^2F_1^2F_2^2 + 10395F_1^6 - F_0^5F_6 - 378F_0^3F_1^2F_4 - 1260F_0^3F_1F_2F_3 - 280F_0^3F_2^3 - 17325F_0F_1^4F_2}{F_0^{13}}\right] \qquad (3.3.44(h))$$

where: $$T_N = \frac{T_c}{(1+\alpha)CR}\left[\frac{1}{1+\frac{T_a}{(1+\alpha)CR}}\right] \qquad (3.3.45(a))$$

$$A_2 = \left\{1 + \frac{2.1}{2!}\left(\frac{1}{\gamma}\right) + \frac{2^2.1.3}{3!}\left(\frac{1}{\gamma}\right)^2 + \frac{2^3.1.3.5}{4!}\left(\frac{1}{\gamma}\right)^3 + \text{-----}\right\} \qquad (3.3.45(b))$$

$$\gamma = \frac{CR}{T_a}\left[\frac{T_a}{CR} + 1 + \alpha\right]^2 \qquad (3.3.45(c))$$

$$A_1 = \gamma - A_2 \qquad (3.3.45(d))$$

$$F_n = \frac{A_2^n \exp\left(-A_2 T_N \frac{\mathring{t}_1}{T_c}\right)}{1+\exp\left(\frac{-A_2 T_N}{2}\right)} - \frac{A_1^n \exp\left(-A_1 T_N \frac{\mathring{t}_1}{T_c}\right)}{1+\exp\left(\frac{-A_1 T_N}{2}\right)} \qquad (3.3.45(e))$$

$$D = 1 - 2\left[1+\exp\left(\frac{-A_1 T_N}{2}\right)\right]^{\frac{A_2}{A_1-A_2}}\left[1+\exp\left(\frac{-A_2 T_N}{2}\right)\right]^{\frac{-A_1}{A_1-A_2}} \qquad (3.3.45(f))$$

$\mathring{t}_1$ is the unmodulated position of the leading-edge of the pulse, (i.e. $\mathring{t}_1 = t_1/_{M=0}$) and is given by the numerical solution of the following expression:

$$\frac{2\left(\frac{A_2}{A_2-A_1}\right)}{1+\exp\left(\frac{-A_1 T_N}{2}\right)}\exp\left(-A_1 T_N \frac{\mathring{t}_1}{T_c}\right) + \frac{2\left(\frac{A_1}{A_1-A_2}\right)}{1+\exp\left(\frac{-A_2 T_N}{2}\right)}\exp\left(-A_2 T_N \frac{\mathring{t}_1}{T_c}\right) = 1 \qquad (3.3.45(g))$$

$$b_n = (-1)^n a_n \qquad (3.3.46)$$

The numerical methods used in evaluating the coefficients a_n and b_n are described in Appendix 3. Figs. 3.3.10(a), (b), (c) and (d) show

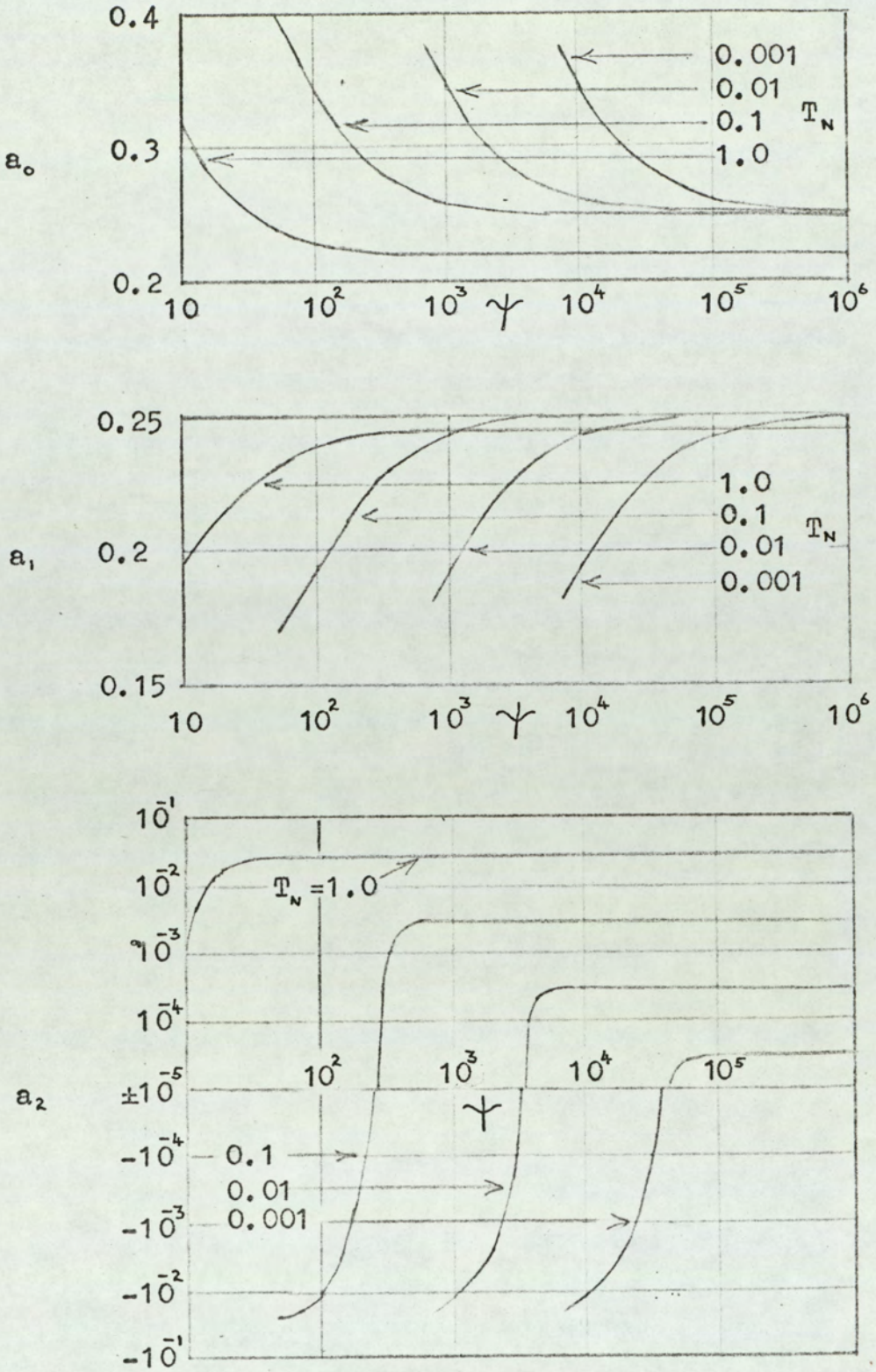

Fig.3.3.10(a). Coefficients a_o, a_1 and a_2 for double-edge modulation system with bandwidth-limited integrator amplifier.

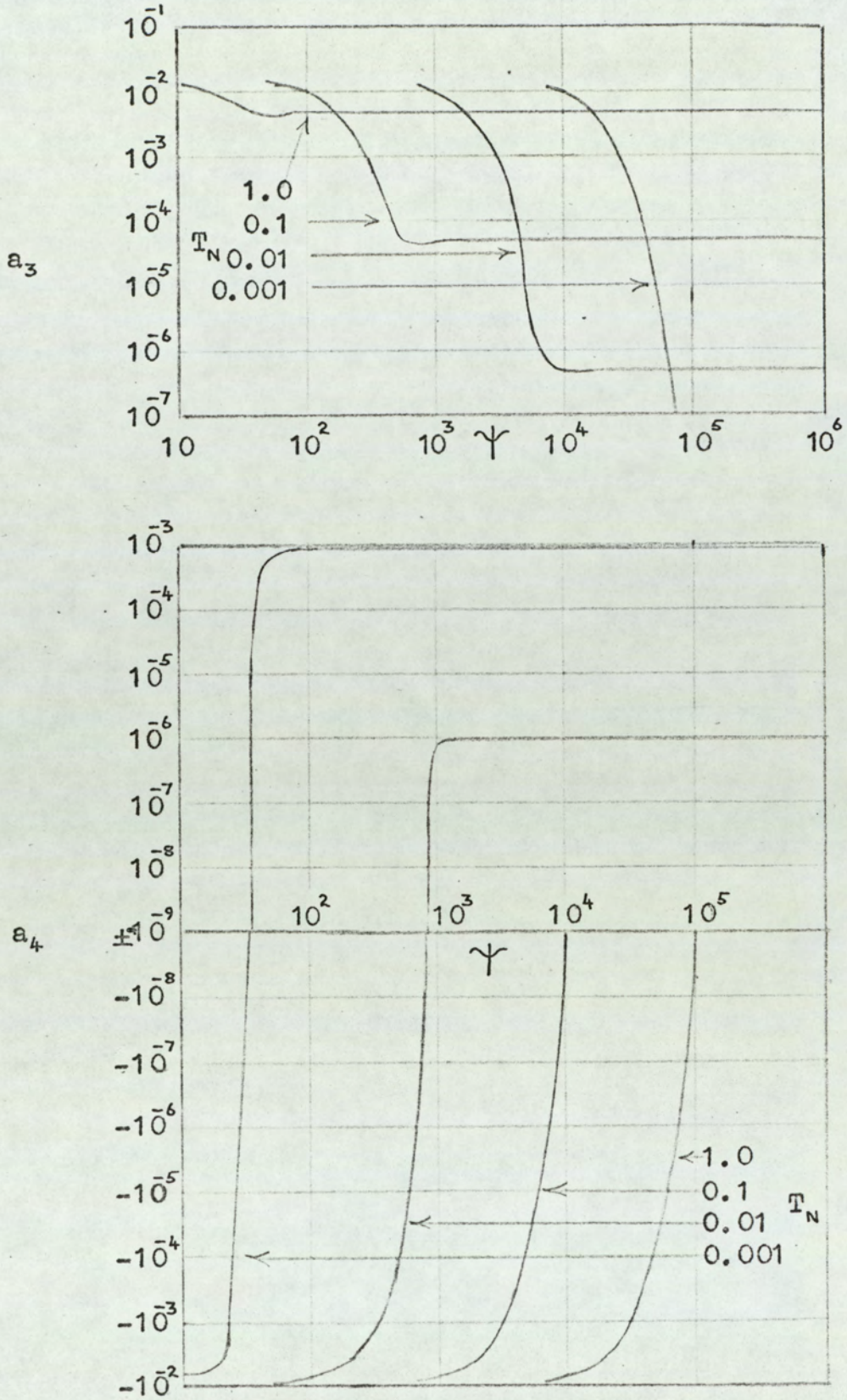

Fig.3.3.10(b). Coefficients a_3 and a_4 for double-edge modulation system with bandwidth-limited integrator amplifier.

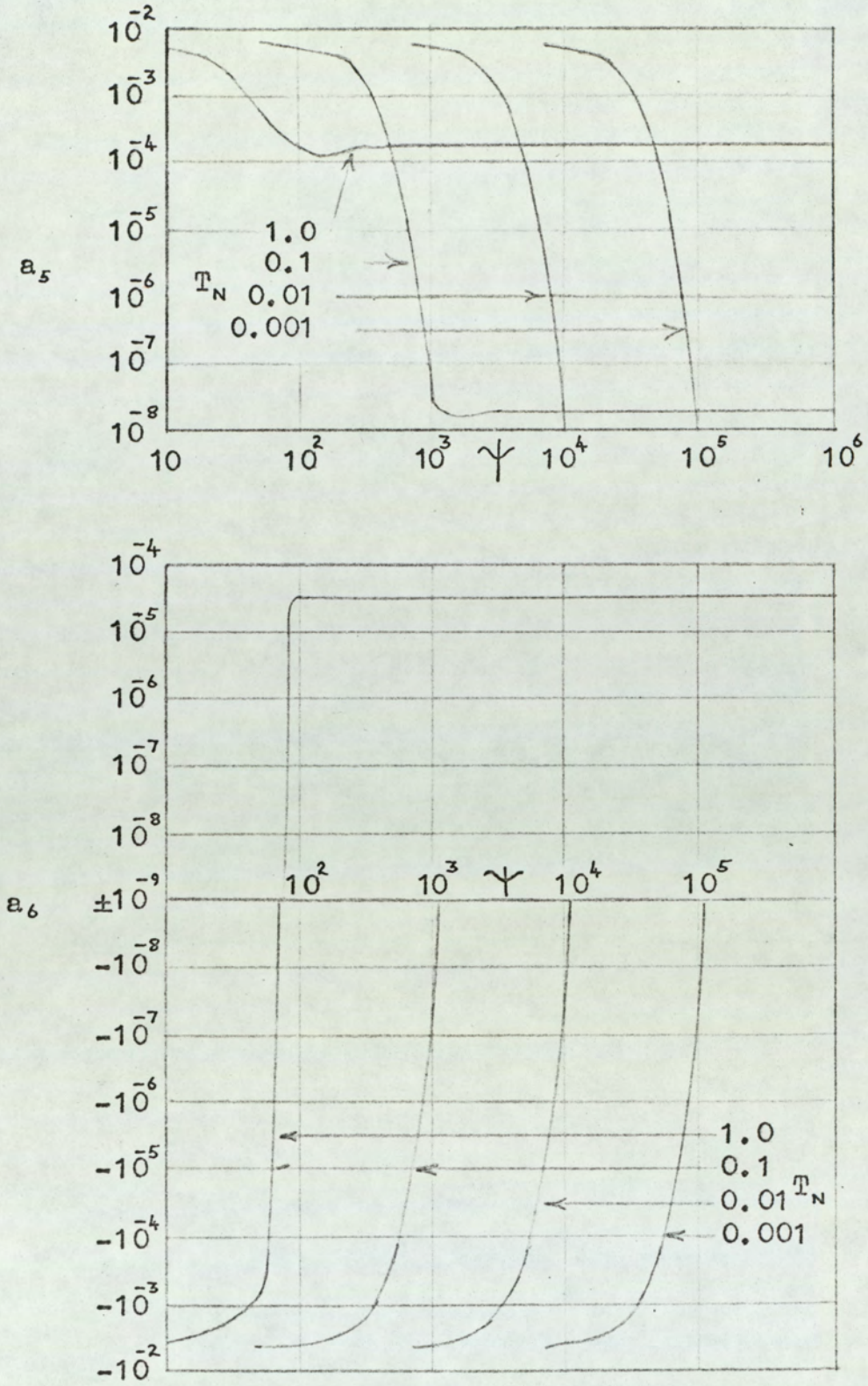

Fig.3.3.10(c). Coefficients a_5 and a_6 for double-edge modulation system with bandwidth-limited integrator amplifier.

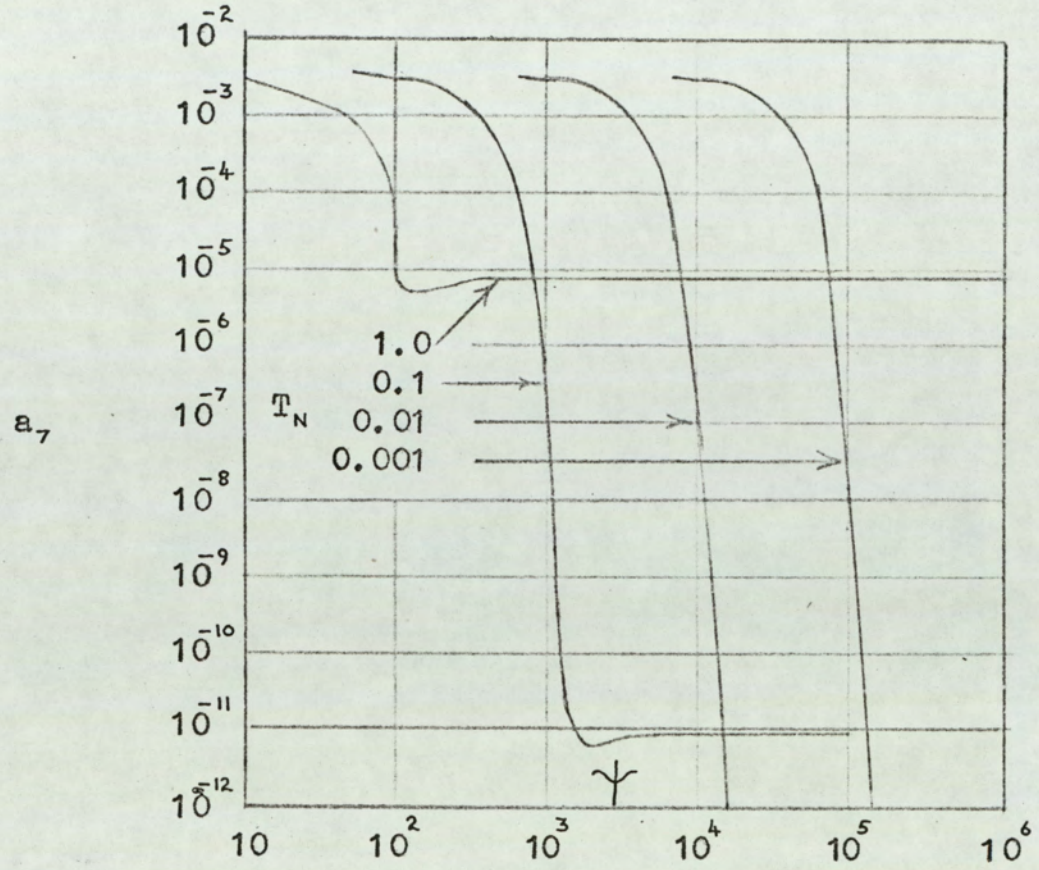

Fig.3.3.10(d). Coefficient a_7 for double-edge modulation system with bandwidth-limited integrator amplifier.

the coefficients a_o to a_7 plotted as functions of the normalised time constant T_N and the parameter Υ . The graphs of the coefficients have the same general form as those for single-edge modulation but they are numerically smaller. The value of the coefficients change rapidly when particular values of Υ are exceeded, for the reasons discussed in section 3.3.1 for single-edge modulation. Care must be taken in the interpretation of figs. 3.3.10 (a), (b), (c) and (d), as was discussed in relation to single-edge modulation (See equations 3.3.21(a) and (b)).

Demodulation of the pulse-length modulated wavetrain at the output of the level detector is equivalent to taking the average value of the waveform over one cycle of the repetition frequency. Therefore, from fig. 3.3.9, the amplitude of the demodulated wavetrain is:

$$V_{av} = 2\left(\frac{t_2}{T_c} - \frac{1}{2} - \frac{t_1}{T_c}\right) \qquad (3.3.47)$$

Substituting equations 3.3.42 and 3.3.43 in the above expression gives:

$$V_{av} = 2\sum_{n=0}^{\infty}(b_n - a_n)M^n \qquad (3.3.48)$$

But it has been shown that $b_n = (-1)^n a_n$

$$\therefore \quad V_{av} = -4\sum_{n=1}^{\infty} a_{2n-1} . M^{2n-1} \qquad (3.3.49)$$

Equation 3.3.49 shows that the amplitude of the demodulated wavetrain is zero when the modulation index is zero. Also, since only odd powers of M occur in the expression for V_{av}, the system transfer function will be symmetrical about the origin.

It has been implicitly assumed that the preceding analysis is valid for all values of modulation index. That this assumption is not valid may be seen from fig. 3.3.9. As the modulating input voltage increases in the positive direction, so the position of the leading edge tends towards $\frac{T_c}{2}$, and eventually the condition is reached where $t_1 = \frac{T_c}{2}$. The analytical expressions that have been developed are only valid for $t_1 < \frac{T_c}{2}$, since it is assumed that t_1 is determined by the integrator waveform for the period 0 to $\frac{T_c}{2}$ (i.e. equation 3.3.29). When t_1 is greater than $\frac{T_c}{2}$, then both t_1 and t_2 are governed by the integrator waveform for the period $\frac{T_c}{2}$ to T_c (i.e. equation 3.3.30). Thus, the analytical expressions will give an incorrect result when the modulating input voltage is such that t_1 is greater than $\frac{T_c}{2}$. This effect is illustrated by fig. 3.3.11. Since the integrator output waveform is symmetrical, a similar effect exists when the negative input voltage is such that t_2 is greater than T_c. From fig. 3.3.9, t_1 becomes equal to $\frac{T_c}{2}$ when the positive input voltage is equal and opposite to the amplitude of the integrator output waveform at time $t = \frac{T_c}{2}$. Therefore the maximum input voltage $V_{in}(max)$, for which the theory is valid, may be obtained by setting $t = \frac{T_c}{2}$ in equation 3.3.29.

$$V_{in}(max) = -V_2\left(\frac{T_c}{2}\right) = V_2(0)$$

$$= -\alpha V_1 \left\{ 1 - \frac{2\left(\frac{k_2}{k_2 - k_1}\right)}{1 + \exp\left(\frac{-k_1 T_c}{2}\right)} - \frac{2\left(\frac{k_1}{k_1 - k_2}\right)}{1 + \exp\left(\frac{-k_2 T_c}{2}\right)} \right\} \qquad (3.3.50)$$

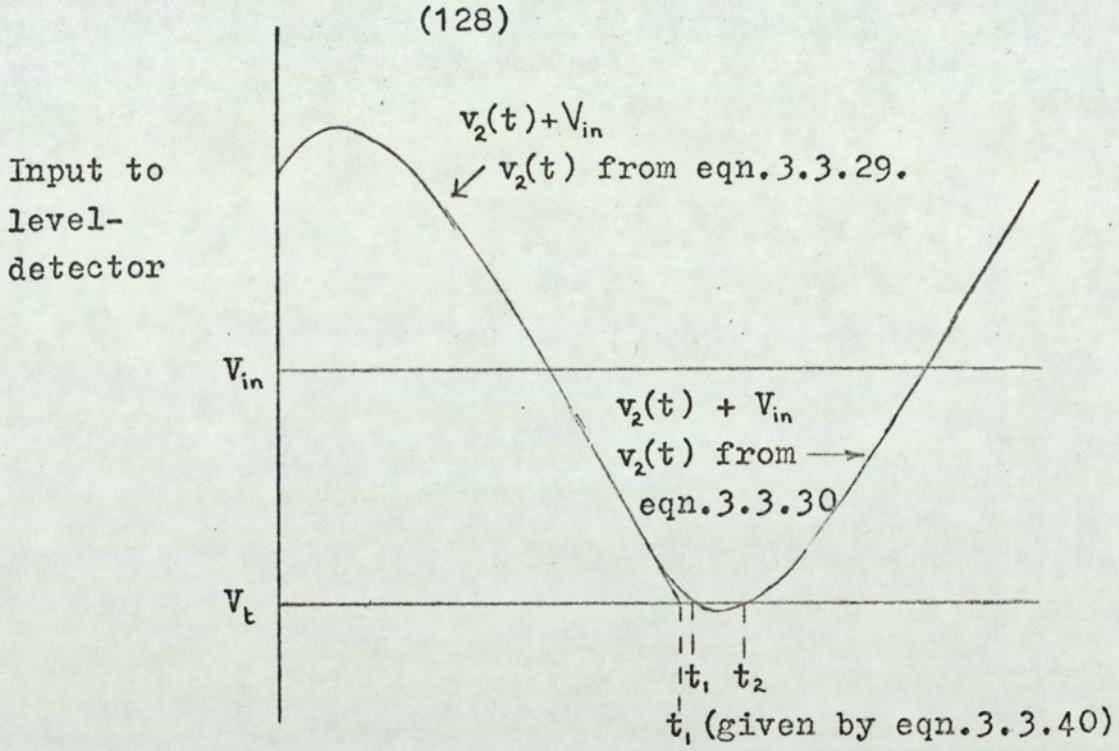

Fig.3.3.11. Level-detector input waveform.

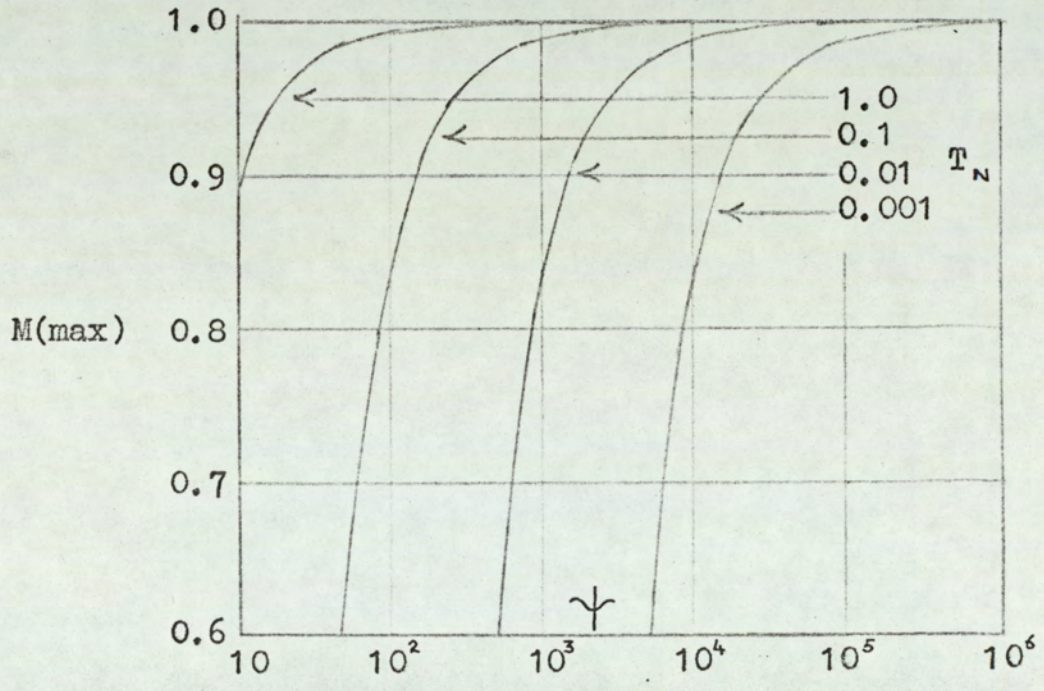

Fig.3.3.12. Maximum modulation index for which the analytical expressions are valid.

This value of maximum input voltage may be expressed as an equivalent modulation index, M(max).

$$M(max) = \frac{V_{in}(max)}{\hat{V}_{in+}} \qquad (3.3.51)$$

Therefore, from equations 3.3.34 and 3.3.39

$$M(max) = \frac{1 - \frac{2\left(\frac{k_2}{k_2 - k_1}\right)}{1+\exp\left(\frac{-k_1 T_c}{2}\right)} - \frac{2\left(\frac{k_1}{k_1 - k_2}\right)}{1+\exp\left(\frac{-k_2 T_c}{2}\right)}}{1-2\left[1+\exp\left(\frac{-k_1 T_c}{2}\right)\right]^{\frac{k_2}{k_1 - k_2}}\left[1+\exp\left(\frac{-k_2 T_c}{2}\right)\right]^{\frac{-k_1}{k_1 - k_2}}} \qquad (3.3.52)$$

M(max) may be expressed as a function of the two parameters T_N and Υ by substituting equations A3.6, A3.7, A3.14(a), (b) and (c) (from Appendix 3) in equation 3.3.52.

$$M(max) = \frac{1 - \frac{2\left(\frac{A_2}{A_2 - A_1}\right)}{1+\exp\left(\frac{-A_1 T_N}{2}\right)} - \frac{2\left(\frac{A_1}{A_1 - A_2}\right)}{1+\exp\left(\frac{-A_2 T_N}{2}\right)}}{1-2\left[1+\exp\left(\frac{-A_1 T_N}{2}\right)\right]^{\frac{A_2}{A_1 - A_2}}\left[1+\exp\left(\frac{-A_2 T_N}{2}\right)\right]^{\frac{-A_1}{A_1 - A_2}}} \qquad (3.3.53)$$

where T_N, A_2 and A_1 are given by equations 2.3.45(a), (b) and (d) respectively. Fig. 3.3.12 shows M(max) plotted as a function of the parameters T_N and Υ.

A further point arises from the discussion of the maximum input level for which the theory is valid. It was shown that when the positive input exceeds $V_{in}(max)$ then both t_1 and t_2 are governed by the integrator waveform for the period $\frac{T_c}{2}$ to T_c. Now, the

power series representation of t_2 should yield two values for t_2 under these conditions, the smaller of these values being the effective value of t_1. It is obviously not possible for the power series to give two values of t_2 for a given value of modulation index. One attempt to overcome this problem is to represent the integrator waveform as a Fourier series which may be time shifted so that the peak value of the waveform occurs at the time origin. However, it is not then possible to use Maclaurin's theorem to obtain a power series for the switching points, since a discontinuity exists in the first differential of the integrator waveform and further differentials would be meaningless.

In section 3.1.1 the static error E_1 in the amplitude V_{av} of the demodulated wavetrain was defined as:

$$E_1 = V_{av} + M \qquad (3.3.54)$$

Therefore, from equation 3.3.49

$$E_1 = M - 4 \sum_{n=1}^{\infty} a_{2n-1} M^{2n-1} \qquad (3.3.55)$$

It is not practicable to present graphs of E_1 as a function of the system parameters for all values of modulation index, and graphs will be drawn for the single value of $M = 0.5$. The system transfer function is symmetrical about the origin, so the error for $M = -0.5$ will be equal and opposite to the error for $M = 0.5$. The error E_1 for $M = 0$ is zero, since no constant term exists in the expression for V_{av}. By definition, the error E_1 for full modulation is zero; thus a knowledge of the error for $M=0.5$ will give a reasonable indication of the manner in which the error depends on the system parameters at other values of modulation index. Fig. 3.3.13 shows the static error E_1, as a function of the normalised time constant

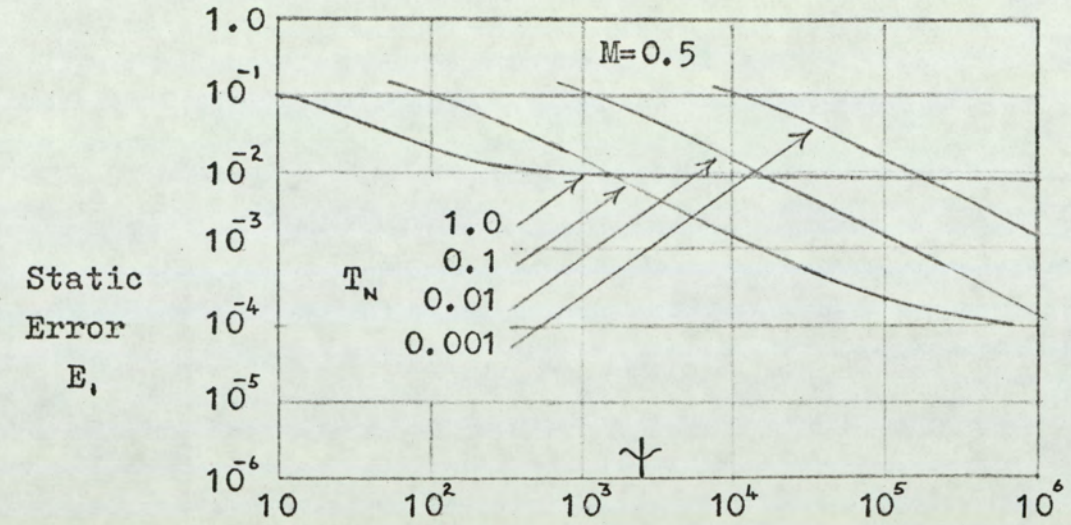

Fig.3.3.13. Static error E_1 for double-edge modulation system with bandwidth-limited integrator amplifier.

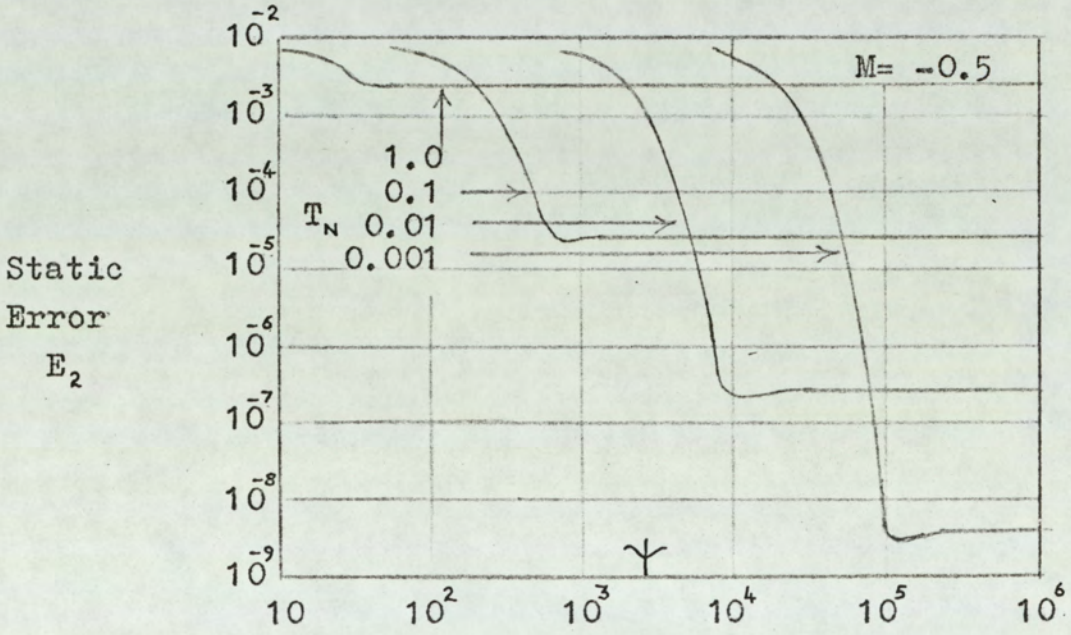

Fig.3.3.14. Static error E_2 for double-edge modulation system with bandwidth-limited integrator amplifier.

T_N and the factor Ψ, for M=0.5. It will be noted that the static error increases as the factor Ψ is decreased.

For reasons discussed in section 3.1.2, the error in the amplitude of the demodulated wavetrain may also be expressed as the difference between the amplitude of V_{av} and the component which is directly proportional to the modulation index M. Therefore, from equation 3.3.49:

$$E_2 = -4 \sum_{n=2}^{\infty} a_{2n-1} . M^{2n-1} \qquad (3.3.56)$$

Since it is not practicable to plot graphs of error E_2 against system parameters for all values of modulation index it is necessary to select a particular value of M. Now, for a double-edge pulse-length modulation system with finite integrator gain and infinite amplifier bandwidth, the error E_2 is a maximum for full modulation (See fig. 3.1.11, section 3.1.2). Thus graphs of error E_2 for the system utilising a bandwidth limited amplifier would be most useful if plotted for M=1. Unfortunately, the analytical expressions developed for E_2 are not valid for full modulation; a lower value of M must therefore be chosen. Fig. 3.3.14 shows the error E_2 as a function of the normalised time constant T_N and the parameter Ψ for a modulation index of M = -0.5. Due to the symmetry of the transfer function about the origin, the error for M = +0.5 will be equal and opposite to the error for M = -0.5. The error for M=0 is zero, since no constant term exists in the expression for the amplitude V_{av} of the demodulated wavetrain. Fig. 3.3.14 shows that the system static error E_2 increases with decreasing values of Ψ.

As was discussed in section 3.1.2, an important parameter in the design of a pulse length modulation system is the peak amplitude

$\hat{v}_2(t)$ of the sampling waveform, since it determines the accuracy required of the level-detector threshold voltage. Fig. 3.3.15 shows the ratio $\frac{\hat{v}_2(t)}{V_1}$, from equation 3.3.39, plotted as a function of the system parameters.

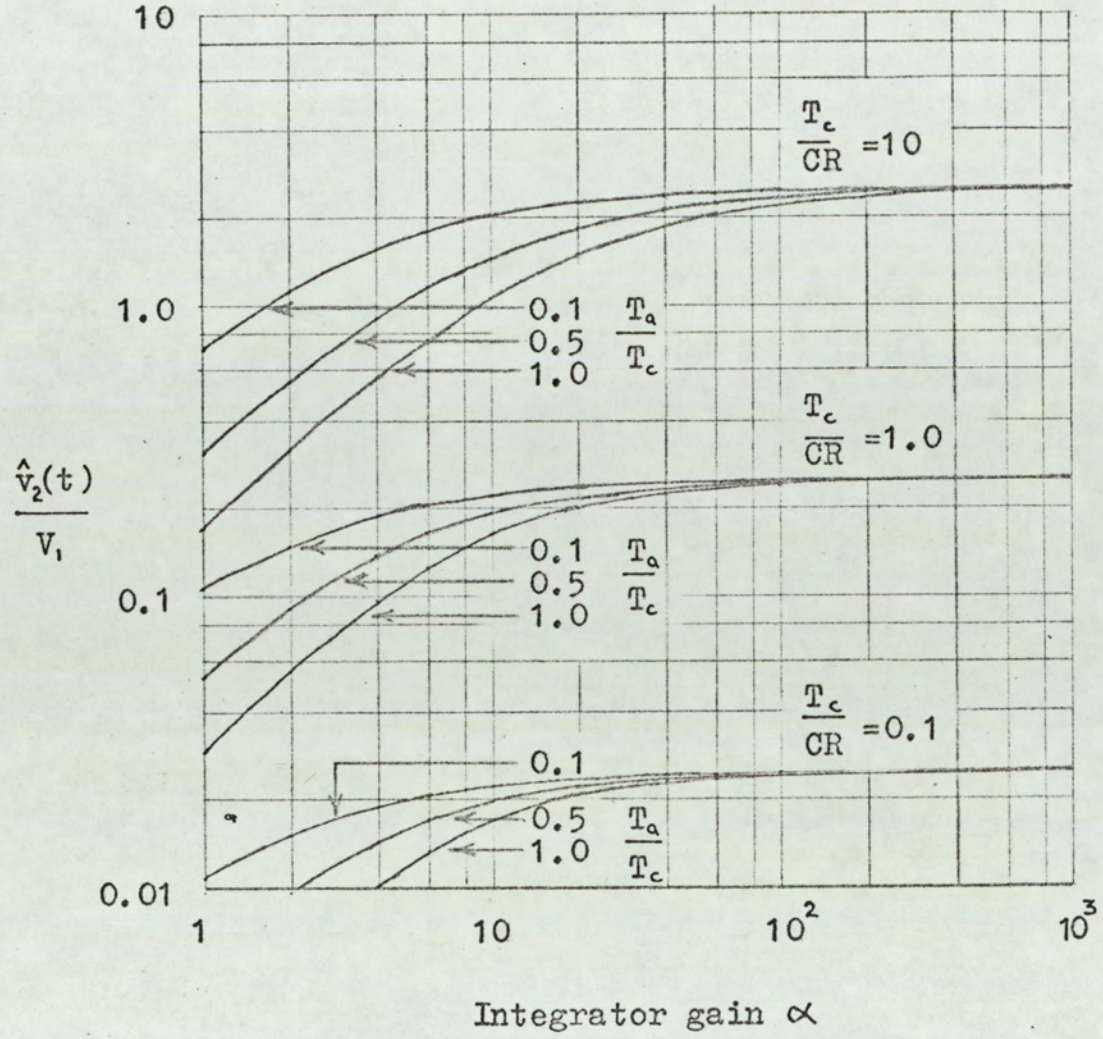

Fig.3.3.15. Peak integrator output for double-edge modulation system with bandwidth-limited integrator amplifier.

3.3.3 Conclusions

Expressions have been derived for the static error in pulse-length modulation systems which utilise a bandwidth-limited amplifier in the integrator section. The error equations have been expressed in terms of three variables: the normalised time constant T_N, the modulation index M and the parameter Υ,

$$\text{where } \Upsilon = \frac{CR}{T_a}\left[\frac{T_a}{CR} + 1 + \alpha\right]^2$$

The transfer function of the single-edge modulation system is not symmetrical about the origin. In general, a constant term exists in the demodulated output waveform when the modulation index is zero. However, it is shown that under certain conditions the effect of the finite amplifier bandwidth is to reduce this constant term to zero. The transfer function of the double-edge modulation system is symmetrical about the origin, and the amplitude of the demodulated system output is zero when the modulation index is zero.

The magnitude of the amplifier time constant T_a that can be tolerated without significantly affecting the system performance is a function of the other system parameters. For this reason, a clearer indication of the effects of the finite amplifier bandwidth can be gained by applying the analytical results to a practical example (See section 5).

3.4 Static error due to hysteresis in the level detector threshold level

Many of the circuits used as level detectors exhibit a hysteresis effect in that the threshold level for positive-going input voltages differs from that for negative-going input voltages. The transfer function of a hysteretic level detector is shown in fig. 3.4.1

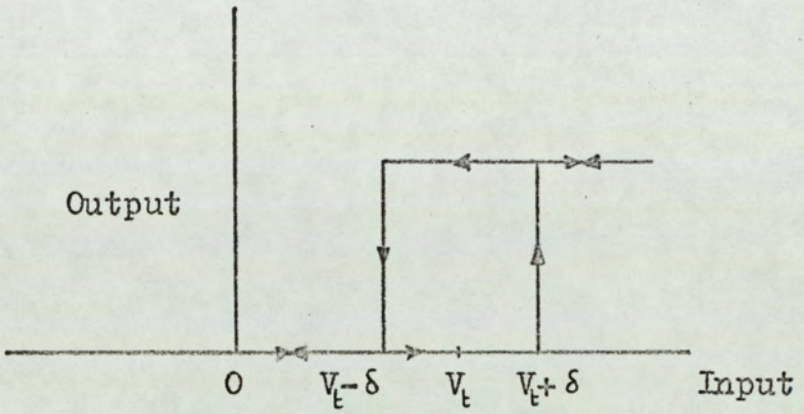

Fig.3.4.1. Transfer function of hysteretic level-detector.

In the design of a pulse-length modulation system it is required to know what effect the level-detector hysteresis has on the system performance.

3.4.1 Single-edge modulation

Consider the single-edge modulation system of fig. 2.3(a) utilising a hysteretic level detector with a transfer characteristic as shown in fig. 3.4.1. It will be assumed that the integrator has finite gain but is ideal in all other respects. The output $v_2(t)$ of the integrator is given by equation 3.1.1 of

section 3.1.1 and is rewritten below for convenience.

$$v_2(t) = -\alpha V_1 \left[1 - \exp\left(\frac{-t}{(1+\alpha)CR}\right)\right] \qquad (3.4.1)$$

The integrator output waveform is added to the modulating input voltage V_{in} and the sum applied to the input of the level detector. The output of the level detector changes state whenever the sum of the modulating input voltage and the integrator output voltage crosses the effective threshold level. The waveforms associated with the level detector are shown in fig. 3.4.2. It can be seen that the positive hysteresis $(V_t + \delta)$ does not affect the position of the trailing edges of the pulses. The position t_1 of the leading edge of the pulse is defined by the expression:

$$v_2(t_1) + V_{in} = V_t - \delta \qquad (3.4.2)$$

Since the hysteresis does not affect the position of the pulse trailing edge, the level detector can be considered as non-hysteretic but with an effective threshold level of $V_t - \delta$. Obviously this effective threshold level can be set to give identical conditions to those for a non-hysteretic level detector. Thus, hysteresis in the level detector threshold will have no effect on the system error, provided that the effective threshold level $(V_t - \delta)$ is set to the value required for a level detector with zero hysteresis (See section 3.1.1).

Fig. 3.4.2 shows that, for positive values of modulating input voltage, full modulation corresponds to $t_1 = T_c$. Full modulation for negative values of modulating input voltage corresponds to $t_1 = 0$. However, full modulation cannot be achieved in a continuous manner for negative values of V_{in}.

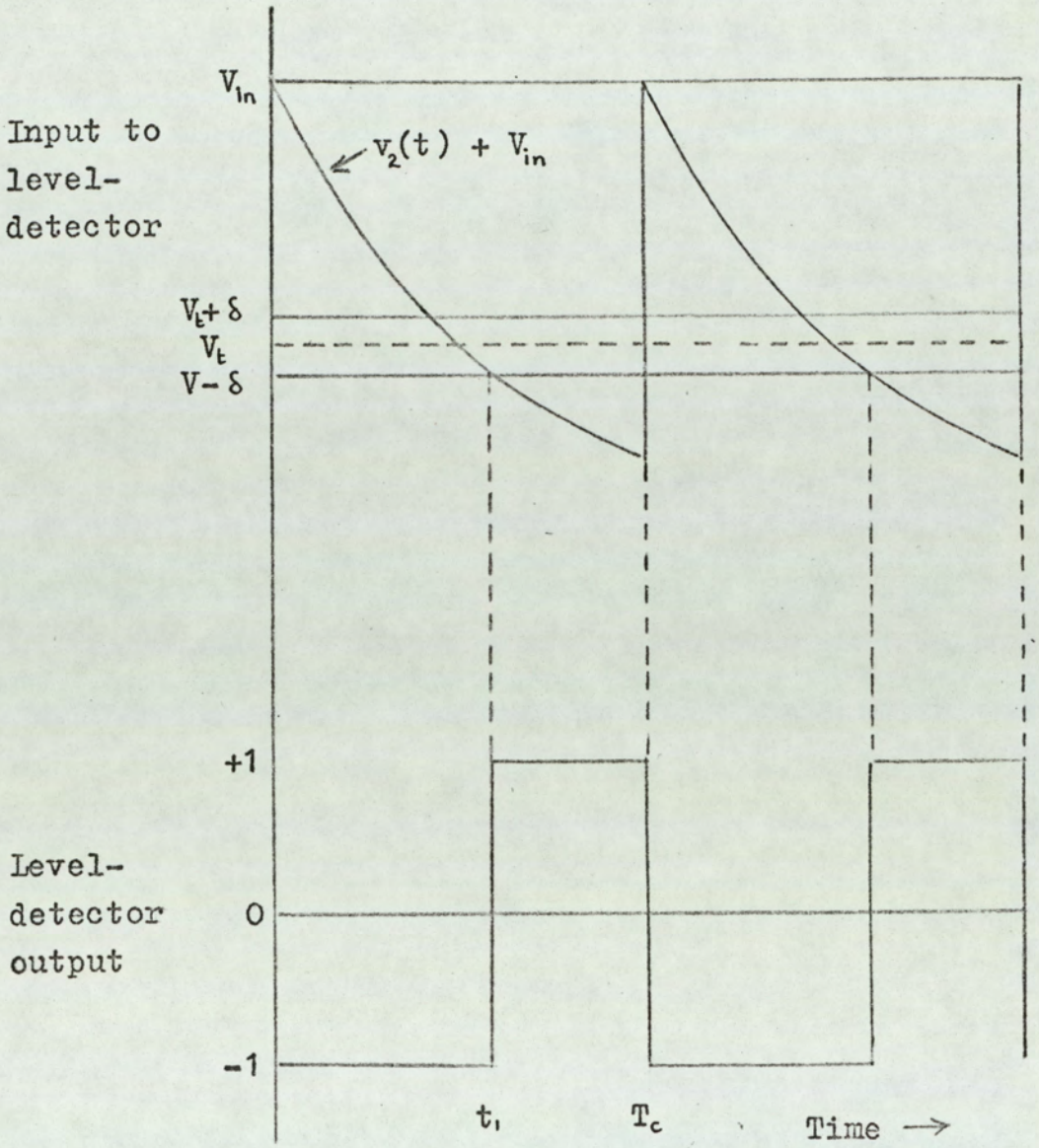

Fig.3.4.2. Waveforms for single-edge modulation system with hysteretic level-detector.

As V_{in} is increased negatively, the position t_1 of the leading edge approaches zero, until the condition shown in fig. 3.4.3 is reached. If the modulating input voltage is further increased negatively, then t_1 changes abruptly from some finite value to zero, since the sum of the integrator output voltage and the modulating input voltage does not cross the upper threshold level $V_t + \delta$. Thus, continuous modulation is achieved for negative values of V_{in} only if the sum of V_{in} and the integrator output voltage at time $t=0_+$ is greater than the upper effective threshold level, $V_t + \delta$. The amplitude of the integrator output waveform is zero at time $t=0_+$, so the maximum negative input voltage $V_{in-}(max)$ for continuous modulation is given by:

$$V_{in-}(max) = V_t + \delta \qquad (3.4.3)$$

It was shown in section 3.1.1, for the system with a non-hysteretic level detector, that if the positive and negative input voltages required to produce full modulation are to be of equal amplitude, then the level detector threshold level must be set to half the peak value of the integrator output waveform. Under these conditions, equation 3.1.10 gives the following input voltage $\hat{V}_{in+}$, for full modulation:

$$\hat{V}_{in+} = \frac{1}{2} \alpha V_1 \left[1 - \exp\left(\frac{-T_c}{(1+\alpha)CR} \right) \right] \qquad (3.4.4)$$

Therefore, for a system with a hysteretic level detector, if the effective threshold level $V_t - \delta$ is set to half the peak value of the integrator output waveform, the positive input voltage required to produce full modulation is given by equation 3.4.4 and the effective threshold level is:

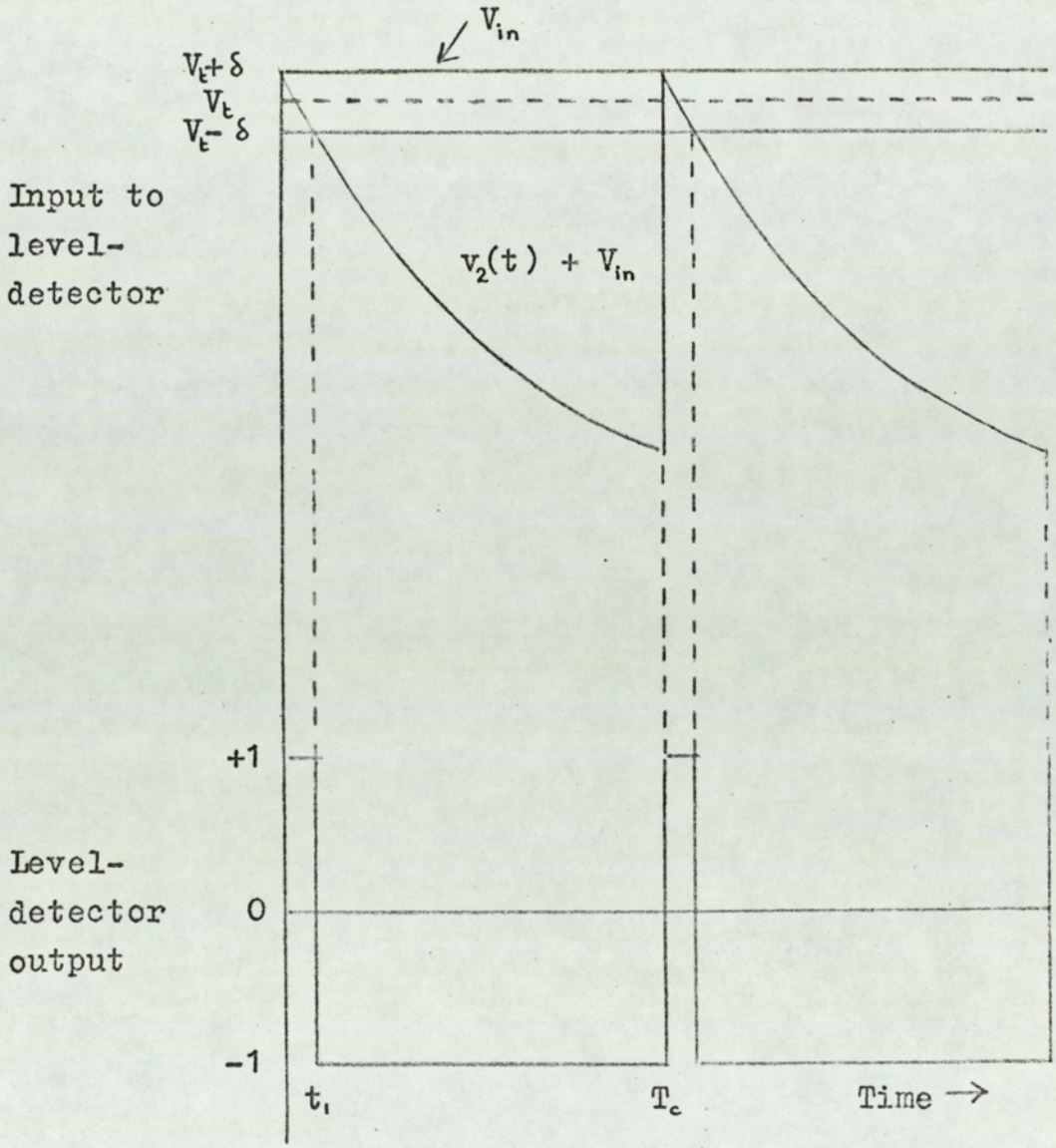

Fig.3.4.3. Limiting condition for negative values of modulating input voltage V_{in}.

$$V_t - \delta = -\frac{1}{2}\alpha V_1\left[1-\exp\left(\frac{-T_c}{(1+\alpha)CR}\right)\right] \qquad (3.4.5)$$

The maximum negative input $V_{in-}(max)$ can now be expressed as a modulation index:

$$M_-(max) = \frac{V_{in-}(max)}{\hat{V}_{in}} \qquad (3.4.6)$$

Substituting equations 3.4.3, 3.4.4 and 3.4.5 in equation 3.4.6 gives:

$$M_-(max) = -1 + \frac{4\delta}{\alpha V_1\left[1-\exp\left(\frac{-T_c}{(1+\alpha)CR}\right)\right]} \qquad (3.4.7)$$

The above expression for the maximum negative modulation index for continuous modulation may be rewritten as:

$$M_-(max) = -1 - \frac{4\delta}{\hat{v}_2(t)} \qquad (3.4.8)$$

where $\hat{v}_2(t)$ is the peak output of the integrator.

Thus, hysteresis in the level detector has no effect on the system error, but it sets a limit of less than unity on the maximum negative value of the modulation index.

3.4.2 Double-edge modulation

Consider the double-edge modulation system of fig. 3.1(a) where the level detector has a transfer function as shown in fig. 3.4.1. As for the single-edge modulation system, it will be assumed that the integrator has finite voltage gain but is ideal in all other respects. The output of the integrator $v_2(t)$ is given by equations 3.1.23 and 3.1.24 of section 3.1.2, which are rewritten below for convenience.

$$v_2(t) = -\alpha V_1 \left\{ 1 - \frac{2\exp\left(\frac{-t}{(1+\alpha)CR}\right)}{1+\exp\left(\frac{-T_c}{2(1+\alpha)CR}\right)} \right\} \quad , 0 \leq t \leq \frac{T_c}{2} \qquad (3.4.9)$$

$$v_2(t) = -\alpha V_1 \left\{ -1 + \frac{2\exp\left(\frac{-(t_2-\frac{T_c}{2})}{2(1+\alpha)CR}\right)}{1+\exp\left(\frac{-T_c}{2(1+\alpha)CR}\right)} \right\} \quad , \frac{T_c}{2} \leq t \leq T_c \qquad (3.4.10)$$

The integrator output voltage $v_2(t)$ is added to the modulating input voltage V_{in} and the sum is applied to the input of the level detector. The output of the level detector changes state whenever the sum of the input voltage V_{in} and the integrator output voltage crosses level $V_t + \delta$ for positive - going voltages, and $V_t - \delta$ for negative - going voltages. The waveforms associated with the level detector are shown in fig. 3.4.4. The positions of the leading and trailing edges of the level detector output pulse, t_1 and t_2 respectively, are defined by:

$$v_2(t_1) + V_{in} = V_t - \delta \qquad (3.4.11)$$

$$v_2(t_1) + V_{in} = V_t + \delta \qquad (3.4.12)$$

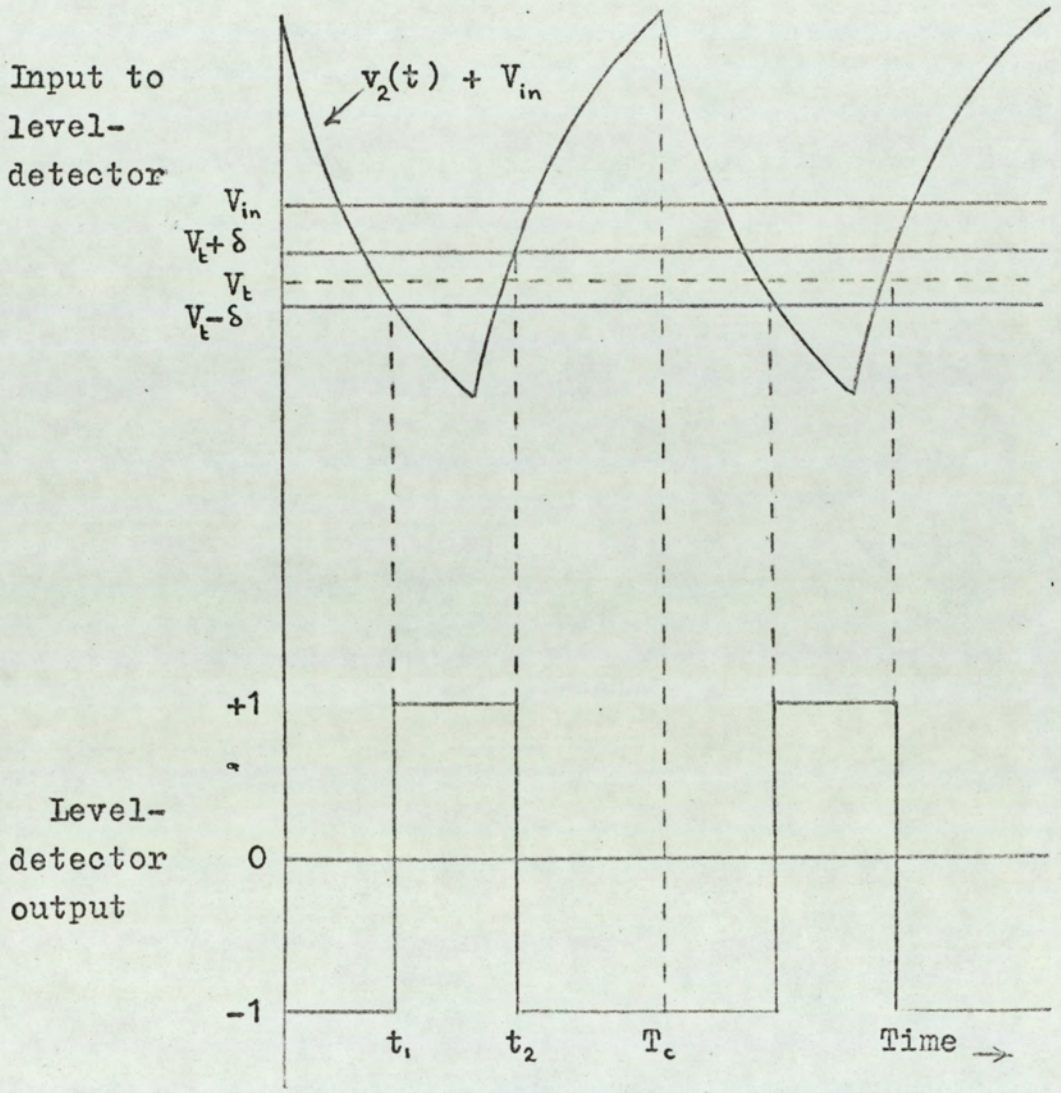

Fig.3.4.4. Waveforms for double-edge modulation system with hysteretic level-detector.

Fig. 3.4.4 shows that, as the modulating input voltage increases in the positive direction so the position t_1 of the leading edge of the pulse tends to $\frac{T_c}{2}$. Eventually, the condition is reached where $t_1 = \frac{T_c}{2}$; however, as a result of the hysteresis, the position t_2 of the trailing edge is not equal to $\frac{T_c}{2}$. If the input voltage V_{in} increases further, the pulse length $(t_2 - t_1)$ abruptly changes to zero, since the sum of the integrator waveform and the modulating input no longer crosses the lower threshold level $V_t - \delta$. Similarly, for negative values of input voltage a condition is reached where $t_2 = T_c$, but t_1 is not zero. Further increase of V_{in} in the negative direction will cause the pulse length $(t_2 - t_1)$ to change abruptly to T_c, since the sum of the input voltage V_{in} and the integrator output voltage no longer crosses the upper threshold level $V_t + \delta$. Thus, the maximum positive value of input voltage $\hat{V}_{in+}$ for which the modulation process is continuous, from fig. 3.4.4, is:

$$\hat{V}_{in+} = V_t - \delta - v_2\left(\frac{T_c}{2}\right) \qquad (3.4.13)$$

where $v_2(\frac{T_c}{2})$ is the integrator output voltage at time $t = \frac{T_c}{2}$. Due to the symmetry of the integrator output waveform, $v_2(\frac{T_c}{2})$ is equal and opposite to the peak positive integrator output $\hat{v}_2(t)$ which occurs at time $t = 0$.

$$\therefore \quad \hat{V}_{in+} = V_t - \delta + \hat{v}_2(t) \qquad (3.4.14)$$

Similarly, the maximum negative value of input $\hat{V}_{in-}$ for continuous modulation is:

$$\hat{V}_{in-} = V_t + \delta - \hat{v}_2(t) \qquad (3.4.15)$$

The conditions of input given by equations 3.4.14 and 3.4.15 will be defined as full modulation, even though the pulse lengths corresponding to these inputs are not zero and T_c. If the maximum positive input voltage $\hat{V}_{in+}$ is to be equal and opposite to the maximum negative input $\hat{V}_{in-}$ then, from equations 3.4.14 and 3.4.15,

$$V_t = 0 \quad \text{for} \quad \hat{V}_{in+} = -\hat{V}_{in-} \tag{3.4.16}$$

Equations 3.4.11 and 3.4.12 now become:

$$v_2(t_1) + V_{in} = -\delta \tag{3.4.17}$$

$$v_2(t_2) + V_{in} = \delta \tag{3.4.18}$$

Dividing equations 3.4.17 and 3.4.18 by $\hat{V}_{in+}$, and solving for t_1 and t_2 gives:

$$\frac{t_1}{T_c} = -\frac{(1+\alpha)CR}{T_c}\left\{\log\frac{1}{2}\left[1-\frac{\delta}{\alpha V_1}\right]\left[1+\exp\left(\frac{-T_c}{2(1+\alpha)CR}\right)\right] + \log\left[1-M\phi K\right]\right\} \tag{3.4.19}$$

$$\frac{t_2}{T_c} = \frac{1}{2} - \frac{(1+\alpha)CR}{T_c}\left\{\log\frac{1}{2}\left[1-\frac{\delta}{\alpha V_1}\right]\left[1+\exp\left(\frac{-T_c}{2(1+\alpha)CR}\right)\right] + \log\left[1+M\phi K\right]\right\} \tag{3.4.20}$$

where: $M = \dfrac{V_{in}}{\hat{V}_{in+}}$, the modulation index.

$$K = \frac{1-\exp\left(\dfrac{-T_c}{2(1+\alpha)CR}\right)}{1+\exp\left(\dfrac{-T_c}{2(1+\alpha)CR}\right)} \tag{3.4.21}$$

$$\phi = 1 + \frac{\dfrac{\delta}{\alpha V_1}(K-1)}{K\left(1-\dfrac{\delta}{\alpha V_1}\right)} \tag{3.4.22}$$

The modulation-index modifying function ϕ may be expressed in terms of the peak output voltage $\hat{v}_2(t)$ of the integrator. From equation 3.4.22 and equation 3.4.9 with time t = 0:

$$\phi = 1 + \frac{K-1}{\frac{\hat{v}_2(t)}{\delta} - K} \qquad (3.4.23)$$

The form of equation 3.4.23 is more convenient for design purposes since the ratio $\frac{\delta}{\hat{v}_2(t)}$ is easier to visualise in terms of the system, than the ratio $\frac{\delta}{\alpha V_1}$. Fig. 3.1.12 of section 3.1.2 shows the peak integrator output $\hat{v}_2(t)$ plotted as a function of the system parameters.

Demodulation of the length-modulated wavetrain at the level-detector output is equivalent to taking the average value of the waveform over one cycle of the repetition frequency. Therefore, from fig. 3.4.4, the amplitude V_{av} of the demodulated wavetrain is:

$$V_{av} = 2\left(\frac{t_2}{T_c} - \frac{1}{2} - \frac{t_1}{T_c}\right) \qquad (3.4.24)$$

Substituting equations 3.4.19 and 3.4.20 in equation 3.4.24:

$$V_{av} = -\frac{2(1+\alpha)CR}{T_c} \log\left(\frac{1+M\phi K}{1-M\phi K}\right) \qquad (3.4.25)$$

The logarithmic term in equation 3.4.25 may be expanded as an infinite series:

$$V_{av} = -\frac{4(1+\alpha)CR}{T_c} \sum_{n=1}^{\infty} \frac{1}{(2n-1)} (M\phi K)^{2n-1} \qquad (3.4.26)$$

Comparing equations 3.4.25 and 3.4.26 with the corresponding expressions for the amplitude of the demodulated wavetrain for the

double-edge modulation system with a non-hysteretic level detector (equation 3.1.36 and 3.1.37) shows that the effect of the level detector hysteresis is simply to modify the effective value of the modulation index from M to $M\phi$.

The static error E_1 in the amplitude of the demodulated wavetrain was defined in section 3.1.1 as:

$$E_1 = V_{av} + M \qquad (3.4.27)$$

Equation 3.4.27 may be rewritten as:

$$E_1 = V_{av} + M\phi + M(1-\phi) \qquad (3.4.28)$$

The term $V_{av} + M\phi$ in equation 3.4.28 is identical, in form, to equation 3.1.16 for the static error E_1 in a double-edge modulation system with a non-hysteretic level detector. The only difference is that the modulation index M is replaced with $M\phi$. Thus, fig. 3.1.10 of section 3.1.2 may be used to determine the value of $V_{av} + M\phi$ by simply replacing the modulation index M with the modified modulation index $M\phi$. Fig. 3.4.5 shows the factor $(1-\phi)$ plotted as a function of the normalised time constant $\frac{T_c}{(1+\alpha)\,CR}$ and the ratio $\frac{\delta}{\hat{v}_2(t)}$. The term $M(1-\phi)$ can readily be evaluated from fig. 3.4.5. Thus, the static error E_1 for a double-edge modulation system with a hysteretic level detector has been expressed as the static error of an equivalent double-edge modulation with a non-hysteretic level detector, plus an additional error term $M(1-\phi)$. Figs. 3.1.10 and 3.4.5 show that the two terms in equation 3.4.28 have the same sign. Since the modulation index modifying factor ϕ is nearly equal to unity for practical values of level detector hysteresis, the term $(V_{av}+M\phi)$ in equation 3.4.28 will be very little different from the error E_1 of a

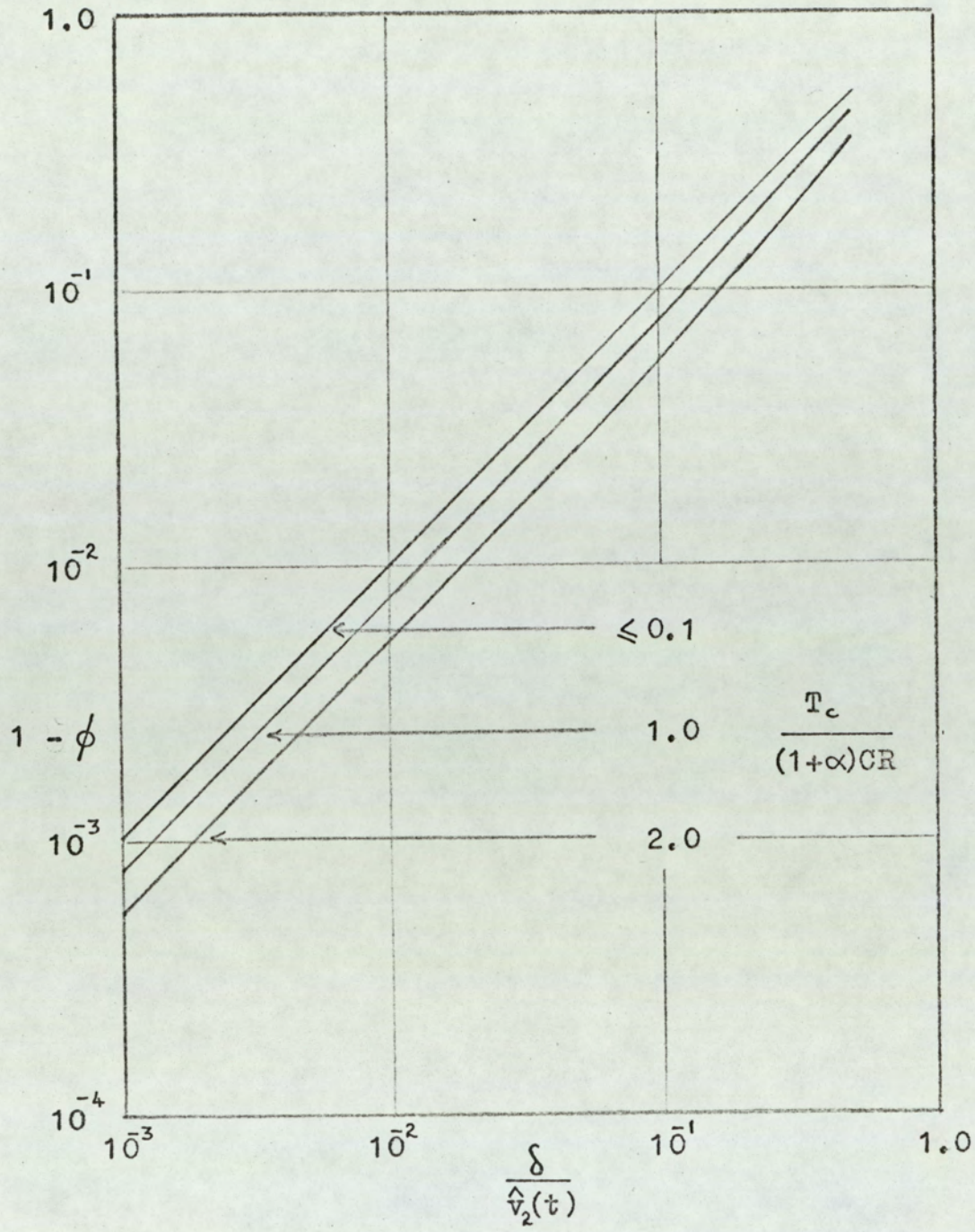

Fig.3.4.5. Modulation index modifying function ϕ for double-edge modulation system with hysteretic level-detector.

non-hysteretic system. However, the term $M(1-\phi)$ will certainly be significant compared with $(V_{av} + M\phi)$, so level-detector hysteresis can cause an appreciable increase in the system static error E_1. When designing a system, the manner in which E_1 is defined should be borne in mind since the definition used perhaps gives an erroneous indication of system error. The error E_1 is defined as the deviation of the system transfer function from the ideal one where $V_{av} = -M$, as shown in fig. 3.4.6. From this diagram it can be seen that care is required in interpreting the significance of E_1, since it does not give a true indication of the system linearity. In many systems, the increase in E_1 will not matter, since, from fig. 3.4.5, the increased error may be interpreted as a decrease in system gain.

For reasons discussed in section 2.1.2, the error in the amplitude V_{av} of the demodulated wavetrain may also be expressed as the difference between the amplitude of V_{av} and the component of the demodulated wavetrain that is directly proportional to the modulation index M. Therefore, from equations 3.4.25 and 3.4.26:

$$E_2 = -\frac{2(1+\alpha)CR}{T_c}\left\{\log\left(\frac{1+M\phi K}{1-M\phi K}\right) - 2M\phi K\right\} \qquad (3.4.29)$$

$$\text{or} \quad E_2 = -\frac{4(1+\alpha)CR}{T_c}\sum_{n=2}^{\infty}\frac{1}{(2n-1)}(M\phi K)^{2n-1} \qquad (3.4.30)$$

Comparing equations 3.4.29 and 3.4.30 with the corresponding expressions for the double-edge modulation system with a non-hysteretic level detector (equations 3.1.39 and 3.1.40) it will be noted that they are identical in form. Therefore, fig. 3.1.11

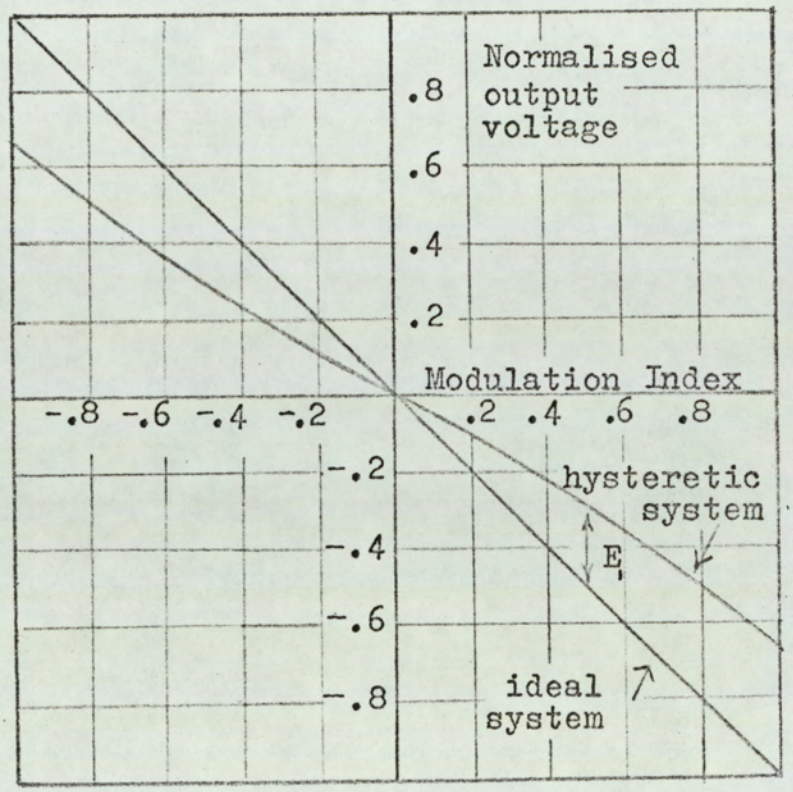

Fig.3.4.6. Definition of static error E_1 for double-edge modulation system with hysteretic level-detector.

for the error E_2 in the double-edge modulation system with no hysteresis may be used to determine the error E_2 in the system with hysteresis by replacing the modulation index M in fig. 3.1.11 with the modified modulation index $M\phi$.

3.4.3 Conclusions

Expressions have been derived for the static error in pulse length modulation systems which utilise a hysteretic level detector. The error equations are expressed in terms of the error of equivalent systems with non-hysteretic level detectors.

It is shown that, for a single-edge modulation system, the level-detector hysteresis has no effect on the system error provided that the effective threshold $V_t - \delta$ is set to the value required for the threshold of a system with zero hysteresis. Under these conditions, the only effect of hysteresis is to limit the maximum negative value of the modulation index for which the modulation process is continuous.

For the double-edge modulation system, level-detector hysteresis reduces the effective modulation index. This reduces the maximum value of the demodulated system output. When the modulation index M is unity, the system output corresponds to the output of a non-hysteretic system with a modulation index of $M\phi$.

Hysteresis is inherent in the operation of many forms of level detector. However, some types of level detector do not possess hysteresis (e.g. A high-gain, wide-band saturating amplifier). In practice, it is often convenient to introduce a small amount of hysteresis into this type of level detector to avoid 'jitter' of the pulse edges at high levels of modulation. The 'jitter' is due to a tendency to oscillation in the high-gain, wide-band type of circuit. Any oscillation can, of course, be avoided by careful design and component layout, but it is often more practical to overcome the problem by introducing hysteresis.

3.5 General discussion of the results of the static analyses

A number of interesting general observations can be made from preceding analyses of static error in pulse-length modulation systems. In all the cases analysed, it was found that the amplitude V_{av} of the demodulated wavetrain could be represented by power series of form:

$$V_{av} = \sum_{n=0}^{\infty} a_n . M^n \qquad \text{for single-edge modulation}$$

$$V_{av} = \sum_{n=1}^{\infty} a_{2n-1} M^{2n-1} \qquad \text{for double-edge modulation}$$

where M is the modulation index and the coefficients a_n are functions of the system parameters. The power series for double-edge modulation does not contain a constant term, so the amplitude of the demodulated wavetrain is zero when the modulation index is zero; this is not the case for single-edge modulation. The power series for single-edge modulation has terms involving all positive powers of M, whereas the series for double-edge modulation contains only positive odd powers of M. Consequently the transfer function of the double-edge modulation system is symmetrical about the origin. In general, the system static error is smaller for double-edge modulation systems, and the reason for this may be demonstrated diagrammatically as shown in fig. 3.5.1. The points t_1 and t_2 represent the non-ideal case where the sampling waveform is not linearly related to time. It will be noted that, for double-edge modulation, the error in t_1 cancels the error in t_2 to some extent. With single-edge modulation there is no cancellation of error.

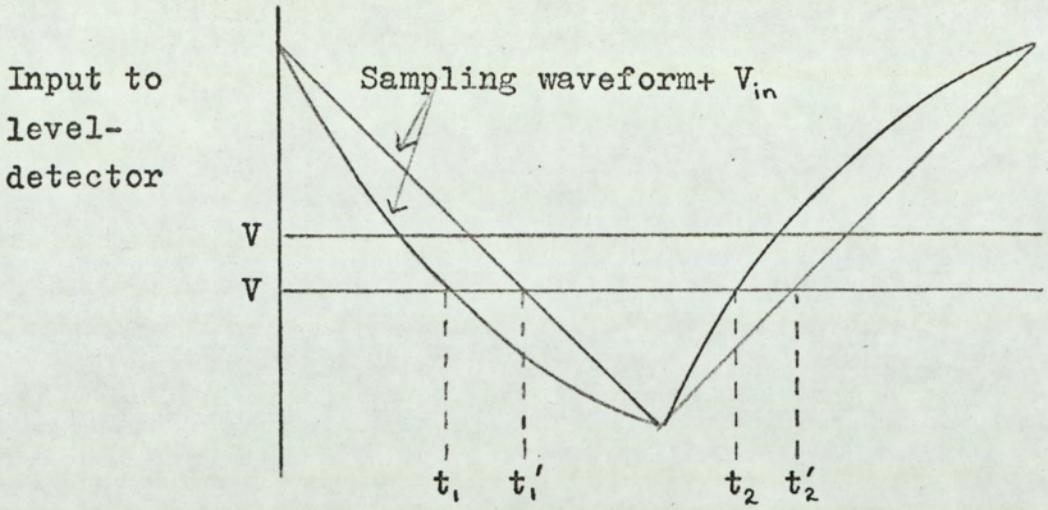

(a)

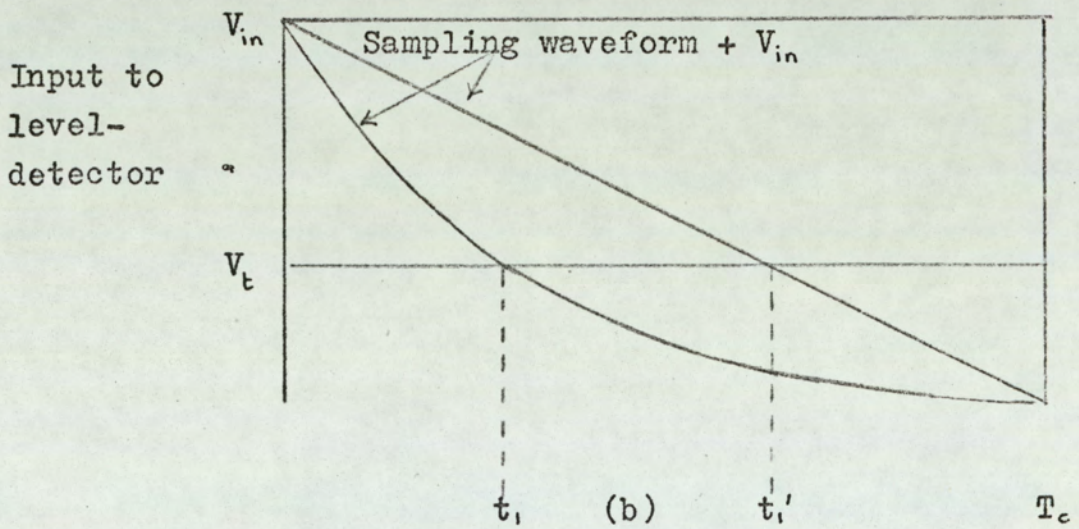

Fig.3.5.1. Error in level-detector switching instants

(a) Double-edge modulation

(b) Single-edge modulation

For all the cases considered, it has been shown that the level-detector threshold should be set at zero for double-edge modulation, and to some finite value (which depends on the system parameters) for single-edge modulation. Since it is normally simpler to design a level detector with a threshold of zero volts, this is a practical advantage of double-edge modulation.

4. Spectrum Analysis

4.1. General Theory

The method of spectrum analysis which is based on setting up the Fourier series for a train of unmodulated pulses, and then applying the modulation to the appropriate parameter, lacks mathematical rigour. This is due to the non-periodicity of a pulse-length modulated wavetrain produced by natural sampling. The method of analysis used in this section is based on that used by Fitch[11] and Stuart[49] for the spectrum analysis of pulse-length modulation with ideal sampling waveforms. It may be shown[11,49] that the frequency spectrum of 2N + 1 pulses, whose edges are position modulated, is given by the expression:

$$F(t)=\frac{1}{2\pi}\int_{-\infty}^{\infty}\frac{\sin\left(N+\frac{1}{2}\right)\omega T_c}{\sin\left(\frac{\omega T_c}{2}\right)}\;\frac{1}{j\omega}\left[\exp\left(j\omega\left[t-\frac{T_o}{2}+t_{dl}\right]\right)-\exp\left(j\omega\left[t-\frac{T_o}{2}-t_{dt}\right]\right)\right]d\omega \qquad (4.1.1)$$

where ω = angular frequency

T_o = unmodulated pulse length

t_{dl} and t_{dt} are the time deviations from the unmodulated positions, of the leading and trailing pulse edges respectively

T_c = pulse period = $\frac{2\pi}{\omega_c}$

Fig. 4.1.(a). shows the manner in which the unmodulated wavetrain is defined, and fig. 4.1.(b). the manner in which the time deviations of the pulse edges are defined. The general expression for the frequency spectrum of 2N + 1 length-modulated pulses (equation 4.1.1.) is the basis of all the following analyses.

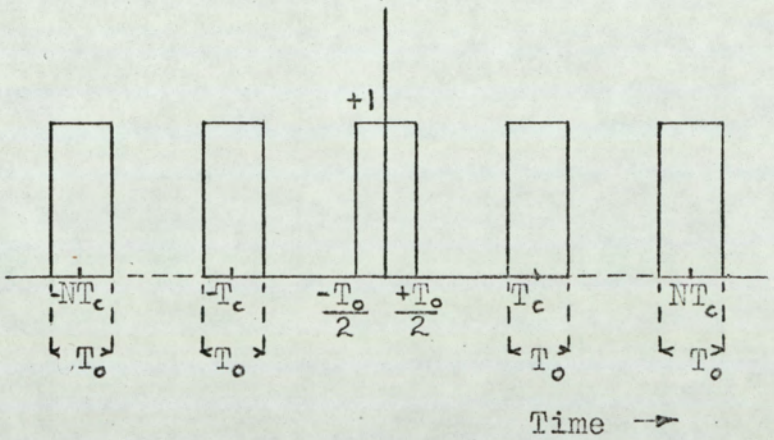

Fig.4.1.1(a) Unmodulated pulse-train

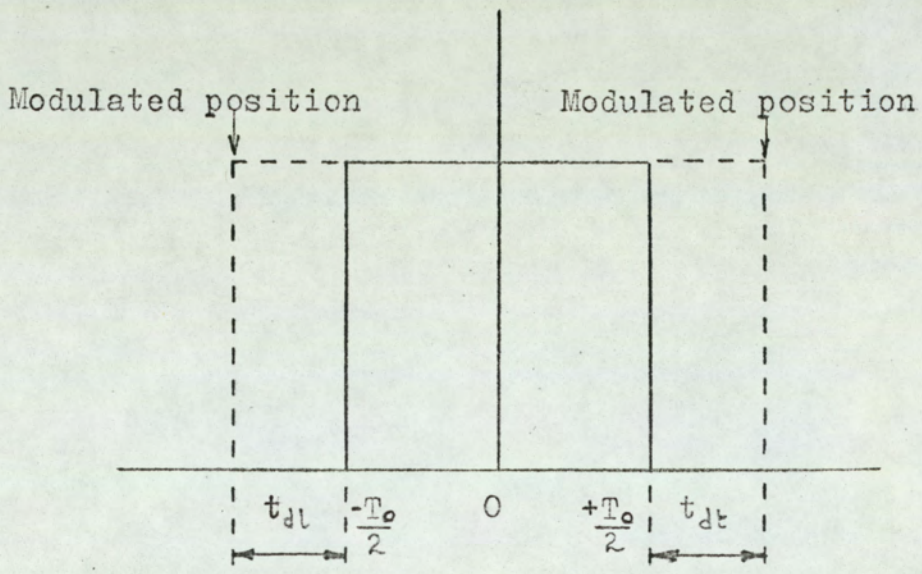

Fig.4.1.1(b) Modulated pulse

4.2. Distortion due to Finite Operational Integrator Gain

4.2.1. Single-edge Modulation

It is shown in section 3.1.1. (equation 3.1.12.) that the position t_1 of the leading edge of the pulse in a single-edge modulation system, with finite integrator gain, is given by the expression:

$$\frac{t_1}{T_c} = -\frac{(1+\alpha)CR}{T_c}\left\{\log\frac{1}{2}\left[1-\exp\left(\frac{-T_c}{(1+\alpha)CR}\right)\right]+\log\left(1-M.K\right)\right\} \qquad (4.2.1(a))$$

where:
$$K = \frac{1-\exp\left(\frac{-T_c}{(1+\alpha)CR}\right)}{1+\exp\left(\frac{-T_c}{(1+\alpha)CR}\right)} \qquad (4.2.1(b))$$

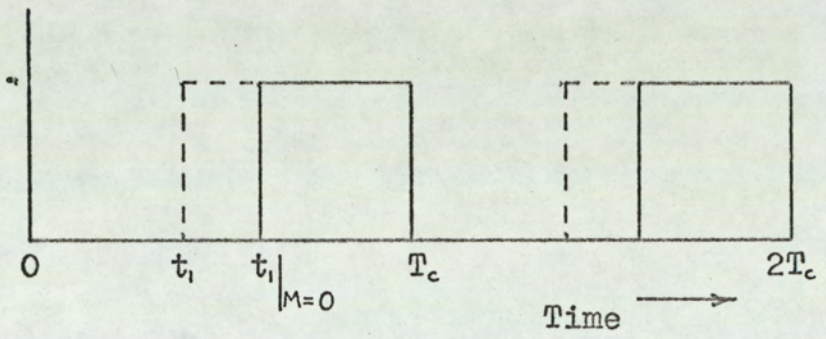

Fig.4.2.1. Single-edge pulse-length modulated wavetrain.

The trailing edges of the pulses occur at periodic intervals of nT_c as shown in fig. 4.2.1. From equation 4.2.1. and fig. 4.2.1. the time deviation of the leading edge is:

$$t_{d1} = t_1\Big|_{M=0} - t_1$$

$$\therefore \quad \frac{t_{d1}}{T_c} = \frac{(1+\alpha)CR}{T_c} \log\left(1 - M.K\right) \tag{4.2.2}$$

The time deviation of the trailing edge is zero

$$\frac{t_{dt}}{T_c} = 0 \tag{4.2.3}$$

The unmodulated pulse length T_o is:

$$T_o = T_c - t_1\Big|_{M=0}$$

$$\therefore \quad \frac{T_o}{T_c} = 1 + \frac{(1+\alpha)CR}{T_c} \log \frac{1}{2}\left[1 + \exp\left(\frac{-T_c}{(1+\alpha)CR}\right)\right] \tag{4.2.4}$$

If the modulating input to the system is a cosine wave of frequency ω_m, then the modulation index is a time function $M.\cos \omega_m t$. The expression for the time deviation of the leading pulse edge becomes:

$$\frac{t_{d1}}{T_c} = \frac{(1+\alpha)CR}{T_c} \log\left[1 - M.K.\cos\left(\omega_m t\right)\right] \tag{4.2.5}$$

Substituting equations 4.2.3., 4.2.4. and 4.2.5. in equation 4.1.1. gives the following expression for the frequency

spectrum of a single-edge pulse-length modulated wavetrain of 2N + 1 pulses where the sampling waveform is produced by an operational integrator having finite gain.

$$F(t)=\frac{1}{2\pi}\int_{-\infty}^{\infty}\frac{\sin\left(N+\frac{1}{2}\right)\omega T_c}{\sin\left(\frac{\omega T_c}{2}\right)}\cdot\frac{1}{j\omega}\left\{-\exp\left[j\omega\left(t-\frac{T_o}{2}\right)\right]+\right.$$

$$\left.\exp\left[j\omega\left(t+\frac{T_o}{2}-(1+\alpha)CR.\log\left[1-M.K.\cos(\omega_m t)\right]\right)\right]\right\}d\omega \qquad (4.2.6)$$

The limit of equation 4.2.6. as N tends to infinity will not be derived here since the limiting process of similar expressions is considered in detail elsewhere[49,56]. Following the methods given in references 49 and 56, the limit of equation 4.2.6. is:

$$F(t)=\frac{1}{2\pi j}\sum_{p=-\infty}^{\infty}\frac{1}{p}\left\{-\exp\left[jp\omega_c\left(t-\frac{T_o}{2}\right)\right]+\right.$$

$$\left.\exp\left[jp\omega_c\left(t+\frac{T_o}{2}+(1+\alpha)CR.\log\left[1-M.K.\cos(\omega_m t)\right]\right)\right]\right\} \qquad (4.2.7)$$

where ω_c = angular repetition frequency of the pulse train. Making use of the expansion[57]:

$$\log\left(r^2+s^2-2r.s.\cos\theta\right)=2\log(r)-2\sum_{n=1}^{\infty}\left(\frac{s}{r}\right)^n.\frac{\cos(n\theta)}{n} \qquad (4.2.8)$$

for $\frac{s}{r}<1$

the frequency spectrum given by equation 4.2.7. may be rewritten as:

$$F(t)=\frac{1}{2\pi j}\sum_{p=-\infty}^{\infty}\frac{1}{p}\left\{-\exp\left[jp\omega_c\left(t-\frac{T_o}{2}\right)\right]+\right.$$

$$\left.\exp\left[jp\omega_c\left(t+\frac{T_o}{2}-\sum_{n=0}^{\infty}k_n\cos(n\omega_m t)\right)\right]\right\} \qquad (4.2.9)$$

where

$$k_o=-(1+\alpha)CR.\log\left\{\frac{\frac{1}{2}(M.K)^2}{1-\sqrt{\left[1-(M.K)^2\right]}}\right\} \qquad (4.2.10(a))$$

$$k_n=(1+\alpha)CR\frac{2}{n}\left\{\frac{1}{M.K}-\sqrt{\left[\left(\frac{1}{M.K}\right)^2-1\right]}\right\}^n \qquad (4.2.10(b))$$

It is shown in Appendix 4 that manipulation of equation 4.2.9. in the general form is very complex. In order to ease the problem somewhat, the assumption is made that the non-linearity of the sampling waveform is such that an adequate representation is obtained by taking only the first three terms containing harmonics of the modulation frequency. Therefore equation 4.2.9. becomes:

$$F(t) \triangleq \frac{1}{2\pi j} \sum_{p=-\infty}^{\infty} \frac{1}{p} \left\{ -\exp\left[jp\omega_c\left(t - \frac{T_o}{2}\right)\right] + \right.$$

$$\left. \exp\left[jp\omega_c\left(t + \frac{T_o}{2} - \sum_{n=0}^{3} k_n . \cos(n\omega_m t)\right)\right] \right\} \qquad (4.2.11)$$

The rearrangement of equation 4.2.1.. into a useful form is considered in detail in Appendix 4, and only the result is quoted here.

$$F(t) \triangleq \frac{1}{T_c}\left[T_o - k_o - k_1.\cos(\omega_m t) - k_2.\cos(2\omega_m t) - k_3\cos(3\omega_m t)\right] -$$

$$\frac{1}{\pi} \sum_{p=1}^{\infty} \frac{1}{p} \sin\left(p\omega_c\left(t - \frac{T_o}{2}\right)\right) +$$

$$\frac{1}{\pi} \sum_{p=1}^{\infty} \frac{1}{p} \left\{ \sum_{\substack{e,f,g \\ =-\infty}}^{\infty} J_e(p\omega_c k_1)\, J_f(p\omega_c k_2)\, J_g(p\omega_c k_3) \times \right.$$

$$\left. \sin\left[\left(p\omega_c + [e+2f+3g]\,\omega_m\right)t + p\omega_c\left(\frac{T_o}{2} - k_o\right) - (e+f+g)\frac{\pi}{2}\right] \right\} \qquad (4.2.12)$$

Thus the frequency spectrum consists of a constant term $\frac{1}{T_c}(T_o - k_o)$, and components at the modulation frequency and its harmonics. Components are also present at all the harmonics $p\omega_c$ of the repetition frequency plus sidebands

$p\omega_c \pm (e + 2f + 3g)\omega_m$.

The amplitude of the components at the modulation frequency and its harmonics are not linearly related to the modulation index as can be seen from equation 4.2.10(b). Fig. 4.2.2. shows the peak amplitude of the modulation frequency component $\frac{k_1}{T_c} \cdot \cos(\omega_m t)$ plotted as a function of the normalised time constant $\frac{T_c}{(1+\alpha)CR}$ and the modulation index M . It will be noted that for values of $\frac{T_c}{(1+\alpha)CR}$ less than 0.1, the modulation frequency component is very nearly equal to $\frac{M}{2}$.

The second and third harmonic distortion factors, DF_2 and DF_3 respectively, are defined as:

$$DF_2 = \frac{k_2}{k_1} \qquad (4.2.13)$$

$$DF_3 = \frac{k_3}{k_1} \qquad (4.2.14)$$

Subsituting equation 4.2.10(b) in equations 4.2.13. and 4.2.14 gives:

$$DF_2 = \frac{1}{2}\left\{ \frac{1}{MK} - \sqrt{\left[\left(\frac{1}{MK}\right)^2 - 1\right]}\right\} \qquad (4.2.15)$$

$$DF_3 = \frac{1}{3}\left\{ \frac{1}{MK} - \sqrt{\left[\left(\frac{1}{MK}\right)^2 - 1\right]}\right\}^2 \qquad (4.2.16)$$

Fig. 4.2.3. shows the harmonic distortion factors DF_2 and DF_3 as functions of the normalised time constant $\frac{T_c}{(1+\alpha)CR}$

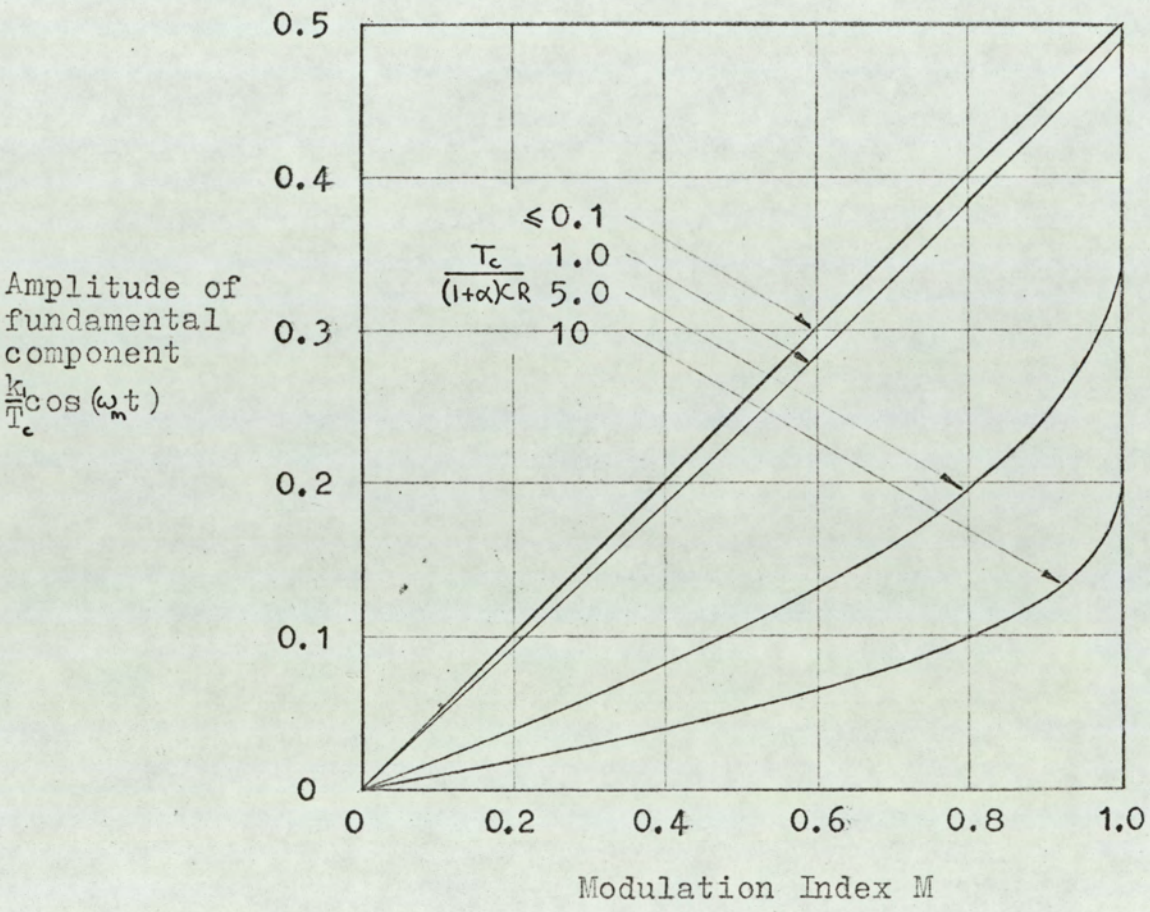

Fig.4.2.2. Amplitude of fundamental component for single-edge modulation system with finite gain integrator.

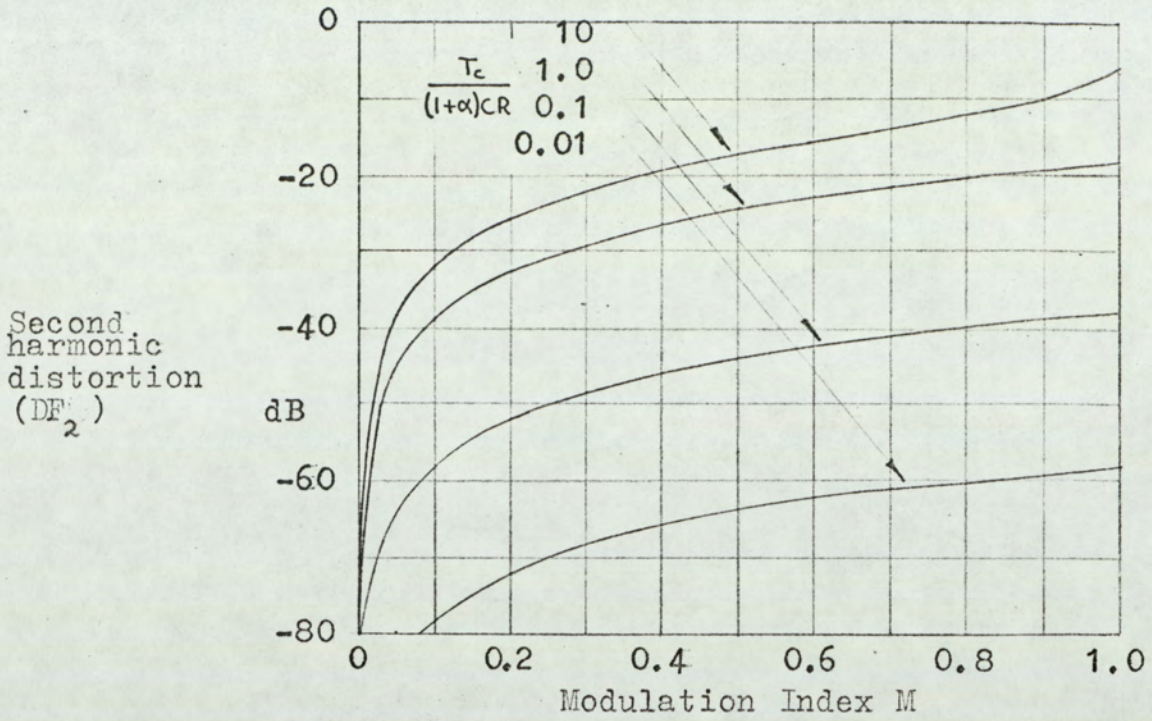

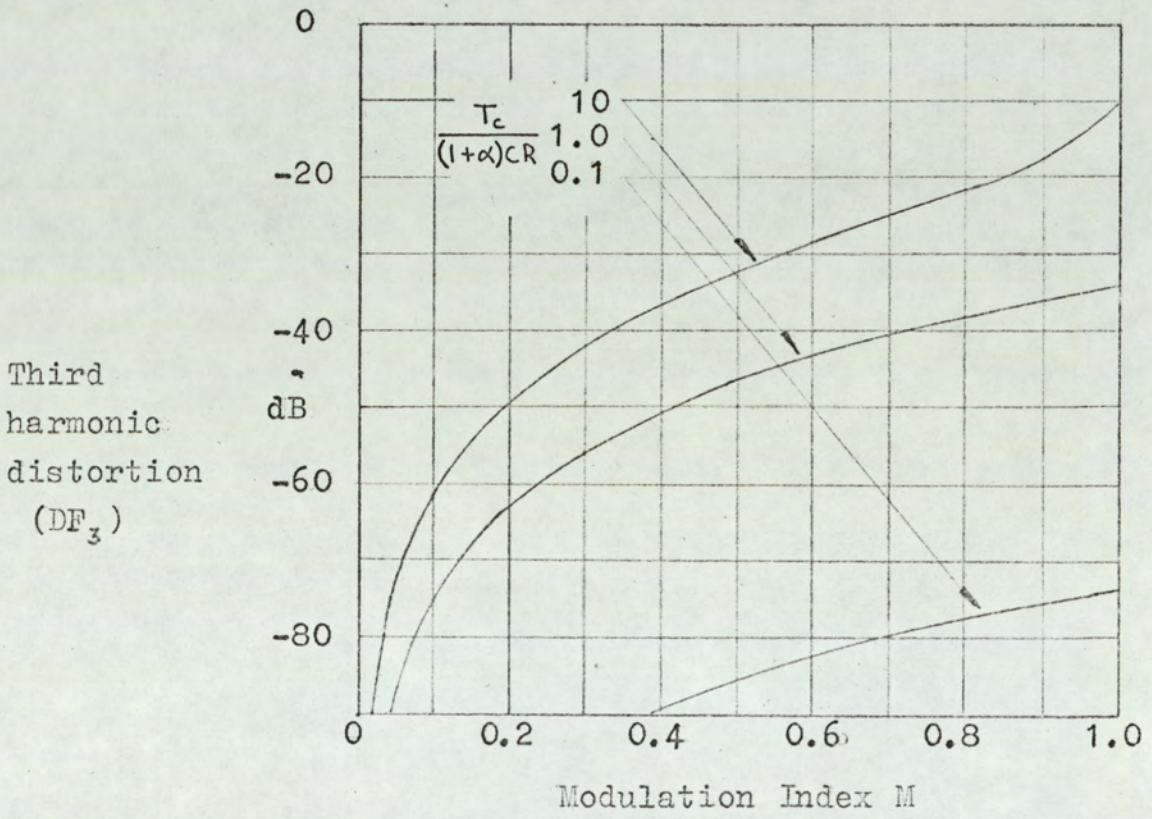

Fig.4.2.3. Harmonic distortion in single-edge modulation system with finite integrator gain.

and the modulation index M .

In order to present graphs of the amplitudes of the components at the repetition frequency and the sideband frequencies, it is necessary to choose a reference level. The most obvious one is the amplitude of the modulation frequency component at full modulation. However, for some of the system imperfections considered in the static analysis section, the results are not valid at full modulation. Since these results are required for the spectrum analyses, it is convenient to define a reference level which can be used as a basis for presenting graphical results for all the spectrum analyses. For this reason, the amplitude of the modulation frequency component $\frac{k_1}{T_c} \cdot \cos(\omega_m t)$ is chosen as the reference level. Fig. 4.2.4(a), (b) and (c) shows the relative amplitudes of the repetition frequency components and the sideband components as function of the normalised time constant $\frac{T_c}{(1+\alpha)CR}$ and the modulation index M . For values of normalised time constant less than 0.1, the finite integrator gain has negligible effect on the amplitude of the components. However, for $\frac{T_c}{(1+\alpha)CR}$ greater than 0.1, the effect on the higher order sideband components is quite marked.

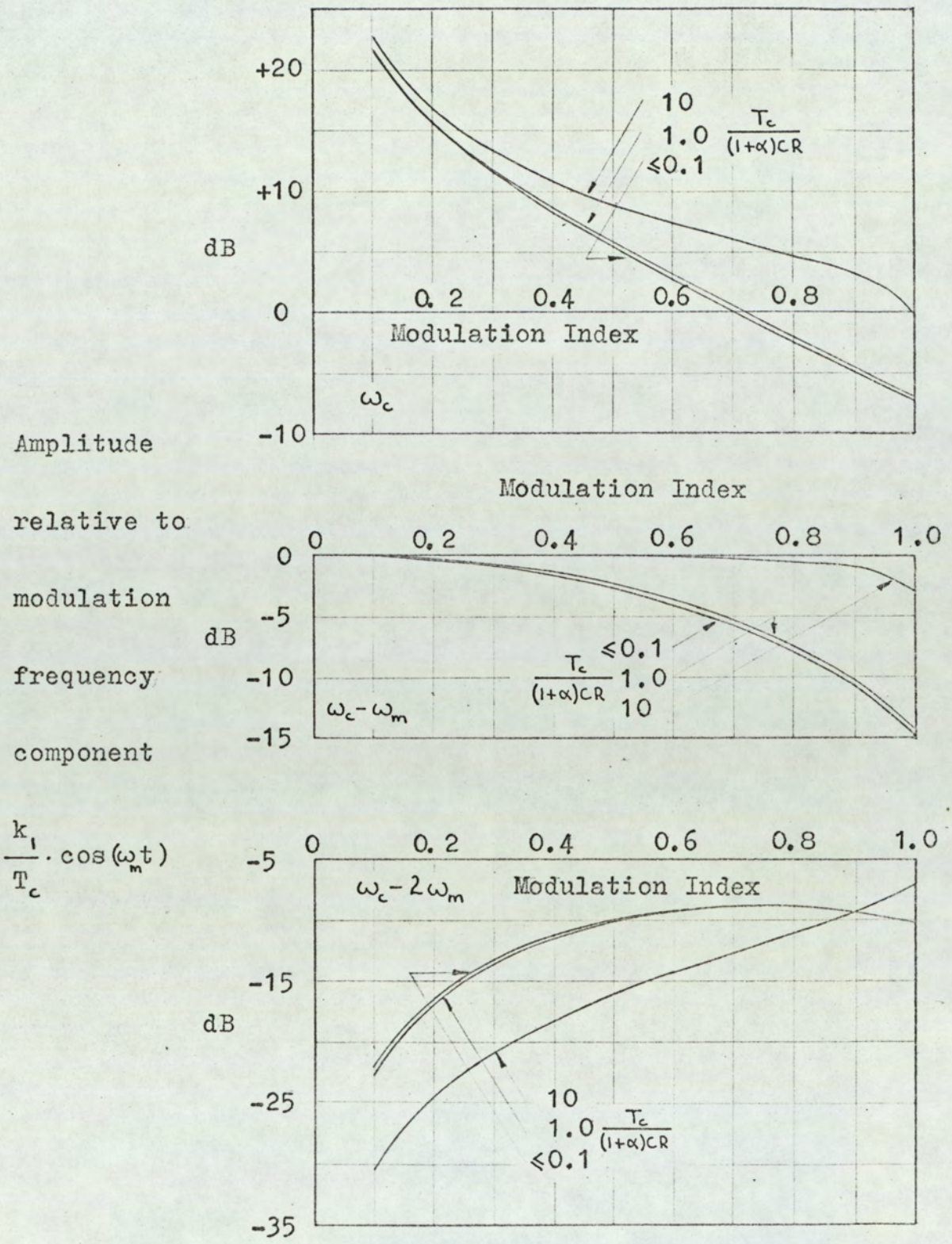

Fig.4.2.4(a). Amplitude of components at the repetition frequency and sidebands for single-edge modulation system with finite gain integrator.

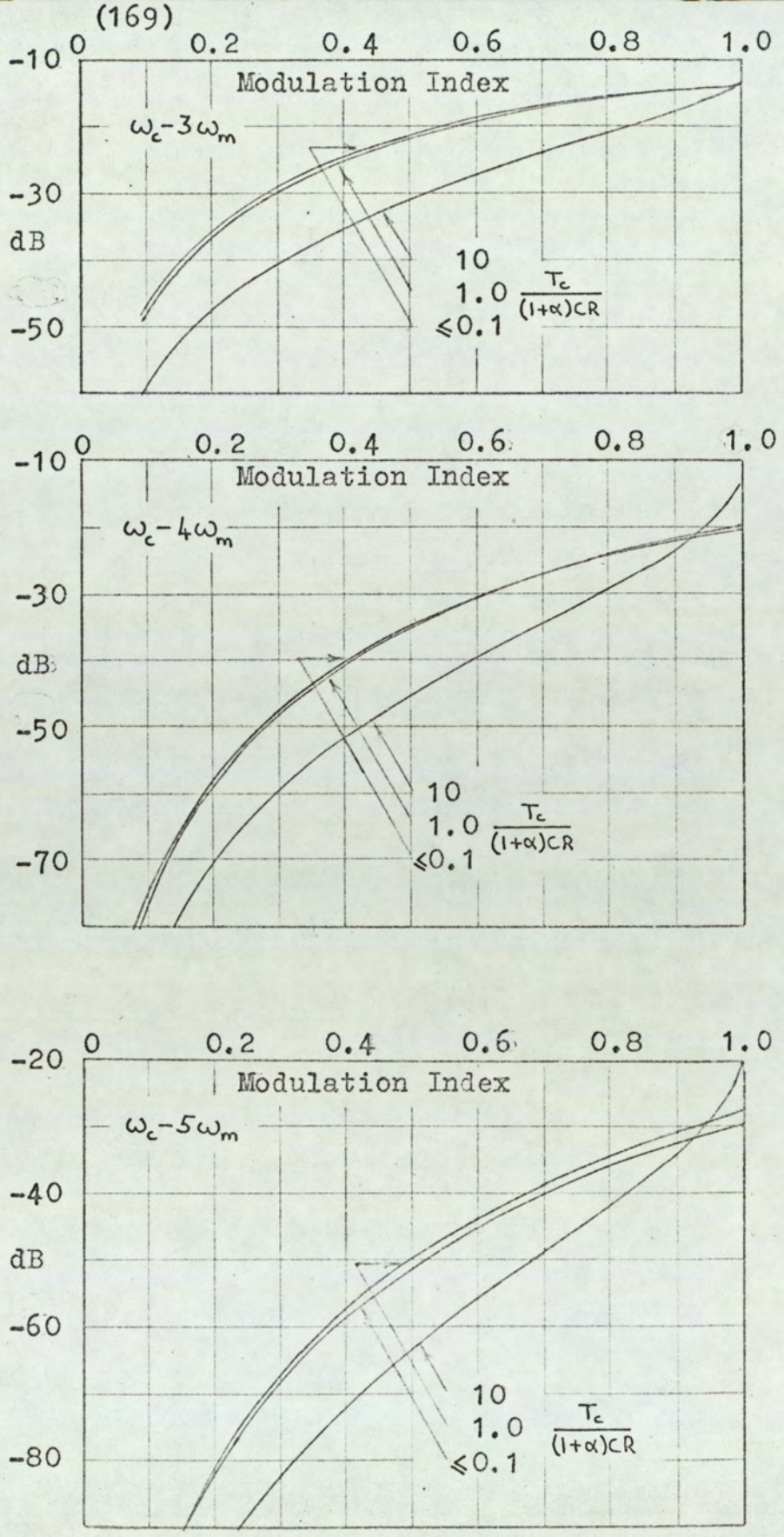

Amplitude relative to modulation frequency component $\frac{k_1}{T_c}\cos(\omega_m t)$

Fig.4.2.4(b). Amplitude of sideband components for single-edge modulation system with finite integrator gain.

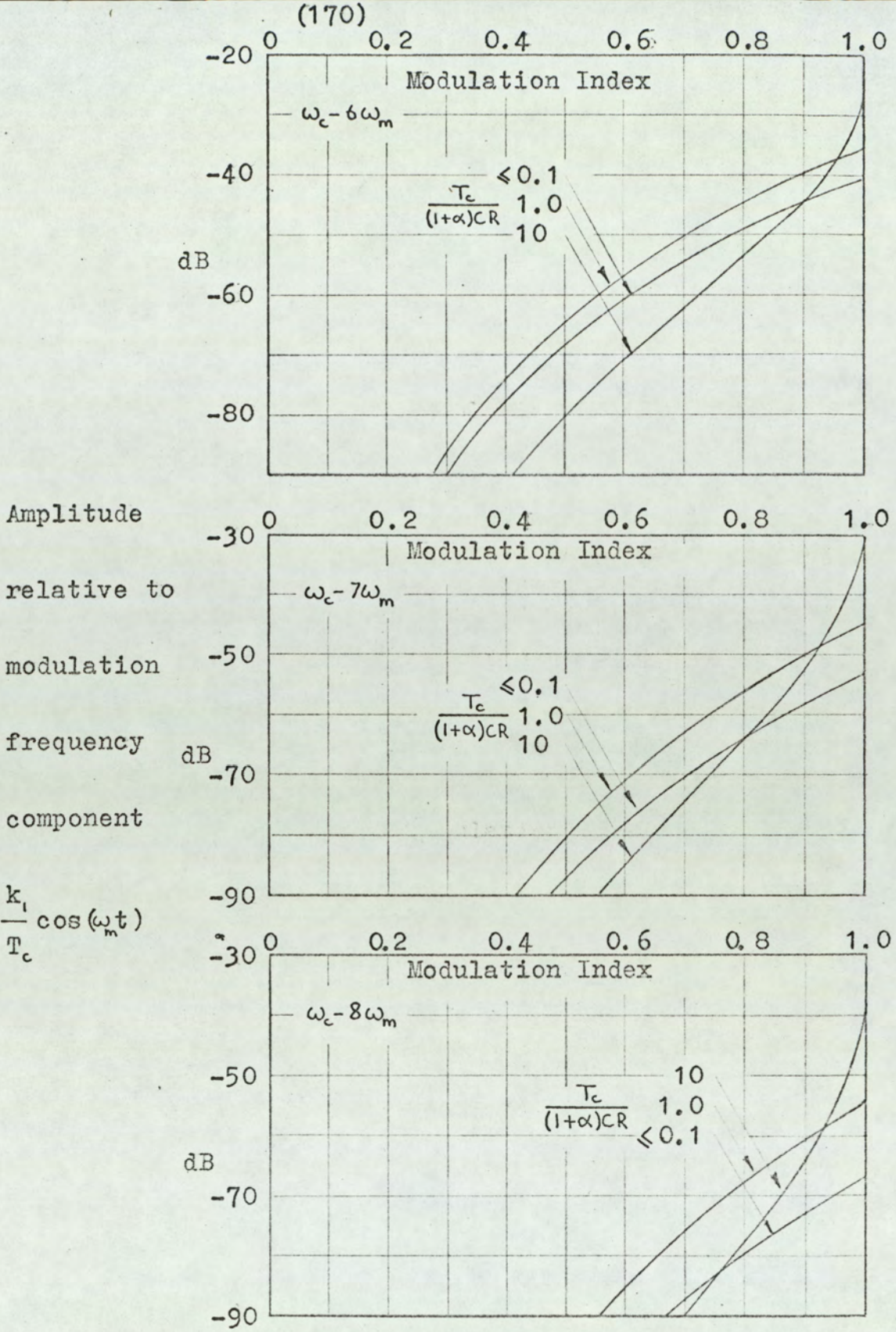

Amplitude relative to modulation frequency component $\frac{k_1}{T_c}\cos(\omega_m t)$

Fig.4.2.4(c). Amplitude of sideband components for single-edge modulation system with finite integrator gain.

4.2.2. Double-edge Modulation

It is shown in section 3.1.2. (equations 3.1.33. and 3.1.34.) that the positions of the leading and trailing edges of the pulses, t_1 and t_2 respectively, in a double-edge modulation system with finite integrator gain are given by the expressions:

$$\frac{t_1}{T_c} = -\frac{(1+\alpha)CR}{T_c}\left\{\log\frac{1}{2}\left[1+\exp\left(\frac{-T_c}{(1+\alpha)CR}\right)\right]+\log\left(1-M.K\right)\right\} \qquad (4.2.18(a))$$

$$\frac{t_2}{T_c} = \frac{1}{2}-\frac{(1+\alpha)CR}{T_c}\left\{\log\frac{1}{2}\left[1+\exp\left(\frac{-T_c}{(1+\alpha)CR}\right)\right]+\log\left(1+M.K\right)\right\} \qquad (4.2.18(b))$$

$$K = \frac{1-\exp\left(\frac{-T_c}{2(1+\alpha)CR}\right)}{1+\exp\left(\frac{-T_c}{2(1+\alpha)CR}\right)} \qquad (4.2.19)$$

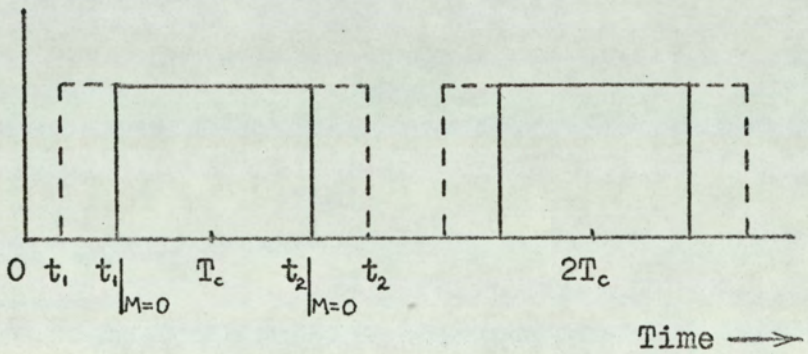

Fig.4.2.5. Double-edge pulse-length modulated wavetrain.

From fig. 4.2.5., equation 4.2.18(a). and equation 4.2.18(b), the time deviations t_{dl} and t_{dt}, of the leading and trailing pulse edges respectively, are:

$$t_{dl} = t_1\Big|_{M=0} - t_1 \qquad (4.2.20(a))$$

$$\frac{t_{dl}}{T_c} = \frac{(1+\alpha)CR}{T_c}\log\left(1-M.K\right) \qquad (4.2.20(b))$$

$$t_{dt} = t_2 - t_2\Big|_{M=0} \qquad (4.2.21(a))$$

$$\frac{t_{dt}}{T_c} = -\frac{(1+\alpha)CR}{T_c}\log\left(1+M.K\right) \qquad (4.2.21(b))$$

The unmodulated pulse length T_o is:

$$T_o = t_2\Big|_{M=0} - t_1\Big|_{M=0} \qquad (4.2.22(a))$$

$$T_o = \frac{T_c}{2} \qquad (4.2.22(b))$$

If the modulating input to the system is a cosine wave, then the modulation index is a time function $M.\cos(\omega_m t)$. The expressions for the time deviations of the leading and trailing pulse edges become:

$$t_{dl} = (1+\alpha)CR.\log\left[1-M.K.\cos(\omega_m t)\right] \qquad (4.2.23)$$

$$t_{dt} = -(1+\alpha)CR\log\left[1+M.K\cos(\omega_m t)\right] \qquad (4.2.24)$$

Substituting equations 4.2.22., 4.2.23., and 4.2.24. in equation 4.1.1. gives the following expression for the frequency spectrum of a double-edge pulse-length modulated wavetrain of 2N + 1 pulses, where the sampling waveform is produced by a finite gain integrator.

$$F(t) = \frac{1}{2\pi}\int_{-\infty}^{\infty} \frac{\sin\left(N+\frac{1}{2}\right)\omega T_c}{\sin\left(\frac{\omega T_c}{2}\right)} \cdot \frac{1}{j\omega} \times$$

$$\left\{\exp\left[j\omega\left(t + \frac{T_c}{4} + (1+\alpha)CR.\log\left[1 - M.K.\cos(\omega_m t)\right]\right)\right]\right.$$

$$\left.\exp\left[j\omega\left(t - \frac{T_c}{4} + (1+\alpha)CR.\log\left[1 + M.K.\cos(\omega_m t)\right]\right)\right]\right\} d\omega \qquad (4.2.25)$$

The limit of equation 4.2.25. as N tends to infinity will not be derived here since the limiting process for similar expressions is considered in detail in the literature[49,56]. Following the methods given in references 49 and 56 the limit of equation 4.2.25. is:

$$F(t) = \frac{1}{j2\pi}\sum_{p=-\infty}^{\infty} \frac{1}{p}\left\{\exp\left[jp\omega_c\left(t + \frac{T_c}{4} + (1+\alpha)CR.\log\left[1 - M.K.\cos(\omega_m t)\right]\right)\right] -\right.$$

$$\left.\exp\left[jp\omega_c\left(t - \frac{T_c}{4} + (1+\alpha)CR.\log\left[1 + M.K.\cos(\omega_m t)\right]\right)\right]\right\} \qquad (4.2.26)$$

where $\omega_c = \frac{2\pi}{T_c}$, the angular repetition frequency of the pulse train.

Making use of the expansion[57]:

$$\log\left(r^2+s^2+2r.s\right) = 2\log(r) - 2\sum_{n=1}^{\infty}\left(\frac{s}{r}\right)^n \frac{\cos(n\theta)}{n} \qquad (4.2.27)$$

for $\left|\frac{s}{r}\right| < 1$

the frequency spectrum given by equation 4.2.26. may be rewritten as:

$$F(t)=\frac{1}{2\pi j}\sum_{p=-\infty}^{\infty}\frac{1}{p}\left\{\exp\left[jp\omega_c\left(t+\frac{T_c}{4}-\sum_{n=0}^{\infty}k_n.\cos(n\omega_m t)\right)\right]-\right.$$

$$\left.\exp\left[jp\omega_c\left(t-\frac{T_c}{4}-\sum_{n=0}^{\infty}(-1)^n k_n.\cos(n\omega_m t)\right)\right]\right\} \qquad (4.2.28)$$

where

$$k_o = -(1+\alpha)CR.\log\left\{\frac{\frac{1}{2}(M.K)^2}{1-\sqrt{\left[1-(M.K)^2\right]}}\right\} \qquad (4.2.29(a))$$

$$k_n = (1+\alpha)CR\,\frac{2}{n}\left\{\frac{1}{MK}-\sqrt{\left[\left(\frac{1}{MK}\right)^2-1\right]}\right\}^n \qquad (4.2.29(b))$$

It is shown in Appendix 5 that manipulation of equation 4.2.28. in the general form is extremely difficult. In order to ease the problem, the assumption is made that the non-linearity of the sampling waveform is such that an adequate representation is obtained by taking only the first three terms containing harmonics of the modulation frequency. Therefore equation 4.2.28. becomes:

$$F(t) \triangleq \frac{1}{2\pi j} \sum_{p=-\infty}^{\infty} \frac{1}{p} \left\{ \exp\left[jp\omega_c \left(t - \frac{T_c}{4} - \sum_{n=0}^{3} k_n . \cos(n\omega_m t) \right) \right] \right.$$

$$\left. - \exp\left[jp\omega_c \left(t - \frac{T_c}{4} - \sum_{n=0}^{3} (-1)^n \, k_n . \cos(n\omega_m t) \right) \right] \right\} \qquad (4.2.30)$$

The rearrangement of equation 4.2.30 into a useful form is considered in detail in Appendix 5, and only the result is quoted here:

$$F(t) \triangleq \frac{1}{2} - \frac{k_1}{T_c} \cos(\omega_m t) \; \frac{k_3}{T_c} \cos(3\omega_m t) \; +$$

$$\frac{2}{\pi} \sum_{p=1}^{\infty} \frac{1}{p} \left\{ \sum_{\substack{e,f,g \\ =-\infty}}^{\infty} J_e(p\omega_c k_1) \, J_f(p\omega_c k_2) \, J_g(p\omega_c k_3) \times \right.$$

$$\left. \sin\left[\frac{\pi}{2}(p-e-g) \right] \cos\left[\left(p\omega_c + [e+2f+3g]\omega_m \right) t - p\omega_c k_o - f\frac{\pi}{2} \right] \right\} \qquad (4.2.31)$$

where e, f and g are integer variables, and the summation involving e, f and g is over all positive and negative combinations of the integer variables.

The constant term ($\frac{1}{2}$), in the spectrum, arises from the manner in which the pulse train is specified. If the pulse train had been specified as having an amplitude of ± 1 instead of 0 and 1, then the constant term would be zero. It is of interest to note that only odd harmonics of the modulation frequency are present in the frequency spectrum. Components

are also present at all the harmonics $p\omega_c$ of the repetition frequency, plus sideband components at $p\omega_c \pm (e + 2f + 3g)\omega_m$. The sidebands of most interest in a pulse-length modulation system for use as an amplifier are the lower sidebands of the repetition frequency (i.e. $p = 1$). Now, as a result of the term $\sin \frac{\pi}{2} (p - e - g)$, sidebands of the repetition frequency only exist when $(e + g)$ is an even number. For even values of $(e + g)$, the only sidebands present are those corresponding to even harmonics of the modulation frequency (i.e. $\omega_c - 2\omega_m$, $\omega_c - 4\omega_m$, $\omega_c - 6\omega_m$, etc.).

The amplitudes of the components at the modulation frequency and its harmonics are not linearly related to the modulation index, as can be seen from equations 4.2.29(b). and 4.2.31. The amplitude of the modulation frequency component $\frac{k_1}{T_c}$ is shown in fig. 4.2.6. as a function of the modulation index . . . . and the normalised time constant $\frac{T_c}{(1 + \alpha)CR}$. The diagram shows that, even when the normalised time constant is as large as 1.0, the amplitude of the fundamental component is still very close to the ideal value of $\frac{M}{2}$.

The second harmonic distortion is zero since no second harmonic term exists in the frequency spectrum. The third harmonic distortion factor DF_3 is defined as:

$$DF_3 = \frac{k_3}{k_1} \qquad (4.2.32)$$

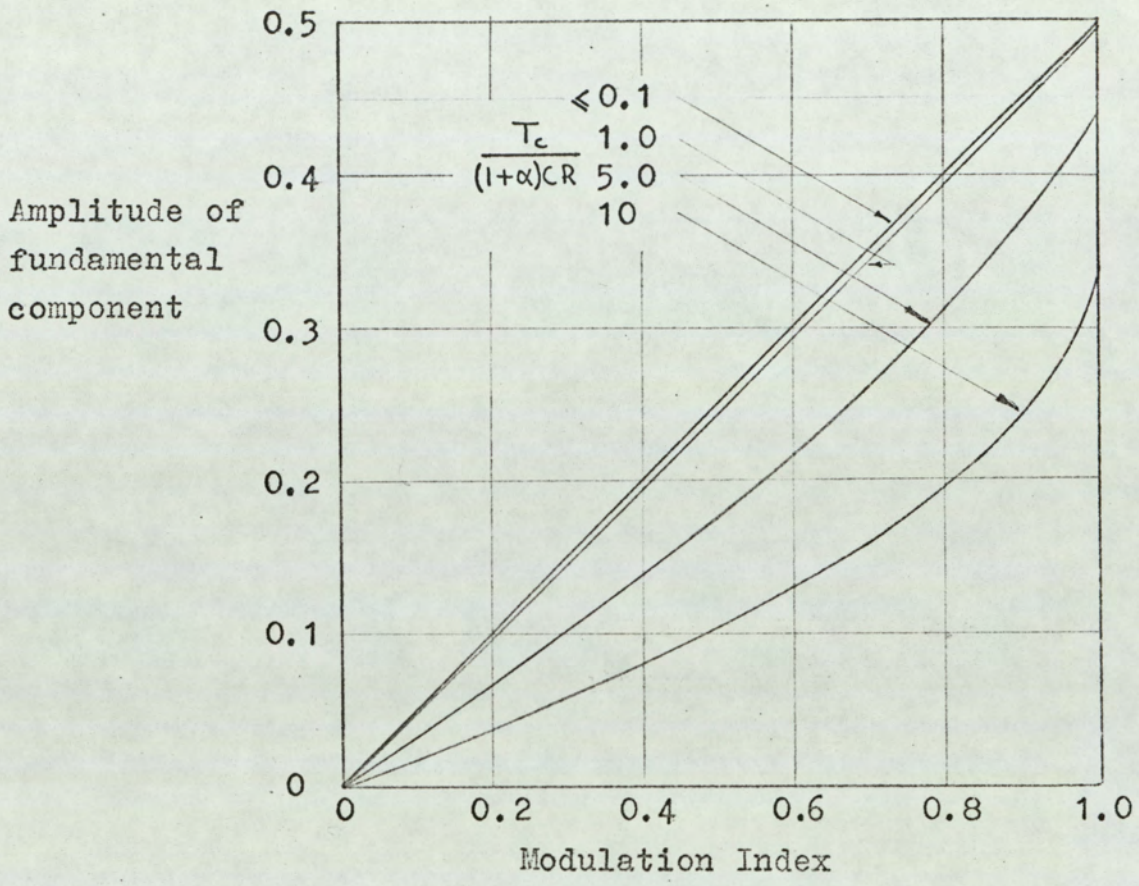

Fig.4.2.6. Amplitude of fundamental component for double-edge modulation system with finite integrator gain

Substituting equations 3.2.29(b). in equation 3.2.32. gives:

$$DF_3 = \frac{1}{3}\left\{\frac{1}{MK} - \sqrt{\left[\left(\frac{1}{MK}\right)^2 - 1\right]}\right\} \qquad (4.2.33)$$

Fig. 4.2.7. shows the third harmonic distortion factor DF_3 plotted as a function of the normalised time constant $\frac{T_c}{(1+\alpha)CR}$ and the modulation index M.

Figs. 4.2.8(a). and (b) show the relative amplitudes of the repetition frequency component and the sideband components. the reference level is the amplitude of the modulation frequency component $\frac{k_1}{T_c}\cos(\omega_m t)$. The reasons for choosing this particular reference level are discussed in section 4.2.1. The effect of the finite integrator gain is most marked on the higher order sidebands (i.e. $\omega_c - 6\omega_m$, $\omega_c - 8\omega_m$). For values of normalised time constant less than 0.1, the effect is negligible, but for values greater than 1.0, a significant increase in the level of the sidebands is produced.

Numerical evaluation of the various sideband components from equation 4.2.31. entails a considerable amount of computation since there are a large number of combinations of e, f and g which give rise to terms that make a significant contribution to a particular sideband component. All of these contributions must be added in the correct phase in order to calculate the amplitude of the particular sideband. The problems involved are discussed in more detail in Appendix 5.

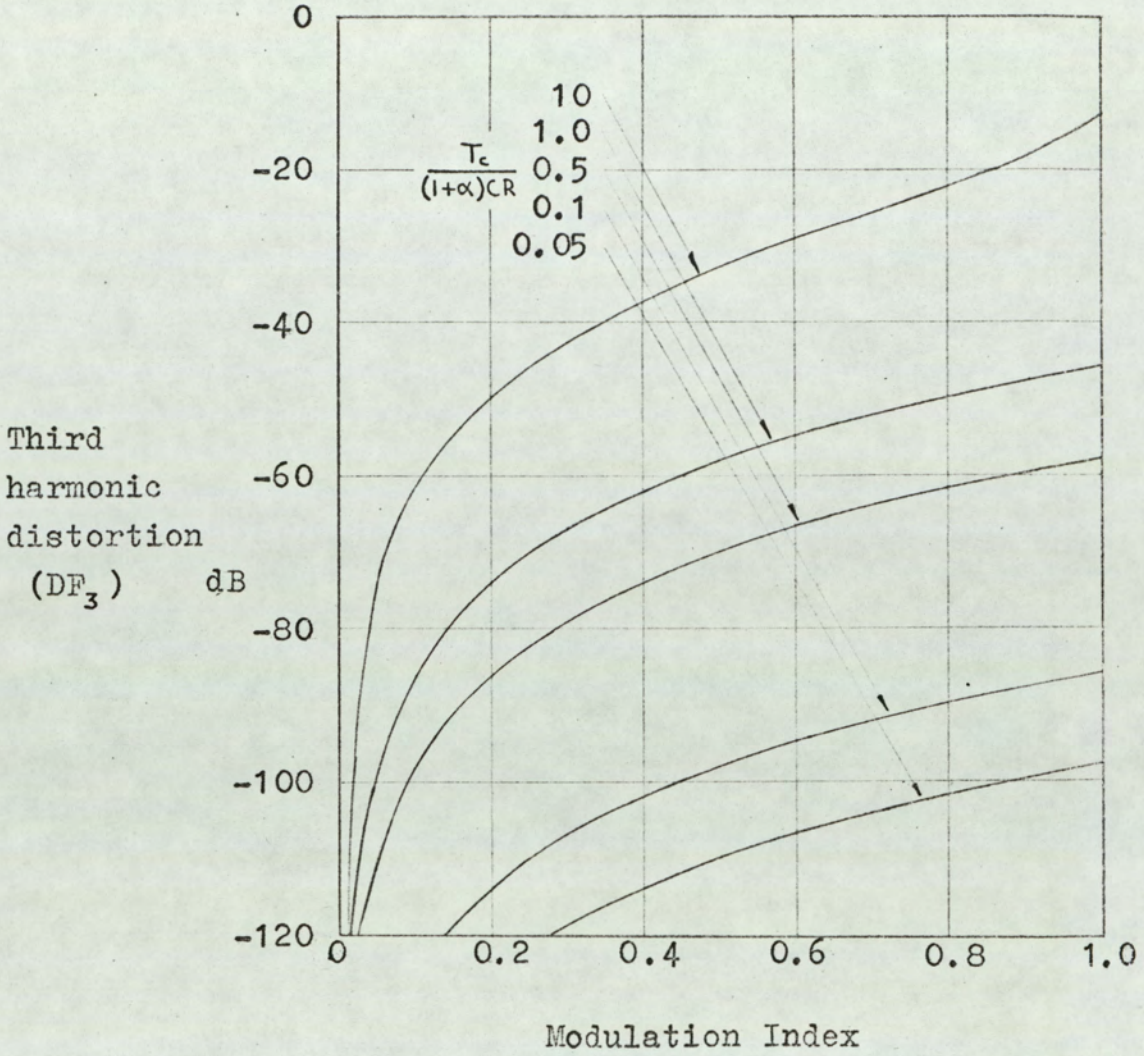

Fig.4.2.7. Third harmonic distortion in a double-edge modulation system with finite integrator gain.

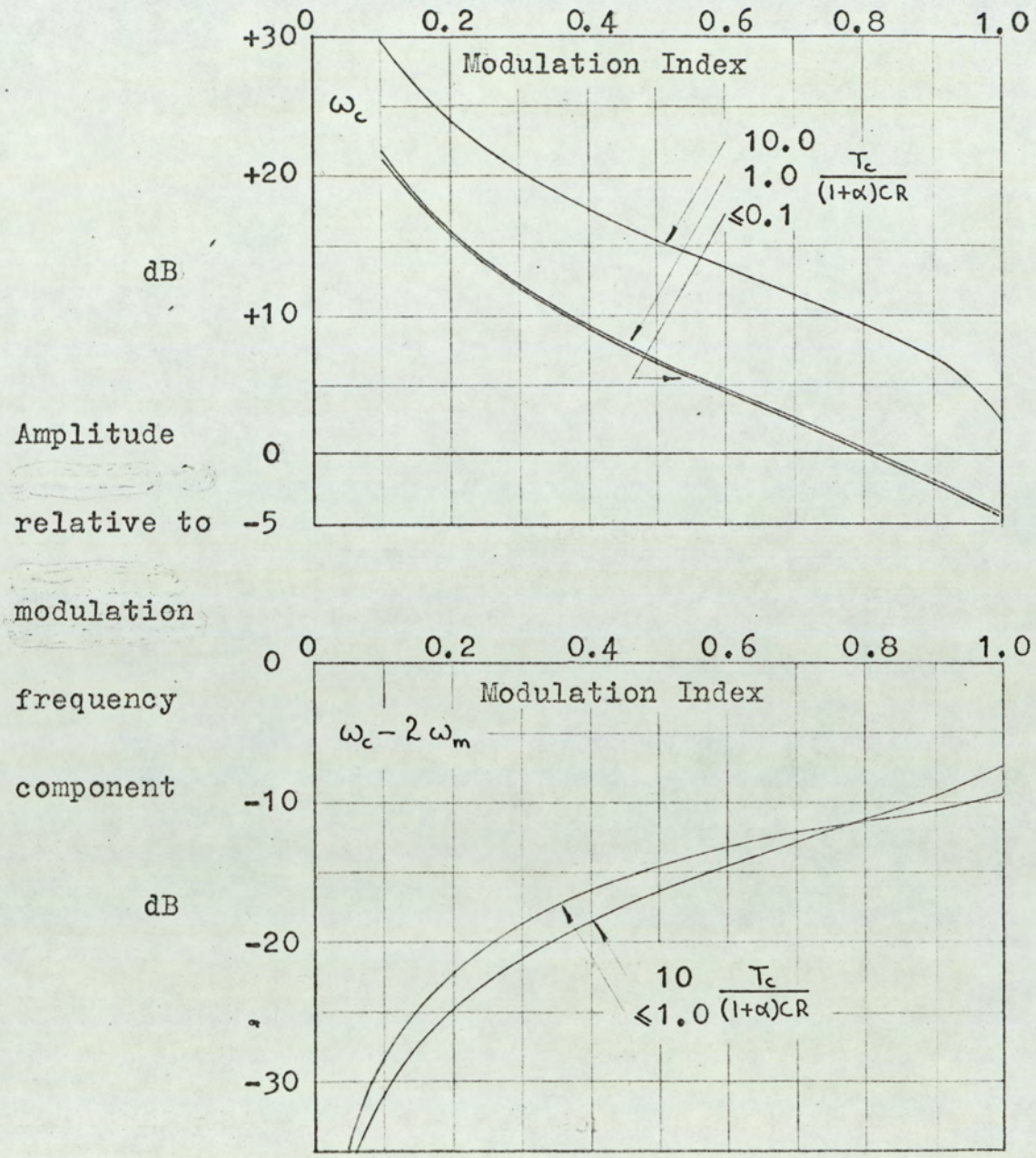

Fig.4.2.8(a). Amplitude of components at the repetition frequency and sidebands for double-edge modulation system with finite integrator gain.

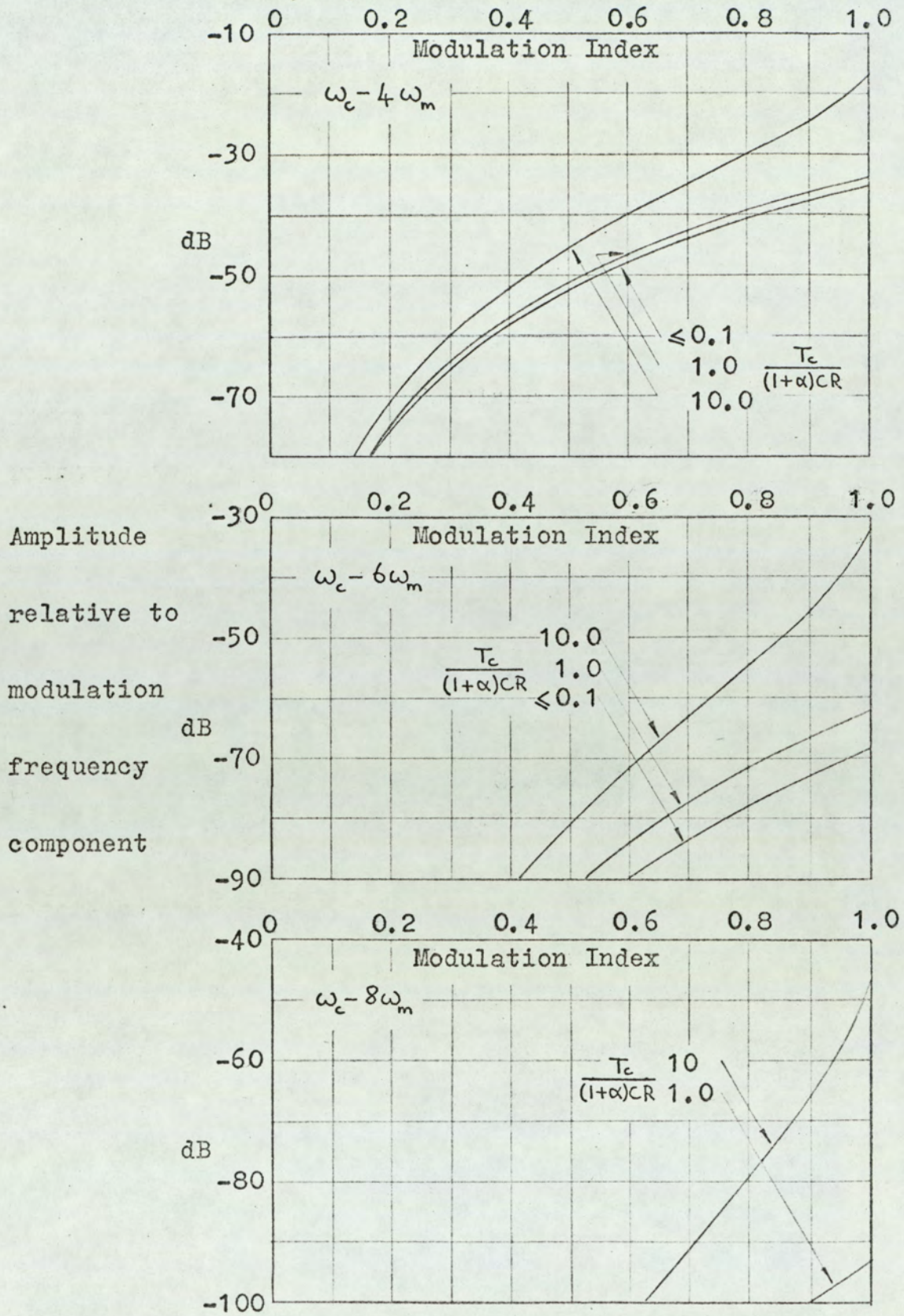

Amplitude relative to modulation frequency component

Fig.4.2.8(b). Amplitude of sideband components for double-edge modulation system with finite integrator gain.

4.2.3. Conclusions

Expressions have been derived for the frequency spectra of the outputs of pulse-length modulation systems which utilise finite gain operational integrators. The spectrum of the output of the single-edge modulation system contains a component at the modulation frequency and components at harmonics of the modulation frequency. The component at the modulation frequency increases towards the value of O.25 as the normalised time constant $\frac{T_c}{(1+\alpha)CR}$ is reduced. The harmonic distortion components decrease with decreasing values of $\frac{T_c}{(1+\alpha)CR}$. Terms also exist at all harmonics $p\omega_c$ of the pulse repetition frequency, together with sidebands of the form $p\omega_c \pm n\omega_m$ associated with each harmonic. It is shown that for values of normalised time constant less than 0.1, the finite integrator gain has negligible effect on the amplitude of the sideband components.

The spectrum for the double-edge modulation system contains a component at the modulation frequency and components at only odd harmonics of the modulation frequency. The spectrum also contains terms at all harmonics $p\omega_c$ of the pulse repetition frequency, plus sidebands of the form $p\omega_c \pm n\omega_m$. From the point of view of distortion, the most important sideband components are the lower sidebands of the repetition frequency (i.e. $\omega_c - n\omega_m$). For double-edge modulation these components only exist when n is even.

Comparison of the results of the analysis of the single-

edge modulation system and the results for the double-edge modulation system shows that the harmonic distortion and sideband components are significantly smaller for double-edge modulation. Adding to this the fact that not all the harmonic distortion and sideband components are present with double-edge modulation, it can be seen that double-edge modulation is inherently superior to single-edge modulation.

4.3. Distortion due to Finite Input and Output Resistance of the Integrator Amplifier

4.3.1. Single-edge Modulation

It is shown in section 3.2.1. (equation 3.2.9.) that the position t_1 of the leading edge of the pulse in a single-edge modulation system, with finite values of amplifier input and output resistance, is given by the expression:

$$\frac{t_1}{T_c} = -\frac{T_e}{T_c}\left\{\log\frac{1}{2}\left[1-\exp\left(\frac{-T_c}{T_e}\right)\right]+\log\left(1-M.K\right)\right\} \qquad (4.3.1)$$

where

$$T_e = \frac{(1+\alpha)CR}{1+R/R_1} + CR_o \qquad (4.3.2)$$

$$K = \frac{1-\exp\left(\frac{-T_c}{T_e}\right)}{1-\exp\left(\frac{-T_c}{T_e}\right)} \qquad (4.3.3)$$

Comparing the above expression for t_1 with the corresponding one for a system with infinite amplifier input resistance and zero output resistance (equation 4.2.1(a).) shows that the effect of the finite resistances is simply to modify the normalised time constant from $\frac{T_c}{(1+\alpha)CR}$ to $\frac{T_c}{T_e}$. As a result of this similarity, the expression for the frequency spectrum can be written down by inspection of equations 4.2.12., 4.2.10(a) and (b) of section 4.2.1.

$$F(t) \triangleq \frac{1}{T_c}\left[T_o - k_o - k_1\cos(\omega_m t) - k_2\cos(2\omega_m t) - k_3\cos(3\omega_m t)\right] -$$

$$\frac{1}{\pi}\sum_{p=1}^{\infty}\frac{1}{p}\sin\left[p\omega_c\left(t-\frac{T_o}{2}\right)\right] -$$

$$\frac{1}{\pi}\sum_{p=1}^{\infty}\frac{1}{p}\left\{\sum_{\substack{e,f,g\\=-\infty}}^{\infty} J_e(p\omega_c k_1)\, J_f(p\omega_c k_2)\, J_g(p\omega_c k_3) \times \right.$$

$$\left.\sin\left[\left(p\omega_c+[e-2f-3g]\omega_m\right)t + p\omega_c\left(\frac{T_o}{2}-k_o\right)-(e-f-g)\frac{\pi}{2}\right]\right\} \qquad (4.3.4)$$

where

$$k_o = -T_e.\log\left\{\frac{\frac{1}{2}(M.K)^2}{1-\sqrt{\left[1-(M.K)^2\right]}}\right\} \qquad (4.3.5(a))$$

$$k_n = T_e\frac{2}{n}\left\{\frac{1}{M.K} - \sqrt{\left[\left(\frac{1}{M.K}\right)^2 - 1\right]}\right\} \qquad (4.3.5(b))$$

$$T_o = T_c + T_e.\log\frac{1}{2}\left[1+\exp\left(\frac{-T_c}{T_e}\right)\right] \qquad (4.3.5(c))$$

Since the spectrum for the system with finite values of amplifier input and output resistance has the same form as the spectrum for the system with infinite amplifier input resistance and zero output resistance, figs. 4.2.2., 4.2.3., 4.2.4(a)., (b) and (c) may be used to determine the amplitude of the spectral components. It is merely necessary to replace $\frac{T_c}{(1+\alpha)CR}$ in the diagrams with the modified normalised time constant $\frac{T_c}{T_e}$. The forms of the diagrams of the various spectral components are discussed

in section 4.2.1. This discussion is valid for the system with finite amplifier input and output resistance, bearing in mind that the normalised time constant is modified by the amplifier resistances.

The effects of the finite amplifier resistances on the normalised time constant $\frac{T_c}{T_e}$ are readily deduced from equation 4.3.2. The finite value of amplifier input resistance increases the value of the normalised time constant, hence increasing the system harmonic distortion (see fig. 4.2.3.). The finite value of output resistance decreases the normalised time constant, hence decreasing the system harmonic distortion. The effect of the finite resistances on the sideband components cannot be stated in general terms since the form of the effect is dependent on the modulation index M. (see figs. 4.2.4(a), (b) and (c).)

4.3.2. Double-edge Modulation

It is shown in the static analysis of a double-edge pulse-length modulation system with finite values of amplifier input and output resistance (section 3.2.2., equations 3.2.30. and 3.2.31.), that the positions of the leading and trailing edges of the pulses, t_1 and t_2 respectively are given by the expressions:

$$\frac{t_1}{T_c} = -\frac{T_e}{T_c}\left\{\log\frac{1+\exp\left(\frac{-T_c}{2T_e}\right)}{2\left(1+\frac{CR_o}{\alpha T_e}\right)} + \log\left(1-M\phi K\right)\right\} \qquad (4.3.6)$$

$$\frac{t_2}{T_c} = \frac{1}{2} - \frac{T_e}{T_c}\left\{\log\frac{1+\exp\left(\frac{-T_c}{2T_e}\right)}{2\left(1+\frac{CR_o}{T_e}\right)} + \log\left(1+M\phi K\right)\right\} \qquad (4.3.7)$$

where

$$\phi = \frac{1-\frac{2\left(1+\frac{CR_o}{\alpha T_e}\right)}{1+\exp\left(\frac{-T_c}{2T_e}\right)}}{1-\frac{2}{1+\exp\left(\frac{-T_c}{2T_e}\right)}} \qquad (4.3.8)$$

$$T_e = \frac{(1+\alpha)CR}{1+R/R_1} + CR_o \qquad (4.3.9)$$

$$K = \frac{1-\exp\left(\frac{-T_c}{2T_e}\right)}{1+\exp\left(\frac{-T_c}{2T_e}\right)} \qquad (4.3.10)$$

It is shown in the spectrum analysis of double-edge pulse-length modulations systems with finite integrator gain (section 4.2.2., equation 4.2.20(a).) that the time deviation t_{dl} of the leading edge of the pulse is given by:

$$t_{dl} = t_1\Big|_{M=0} - t_1$$

Substituting equation 4.3.6. in the above expression gives:

$$\frac{t_{dl}}{T_c} = \frac{T_e}{T_c} \log\left(1 - M\phi K\right) \qquad (4.3.11)$$

The time deviation t_{dt} of the pulse trailing edge is given by equation 4.2.21(a) of section 4.2.2.

$$t_{dt} = t_2 - t_2\Big|_{M=0}$$

Therefore, from equation 4.3.7.:

$$\frac{t_{dt}}{T_c} = -\frac{T_e}{T_c} \log\left(1 + M\phi K\right) \qquad (4.3.12)$$

Equation 4.2.22(a) (section 4.2.2.) expresses the unmodulated pulse length as:

$$T_o = t_2\Big|_{M=0} - t_1\Big|_{M=0}$$

Substituting equations 4.3.6. and 4.3.7. in the above expression gives:

$$T_o = \frac{T_c}{2} \qquad (4.3.13)$$

Comparison of equations 4.3.11., 4.3.12., and 4.3.13., with the corresponding expressions for the double-edge modu-

lation system with infinite amplifier input resistance and zero output resistance (equations 4.2.20(b)., 4.2.21(b). and 4.2.22(b), section 4.2.2.) shows that the expressions are identical in form. The effect of the finite resistances is to modify the normalised time constant from $\frac{T_c}{(1+\alpha)CR}$ to $\frac{T_c}{T_e}$, and to modify the modulation index from M to $M\phi$. As a result of this similarity, the frequency spectrum may be written down by inspection of equation 4.2.31. (section 4.2.2.) for the spectrum of a system with infinite amplifier input resistance and zero output resistance. Therefore:

$$F(t) \triangleq \frac{1}{2} - \frac{k_1}{T_c}\cos(\omega_m t) - \frac{k_3}{T_c}\cos(3\omega_m t) +$$

$$\frac{2}{\pi}\sum_{p=1}^{\infty}\frac{1}{p}\left\{\sum_{\substack{e,f,g\\=-\infty}}^{\infty} J_e(p\omega_c k_1)\, J_f(p\omega_c k_2)\, J_f(p\omega_c k_3) \times \right.$$

$$\left. \sin\left[\frac{\pi}{2}(e-f-g)\right]\cos\left[\left(p\omega_c-[e-2f-3g]\omega_m\right)t - p\omega_c k_o - f\frac{\pi}{2}\right]\right\} \qquad (4.3.14)$$

where

$$k_o = -T_e \log\left\{\frac{\frac{1}{2}(M\phi K)^2}{1-\sqrt{[1-(M\phi K)^2]}}\right\} \qquad (4.3.15(a))$$

$$k_n = T_e \frac{2}{n}\left\{\frac{1}{M\phi K} - \sqrt{\left[\left(\frac{1}{M\phi K}\right)^2 - 1\right]}\right\}^n \qquad (4.3.15(b))$$

The above expression for the frequency spectrum is an approximation. The reasons for deriving an approximate

expression are discussed in section 4.2.2. Since the finite amplifier resistances simply modify the normalised time constant and the modulation index, the various components in the frequency spectrum can be evaluated from figs. 4.2.6., 4.2.7., 4.2.8(a). and (b) for the system with infinite amplifier input resistance and zero output resistance. It is merely necessary to replace the system parameters $\frac{T_c}{(1+\alpha)CR}$ and M, in the diagrams, with the modified parameters $\frac{T_c}{T_e}$ and $M\phi$ respectively. The forms of the diagrams of the various spectral components are discussed in section 4.2.2., and this discussion is valid for the system with finite values of amplifier input and output resistance, bearing in mind that the system parameters are modified by the amplifier resistances. A further point which must be considered is that the expressions derived, in the static analysis section, for the position of the leading and trailing edges of the pulse are not valid for all values of modulation index. Fig. 3.2.11. of section 3.2.2. shows the maximum value of the modulation index for which the analytical expressions for the positions of the pulse edges are valid. This maximum value of the modulation index also applies to the spectrum analysis since the spectrum analysis has been derived from the results of the static analysis.

The modulation index modifying factor ϕ may be evaluated from fig. 3.2.9. of the static analysis section (section 3.2.2.). Interpretation of fig. 3.2.9. is facilitated by making reference to equations 3.2.39. and 3.2.40. (section 3.2.2.) which express the parameters $\frac{CR_0}{\alpha T_e}$ and $\frac{T_c}{T_e}$

directly in terms of the system parameters.

$$\frac{C R_o}{\alpha T_e} = \frac{1}{\alpha\left[\frac{(1+\alpha)^{R}/R_o}{1+{}^{R}/R_1} + 1\right]} \qquad (4.3.16)$$

$$\frac{T_c}{T_e} = \frac{T_c}{CR}\left[\frac{1}{\frac{(1+\alpha)}{1+{}^{R}/R_1} + \frac{R_o}{R}}\right] \qquad (4.3.17)$$

The factor ϕ increases with increasing values of amplifier output resistance R_o thus increasing the effective modulation index $M\phi$ and the system harmonic distortion (see fig. 4.2.7., section 4.2.2.). However, the output resistance decreases the normalised time constant $\frac{T_c}{T_e}$ which leads to a decrease in harmonic distortion. It is not possible to say, in general terms, what overall effect the output resistance has, since this depends on the other system parameters. However, fig. 3.2.9. (section 3.2.2.) shows that relatively large values of amplifier output resistance can be tolerated without making ϕ significantly greater than unity.

The finite value of amplifier input resistance increases the normalised time constant $\frac{T_c}{T_e}$ and hence increases the system harmonic distortion. The second effect of the input resistance is to increase the value of the modulation index modifying factor ϕ which also leads to an increase in harmonic distortion.

Due to the manner in which the various parameters interact, the overall effect of the finite amplifier resistances on the sideband frequency components cannot be stated in

general terms. When designing a system it is therefore necessary to examine the effect of the resistances for the particular values of the other system parameters that are to be used in the design.

4.3.3. Conclusions

The spectra of pulse-length modulated wavetrains, produced by systems with finite values of amplifier input resistance, output resistance and gain, have been derived in terms of the spectra for systems with ideal values of amplifier input and output resistance. The effect of the amplifier input and output resistance on the overall system performance cannot be stated in general terms since the nature of the effect depends on the actual values of the system parameters. The most striking feature of the results is that a relatively large value of output resistance can be tolerated without producing any significant effect on the system performance. In the design of a system it would seem, from the analytical results, that amplifier output resistance is not a parameter which will give rise to practical problems. If the effect of the amplifier output resistance is negligible then the amplifier input resistance simply reduces the effective integrator time constant from $(1+\alpha)CR$ to $\frac{(1+\alpha)CR}{1+R/R_1}$. With the aid of the analytical results, the choice of values of the parameters to give a specified level of harmonic and sideband distortion is a straightforward matter.

4.4. Generalised Spectrum Analysis of Non-linear Pulse-Length Modulation

The frequency spectrum of $2N + 1$ length-modulated pulses is given by equation 4.1.1. of section 4.1. In a linear system, the time deviations of the pulse edges are linearly related to the modulating signal and the analysis is straightforward[11,49,51]. In a non-linear system, however, the time deviations will not be directly proportional to the modulating signal. It is the objective of this section to develop a generalised spectrum analysis for non-linear systems.

For all the cases analysed in the static analysis section, it is shown that the positions of the pulse edges can be represented by power series in terms of the modulation index M. It will be assumed that, for any non-linear pulse-length modulation system, the positions of the leading and trailing pulses edges, t_1 and t_2 respectively, can be represented by the power series:

$$\frac{t_1}{T_c} = \alpha_0 - \sum_{n=1}^{\infty} \alpha_n M^n \qquad (4.4.1)$$

$$\frac{t_2}{T_c} = \beta_0 + \sum_{n=1}^{\infty} \beta_n M^n \qquad (4.4.2)$$

The signs of the coefficients, α_n and β_n, are defined so that the pulse-length increases for positive values of modulation index M. From fig. 4.4.1., equation 4.4.1., and equation 4.4.2., the time deviations of the pulse edges are:

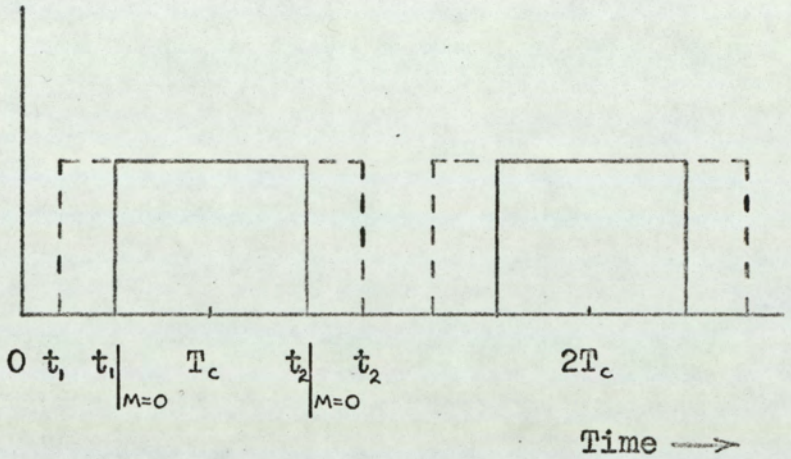

Fig. 4.4.1.

$$\frac{t_{dl}}{T_c} = \frac{t_1}{T_c}\bigg|_{M=0} - \frac{t_1}{T_c} \qquad (4.4.3(a))$$

$$\therefore \quad \frac{t_{dl}}{T_c} = \sum_{n=1}^{\infty} \alpha_n M^n \qquad (4.4.3(b))$$

where t_{dl} is the time deviation of the pulse leading edge.

$$\frac{t_{dt}}{T_c} = \frac{t_2}{T_c} - \frac{t_2}{T_c}\bigg|_{M=0} \qquad (4.4.4(a))$$

$$\frac{t_{dt}}{T_c} = \sum_{n=1}^{\infty} \beta_n M^n \qquad (4.4.4(b))$$

where t_{dt} is the time deviation of the pulse trailing edge.

The unmodulated pulse length T_o is:

$$\frac{T_o}{T_c} = \frac{t_2}{T_c}\bigg|_{M=0} - \frac{t_1}{T_c}\bigg|_{M=0} \qquad (4.4.5)$$

$$\frac{T_o}{T_c} = \beta_o - \alpha_o \qquad (4.4.5)$$

If the system modulating input is a cosine wave, then the modulation index is a time function $M\cos(\omega_m t)$, and the expressions for the time deviations of the pulse edges become:

$$\frac{t_{dl}}{T_c} = \sum_{n=1}^{\infty} \alpha_n M^n \cos^n(\omega_m t) \qquad (4.4.6)$$

$$\frac{t_{dt}}{T_c} = \sum_{n=1}^{\infty} \beta_n M^n \cos^n(\omega_m t) \qquad (4.4.7)$$

Substituting equations 4.4.5., 4.4.4., and 4.4.7. in equation 4.1.1. (section 4.1.) gives the following expression for the frequency spectrum of 2N + 1 pulses whose length is modulated in a non-linear manner.

$$F(t) = \frac{1}{2\pi}\int_{-\infty}^{\infty} \frac{\sin\left(N+\frac{1}{2}\right)\omega T_c}{\sin\left(\frac{\omega T_c}{2}\right)} \cdot \frac{1}{j\omega} \times$$

$$\left\{ \exp\left(j\omega\left[t + \frac{T_o}{2} + T_c \sum_{n=1}^{\infty} \alpha_n M^n \cos^n(\omega_m t)\right]\right) - \right.$$

$$\left. \exp\left(j\omega\left[t - \frac{T_o}{2} - T_c \sum_{n=1}^{\infty} \beta_n M^n \cos^n(\omega_m t)\right]\right)\right\} \qquad (4.4.8)$$

The limit of equation 4.4.8., as N tends to infinity, will not be derived here since the limiting process for similar

expressions is considered in detail in the literature[49,56]. Following the methods of references 49 and 56 the limit of equation 4.4.8. is:

$$F(t)=\frac{1}{j2\pi}\sum_{p=-\infty}^{\infty}\frac{1}{P}\left\{\exp\left[jp\omega_c\left(t-\frac{T_o}{2}-T_c\sum_{n=1}^{\infty}\alpha_n M^n\cos^n(\omega_m t)\right)\right]-\right.$$

$$\left.\exp\left[jp\omega_c\left(t-\frac{T_o}{2}-T_c\sum_{n=1}^{\infty}\beta_n M^n\cos^n(\omega_m t)\right)\right]\right\} \qquad (4.4.9)$$

where

$\omega_c = \frac{2\pi}{T_c}$, the angular pulse repetition frequency.

One possible approach to the problem of obtaining a useful expression from equation 4.4.9. is to convert the power series in terms of $M^n\cos^n(\omega_m t)$ into a Fourier series of the form $k_n.\cos(n\omega_m t)$. This is the procedure that is used in section 4.2. except that the Fourier series is obtained directly from the closed form of the expressions for the time-deviations of the pulse edges rather than from the power series. This approach to the problem leads to expressions which require a considerable amount of computation in order to evaluate the amplitudes of the various components. This is because the expression for the spectrum contains terms of the form:

$$\sum_{\substack{e,f\ldots n\\=-\infty}}^{\infty} J_e(A_1)\,J_f(A_2)\ldots J_n(A_n)\cos\left[p\omega_c t+(e+2f+\ldots)+\phi(e,f,\ldots n)\right]$$

(4.4.10)

The major problem with this form of analysis is that there are a large number of combinations of the integers e, f ..... n which give rise to terms making a significant contribution to a particular sideband component. For each combination of the integers, the product of the Bessel functions must be evaluated and the resulting contributions to the sideband added together with account taken of the phase angle ϕ (e, f, ... n). In fact, equation 4.4.10. is simplified since, in the general form, there are an infinite number of Bessel function terms rather than the finite number, J_e, J_f .... J_n. This comment leads to a further problem - that of deciding how many of the Bessel function terms should be considered, and also deciding what limits should be taken for the integers e, f, ... n if no significant contributions to a particular sideband are to be neglected.

As a result of the compexity of the computational problem involved in the Bessel function analysis, it is worthwhile considering a different approach. Equation 4.4.9., for the spectrum, may be written in terms of only positive values of the integer p; the term corresponding to p = 0 being disregarded temporarily.

$$F(t)=\frac{1}{\pi}\sum_{p=1}^{\infty}\frac{1}{p}\left\{\sin\left[p\omega_c\left(t+\frac{T_o}{2}+T_c\sum_{n=1}^{\infty}\alpha_n M^n.\cos^n(\omega_m t)\right)\right]-\right.$$

$$\left.\sin\left[p\omega_c\left(t-\frac{T_o}{2}-T_c\sum_{n=1}^{\infty}\beta_n M^n\cos^n(\omega_m t)\right)\right]\right\} \qquad (4.4.11)$$

Noting that $\omega_c = \frac{2\pi}{T_c}$, equation 4.4.11. may be rewritten as:

$$F(t)=\frac{1}{\pi}\sum_{p=1}^{\infty}\frac{1}{p}\left\{\sin\left[p\omega_c\left(t+\frac{T_o}{2}\right)\right]\cos\left[p2\pi\sum_{n=1}^{\infty}\alpha_n M^n\cos^n(\omega_m t)\right]\right.$$

$$\cos\left[p\omega_c\left(t-\frac{T_o}{2}\right)\right]\sin\left[p2\pi\sum_{n=1}^{\infty}\alpha_n M^n\cos^n(\omega_m t)\right]-$$

$$\sin\left[p\omega_c\left(t-\frac{T_o}{2}\right)\right]\cos\left[p2\pi\sum_{n=1}^{\infty}\beta_n M^n\cos^n(\omega_m t)\right]-$$

$$\left.\cos\left[p\omega_c\left(t-\frac{T_o}{2}\right)\right]\sin\left[p2\pi\sum_{n=1}^{\infty}\beta_n M^n\cos^n(\omega_m t)\right]\right\} \qquad (4.4.12)$$

The trigonometric expressions containing power series in terms of $M^n \cos^n(\omega_m t)$ may be rewritten as further power series as shown below:

$$\cos\left[p2\pi\sum_{n=1}^{\infty}\alpha_n M^n\cos^n(\omega_m t)\right]=\sum_{k=0}^{\infty}A_k\cos^k(\omega_m t) \qquad (4.4.13(a))$$

$$\cos\left[p2\pi\sum_{n=1}^{\infty}\beta_n M^n\cos^n(\omega_m t)\right]=\sum_{k=0}^{\infty}B_k\cos^k(\omega_m t) \qquad (4.4.13(b))$$

$$\sin\left[p2\pi\sum_{n=1}^{\infty}\alpha_n M^n\cos^n(\omega_m t)\right]=\sum_{k=0}^{\infty}C_k\cos^k(\omega_m t) \qquad (4.4.13(c))$$

$$\sin\left[p2\pi\sum_{n=1}^{\infty}\beta_n M^n\cos^n(\omega_m t)\right]=\sum_{k=0}^{\infty}D_k\cos^k(\omega_m t) \qquad (4.4.13(d))$$

Now the right-hand sides of equations 4.4.13(a), (b), (c) and (d) may be expanded as Fourier series to give:

$$\cos\left[p2\pi\sum_{n=1}^{\infty}\alpha_n M^n\cos^n(\omega_m t)\right]=\frac{E_o}{2}+\sum_{n=0}^{\infty}E_n\cos(n\omega_m t) \qquad (4.4.14(a))$$

$$\cos\left[p2\pi\sum_{n=1}^{\infty}\beta_n M^n\cos^n(\omega_m t)\right]=\frac{F_o}{2}+\sum_{n=0}^{\infty}F_n\cos(n\omega_m t) \qquad (4.4.14(b))$$

$$\sin\left[p2\pi\sum_{n=1}^{\infty}\alpha_n M^n\cos^n(\omega_m t)\right]=\frac{G_o}{2}+\sum_{n=0}^{\infty}G_n\cos(n\omega_m t) \qquad (4.4.14(c))$$

$$\sin\left[p2\pi\sum_{n=1}^{\infty}\beta_n M^n\cos^n(\omega_m t)\right]=\frac{H_o}{2}+\sum_{n=0}^{\infty}H_n\cos(n\omega_m t) \qquad (4.4.14(d))$$

The constant terms are defined in the manner shown for convenience in later equations.

Equations 4.4.14(a), (b), (c) and (d) may be substituted in equation 4.4.12. and the resulting expression rearranged to give:

$$F(t)=\frac{1}{2\pi}\sum_{p=1}^{\infty}\frac{1}{p}\sum_{n=-\infty}^{\infty}\left\{\sqrt{\left(\gamma_n^2-\delta_n^2\right)}\sin\left[\left(p\omega_c-n\omega_m\right)t+\phi_n\right]\right\} \qquad (4.4.15)$$

where

$$\gamma_n=\left(E_n-F_n\right)\cos\left(\frac{p\omega_c T_o}{2}\right)+\left(H_n-G_n\right)\sin\left(\frac{p\omega_c T_o}{2}\right) \qquad (4.4.16(a))$$

$$\delta_n=\left(H_n+G_n\right)\cos\left(\frac{p\omega_c T_o}{2}\right)+\left(E_n+F_n\right)\sin\left(\frac{p\omega_c T_o}{2}\right) \qquad (4.4.16(b))$$

$$\phi_n=\tan^{-1}\left(\frac{\delta_n}{\gamma_n}\right) \qquad (4.4.16(c))$$

$$E_{-n}=E_n\ ,\ F_{-n}=F_n\ ,\ G_{-n}=G_n\ ,\ H_{-n}=H_n \qquad (4.4.16(d))$$

The term corresponding to p = 0 has been disregarded in the expressions for the frequency spectrum from equation 4.4.10. onwards. Since equation 4.4.9. for the complete frequency spectrum is indeterminate when p = 0, it is necessary to apply L'Hopital's rule for the limit of a quotient. This gives:

$$F(t)\Big|_{p=0}=\frac{T_o}{T_c}+\sum_{n=1}^{\infty}\left(\alpha_n+\beta_n\right)M^n\cos^n\left(\omega_m t\right) \qquad (4.4.17)$$

The power series in terms of $M^n\cos^n(\omega_m t)$ may be expressed as a Fourier series:

$$F(t)\Big|_{p=0} = \frac{T_o}{T_c} + \frac{K_o}{2} + \sum_{v=1}^{\infty} K_v \cdot \cos(v\omega_m t) \qquad (4.4.18)$$

Therefore, from equations 4.4.15. and 4.4.18. the complete frequency spectrum for non-linear pulse-length modulation is:

$$F(t) = \frac{T_o}{T_c} + \frac{K_o}{2} + \sum_{v=1}^{\infty} K_v \cdot \cos(v\omega_m t) +$$

$$\frac{1}{2\pi} \sum_{p=1}^{\infty} \frac{1}{p} \sum_{n=-\infty}^{\infty} \left\{ \sqrt{(\gamma_n^2 - \delta_n^2)} \sin\left[(p\omega_c + n\omega_m)t - \phi_n \right] \right\} \qquad (4.4.19)$$

The derivation of the expressions for the coefficients E_n, F_n, G_n, H_n, and K_v is considered in detail in Appendix 6, and only the results are given here.

$$E_o = \sum_{u=0}^{\infty} A_{2u} \frac{1}{2^{2u-1}} \binom{2u}{u} \qquad (4.4.20(a))$$

$$E_{2n-1} = \sum_{u=n}^{\infty} A_{2u-1} \frac{1}{2^{2u-2}} \binom{2u-1}{u-n} \qquad (4.4.20(b))$$

$$E_{2n} \sum_{u=n}^{\infty} A_{2u} \frac{1}{2^{2u-1}} \binom{2u}{u-n} \qquad (4.4.20(c))$$

$$F_o = \sum_{u=0}^{\infty} B_{2u} \frac{1}{2^{2u-1}} \binom{2u}{u} \qquad (4.4.21(a))$$

$$F_{2n-1} = \sum_{u=n}^{\infty} B_{2u-1} \frac{1}{2^{2u-2}} \binom{2u-1}{u-n} \qquad (4.4.21(b))$$

$$F_{2n} = \sum_{u=n}^{\infty} B_{2u} \frac{1}{2^{2u-1}} \binom{2u}{u-n} \qquad (4.4.21(c))$$

$$G_o = \sum_{u=0}^{\infty} C_{2u} \frac{1}{2^{2u-1}} \binom{2u}{u} \qquad (4.4.22(a))$$

$$G_{2n-1} = \sum_{u=n}^{\infty} C_{2u-1} \frac{1}{2^{2u-2}} \binom{2u-1}{u-n} \qquad (4.4.22(b))$$

$$G_{2n} = \sum_{u=n}^{\infty} C_{2u} \frac{1}{2^{2u-1}} \binom{2u}{u-n} \qquad (4.4.22(c))$$

$$H_o = \sum_{u=0}^{\infty} D_{2u} \frac{1}{2^{2u-1}} \binom{2u}{u} \qquad (4.4.23(a))$$

$$H_{2n-1} = \sum_{u=n}^{\infty} D_{2u-1} \frac{1}{2^{2u-2}} \binom{2u-1}{u-n} \qquad (4.4.23(b))$$

$$H_{2n} = \sum_{u=n}^{\infty} D_{2u} \frac{1}{2^{2u-1}} \binom{2u}{u-n} \qquad (4.4.23(c))$$

where:

$$A_k = -\frac{(2\pi p)^2}{k} \sum_{q=0}^{k-2} \left\{ M^{k-q} A_q \sum_{r=q+1}^{k-1} \frac{(r-q)(k-r)}{r} \alpha_{k-r} \alpha_{r-q} \right\} \qquad (4.4.24(a))$$

$$A_0 = 1 \qquad (4.4.24(b))$$

$$A_1 = 0 \qquad (4.4.24(c))$$

$$C_k = M^k p 2\pi \alpha_k - \frac{(2\pi p)^2}{k} \sum_{q=0}^{k-2} \left\{ M^{k-q} C_q \sum_{r=q+1}^{k-1} \frac{(r-q)(k-r)}{r} \alpha_{k-r} \alpha_{r-q} \right\} \qquad (4.4.25(a))$$

$$C_0 = 0 \qquad (4.4.25(b))$$

$$C_1 = M p 2\pi \alpha_1 \qquad (4.4.25(c))$$

$$B_k = -\frac{(2\pi p)^2}{k} \sum_{q=0}^{k-2} \left\{ M^{k-q} B_q \sum_{r=q+1}^{k-1} \frac{(r-q)(k-r)}{r} \beta_{k-r} \beta_{r-q} \right\} \qquad (4.4.26(a))$$

$$B_0 = 1 \qquad (4.4.26(b))$$

$$B_1 = 0 \qquad (4.4.26(c))$$

$$D_k = M^k p 2\pi \beta_k - \frac{(2\pi p)^2}{k} \sum_{q=0}^{k-2} \left\{ M^{k-q} D_q \sum_{r=q+1}^{k-1} \frac{(r-q)(k-r)}{r} \beta_{k-r} \beta_{r-q} \right\} \qquad (4.4.27(a))$$

$$D_0 = 0 \qquad (4.4.27(b))$$

$$D_1 = M p 2\pi \beta_1 \qquad (4.4.27(c))$$

$$K_o = \sum_{w=1}^{\infty} \left(\alpha_{2w} + \beta_{2w}\right) M^{2w} \frac{1}{2^{2w-1}} \binom{2w}{w} \qquad (4.4.28(a))$$

$$K_{2v-1} = \sum_{w=v}^{\infty} \left(\alpha_{2w-1} + \beta_{2w-1}\right) M^{2w-1} \frac{1}{2^{2w-2}} \binom{2w-1}{w-v} \qquad (4.4.28(b))$$

$$K_{2v} = \sum_{w=v}^{\infty} \left(\alpha_{2w} + \beta_{2w}\right) M^{2w} \frac{1}{2^{2w-1}} \binom{2w}{w-v} \qquad (4.4.28(c))$$

At first sight, the expressions developed for the spectrum appear formidable and would seem to have little advantage over the Bessel function type of analysis. However there is an important point in favour of this series analysis. Consider the components at the pulse repetition frequency $p\omega_c$ and the sideband frequencies $(p\omega_c \pm n\omega_m)$. The amplitude of each sideband component is specified by only one term, namely $(\gamma_n^2 + \delta_n^2)$. Equations 4.4.16(a). and (b) express $(\gamma_n^2 + \delta_n^2)$ in terms of the coefficients E_n, F_n, G_n and H_n. Since these coefficients are defined by convergent series (equations 4.4.20. 4.4.21., 4.4.22. and 4.4.23 respectively) the amplitude of the sideband components can be calculated to any required accuracy by taking sufficient terms in the series. Thus, the series analysis overcomes the major disadvantage of the Bessel function type of analysis (i.e. that of deciding how many of the Bessel function terms must be considered, and the limits that must be placed on the order of the Bessel functions).

Although the series analysis presented may not be the best approach to the problem of analysing non-linear pulse-length modulation, it does demonstrate that methods can be developed which are superior to the Bessel function analysis. The Bessel function analysis is an extension of the methods used for analysis of linear pulse-length modulation, and is not really adequate. It is possible that the series analysis could be simplified since the expressions for the various coefficients have the same general form. A further point which requires investigation is the implicit assumption that the series for the coefficients, E_n, F_n, G_n and H_n are convergent. In all the practical problems for which the analysis has been used, the series have converged rapidly. Figs. A6.1 and A6.2. in Appendix 6 shows the flow chart which was used as a basis for a computer programme to evaluate the spectral components.

4.5. Distortion due to Finite Bandwidth of the Integrator Amplifier

4.5.1. Single-edge Modulation

It is shown in the static analysis of a single-edge pulse-length modulation system with finite amplifier bandwidth that the position t_1 of the pulse leading-edge can be represented by the following power series:

$$\frac{t_1}{T_c} = \sum_{n=0}^{\infty} a_n M^n \qquad (4.5.1)$$

Analytical expressions for the coefficients a_n are given in section 3.3.1. (equations 3.3.18., 3.3.19., and 3.3.20.). The coefficients are also shown in graphical form in figs. 3.3.3(a)., (b), (c) and (d). It is also shown in the static analysis that the trailing-edge of the pulses occur at periodic intervals of T_c.

$$\frac{t_2}{T_c} = 1 \qquad (4.5.2)$$

Equation 4.5.1. for the position of the pulse leading-edge is in the form required for the generalised spectrum analysis. Comparison of equations 4.5.1. and 4.5.2. with equations 4.4.1. and 4.4.2. of section 4.4. shows that in order to use the generalised spectrum analysis, the following substitutions must be made in the expressions for the spectrum:

$$\alpha_o = a_o \qquad (4.5.3(a))$$

$$\alpha_n = -a_n \qquad (4.5.3(b))$$

$$\beta_o = 1 \qquad (4.5.3(c))$$

$$\beta_n = 0 \qquad (4.5.3(d))$$

Due to the number of variables involved, it is not practical to present graphs of the spectral components for all values of modulation index M. Thus, it is necessary to select a single value of modulation index for which the components of the frequency spectrum may be evaluated. Since the distortion is likely to be greatest for full modulation (i.e. $M = 1$) this would be the most useful value. However, the static analysis for the double-edge modulation system with finite amplifier bandwidth is not valid for $M = 1$. In order to compare the single-edge modulation and double-edge modulation systems, it is convenient if the spectra for the two systems are evaluated for the same value of modulation index. For this reason a value of $M = 0.5$ is used. The frequency spectrum of the single-edge modulation system with finite bandwidth was evaluated from the generalised spectrum analysis by means of a digital computer.

The amplitudes of the various components of the spectrum may be plotted as functions of the parameters T_N and Ψ. The normalised time constant T_N is given by equation 3.3.19(a). of the static analysis section.

$$T_N = \frac{T_c}{(1+\alpha)CR}\left[\frac{1}{1+\frac{T_a}{(1+\alpha)CR}}\right] \qquad (4.5.4(a))$$

and the factor Ψ by equation 3.3.19(c)

$$\Psi = \frac{CR}{T_a}\left[\frac{T_a}{CR}+1+\alpha\right]^2 \qquad (4.5.4(b))$$

As was discussed in section 3.3.1., care is required in interpreting the parameter Ψ since it has a minimum value which is a function of the integrator gain α. This minimum value occurs when:

$$\frac{T_a}{CR} = 1+\alpha \qquad (4.5.5(a))$$

and the magnitude of the term Ψ is given by:

$$\Psi_{min} = 4(1+\alpha) \qquad (4.5.5(b))$$

Thus, for a particular value of α, as the term $\frac{T_a}{CR}$ is increased, so the term Ψ decreases to the minimum value and then increases again.

Fig. 4.5.1. shows the amplitude of the modulation frequency component as a function of T_N and Ψ. The amplitude of the component approaches the ideal value of 0.25 as the normalised time constant T_N is reduced. 0.25 is the ideal value since the amplitude of the pulse train was defined as unity, and the modulation index is 0.5. It can be seen that the effect of

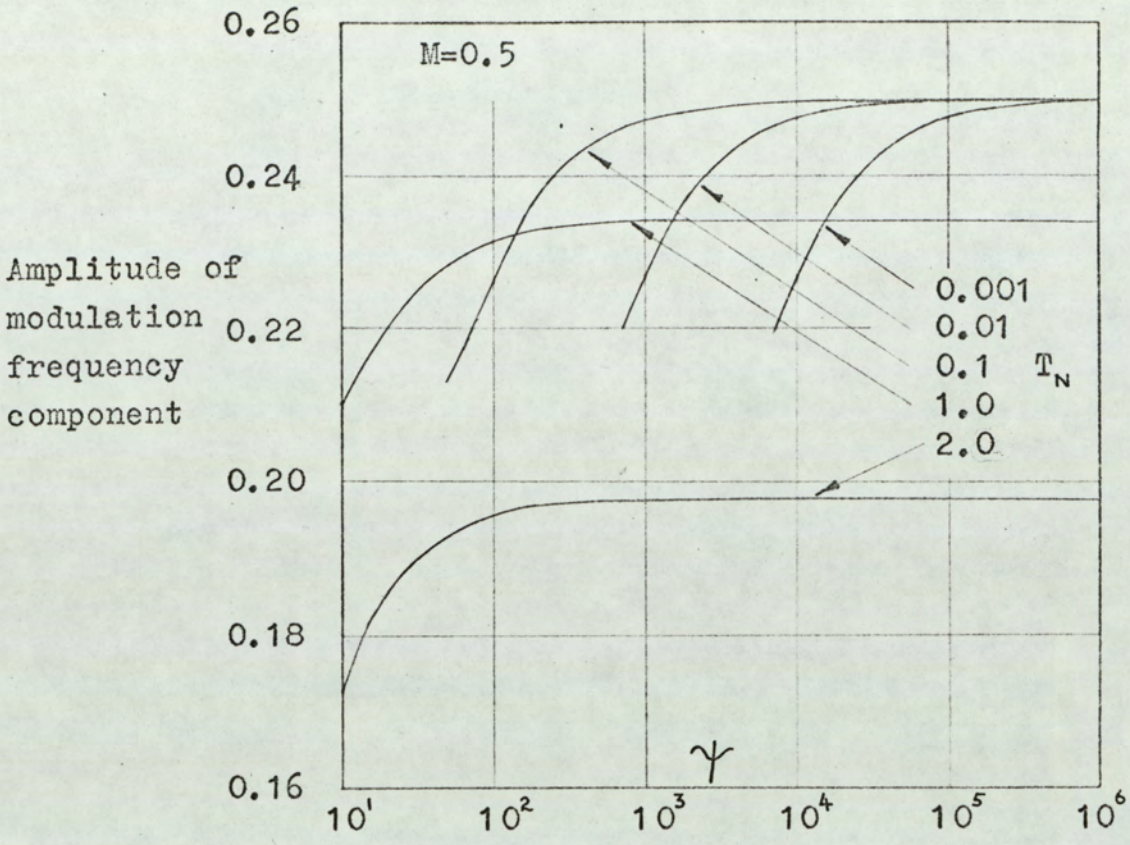

Fig.4.5.1. Amplitude of modulation frequency component for single-edge modulation system with finite bandwidth integrator amplifier.

increasing the amplifier time constant T_a is to reduce the amplitude of the modulation frequency component.

Figs. 4.5.2(a). and (b) show the second, third and fourth harmonic distortion factors for the system. The v^{th} harmonic distortion factor DF_v is defined from the generalised spectrum analysis (equation 4.4.19.) as:

$$DF_v = \frac{K_v}{K_1} \qquad (4.5.6)$$

As Ψ is decreased, the even harmonic distortion factors (i.e. DF_2 and DF_4 decrease to zero and then rapidly increase again. However, it is not possible to make use of this effect to produce a low distortion system since the value of Ψ required to produce zero distortion is a function of the modulation index M. That this is so may be seen from equation 4.4.28., of the generalised spectrum analysis (section 4.4.), for the coefficients K_v of the modulation frequency and harmonic components. The third harmonic distortion factor DF_3 increases as the factor Ψ is decreased.

Figs. 4.5.3(a)., (b) and (c) show the amplitudes of the repetition frequency component and the sideband frequency components as functions of the normalised time constant T and the factor Ψ. The amplitude of the repetition frequency component and the first sideband component both increase as as the factor Ψ is decreased. The amplitudes of the higher order sidebands decrease with decreasing values of Ψ.

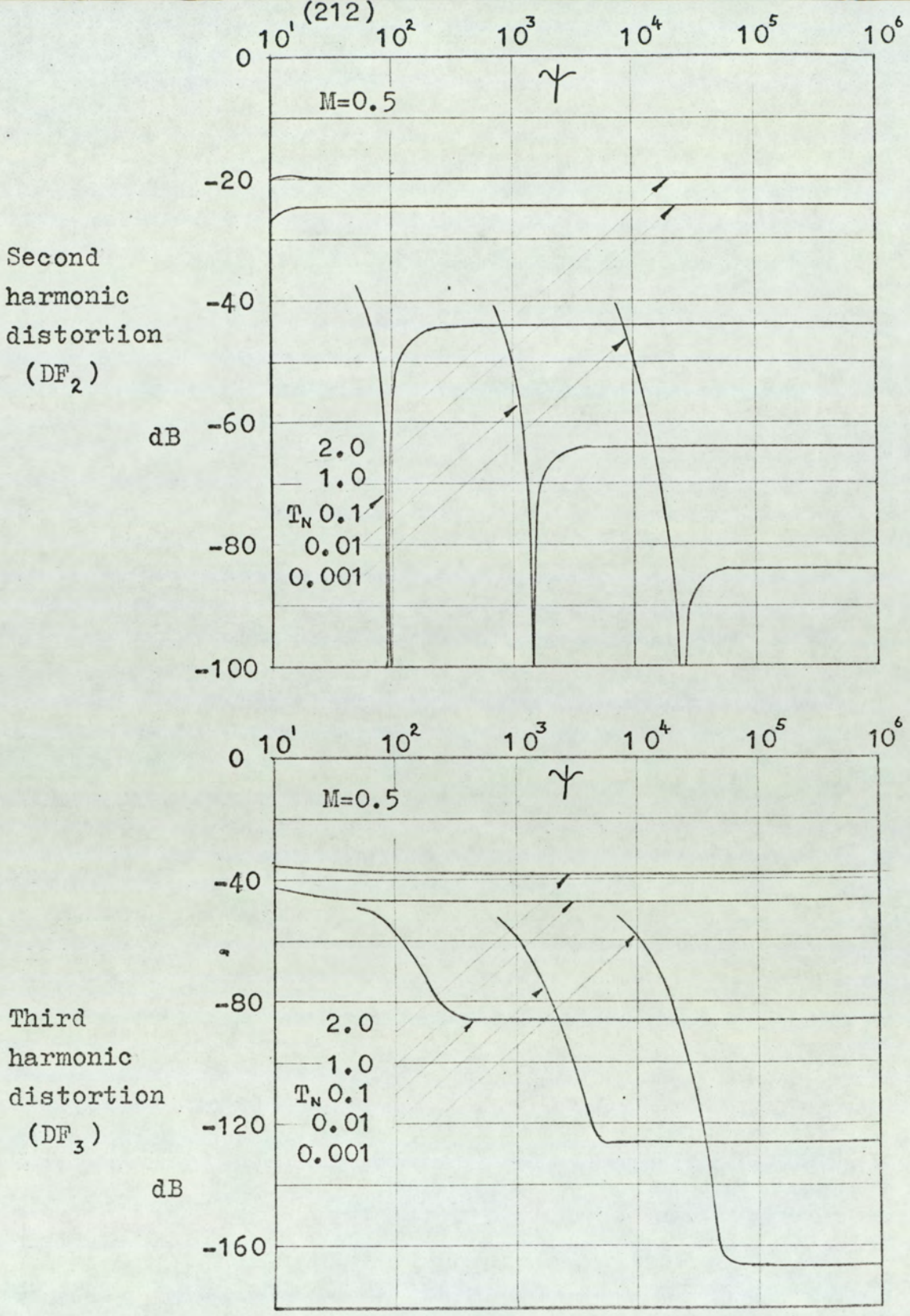

Fig.4.5.2(a). Harmonic distortion in single-edge modulation system with finite bandwidth integrator-amplifier.

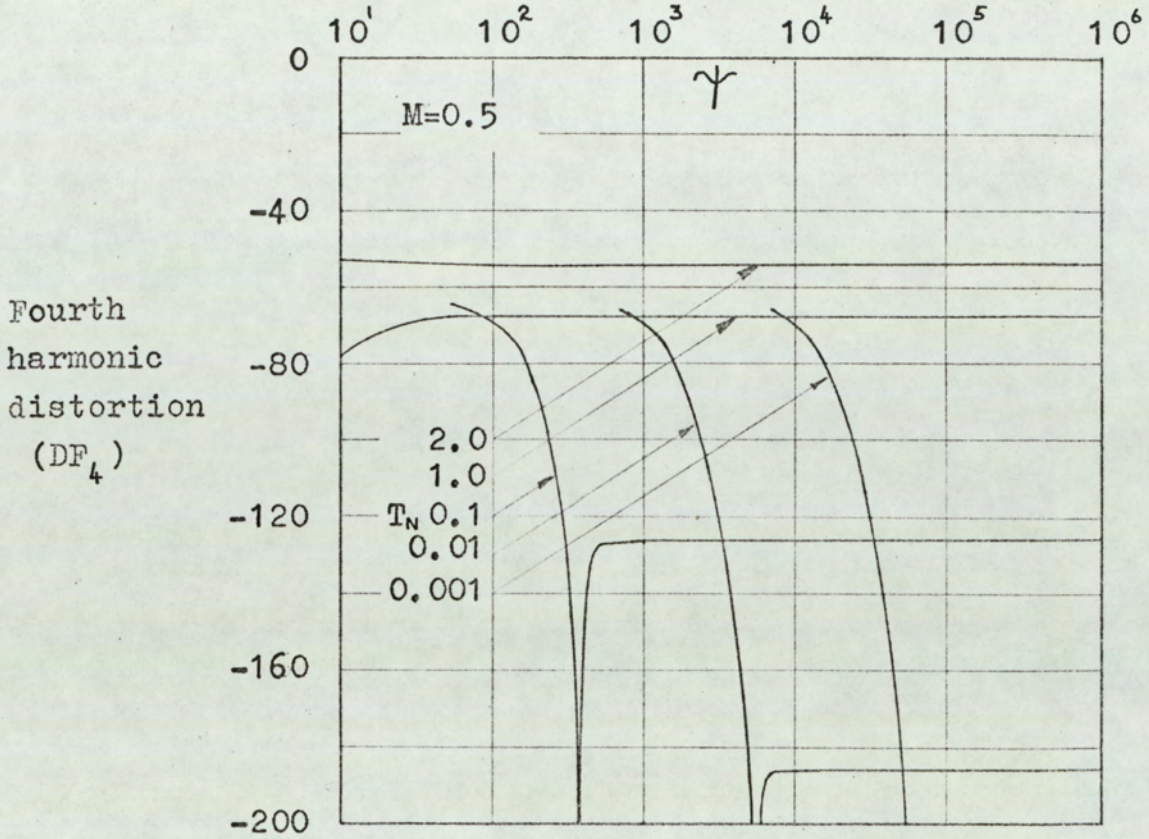

Fig.4.5.2(b). Harmonic distortion in single-edge modulation system with bandwidth limited integrator amplifier.

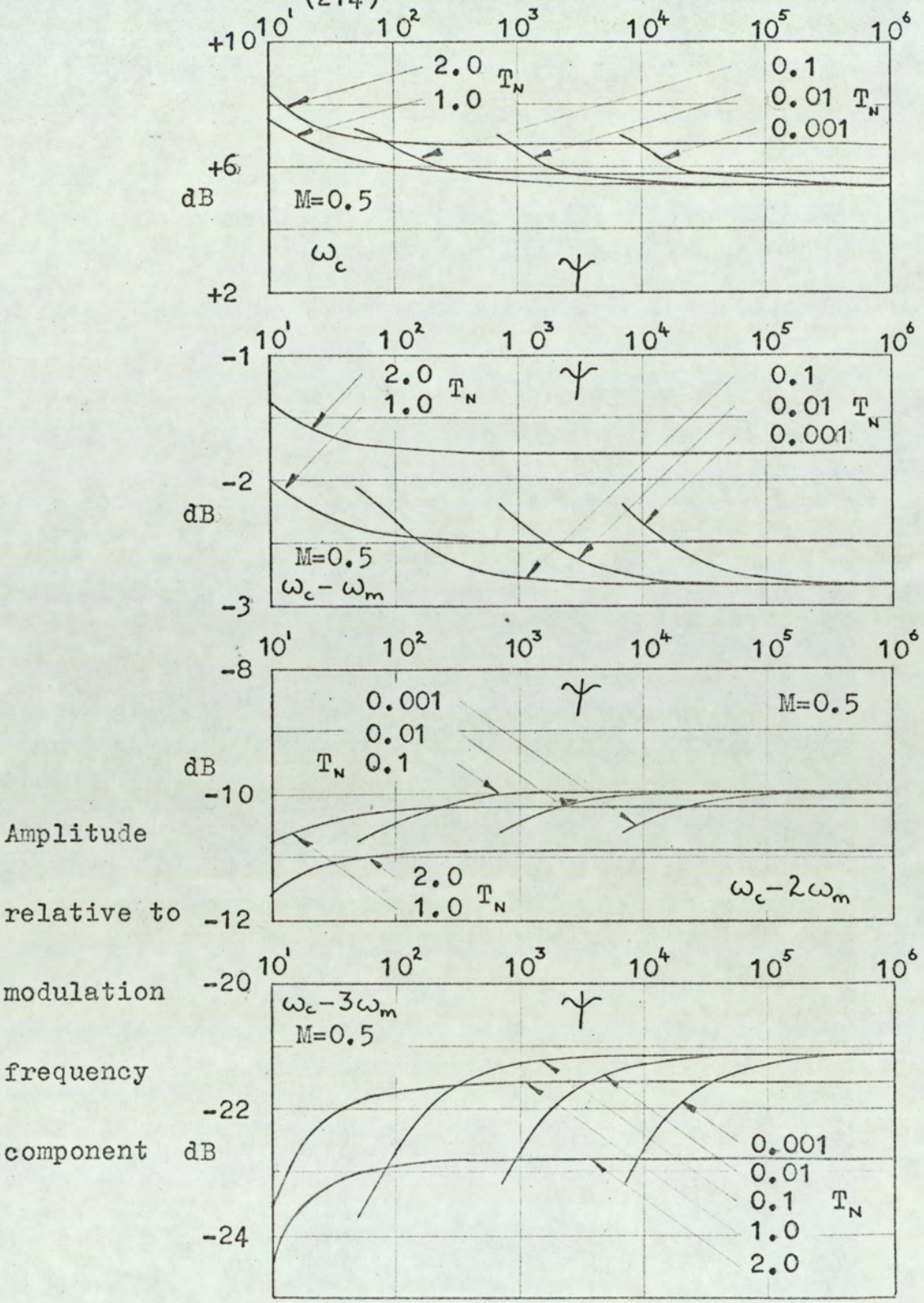

Amplitude relative to modulation frequency component

Fig.4.5.3(a). Amplitude of repetition frequency component and sideband components for single-edge modulation system with bandwidth limited integrator amplifier.

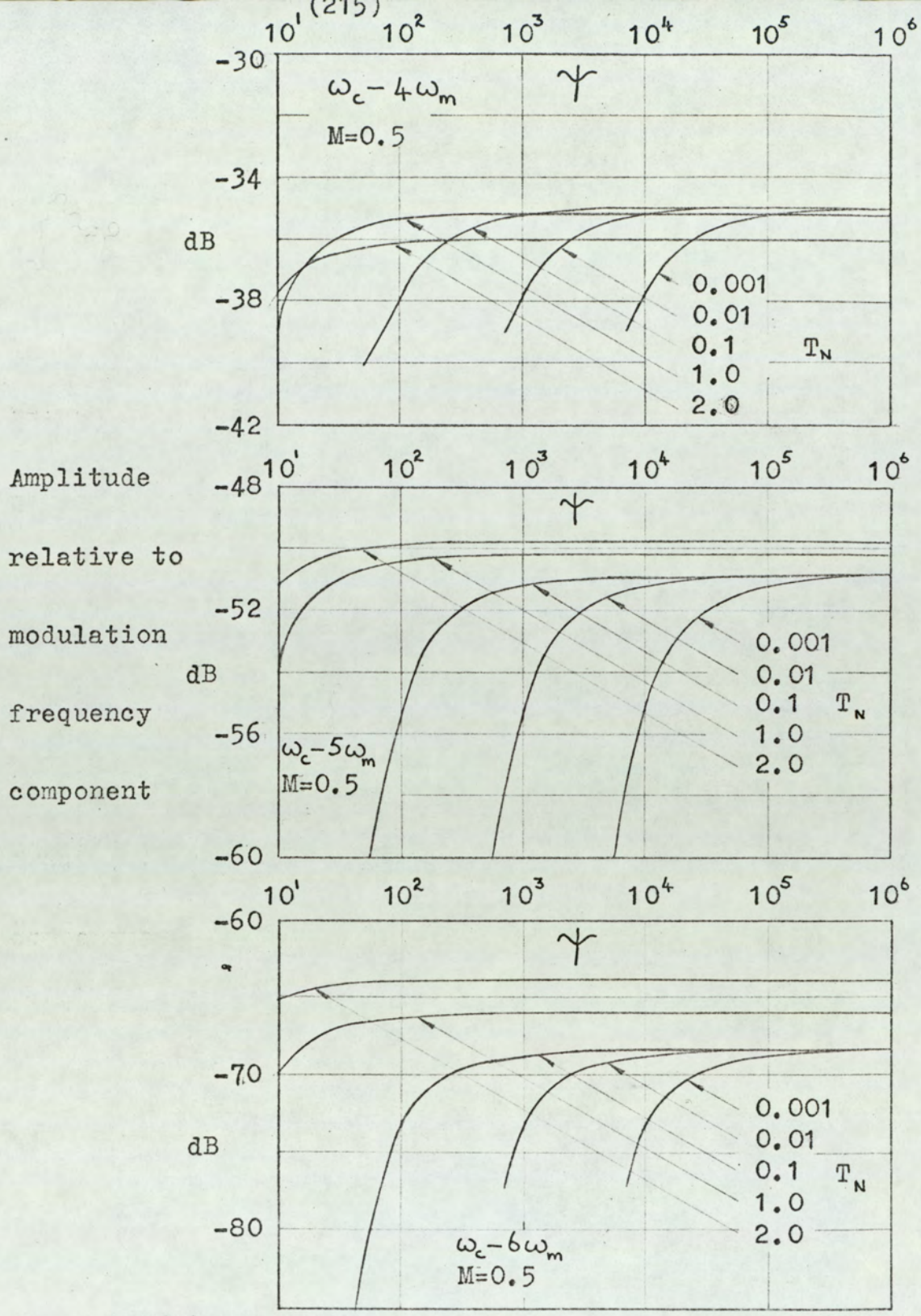

Amplitude relative to modulation frequency component

Fig.4.5.3(b). Amplitude of sideband components for single-edge modulation system with bandwidth limited integrator amplifier.

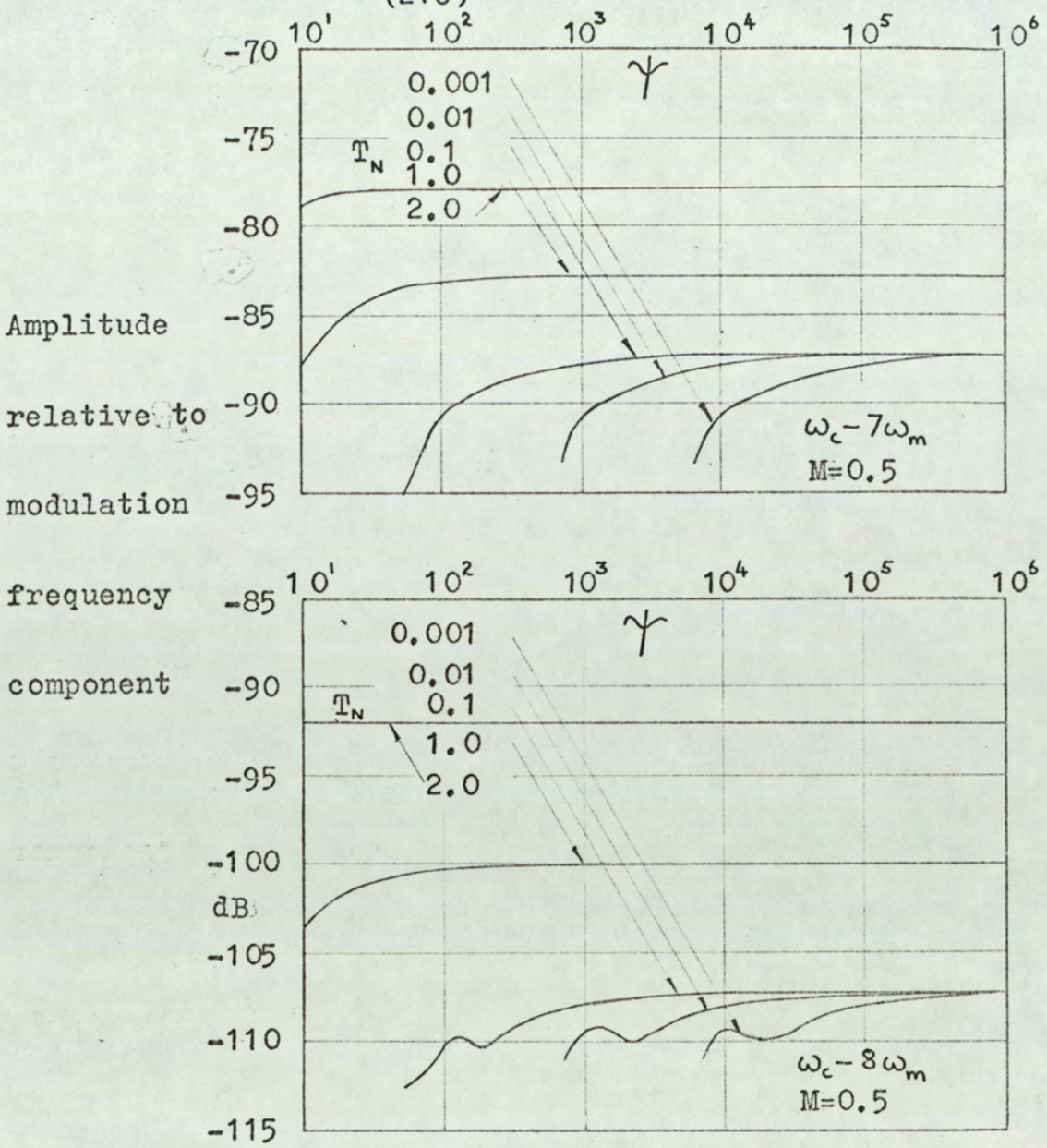

Fig.4.5.3(c). Amplitude of sideband components for single-edge modulation system with bandwidth-limited integrator amplifier.

4.5.2. Double-edge Modulation

It is shown in the static analysis of a double-edge pulse-length modulation system with a finite bandwidth integrator amplifier, (equations 3.3.42., 3.3.43. and 3.3.46.) that the positions of the leading and trailing edges of the pulse may be represented by the following power series:

$$\frac{t_1}{T_c} = \sum_{n=0}^{\infty} a_n M^n \qquad (4.5.7)$$

$$\frac{t_2}{T_c} = \frac{1}{2} + \sum_{n=0}^{\infty} (-1)^n a_n M^n \qquad (4.5.8)$$

where t_1 and t_2 are the positions of the leading and trailing pulse-edges respectively. The expressions for the coefficients a_n are given in equations 3.3.44. and 3.3.45. of section 3.3. The coefficients a_n are also presented in graphical form in figs. 3.3.10(a)., (b), (c) and (d) of section 3.3.

Equations 4.5.7. and 4.5.8. for the positions of the pulse edges are in the form required for the generalised spectrum analysis of section 4.4. Comparing equations 4.5.7 and 4.5.8. with equations 4.4.1. and 4.4.2. of section 4.4. shows that the following substitutions must be made in order to use the generalised spectrum analysis.

$$\alpha_0 = a_0 \qquad (4.5.9(a))$$

$$\alpha_n = -a_n \qquad (4.5.9(b))$$

$$\beta_0 = \frac{1}{2} + a_0 \qquad (4.5.9(c))$$

$$\beta_n = (-1)^n a_n \qquad (4.5.9(d))$$

The number of variables involved makes graphical presentation of the results of the spectrum analysis impractical for all values of modulation index. Therefore, one particular value of must be selected. Since it seems likely that the distortion components would be greatest at full modulation, the ideal value for the modulation index would be unity. However, the analytical expressions for the coefficients a_n in the power series representation of the positions of the pulse edges are not valid for full modulation. The maximum value of modulation index for which the expression are valid is a function of the system parameters as shown in fig. 3.3.12. of the static analysis section (section 3.3.2.). For the range of system parameters chosen, the value of $M = 0.5$ ensures that the expressions describing the positions of the pulse edges are valid. Thus the various components in the frequency spectrum can be evaluated by means of the static analysis of section 4.4. The amplitudes of the spectral components can be presented graphically as functions of the normalised time constant T_N (equation 4.5.4(a).) and the factor Ψ (equation 4.5.4(b).). Care is required in interpreting the factor Ψ as is discussed in connection with the single-edge modulation system (see equations 4.5.5(a). and (b)).

Fig. 4.5.4. shows the amplitude of the modulation frequency component as a function of T_N and Υ. As the normalised time constant T_N is reduced so the amplitude of the modulation frequency component approaches the value of 0.25. Since the amplitude of the pulse train is defined as unity, and the modulation index is 0.5, the amplitude of the modulation frequency component in an ideal system is 0.25. The effect of increasing the amplifier time constant T_a is to reduce the amplitude of the modulation frequency component, bearing in mind the remarks regarding the variation of Υ with T_a.

With the double-edge modulation system, no components exist at even harmonics of the modulation frequency. The reason for this may be seen from equation 4.4.28., of the generalised spectrum analysis, which expresses the amplitude of the modulation frequency and harmonic components in terms of the coefficients α_n and β_n. Since $\alpha_n = (-1)^n \beta_n$ (equations 4.5.9(b). and (c)), the coefficients of the even harmonic terms cancel out. Fig. 4.5.5. shows the third and fifth harmonic distortion factors as function of T_N and Υ. The v^{th} harmonic distortion factor DF_v is defined from equation 4.4.19. of the generalised spectrum analysis as:

$$DF_v = \frac{K_v}{K_1} \qquad (4.5.10)$$

The odd harmonic distortion factors decrease as the normalised time constant T_N is decreased. Decreasing the factor Υ increases the harmonic distortion.

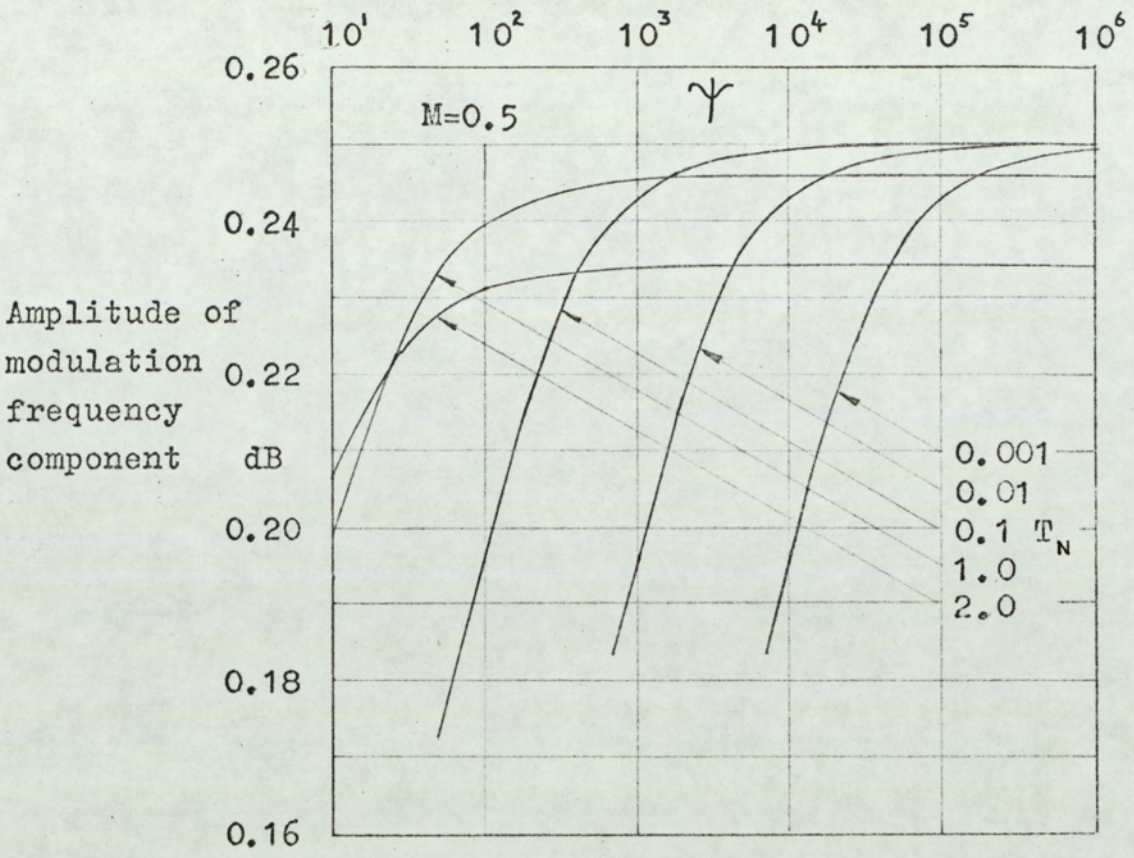

Fig.4.5.4. Amplitude of modulation frequency component for double-edge modulation system with finite-bandwidth integrator amplifier.

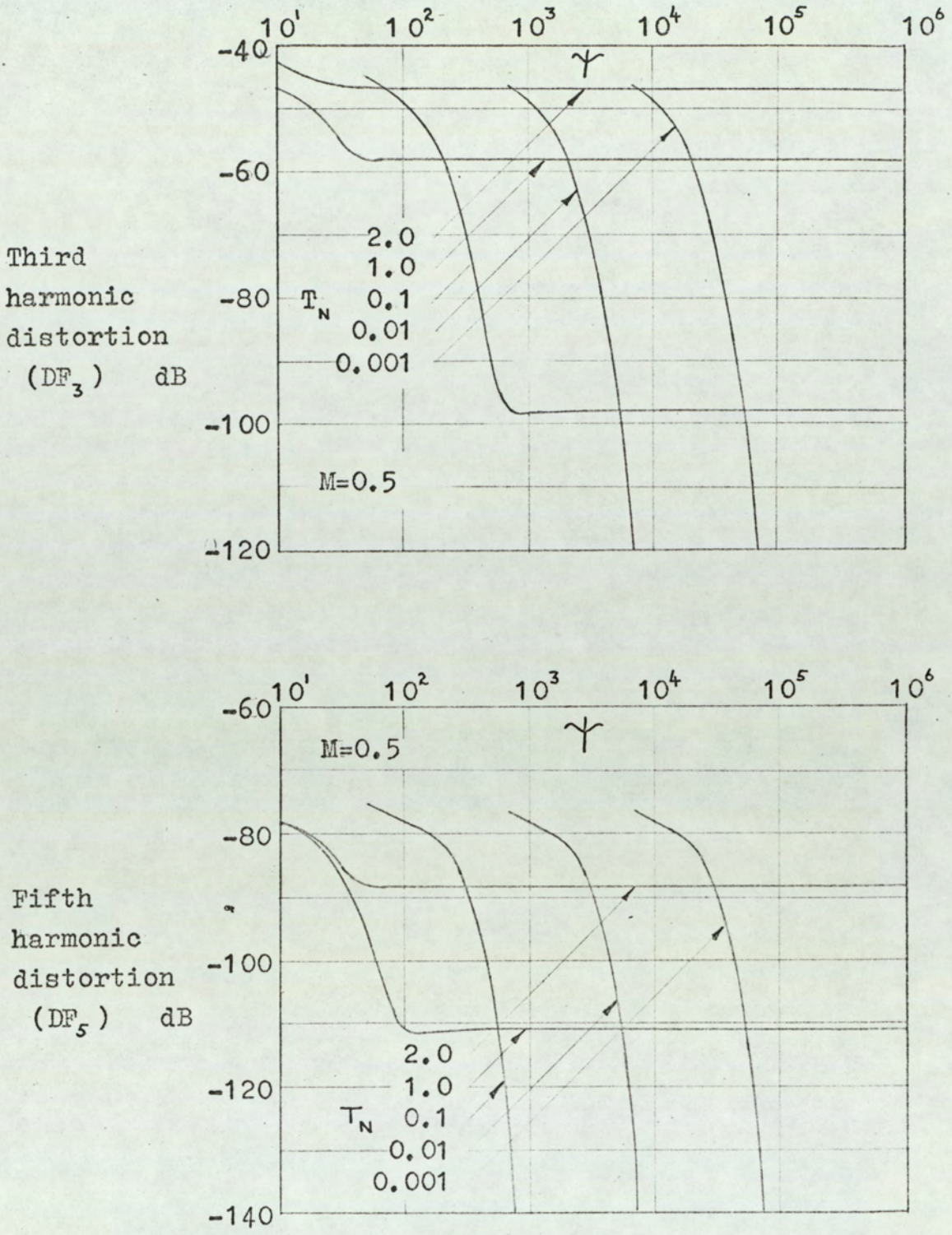

Fig.4.5.5. Harmonic distortion in double-edge modulation system with bandwidth-limited integrator amplifier.

Figs. 4.5.6(a). and (b) show the amplitude of the repetition frequency component and the sideband frequency components as functions of the parameters T_N and Υ. It will be noted that with double-edge modulation, no odd order sidebands exist (i.e. sidebands $\omega_c \pm n\omega_m$, where n is odd). This is due to the relationship between the coefficients β_n and α_n (i.e. $\alpha_n = (-1)^n \beta_n$) which define the time deviations of the leading and trailing edges of the pulses. The amplitude of the repetition frequency component increases with decreasing values of Υ, whilst the amplitude of the sideband component $(\omega_c - 2\omega_m)$ decreases with decreasing values of Υ. The amplitude of the sideband components at $\omega_c - 4\omega_m$, $\omega_c - 6\omega_m$ and $\omega_c - 8\omega_m$ decrease with decreasing values of Υ until the amplitude of the particular sideband component is zero. As Υ is further increased, so the amplitude of the component rapidly increases. However, it is not possible to make use of this effect in the design of a system with small sideband distortion. This is because the values of the system parameters required to make the amplitude of a particular sideband zero, are functions of the modulation index. That this is so may be seen from the equations for the parameters in the generalised spectrum analysis (equations 4.4.19. to 4.4.27. of section 4.4.).

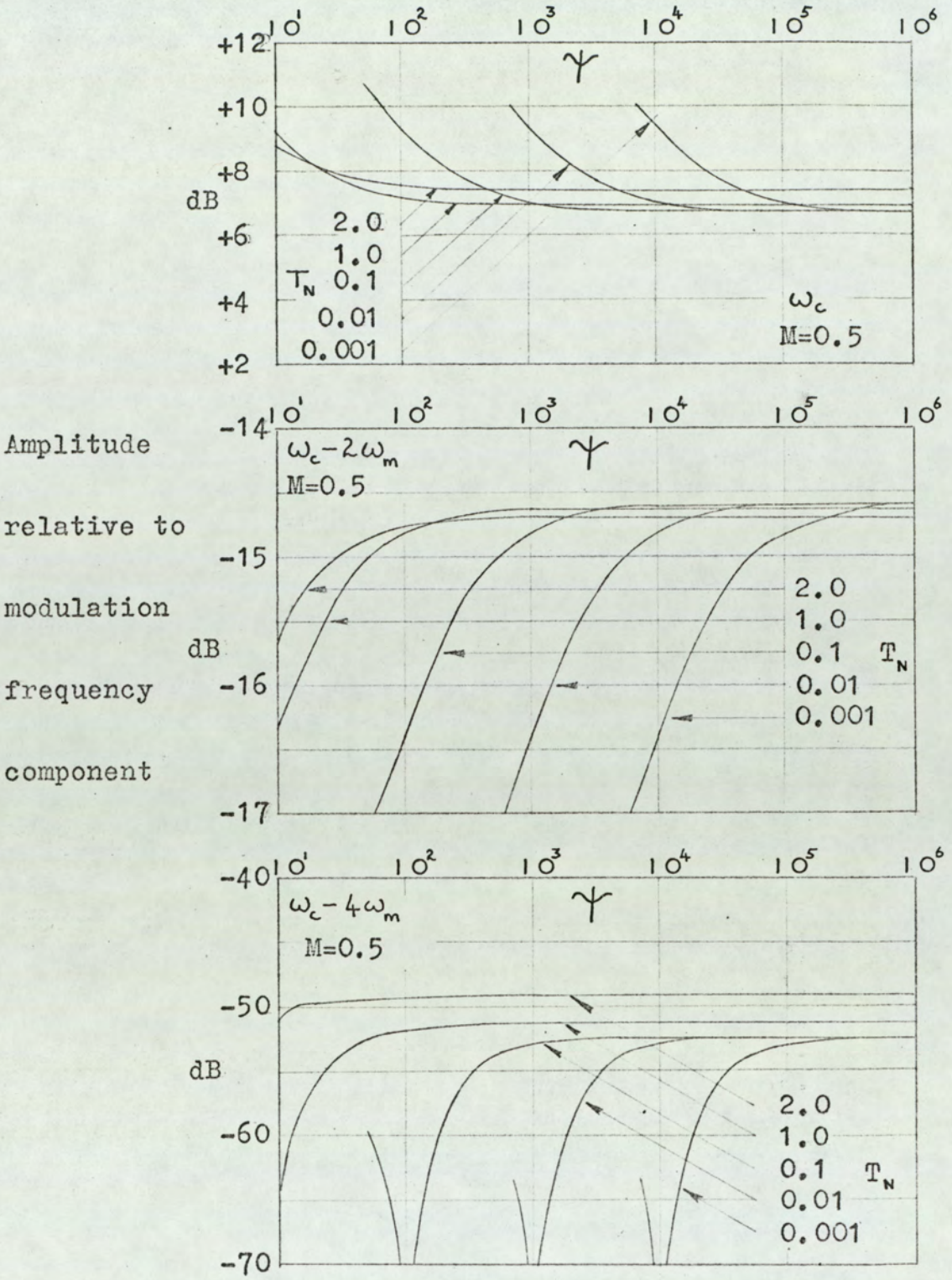

Fig.4.5.6(a). Amplitude of repetition frequency component and sideband frequency components for double-edge modulation system with band-width limited integrator amplifier.

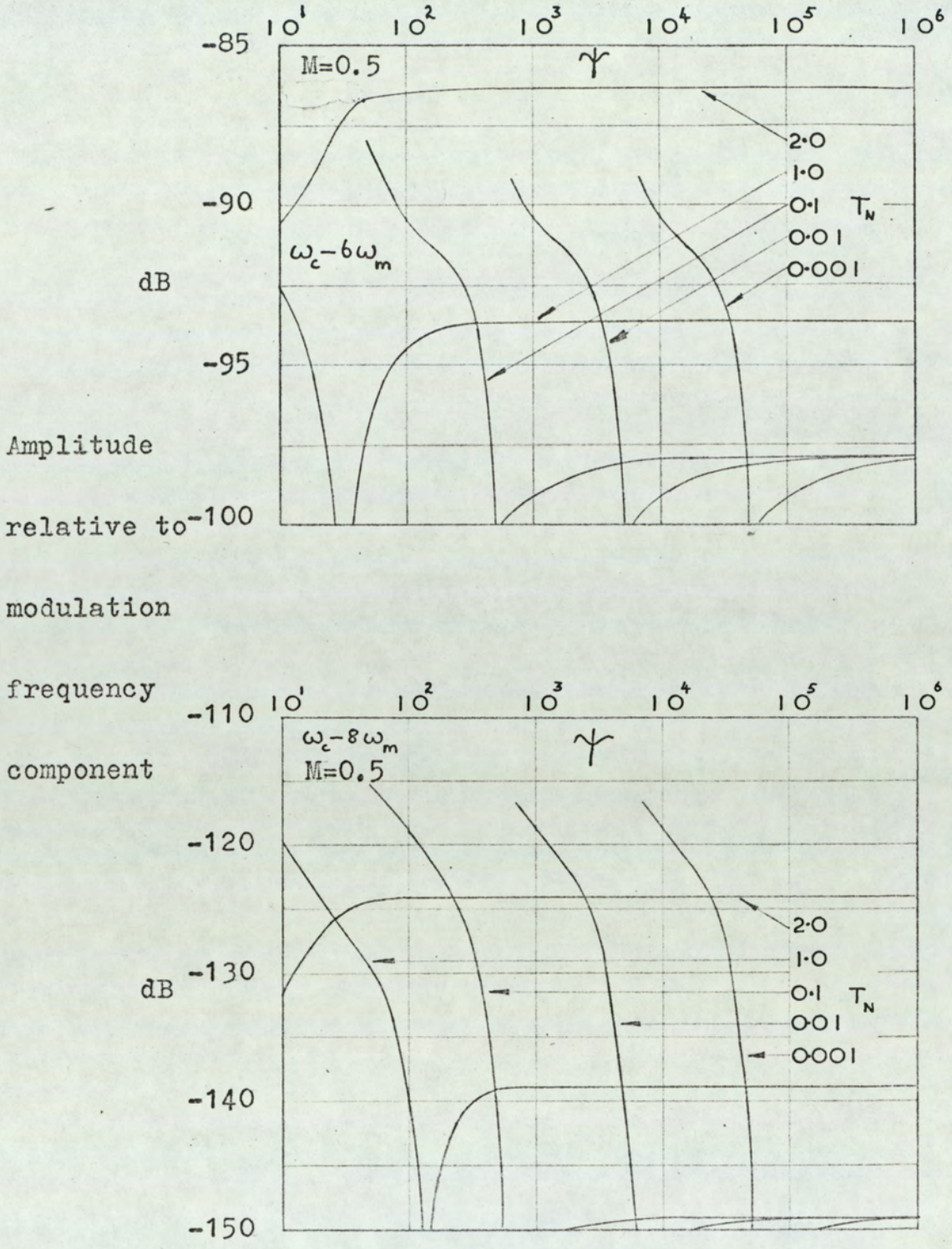

Fig.4.5.6(b). Amplitude of sideband frequency components for double-edge modulation system with bandwidth-limited integrator amplifier.

4.5.3. Conclusions

The spectrum analyses of pulse-length modulation systems which utilise finite bandwidth integrator amplifiers have been carried out by means of the generalised spectrum analysis of section 4.4. The amplitudes of the spectral components have been presented in graphical form as a function of T_N , the normalised time constant, and γ .

In the spectrum for single-edge modulation, components exist at the modulation frequency and at harmonics of the modulation frequency. Terms are also present at all harmonics $p\omega_c$ of the pulse repetition frequency, together with sidebands at $p\omega_c \pm n\omega_m$. The spectrum for double-edge modulation contains a component at the modulation frequency and components at only even harmonics of the modulation frequency. Terms are also present at all the harmonics $p\omega_c$ of the pulse repetition frequency, together with sidebands $p\omega_c \pm n\omega_m$. However, sidebands do not exist for all values of n. From the point of view of sideband distortion, the most important components are the lower order sidebands (i.e. $\omega_c - n\omega_m$). For double-edge modulation, these sidebands exist only when n is even.

For both single-edge modulation and double-edge modulation, the amplitude of the harmonic distortion components decrease as the normalised time constant T_N is decreased. The amplitude of the modulation frequency component approaches the ideal value of 0.25 as T_N is reduced. The value of the amplifier time constant T_N that can be tolerated without producing a significant change in system performance is a

function of the other system parameters. For this reason, a clearer indication of the effects of the finite bandwidth is gained by applying the analytical results to a practical example. (see section 5).

4.6. Distortion due to Hysteresis in the Level-Detector Threshold Voltage

4.6.1. Single-edge Modulation

It is shown in the static analysis section (section 3.4.1.) that hysteresis in the level detector does not modify the positions of the pulse-edges provided that the effective threshold voltage ($V_t - \delta$) is set to the value required for a non-hysteretic system. The only effect of the hysteresis is to impose a limit on the maximum negative modulation index for which the modulation process is continuous (see equation 3.4.8., section 3.4.1.). Since the hysteresis of the level-detector does not affect the positions of the pulse-edges, the frequency spectrum of the modulated waveform is identical to that of a system with a non-hysteretic level-detector. Thus the spectrum analysis of section 4.2.1. is valid for a single-edge pulse-length modulation system with a hysteretic level-detector.

4.6.2. Double-edge Modulation

It is shown in the static analysis of a double-edge modulation system with a non-hysteretic level-detector (section 3.4.2., equations 3.4.19. and 3.4.20.) that the positions of the leading and trailing edges of the pulses are given by the following expressions:

$$\frac{t_1}{T_c} = -\frac{(1+\alpha)CR}{T_c}\left\{\log\frac{1}{2}\left[1-\frac{\delta}{\alpha V_1}\right]\left[1-\exp\left(\frac{-T_c}{2(1+\alpha)CR}\right)\right]+\log\left(1-M\phi K\right)\right\} \qquad (4.6.1)$$

$$\frac{t_2}{T_c} = \frac{1}{2}-\frac{(1+\alpha)CR}{T_c}\left\{\log\frac{1}{2}\left[1-\frac{\delta}{\alpha V_1}\right]\left[1-\exp\left(\frac{-T_c}{2(1+\alpha)CR}\right)\right]+\log\left(1+M\phi K\right)\right\} \qquad (4.6.2)$$

where t_1 and t_2 are the positions of the pulse leading and trailing edges respectively.

and

$$\phi = 1+\frac{K-1}{\frac{\hat{V}_2(t)}{\delta}-K} \qquad (4.6.3)$$

$$K = \frac{1-\exp\left(\frac{-T_c}{2(1+\alpha)CR}\right)}{1+\exp\left(\frac{-T_c}{2(1+\alpha)CR}\right)} \qquad (4.6.4)$$

It is shown in the spectrum analysis of a double-edge pulse-length modulation system with finite integrator gain (section 4.2.2., equation 4.2.20(a).), that the time deviation t_{d1} of the leading edge of the pulse is given by:

$$t_{dl} = t_1\Big|_{M=0} - t_1$$

Substituting equation 4.6.1. in the above expression gives:

$$\frac{t_{dl}}{T_c} = \frac{(1+\alpha)CR}{T_c}\log\left(1-M\phi K\right) \qquad (4.6.5)$$

The time deviation t_{dt} of the pulse trailing edge is given by equation 4.2.21(a). of section 4.2.2.

$$t_{dt} = t_2 - t_2\Big|_{M=0}$$

Therefore, from equation 4.6.2.:

$$\frac{t_{dt}}{T_c} = -\frac{(1+\alpha)CR}{T_c}\log\left(1+M\phi K\right) \qquad (4.6.6)$$

Equation 4.2.22(a). (section 4.2.2.) expresses the unmodulated pulse length T_o as:

$$T_o = t_2\Big|_{M=0} - t_1\Big|_{M=0}$$

Substituting equations 4.6.1. and 4.6.2. in the above expressions gives:

$$T_o = \frac{T_c}{2} \qquad (4.6.7)$$

Comparison of equations 4.6.5., 4.6.6. and 4.6.7. with the corresponding expressions for a double-edge modulation system with zero hysteresis (equations 4.2.20(b), 4.2.21(b)., 4.2.22(b)., section 4.2.2.) shows that the expressions for the two systems are identical in form. The

only effect of the level-detector hysteresis is to modify the value of the modulation index from M to $M\phi$. As a result of this similarity, the expression for the frequency spectrum of the system output may be written down by inspection of equation 4.2.31. (section 4.2.2.) for the spectrum of a double-edge modulation system with finite integrator gain and zero hysteresis.

$$F(t) \triangleq \frac{1}{2} - \frac{k_1}{T_c}\cos(\omega_m t) - \frac{k_3}{T_c}\cos(3\omega_m t) +$$

$$\frac{2}{\pi}\sum_{p=1}^{\infty}\frac{1}{p}\left\{\sum_{\substack{e,f,g\\=-\infty}}^{\infty} J_e(p\omega_c k_1)\,J_f(p\omega_c k_2)\,J_g(p\omega_c k_3)\sin\left[\frac{\pi}{2}(e-f-g)\right]\times\right.$$

$$\left.\cos\left[\left(p\omega_c+\left[e+2f+3g\right]\omega_m\right)t - p\omega_c k_o - f\frac{\pi}{2}\right]\right\} \qquad (4.6.8)$$

where

$$k_o = -(1+\alpha)CR\log\left\{\frac{\frac{1}{2}(M\phi K)^2}{1-\sqrt{\left[1-(M\phi K)^2\right]}}\right\} \qquad (4.6.9(a))$$

$$k_n = (1+\alpha)CR\,\frac{2}{n}\left\{\frac{1}{M\phi K} - \sqrt{\left[\left(\frac{1}{M\phi K}\right)^2 - 1\right]}\right\}^n \qquad (4.6.9(b))$$

The reasons for deriving only an approximate expression for the frequency spectrum are discussed in section 4.2.2. The modulation index modifying factor ϕ is shown as a function of the system parameters in fig. 3.4.5. of the static analysis

(section 3.4.2.). The factor ϕ decreases with increasing values of level-detector hysteresis, which means that the effective modulation index $M\phi$ decreases as the hysteresis is increased. Since the effect of the hysteresis is simply to modify the effective modulation index, the discussion of the results of the spectrum analysis for the non-hysteretic system (section 4.2.2.) is equally valid for the hysteretic system, and will not be repeated here.

4.6.3. Conclusions

Expressions have been derived for the spectra of the outputs of pulse-length modulation systems utilising hysteretic level-detectors. The equations for the frequency spectra are expressed in terms of the spectra of equivalent systems with non-hysteretic level-detectors.

For the single-edge modulation system it is shown, from the results of the static analysis, that if the effective threshold $V_t - \delta$ is set to the value required for a non-hysteretic system, then the hysteresis has no effect on the frequency spectrum. Thus the frequency spectrum of a single-edge modulation system, with a hysteretic level-detector and finite integrator gain, is identical to that of a non-hysteretic system with finite integrator gain. However, the hysteresis sets a limit on the maximum negative value of modulation index for which the modulation process is continuous.

The effect of the hysteresis in the double-edge modulation system is simply to modify the effective modulation index. Therefore the form of the spectrum is identical to that of a non-hysteretic system. However, the reduction of the effective value of modulation index means that the maximum value of the modulation frequency component will be reduced. Under conditions of full modulation (i.e. $M = 1$), the system output will be identical to the output of a non-hysteretic system with a modulation index of $M\phi$.

4.7. Discussion of the Results of the Spectrum Analyses

The frequency spectra for the various single-edge modulation systems analysed all have the same general form. The spectra consist of a constant term and a modulation frequency component, plus terms at harmonics of the modulation frequency. Components also exist at all the harmonics ($p\omega_c$) of the pulse repetition frequency, together with associated sideband components ($p\omega_c \pm n\omega_m$). The terms at harmonics of the modulation frequency constitute harmonic distortion, and are due to the non-linearity of the sampling waveform. In general, the system imperfections (i.e. finite integrator gain, etc.) are found to have only a relatively small effect on the amplitude of the sideband components of the frequency spectrum.

The spectra for the double-edge modulation systems have a number of important differences compared with the spectra for single-edge modulation systems. The first of these differences is that components exist at only odd harmonics of the modulation frequency, and are of smaller amplitude than the corresponding harmonics for the single-edge modulation systems. The fact that only odd harmonics exist in the double-edge modulation spectrum might have been anticipated from the static analyses which show that the d.c. transfer functions of the double-edge modulation systems are symmetrical about the origin. The second difference in the frequency spectra is that sideband components ($\omega_c - n\omega_m$) are present only for even values of the integer n, and the components are smaller than the corresponding ones for

single-edge modulation.

As a result of these differences in the spectra for the two types of modulation, it can be seen that double-edge modulation is inherently superior to single-edge modulation as a technique for high power amplification.

5. Application of the analytical results to a practical system

Since it is difficult to make generalised comments on many of the analytical results, it is worthwhile considering a practical system as this will give a clearer insight into the effects of the various parameters on the system performance.

Given below are values for the major parameters of a typical operational amplifier. In order to demonstrate some of the effects more clearly, a value of voltage gain α has been specified which is rather lower than that obtained from commercial amplifiers.

Voltage gain	=	100
Input resistance R_1	=	40 kΩ
Output resistance R_o	=	200 Ω
3dB bandwidth	=	800 kHz

Let the bandwidth of the system input signal be 17 kHz. In order to estimate the required pulse repetition frequency, the specification is made that no sideband components falling within the system passband must be greater than -60 dB with respect to the modulation frequency component.

Assume initially that the system is ideal in all respects except that the integrator has a finite gain. Now it is shown in sections 4.2.1 (Figs. 4.2.4 (a), (b) and (c)) and section 4.2.2 (Figs. 4.2.8 (a) and (b)) that if the normalised time constant $\frac{T_c}{(1 + \alpha) CR}$ is less than 0.1 then the finite integrator gain has negligible effect on the amplitude of the sideband components. Therefore an initial estimate of the required pulse repetition frequency may be made by assuming that $\frac{T_c}{(1 + \alpha) CR}$ is less

than 0.1. Figs. 4.2.4 (c) and 4.2.8 (b) of section 4.2 show that the required pulse repetition frequencies ω_c are:

$\omega_c \geqslant 9\omega_m$ for a single-edge modulation system

$\omega_c \geqslant 7\omega_m$ for a double-edge modulation system

Now the highest frequency of the input signal has been specified as 17 kHz. Therefore:

$f_c \geqslant$ 160 kHz for single-edge modulation

$f_c \geqslant$ 120 kHz for double-edge modulation

where $f_c = \dfrac{\omega_c}{2\pi}$

A typical value for V_1, the input to the integrator in Figs. 2.1 (a) and 2.1 (b) of section 2, is 5v. The output of the integrator is added to the input signal, and the sum applied to the input of the level detector. The accuracy required for the level detector threshold is obviously directly related to the peak amplitude of the integrator output. A typical value for the maximum output of a solid state operational amplifier is $\pm$5v. Having specified the peak integrator output, the integrator input and the gain, the required value of $\dfrac{T_c}{CR}$ may be obtained from Fig. 3.1.6 and 3.1.12 of section 3.1. Therefore, for a peak to peak integrator output of 5v:

$$\frac{T}{CR} = 1.0 \quad \text{for single-edge modulation}$$

$$\therefore \quad \frac{T_c}{(1 + \alpha)\, CR} \doteq 0.01$$

$$\frac{T_c}{CR} = 1.0 \quad \text{for double-edge modulation}$$

$$\therefore \quad \frac{T_c}{(1 + \alpha)\, CR} \doteq 0.01$$

The static error of the two systems may now be evaluated from figs. 3.1.4, 3.1.5, 3.1.10 and 3.1.11 of section 3.1.

Single-edge modulation

$$\text{Static error } E_1 \quad \begin{cases} = 1.88.10^{-3} & \text{for } M = 0.5 \\ = 2.50.10^{-3} & \text{for } M = 0.0 \\ = 1.87.10^{-3} & \text{for } M = -0.5 \end{cases}$$

$$\text{Static error } E_2 \quad \begin{cases} = 1.87.10^{-3} & \text{for } M = 0.5 \\ = 1.87.10^{-3} & \text{for } M = 0.5 \end{cases}$$

Double-edge modulation

$$\text{Static error } E_1 = 7.81.10^{-7} \text{ for } M = 0.5$$

$$\text{Static error } E_2 = -2.60.10^{-7} \text{ for } M = 0.5$$

Since $\frac{T_c}{(1+\alpha)\,CR} < 0.1$ the finite integrator gain has negligible effect on the amplitude of the sideband components, as may be seen from figs. 4.2.4 and 4.2.8 of section 4.2. The harmonic distortion factors of the systems are evaluated from figs. 4.2.3 and 4.2.7. However, some of the distortion factors do not come within the range of the diagrams so that the precise value cannot be evaluated.

Single-edge modulation

Second harmonic distortion = -58 dB for M = 1

Third harmonic distortion < -90 dB for M = 1

Double-edge modulation

Second harmonic distortion does not exist

Third harmonic distortion < -120 dB for M = 1

Up to this point it has been assumed that the system is ideal except for the finite value of integrator gain. The effect of the finite values of amplifier input resistance R_1 and output resistance R_o must now be considered. In order to evaluate the effect of the finite amplifier resistances on the system performance it is necessary to select a value for the integrator time constant resistance R. Now in the analyses of systems with finite values of amplifier input and output resistance (Section 3.2), two resistance ratios occur in the equations: namely $\frac{R_o}{R}$ and $\frac{R}{R_1}$.

In an ideal system both of these ratios are zero. Therefore the value of R should be chosen so that these ratios are as small as possible. Since $R_1 = 40\ k\Omega$ and $R_o = 200\ \Omega$, a reasonable value for R is $5\ k\Omega$. From equations 3.2.39 and 3.2.40 (Section 3.2) the parameters $\frac{CR_o}{\alpha T_e}$ and $\frac{T_c}{T_e}$ may be evaluated.

$$\frac{T_c}{T_e} = \frac{T_c}{CR}\left[\frac{1}{\frac{(1+\alpha)}{1+R/R_1} + \frac{R_o}{R}}\right]$$

$$\frac{CR_o}{\alpha T_e} \quad \frac{1}{\alpha\left[\frac{(1+\alpha)R/R_o}{1+R/R_1} + 1\right]} = 4\cdot5.10^{-6}$$

$\frac{T_c}{T_e} = 1.11.10^{-2}$ for both the single-edge and the double-edge modulation systems. The effect of the finite output resistance on the normalised time constant $\frac{T_c}{T_e}$ is negligible. The finite input resistance, however, does lead to a significant increase in $\frac{T_c}{T_e}$. It is shown in section 3.2.1 that the static error in a single-edge modulation system with finite values of amplifier input and output

resistance is equal to the error in a system with ideal values of input and output resistance and an effective normalised time constant of $\frac{T_c}{T_e}$. Therefore the single-edge modulation system error may be evaluated from figs. 3.1.4 and 3.1.5 of section 3.1.1. From the diagrams it can be seen that the increase in normalised time constant does not lead to a significant increase in static error.

It is shown in section 3.2.2 (equation 3.2.38) that the demodulated output of a double-edge modulation system with finite values of amplifier resistances is equal to the output of a system with ideal values of resistances operating with an effective modulation index $M\phi$ and a normalised time constant $\frac{T_c}{T_e}$. As a result of this, the static error E_1 in the system output is (equation 3.2.38):

$$E_1 = V_{av} + M\phi + M(1-\phi)$$

The above error expression is equivalent to the error E_1 in a system with ideal amplifier resistances, effective modulation index $M\phi$ and normalised time constant $\frac{T_c}{T_e}$, plus an additional error term $M(1-\phi)$. From fig. 3.2.9 of section 3.2.1, the value of the modulation index modifying factor is $\phi = 1.002$ for the system under consideration. The term $(V_{av} + M\phi)$ in the expression for E_1 may be evaluated from fig. 3.1.10, for the error E_1 in a system with ideal amplifier resistances, by replacing M and $\frac{T_c}{(1+\alpha)\,CR}$ with $M\phi$ and $\frac{T_c}{T_e}$ respectively. From the diagram it can be seen that the modified parameters have negligible effect on the term $(V_{av} + M\phi)$. However, the term $M(1-\phi)$ in the expression for E_1 leads to a large increase in error since the term $V_{av} + M\phi$ is $7.8.10^{-7}$ for $M = 0.5$, while $M(1-\phi)$ is $-1.0.10^{-3}$ for $M = 0.5$. Therefore static error $E_1 \triangleq -1.0.10^{-3}$ for $M = 0.5$.

The system static error E_2 is shown in section 3.2.2, equation 3.2.36, to be equal to the static error E_2 in a system with ideal values of amplifier resistances, but with a modified modulation index $M\phi$ and a normalised time constant $\frac{T_c}{T_e}$. Therefore error E_2 may be evaluated from fig. 3.1.11 by replacing M and $\frac{T_c}{(1+\alpha)\,CR}$, in the diagram, with $M\phi$ and $\frac{T_c}{T_e}$ respectively. From the diagram it can be seen that the modified parameters have an insignificant effect on the static error.

Thus it has been shown that, apart from the error E_1 in the double-edge modulation system, the effect of the finite values of amplifier resistances may be ignored in these particular systems. The input resistance R_1 has more effect on the system performance than R_o. For this reason it may be preferable in some systems to reduce the value of the time constant resistance R, hence decreasing the ratio $\frac{R}{R_1}$.

It is of interest to calculate how large the output resistance must be before it seriously affects the modulation index modifying factor ϕ. From fig. 3.2.9 for the factor ϕ, it can be seen that a value of $\frac{CR_o}{T_e} = 10^{-4}$ is required to bring about a change of approximately 5% in the effective modulation index $M\phi$. Calculation, from equation 3.2.39, of the value of R_o required to make $\frac{CR_o}{\alpha T_e} = 10^{-4}$ gives the value of R_o = 4.5 kΩ. However from fig. 3.2.11, this value of R_o would limit the maximum modulation index for the double-edge modulation system to 0.92. Even with a value of R_o = 4.5 kΩ, the effect of the output resistance on the normalised time constant is less than 1%.

Figs. 3.2.6 and 3.2.7 of section 3.2 show that the finite values of amplifier input and output resistance have a negligible effect on the peak value of the integrator output.

The finite values of amplifier resistance do not significantly effect the static error E_2 of the systems. Therefore the spectra of the system outputs will also be unaffected since the analyses of the frequency spectra are derived from the results of the static analyses. Replacing $\frac{T_c}{(1+\alpha)\,CR}$ with $\frac{T_c}{T_e}$ in figs. 4.2.2, 4.2.3 and 4.2.4 for the spectrum of the single-edge modulation system, shows this statement to be true. The spectrum for the double-edge modulation system is obtained by replacing $\frac{T_c}{(1+\alpha)\,CR}$ and M, in figs. 4.2.6, 4.2.7 and 4.2.8, with $\frac{T_c}{T_e}$ and $M\phi$ respectively.

It is now necessary to consider the effects of the finite amplifier bandwidth on the system performance. The upper turnover frequency of the amplifier is specified as 800 kHz so that the amplifier time constant is 1.25 μsec. For the single-edge modulation system the pulse repetition frequency is 160 kHz, and for the double-edge modulation system it is 120 kHz. Therefore the period T_c of the repetition frequency is 6.25 μsec. for single-edge modulation and 8.34 μsec. for double-edge modulation. The results of the static analyses of systems utilising bandwidth integrator amplifiers (Section 3.3) are presented in terms of the parameters T_N and Υ. The normalised time constant T_N is given by equation 3.3.19 (a) (Section 3.3).

$$T_N = \frac{T_c}{(1+\alpha)CR}\left[\frac{1}{1+\frac{T_a}{(1+\alpha)CR}}\right]$$

The factor Υ is given by equation

$$\Upsilon = \frac{CR}{T_a}\left[\frac{T_a}{CR}+1+\alpha\right]^2$$

Therefore:

For the double-edge modulation system:

$$\Upsilon = 6{\cdot}6.10^4$$
$$T_N = 0{\cdot}989.10^{-2}$$

For the single-edge modulation system:

$$\Upsilon = 5{\cdot}5.10^4$$
$$T_N = 0{\cdot}988.10^{-2}$$

The static error in the single-edge modulation system may be evaluated from figs. 3.3.4 and 3.3.6 (Section 3.3.1).

$$\text{Static error } E_1 = \begin{cases} 1.0.10^{-3} & \text{for } M = 0.5 \\ 7.0.10^{-4} & \text{for } M = 0 \\ -8.0.10^{-4} & \text{for } M = -0.5 \end{cases}$$

$$\text{Static error } E_2 = \begin{cases} < 10^{-4} & \text{for } M = 0.5 \\ < 10^{-4} & \text{for } M = -0.5 \end{cases}$$

The static error in the double-edge modulation system is evaluated from figs. 3.3.13 and 3.3.14 (Section 3.3.2).

$$\text{Static error } E_1 = 2.0.10^{-3} \text{ for } M = 0.5$$
$$\text{Static error } E_2 = 2.6.10^{-7} \text{ for } M = -0.5$$

The effect of the finite amplifier bandwidth on the single-edge modulation system is to decrease the static error. This is mainly because the finite bandwidth decreases the amplitude of the demodulated system output when $M = 0$. The finite bandwidth causes a considerable increase in the static error E_1 of the double-edge modulation system but a negligible change in the static error E_2.

The analytical results for the double-edge modulation system are not valid for all values of modulation index. The maximum value of the modulation index M (max), for which the analytical results are valid, is evaluated from fig. 3.3.12 (Section 3.3.1). The value of M (max) obtained from the diagram is 0.999.

The effect of the finite amplifier bandwidth on the frequency spectra of the systems may be evaluated from figs. 4.5.1 to 4.5.6 (Section 4.5). For the single-edge modulation

system figs. 4.5.1, 4.5.2 and 4.5.3 show that the limited bandwidth has negligible effect on the amplitude of the spectral components, the variation being less than 0.5 dB for all components. It is of interest to calculate how small the amplifier bandwidth can be made before any significant change occurs in the harmonic distortion. From fig. 4.5.2, the third and fourth harmonic distortion factors increase rapidly for values of less than 5.10^3. This value of $\curlywedge$ corresponds to an amplifier time constant of $T_a = 12.5\ \mu$sec. (i.e. an upper 3 dB frequency of 80 kHz).

For the double-edge modulation system figs. 4.5.4, 4.5.5 and 4.5.6 show that the finite bandwidth of the amplifier does not produce a significant change in the amplitude of the spectral components, the variation being less than 0.5 dB. The amplitudes of the harmonic distortion components are such that they do not come within the range of the diagrams. However, from the general form of the curves it can be seen that the limited bandwidth will not affect the amplitude of the components. As with the single-edge modulation system, it is of interest to calculate the value of amplifier time constant that is required to produce a significant change in harmonic distortion. Extrapolating from the curves of fig. 4.5.5 shows that the distortion rises rapidly for values of $\curlywedge$ less than 10^4. This value of $\curlywedge$ corresponds to an amplifier time constant of 8.34 μsec. (i.e. an upper turnover frequency of 120 kHz).

Figs. 3.3.7 and 3.3.15 (Section 3.3) show that the finite amplifier bandwidth has a negligible effect on the peak amplitude of the integrator output waveform for both the single-edge modulation and the double-edge modulation systems.

Thus it has been shown that low distortion pulse-length modulation systems can be designed using only moderate performance operational amplifiers. However, as the required system passband is increased so the problem of providing adequate amplifier bandwidth will become more severe.

The effect of hysteresis in the level detector will now be considered. It is shown in the static analysis section (Section 3.4.1) that hysteresis has no effect on the static error and distortion of a single-edge modulation system provided that certain conditions regarding the level detector threshold are satisfied. These conditions are discussed in section 3.4.1. The only effect of the hysteresis on the system performance is to limit the maximum negative value of modulation index for which the modulation process is continuous. This maximum negative modulation index $M_{-}(max)$ is given by equation 3.4.8.

$$M_{-}(max) = -1 - \frac{4}{\hat{v}_2(t)}$$

For the practical system under consideration the value of $\hat{v}_2(t)$, the peak integrator output voltage, is -5v. If the specification is made that the system must operate with negative values of modulation index up to -0.95, then a hysteresis component of $\pm$ 0.0625v can be tolerated.

The analyses of a double-edge modulation system which utilises a hysteretic level detector(Sections 3.4.2 and 4.6.2) show that the demodulated output of the system is identical to that of a non-hysteretic system with an effective modulation index $M\phi$. This means that under conditions of full modulation (i.e. M = 1) the output of the system is equal to that of a non-hysteretic system with modulation index ϕ. If the specification is made that

$\phi = 0.95$ then, from fig. 3.4.5, a normalised hysteresis of up to $\frac{\delta}{\hat{v}_2(t)} = 0.05$ can be tolerated. The peak to peak integrator output (i.e. $2\hat{v}_2(t)$) is 5v so that the level detector hysteresis must not exceed $\pm$ 0.125v.

It is shown in section 3.4.2 (equation 3.2.38) that the system static error E_1 is given by the expression:

$$E_1 = V_{av} + M\phi + M(1-\phi)$$

The term $(V_{av} + M\phi)$ in the above expression is equal to the static error E_1 of a non-hysteretic system operating with an effective modulation index $M\phi$. (See discussion following equation 3.2.38). Thus $V_{av} + M\phi$ may be evaluated from fig. 3.1.10, for the error E_1 in a non-hysteretic system, by replacing M with $M\phi$. The diagram gives a value of $(V_{av} + M\phi)$, for $M\phi = 0.475$, which is negligibly different from the error E_1 of a non-hysteretic system with $M = 0.5$ (i.e. $E_1 \triangleq 7.8.10^{-7}$). The term $M(1-\phi)$ leads to a large increase in error since its value is 0.025 for a modulation index of $M = 0.5$. Therefore the effect of the level detector hysteresis is to increase the system static error E_1 from $7.8.10^{-7}$ to approximately 0.025. However, care is required in interpreting this large increase in error, as is discussed in section 3.4.2. (See discussion following equation 3.4.28).

Equation 3.4.29 shows that the static error E_2 of a double-edge modulation system with a hysteretic level detector is equal to the static error E_2 of a non-hysteretic system with a modulation index of $M\phi$. Therefore the error E_2 may be evaluated from fig. 3.1.11 by replacing M with $M\phi$. Since ϕ is less than unity the effect of the hysteresis is to reduce the error E_2. However, it must be remembered that the system output is also decreased so that no real advantage is gained from

increasing the level detector hysteresis.

It is shown in section 4.6.2 (Equations 4.6.8 and 4.6.9) that the frequency spectrum of a double-edge modulation system with hysteresis is identical to that of a non-hysteretic system with modulation index $M\phi$. Figs. 4.2.6, 4.2.7 and 4.2.8 for the spectrum of a non-hysteretic system may therefore be used to evaluate the spectrum of the hysteretic system by replacing M with $M\phi$ in the diagrams. Since ϕ is less than unity the effect of the hysteresis is to reduce the harmonic distortion. However, as with the static error E_2, no advantage is gained by increasing the hysteresis since the modulation frequency component is also reduced. If the modulation index of the hysteretic system is adjusted to give the same modulation frequency component output as the non-hysteretic system, then the spectra for the two systems are identical.

In the practical example just considered the system parameters have a negligible effect on the amplitude of the sideband components so that the initial estimate of the required pulse-repetition frequency is adequate. The initial value of the repetition frequency is chosen under the assumtion that, apart from the finite integrator gain, the system is ideal. With some systems it may be found that the effect of the other system parameters, on the sideband components, make the initial value of repetition frequency inadequate. When this is the case it is necessary to choose a higher frequency and repeat the design process.

6. Experimental Work

6.1. Experimental Apparatus

Since the methods used for the analyses of single-edge modulation and double-edge modulation systems are the same for each system, experimental verification of the analytical results is carried out only for double-edge modulation. Figs. 6.1.1(a), (b) and (c) show the circuit for a double-edge modulation system with variable values of integrator gain, amplifier input resistance, amplifier output resistance, amplifier bandwidth and level-detector hysteresis.

The square-wave generator (fig. 6.1.1(a).) consists of a self-starting multivibrator[64] utilising standard integrated logic circuits. The multivibrator is designed to operate at 40 kHz, and the frequency can be adjusted over a small range by means of RV1. The variable resistance RV1 actually varies only one of the two multivibrator time constants so that the mark-space ratio is varied as well as the frequency. However, this does not matter since the output of the multivibrator is connected to the input of a binary circuit. The output of the binary stage has a frequency which is half that of the multivibrator, and an accurately defined mark-space ratio of unity. The discrete component circuit, following the binary stage, increases the amplitude of the square-wave. Thus the frequency of the square-wave generator output is 20 kHz, this value being chosen from consideration of the spectrum analysis equipment available.

The operational integrator is shown in fig. 6.1.1(b). In order to make measurement of the system performance easier,

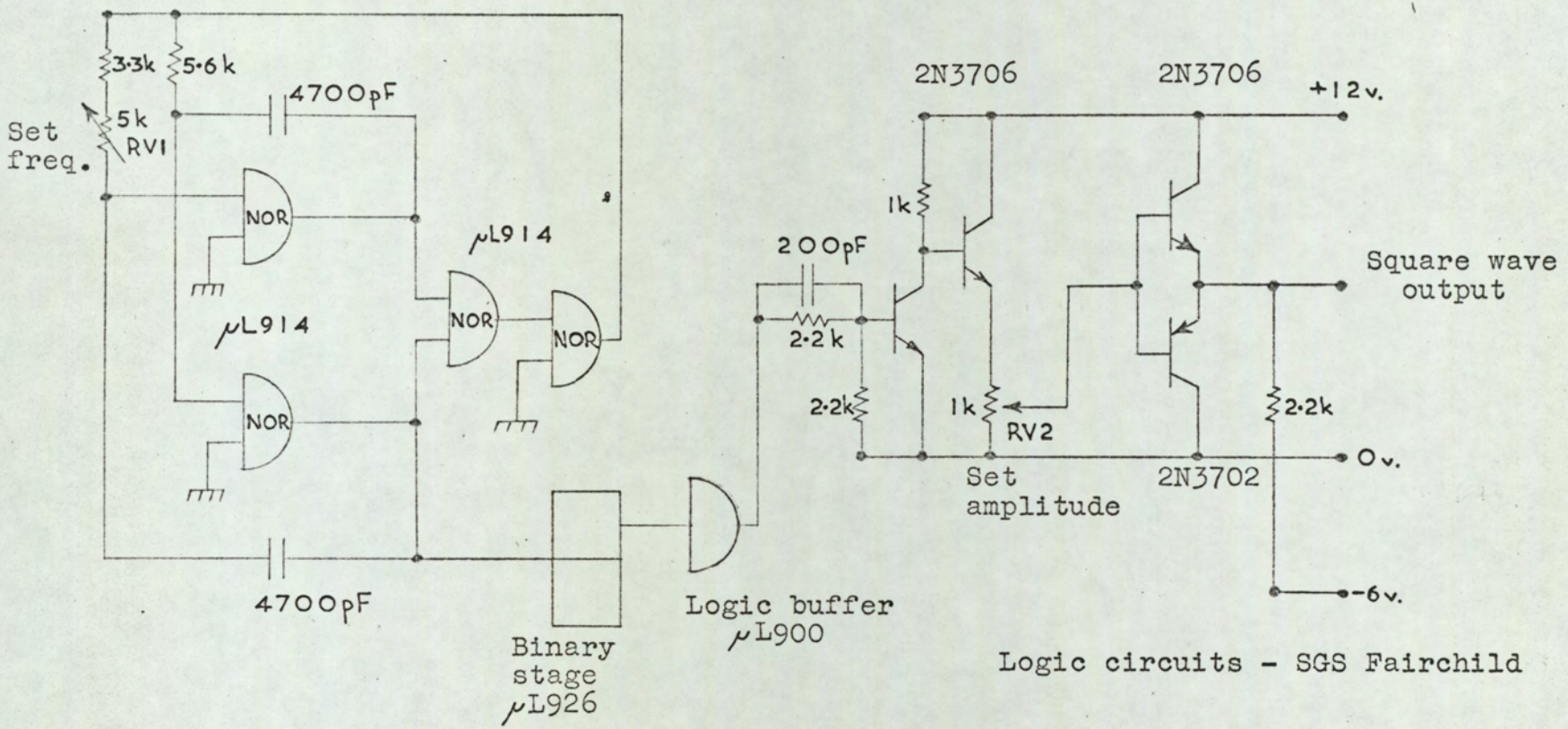

Fig.6.1.1(a). Circuit diagram for square wave generator.

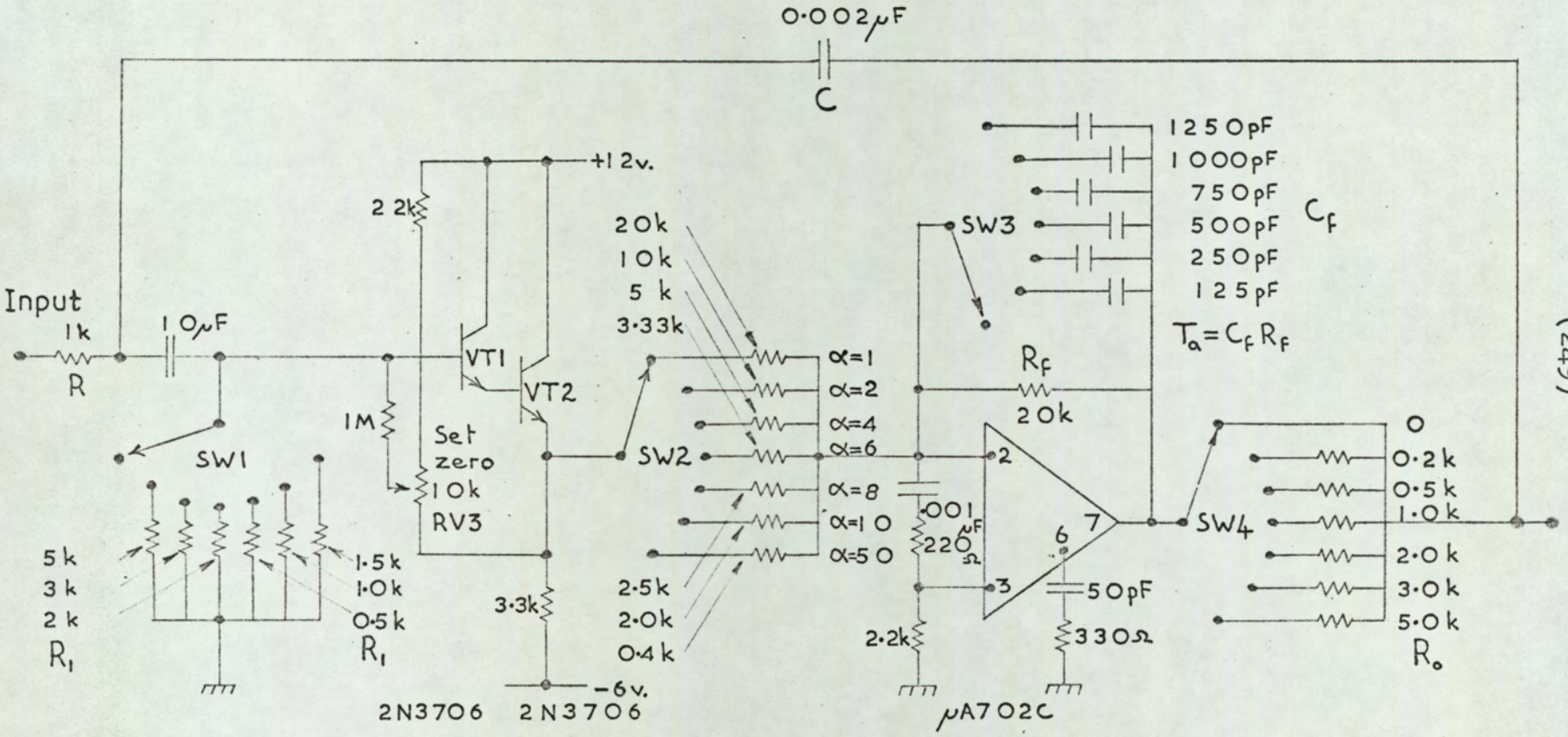

Fig.6.1.1(b). Circuit diagram for operational integrator with variable gain, bandwidth, input resistance and output resistance.

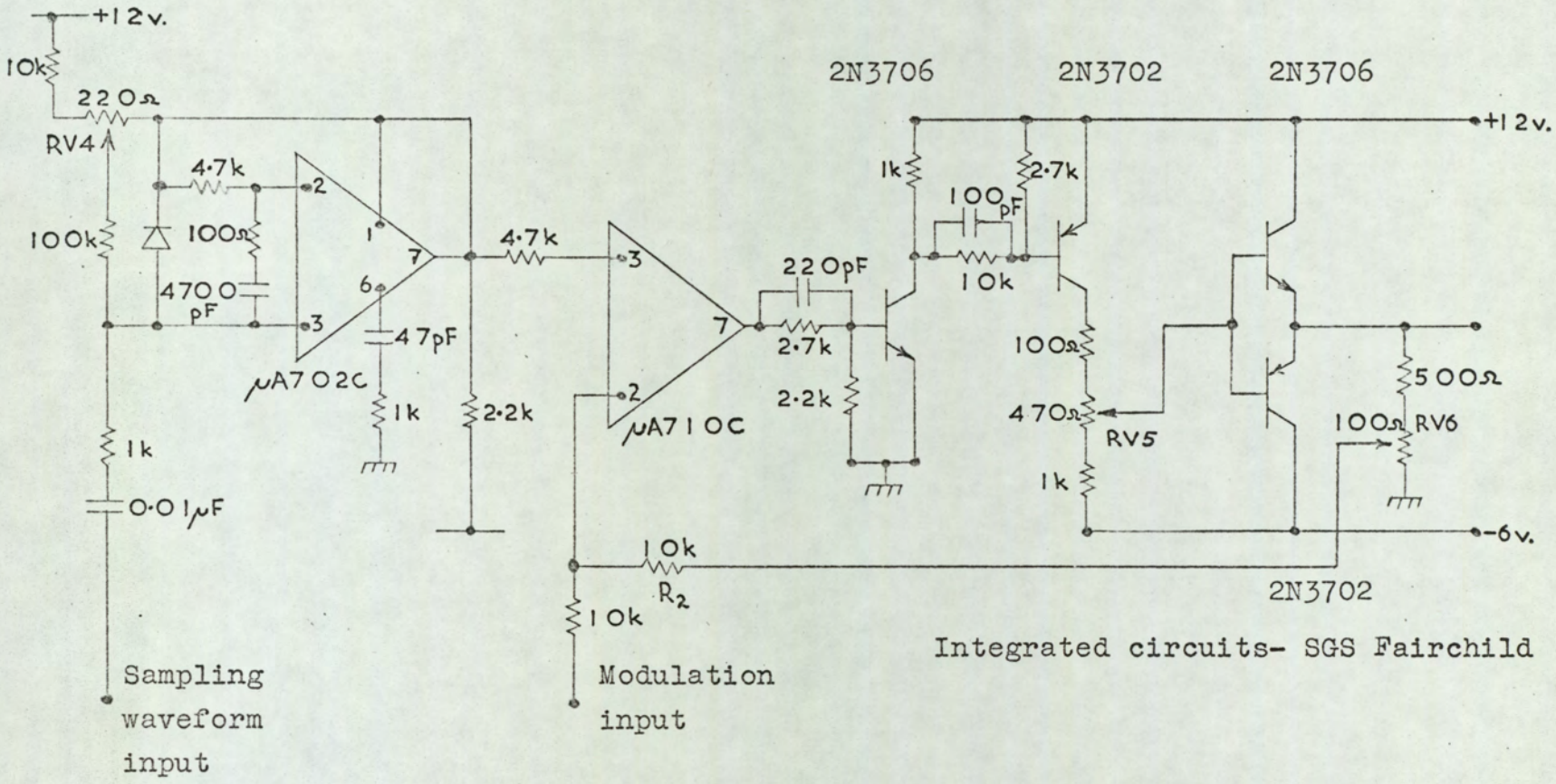

Fig.6.1.1(c). High input resistance level detector with variable hysteresis.

the values of the integrator parameters have been selected to give a markedly non-linear sampling waveform. The value chosen for the normalised time constant $\frac{T_c}{CR}$ is 25.

Since T_c, the period of the square-wave input, is 50 μsec., the time constant CR is 2 μsec. Transistors VT1 and VT2 are a super-alpha pair with high input resistance ($> 1M\Omega$). The high input resistance is required in order to approximate to an ideal system (i.e. amplifier input resistance $R_1 = \infty$). SW1 provides a means of switching finite values of amplifier input resistance R_1 into circuit. The output of the super-alpha pair is connected to the input of an integrated circuit operational amplifier via switched input resistances. These input resistances were adjusted on test to give the values of voltage gain α shown in the circuit diagram. The bandwidth of the amplifier is varied by means of SW3. This method of varying the bandwidth was chosen in preference to introducing a further high input resistance amplifier and switching capacitors to earth (i.e. in the same manner as the amplifier input resistance R_1 is varied), since additional amplifier stages lead to stability problems due to stray capacitances. The operational amplifier with capacitive feedback closely approximates to a single time constant as may be seen by analysing the circuit shown in fig. 6.1.2.

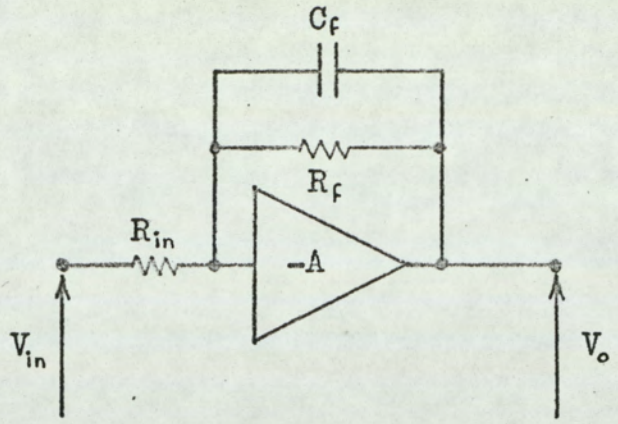

Fig. 6.1.2.

The transfer function of the above circuit is:

$$\frac{V_o}{V_{in}} = \frac{\dfrac{-A}{1+(1+A)\,R_{in}/R_f}}{1+\dfrac{(1+A)\,s\,C_f R_f \cdot R_{in}/R_f}{1+(1+A)\,R_{in}/R_f}} \qquad (6.1.1)$$

The voltage gain A of the μA702C amplifier is 3.10^3. The tests with limited bandwidth were carried out with an integrator gain of 4 (i.e. $R_{in} \triangleq \frac{1}{4} R_f$). Substituting these values in equation 6.1. shows that an accurate approximation to the transfer function is:

$$\frac{V_o}{V_{in}} \simeq \frac{-\alpha}{1 + sT_a} \qquad (6.1.2)$$

where

$$\alpha = \frac{A}{1 + (1+A)^{R_{in}/R_f}}$$

$$T_a = C_f R_f$$

Equation 6.1.2. has the form specified for the bandwidth limited amplifier in the analytical section (section 3.3.1., equation 3.3.1.). The values of effective amplifier time constant $T_a = C_f R_f$ are shown in the circuit diagram. The two capacitance-resistance networks associated with the operational amplifier are to ensure that the amplifier is stable, the values of the components being selected in accordance with the amplifier manufacturers published procedure[65]. Switch SW4 enables finite values of effective amplifier output resistance R_o to be connected into the circuit.

The level-detector circuit is shown in fig. 6.1.1(c). The μA702C integrated circuit is a high gain operational amplifier, and the unity series feedback loop provides a high input resistance. The high input resistance is necessary to avoid loading the output of the integrator when carrying out tests on the effect of finite amplifier output resistance, R_o. The general design of a unity feedback amplifier is discussed in the manufacturers' literature[65] and

will not be considered here. It was shown in the analytical sections that, for a double-edge modulation system, the level-detector threshold should be set to zero. Therefore in the generalised system of fig. 2.1(a) (section 2), the output of the level-detector changes state whenever the sum of the modulating input voltage and the instantaneous integrator output voltage is equal to zero (i.e. the modulating input voltage and integrator output are equal and opposite). The μA710C level-detector shown in the circuit diagram is the differential comparator type (i.e. the output changes state whenever the voltages applied to its two inputs are equal). Therefore the pulse-edges occur when the instantaneous integrator output voltage and the modulating input voltage are equal, as opposed to the generalised system (fig. 2.1(a).) where the pulse-edges occur when the voltages are equal and opposite. However, this difference is of no consequence since it merely introduces a 180^{o} phase change in the demodulated wavetrain. The discrete component circuit following the μA710C level-detector increases the peak to peak output voltage of the system. Potentiometer RV5 is adjusted to make the output waveform symmetrical about zero volts. Hysteresis is provided by the positive feedback network RV6, R_2.

6.2. System Performance with Finite Integrator Gain

With the amplifier input resistance (R_1), amplifier output resistance (R_o) and amplifier time constant (T_a) switches set to the ideal positions (i.e. $R_1 = \infty$, $R_o = 0$, $T_a = 0$) and the hysteresis set to zero, the d.c. transfer function of the system was measured for a range of values of integrator gain α. The pulse-length modulated wavetrain at the system output was demodulated by passing it through a low-pass filter with a pass-band much less than the pulse repetition frequency. For each value of integrator gain, the amplitude of the square wave input was adjusted to give an integrator output of approximately 3v. peak to peak.

Fig. 6.2.1. shows the measured and theoretical system transfer function for a range of values of integrator gain and modulation index. The theoretical curves are calculated from equation 3.1.36. of section 3.1.2.

The components of the frequency spectrum were measured for a range of values of integrator gain and modulation index. Fig. 6.2.2. shows the third harmonic distortion factor DF_3 as a function of the normalised time constant $\frac{T_c}{(1+\alpha)CR}$ and the modulation index. The theoretical curves were calculated from equation 4.2.33. of section 4.2.2. Measurements below - 60 B were not reliable due to the noise level of the spectrum analyser and the harmonic distortion of the modulation signal source. Figs. 6.2.3(a) and (b) show the measured and theoretical values of the sideband components as functions of the normalised time constant $\frac{T_c}{(1+\alpha)CR}$ for $M = 0.5$ and

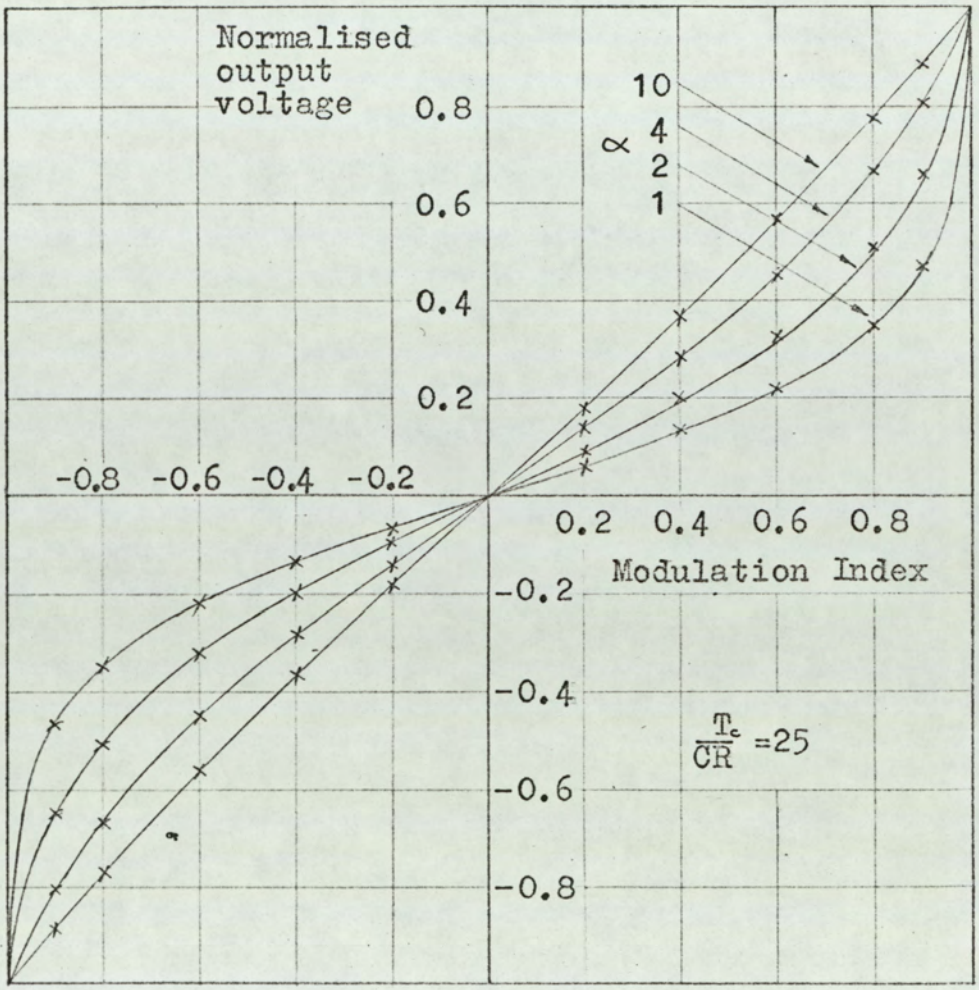

Fig.6.2.1. Transfer function of double-edge modulation system with finite integrator gain.

—— =Theoretical curve

× =Measured value

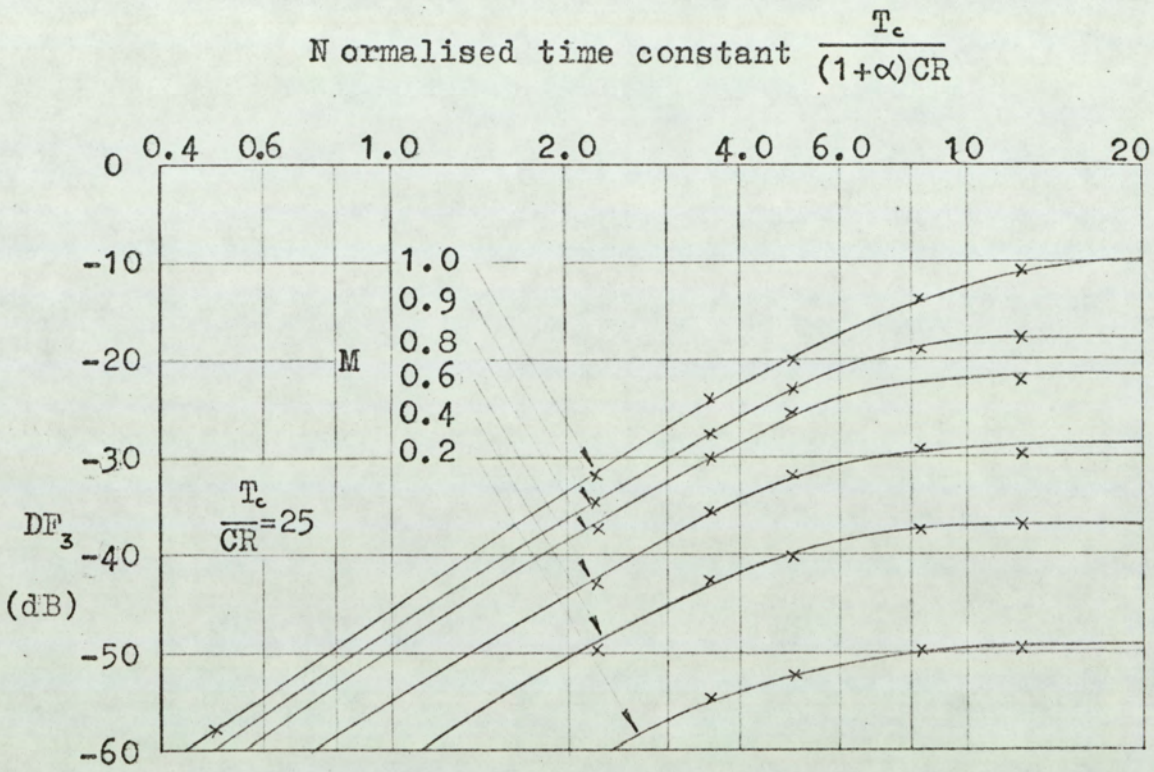

Fig.6.2.2. Third harmonic distortion DF_3 for double-edge modulation system with finite integrator gain.

——=Theoretical curve

× = Measured value

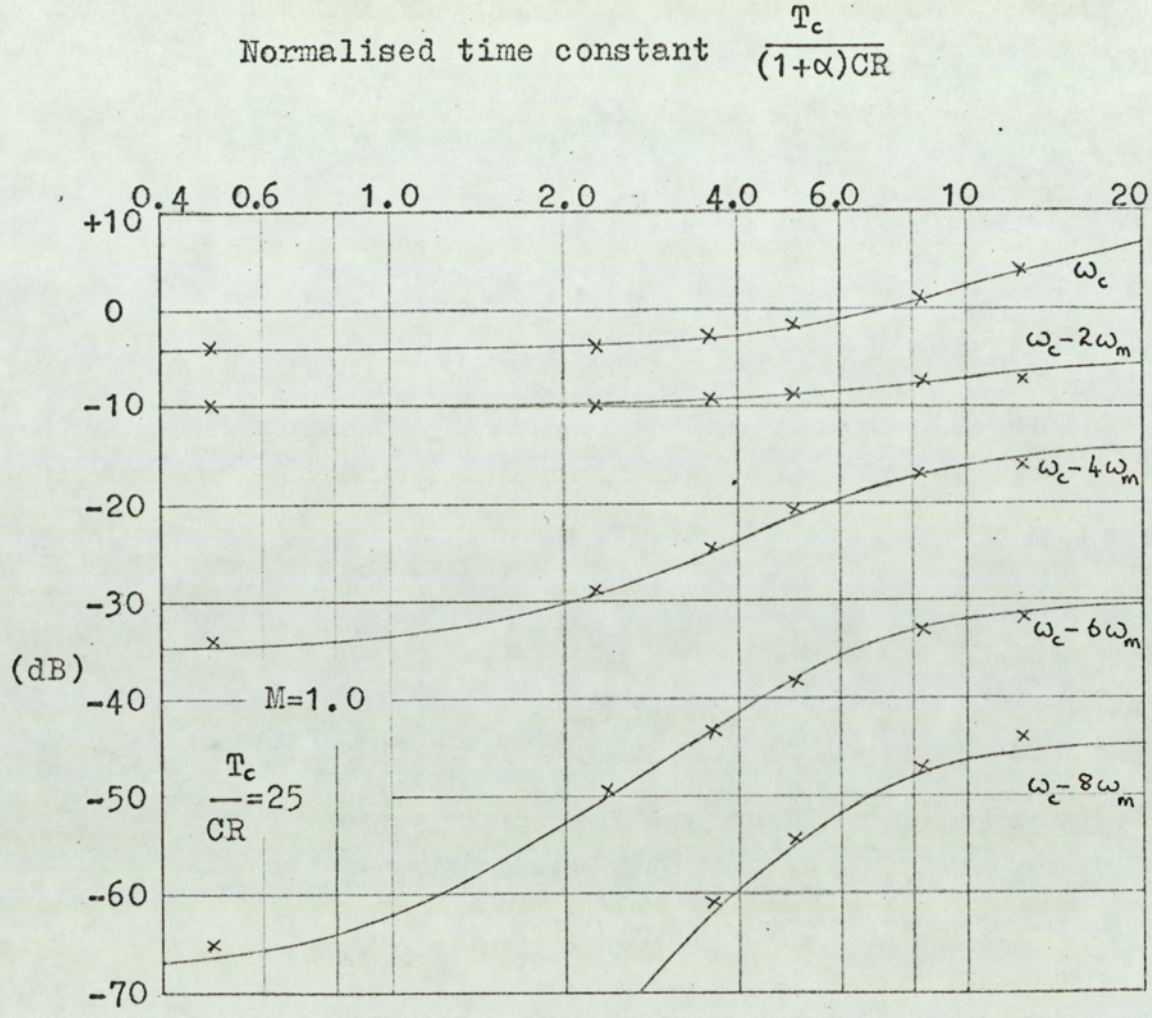

Fig.6.2.3(a). Amplitude of sideband components relative to modulation frequency component for double-edge modulation system with finite integrator gain.

——= Theoretical curve

× = Measured value

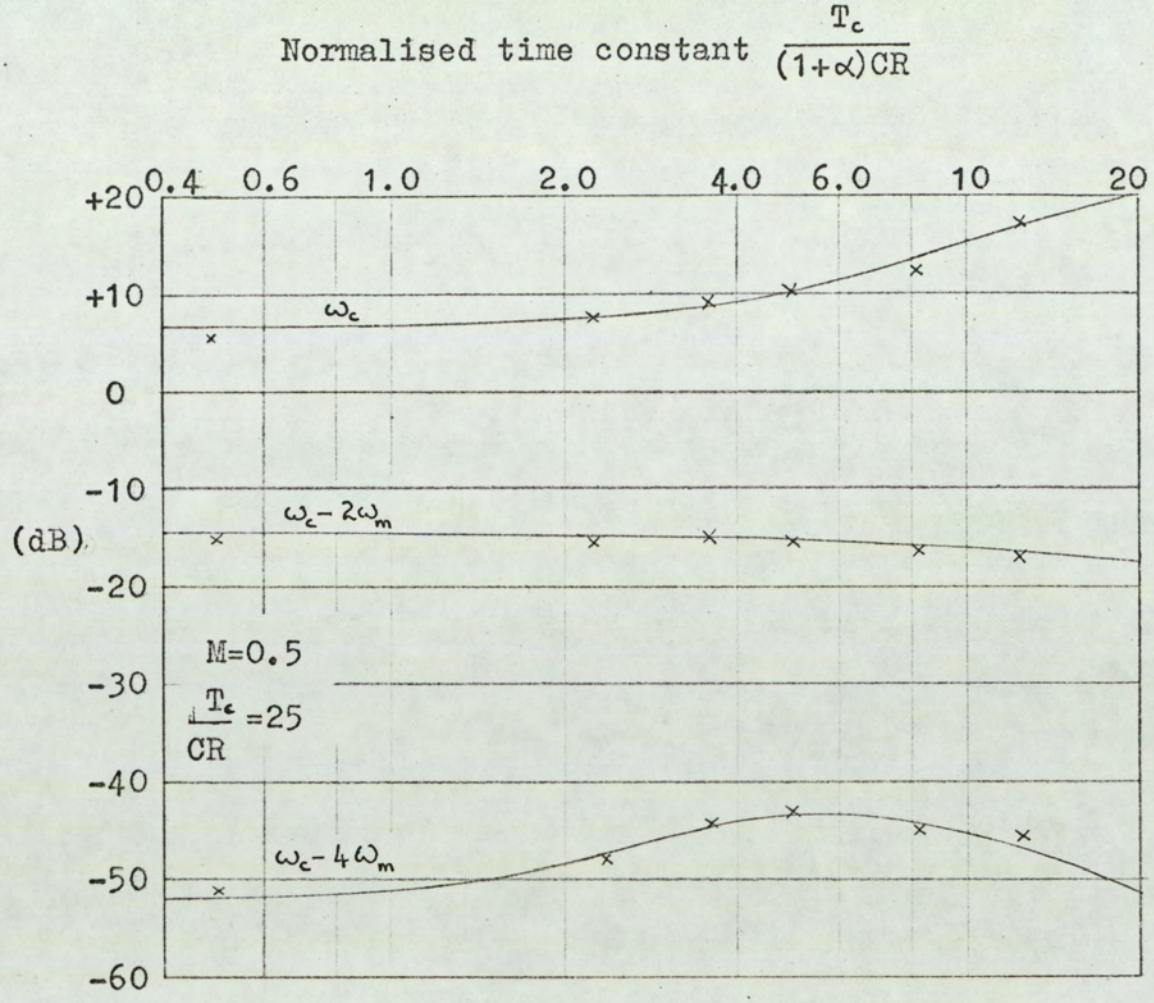

Fig.6.2.3(b). Amplitude of sideband components relative to modulation frequency component for double-edge modulation system with finite integrator gain.

— = Theoretical curve

× = Measured value

$M = 1.0$. The theoretical values of the spectral components were calculated from equation 4. 2. 31. , section 4. 2. 2.

6.3. System Performance with Finite Values of Amplifier Input and Output Resistance

The d.c. transfer function of the system was measured for the range of values of amplifier input resistance R_1 provided by SW1 in the circuit diagram. For the measurements the integrator gain was set to 4.0, the amplifier output resistance set to zero, and the amplifier time constant set to zero. Fig. 6.3.1. shows the measured results together with the theoretical transfer function calculated from equation 3.2.33. of section 3.2.2.

A similar set of measurements were made to determine the system transfer function for finite values of amplifier output resistance, R_o. These measurements were made under two conditions: namely with the amplifier input resistance $R_1 = \infty$, and with the amplifier input resistance R_1 equal to the integrator time constant resistance R. It is shown in section 3.2.2. that the analytical results are not valid for all values of modulation index. The maximum positive value of modulation index for which the theory is valid is defined as that value which causes the leading edge of the pulse to occur at time $\frac{T_c}{2}$ (see discussion preceding equation 3.2.41. of section 3.2.2.). The effect of the finite output resistance is such that under these conditions the trailing-edge of the pulse does not occur at time $\frac{T_c}{2}$. This maximum value of modulation index was checked experimentally. Fig. 6.3.2. shows the measured and theoretical transfer function of the system for a range of values of amplifier output resistance R_o,

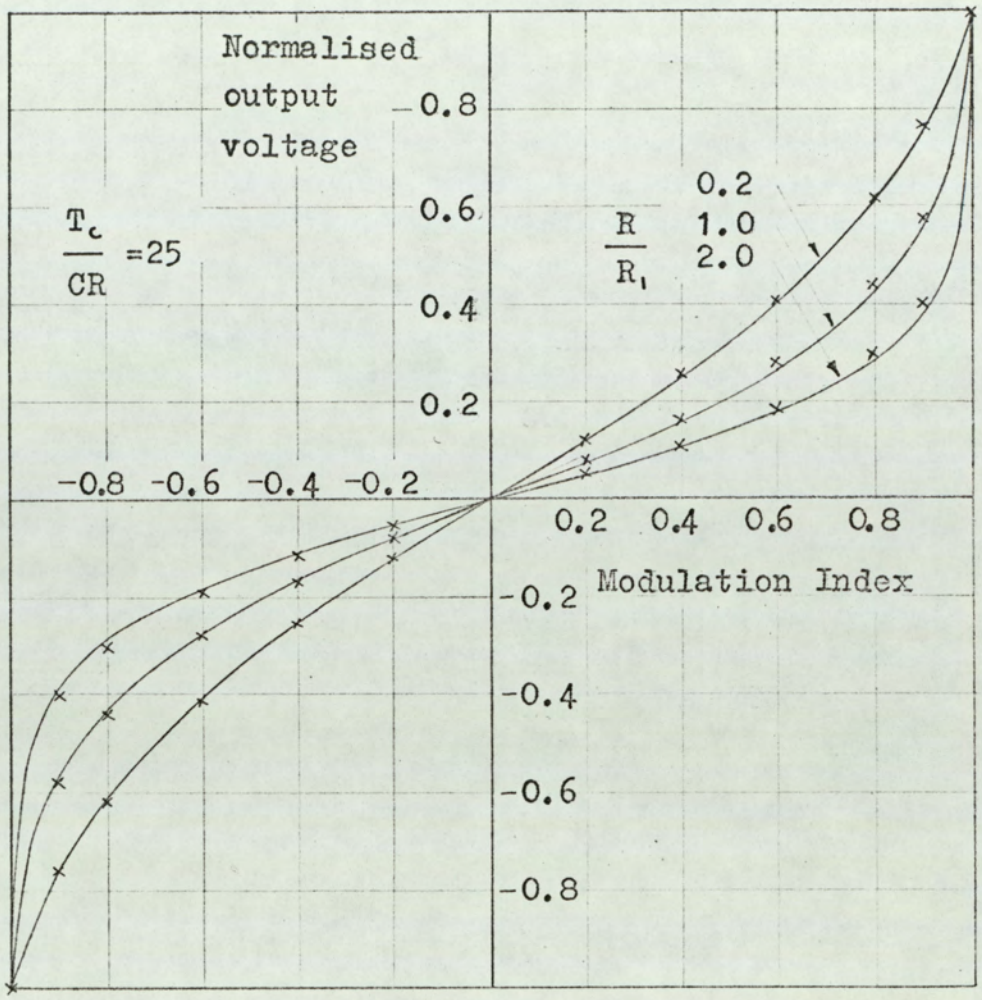

Fig.6.3.1. Transfer function of double-edge modulation system with finite amplifier input resistance.

Integrator gain = 4

—— = Theoretical curve

× = Measured value

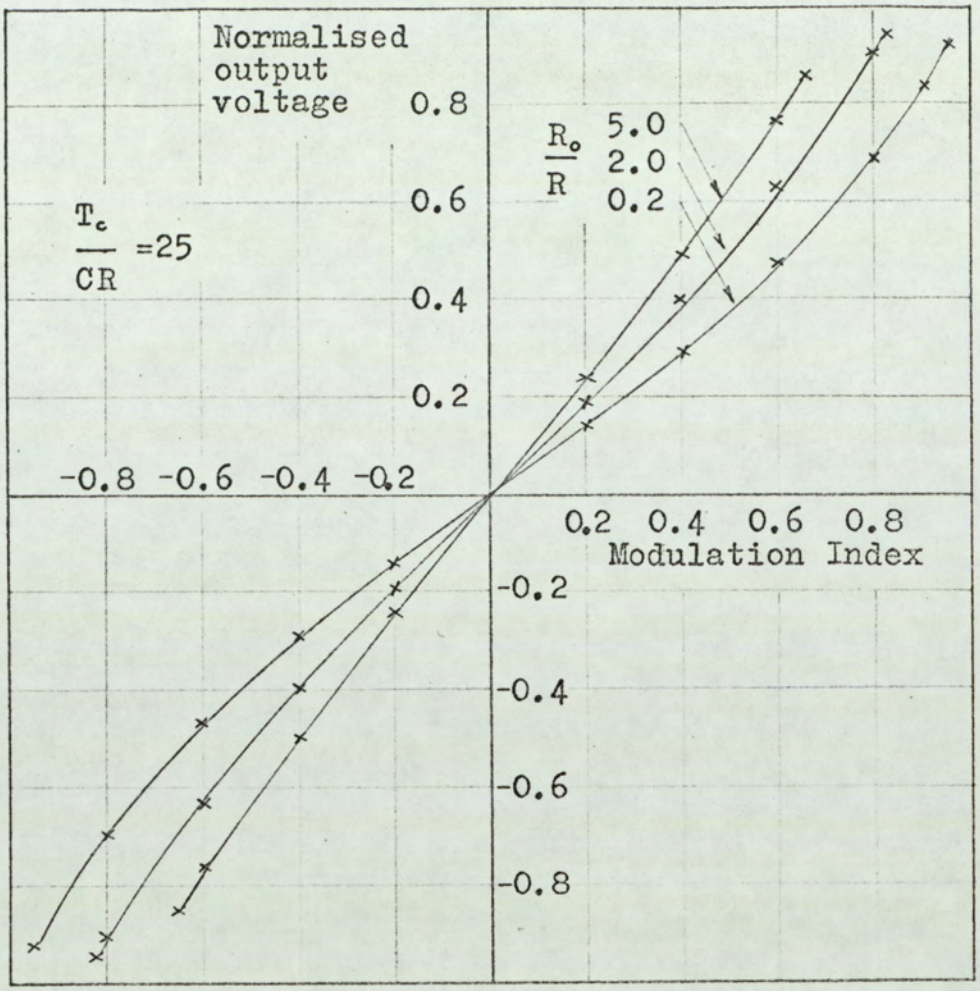

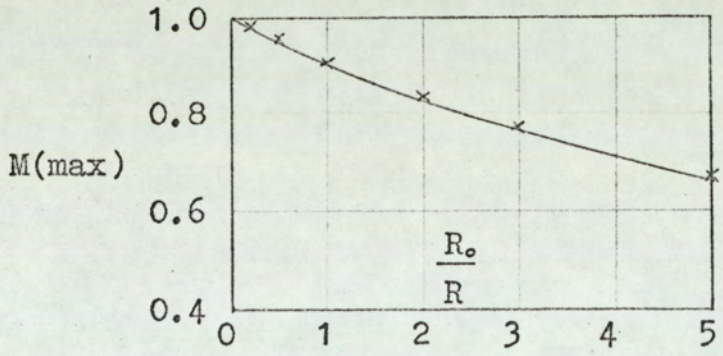

Fig.6.3.2. Transfer funtion and maximum modulation index for double-edge modulation system with finite amplifier output resistance.

Amplifier input resistance R = ∞
Integrator gain = 4

—— = Theoretical curve

× = Measured value

the amplifier input resistance R_1 being infinity. Also shown in fig. 6.3.2. are the measured and theoretical values of maximum modulation index. Fig. 6.3.3. shows the system transfer function for a range of values of output resistance R_o with the amplifier input resistance R_1 equal to the integrator time constant resistance R. The corresponding values of maximum modulation index are also shown in fig. 6.3.3. For both fig. 6.3.2. and fig. 6.3.3., the theoretical transfer function was calculated from equation 3.2.33 (section 3.2.2.), and the theoretical values of modulation index calculated from equation 3.2.43 (section 3.2.2).

The frequency spectrum of the output of a double-edge modulation system, with finite values of amplifier input and output resistance, is given by equation 4.3.14 (section 4.3.2.). Fig. 6.3.4. shows the measured and theoretical values of third harmonic distortion for a range of values of amplifier input resistance and modulation index, the output resistance being zero. Figs. 6.3.5(a). and (b) show the amplitudes of the sideband components as functions of the amplifier input resistance for values of modulation index of 1.0 and 0.5. The measured and theoretical values of third harmonic distortion in the system with finite amplifier output resistance are shown in fig. 6.3.6. The amplitudes of the sideband components are shown in fig. 6.3.7. for a modulation index of 0.5. The measured and theoretical third harmonic distortion in the system having finite values of both amplifier input resistance and output resistance is shown in fig. 6.3.8. for a range of values of modulation index. The

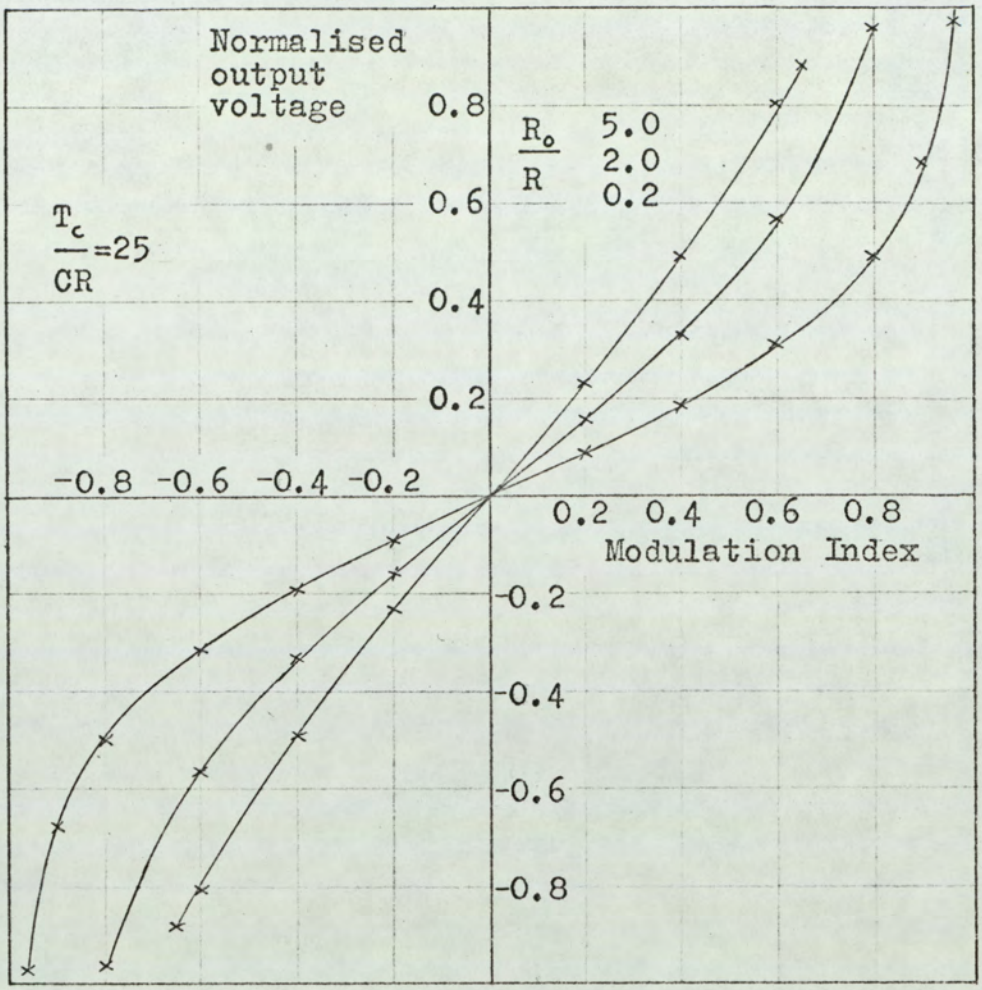

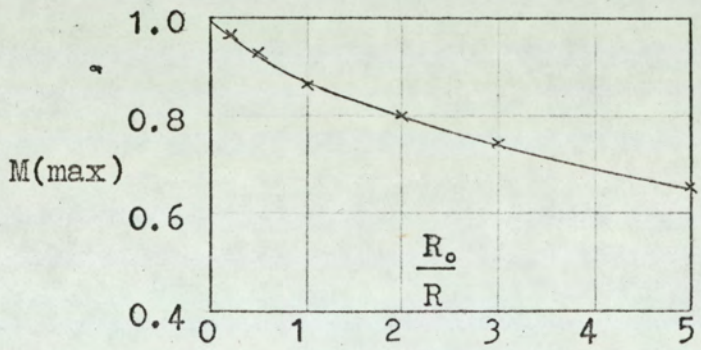

Fig.6.3.3. Transfer function and maximum modulation index for double-edge modulation system with finite amplifier input and output resistance.

Amplifier input resistance R_i= Time constant resistance R
Integrator gain =4

— = Theoretical curve

× = Measured value

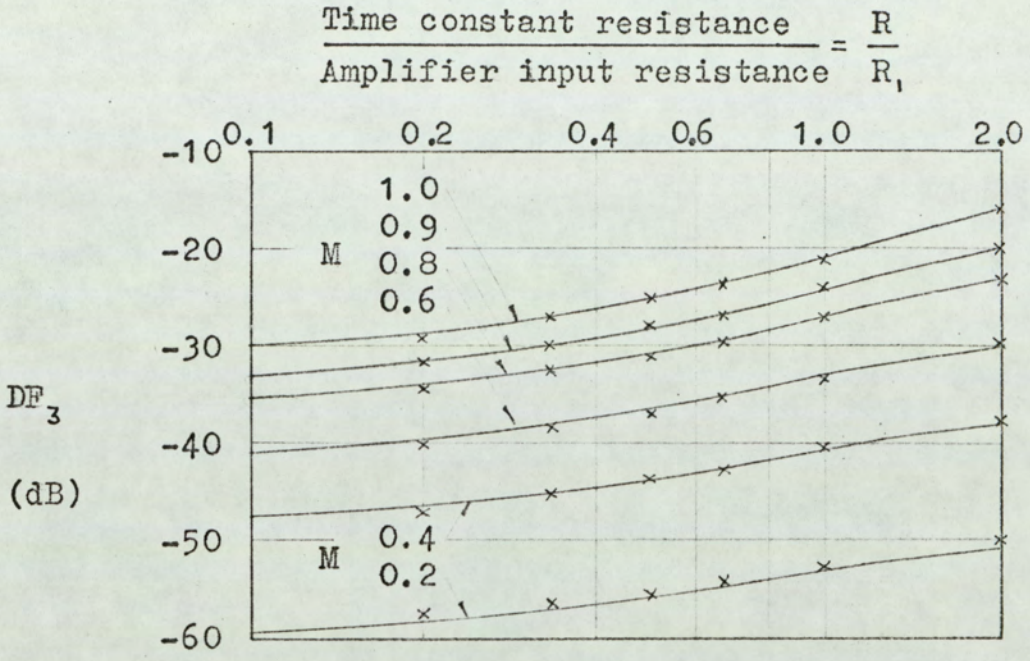

Integrator gain =10

Output resistance R_o =0

$\frac{T_c}{CR}$ =25

Fig.6.3.4. Third harmonic distortion in double-edge modulation system with finite amplifier input resistance

— = Theoretical curve

× = Measured value

$$\frac{\text{Time constant resistance}}{\text{Amplifier input resistance}} = \frac{R}{R_i}$$

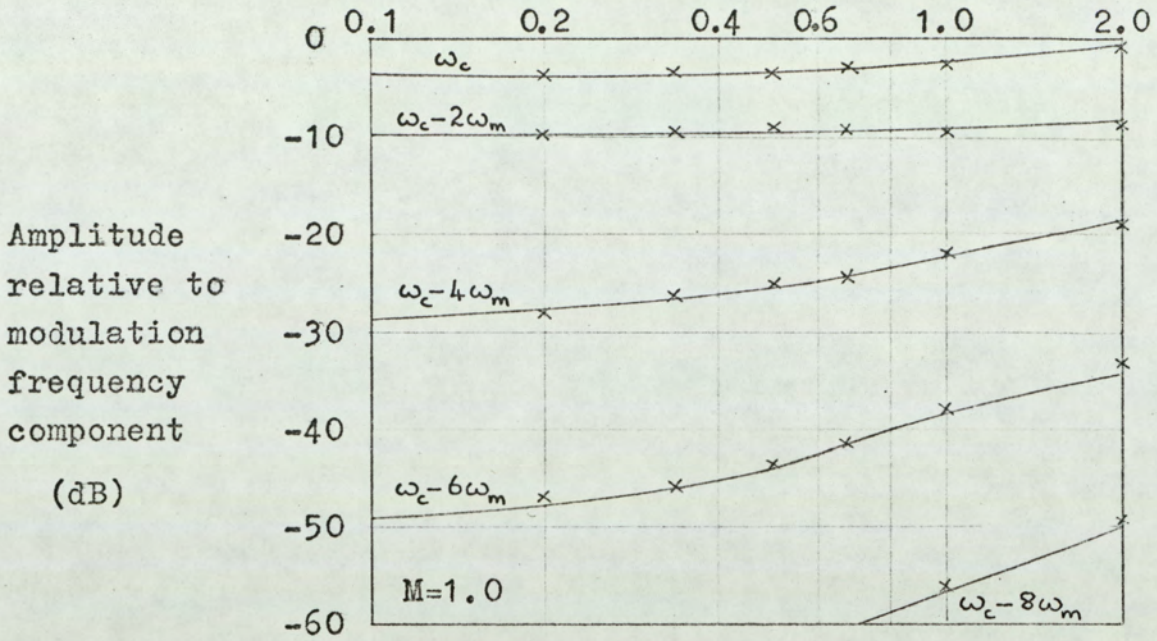

Integrator gain =10

Output resistance $R_o = 0$

$\frac{T_c}{CR} = 25$

Fig.6.3.5(a). Amplitude of sideband components for double-edge modulation system with finite amplifier input resistance.

— = Theoretical curve

× = Measured value

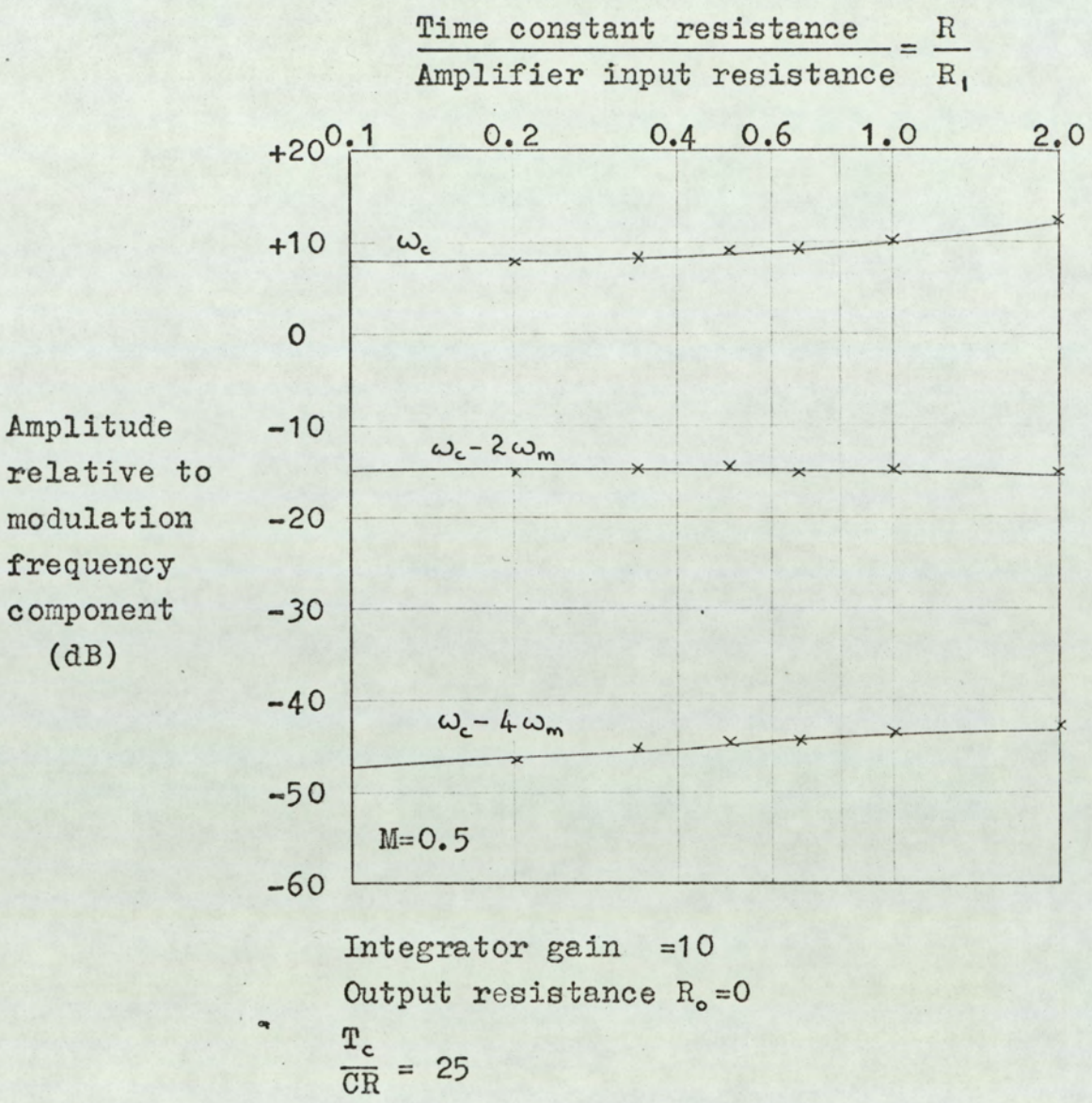

Fig.6.3.5(b). Amplitude of sideband components for double-edge modulation system with finite amplifier input resistance.

—— = Theoretical curve

× = Measured value

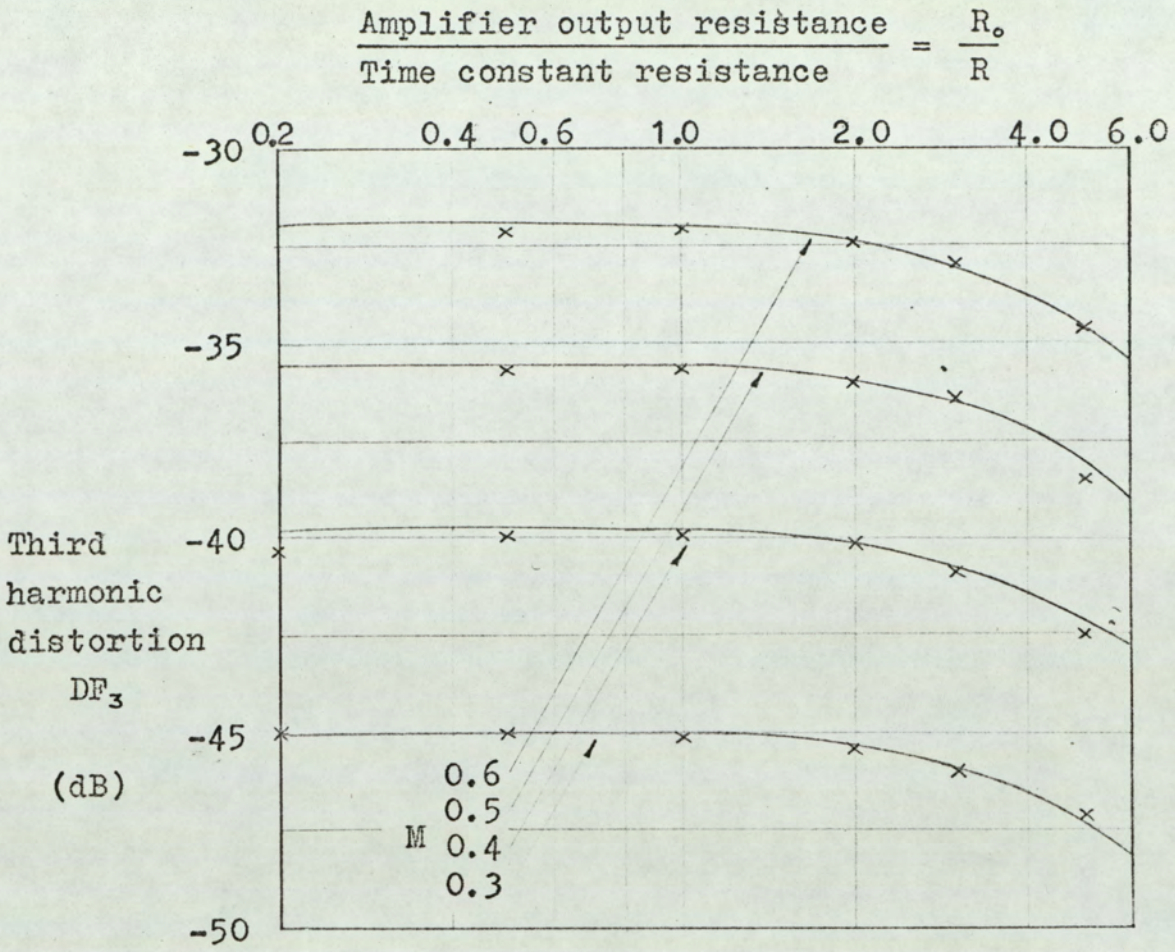

Integrator gain =4

Input resistance $R_1 = \infty$

$\frac{T_c}{CR}$ =25

Fig.6.3.6. Third harmonic distortion for double-edge modulation system with finite amplifier output resistance

—— = Theoretical curve

× = Measured value

$$\frac{\text{Amplifier output resistance}}{\text{Time constant resistance}} = \frac{R_o}{R}$$

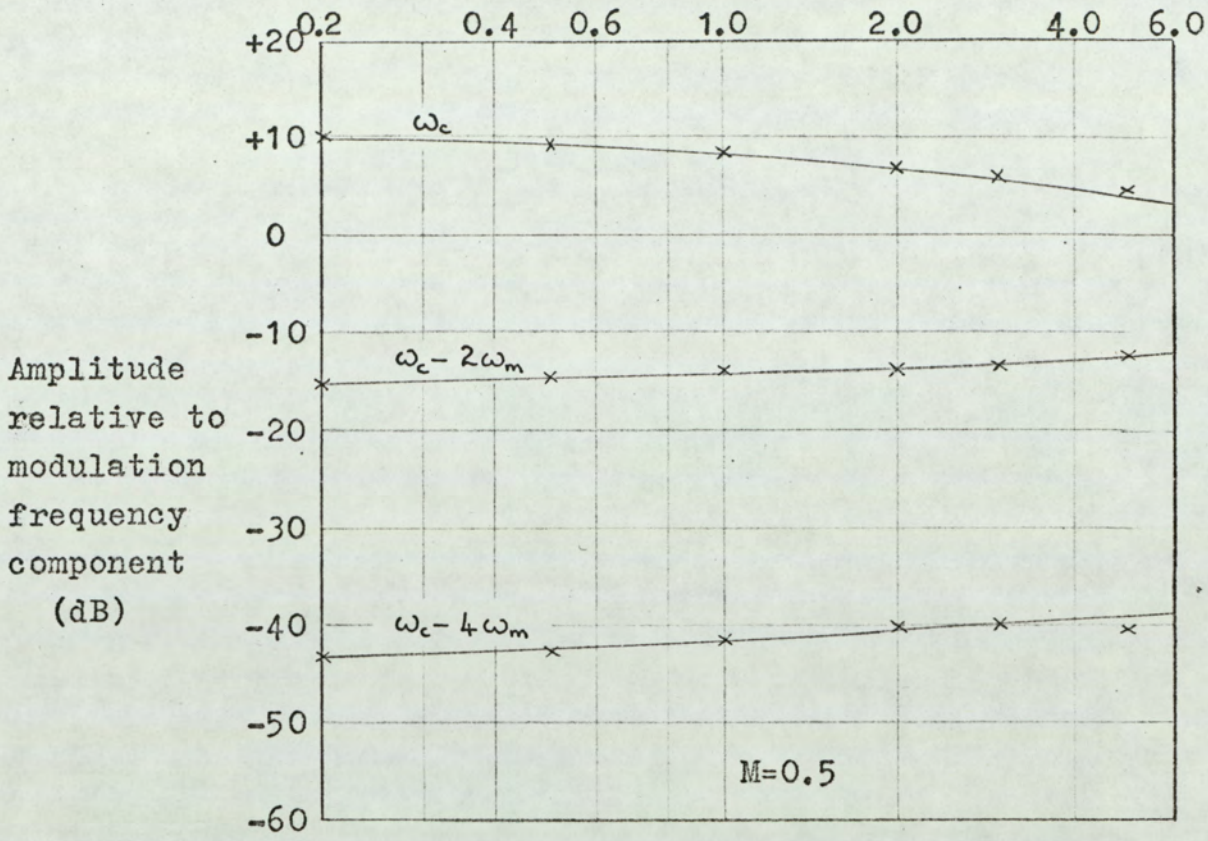

Integrator gain =4

Input resistance $R_1 = \infty$

$\frac{T_c}{CR}$ =25

Fig.6.3.7. Amplitude of sideband components for double-edge modulation system with finite amplifier output resistance.

—— = Theoretical curve

× = Measured value

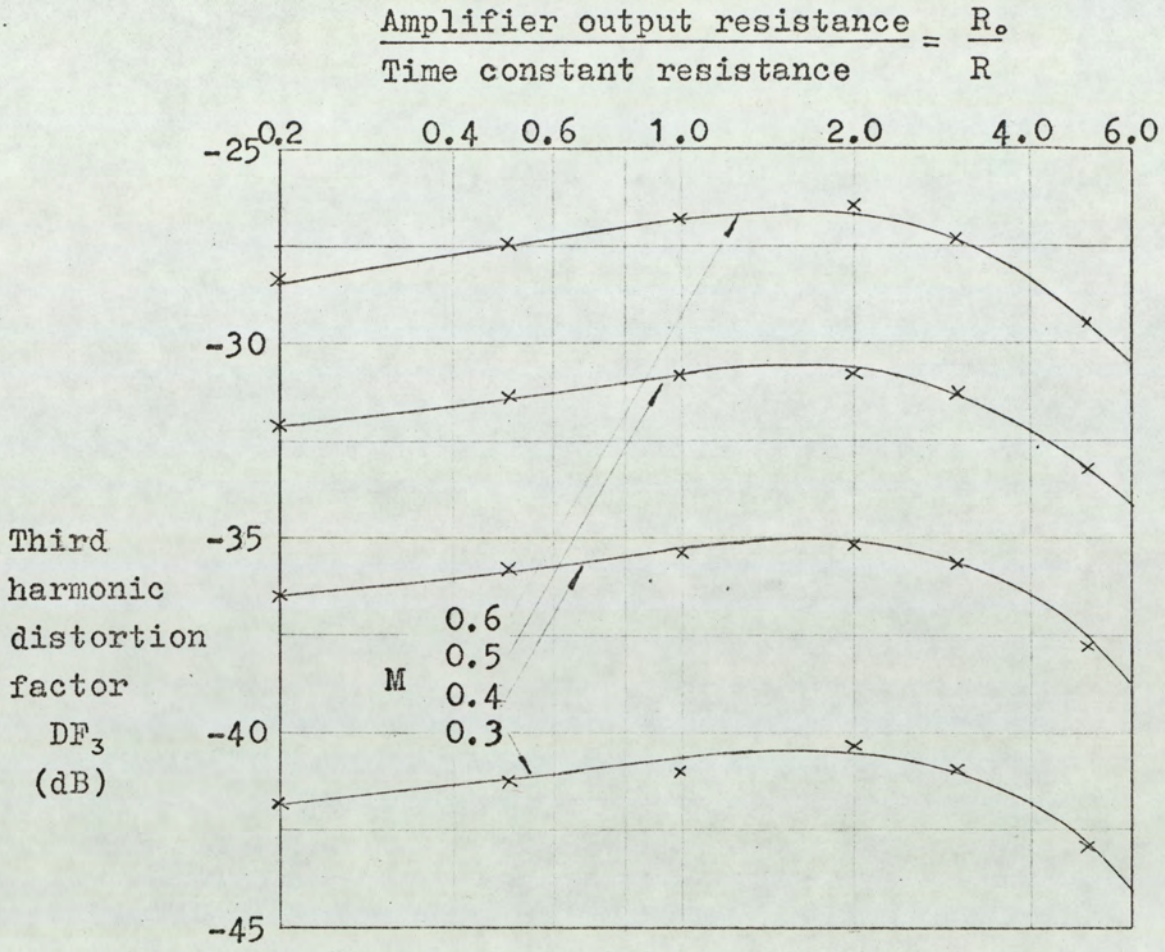

Integrator gain =4

Input resistance R_i = Time constant resistance R

$$\frac{T_c}{CR} = 25$$

Fig.6.3.8. Third harmonic distortion for double-edge modulation system with finite values of amplifier input and output resistance.

—— = Theoretical curve

× = Measured value

amplitudes of the sideband components for the system are shown in fig. 6.3.9. for a modulation index $M = 0.5$.

$$\frac{\text{Amplifier output resistance}}{\text{Time constant resistance}} = \frac{R_o}{R}$$

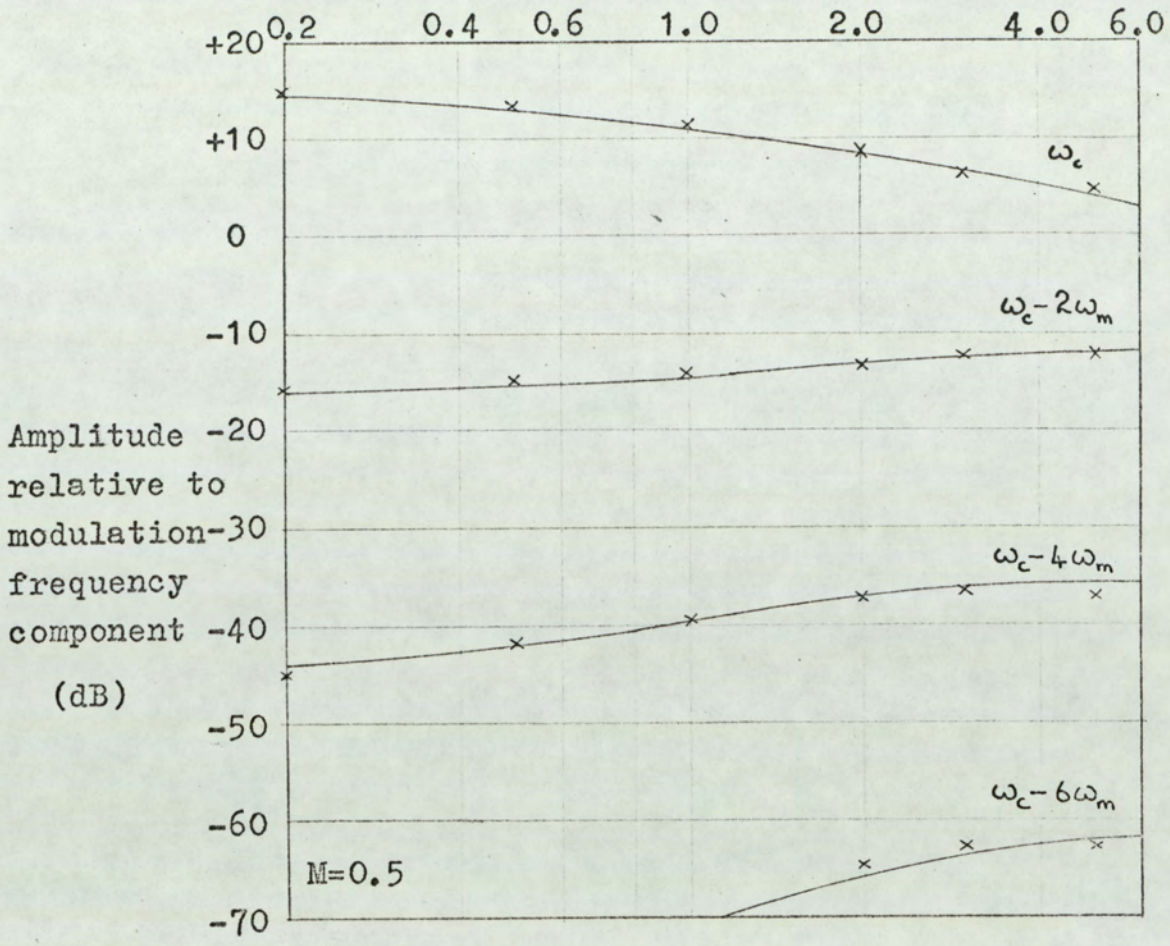

Integrator gain =4

Input resistance R_1 = Time constant resistance R

$$\frac{T_c}{CR} = 25$$

Fig.6.3.9. Amplitude of sideband components for double-edge modulation system with finite values of amplifier input and output resistance.

—— = Theoretical curve

× = Measured value

6.4. System Performance with Finite Amplifier Bandwidth

The d.c. transfer function of the system was measured for selected values of amplifier time constant T_a. For these measurements, the integrator gain was set to 4.0, the input resistance R_1 set to infinity, and the output resistance R_o set to zero. Fig. 6.4.1. shows the theoretical and measured system transfer functions. The theoretical transfer function was calculated from the analytical results of section 3.3.2. (equations 3.3.44., 3.3.45., 3.3.46., and 3.3.47.)

The frequency spectrum for a double-edge modulation system, with a bandwidth-limited integrator amplifier, is evaluated from the results of the static analysis (section 3.3.2.) and the generalised spectrum analysis (section 4.4.). Generalised analytical results are presented in graphical form in section 4.5.2. The measured and theoretical third harmonic distortion of the system output is shown in fig. 6.4.2. for a modulation index of 0.5. The results shown in fig. 6.4.2. may seem, at first sight, to be at variance with the generalised results of section 4.5.2. (fig. 4.5.5.) since the harmonic distortion decreases with increasing values of amplifier time constant T_a. However, in the generalised results it must be remembered that the amplifier time constant T_a also varies the effective normalised integrator time constant T_N (see equation 4.5.4.). The integrator gain is low in the test system so that the increasing values of amplifier time constant T_a lead to an appreciable decrease in the normalised time

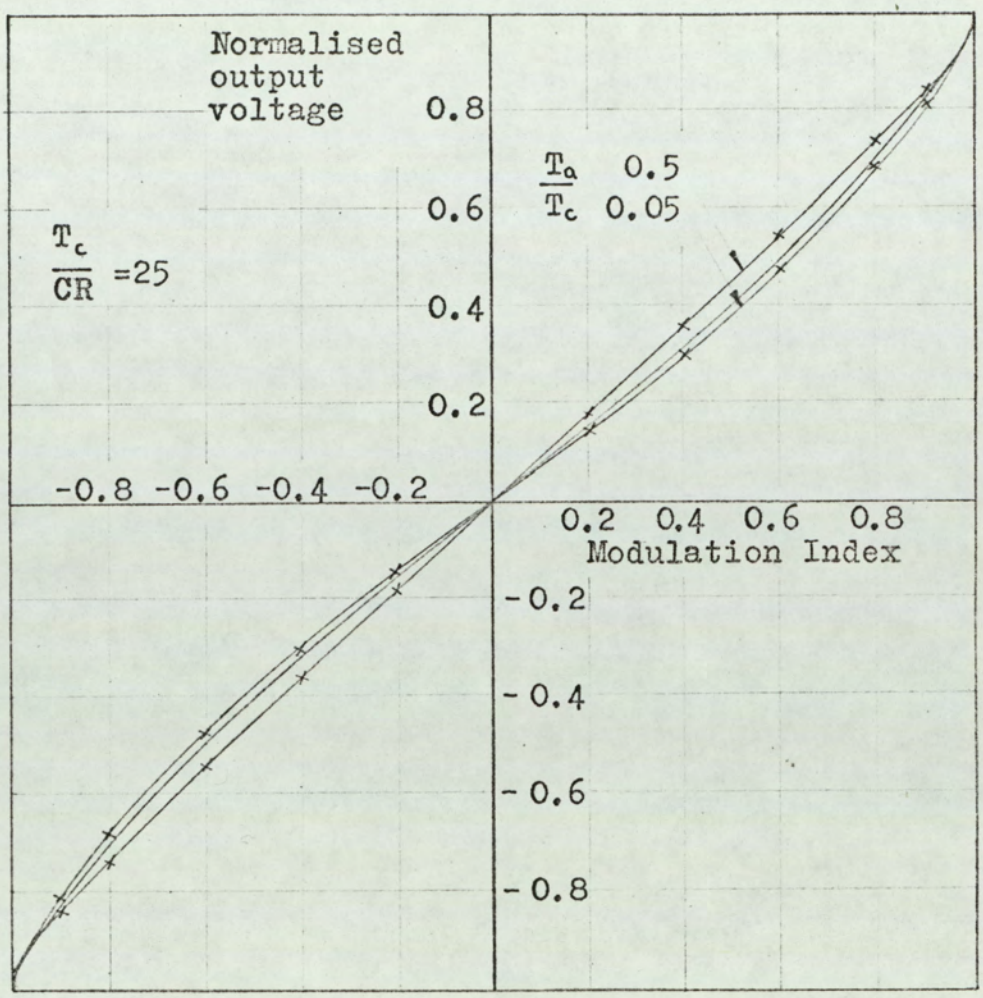

Integrator gain =4

Fig.6.4.1. Transfer function of double-edge modulation system with bandwidth-limited integrator amplifier.

—— = Theoretical curve

× = Measured value

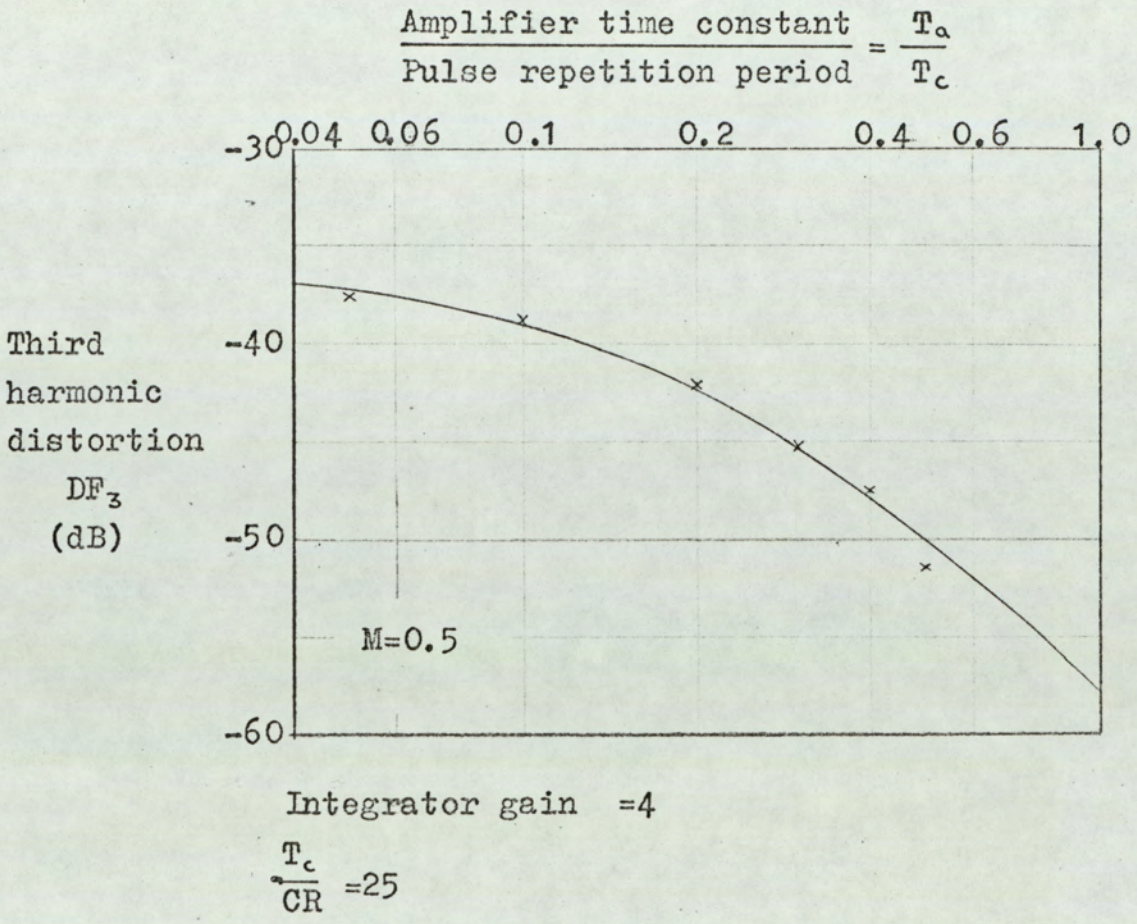

Fig.6.4.2. Third harmonic distortion in double-edge modulation system with bandwidth-limited integrator amplifier.

— = Theoretical curve

× = Measured value

constant T_N. The decreased value of T_N causes a decrease in harmonic distortion. The measured and theoretical values of the sideband components, for a modulation index $M = 0.5$, are shown in fig. 6.4.3. as a function of the amplifier time constant T_a.

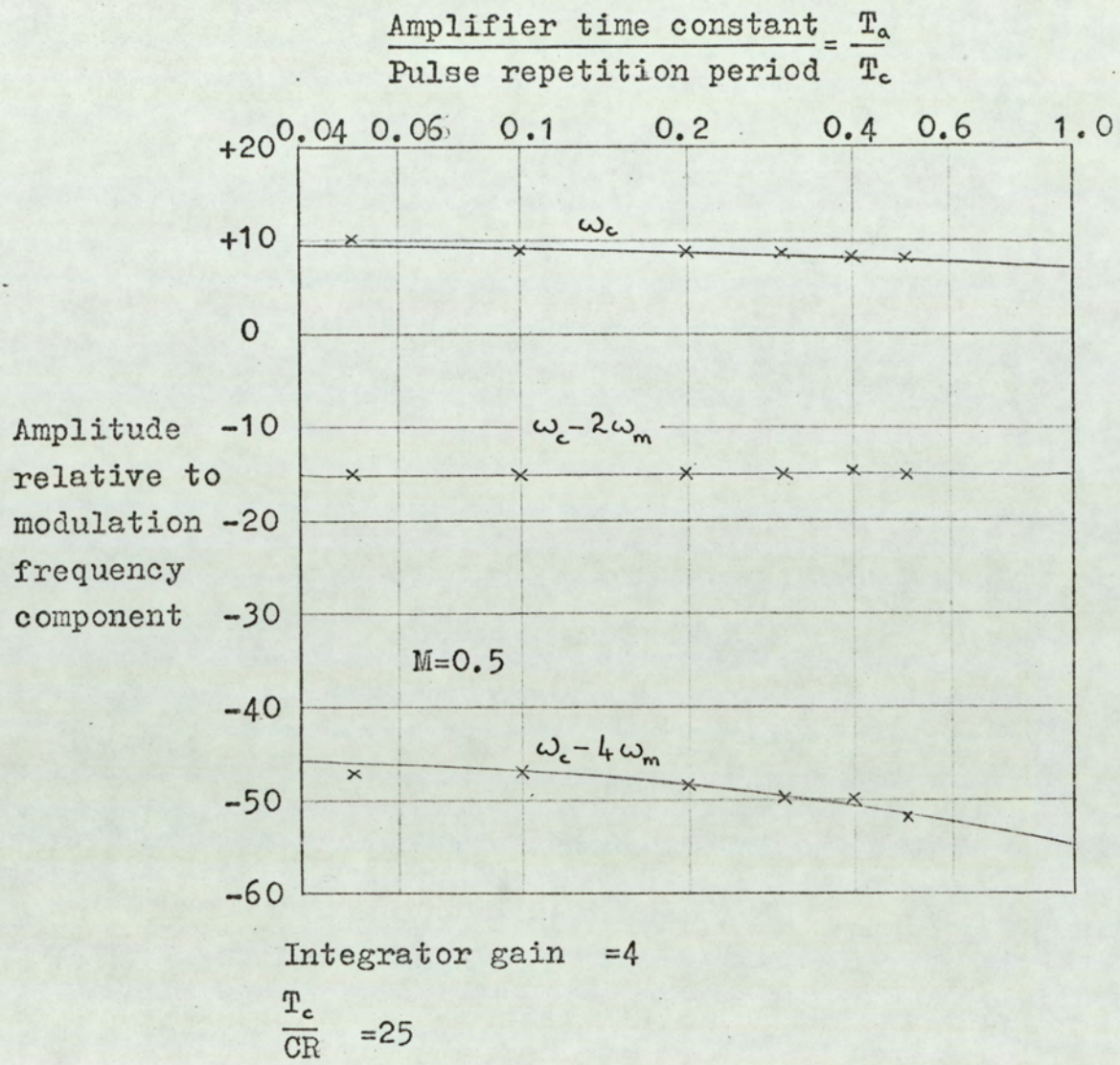

Fig.6.4.3. Amplitude of sideband components for double-edge modulation system with bandwidth-limited integrator amplifier.

—— = Theoretical curve

× = Measured value

6.5. System Performance with a Hysteretic Level-Detector

The d.c. transfer function of the system was measured for a range of values of level detector hysteresis with an integrator gain of 4.0. Full modulation for a double-edge modulation system with hysteresis is defined in section 3.4.2. as that positive value of modulation index which causes the pulse leading edge to occur at time $\frac{T_c}{2}$ (see discussion preceding equation 3.4.13., section 3.4.2.). The effect of the level-detector hysteresis is such that, under these conditions, the trailing edge of the pulse does not occur at time $\frac{T_c}{2}$. This means that for full modulation the system output is less than that of a system with a non-hysteretic level-detector. This effect may be seen in fig. 6.5.1. which shows the measured and theoretical transfer function of the system for selected values of normalised hysteresis $\delta / \hat{v}_2(t)$, where $\hat{v}_2(t)$ is the peak positive value of the integrator output waveform. The output voltage in fig. 6.5.1. is normalised to the value of the system output under conditions of zero hysteresis and full modulation. The theoretical transfer function was calculated from equation 3.4.25., section 3.4.2. The normalised system output for full modulation is shown in fig. 6.5.2. as a function of the normalised hysteresis. As with fig. 6.5.1., the values of system output are normalised to the system output under conditions of zero hysteresis and full modulation.

Fig. 6.5.3. shows the measured and theoretical values

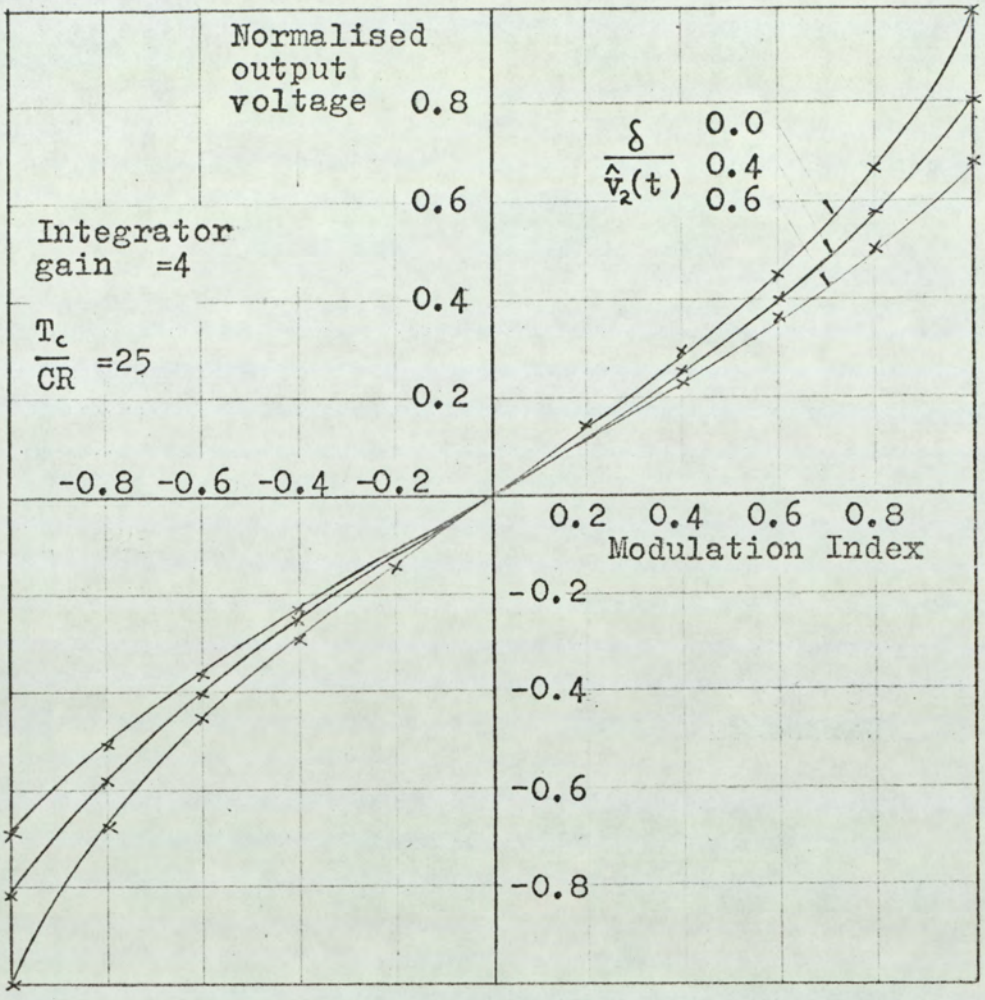

Fig.6.5.1. Transfer function of double-edge modulation system with hysteretic level-detector.

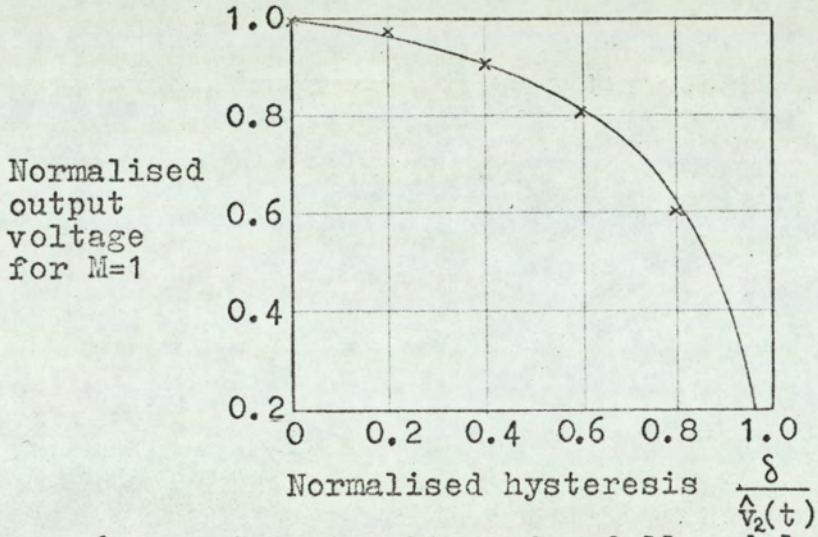

Fig.6.5.2. Output voltage for full modulation normalised to output for $\frac{\delta}{\hat{v}_2(t)}$ =0

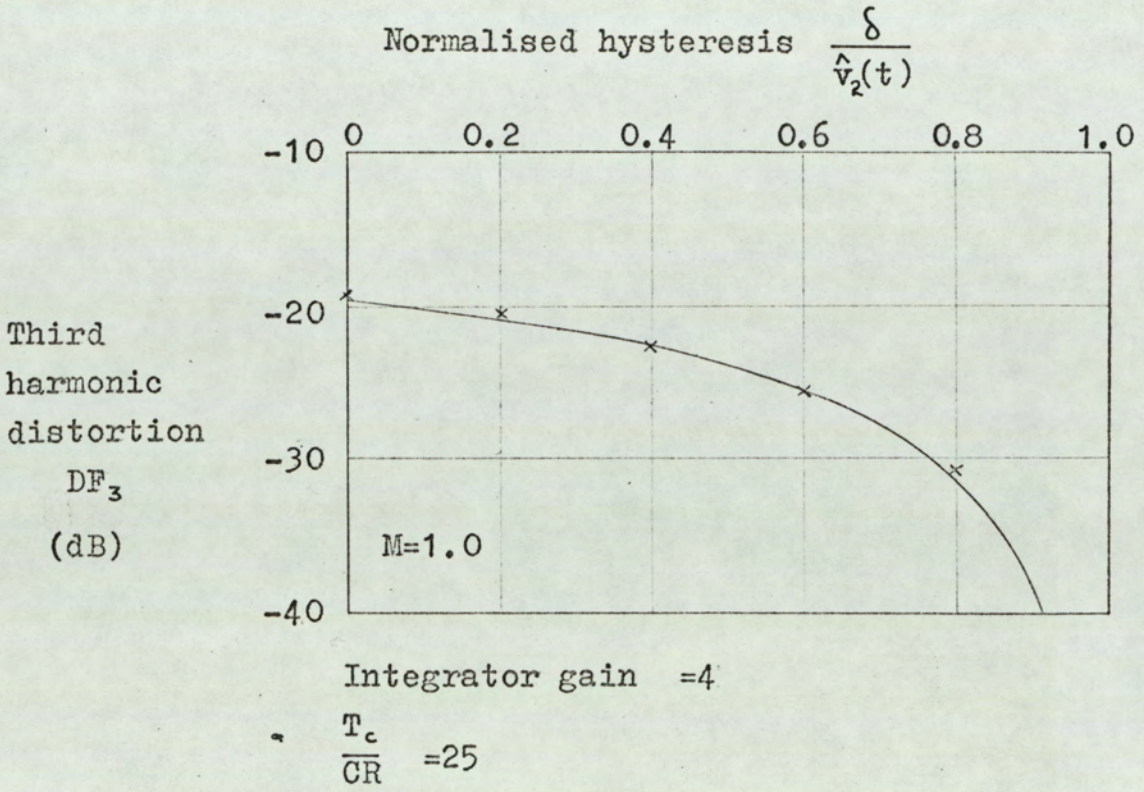

Fig.6.5.3. Third harmonic distortion in double-edge modulation system with hysteretic level-detector.

of third harmonic distortion as a function of the normalised hysteresis. The corresponding sideband amplitudes are shown in fig. 6.5.4. The theoretical values of harmonic distortion and sideband amplitudes were calculated from equations 4.6.8. and 4.6.9. of section 4.6.2.

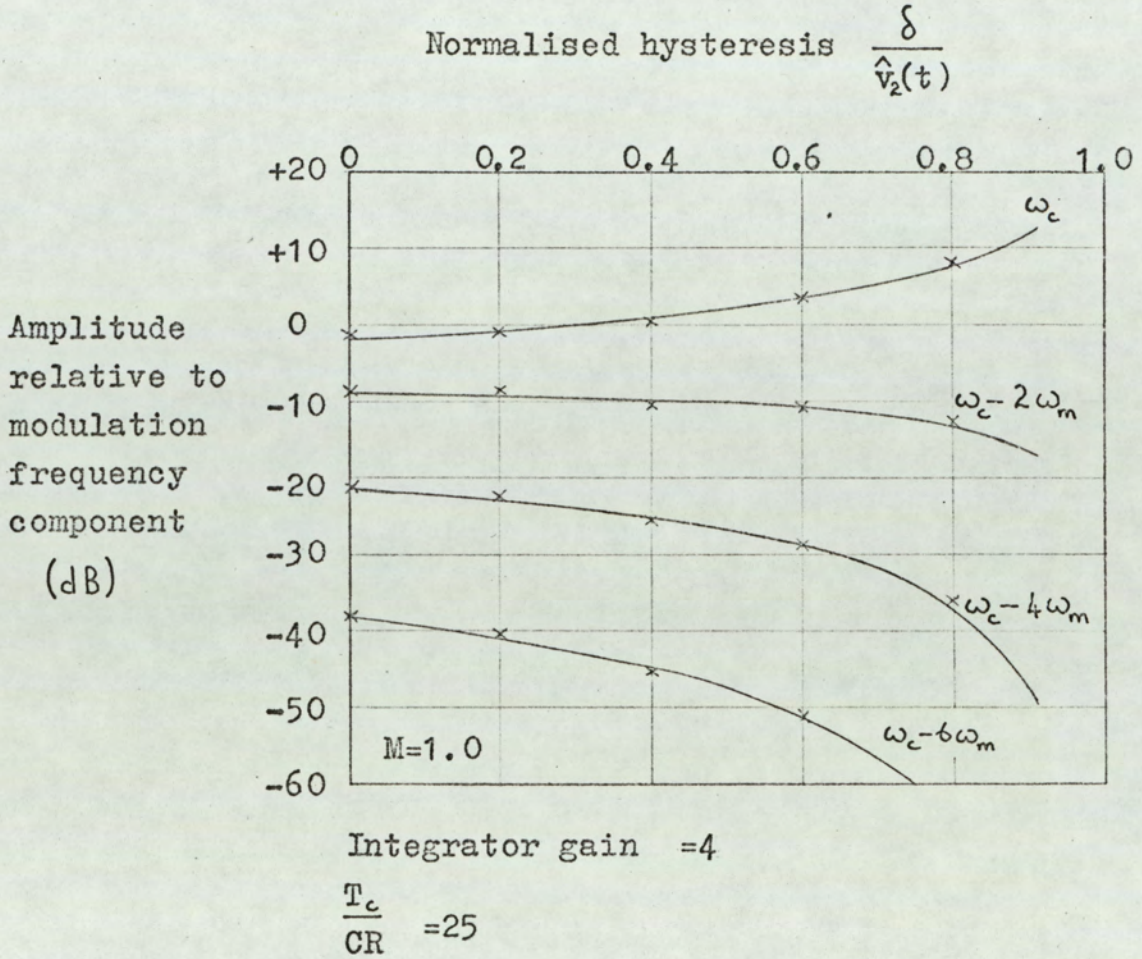

Fig.6.5.4. Amplitude of sideband components for double-edge modulation system with hysteretic level-detector.

6.6. Conclusions

The analytical results of sections 3 and 4 have been compared with the results obtained from an experimental double-edge modulation system. Very close agreement is obtained between the measured and theoretical results. For the measurements made with d.c. inputs the actual measurement error is negligible since a high grade digital voltmeter was used to measure the system input and output voltages. The measured results for the frequency spectrum agree with the theoretical results to within ± 1 dB, which is within the limits of experimental error. The quoted accuracy of the spectrum analyser is ± 0.5 dB so that an experimental error of ± 1 dB is quite reasonable.

CHAPTER III

Analysis of Power Dissipation in the Output Stages of Pulse-length Modulation Amplifiers

1. General

A factor of paramount importance in the choice of pulse-length modulation techniques as a method of linear amplification is that it seems possible to achieve high efficiency. This is, of course, a very desirable state of affairs for high-power amplifiers. Class B operation, which is the only alternative for linear amplification, has a maximum theoretical efficiency of only 78.5% so that the problem of maintaining the amplifier output stage at a reasonable temperature is quite severe at output levels of greater than 100 watts. Cooling of output stages can be an expensive procedure when forced air or water cooling are required.

The calculation of output stage dissipation in a pulse-length modulation system is obviously straightforward for purely resistive loads. However the length-modulated waveform must be filtered if the modulating signal is to be recovered, and it is the introduction of the reactive components of the filter that complicates the analysis. Only a limited amount of published work appears to exist on this particular topic, and the major contributions will be reviewed in chronological order.

Flesher[23] calculates the power dissipation in a common-emitter transistor switching stage by a combination of graphical and analytical techniques. However only the simplest configuration is examined, and the use of diodes to carry the current due to the back e.m.f. of an inductive load is only mentioned briefly. Ettinger and Cooper[25] describe 2 watt and 1 kilowatt pulse-length modulation amplifiers but very little analytical work is presented. The problems of filtering are only mentioned briefly since the amplifiers are intended for driving motors, and

frequency response of the system is not a design criterion. The introduction section of the paper quotes, from an earlier paper by Ettinger[24], an expression for the power dissipation in a common-emitter switching stage, with resistive load. Ohno[30] describes a servo amplifier which uses pulse-length modulation techniques. The theoretical analysis presented deals only with purely resistive loads, and it is assumed that the results apply when the system is used to drive a servo-motor. This assumption is clearly not valid since any electro-mechanical system which operates as a low-pass filter must have reactive components associated with it. Efficiency of the order of 98% for a 250 watt output power into a resistive load is quoted. However this figure appears to be derived from a very much simplified analysis and is not supported by any experimental work. The circuit diagram of a practical system given in the paper has no diodes across the reactive load and no mention is made of the effects of switching this load. Miller[33] presents a more detailed analysis of the effect of the reactive components of the low-pass filter on the power dissipation in a simple thermionic value output stage. The analysis is based on the assumption that all the active components in the output stage (i.e. diodes and valves) can be represented as linear resistances. A further assumption is that the filter input current is d.c. with amplitude proportional to the modulation index of the pulse-length modulated wavetrain. Turnbull and Townsend[44] treat the problem of output stage dissipation in considerably more detail than the previous references. The type of output stage discussed is a complementary transistor pair operated in the common-collector mode as shown in fig. 1.1. The bases of the transistors are switched between the

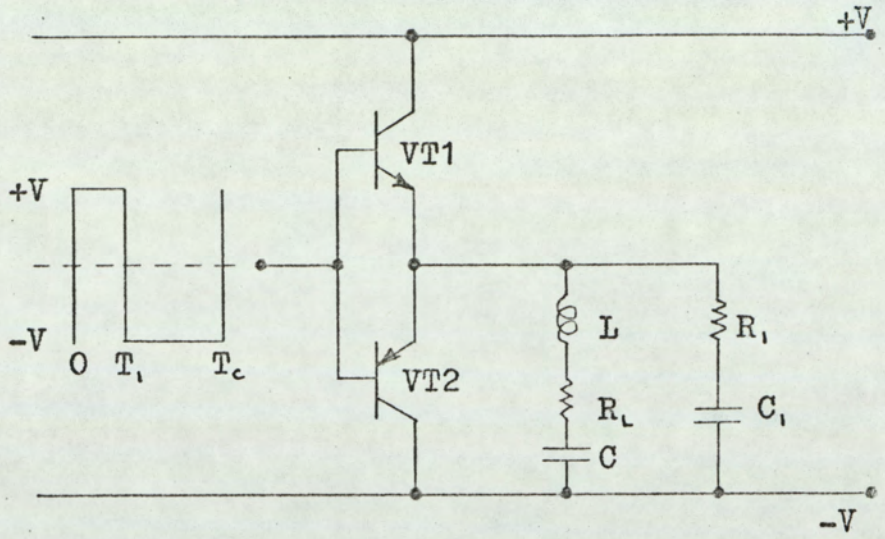

Fig.1.1. Complementary transistor output stage with low-pass filter.

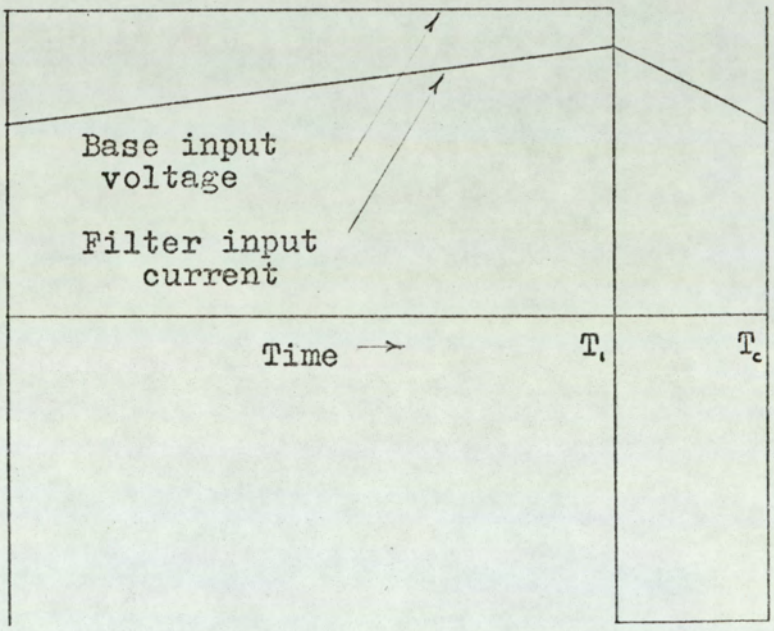

Fig.1.2. Voltage and current waveforms for the circuit shown in fig.1.1.

levels $\pm$ V, and the approximation made that the 'on' transistor can be represented by a 1v. source in series with a resistance of 1Ω. The authors show that for $\omega_c L > R_L$, and $R_1 = \infty$, where ω_c is the pulse repetition frequency, the current into the filter does not change direction during the cycle when the modulation index is sufficiently great. This is illustrated in fig. 1.2. Samain[42] has pointed out that if it is not possible for a transistor to conduct in the reverse direction then the opposite transistor of the output pair will be forced to continue conducting during the time when it has the full supply voltage across it. When this condition exists the efficiency is low. Turnbull and Townsend[44] show that the addition of resistance R_1 and capacitance C_1 in fig. 1.1. can improve the situation if R_1 is chosen so that the combined current into the filter and R_1 is never in the same direction throughout the cycle. Efficiency figures are given for various relationships between the inductance L, the load resistance R_L, R_1 and C_1. It is shown that by limiting the modulation index, and suitably choosing the component values, an overall efficiency comparable with Class B operation can be obtained. Further work by Turnbull and Townsend[45] presents an approximate analysis of the type of output stage shown in fig. 1.3. The diodes D1 and D2 carry the current when it is in the opposite direction to the normal current flow in the 'on' transistor. The analysis is again based on the approximation that the diode and transistor volt-ampere characteristics can be represented by a constant voltage drop in series with a resistance. A further approximation is that only one diode and one transistor conduct during one cycle of the pulse repetition frequency. Dimensional inconsistencies

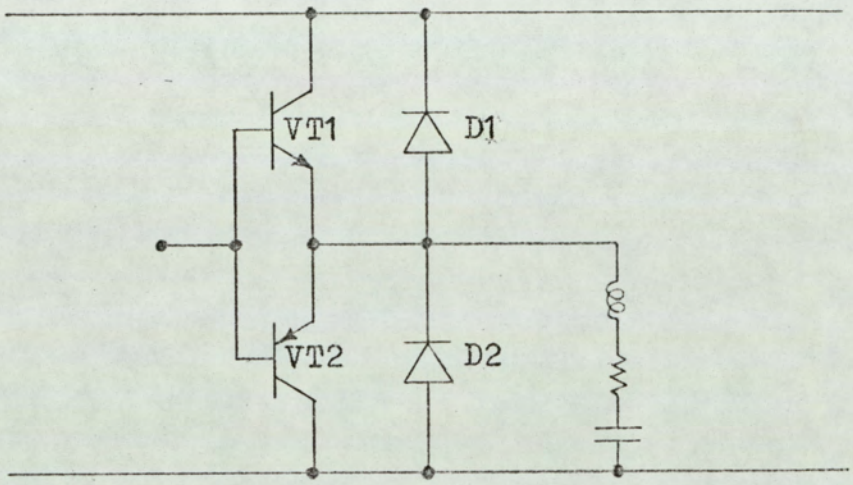

Fig.1.3. Complementary pair output stage with diodes to carry the reverse current.

exist in the power dissipation equations developed in the appendix of the paper. These two papers by Turnbull and Townsend appear to be the only published work which deals, in any detail, with the dissipation in the output stages of pulse-length modulation amplifiers.

The analysis to be presented in this section affords a means of evaluating the power dissipation of the output stage in terms of the static characteristics of the semiconductor elements and the characteristics of the demodulating filter. The basis of the analysis is to obtain an expression for the filter input current as a function of the modulation index. This expression enables the static power dissipation, over one cycle of the pulse-repetition frequency, to be evaluated for each of the elements of the output stage. The modulation index is then varied in a sinusoidal manner and the expressions for power dissipation integrated over one cycle of the modulation frequency to obtain the average power dissipation. This method is only an approximation which improves as the ratio of the pulse-repetition frequency to the modulation frequency increases. A completely rigorous treatment would require that the power dissipation be evaluated from a spectrum analysis of the response of the filter to a sinusoidally pulse-length modulated wavetrain. As was seen in Chapter II, the frequency spectrum of a length-modulated wavetrain is rather complex so that analysis of output stage dissipation on a spectral basis would be extremely involved.

2. Choice of output stage configuration

At the present stage of semiconductor development the junction transistor offers the best combination of high power handling capabilities and fast switching time. For this reason attention will be concentrated on the use of transistors as the switching elements in the output stage. However it is possible that, in the future, the switching time of very high power devices, such as the silicon controlled rectifier, will become comparable with that of transistors. These high power devices will then present an attractive alternative for use in switching output stages.

There are a number of basic configurations of output stages using transistors, and it is necessary to decide which of these configurations offers the best performance. The most simple type is shown in fig. 2.1. This output stage has the obvious drawback that under conditions of zero modulation (i.e. the input waveform has unity mark-space ratio) the mean current flowing in the load is $\frac{1}{2} \cdot \frac{V}{R_L}$, where R_L is the load resistance. This problem may be overcome by making use of the configuration shown in fig. 2.2., where the two transistors switch alternately. (i.e. one transistor is conducting whilst the other is non-conducting). The mean current through the load is zero when the modulation index is zero since the input to the filter and load is switched between $\pm V$.

There are various possible ways in which the transistors can be connected to perform the switching operations shown in fig. 2.2. Consider first, the situation where both transistors are of the same type (i.e. PNP or NPN). Output stage configurations which require operation of the transistors in the common-base mode may be rejected on the grounds that no current gain is available. This leaves

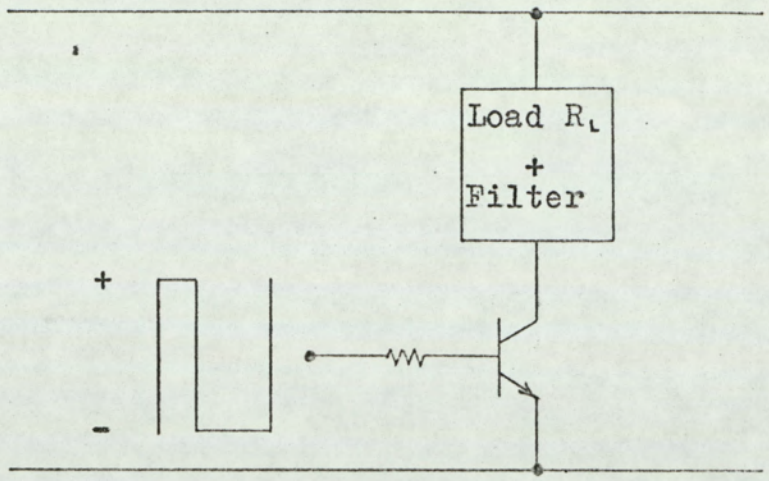

Fig.2.1. Simple switching output stage.

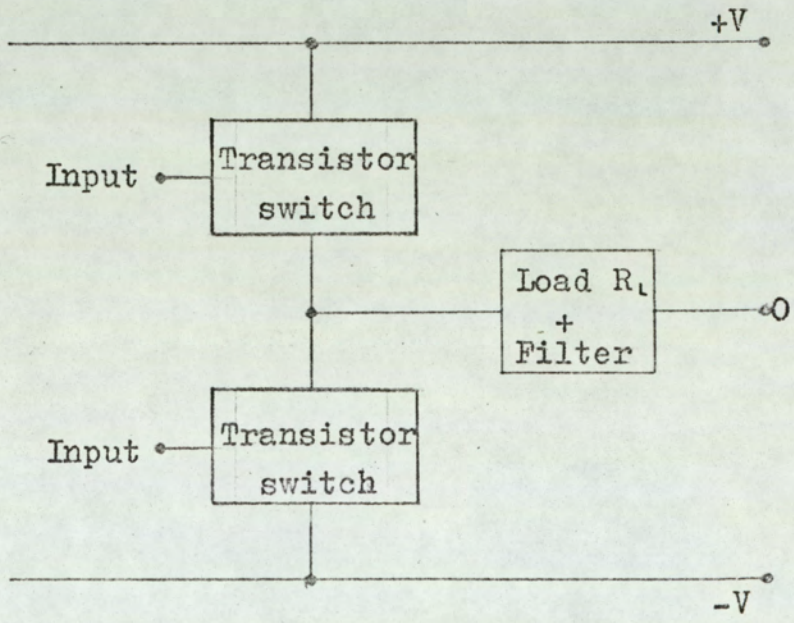

Fig.2.2. Transistor pair output stage.

only the configuration shown in fig. 2.3. The most serious drawback of this type of output stage is as follows. If transistor VT2 is operated as a saturated switch, the stored charge (i.e. the charge in excess of that required to maintain the collector current) causes a time delay when the transistor is switched off[66]. Thus at the point when VT1 is switched on and VT2 is switched off, both transistors will conduct during the period that the excess charge is being removed from the base region of VT2. Since the full supply voltage (2V) is across the transistors, the power dissipation is high. The storage delay time can be reduced to some extent by connecting a capacitor across the input resistor R_b, in order to remove the stored charge more rapidly[67]. However the amount of stored charge is a function of the modulation index since the average collector current depends on the modulation index and the base current is constant. Various techniques have been developed[68] to prevent common-emitter switching stages from entering the saturation region, but they are not really suitable for high power switching where the transistor must be maintained very close to saturation to avoid excessive dissipation. A further drawback of the circuit shown in fig. 2.3 is that with many high power transistors a current gain of the order of 10 to 20 must be assumed in order to ensure saturation. This means that the power dissipated in the base input resistor (R_b) may be large. In a high power amplifier this problem could be quite serious.

Since complementary pairs of transistors are now becoming available it is possible to use the configuration shown in fig. 2.4. Both of the transistors are operated in the common-collector mode so that no problems are

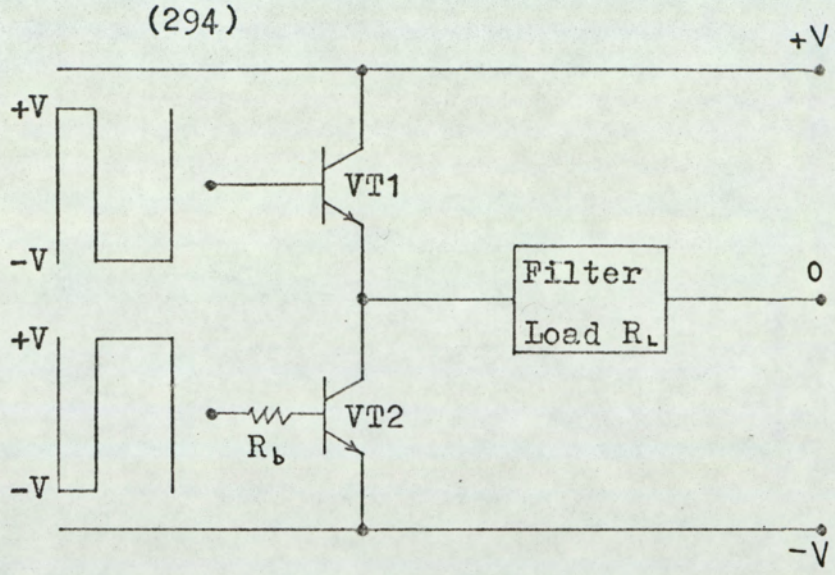

Fig.2.3. Output stage utilising NPN transistors.

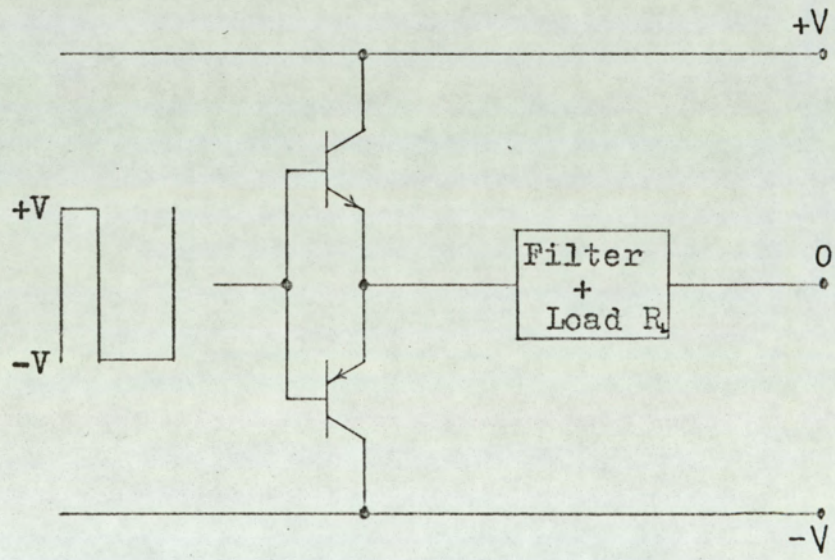

Fig.2.4. Output stage utilising a complementary transistor pair.

are encountered due to storage of excess charge. Furthermore base input resistors are not required which overcomes the second of the problems associated with the saturated common-emitter stage in fig. 2.3. The complementary pair circuit does, however, have the disadvantage that the voltage dropped across the transistors is slightly larger than the voltage drop across a saturated transistor. In spite of this the circuit shown in fig. 2.4 appears to offer the best possibilities.

The low-pass filter connected between the load and the switching transistors must provide high attenuation to frequencies outside the system pass-band, and also present a high impedance to these frequencies in order to prevent large switching currents. The second of these requirements indicates that the filter must have a series input inductance.

3. Performance of low-pass filters with switched input voltages

3.1 Time-domain analysis of filter performance

In order to calculate the power dissipation in the switching elements of the output stage it is necessary to derive expressions for the filter input current as a function of the filter parameters and the mark-space ratio of the voltage waveform applied to the filter input. Since the output impedance of the switching elements is small, the source impedance for the filter is assumed to be zero.

The most simple type of filter is an inductance L in series with the load resistance R_L as shown in fig. 3.1.1. The filter input current, in response to a positive step function voltage input V_1, is given by eqn. 3.1.1.

$$i(t) = \frac{V_1}{R_L}\left\{1 - \exp\left(-t\,\frac{R_L}{L}\right)\right\} \qquad (3.1.1.)$$

The input current in response to the rectangular wavetrain input, shown in fig. 3.1.2., is obtained by synthesising the wavetrain from a series of positive and negative step functions with appropriate time delays. From eqn. 3.1.1. and fig. 3.1.2., the filter input current is:

$$i(t) = \frac{V_1}{R_L}\left\{1 - \exp\left[-\left(t + NT_c\right)\frac{R_L}{L}\right]\right\} + \frac{2V_1}{R_L}\sum_{n=0}^{N-1}\left\{1 - \exp\left[-\left(t + nT_c\right)\frac{R_L}{L}\right]\right\} -$$

$$\frac{2V_1}{R_L}\sum_{n=0}^{N-1}\left\{1 - \exp\left[-\left(t + T_c - T_1 + nT_c\right)\right]\right\} \qquad (3.1.2)$$

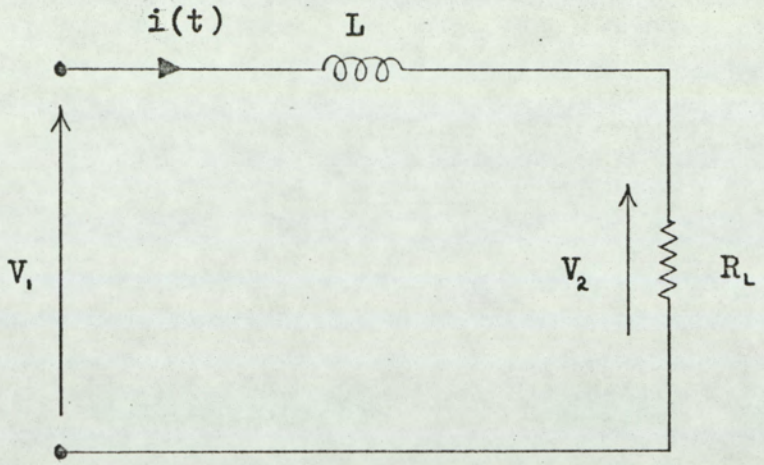

Fig.3.1.1. Simple LR low-pass filter

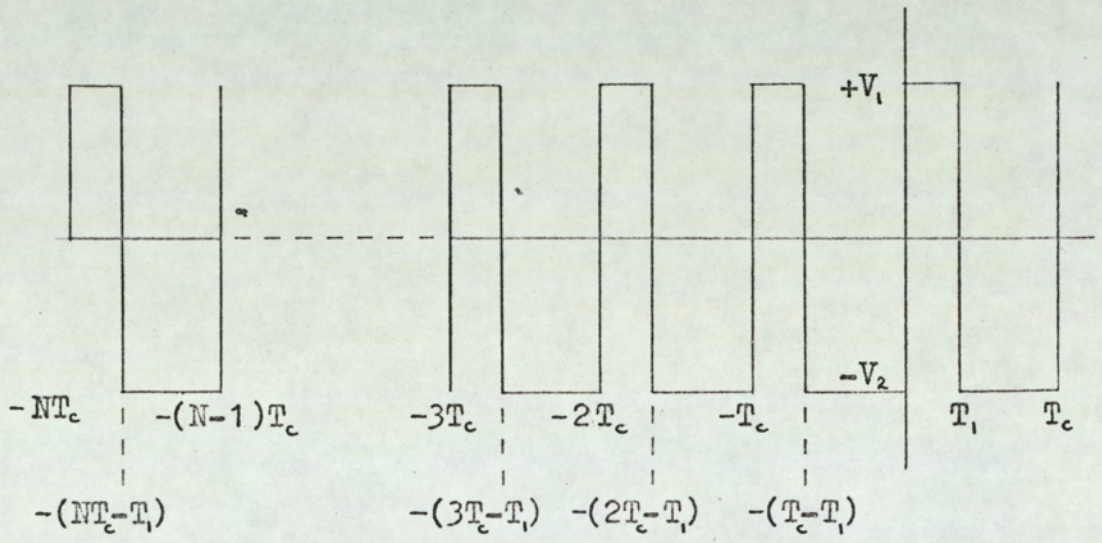

Fig.3.1.2. Voltage wavetrain applied to the filter input.

The above expression may be rearranged to give:

$$i(t)=\frac{V_1}{R}\left\{1-\left[\exp\left(-t\,\frac{R_L}{L}\right)\right]\left[\exp\left(-NT_c\,\frac{R_L}{L}\right)+2\left[1-\exp\left(-\left(T_c-T_1\right)\right)\frac{R_L}{L}\right]\times\right.$$

$$\left.\sum_{n=0}^{N-1}\exp\left(-nT_c\,\frac{R_L}{L}\right)\right]\right\} \qquad (3.1.3)$$

The summation term in eqn. 3.1.3. is a geometrical progression and may be expressed in closed form. Therefore

$$i(t)=\frac{V_1}{R_L}\left\{1-\left[\exp\left(-t\,\frac{R_L}{L}\right)\right]\left[\exp\left(-NT_c\,\frac{R_L}{L}\right)+2\left[1-\exp\left(-\left(T_c-T_1\right)\frac{R_L}{L}\right)\right]\times\right.\right.$$

$$\left.\left.\frac{1-\exp\left(-NT_c\,\frac{R_L}{L}\right)}{1-\exp\left(-T_c\,\frac{R_L}{L}\right)}\right\}\right. \qquad (3.1.4)$$

The expression for the filter current in response to an infinite wavetrain is given by allowing N to tend to infinity in eqn. 3.1.4. Thus:

$$i(t)=\frac{V_1}{R_L}\left\{1-2\exp\left(-t\,\frac{R_L}{L}\right)\,\frac{1-\exp\left[-\left(T_c-T_1\right)\frac{R_L}{L}\right]}{1-\exp\left[-T_c\,\frac{R_L}{L}\right]}\right\} \qquad (3.1.5)$$

for $0 \leqslant t \leqslant T_1$

The input current for the period $T_1 \leqslant t \leqslant T_c$ is obtained by adding, to eqn. 3.1.5., a term corresponding to the filter current in response to a step input of $-2V_1$ occuring at time $t=T_1$.

Therefore:

$$i(t) = \frac{V_1}{R_L}\left\{-1 - 2\exp\left(-t\frac{R_L}{L}\right)\frac{1-\exp\left(T_1\frac{R_L}{L}\right)}{1-\exp\left(-T_c\frac{R_L}{L}\right)}\right\} \qquad (3.1.6)$$

$$\text{for} \quad T_1 \leqslant t \leqslant T_c$$

For a sinusoidal input to the filter the voltage transfer function 3dB frequency ω_o is:

$$\omega_o = \frac{R_L}{L} \qquad (3.1.7)$$

T_c is the period of the pulse repetition frequency ω_c. Therefore:

$$T_c = \frac{2\pi}{\omega_c} \qquad (3.1.8)$$

If the pulse-length modulated wavetrain applied to the filter input is produced by a system having a linear sampling waveform (i.e. the pulse length T_1 is directly proportional to the modulating input voltage), then the modulation index M may be defined as:

$$M = 2\frac{T_1}{T_c} - 1 \qquad (3.1.9)$$

Substituting eqns. 3.1.7., 3.1.8 and 3.1.9. in eqns. 3.1.5. and 3.1.6. enables the filter input current to be expressed as:

$$i(t) = \frac{V_1}{R_L}\left\{1 - 2\exp\left(-2\pi\frac{\omega_o}{\omega_c}\cdot\frac{t}{T_c}\right)\frac{1-\exp\left[-\frac{\omega_o}{\omega_c}(1-M)\pi\right]}{1-\exp\left|-2\pi\frac{\omega_o}{\omega_c}\right|}\right\} \qquad (3.1.10)$$

$$\text{for} \quad 0 \leqslant \frac{t}{T_c} \leqslant \frac{M+1}{2}$$

$$i(t) = \frac{V_1}{R_L}\left\{-1-2\exp\left(-2\pi\,\frac{\omega_o}{\omega_c}\cdot\frac{t}{T_c}\right)\frac{1-\exp\left[-\frac{\omega_o}{\omega_c}(1-M)\pi\right]}{1-\exp\left[-2\pi\,\frac{\omega_o}{\omega_c}\right]}\right\} \qquad (3.1.11)$$

for $\qquad \frac{M+1}{2} \leqslant \frac{t}{T_c} \leqslant 1$

Now it is shown in Chapter II that if the sideband components falling within the system pass-band are to be less than -60dB with respect to the modulation frequency component, then for a double-edge modulation system, the pulse repetition frequency (ω_c) must be greater than $7\omega_m$. The frequency ω_m is the highest modulation frequency the system is required to handle. Therefore allowing a small factor, the smallest value of pulse-repetition frequency likely to be used in a practical system is $\omega_c = 5\omega_m$. In the design of a system, the 3dB frequency of the low-pass filter will be made equal to the highest modulating frequency required. Therefore the maximum value of the ratio ω_o/ω_c is $1/5$.

Fig 3.1.3. shows the normalised filter input current $\frac{R_L}{V_1}\cdot i(t)$, given by eqns. 3.1.10 and 3.1.11, for various values of modulation index M. The diagram shows that the filter current is an approximately triangular wave superimposed on a normalised current of M. This observation however, is not particularly obvious from eqns. 3.1.10 and 3.1.11.

Before proceeding further with this point a time-domain analysis of a slightly more complex filter will be carried out using the same techniques as for the simple LR

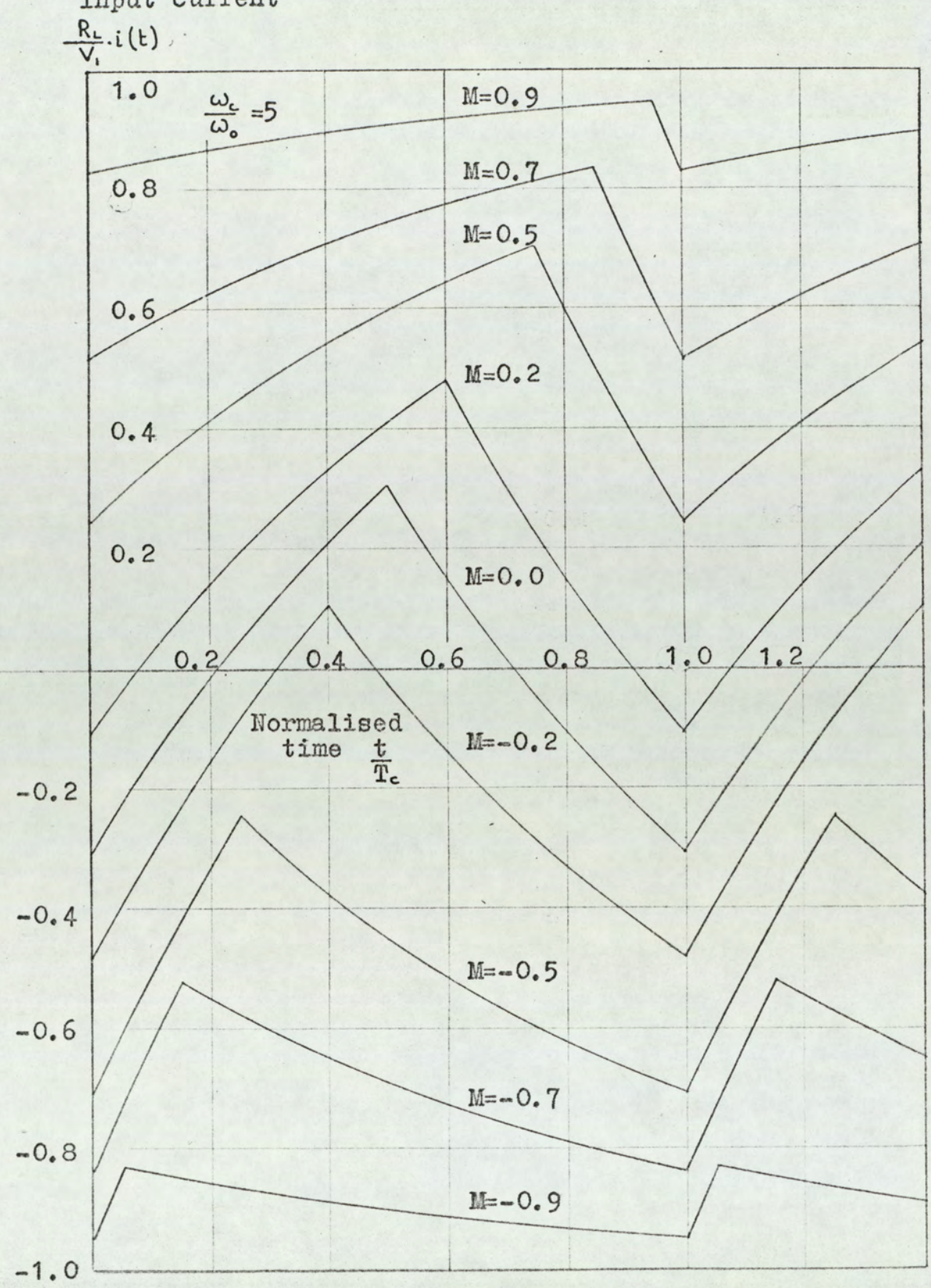

Fig.3.1.3. Normalised input current for a simple LR filter.

filter. The obvious extension of the LR filter is to connect a capacitor across the load resistance R_L, as shown in fig. 3.1.4., to further attenuate the high frequency components which appear across the load.

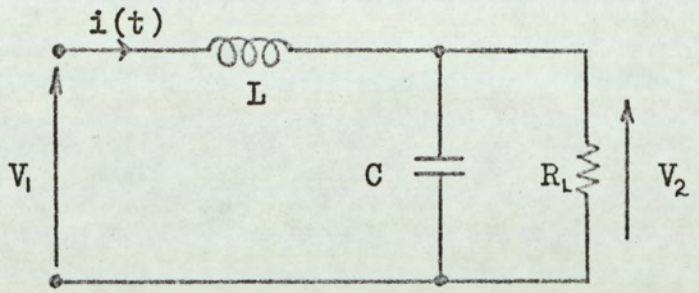

Fig.3.1.4. Single-section LCR low-pass filter.

In order to obtain constancy of amplitude response, the values of the filter components are chosen to give the maximally-flat (or Butterworth) characteristic. It may be shown that the voltage transfer function $G(\omega)$ of the filter is given by the expression:

$$\left|G(\omega)\right| = \frac{1}{\sqrt{\left[1 - 2\omega^2 LC + \omega^4 L^2 C^2 + \omega^2 \frac{L^2}{R_L^2}\right]}} \qquad (3.1.12)$$

For maximally-flat amplitude response:

$$2\omega^2 LC = \omega^2 \frac{L^2}{R_L^2}$$

Therefore:
$$L = 2CR_L^2 \qquad (3.1.13)$$

and the maximally-flat transfer function is:

$$\left|G(\omega)\right| = \frac{1}{\sqrt{\left[1 + \omega^4 L^2 C^2\right]}} \qquad (3.1.14)$$

From eqn. 3.1.14., the 3dB frequency (ω_o) of the filter is given by the expression:

$$\omega_o = \frac{1}{\sqrt{(LC)}} = \frac{1}{\sqrt{(2)}CR_L} \qquad (3.1.15)$$

The above equation for the filter turnover frequency is at variance with the result quoted by Miller[33] (i.e. $\omega_o = \frac{\sqrt{2}}{CR_L}$) for the same filter. Analysis of the maximally-flat filter shows that the filter input current, in response to a step function voltage input V_1, may be expressed as:

$$i(t) = \frac{V_1}{R_L}\left\{1 - \frac{1}{2}\left[\exp\left(\frac{-t}{2CR_L}\right)\right]\left[\exp\left(\frac{-jt}{2CR_L}\right) + \exp\left(\frac{-jt}{2CR_L}\right)\right]\right\} \qquad (3.1.16)$$

The response of the filter to the rectangular wavetrain shown in fig. 3.1.2. is obtained from the step response by the same methods as were used for the simple LR filter. Since the methods are identical, only the results are given here.

$$\frac{R_L.i(t)}{V_1} = 1 - \frac{2.\exp\left(-\mu\frac{t}{T_c}\right)}{1+\exp(-2\mu)-2\exp(-\mu).\cos(\mu)} \times$$

$$\left\{\cos\left(\mu\frac{t}{T_c}\right)\left[1-\exp(-\mu)\cos(\mu)-\exp\left[-(1-M)\frac{\mu}{2}\right]\cos\left[(1-M)\frac{\mu}{2}\right]+\exp\left[-\mu\left(1+\frac{1-M}{2}\right)\right]\sin\left[(M-1)\frac{\mu}{2}\right]\right]-\right.$$

$$\left.\sin\left(\mu\frac{t}{T_c}\right)\left[\exp(-\mu)\sin(\mu)-\exp\left[-(1-M)\frac{\mu}{2}\right]\sin\left[(1-M)\frac{\mu}{2}\right]-\exp\left[-\mu\left(1+\frac{1-M}{2}\right)\right]\sin\left[(M-1)\frac{\mu}{2}\right]\right]\right\}$$

$$\text{for} \quad 0 \leqslant \frac{t}{T_c} \leqslant \frac{M+1}{2} \qquad (3.1.17)$$

The normalised filter input current for the period $T_1 \leqslant t \leqslant T_c$ is obtained by adding to eqn. 3.1.17 a term corresponding to the filter current in response to a negative step input of $2V_1$ occuring at time $t=T_1$.

Therefore:

$$\frac{R_L i(t)}{V_1} = -1 - \frac{2\exp\left(-\nu\frac{t}{T_c}\right)}{1+\exp(-2\nu)-2\exp(-\nu)\cos(\nu)} \times$$

$$\left\{\cos\left(\nu\frac{t}{T_c}\right)\left[1-\exp(-\nu)\cos(\nu)-\exp\left[-(1-M)\frac{\nu}{2}\right]\cos\left[(1-M)\frac{\nu}{2}\right]+\exp\left[-\nu\left(1-\frac{1-M}{2}\right)\right]\cos\left[(M-1)\frac{\nu}{2}\right]\right]-\right.$$

$$\left.\sin\left(\nu\frac{t}{T_c}\right)\left[\exp(-\nu)\sin(\nu)-\exp\left[-(1-M)\frac{\nu}{2}\right]\sin\left[(1-M)\frac{\nu}{2}\right]-\exp\left[-\nu\left(1+\frac{1-M}{2}\right)\right]\sin\left[(M-1)\frac{\nu}{2}\right]\right]\right\}$$

$$+2\exp\left[-\nu\frac{t}{T_c}+\frac{\nu}{2}(M+1)\right]\cos\left[\nu\cdot\frac{t}{T_c}-\frac{\nu}{2}(M+1)\right] \quad \text{for } \frac{M+1}{2} \leq \frac{t}{T_c} \leq 1 \qquad (3.1.18)$$

$$M = \frac{2T_1}{T_c} - 1 \qquad (3.1.19(a))$$

$$\nu = \sqrt{(2)}\,\pi\,\frac{\omega_o}{\omega_c} \qquad (3.1.19(b))$$

As discussed in connection with the LR filter, the maximum value of the ratio ω_o/ω_c is likely to be of the order of $\frac{1}{5}$ for a practical system. Fig. 3.1.5 shows the normalised filter current $\frac{R_L}{V_1} i(t)$ plotted as a function of normalised time $\frac{t}{T_c}$. The diagram shows that the current is closely approximated by a triangular wave superimposed on a normalised current of M. From the point of view of analysing the power dissipation in the output stage it would clearly be advantageous to have an approximate expression for the filter current in this form. If the exponential and trigonometric terms in eqns. 3.1.17 and 3.1.18. are written as power series then truncation of the resulting expressions should yield the required form. However the expressions are too complex to make this procedure practicable. Obviously the

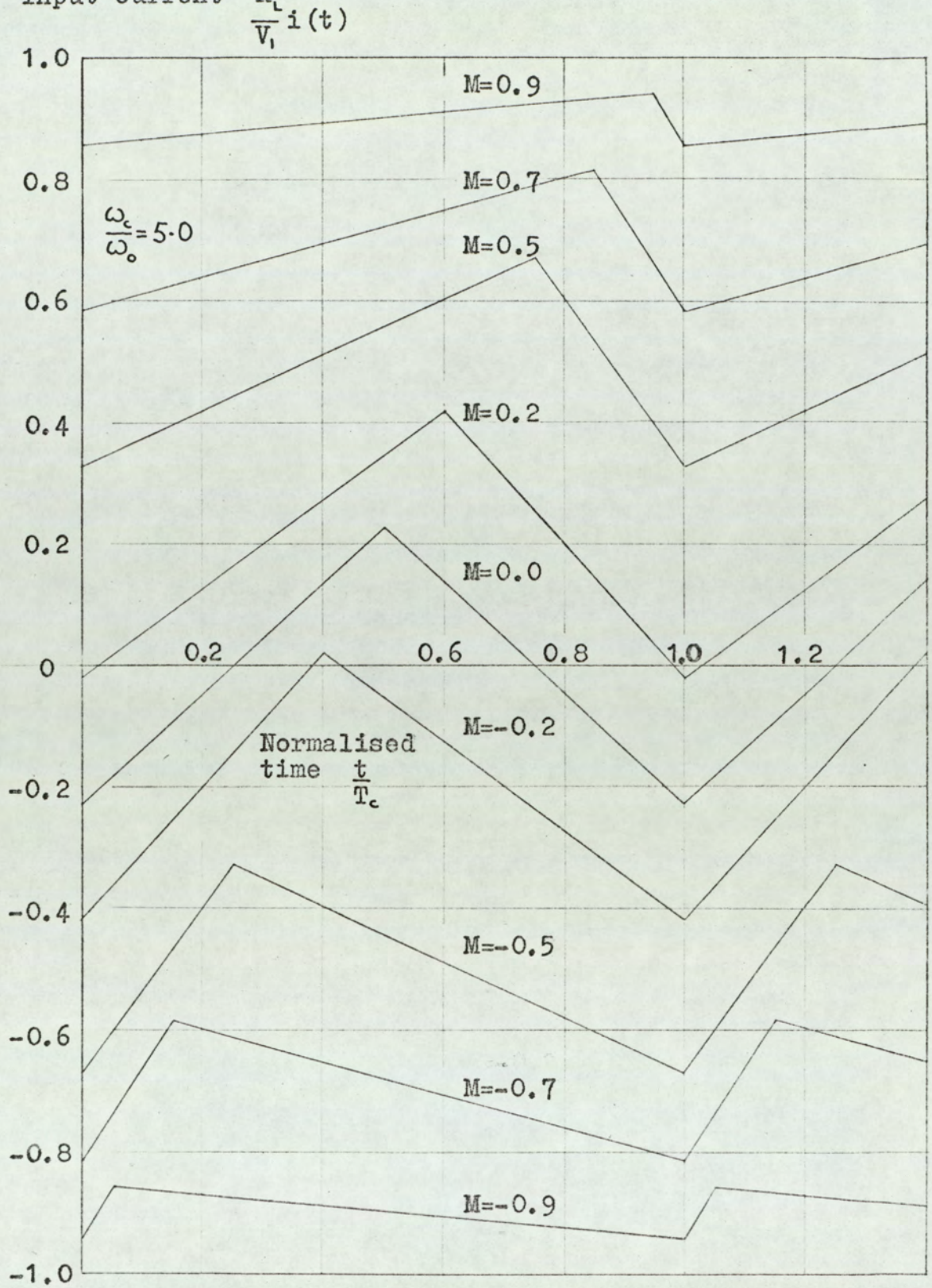

Fig.3.1.5. Normalised input current for maximally-flat single-section LCR filter.

complexity of the analysis in the time domain will increase as more sophisticated filter circuits are used. For this reason, analysis in the frequency domain will be applied to the problem.

3.2 Frequency-domain analysis of filter performance

Fourier analysis of the filter input voltage waveform shown in fig. 3.2.1. gives the following expression for the frequency spectrum.

$$f(t) = V_1 \left\{ \left(\frac{2T_1}{T_c} - 1 \right) + \frac{2T_1}{T_c} \sum_{n=\pm 1}^{\pm\infty} \frac{\sin\left(\frac{n\omega_c T_1}{2}\right)}{\frac{n\omega_c T_1}{2}} \exp(jn\omega_c t) \right\} \qquad (3.2.1)$$

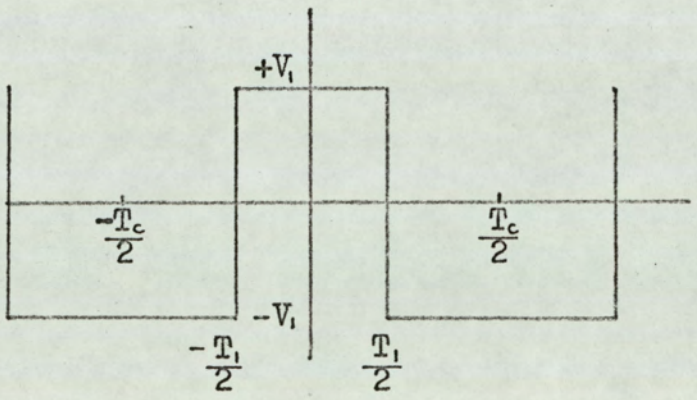

Fig.3.2.1. Filter input voltage waveform.

Rearranging the limits of the summation in eqn. 3.2.1. gives:

$$f(t) = V_1 \left\{ M + 2(M+1) \sum_{n=1}^{\infty} \frac{\sin\left[\frac{n\pi}{2}(M+1)\right]}{\frac{n\pi}{2}(M+1)} \cos(n\omega_c t) \right\} \qquad (3.2.2)$$

where: Modulation index

$$M = 2\frac{T_1}{T_c} - 1 \qquad (3.2.3)$$

For a sinusoidal input $V_1(\omega)$, the input current of the simple LR filter, shown in fig. 3.1.1., is given by the following expression:

$$\frac{i R_L}{V_1(\omega)} = \frac{1}{\sqrt{\left[1 + \left(\frac{\omega}{\omega_o}\right)^2\right]}} \angle\theta \qquad 3.2.4$$

where:

$$\theta = \tan^{-1}\left(\frac{-\omega}{\omega_o}\right) \qquad (3.2.5)$$

$$\omega_o = R_L/L \qquad (3.2.6)$$

Therefore, from eqns. 3.2.2. and 3.2.4., the normalised filter input current for, in response to the rectangular input voltage wavestrain, is:

$$\frac{R_L}{V_1} \cdot i(t) = M+2(M+1) \sum_{n=1}^{\infty} \frac{1}{\sqrt{\left[1+\left(\frac{n\omega_c}{\omega_o}\right)^2\right]}} \frac{\sin\left[\frac{n\pi}{2}(M+1)\right]}{\frac{n\pi}{2}(M+1)} \cos\left[n\omega_c t + \theta_n\right] \qquad (3.2.7)$$

where $$\theta_n = \tan^{-1}\left(\frac{-n\omega_c}{\omega_o}\right) \qquad (3.2.8)$$

If $n\omega_c \gg \omega_o$ then eqn. 3.2.7. may be written as:

$$\frac{R_L}{V_1} i(t) \triangleq M+2(M+1) \sum_{n=1}^{\infty} \frac{\omega_o}{n\omega_c} \frac{\sin\left[\frac{n\pi}{2}(M+1)\right]}{\frac{n\pi}{2}(M+1)} \sin(n\omega_c t) \qquad (3.2.9)$$

As was discussed in section 3.1., the maximum value of likely to be used in a practical pulse-length modulation system, is $\frac{1}{5}$.

Therefore the maximum error in the approximation

$$\frac{\omega_o}{n\omega_c} \triangleq \frac{1}{\sqrt{\left[1+\left(\frac{n\omega_c}{\omega_o}\right)^2\right]}}$$

is 1.95%. The maximum error in the phase angle approximation $\theta_n \triangleq -\frac{\pi}{2}$ is 12.6%. However it will be noted that the Fourier coefficients in eqn. 3.2.9. decrease as $1/n^2$ which is a characteristic of the frequency

spectrum for a triangular wave. Before pursuing this point further, the frequency spectrum will be derived for the input current of the single-section maximally-flat LCR filter shown in fig. 3.1.5.

The normalised input current of the LCR filter, for a sinusoidal input voltage $V_1(\omega)$, is given by:

$$\frac{i.R_L}{V_1(\omega)} = \frac{\sqrt{\left\{1+\frac{\omega}{2\omega_o^2}\left[1+\frac{\omega^2}{\omega_o^2}\right]^2\right\}}}{1+\left(\frac{\omega}{\omega_o}\right)^4} \angle\theta \qquad (3.2.10)$$

where: $$\theta = \tan^{-1}\left\{\frac{-\omega}{\sqrt{2}.\omega_o}\left[1+\frac{\omega^2}{\omega_o^2}\right]\right\} \qquad (3.2.11)$$

$$\omega_o = \frac{1}{\sqrt{2}\,CR_L} \qquad (3.2.12)$$

From eqns. 3.2.2. and 3.2.10, the normalised input current for a rectangular voltage wavetrain input, is:

$$\frac{R_L}{V_1} i(t) = M+2(M+1)\sum_{n=1}^{\infty} \frac{\left\{1+\frac{1}{2}\left(\frac{n\omega_c}{\omega_o}\right)^2\left[1+\left(\frac{n\omega_c}{\omega_o}\right)^2\right]^2\right\}}{1+\left(\frac{n\omega_c}{\omega_o}\right)^4} \times$$

$$\frac{\sin\left[\frac{n\pi}{2}(M+1)\right]}{\frac{n\pi}{2}(M+1)} \cos\left[n\omega_c t+\theta_n\right] \qquad (3.2.13)$$

where: $$\theta_n = \tan^{-1}\left\{\frac{-n\omega_c}{\sqrt{2}\,\omega_o}\left[1+\frac{\omega^2}{\omega_o^2}\right]\right\} \qquad (3.2.14)$$

If $\omega_c \gg \omega_o$, then eqn. 3.2.13 may be rewritten as:

$$\frac{R_L}{V_1} i(t) \triangleq M+2(M+1)\sum_{n=1}^{\infty} \frac{1}{\sqrt{2}} \frac{\omega_o}{n\omega_c} \frac{\sin\left[\frac{n\pi}{2}(M+1)\right]}{\frac{n\pi}{2}(M+1)} \sin(n\omega_c t) \qquad (3.2.15)$$

Since $\omega_c \geqslant 5\omega_m$ in a practical system, the maximum error in the approximation

$$\frac{\left\{1+\frac{1}{2}\left(\frac{n\omega_c}{\omega_o}\right)^2\left[1+\left(\frac{n\omega_c}{\omega_o}\right)^2\right]^2\right\}}{1+\left(\frac{n\omega_c}{\omega_o}\right)^4} \triangleq \frac{1}{\sqrt{2}}\ \frac{\omega_o}{n\omega_c}$$

is 3.6%. The maximum error in the approximation $\theta_n \triangleq -\frac{\pi}{2}$ is 0.67%. It should be noted that the errors in the approximations for the Fourier coefficients and the phase angle give only a general indication of how accurately the approximate frequency spectrum describes the normalised filter input current. The Fourier coefficients in eqn. 3.2.15 decrease as $1/n^2$ which is characteristic of the frequency spectrum for a triangular wave.

It was shown in the time-domain analysis of the LR filter and the maximally-flat LCR filter that the input currents closely approximated to a triangular waveform superimposed on a constant term M. The triangular wave is as shown in fig. 3.2.2.

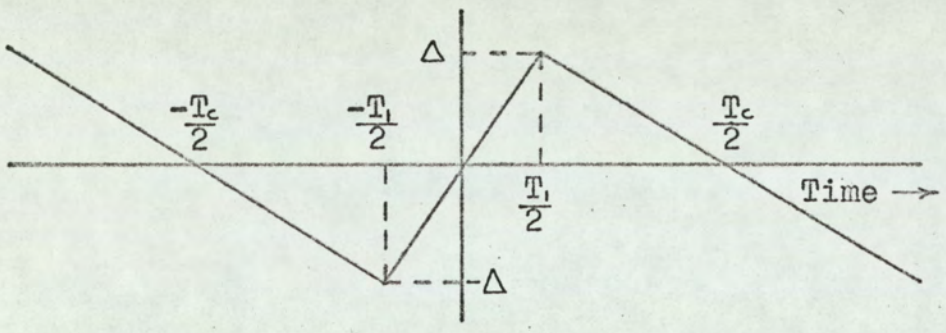

Fig.3.2.2.

Fourier analysis of the waveform gives the following expression for the frequency spectrum.

$$f(t)=\sum_{n=1}^{\infty}\frac{8\Delta}{n^2\pi^2(1-M)(1+M)}\sin\left[\frac{n\pi}{2}(M+1)\right]\sin(n\omega_c t) \qquad (3.2.16)$$

where

$$M=2\frac{T_1}{T_c}-1$$

If the waveform shown in fig. 3.2.2. is superimposed on a constant term M, then the spectrum becomes:

$$f(t)=M+\sum_{n=1}^{\infty}\frac{8\Delta}{n^2\pi^2(1-M)(1+M)}\sin\left[\frac{n\pi}{2}(M+1)\right]\sin(n\omega_c t) \qquad (3.2.17)$$

Comparison of eqns. 3.2.9. and 3.2.15, for the normalised input current of the LR and the maximally-flat LCR filters respectively, with eqn. 3.2.17 reveals that the expressions all have the same form. It is now possible to obtain simplified expressions for the filter input current in the form of a triangular wave plus a constant term. The peak excursion Δ of the triangular component is related to the filter constants by equating the approximate frequency spectrum for the filter current to the spectrum for the triangular wave.

From eqn. 3.2.9. for the LR filter, and eqn. 3.2.17 for the triangular wave:

$$M+2(M+1)\sum_{n=1}^{\infty}\frac{\omega_o}{n\omega_c}\frac{\sin\left[\frac{n\pi}{2}(M+1)\right]}{\frac{n\pi}{2}(M+1)}\sin(n\omega_c t)\equiv$$

$$M+\sum_{n=1}^{\infty}\frac{8\Delta}{n^2\pi^2(1-M)(1+M)}\sin\left[\frac{n\pi}{2}(M+1)\right]\sin(n\omega_c t) \qquad (3.2.18)$$

Therefore: $$\Delta=\frac{\omega_o}{\omega_c}\frac{\pi}{2}(1-M)(1+M) \qquad (3.2.19)$$

where $\omega_o=R_L/L$

Similarly, from eqn. 3.2.15 for the LCR filter:

$$\Delta = \frac{\mu}{4}(1-M)(1+M) \qquad (3.2.20)$$

where: $$\mu = \sqrt{2}\,\pi\,\frac{\omega_o}{\omega_c}$$

and $$\omega_o = \frac{1}{\sqrt{2}\,CR_L}$$

Thus the normalised input current for the two filters may be approximately represented by the waveform shown in fig. 3.2.3. The equations defining the

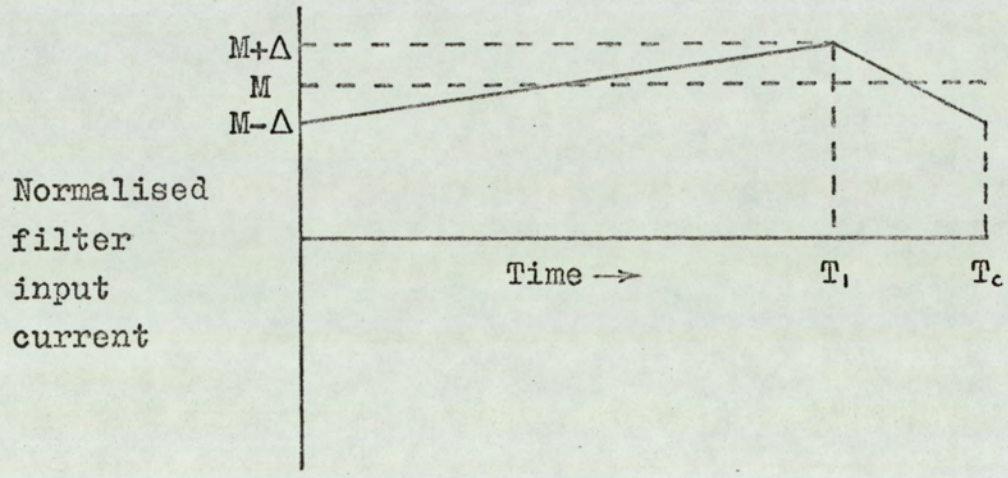

Fig.3.2.3.

waveform are as follows:

$$\frac{R_L}{V_1}\,i(t) = M-\Delta\left(2\frac{t}{T_1}-1\right) \qquad \text{for } 0 \leqslant t \leqslant T_1 \qquad (3.2.21(a))$$

$$\frac{R_L}{V_1}\,i(t) = M+\Delta\left[1-\frac{2}{T_c-T_1}(t-T_1)\right] \qquad \text{for } T_1 \leqslant t \leqslant T_c \qquad (3.2.21(b))$$

Since $M = 2\frac{T_1}{T_c} - 1$, eqns. 3.2.31(a) and (b) may be rewritten as:

$$\frac{R_L}{V_1} i(t) = M + \Delta\left(\frac{4}{M+1} \cdot \frac{t}{T_c} - 1\right) \qquad \text{for } 0 \leq \frac{t}{T_c} \leq \frac{M+1}{2} \qquad (3.2.22(a))$$

$$\frac{R_L}{V_1} i(t) = M + \Delta\left(\frac{3+M}{1-M} - \frac{4}{1-M} \cdot \frac{t}{T_c}\right) \qquad \text{for } \frac{M+1}{2} \leq \frac{t}{T_c} \leq 1 \qquad (3.2.22(b))$$

Fig. 3.2.4. shows the error in the triangular approximation for the input current of the two filters considered. The exact expressions for the input current are given by eqns. 3.1.10, 3.1.11, 3.1.17 and 3.1.18 of the time domain analysis section (Section 3.1). The error has been expressed as a percentage of the peak excursion of the current, (i.e. $M+\Delta$). It can be seen that the triangular wave approximation for the LCR filter is quite accurate, the maximum error being of the order of 3%. The approximation for the simple LR filter is not so accurate, the maximum error being 16%. However, both of the curves shown in fig. 3.2.4. represent the "worst case" condition for the approximation since the error decreases as the modulation index M increases (e.g. With M=0.5, the error falls to 6% for the LR filter). A further point is that the accuracy of the approximation will improve as the ratio of the pulse repetition frequency (ω_c) to the filter turnover frequency (ω_o) increases. The value of ω_c/ω_o used in the error calculations is 5.0, which, as mentioned earlier, is the smallest value likely to be used in a practical system.

Since any filter used in a pulse-length modulation system must have a series input inductance if large switching currents are to be avoided, it is a reasonable assumption that the triangular approximation to the input current will be valid for the majority of filters. It

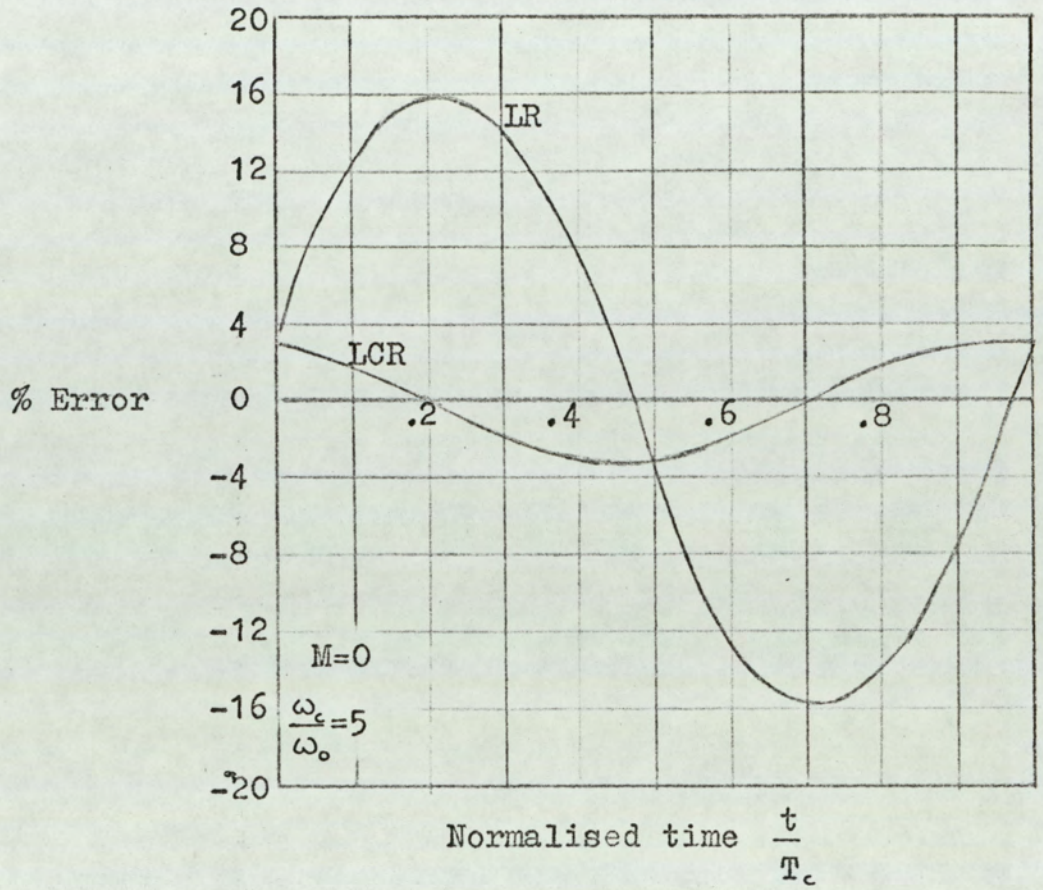

Fig.3.2.4. Error in the approximate expression for the normalised filter input current.

Error defined as $$\frac{\left(\frac{R_L}{V_1}i(t)\right)-\left(\frac{R_L}{V_1}i(t)\right)_{approx.}}{\text{Peak swing of } \frac{R_L}{V_1}i(t)}$$

is also reasonable to expect that peak excursion (Δ) of the triangular component will have the same form as that obtained for the two filters analysed. Therefore the general expression for Δ is:

$$\Delta = \lambda(1-M)(1+M) \qquad (3.2.23)$$

where λ is a function of the filter components.

4. Static analysis of power dissipation in the output stage

It is the objective of this section to derive expressions for the static power dissipation in the various switching elements of the output stage by making use of the approximate expression for filter current obtained in section 3.2. The discussion in section 2 indicated that the output stage configuration which offers the best possibilities is the common-collector complementary pair shown in fig. 4.1. The triangular wave approximation to the filter input current is shown in fig. 4.2. Consider the situation, in fig. 4.2, where the modulation index $M=M_1$. During the period $t\doteq 0$ to $t=T_1$, transistor VT1 in fig. 4.1. is conducting whilst transistor VT2 is turned off. In order to simplify the analytical work the assumption is made that the current gain of the transistors is such that the emitter current is insignificantly different from the collector current. Therefore the instantaneous power dissipation in VT1 is given by the product of the instantaneous filter input current and the instantaneous collector-emitter voltage of VT1. The power dissipation in transistor VT2 is the product of the transistor leakage current and the collector-emitter voltage. The power dissipation due to the leakage current will be neglected since the leakage in modern silicon transistors is very small. At time $t=T_1$ the voltage applied to the bases of the transistors switches to $-V_2$. However the filter input current does not change direction. This means that transistor VT2 cannot conduct since the current is in the opposite direction to the normal current flow in a transistor. The back e.m.f. of the filter thus drives the emitters of the transistors negative with respect to the negative supply

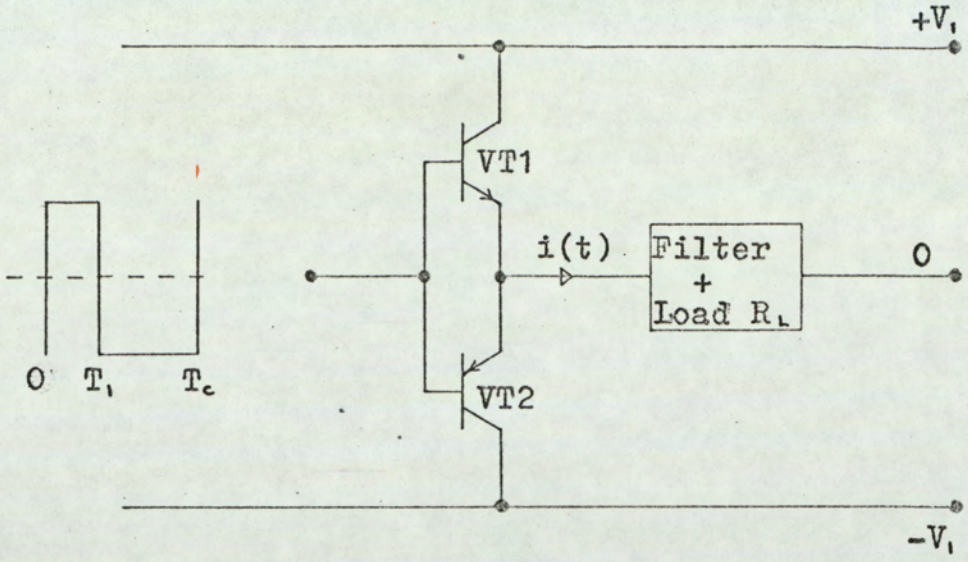

Fig.4.1. Common collector complementary pair output stage.

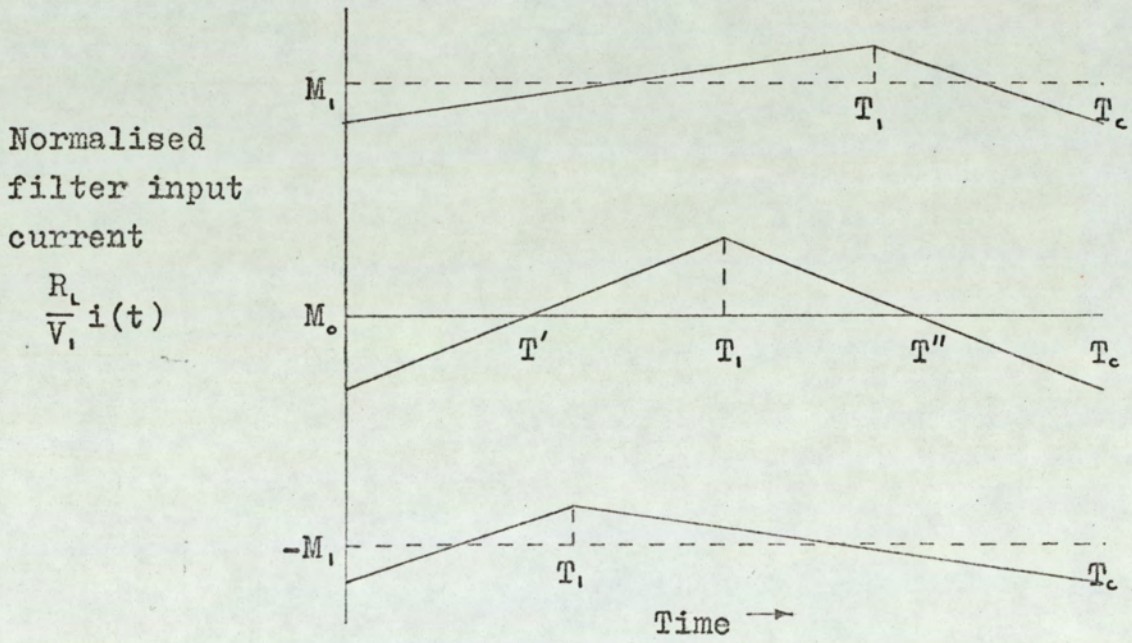

Fig.4.2. Normalised filter input current.

line until the base-emitter junction of VT1 becomes forward-biased and VT1 conducts. Thus transistor VT1 is forced to conduct throughout the period t=0 to T_c. The power dissipation during the period T_1 to T_c is high since the collector-emitter voltage is approximately equal to the supply voltage $2V_1$. For negative values of modulation index (e.g. $-M_2$ in fig. 4.2) transistor VT2 will be forced to conduct throughout the cycle. At intermediate values of modulation index (e.g. $M = M_o$ in fig. 4.2) both transistors will conduct at different times during the cycle. However the power dissipation will still be large since during the period 0 to T' transistor VT2 will be forced to conduct with nearly the full supply voltage across it. Also transistor VT1 is forced to conduct with approximately the full supply voltage between collector and emitter during the period T'' to T_c. This mode of operation is clearly inefficient. Turnbull and Townsend[44] have carried out an approximate analysis of the operation, and have shown that the efficiency is slightly lower than that of a conventional Class B output stage.

One method of overcoming this problem is presented by Miller[33] and consists of connecting diodes across the transistors to carry the reverse direction currents. The circuit arrangement is shown in fig. 4.3. Consider the operation of the circuit when the modulation index $M=M_1$ as shown in fig. 4.2. As before transistor VT1 conducts for the period t=0 to $t=T_1$. At time T_1 the base input voltage switches to $-V_2$ but the filter input current does not change direction so that VT2 is unable to conduct. Since VT2 does not conduct, the back e.m.f. of the filter forces the emitters negative with respect to the negative supply line until diode D_2 becomes forward biased and

Fig.4.3. Output stage with diodes to conduct reverse current.

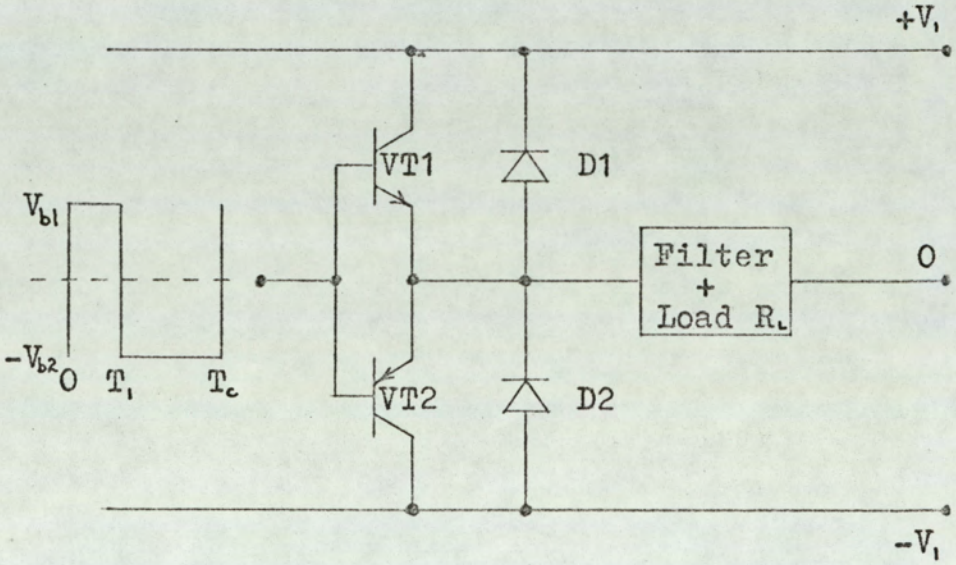

conducts the filter current. Care must be taken in the design to ensure that the voltage drop across D_2 is insufficient to forward bias the base-emitter junction of transistor VT1. This problem is discussed in more detail later in the section. It can be seen that this system is inherently more efficient than the previous one since neither of the transistors conduct with the full supply voltage between collector and emitter. Fig. 4.4. shows the manner in which the period of conduction of each of the output stage elements varies with modulation index. Also shown in fig. 4.4 are the voltage waveforms appearing at the filter input. From the diagram it can be seen that as the modulation index is increased positively so the period T' decreases and the period T" increases. Eventually the condition is reached where T' is zero, and T" is equal to T_c. From figs. 4.4 and 3.2.3., the value of modulation index required to bring about this condition is $M=\Delta$, where 2Δ is the peak to peak value of the normalised filter input current. As the modulation index M is increased in the negative direction so the period T' increases and period T" decreases. When the condition that M=- is reached, then $T'=T_1$ and $T''=T_1$. Expressions for the two periods T' and T" may be calculated from the equations for the triangular wave approximation for the filter current derived in section 3.2.

From fig. 4.4 the period T' is defined by the condition that the normalised filter input current $\frac{R_L}{V_1} i(t) = 0$. Therefore, setting $\frac{R_L}{V_1} i(t) = 0$ and t=T' in eqn. 3.2.22(a) for the triangular wave approximation to the normalised

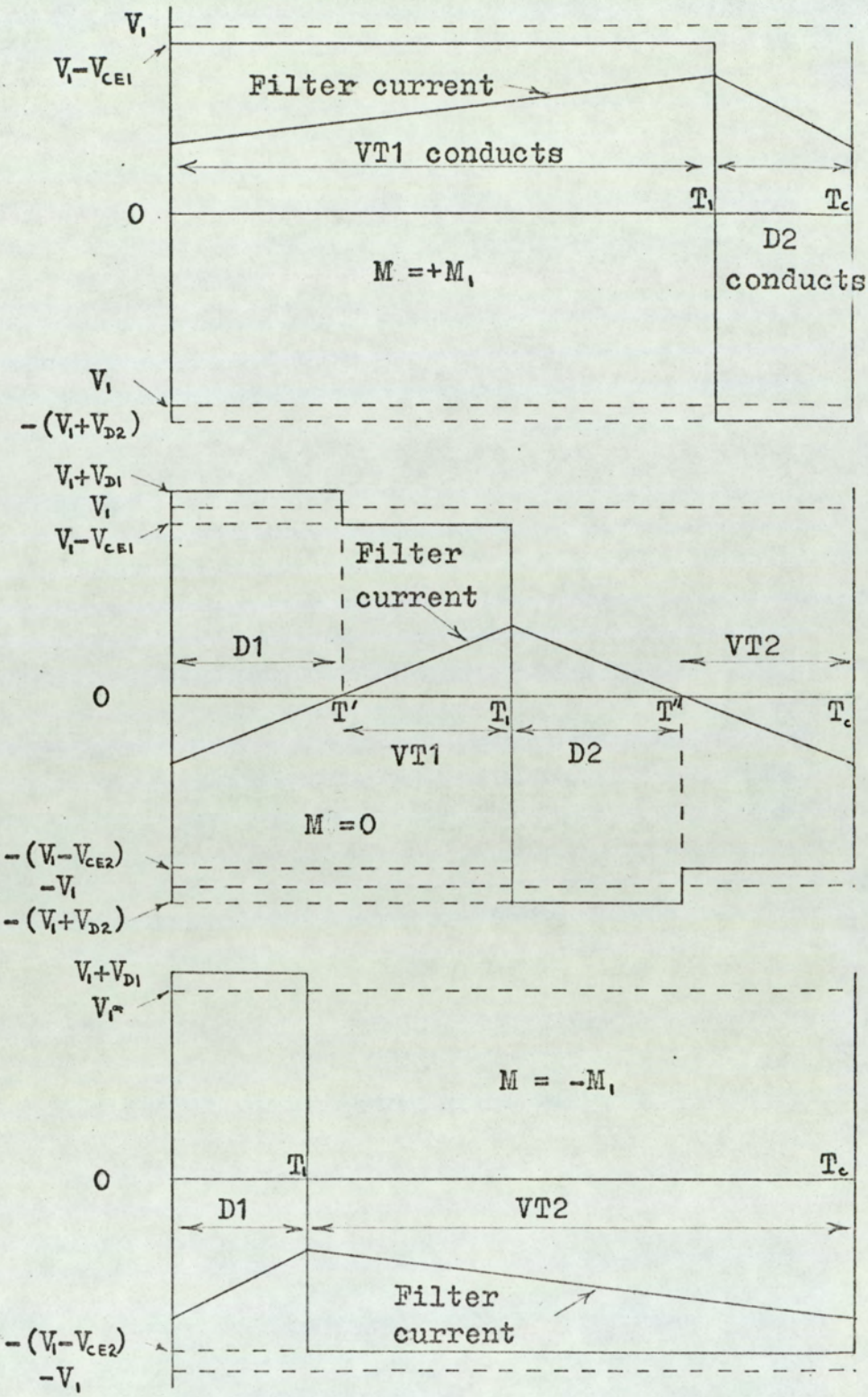

Fig.4.4. Filter input voltage and current waveforms showing the period of conduction of the output stage elements.

filter current gives:

$$0 = M - \Delta\left(\frac{4}{M+1}\,\frac{T'}{T_c} - 1\right)$$

$$\therefore \quad \frac{T'}{T_c} = \left(1 - \frac{M}{\Delta}\right)\left(\frac{M+1}{4}\right) \qquad (4.1)$$

Now, as was just discussed, the period T' tends to zero as the modulation index is increased. The limiting condition is obtained by setting $T'/T_c = 0$ in eqn. 4.1. The non-trivial solution to the equation gives:

$$M = \Delta \quad \text{for} \quad \frac{T'}{T_c} = 0 \qquad (4.2)$$

This is the result derived by inspection of fig. 4.4. As the modulation index is increased negatively so the period T' tends to T_1. Therefore setting $T'/T_c = T_1/T_c$ in eqn. 4.1, and substituting for T_1/T_c from the expression $M = 2\,T_1/T_c - 1$ gives:

$$M = -\Delta \quad \text{for} \quad \frac{T'}{T_c} = \frac{T_1}{T_c} \qquad (4.3)$$

Thus eqn. 4.1 for the period T' is valid for $-\Delta \leqslant M \leqslant \Delta$

From fig. 4.1, the period T" is defined by the condition that the normalised filter current is zero. Therefore setting $\frac{R_L}{V_1} i(t) = 0$ and t=T" in eqn. 3.2.22(b) for the approximate filter current gives:

$$\frac{T''}{T_c} = \frac{1-M}{4}\left[\frac{M}{\Delta} + \frac{3+M}{1-M}\right] \qquad (4.4)$$

Now as the modulation index is increased negatively so T" tends to T_1. The limiting condition is obtained by setting $T''=T_1$ in eqn. 4.4, and substituting for T_1/T_c from the expression $M = 2\,T_1/T_c - 1$.
This gives:

$$M = -\Delta \quad \text{for} \quad \frac{T''}{T_c} = \frac{T_1}{T_c} \qquad (4.5)$$

Increasing the modulation index positively causes T'' to approach T_c. Setting $T''=T_c$ in eqn. 4.4. gives the limiting condition as:

$$M = \Delta \quad \text{for} \quad \frac{T''}{T_c} = 1 \qquad (4.6)$$

Therefore eqn. 4.4., for the period T'', is valid for

$$-\Delta \leqslant M \leqslant \Delta$$

The values of the periods T' and T'' outside the range $-\Delta \leqslant M \leqslant \Delta$ may be deduced from fig. 4.4.

$$\frac{T'}{T_c} = 0 \text{ , and } \frac{T''}{T_c} = 1 \qquad \text{for} \quad M \gg \Delta \qquad (4.7)$$

$$\frac{T'}{T_c} = \frac{T_1}{T_c} \text{ , and } \frac{T''}{T_c} = \frac{T_1}{T_c} \qquad \text{for} \quad M \leqslant -\Delta \qquad (4.8)$$

Now that analytical expressions have been obtained for T' and T'' it is possible to evaluate the power dissipated in each of the elements of the output stage.

The power dissipation is expressed as the average value of the product of the instantaneous voltage across the device and the instantaneous current taken over one cycle of the pulse repetition frequency (i.e. over the period 0 to T_c).

Therefore from figs. 4.3 and 4.4:

Average power dissipation in transistor VT1 = $\overline{P}_{VT1}$

$$\overline{P}_{VT1} = \frac{1}{T_c}\int_{T'}^{T_1} i(t).V_{cE1}(t).dt \qquad (4.9)$$

Average power dissipation in diode D1 = $\overline{P}_{D1}$

$$\overline{P}_{D1} = \frac{1}{T_c}\int_{0}^{T'} i(t).V_{D1}(t).dt \qquad (4.10)$$

Average power dissipation in transistor VT2 = $\bar{P}_{VT2}$

$$\bar{P}_{VT2} = \frac{-1}{T_c}\int_{T''}^{T_c} i(t).V_{CE2}(t).dt \qquad (4.11)$$

Average power dissipation in diode D2 = $\bar{P}_{D2}$

$$\bar{P}_{D2} = \frac{1}{T_c}\int_{T_1}^{T''} i(t).V_{D2}(t).dt \qquad (4.12)$$

where: i(t) is the instantaneous filter input current

$V_{CE1}(t)$ and $V_{CE2}(t)$ are the instantaneous collector-emitter voltages during conduction of VT1 and VT2 respectively.

$V_{D1}(t)$ and $V_{D2}(t)$ are the instantaneous voltages across diodes D_1 and D_2 respectively.

The negative signs in the expressions for $\bar{P}_{D1}$ and $\bar{P}_{VT2}$ are required since the filter input current is negative during the period of conduction of D1 and VT2. In order to evaluate the expressions for the power dissipation in the output stage elements it is necessary to relate the voltage drops across the devices to the current.

The terminal voltages and currents for an idealised junction transistor may be represented[69,70] by the following expressions:

$$I_E = I_{ES}\left[\exp\left(\frac{qV'_{EB}}{kT}\right)-1\right] - \alpha_R I_{CS}\left[\exp\left(\frac{qV'_{CB}}{kT}\right)-1\right] \qquad (4.13)$$

$$I_c = -\alpha_F I_{ES}\left[\exp\left(\frac{qV'_{EB}}{kT}\right)-1\right] + I_{CS}\left[\exp\left(\frac{qV'_{CB}}{kT}\right)-1\right] \qquad (4.14)$$

where:

I_{ES} = The emitter junction saturation current with the collector connected to the base.

I_{cs} = The collector junction saturation current with the emitter connected to the base.

α_F = Large-signal forward-injection common-base short-circuit current gain

α_R = Large-signal reverse-injection common-base short-circuit current gain

V'_{EB} =Emitter-base voltage taken as positive for a forward-biased junction

V'_{cB} =Collector-base voltage taken as positive for a forward-biased junction.

k = Boltzmann's constant ($1.3805.10^{-23}$ joules/degree)

T = Absolute temperature

q = Magnitude of the electronic charge ($1.602.10^{-19}$ coulomb)

Under normal operating conditions the collector-base junction is reverse biased. If the reverse bias is greater than a few tens of millivolts then the large-signal volt-ampere characteristics reduce to:

$$I_E \triangleq I_{ES}\left[\exp\left(\frac{qV'_{EB}}{kT}\right)-1\right]+\alpha_R I_{cs} \qquad (4.15)$$

$$I_c \triangleq -\alpha_F I_E-(1-\alpha_F\alpha_R)I_{cs} \qquad (4.16)$$

With the complementary common-collector output stage shown in fig. 4.3, the collector-base junctions will always be reverse-biased if the voltage applied to the bases is less than the supply voltage. The terms $\alpha_R I_{cs}$ and $(1-\alpha_F\alpha_R)I_{cs}$ in eqns. 4.15 and 4.16 are usually very small compared with typical normal-region emitter currents, and may be neglected. If the assumption is made that the forward current gain of the transistor is sufficiently large for

the collector and emitter currents to be regarded as equal (i.e. $\alpha_F \simeq 1$) then:

$$I_E \simeq I_{ES}\left[\exp\left(\frac{q V'_{EB}}{kT}\right) - 1\right] \qquad (4.17)$$

$$I_C \simeq I_E \qquad (4.18)$$

The current-voltage relationship for an idealised junction diode[70] is given by the expression:

$$I_D = I_s\left[\exp\left(\frac{q V'_D}{kT}\right) - 1\right] \qquad (4.19)$$

where I_S = diode saturation current

V'_D = voltage across the diode

Experimental work, which is described later in this chapter, shows that the simple mathematical models of the transistor and diode are not sufficiently accurate. Considerably better agreement is obtained between the measured and theoretical characteristics if a linear resistance is included in series with the ideal diode and transistor as shown in fig. 4.5

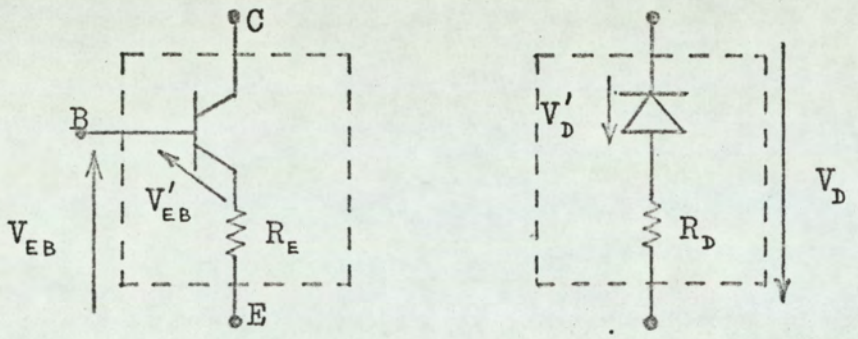

Fig.4.5. Idealised transistor and diode with added series resistance.

The volt-ampere characteristics for the modified transistor and diode may be written down from eqns. 4.17 4.19 and fig. 4.5

$$V_{EB} = I_E . R_E + \frac{kT}{q} \log\left[1 + \frac{I_E}{I_{ES}}\right] \qquad (4.20)$$

$$V_D = I_D R_D + \frac{kT}{q} \log\left[1 + \frac{I_E}{I_s}\right] \qquad (4.21)$$

The instantaneous power dissipation in the output stage diodes is simply the product of the current flowing (i.e. the filter input current) and the voltage drop across the diode as given by eqn. 4.21. The power dissipation in the transistors is made up of two components. One component being the product of the filter input current and the emitter-base voltage of the transistor. The second component is the product of the filter current and the collector-base voltage. From fig. 4.3 the collector-base voltage V_{CB1} of transistor VT1 during the conduction period is:

$$V_{CB1} = V_1 - V_{b1} \qquad (4.22)$$

The collector-base voltage of transistor VT2 during the conduction period is:

$$V_{CB2} = V_1 - V_{b2} \qquad (4.23)$$

Thus eqns. 4.9, 4.10, 4.11 and 4.12, for the average power dissipation in the elements of the output stage, may be written as:

$$\bar{P}_{VT1} = \frac{1}{T_c} \int_{T'}^{T_1} i(t)\left[i(t) R_{E1} + \frac{kT}{q} \log\left(1 + \frac{i(t)}{I_{ES1}}\right) + V_{CB1}\right] dt \qquad (4.24)$$

$$\bar{P}_{D1} = \frac{-1}{T_c}\int_0^{T'} i(t)\left[-i(t)R_{D1} + \frac{kT}{q}\log\left(1+\frac{-i(t)}{I_{S1}}\right)\right] dt \qquad (4.25)$$

$$\bar{P}_{VT2} = \frac{-1}{T_c}\int_{T''}^{T_c} i(t)\left[-i(t)R_{E2} + \frac{kT}{q}\log\left(1+\frac{-i(t)}{I_{ES2}}\right) + V_{cB2}\right] dt \qquad (4.26)$$

$$\bar{P}_{D2} = \frac{1}{T_c}\int_{T_1}^{T''} i(t)\left[\, i(t)R_{D2} + \frac{kT}{q}\log\left(1+\frac{i(t)}{I_{S1}}\right)\right] dt \qquad (4.27)$$

where i(t) is the filter input current as given by eqns. 3.2.22(a) and (b) of section 3.2.
The integration and rearrangement of the power dissipation expressions is covered in detail in Appendix 7., and only the results are quoted here.

For $M \gg \Delta$

$$\bar{P}_{VT1} = \frac{kT}{q}\frac{I_{ES1}^2(M+1)}{4I\Delta}\left\{b_2\left(\frac{b_2}{2}-1\right)\log b_2 - b_1\left(\frac{b_1}{2}-1\right)\log b_1 - b_2\left(\frac{b_2}{4}-1\right)+b_1\left(\frac{b_1}{4}-1\right)\right\} +$$

$$\frac{I V_{cB1} M(M+1)}{2} + I^2 R_{E1}\Delta^2\frac{M+1}{2}\left[\left(\frac{M}{\Delta}\right)^2+\frac{1}{3}\right] \qquad (4.28(a))$$

where: $b_1 = 1+\frac{I}{I_{ES1}}(M-\Delta)$ $\qquad$ $b_2 = 1+\frac{I}{I_{ES1}}(M-\Delta)$

$$\bar{P}_{D1} = 0 \qquad (4.28(b))$$

$$\bar{P}_{VT2} = 0 \qquad (4.28(c))$$

$$\bar{P}_{D2} = \frac{kT}{q}\,\frac{I_{S2}^2(1-M)}{4I\Delta}\left\{c_1\left(\frac{c_1}{2}-1\right)\log c_1 - c_2\left(\frac{c_2}{2}-1\right)\log c_2 - c_1\left(\frac{c_1}{4}-1\right)+c_2\left(\frac{c_2}{4}-1\right)\right\}+$$

$$I^2 R_{D2}\,\Delta^2\,\frac{(1-M)}{2}\left[\left(\frac{M}{\Delta}\right)^2+\frac{1}{3}\right] \qquad (4.28(d))$$

where: $c_1 = 1+\frac{I}{I_{S2}}(M+\Delta)$ $\qquad$ $c_2 = 1+\frac{I}{I_{S2}}(M-\Delta)$

For $-\Delta \leq M \leq \Delta$

$$\bar{P}_{VT1} = \frac{kT}{q}\,\frac{I_{ES1}^2(M+1)}{4I\Delta}\left\{b_2\left(\frac{b_2}{2}-1\right)\log b_2 - b_2\left(\frac{b_2}{4}-1\right)-\frac{3}{4}\right\}+$$

$$I V_{CB1}\left[\frac{(M+1)(M+\Delta)^2}{8\Delta}\right]+\frac{I^2 R_{E1}\,\Delta^2(M+1)}{12}\left(1+\frac{M}{\Delta}\right)^3 \qquad (4.29(a))$$

where: $b_2 = 1+\frac{I}{I_{ES1}}(M+\Delta)$

$$\bar{P}_{D1} = \frac{kT}{q}\,\frac{I_{S1}^2(M+1)}{4I\Delta}\left\{a_1\left(\frac{a_1}{2}-1\right)\log a_1 - a_1\left(\frac{a_1}{4}-1\right)-\frac{3}{4}\right\}+$$

$$\frac{I^2 R_{D1}\,\Delta^2(M+1)}{12}\left(1-\frac{M}{\Delta}\right)^3 \qquad (4.29(b))$$

where $a_1 = 1-\frac{I}{I_{S1}}(M-\Delta)$

$$\bar{P}_{VT2} = \frac{kT}{q}\,\frac{I_{ES2}^2(1-M)}{4I\Delta}\left\{d_2\left(\frac{d_2}{2}-1\right)\log d_2 - d_2\left(\frac{d_2}{4}-1\right)-\frac{3}{4}\right\}+$$

$$I V_{CB2}\left[\frac{(1-M)(M-\Delta)^2}{8\Delta}\right]+\frac{I^2 R_{E2}\,\Delta^2(1-M)}{12}\left(1-\frac{M}{\Delta}\right)^3 \qquad (4.29(c))$$

where: $d_2 = 1-\frac{I}{I_{ES1}}(M-\Delta)$

$$\bar{P}_{D2} = \frac{kT}{q}\,\frac{I_{S2}^2(1-M)}{4I\Delta}\left\{c_1\left(\frac{c_1}{2}-1\right)\log c_1 - c_1\left(\frac{c_1}{4}-1\right)-\frac{3}{4}\right\}$$

$$\frac{I^2 R_{D2}\,\Delta^2(1-M)}{12}\left(1+\frac{M}{\Delta}\right)^3 \qquad (4.29(d))$$

where: $c_1 = 1+\frac{I}{I_{S2}}(M+\Delta)$

For $M \leq -\Delta$

$$\bar{P}_{VT1} = 0 \qquad (4.30(a))$$

$$\bar{P}_{D1} = \frac{kT}{q}\frac{I_{S1}^2(1-M)}{4I\Delta}\left\{a_1\left(\frac{a_1}{2}-1\right)\log a_1 - a_2\left(\frac{a_2}{2}-1\right)\log a_2 - a_1\left(\frac{a_1}{4}-1\right) + a_2\left(\frac{a_2}{4}-1\right)\right\} +$$

$$\frac{I^2 R_{D1}\Delta^2(M+1)}{2}\left[\left(\frac{M}{\Delta}\right)^2 + \frac{1}{3}\right] \qquad (4.30(b))$$

where $a_1 = 1 - \frac{I}{I_{S1}}(M-\Delta)$, $a_2 = 1 - \frac{I}{I_{S1}}(M+\Delta)$

$$\bar{P}_{VT2} = \frac{kT}{q}\frac{I_{ES2}^2(1-M)}{4I\Delta}\left\{d_2\left(\frac{d_2}{2}-1\right)\log d_2 - d_1\left(\frac{d_1}{2}-1\right)\log d_1 - d_2\left(\frac{d_2}{4}-1\right) + d_1\left(\frac{d_1}{4}-1\right)\right\} -$$

$$\frac{V_{CB2} I M(1-M)}{2} + \frac{I^2 R_{E2}\Delta^2(1-M)}{2}\left[\left(\frac{M}{\Delta}\right)^2 + \frac{1}{3}\right] \qquad (4.30(c))$$

where $d_1 = 1 - \frac{I}{I_{ES2}}(M+\Delta)$, $d_2 = 1 - \frac{I}{I_{ES2}}(M-\Delta)$

$$\bar{P}_{D2} = 0 \qquad (4.30(d))$$

In the above equations I is the maximum current that can be passed through the load.

$$I = \frac{V_1}{R_L} \qquad (4.31)$$

It has been assumed throughout the analysis that only one of the output stage elements is conducting at any given time. However this may not be the case unless care is taken in the design of the output stage. Consideration of the circuit diagram of fig. 4.3, and the associated waveforms of fig. 4.4., shows that, for sufficiently large positive values of modulation index, diode D_2 should conduct the filter current during the period $t=T_1$ to T_C. Fig. 4.4. shows that when diode D_2 is conducting, the filter input voltage is $-(V_1 + V_{D2})$ Under these conditions the base-emitter voltage for transistor

VT1 is $(V_1 + V_{D2} - V_b)$. Now in a practical system V_b is likely to be slightly less than V_1 which means that base-emitter voltage of VT1 is slightly greater than the voltage V_{D2} dropped across D_2. This forward bias on VT1 may well be sufficient to cause transistor VT1 to conduct a significant proportion of the filter current during the period $t=T_1$ to T_c. Since the collector-emitter voltage of VT1 will be approximately equal to the supply voltage 2V during this period, inefficient operation will result. Similar reasoning applies to the forward base-emitter voltage of transistor VT2 for sufficiently large negative values of modulation index. This problem may be reduced by the circuit arrangement shown in fig. 4.6 where the diodes D3 and D4 increase the effective emitter-base voltage required by transistors VT1 and VT2 respectively. Thus the conditions for the correct operation of the circuit are:

$$V_{D2} + (V_1 - V_{b2}) < V_{BE1} + V_{D3} \qquad (4.32)$$

$$V_{D1} + (V_1 - V_{b1}) < V_{BE2} + V_{D4} \qquad (4.33)$$

where V_{BE1}, V_{D3}, V_{BE2} and V_{D4} are the forward bias voltages necessary to cause a significant current flow in VT1, D3, VT2, and D4 respectively.

Diodes D3 and D4 are in series with transistors VT1 and VT2 and hence conduct when the respective transistors conduct. Therefore the average power dissipation in the diodes may be written down by inspection of eqns. 4.28(a) and (c), 4.29(a) and (c), 4.30(a) and (c) for the power dissipation in the transistors.

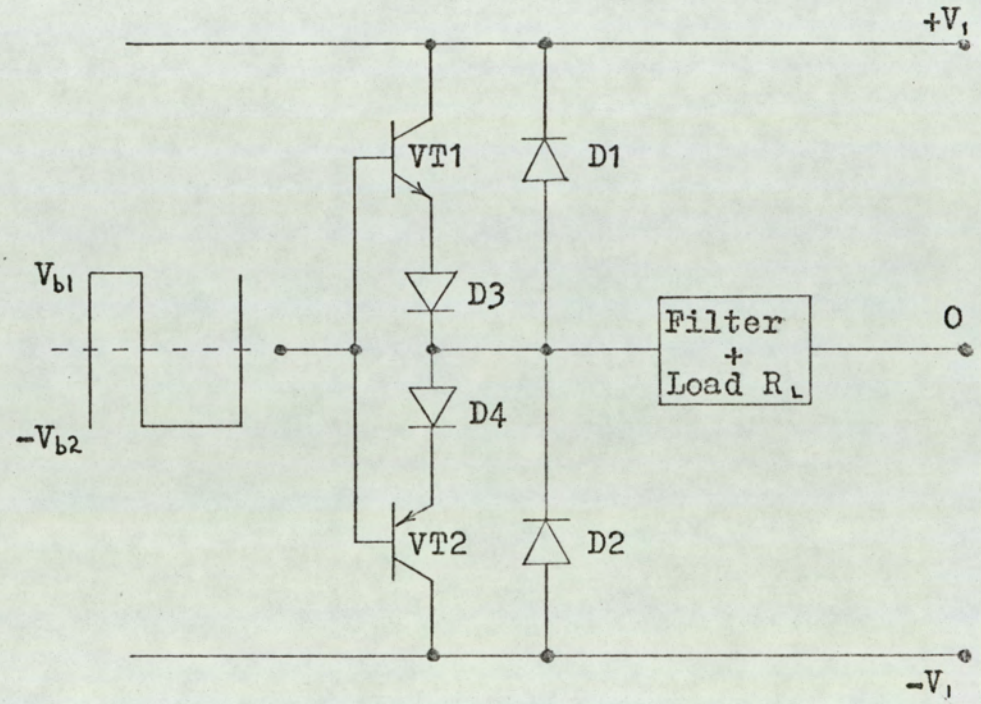

Fig.4.6. Output stage with additional diodes D3 and D4.

For $M \geq \Delta$

$$\bar{P}_{D3} = \frac{kT}{q}\frac{I_{s3}(M+1)}{4I\Delta}\left\{f_2\left(\frac{f_2}{2}-1\right)\log f_2 - f_1\left(\frac{f_1}{2}-1\right)\log f_1 - f_2\left(\frac{f_2}{4}-1\right)+f_1\left(\frac{f_1}{4}-1\right)\right\} +$$

$$I^2 R_{D3}\Delta^2\frac{M+1}{2}\left[\left(\frac{M}{\Delta}\right)^2+\frac{1}{3}\right] \qquad (4.34(a))$$

where: $f_1 = 1+\frac{I}{I_{s3}}(M-\Delta)$ $\qquad$ $f_2 = 1+\frac{I}{I_{s3}}(M+\Delta)$

$$\bar{P}_{D4} = 0 \qquad (4.34(b))$$

For $-\Delta \leq M \leq \Delta$

$$\bar{P}_{D3} = \frac{kT}{q}\frac{I_{s3}^2(M+1)}{4I\Delta}\left\{f_2\left(\frac{f_2}{2}-1\right)\log f_2 - f_2\left(\frac{f_2}{4}-1\right)-\frac{3}{4}\right\}+\frac{I^2 R_{D3}\Delta^2(M+1)}{12}\left(1+\frac{M}{\Delta}\right)^3 \qquad (4.35(a))$$

where: $f_2 = 1+\frac{I}{I_{s3}}(M+\Delta)$

$$\bar{P}_{D4} = \frac{kT}{q}\frac{I_{s4}^2(1-M)}{4I\Delta}\left\{g_2\left(\frac{g_2}{2}-1\right)\log g_2 - g_2\left(\frac{g_2}{4}-1\right)-\frac{3}{4}\right\}+\frac{I^2 R_{D4}\Delta^2(1-M)}{12}\left(1-\frac{M}{\Delta}\right)^3 \qquad (4.35(b))$$

where: $g_2 = 1+\frac{I}{I_{s4}}(M-\Delta)$

For $M \leq \Delta$

$$\bar{P}_{D3} = 0 \qquad (4.36(a))$$

$$\bar{P}_{D4} = \frac{kT}{q}\frac{I_{s4}^2(1-M)}{4I\Delta}\left\{g_2\left(\frac{g_2}{2}-1\right)\log g_2 - g_1\left(\frac{g_1}{2}-1\right)\log g_1 - g_2\left(\frac{g_2}{4}-1\right)+g_1\left(\frac{g_1}{4}-1\right)\right\} +$$

$$\frac{I^2 R_{D4}\Delta^2(1-M)}{2}\left[\left(\frac{M}{\Delta}\right)^2+\frac{1}{3}\right] \qquad (4.36(b))$$

where: $g_1 = 1-\frac{I}{I_{s4}}(M+\Delta)$ $\qquad$ $g_2 = 1-\frac{I}{I_{s4}}(M-\Delta)$

Thus expressions have been developed for the average power dissipation in all the elements of the output stage. The equations are expressed in terms of the modulation index M, the parameters of the particular element, and the peak to peak excursion (2Δ) of the triangular wave approximation to the normalised filter current. It is shown that the diodes D1 and D2 modify the voltage waveform at the filter input. However the assumption is made that this modification of the waveform has negligible effect on the filter current so that the triangular wave approximation is still valid. Due to the number of independent variables involved in the power dissipation equations it is not practicable to present generalised graphs of power dissipation for the various output stage elements. However application of the analytical expressions to a practical system is a straightforward matter, although somewhat time consuming due to the complexity of the equations.

5. Quasi-dynamic analysis of power dissipation in the output stage

The difficulty of performing a rigorous analysis of power dissipation in the output stage for time-varying modulation is discussed in section 1. However an approximate analysis may be carried out on a quasi-dynamic basis. In section 4 expressions are derived relating the average power dissipation, over one cycle of the pulse repetition frequency, to the circuit parameters and the modulation index M. If the modulation index, in these expressions, is allowed to vary in a sinusoidal manner then the average power dissipation may be evaluated by integrating over one cycle of the modulation frequency. The innaccuracy of the method lies in the fact that the expressions for the filter input current were derived by assuming that the rectangular wavetrain applied to the filter input started at an infinite time before time zero. The accuracy of the quasi-dynamic analysis will thus improve as the ratio of the pulse repetition frequency to the modulation frequency increases. Now it was shown in the static analysis that the power dissipated in each of the active elements of the output stage is governed by one of three different expressions, depending on the value of the modulation index. (See eqns. 4.28, 4.29, 4.30, 4.34, 4.35 and 4.36). The three ranges of modulation index for which the power dissipation expressions are defined are $M \geqslant \Delta$, $-\Delta \leqslant M \leqslant \Delta$, and $M \leqslant -\Delta$. If the system input is a cosine wave (i.e. $M(t) = M.\cos(\omega_m t)$) then these limit values of modulation index may be related to time as shown in fig. 5.1. Now Δ, the peak value of

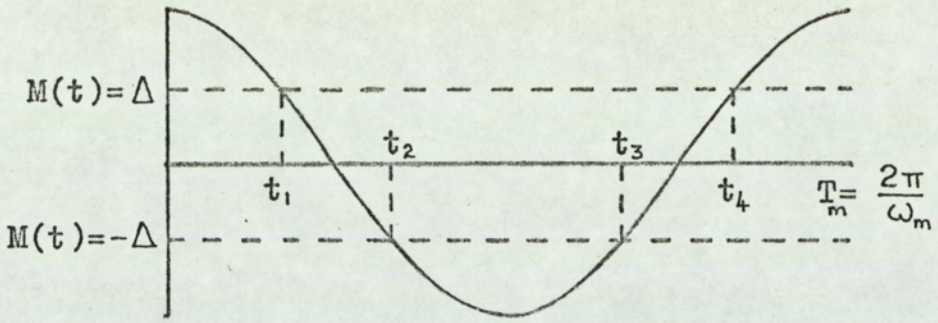

Fig.5.1. Instantaneous modulation index $M.\cos(\omega_m t)$

the triangular component of the filter current (see fig. 3.2.3.) is a function of the modulation index. It is shown in section 3.2, eqn. 3.2.23, that the factor is given by the expression:

$$\Delta = \lambda(1-M)(1+M) \qquad (5.1)$$

where λ is a function of the filter parameters. Since the modulation index is time varying, eqn. 5.1 may be rewritten as:

$$\Delta(t) = \lambda(1-M(t))(1+M(t)) \qquad (5.2)$$

The instants t_1 and t_2 in fig. 5.1 are defined by the expressions:

$$M(t_1) = \Delta(t_1) \qquad (5.3)$$

$$M(t_2) = \Delta(t_2) \qquad (5.4)$$

Substituting eqn. 5.2 in eqns. 5.3. and 5.4., and setting $M(t) = M\cos(\omega_m t)$, leads to the following expressions for t_1 and t_2.

$$\frac{t_1}{T_m} = \frac{1}{2\pi}\cos^{-1}\left\{\frac{1}{2M\lambda}\left[-1+\sqrt{(1+4\lambda^2)}\right]\right\} \qquad (5.5)$$

$$\frac{t_2}{T_m} = \frac{1}{2\pi}\cos^{-1}\left\{\frac{1}{2M\lambda}\left[1-\sqrt{(1-4\lambda^2)}\right]\right\}$$

$$= 0{\cdot}5 - \frac{t_1}{T_m} \qquad (5.6)$$

As a result of the symmetry of fig. 5.1, expressions for the instants t_3 and t_4 could be derived from eqns. 5.5 and 5.6. However it is shown later in this section that these expressions are not required.

For small values of modulation index the condition $M(t) = \Delta(t)$ may not occur. The limit condition is when the peak value of the modulation index $M(t)$ is equal to $\Delta(t)$. Therefore:

$$M = \lambda(1-M)(1+M)$$

which gives $$M_{min} = \frac{1}{2\lambda}\left[-1+\sqrt{(1+4\lambda^2)}\right] \qquad (5.7)$$

where M_{min} is the minimum value of the modulation index for which eqns. 5.5. and 5.6 are valid.
From fig. 5.1. it can be seen that when $M = M_{min}$ then $t_1 = 0$ and $t_2 = T_m/2$. Although t_1 and t_2 do not actually exist for $M < M_{min}$ it is convenient to make the definition:

$$\frac{t_1}{T_m} = 0 \quad \text{and} \quad \frac{t_2}{T_m} = \frac{1}{2} \quad \text{for} \quad M \leq M_{min} \qquad (5.8)$$

The average power dissipation, over one cycle of the modulation frequency ω_m, in each of the elements of the output stage can now be expressed by the general equation:

$$P=\frac{1}{T_m}\left\{\int_0^{t_1} P_1(t).dt+\int_{t_1}^{t_2} P_2(t).dt+\int_{t_2}^{t_3} P_3(t).dt+\int_{t_3}^{t_4} P_2(t).dt+\int_{t_4}^{T_m} P_1(t).dt\right\} \qquad (5.9)$$

where: $P_1(t)$ is the power dissipation in the element for $M(t) \gg \Delta(t)$

$P_2(t)$ is the power dissipation in the element for $-\Delta(t) \leq M(t) \leq \Delta(t)$

$P_3(t)$ is the power dissipation in the element for $M(t) \leq -\Delta(t)$

Since the time varying modulation index $M.\cos(\omega_m t)$ is symmetrical about time $t = T_m/2$ eqn. 5.9 reduces to:

$$P=\frac{2}{T_m}\left\{\int_0^{t_1} P_1(t).dt+\int_{t_1}^{t_2} P_2(t).dt+\int_{t_2}^{T_m/2} P_3(t).dt\right\} \qquad (5.10)$$

Now it is shown in the static analysis of power dissipation that, for some ranges of modulation index, the power dissipation in a particular element of the output stage is zero. (e.g. From eqn. 4.30(a) the power dissipation in transistor VT1 is zero for $M \leq -\Delta$).
Therefore, from eqns. 4.28, 4.29, 4.30, 4.34, 4.35, 4.36 and 5.10, the power dissipation in each of the output stage elements may be expressed as:

$$P_{VT1}=\frac{2}{T_m}\left\{\int_0^{t_1} \overline{P}_{VT1}(t).dt+\int_{t_1}^{t_2} \overline{P}_{VT1}(t).dt\right\} \qquad (5.11(a))$$

$$P_{D3}=\frac{2}{T_m}\left\{\int_0^{t_1} \overline{P}_{D3}(t).dt+\int_{t_1}^{t_2} \overline{P}_{D3}(t).dt\right\} \qquad (5.11(b))$$

$$P_{D1} = \frac{2}{T_m}\left\{\int_{t_1}^{t_2} \bar{P}_{D1}(t).dt + \int_{t_2}^{T_m/2} \bar{P}_{D1}(t).dt\right\} \qquad (5.11(c))$$

$$P_{VT2} = \frac{2}{T_m}\left\{\int_{t_1}^{t_2} \bar{P}_{VT2}(t).dt + \int_{t_2}^{T_m/2} \bar{P}_{VT2}(t).dt\right\} \qquad (5.11(d))$$

$$P_{D4} = \frac{2}{T_m}\left\{\int_{t_1}^{t_2} \bar{P}_{D4}(t).dt + \int_{t_2}^{T_m/2} \bar{P}_{D4}(t).dt\right\} \qquad (5.11(e))$$

$$P_{D2} = \frac{2}{T_m}\left\{\int_{0}^{t_1} \bar{P}_{D2}(t).dt + \int_{t_1}^{t_2} \bar{P}_{D2}(t).dt\right\} \qquad (5.11(f))$$

The expressions for the time dependent power dissipation are obtained by replacing M with $M.\cos(\omega_m t)$ in the expressions for the static power dissipation. The appropriate static power dissipation expression may be identified by the limits of the integration.

i.e. For 0 to t_1 , $M \geqslant \Delta$ (5.12(a))

For t_1 to t_2 , $-\Delta \leqslant M \leqslant \Delta$ (5.12(b))

For t_2 to $T_m/2$, $M \leqslant -\Delta$ (5.12(c))

Integration of the static power dissipation expressions (eqns. 4.28,4.29,4.30,4.34,4.35, and 4.36) is a formidable task when M is replaced by $M.\cos(\omega_m t)$ and the results are likely to be so complex as to preclude evaluation without the use of a digital computer. For this reason numerical integration is used to evaluate eqns. 5.11(a) to (f). With this in mind, a number of useful observations can be made from the static power dissipation expressions.

Comparison of eqns. 4.28(a), 4.29(a) and 4.30(a) for the power dissipation in transistor VT1 with eqns. 4.34(a), 4.35(a) and 4.36(a) for the power dissipation in the associated series diode D3 shows that the corresponding expressions for each element have the same form. The only difference in the expressions is in the constants relating to the particular element. Similarly the expressions for the dissipation in transistor VT2 and associated diode D4 have the same form. Furthermore comparison of eqns. 4.28(a), 4.29(a) and 430(a) with eqns. 4.30(c), 4.29(c) and 4.28(c) respectively, shows that the dissipation in transistor VT1 for positive values of modulation index has the same form as the expressions for the dissipation in transistor VT2 with negative values of modulation index. Therefore, as a result of the symmetry of the modulation, the expressions for the average power dissipation in transistors VT1 and VT2 onver one cycle of the modulation frequency will have the same form. This means that when calculating the average power dissipation in VT2 it is only necessary to substitute the constants relating to VT2 in the expression for the power dissipation in transistor VT1. Therefore the average power dissipation in the four series elements may all be evaluated by integration of the expressions for the dissipation in transistor VT1 (i.e. eqns. 4.28(a) and 4.29(a with $M.\cos(\omega_m t)$ replacing M) with the appropriate constant substituted in place of those relating to VT1. The limits of the integration are given by eqn. 5.11(a). Comparison of eqns. 4.28(b), 4.29(b) and 4.30(b) with eqns. 4.30(d), 4.29(d) and 4.28(d) respectively shows that the power dissipation in diode D1 for positive values of modulation index has the same form as the dissipation in D2 for negativ

values of modulation index. Therefore, as a result of the symmetry of the modulation, the average power dissipation in diode D2 may be evaluated by integrating the expressions for the dissipation in diode D1, with the constants for D2 replacing those relating to D1. The limits for the integration are given by eqn. 5.11(c). These observations considerably simplify the writing of a computer program to evaluate the average power dissipation in each of the elements.

Figs. 5.2(a) and (b) show the flowchart used as the basis of the computer program. Simpson's method[60] is used to perform the integration. The integration is reiterated with the mesh size halved for each iteration, until two successive evaluations of the integral agree to one part in 10^3. The flowchart is split into two sections: namely fig. 5.2(a) which evaluates the average power dissipation in the series elements of the output stage, and fig. 5.2(b) which evaluates the dissipation in the shunt diodes D1 and D2 of fig. 4.3. Since the first section (i.e. fig. 5.2(a)) evaluates the dissipation for diodes and transistors, it is necessary to specify in the data, that $V_{CB} = 0$ for the diodes.

Due to the number of independent variables it is not practicable to present generalised graphs of power dissipation in each of the output stage elements. However the theory is applied to an experimental system in section 6.4. , and the results give a reasonable indication of the variation of power dissipation with modulation index.

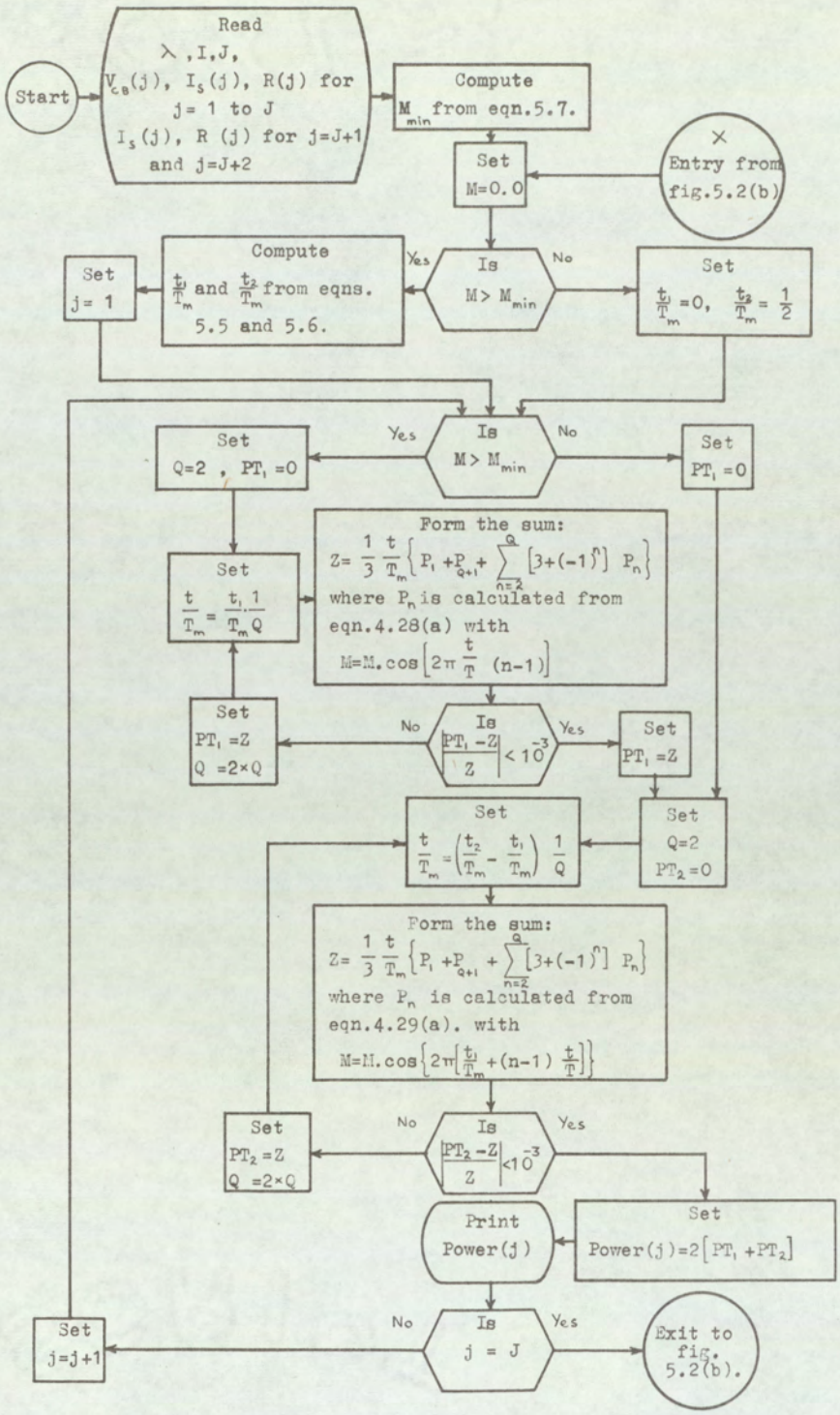

Fig.5.2(a). Flowchart for calculating average power dissipation in series elements of output stage.

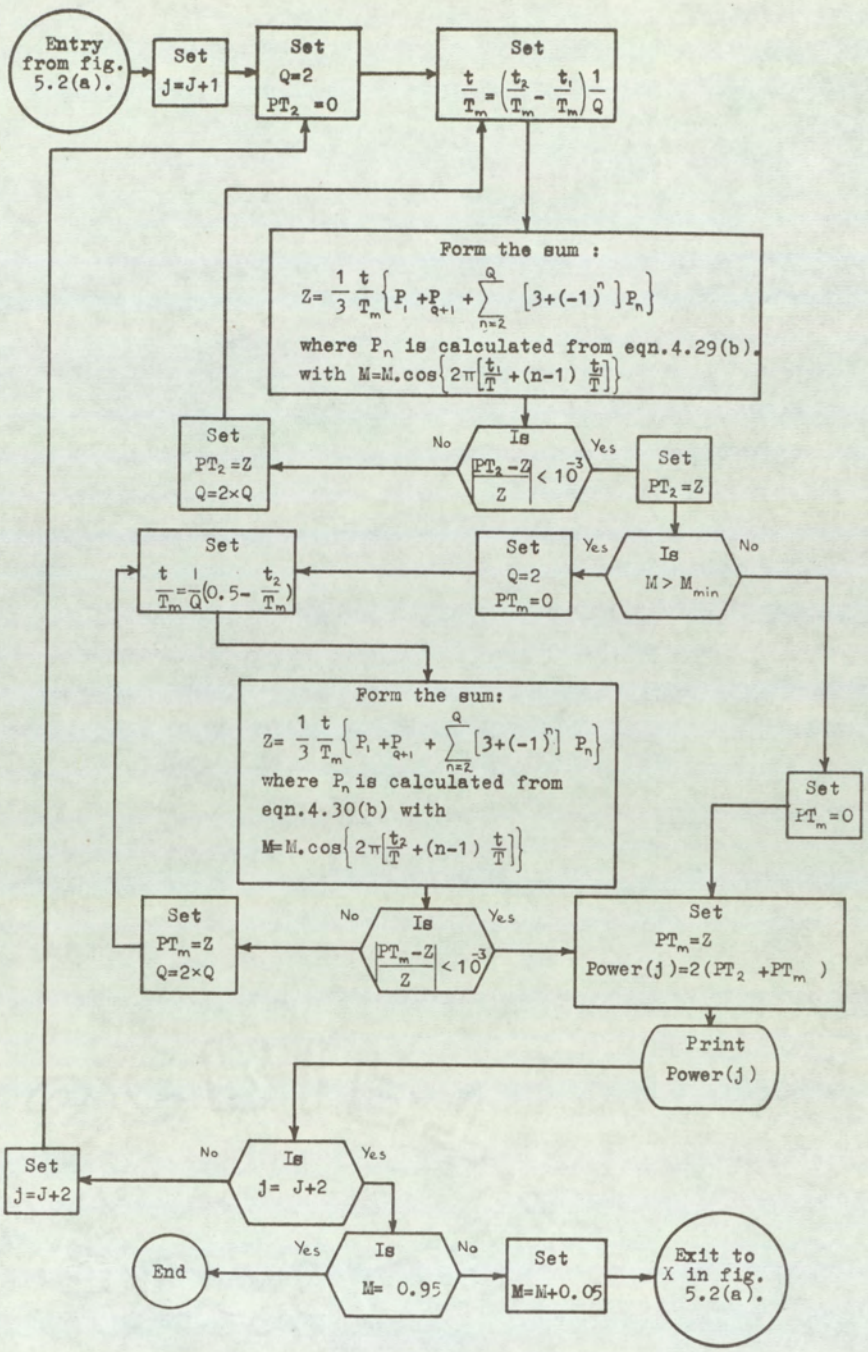

Fig.5.2(b). Flowchart for calculating average power dissipation in shunt diodes of the output stage.

6. Experimental work

6.1. Determination of diode and transistor parameters

Eqn. 4.19 for the voltage-current characteristic of an idealised junction diode shows that if the diode is reverse-biased by a few volts then the diode current will be very nearly equal to the saturation current I_s. This method would seem to be the most convenient way of determining I_s. In practice, however, the current does not reach a constant value as the reverse bias is increased. This effect is discussed in some detail in the literature (Reference(71), Chapter 4,) and is, in general, attributable to carrier generation in the space-charge region. The total current accounted for by generation in the space-charge layer is proportional to the rate of thermal generation of carriers, and to the colume of the space-charge layer. Consequently, this reverse current component has the same dependence on the reverse-bias voltage as does the width of the space-charge layer, and falls in the range $V^{\frac{1}{2}}$ for abrupt junctions to $V^{\frac{1}{3}}$ for graded junctions. It is pointed out in reference (71) that considerably better agreement between the measured characteristics and the idealised model may be obtained by deducing the saturation current I_s from the measured forward characteristics.

Table 6.1 shows a range of measured values of forward voltage and current for a typical silicon power diode (IN3880). Eqn. 4.19 for the idealised diode shows that it should be sufficient to determine the saturation current from one set of readings of forward voltage and current. However, Table 6.1. shows that

Measured current (Amp)	Measured voltage (volts)	Apparent value of I_s (Amps)
0.1	0.5886	$5.95.10^{-12}$
0.2	0.6219	$3.14.10^{-12}$
0.3	0.6390	$2.38.10^{-12}$
0.4	0.6525	$1.85.10^{-12}$
0.6	0.6681	$1.49.10^{-12}$
0.8	0.6765	$1.41.10^{-12}$
1.0	0.6820	$1.42.10^{-12}$
1.2	0.6898	$1.25.10^{-12}$
1.4	0.6940	$1.23.10^{-12}$
1.5	0.6992	$1.07.10^{-12}$

Table 6.1.

the apparent value of I_s (calculated from eqn. 4.19 for each set of values of forward current and voltage) decreases with increasing values of forward voltage and current. If the calculated value of the saturation current at 0.1A. is taken as reference than theoretical values of diode forward voltage may be calculated from eqn. 4.19. The results are shown in fig. 6.1 where it can be seen that the calculated diode voltages are lower than the measured values, and that the difference increases as the current increases. This effect could be accounted for by including a resistance in series with the idealised model of the diode. Reference (71) (Chapter 4) discusses various factors which contribute to the effect of an apparent series resistance.

The voltage drop across a diode with series resistance is obtained from eqn. 4.19 for the idealised diode.

$$V_D = I_D R_D + \frac{kT}{q} \log\left(1 + \frac{I}{I_s}\right) \qquad (6.1)$$

where R_D is the series resistance.
The measured values of voltage and current necessary to determine the diode paramters may be chosen such that $I_D \gg I_s$. The equation for the diode voltage can then be written as:

$$V_D \simeq I_D R_D + \frac{kT}{q} \log\left(\frac{I}{I_s}\right) \qquad (6.2)$$

Since small errors in the measured values of V_D and I_D could lead to large errors in the calculated values of the diode parameters, the minimum square error method is applied to the measured data to reduce the effect of random errors. A further advantage of doing this is that, although the model may not completely describe the diode characteristics, the minimum square error method

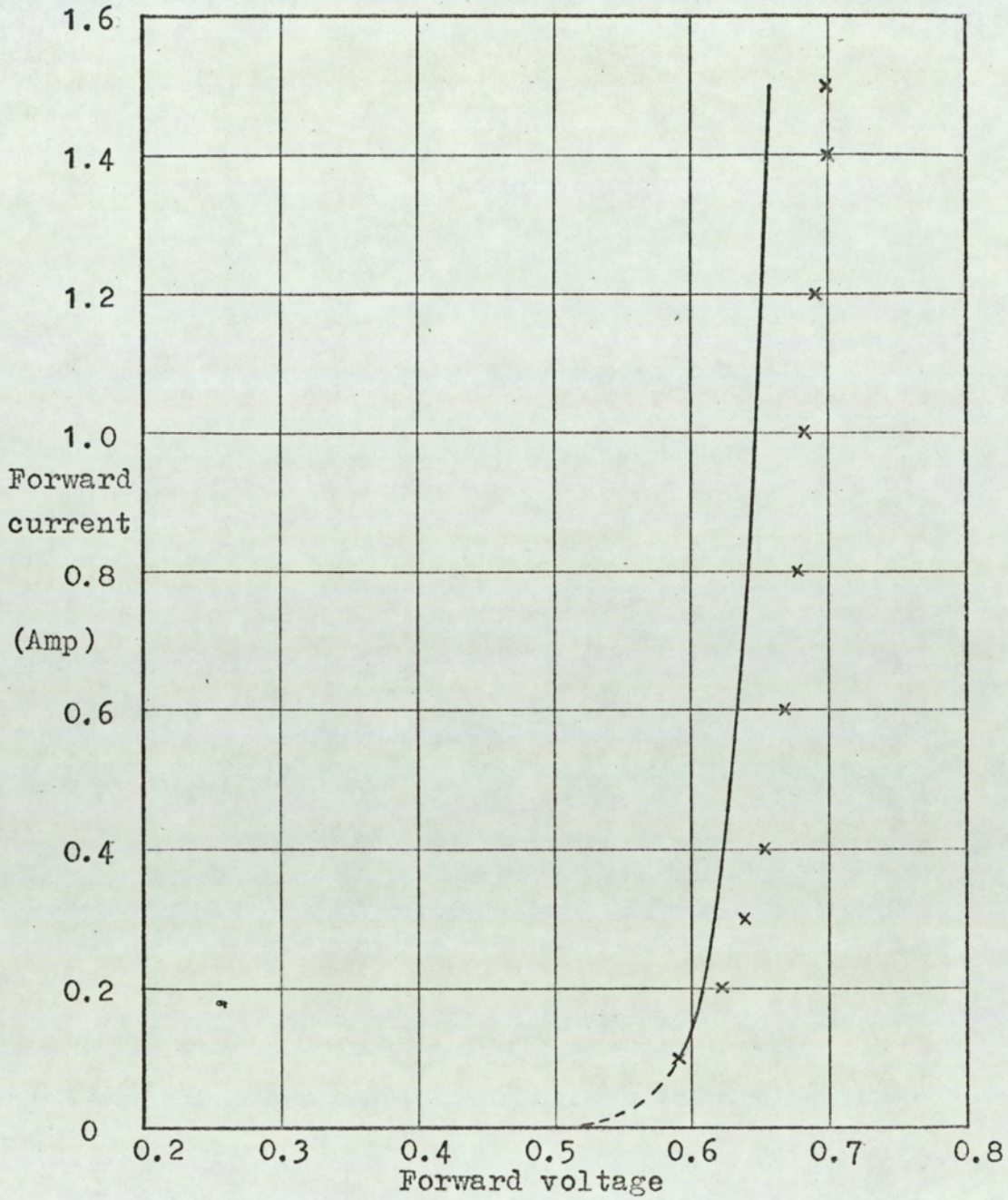

—=curve calculated from $I \simeq I_s \exp(\frac{qV}{kT})$ with I_s calculated from measured results at I = 0.1 A.

× = measured result

Fig.6.1. Characteristic for 1N3880 silicon diode (D3 in output stage).

will give the "best fit" values for the diode paramters. The theory for the method is given in Appendix 8. Since the expression for the base-emitter voltage of an idealised junction transistor (eqn. 4.17) is identical to eqn. 4.19 for the diode, a resistance R_E may be included in the emitter of the idealised transistor. Therefore; from eqn. 4.19, the base-emitter voltage of the transistor is:

$$V_{EB} = I_E R_E + \frac{kT}{q} \log\left(1 + \frac{I_E}{I_{ES}}\right) \qquad (6.3)$$

The minimum square error theory developed in Appendix 8 can be applied to the measured values of voltage and current for the transistor.

Figs. 6.2, 6.3 and 6.4 show the measured and theoretical characteristics of the NPN transistor and two of the diodes used in the tests on the output stage to be described later in the section. The results obtained by applying minimum square error theory to the model with a series resistance agree quite closely with the measured results. A range of characteristics could be obtained from the idealised diode diode model since the apparent value of the saturation current is a function of the forward current as was shown in Table 6.1. The curves (a) and (c) in figs. 6.2, 6.3 and 6.4 are obtained from the idealised diode model using values of I_S calculated from the measured results at 0.1A and 1.5A. These two values of current are the extremities of the measured range of voltage and current for the devices. It has been assumed in all the analytical work of this section that the device remains at ambient temperature irrespective of the power dissipated. This condition is not met in practice, and probably accounts for the difference between the results obtained from the model

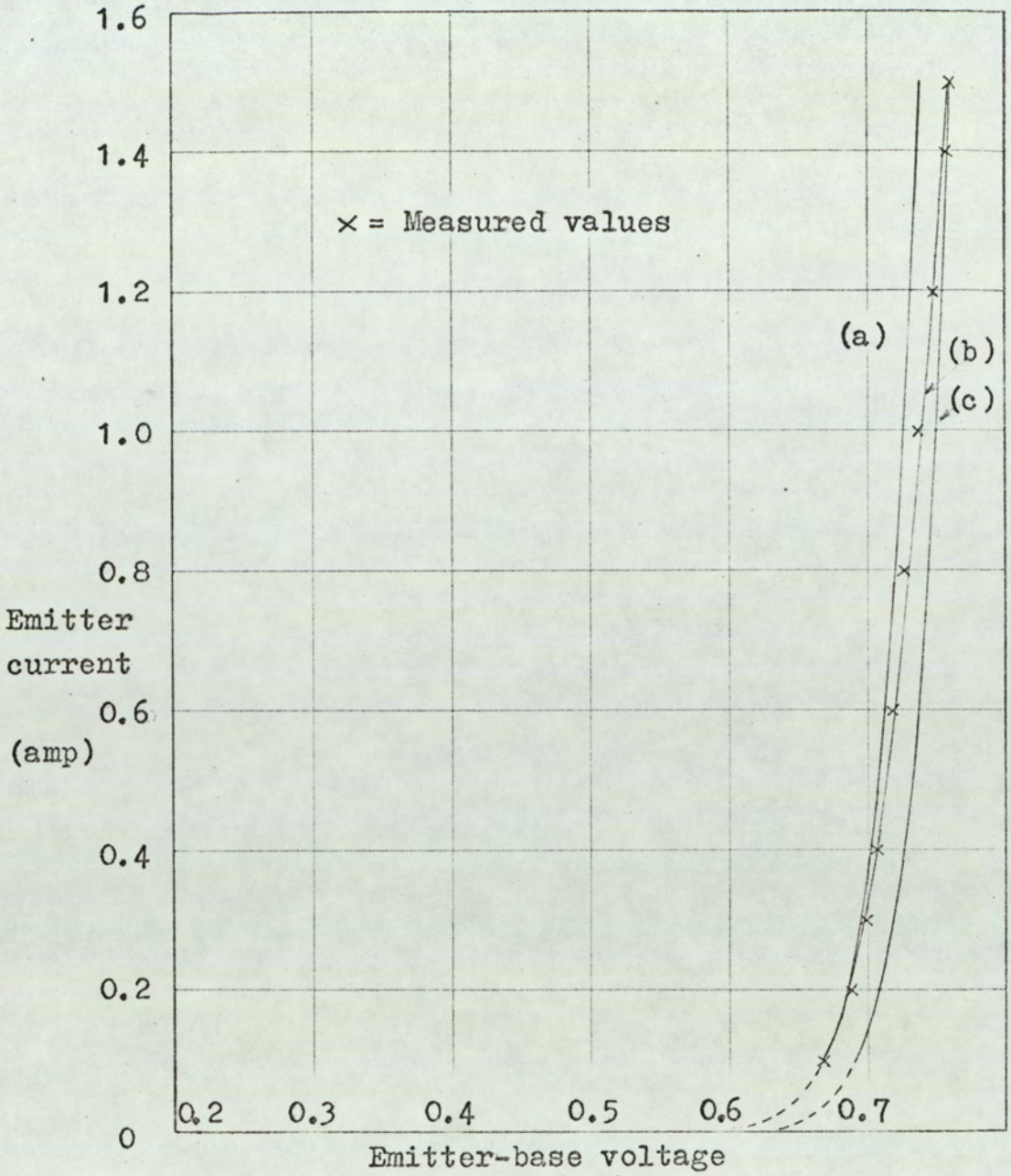

Curve(a) Calculated from $I_E \triangleq I_{ES} \exp(\frac{qV}{kT})$ with I_{ES} calculated from measured results at I_E=0.1 A.

Curve(b) Calculated from minimum square error theory, R_{VT1}=0.0153Ω, I_{ES1}=2.707.10^{-13} A.

Curve(c) Calculated from $I_E \triangleq I_{ES} \exp(\frac{qV}{kT})$ with I_{ES} calculated from measured results at I_E =1.5 A.

Fig.6.2. Input characteristic for CP406 silicon power transistor (VT1 in the output stage).

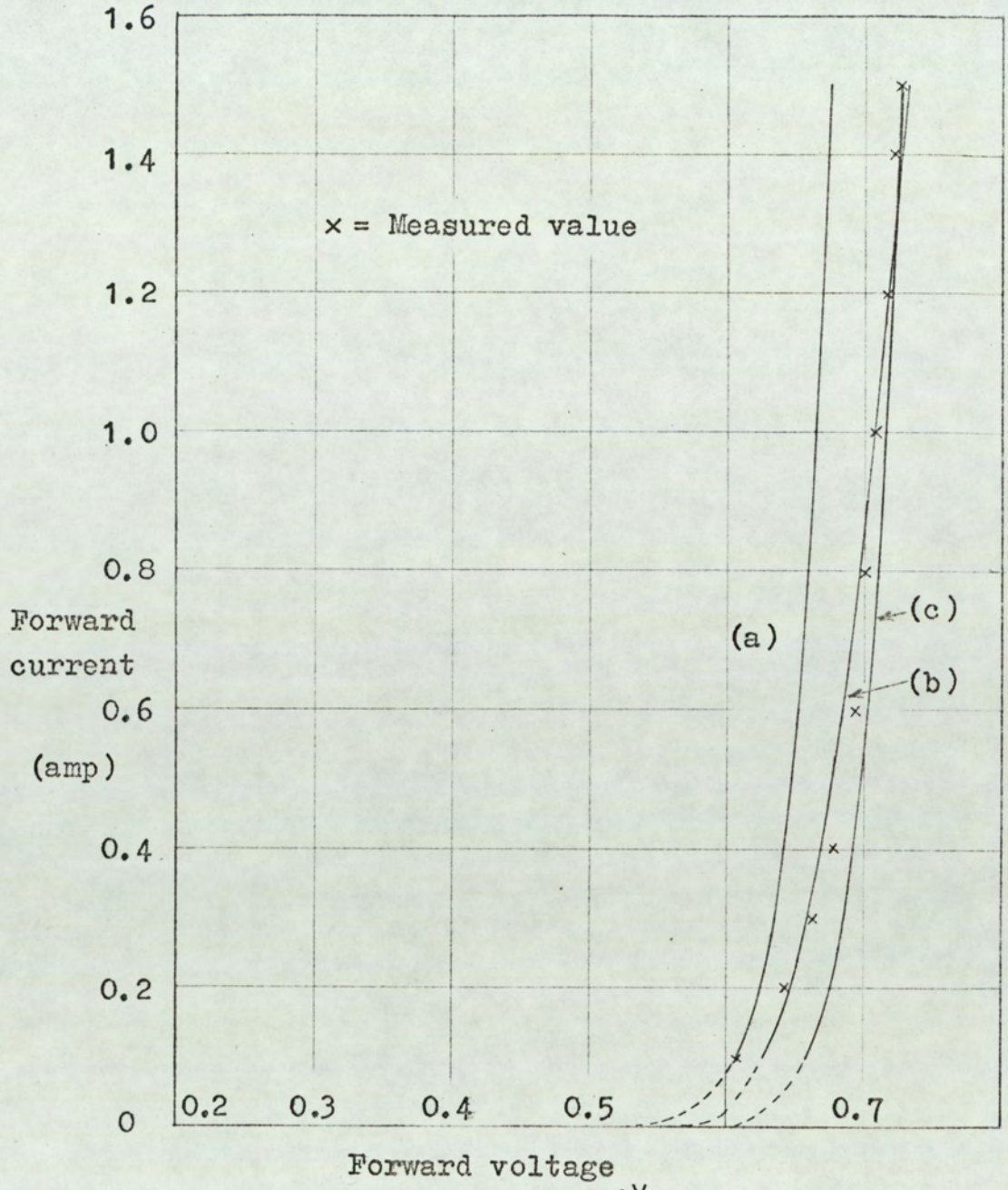

Curve(a) Calculated from $I \triangleq I_s \exp(\frac{qV}{kT})$ with I_s calculated from measured results at I =0.1 A.

Curve(b) Calculated from minimum square error theory, $R_{D1}=0.0263\Omega$, $I_{s1}=1.509.10^{-12}$ A.

Curve(c) Calculated from $I \triangleq I_s \exp(\frac{qV}{kT})$ with I_s calculated from measured results at I =1.5 A.

Fig.6.3. Characteristic of 1N3880 silicon diode (D1 in output stage).

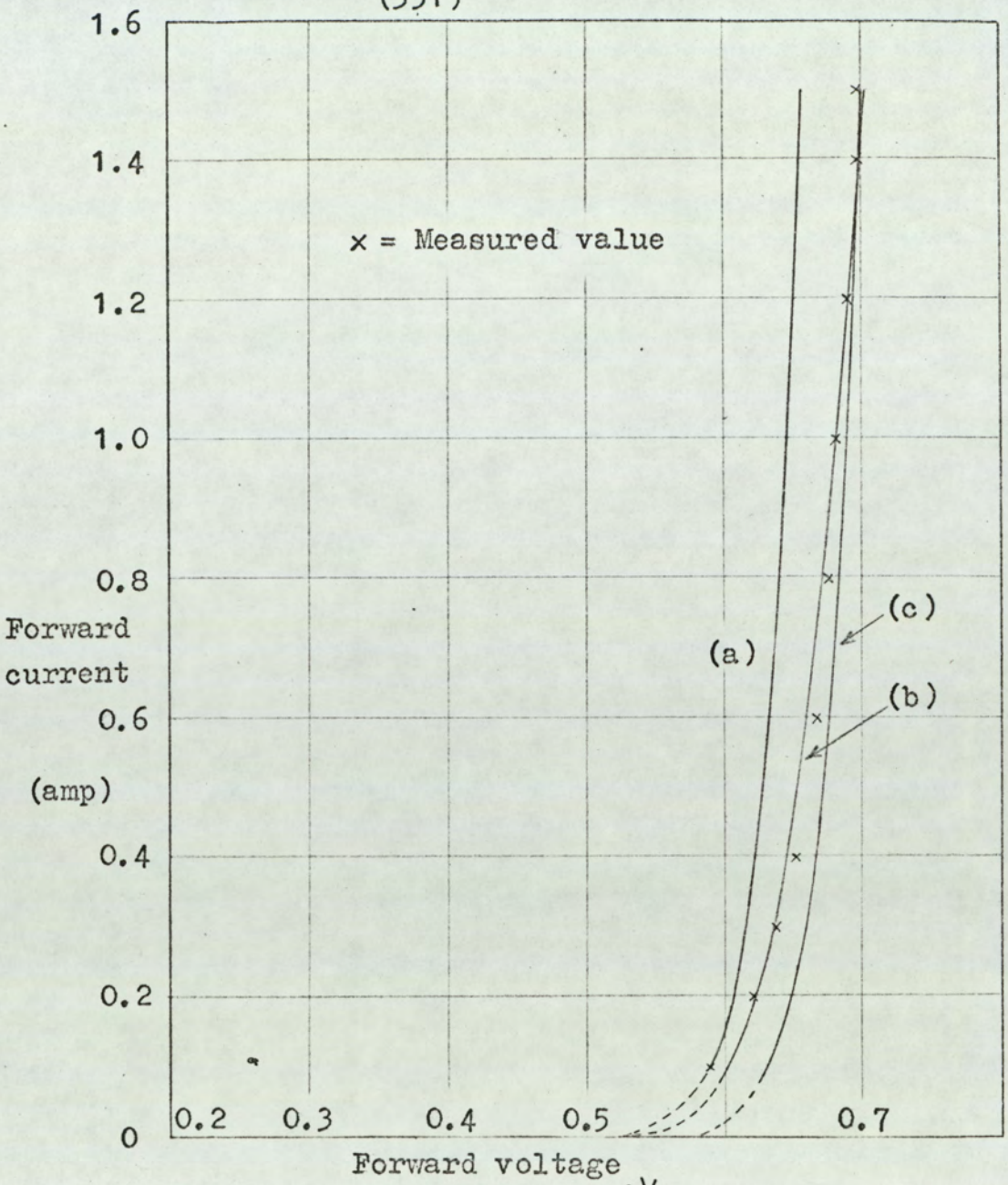

Curve(a) Calculated from $I \triangleq I_s \exp(\frac{qV}{kT})$ with I_s calculated from measured results at I =0.1 A.

Curve(b) Calculated from minimum square error theory, $R_{D3} = 0.0222\Omega$, $I_{S3} = 3.547.10^{-12}$ A.

Curve(c) Calculated from $I \triangleq I_s \exp(\frac{qV}{kT})$ with I_s calculated from measured results at I= 1.5A.

Fig.6.4. Characteristic for 1N3880 silicon diode (D3 in output stage).

and those obtained by measurement. This hypothesis is strengthened by the fact that the results for the power transistor are in better agreement than those obtained for the diodes which have a smaller surface area than the transistor. For a given power dissipation, the temperature of the transistor will be lower than that of the diodes since the transistor has a larger surface area.

6.2 Design of the output stage and low-pass filter

The type of filter used in the experimental work was the single-section maximally flat LCR filter shown in fig. 3.1.4. For ease of experimental measurement a fairly low value of pulse-repetition frequency was chosen (25 kHz). The filter was designed with a turnover-frequency ($\frac{\omega_o}{2\pi}$) of 5kHz. With these values of pulse repetition frequency and filter turnover-frequency the ratio ω_c/ω_o has the value 5.0, which, as discussed in section 3.1., is the smallest value likely to be used in a practical system. The value chosen for the load resistance R_L is 10 Ω as this enables reasonable power levels to be attained with values of supply voltage well within the capabilities of modern power transistors. The values of capacitance and inductance necessary for maximally-flat amplitude-response of the LCR filter are calculated from eqns. 3.1.13 and 3.1.15. The calculated values are as follows:

$L = 450\mu H$

$C = 2.25\mu F$

$R_L = 10\Omega$

$\omega_o = 5.0$ kHz.

In order to avoid problems resulting from the non-linearity of iron-cored coils at the frequency and current used in the tests, the inductor was wound on an air-cored former of the type shown in fig. 6.2.1. Expressions for the inductance of a multilayer coil, with a diameter much greater than the length, are given in the literature [72] and will not be repeated here. The coil former shown in fig. 6.2.1. is completely filled when wound with 68 turns of 15 s.w.g. enamelled copper wire. The measured inductance of a coil manufactured in accordance with fig. 6.2.1. was 452μH which compares favourably

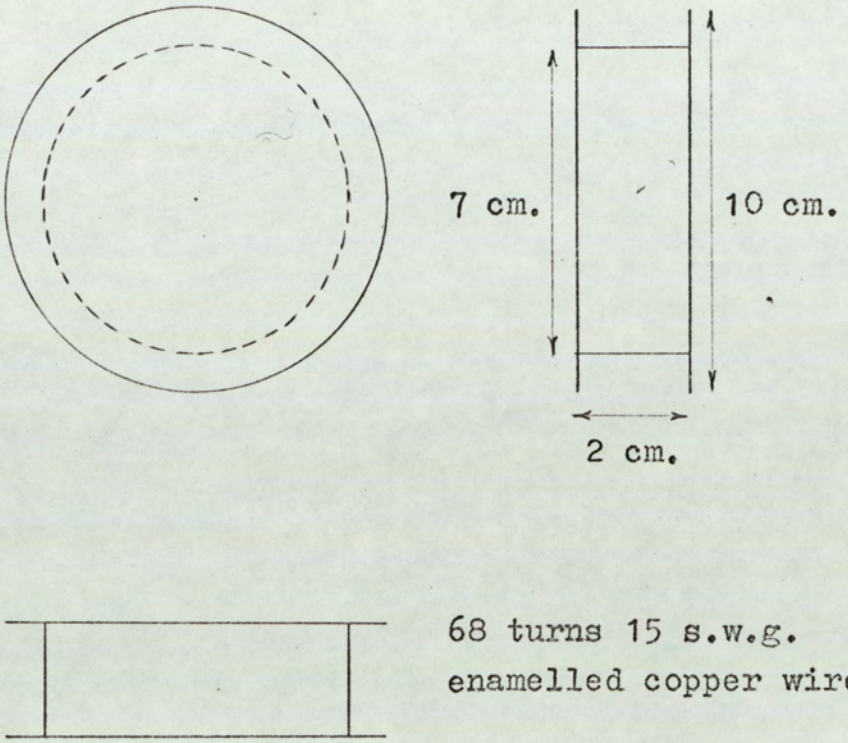

Fig.6.2.1. Coil former for filter inductance.

with the theoretical value of 450μH.

The circuit diagram of the output stage, driver stages and filter is shown in fig. 6.2.2. This circuit does not necessarily represent the optimum configuration for the driver stages since the design objective was simply to supply a waveform, having short rise and fall times and well defined voltage levels, to the bases of the output transistors. Circuit economy was not a design criterion. It is necessary to have two diodes in series with the emitter of the PNP germanium transistor (VT2) in order to ensure that it does not conduct during the wrong period (See section 4, eqns. 4.32 and 4.33).

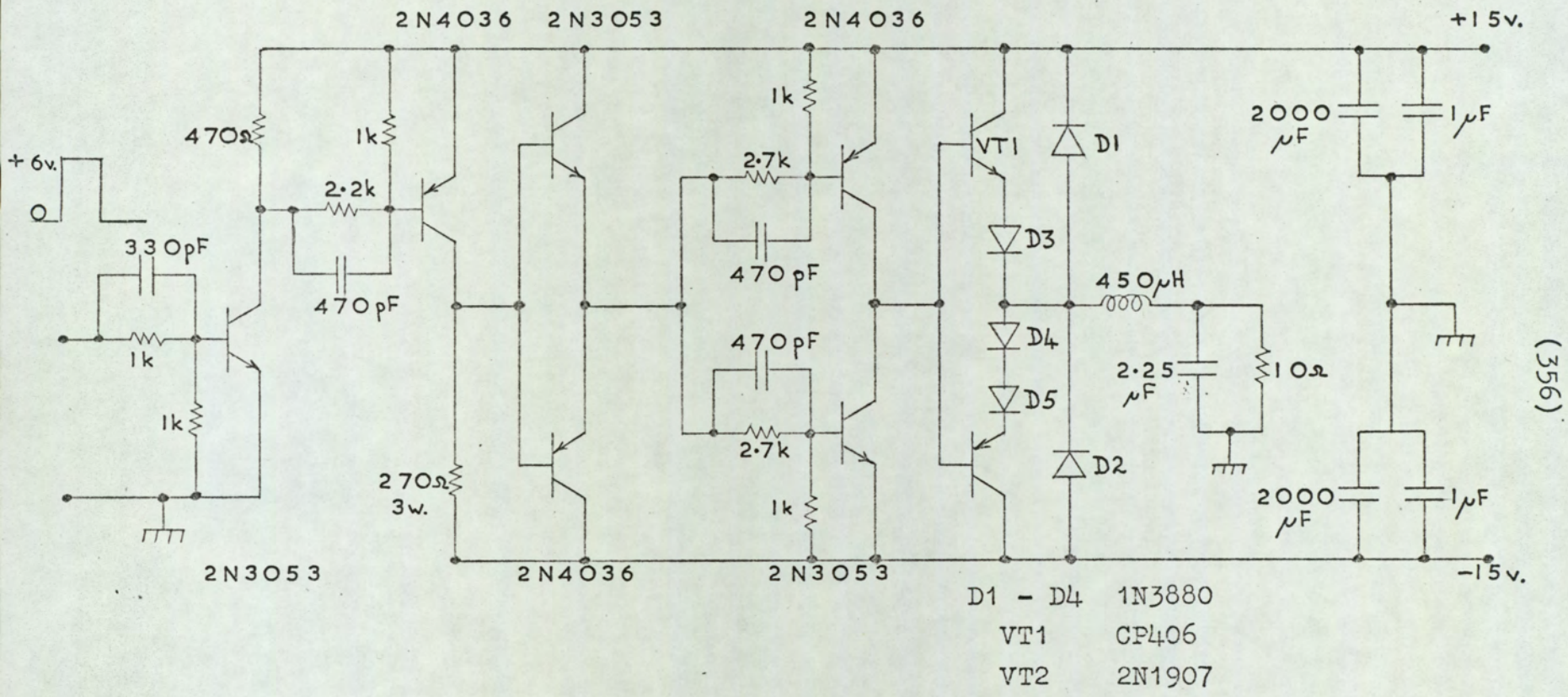

Fig.6.2.2. Circuit diagram of output stage, driver stages and low-pass filter.

6.3 Measurement of static power dissipation in the output stage

Ettinger[24] reviews a number of methods of measuring power dissipation in switching transistors, and concludes that two of the techniques are more suitable than the others. The first method is that of measuring the case temperature of the diodes and transistors under operating conditions. The case temperature of the device may be related to average power dissipation by producing a calibration curve of temperature against power dissipation under d.c. conditions. This method would seem to be capable of reasonable accuracy. However a number of drawbacks arise in practice. The maximum temperature rise in each of the output stage elements is of the order of 15°C to 30°C. In order to measure the power dissipation down to say, one tenth of the maximum value, it is necessary to measure temperature rises of the order of 1.5°C to 3°C. Thermocouples may be attached to the cases of the devices to measure the tem perature rise. However the output of a copper-constantan thermocouple is only 40 μV/°C which makes accurate temperature measurement rather difficult. Kendall, Dixon and Schutte[73] show that much greater sensitivity may be obtained from thermocouples manufactured from semiconductor materials. The germanium thermocouple described by the authors has a sensitivity (2mV/°C) of the order of 35 times that of chromel-constantan thermocouple. As far as is known, semi-conductor thermocouples were not commercially available at the time the work was carried out. Loeffler[74] compares thermocouples, resistance temperature detectors and thermistors. He concludes that thermistors are desirable where measurements are required over relatively short temperature ranges.

However many thermistors are glass encapsulated which makes the problem of obtaining good thermal contact with the diode or transistor more difficult than with thermocouples. A further problem is that the thermistor measures absolute temperature rather than the difference between the ambient temperature and the temperature of the device case. This means that the ambient temperature must be controlled to better than $0.1^{o}C$ if temperature rises of the order $1.5^{o}C$ are to be made with reasonable accuracy. Both thermocouples and thermistors were tested in practice but the results obtained at low power levels were not sufficiently reproducible to be of use.

The second method advocated by Ettinger[24] is to photograph the current and voltage waveforms associated with each device, and multiply ordinates to obtain graphs of instantaneous power. These graphs can then be integrated, by means of a planimeter, to obtain the average power dissipation over one cycle of the pulse repetition-frequency.

An extension of this method is described by Flood and Rayner[75]. The technique used by these authors is to obtain curves of instantaneous power by electronic multiplication of the instantaneous values of the voltage and current waveforms. They overcome the problem of multiplying large bandwidth signals in real-time by using a conventional analogue multiplier operating on the reconstituted signal outputs of a two-channel sampling oscilloscope. A number of practical problems were encountered when applying this technique to the output stage shown in fig. 6.2.2. The major problems were drift in the reconstituted oscilloscope outputs, and the difficulty of measuring the voltages across the series

diodes (D3, D4 and D_5) without intdroducing spurious "ringing" into the voltage and current waveforms. Since the expressions for the power dissipated in transistor VT1, with a modulation index of +M are identical to the expressions for the power dissipated in transistor VT2 with a modulation index of -M, it is only necessary to measure the dissipation in the elements of half the output stage. Figs. 6.3.1, 6.3.2 and 6.3.3. show the measured and theoretical values of power dissipation in transistor VT1, diode D1 and dode D3 respectively. The measured values were obtained by integrating the curves of instantaneous power obtained from oscillographs of the instantaneous voltage and current associated with each device. The theoretical curves were calculated from eqn.s 4.28, 4.29,4.30,4.34, 4.35 and 4.36 of section 4. The value of I, in the equations, was measured in circuit since the voltages dropped across the output stage elements are significant compared with the supply voltage, and error would be introduced by taking the value $I = V_1/R_L = 1{\cdot}5\,A$. The measured and theoretical results agree within the limits of experimental error. The major source of error in the experimental method is in taking readings of voltage and current from the oscillographs. This is particularly so when the current through a particular element is small, since a certain amount of "ringing" occured on the current waveform which makes accurate measurement difficult. This effect may be observed in figs. 6.3.4.(a) and (b) which are photographs of the filter input voltage and the currents flowing through the output stage elements for a range of values of modulation index M.

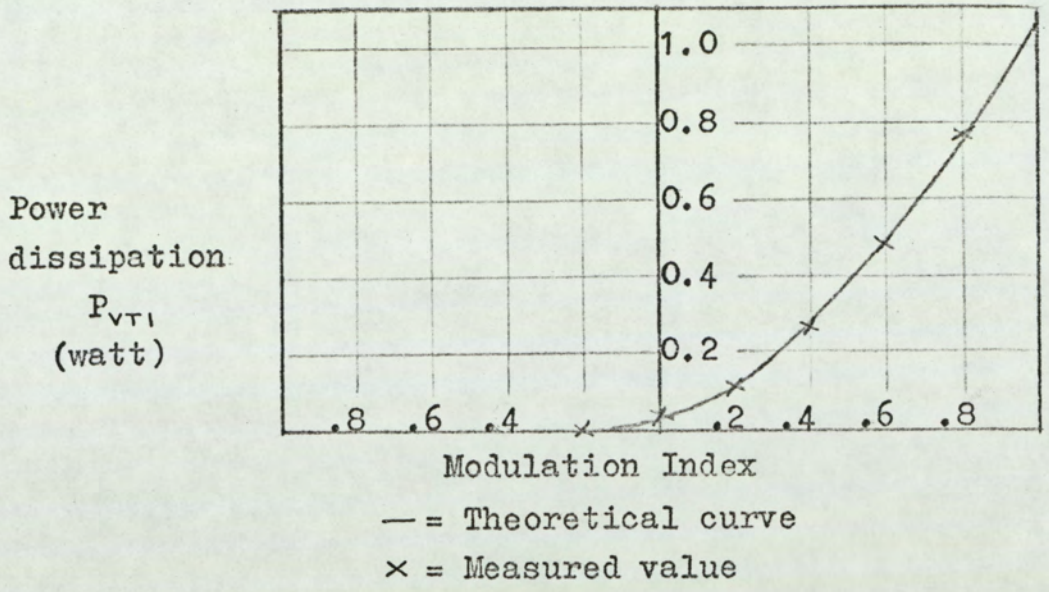

Fig.6.3.1. Static power dissipation in transistor VT1.

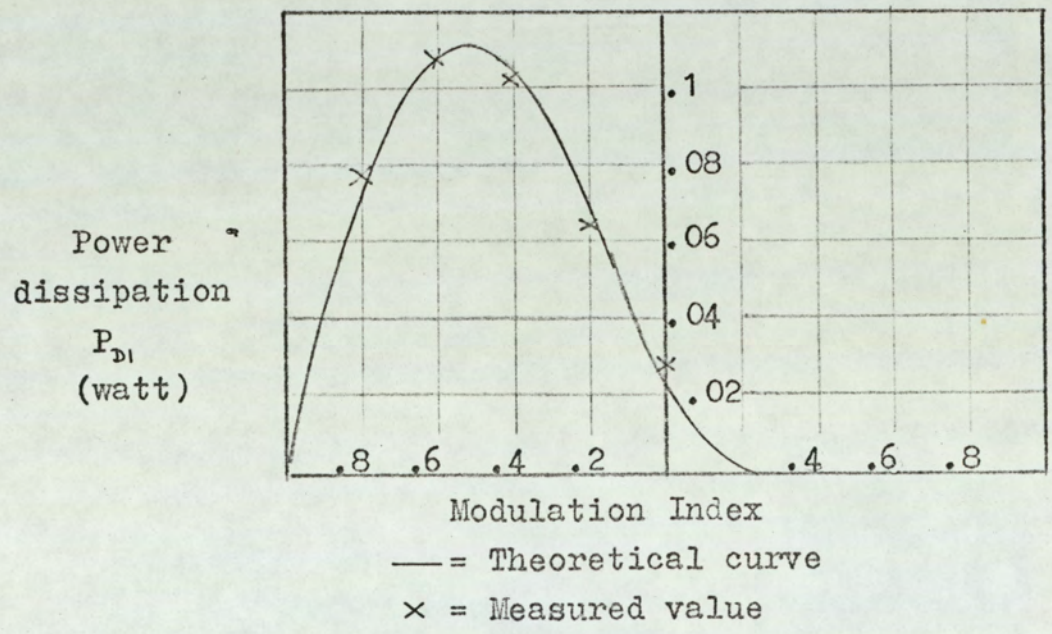

Fig.6.3.2. Static power dissipation in diode D1.

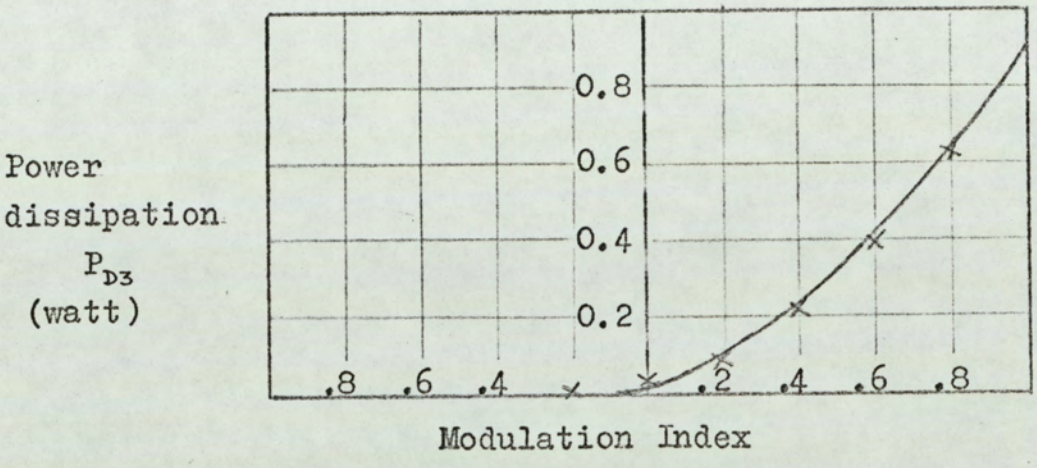

Fig.6.3.3. Static power dissipation in diode D3.

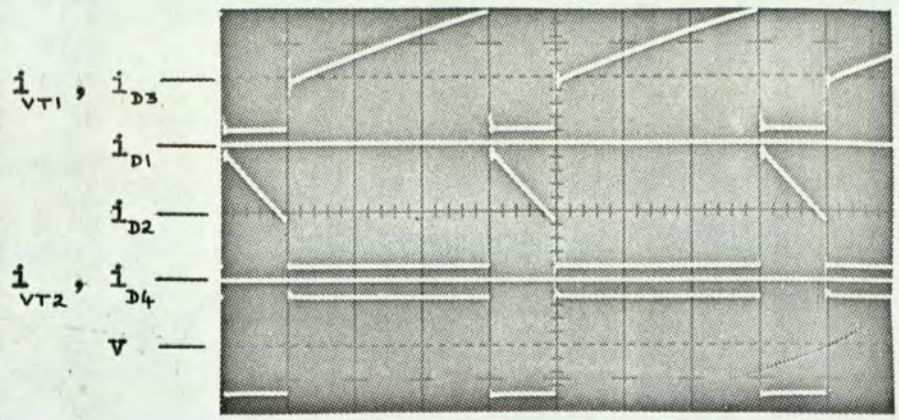

M = 0.5

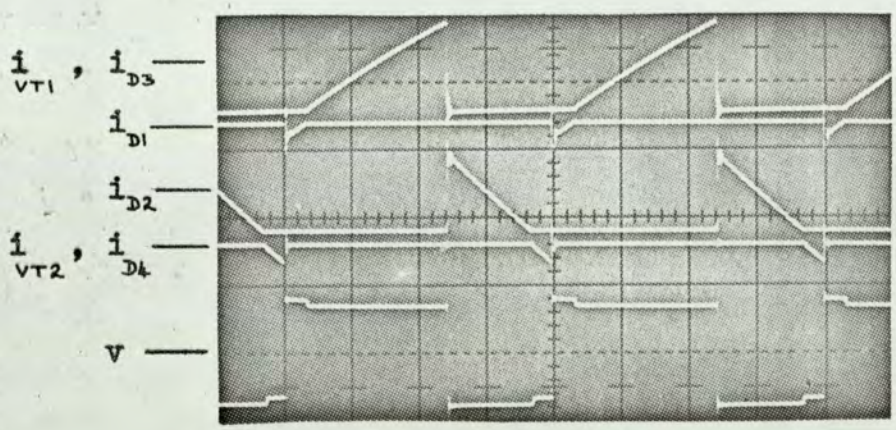

M = 0.2

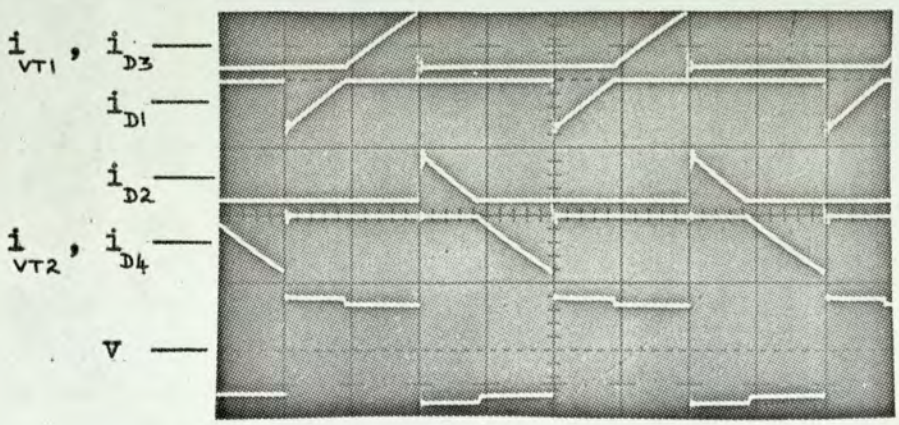

M = 0.0

v= 20v/ div. i= 0.5A/ div. t= 10 sec/div.

Fig.6.3.4(a). Output stage voltage and current waveforms

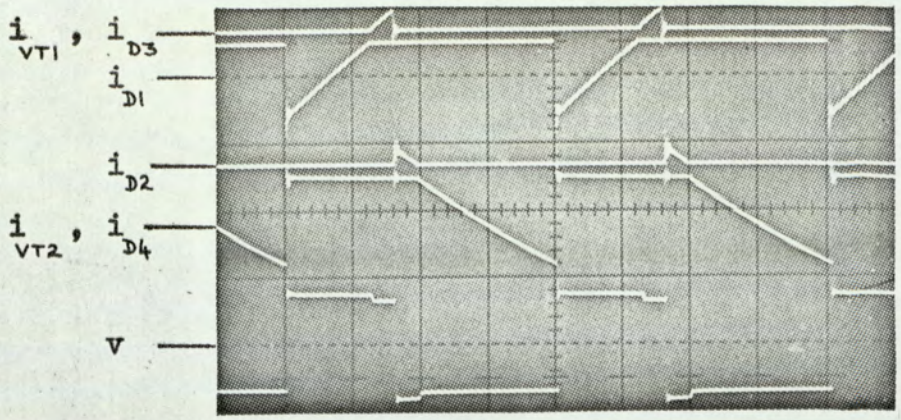

M = -0.2

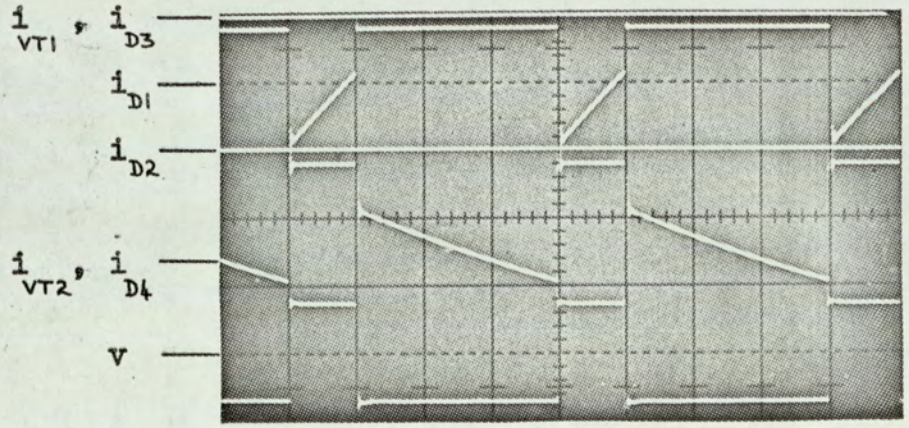

M =-0.5

v = 20 v/ div. i = 0.5 A/ div. t = 10 sec/div.

Fig.6.3.4(b). Output stage voltage and current waveforms.

6.4 Measurement of power dissipation in the output stage for sinusoidal modulation

In order to examine the power dissipation in the output stage under conditions of sinusoidal modulation, the output stage and drive unit, shown in fig. 6.2.2., were connected to the output of the pulse-length modulation system shown in Chapter III (fig. 6.1.1(a) (b) and (c)). The frequency of the square-wave generator was changed to 20kHz since this is the pulse-repetition frequency for which the output stage was designed.

The problem of measuring the average power dissipation in the ouput stage for sinusoidal modulation is much more severe than when using d.c. modulation. The method based on obtaining graphs of instantaneous power in the output stage elements is not practicable since the average power over one cycle of the modulation frequency is required. For this reason the technique used was that of measuring the case temperatures of the devices. The case temperatures are related to average power dissipation by means of calibration curves produced by dissipating known d.c. power levels in the elements. As discussed in section 6.3 this method is subject to rather large random errors due to the small temperature changes in the elements at low power levels. In order to minimise these errors thermocouples were bolted to the case of each element to obtain good thermal contact, and the complete output stage operated in a temperature-controlled enclosure. Fig. 6.4.1. shows the experimental results, measured at a modulation frequency of 100c/s, together with the theoretical curves calculated using the numerical integration procedure shown in figs. 5.2(a) and (b). Taking into account the difficulty of making

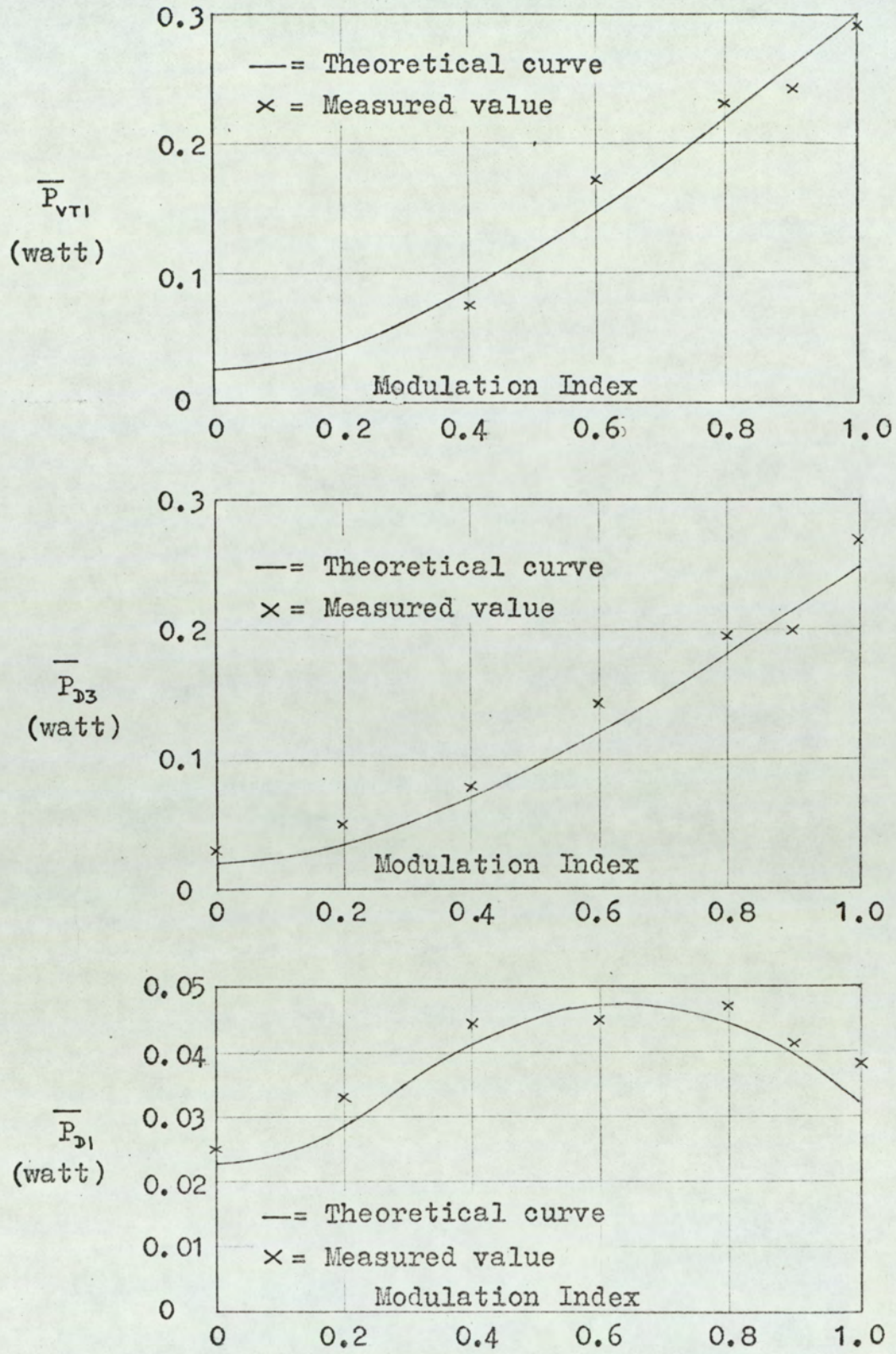

Fig.6.4.1. Average power dissipation in the output stage for sinusoidal modulation.

accurate measurements with the case temperature method, the agreement between the measured and theoretical results is reasonable.

7. Discussion of the analytical and experimental results for the output stage power dissipation

The power dissipation in a pulse-length modulation amplifier output stage has been analysed for both d.c. and sinusoidal modulation. The equations for the dissipation are expressed in terms of the characteristics of the output stage elements and the low-pass filter characteristics. It is shown ,for two particular types of filter, that the filter input current can be approximated by a triangular wave superimposed on a term directly proportional to the modulation index. It is also postulated that this approximation to the input current is valid for the majority of filters having a series input inductance. Introduction of the approximate expression for the filter input current considerably simplifies the evaluation of output stage dissipation. However, in spite of this simplification, the expressions for the power dissipation are still very complex, and contain too many independent variables to make presentation of generalised graphs of power dissipation practicable.

Results obtained from measurements on a practical system are compared with the analytical results and found to agree within the limits of experimental error. An interesting feature of the results is that the power dissipation in the shunt diodes is considerably less than that in the series diodes. (See figs. 6.3.1, 6.3.2., 6.3.3. and 6.4.1.). The reason for this is that when the shunt diode current is large, the period of conduction is short so that the average power dissipation is small (See figs. 6.3.1(a) and (b).).

With the system used in the experimental work, the peak value of the modulation frequency component appearing

across the load resistance is approximately equal to the supply voltage V, under conditions of full modulation. Therefore the system can deliver a maximum power output of $\left(\frac{15}{\sqrt{2}}\right)^2 \cdot \frac{1}{10}$ = 12.25 watts. From fig. 6.4.1. the total power loss in half of the output stage (i.e. VT1, D1 and D3) is 0.3+0.25+0.032 = 0.582 watts. If it is assumed that the power dissipation in the other half of the output stage is also 0.582 watts, then the output stage efficiency is 92% at full modulation. Greater efficiency can be obtained by increasing the supply voltage (V_1) and the load resistance (R_L) such that the peak current through the load (i.e. $I = V_1/R_L$) remains constant. Under these conditions the power dissipation in the output stage elements is unchanged but the available output power is increased. Therefore, in the design of a system, the supply voltage should be made as high as possible in order to reduce the load current and hence increase the efficiency.

CHAPTER IV

The Generation of Non-linear Functions by means of Pulse-length Modulation

1. General

In the analysis of error in practical pulse-length modulation systems (Chapter II) it is shown that the amplitude of the demodulated system output is proportional to some non-linear function of the modulating input when the sampling waveform is not a linear time function. The objective of this chapter is to examine the possibility of making use of this phenomenon to produce systems having a prescribed non-linear transfer function.

Very little work appears to have been published on the use of pulse-length modulation for this purpose. Schmid[76] describes a method for producing a system with a sine (or cosine) transfer function. The principle of operation is to use a length-modulated pulse to gate a sinusoidal input to an integrator. Thus the output of the integrator is:

$$\int_0^{t_1} \sin(\omega t).dt = \frac{-1}{\omega} \cos(\omega t_1) \qquad (1.1)$$

where t_1 is the length of the gating pulse.
If the pulse length t_1 is made directly proportional to the modulating input (V_{in}) then the integrator output is proportional to $\cos(\omega k V_{in})$. The system therefore has a cosine transfer function. A limited amount of analytical work is given in the paper, and a cursory examination is made of the problems introduced by time-varying system inputs. A later paper by Schmid[77] describes a more sophisticated version of the system. He also shows that any required transfer function can be achieved if a waveform can be generated having a time-function proportional to the derivative of the required transfer function. Klein and den Hertog[78] utilise pulse-length modulation with non-linear sampling waveforms to produce non-linear transfer

functions. They state that incorporation of a non-linear pulse-length modulator in the feedback loop of an operational amplifier gives rise to a system having a transfer function directly proportional to the time-function of the sampling waveform. The description of the operation of the system is based largely on intuitive reasoning rather than on mathematical analysis. However the method described by these authors appears to offer interesting possibilities, and the work to be described in the following sections is an attempt to establish a theoretical basis for the system.

2. Static analysis of pulse-length modulation systems with non-linear sampling waveforms

The basic pulse-length modulation system is shown in fig. 2.1. The output of the differential level-detector changes state whenever the instantaneous value of the sampling waveform $v_2(t)$ is equal to the modulating input voltage V_1. If the switching instants of the level-detector are denoted as t_1 and t_2 then:

$$V_1 = v_2(t_1) \qquad (2.1)$$

$$V_1 = v_2(t_2) \qquad (2.2)$$

Solution of the above equations for t_1 and t_2 will give expressions for the switching instants which involve the time inverse of the sampling waveform time function. This point is clarified if the sampling waveform $v_2(t)$ is defined by a specific function (e.g. $v_2(t) = V_2\sin(\omega_c t)$. Substituting $v_2(t) = V_2.\sin(\omega_c t)$ in eqns. 2.1 and 2.2, and solving for the switching instants, gives:

$$\frac{t_1}{T_c} = \frac{1}{2\pi}\sin^{-1}\left(\frac{V_1}{V_2}\right) \qquad (2.3)$$

$$\frac{t_2}{T_c} = \frac{1}{2\pi}\sin^{-1}\left(\frac{V_1}{V_2}\right) \qquad (2.4)$$

where:

$$T_c = \frac{2\pi}{\omega_c}$$

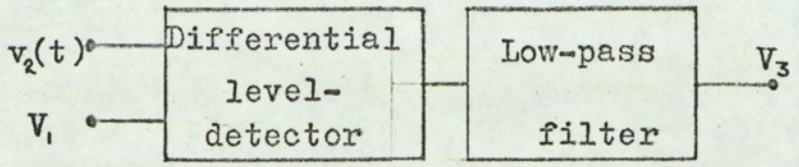

Fig.2.1. Basic pulse-length modulation system

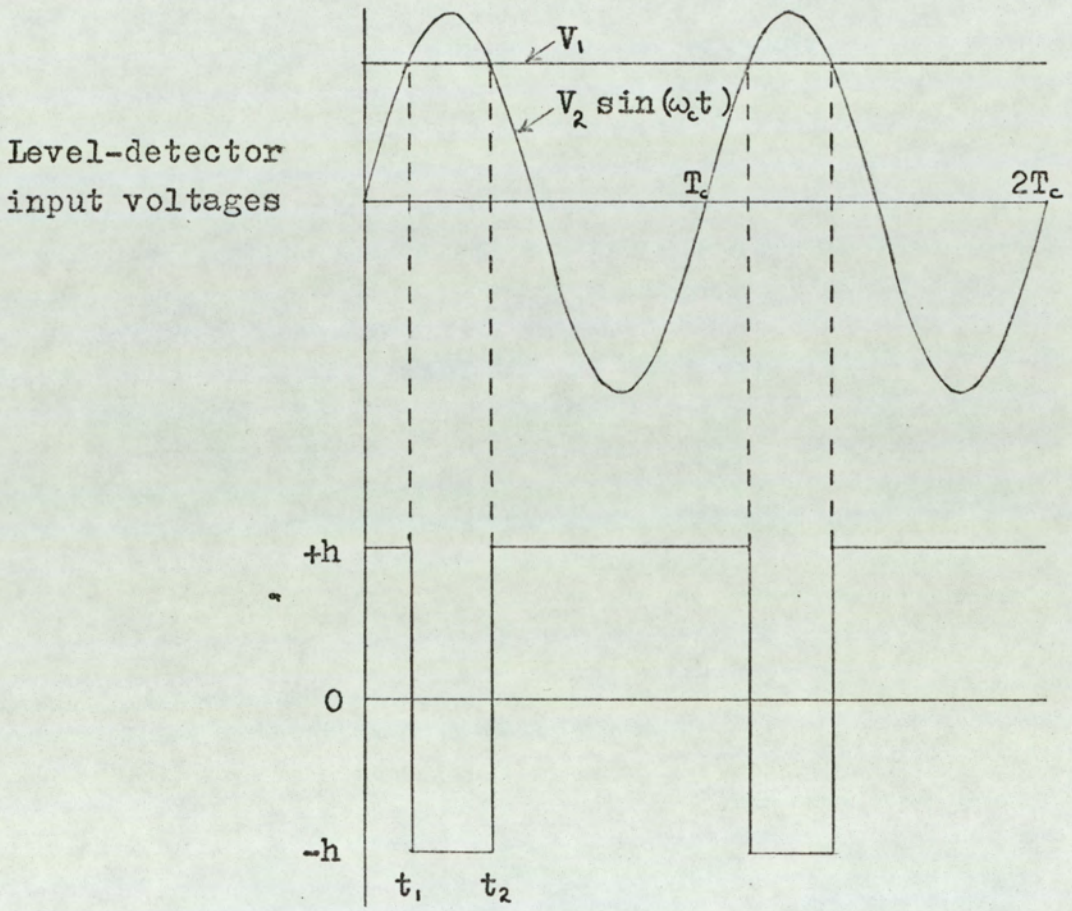

Fig.2.2. Waveforms for system with sinusoidal modulation.

The waveforms associated with the system are shown in fig. 2.2. As a result of the symmetry of the sinusoidal sampling waveform, the expression for t_2 may be rewritten as:

$$\frac{t_2}{T_c} = 0{\cdot}5 - \frac{t_1}{T_c} \qquad (2.5)$$

Passing the length-modulated waveform through the low-pass filter shown in fig. 2.1 is equivalent to taking the average value of the waveform. Therefore, from fig. 2.2:

$$V_3 = 2h\left[\frac{t_1}{T_c} - \frac{t_2}{T_c} + 0{\cdot}5\right] \qquad (2.6)$$

Substituting eqns. 2.3 and 2.5 in eqn. 2.6 gives the following expression for the demodulated output of a pulse-length modulation system with a sinusoidal sampling waveform:

$$V_3 = \frac{2h}{\pi} \sin^{-1}\left(\frac{V_1}{V_2}\right) \qquad (2.7)$$

Thus the system transfer function is proportional to the time inverse of the sampling waveform. Pulse-length modulation can therefore be used to produce a prescribed non-linear transfer function provided that a high frequency waveform can be generated which is the time inverse of the required transfer function. A further application is in generating very low frequency waveforms. If the system modulating input is a low-frequency triangular wave then, from eqn. 2.7, the system output is a $\sin^{-1}$ waveform having the same frequency as the triangular wave. Fig. 2.3 shows the waveforms of a system operating in this manner. In a practical system the ratio of the sampling waveform frequency to the modulating frequency would be much greater.

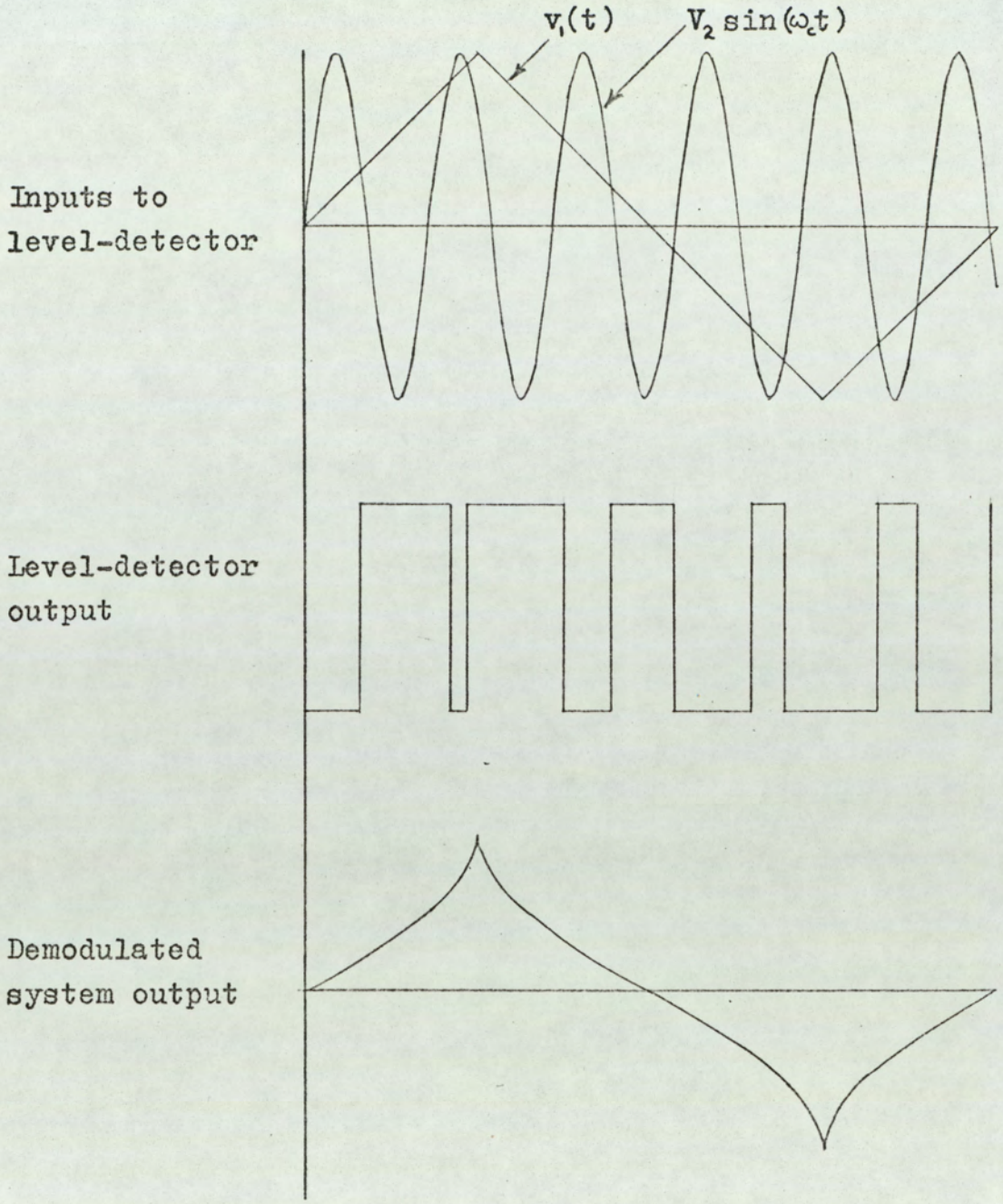

Fig.2.3. System waveforms for sinusoidal sampling waveform and triangular input waveform.

The pulse-length modulation technique for generating non-linear transfer functions would be more useful if the system transfer function could be made directly proportional to the sampling waveform time function rather than proportional to the time inverse of the waveform. This condition may be readily achieved by incorporating the modulation system in the feedback loop of a high gain operational amplifier as shown in fig. 2.4.

Let the transfer function of the pulse-length modulation section be:

$$V_3 = F(V_o) \qquad (2.8)$$

where $F(V_o)$ is a function of the overall system output V_o. Analysis of the system leads to the following expression relating the input voltage (V_{in}) and the output voltage (V_o).

$$V_{in} = -\frac{R_1}{R_2} F(V_o) - \frac{V_o}{\alpha}\left[1 + \frac{R_1}{R_2}\right] \qquad (2.9)$$

If the amplifier gain (α) is large then eqn. 2.9. reduces to:

$$V_{in} \doteq -\frac{R_1}{R_2} \cdot F(V_o) \qquad (2.10)$$

It was shown previously that the transfer function of the pulse-length modulation section is proportional to the time inverse of the sampling waveform $v_2(t)$. Now it can be seen that solving eqn. 2.10 for V_o involves inverting the function $F(V_o)$ which is itself proportional to the time inverse of $v_2(t)$. Therefore the complete system transfer function has the same form as the time function of the sampling waveform. This observation is

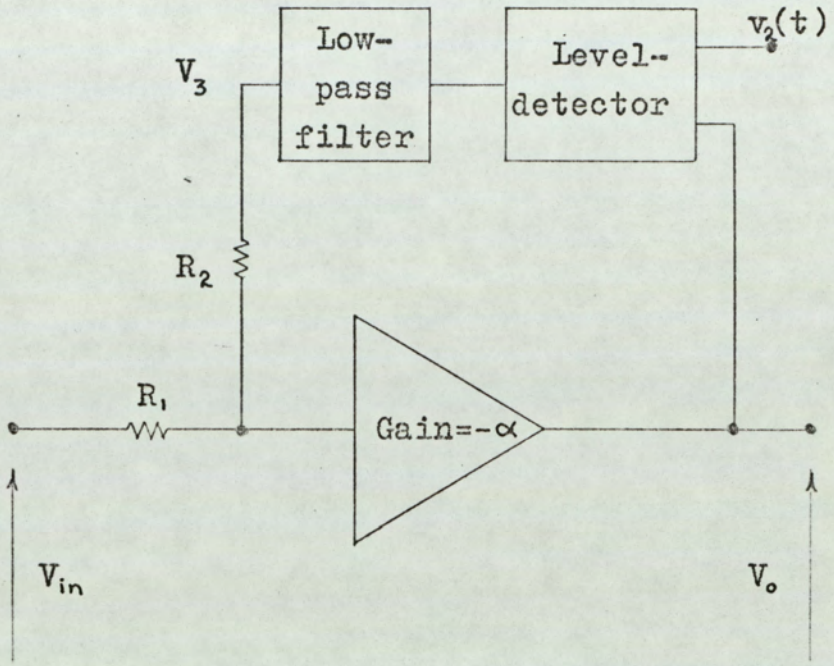

Fig.2.4. Non-linear amplifier utilising pulse-length modulation.

clarified by considering a particular function for the sampling waveform (eg. $v_2(t) = V_2 \sin(\omega_c t)$).

From eqn. 2.7, for the transfer function of a pulse-length modulation system with a sinusoidal sampling waveform, eqn. 2.8 may be written as:

$$F(V_o) = \frac{2h}{\pi} \sin^{-1}\left(\frac{V_4}{V_2}\right) \qquad (2.11)$$

Substituting eqn. 2.11 in eqn. 2.10 and solving for V_o, gives:

$$V_o = -V_2 \sin\left[V_{in} \frac{R_2}{R_1} \cdot \frac{\pi}{2h}\right] \qquad (2.12)$$

Thus the system transfer function has the same form as the time function of the sampling waveform. Fig. 2.5 shows the system output evaluated from eqn. 2.12 for a triangular wave input.

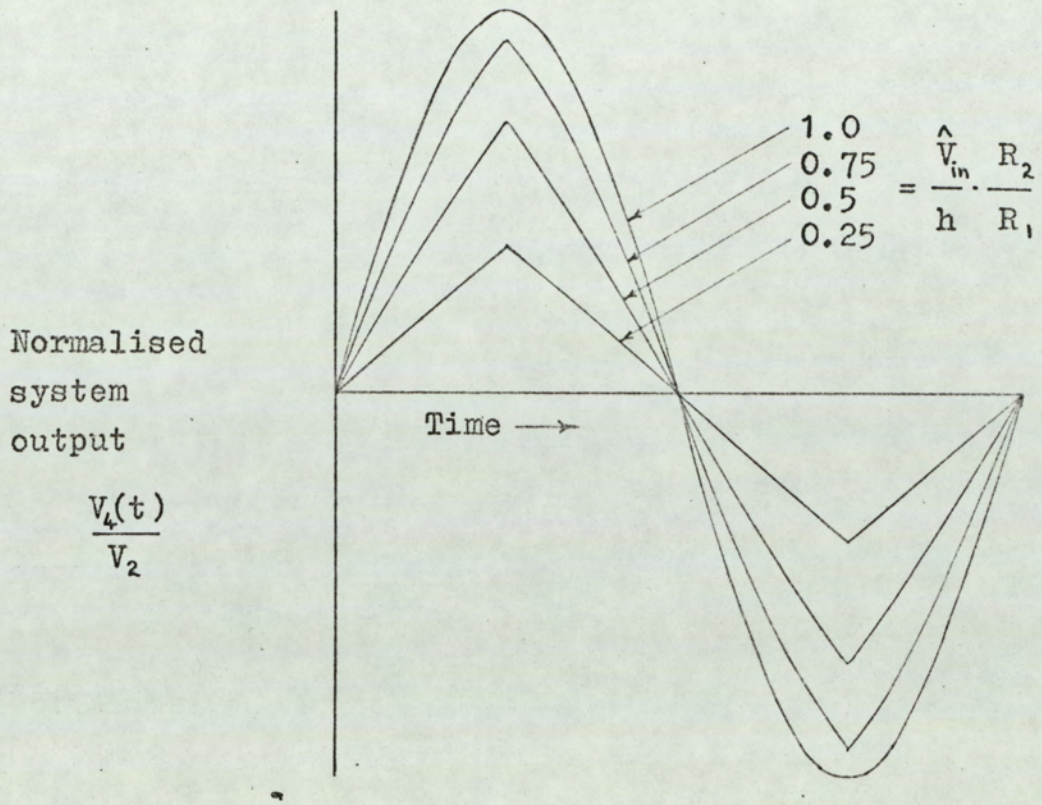

Fig.2.5. Output of system shown in fig.1.4. for a triangular wave input and a sinusoidal sampling waveform.

3. Spectrum analysis of a pulse-length modulation system with a non-linear sampling waveform.

The generalised spectrum analysis of non-linear pulse-length modulation developed in Chapter II could be used to evaluate the frequency spectrum for the output of the basic modulation system shown in fig. 2.1. However this analysis applies to sinusoidal modulating inputs only. Since the major application of these techniques is expected to be in low-frequency function generation, a spectrum analysis is required for triangular wave modulating inputs. Furthermore, for reasons discussed in section 2, the system with the pulse-length modulator in the feedback loop of an operational amplifier is likely to find greater application than the basic system. Therefore the spectrum analysis will be concentrated on the feedback system with a triangular wave modulating input.

Substituting eqn. 2.8 in eqn. 2.10 gives the following result:

$$V_{in} = -\frac{R_1}{R_2} \cdot V_3 \qquad (3.1)$$

Thus the demodulated output (V_3) of the pulse-length modulation section is directly proportional to the input V_{in}, and is independent of the particular sampling waveform being used. It is therefore possible to carry out a generalised spectrum analysis of the system when operating with a triangular wave input. The frequency spectrum of a pulse-length modulated wavetrain of 2N+1 pulses is given in Chapter II (Section 4.1, eqn. 4.1.1) and is rewritten below for convenience.

$$F(t)=\frac{1}{2\pi}\int_{-\infty}^{\infty}\frac{\sin\left(N+\frac{1}{2}\right)\omega T_c}{\sin\left(\frac{\omega T_c}{2}\right)}\;\frac{1}{j\omega}\left\{\exp\left(j\omega\left[t+\frac{T_o}{2}+t_{dl}\right]\right)-\exp\left(j\omega\left[t-\frac{T_o}{2}-t_{dt}\right]\right)\right\}d\omega \qquad (3.2)$$

where: T_c is the period of the pulse-repetition frequency ω_c

T_o is the unmodulated pulse-length

t_{dl} and t_{dt} are the time deviations of the leading and trailing pulse edges respectively.

In order to evaluate the frequency spectrum from eqn. 3.2. it is necessary to develop expressions for the time deviations of the pulse edges.

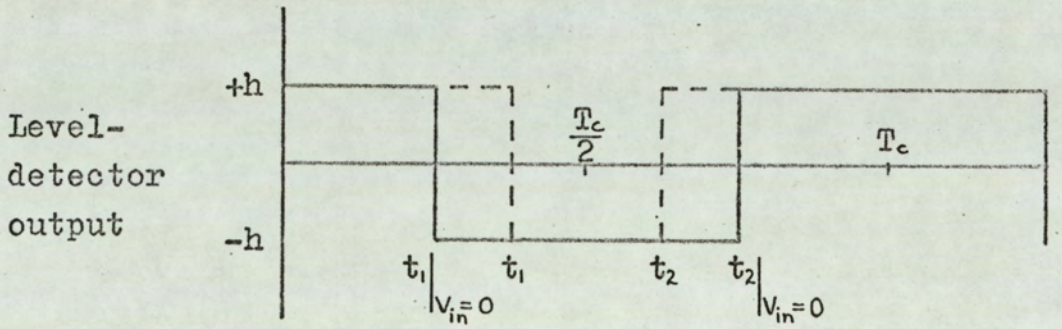

Fig. 3.1.

From fig. 3.1. the time deviations may be expressed as:

$$t_{dl}=t_2\big|_{V_{in}=0}-t_2 \qquad (3.3)$$

$$t_{dt}=t_1-t_1\big|_{V_{in}=0} \qquad (3.4)$$

If the sampling waveform is symmetrical about its peak value (e.g. a sine wave) then:

$$t_2 = T_c - t_1 \qquad (3.5)$$

Fig. 3.1. shows that the unmodulated pulse-length T_o is given by:

$$T_o = T_c - \left[t_2\Big|_{V_{in}=0} - t_1\Big|_{V_{in}=0} \right] \qquad (3.6)$$

Now if the average value of the output of the pulse-length modulation section is to be zero when the modulating input V_{in} is zero then, from fig. 3.1:

$$T_o = \frac{T_c}{2} \qquad (3.7)$$

Substituting eqns. 3.5 and 3.7 in eqn. 3.6 gives the following expressions for the unmodulated positions of the pulse-edges:

$$t_1\Big|_{V_{in}=0} = \frac{T_c}{4} \qquad (3.8)$$

$$t_2\Big|_{V_{in}=0} = 3\,\frac{T_c}{4} \qquad (3.9)$$

Substituting eqns. 3.5., 3.8 and 3.9 in eqns. 3.3. and 3.4 gives:

$$\frac{t_{dl}}{T_c} = \frac{1}{4} - \frac{t_2}{T_c} \qquad (3.10)$$

$$\frac{t_{dt}}{T_c} = \frac{1}{4} - \frac{t_1}{T_c} \qquad (3.11)$$

Now the demodulated output (V_3) of the pulse-length modulation section is equal to the average value of the modulated waveform. Therefore, from fig. 3.1

$$V_3 = 2h\left[\frac{t_1}{T_c} - \frac{t_2}{T_c} + 0{\cdot}5\right] \qquad (3.12)$$

Furthermore, eqn. 3.1. shows that V_3 is directly proportional to the modulating input V_{in}. Thus:

$$-\frac{R_2}{R_1} V_{in} = 2h\left[\frac{t_1}{T_c} - \frac{t_2}{T_c} + 0{\cdot}5\right] \qquad (3.13)$$

Substituting eqn. 3.5. in eqn. 3.13, and solving for $\frac{t_1}{T_c}$ gives:

$$\frac{t_1}{T_c} = -\frac{V_{in}}{4h} \cdot \frac{R_2}{R_1} + \frac{1}{4} \qquad (3.14)$$

Substituting eqn. 3.14 in eqns. 3.10 and 3.11 for the time deviations of the pulse-edges gives:

$$\frac{t_{dt}}{T_c} = \frac{t_{dl}}{T_c} = \frac{V_{in}}{4h} \cdot \frac{R_2}{R_1} \qquad (3.15)$$

Since the maximum time deviation of each pulse-edge is $\pm\frac{T_c}{4}$, the peak value ($\hat{V}_{in}$) of the modulating input is:

$$\hat{V}_{in} = h\,\frac{R_1}{R_2} \qquad (3.16)$$

If the modulating input voltage V_{in} is a triangular wave, as shown in fig. 3.2., then eqn. 3.14 becomes:

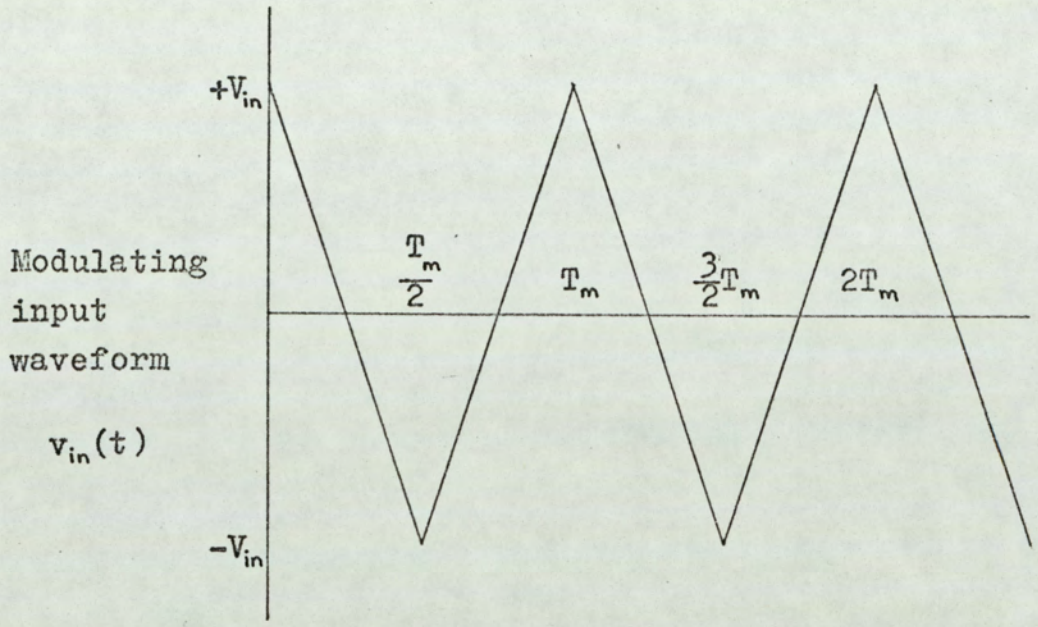

$$v_{in}(t) = V_{in}\left(1-4\,\frac{t}{T_m}\right) \quad \text{for} \quad 0 < t < \frac{T_m}{2}$$

$$v_{in}(t) = V_{in}\left(-3+4\,\frac{t}{T_m}\right) \quad \text{for} \quad \frac{T_m}{2} < t < T_m$$

Fig.3.2. Triangular modulating input waveform.

$$\frac{t_{dl}}{T_c} = \frac{t_{dt}}{T_c} = \frac{M}{4}\left[1 - 4\frac{t}{T_m}\right] \qquad (3.16)$$

for $0 \leqslant t \leqslant \frac{T_m}{2}$

$$\frac{t_{dl}}{T_c} = \frac{t_{dt}}{T_c} = \frac{M}{4}\left[-3 + 4\frac{t}{T_m}\right] \qquad (3.17)$$

for $\frac{T_m}{2} \leqslant t \leqslant T_m$

where $M = V_{in}/\hat{V}_{in}$ is the modulation index.

It is now possible to evaluate the frequency spectrum for the output of the pulse-length modulation section by substituting eqns. 3.7, 3.16 and 3.17 in eqn. 3.2. and then allowing N to tend to infinity. The limit of eqn. 3.2. as N approaches infinity will not be derived here since the limiting process for similar equations is covered in detail in the literature[49,56]. Using the methods of references (49,56), eqn. 3.2. becomes:

$$F(t) = \frac{1}{2\pi j}\sum_{n=-\infty}^{\infty}\frac{1}{n}\left\{\exp\left[jn\omega_c\left(t + \frac{T_c}{4} + t_{dt}\right)\right] - \exp\left[jn\omega_c\left(t - \frac{T_c}{4} - t_{dt}\right)\right]\right\} \qquad (3.18)$$

where t_{dt} and t_{dl} are given by eqns. 3.16 and 3.17. The rearrangement of eqn. 3.18 into a useful form is carried out in Appendix 9., and only the result is given here.

$$F(t) = 4h\frac{t_{dl}}{T_c} -$$

$$2h\sum_{n=1}^{\infty}\frac{4}{(n\pi)^2 M}\sin\left(\frac{n\pi}{2}\right)\sin\left(\frac{n\pi}{2}M\right)\cos(n\omega_c t) +$$

$$2h\sum_{n=1}^{\infty}\sum_{p=\pm1}^{\pm\infty}\frac{2}{(n\pi)^2 M\left(\frac{p}{nM}\right)^2-1}\left\{\left[1-\cos(p\pi)\right]\cos\left(\frac{n\pi}{2}\right)\cos\left(\frac{n\pi}{2}M\right)-\right.$$

$$\left.\left[1+\cos(p\pi)\right]\sin\left(\frac{n\pi}{2}\right)\sin\left(\frac{n\pi}{2}M\right)\right\}\cos(n\omega_c+p\omega_m)t \qquad (3.19)$$

where t_{dl}/T_c is given by eqns. 3.16 and 3.17.
The spectrum given by eqn. 3.19 consists of an undistorted triangular wave component ($4h\,t_{dl}/T_c$), and terms at all odd harmonics ($n\omega_c$) of the pulse repetition frequency. Sideband components ($n\omega_c \pm p\omega_m$) exist for all values of the integer n. However these sidebands are not present for all values of the integer p. The sidebands of most interest are the lower order sidebands of the pulse repetition frequency (i.e. n=1) since some of these fall within the system pass-band and cause distortion. For n=1, sidebands exist for only even values of p. Evaluation of the sideband amplitude for the special case $\left[(p/nM)^2-1\right]=0$ must be carried out by applying L'Hopital's rule to eqn. 3.19 However, this condition does not occur when considering sidebands of only the repetition frequency, so the

expression for the amplitude will not be derived. Fig. 3.3. shows the amplitudes of the sideband components as a function of the modulation index M. When making use of this diagram it should be remembered that ω_m is only the fundamental frequency of the triangular input waveform, and the system bandwidth must be sufficient to pass the triangular wave without significant distortion. If the specification is made that the sideband distortion must be less than -60dB, then fig. 3.3. shows that the frequency of the sideband ($\omega_c - 20\omega_m$) must be greater than the highest harmonic required for the triangular wave. Assuming that harmonics up to $10\omega_m$ will adequately represent the triangular wave, the following relationship is obtained:

$$\omega_c - 20\omega_m \geqslant 10\omega_m$$

Therefore:

$$\omega_c \geqslant 30\omega_m \qquad (3.20)$$

Thus, a practical function generation system based on the schematic circuit shown in fig. 2.4, can now be designed.

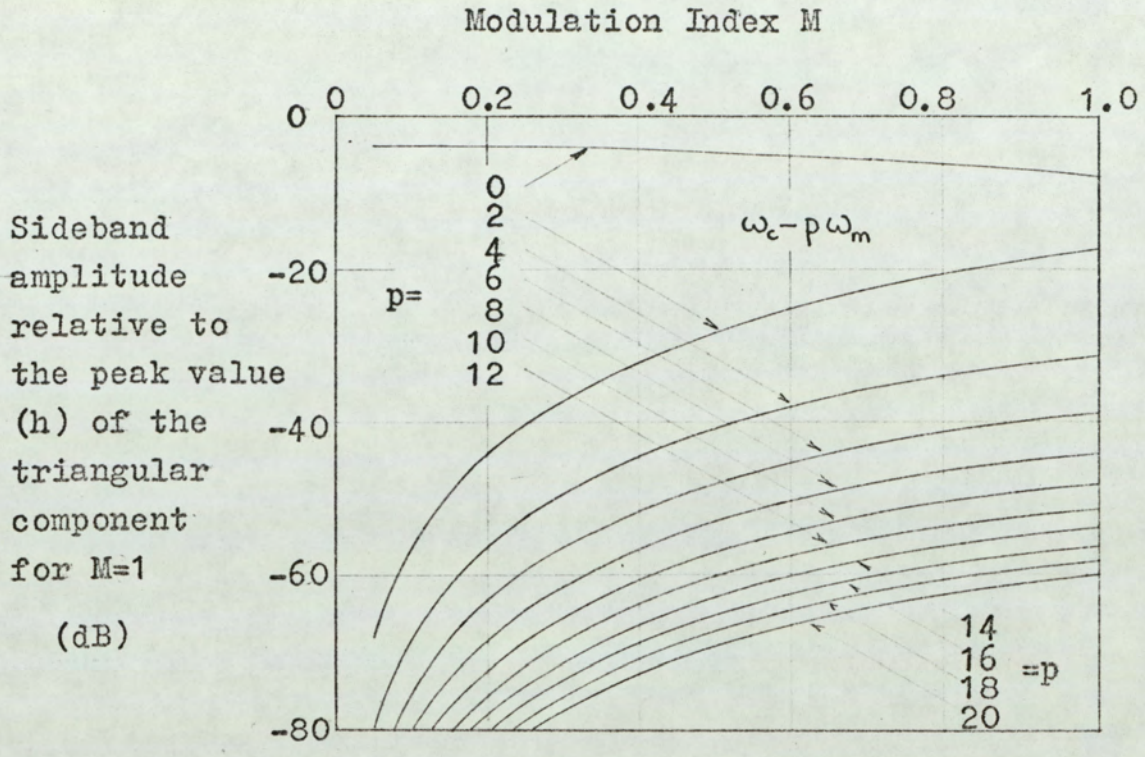

Fig.3.3. Sideband amplitude for triangular wave modulation.

4. Experimental work

The experimental verification of the analytical work of the previous sections is divided into two parts. The first part is measurement of the frequency spectrum for a pulse-length modulation system with triangular wave modulation. The second part is a brief examination of the performance of a practical system based on the schematic circuit shown in fig. 2.4.

The circuit shown in fig. 4.1. was used to produce a pulse-length modulated wavetrain with triangular modulation. Since the sampling waveform is triangular, the time deviations of the pulse edges are directly proportional to the amplitude of the modulating waveform. Thus triangular modulation is achieved by using a triangular modulating waveform. This method of achieving the required modulation was chosen in order to ensure that the measured results were due to the modulation process rather than spurious effects introduced by the practical realisation of the function generator system shown in fig. 2.4. Very close agreement is obtained between the measured and theoretical results as may be seen from fig. 4.2 where the measured values of the sideband amplitudes are plotted for a range of values of modulation index M. The theoretical curves in the diagram are calculated from eqn. 3.19.

Fig. 4.3 shows a complete function generator system based on the schematic circuit of fig. 2.4. Low-pass filtering of the pulse-length modulated wavetrain is performed by the networks R_1C_1 and R_2C_2. The amplifier at the output of the R_1C_1 network is an operational amplifier with unity series feedback to achieve a high input impedance. The purpose of this amplifier is to prevent

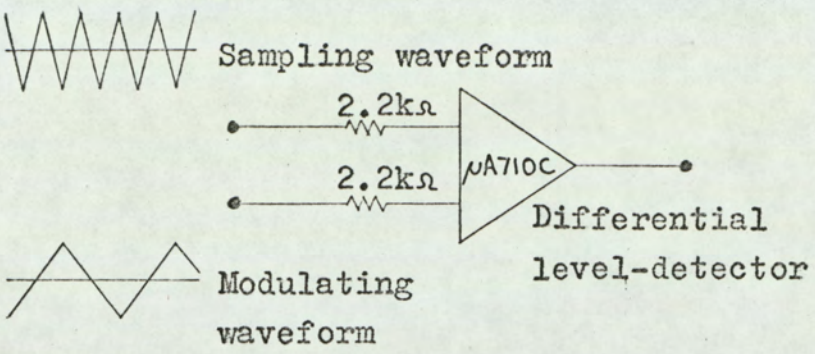

Fig.4.1. Circuit for producing a length-modulated wavetrain with a triangular modulating waveform.

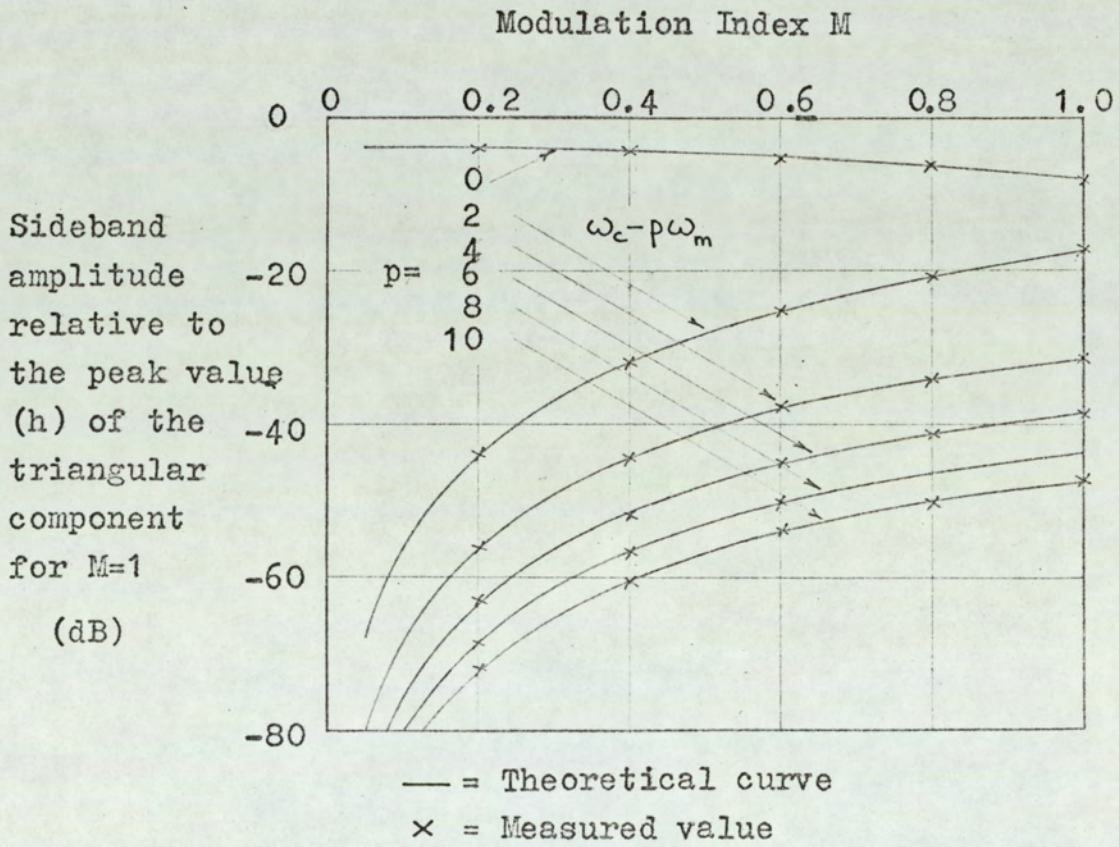

Fig.4.2. Sideband amplitude for triangular wave modulation.

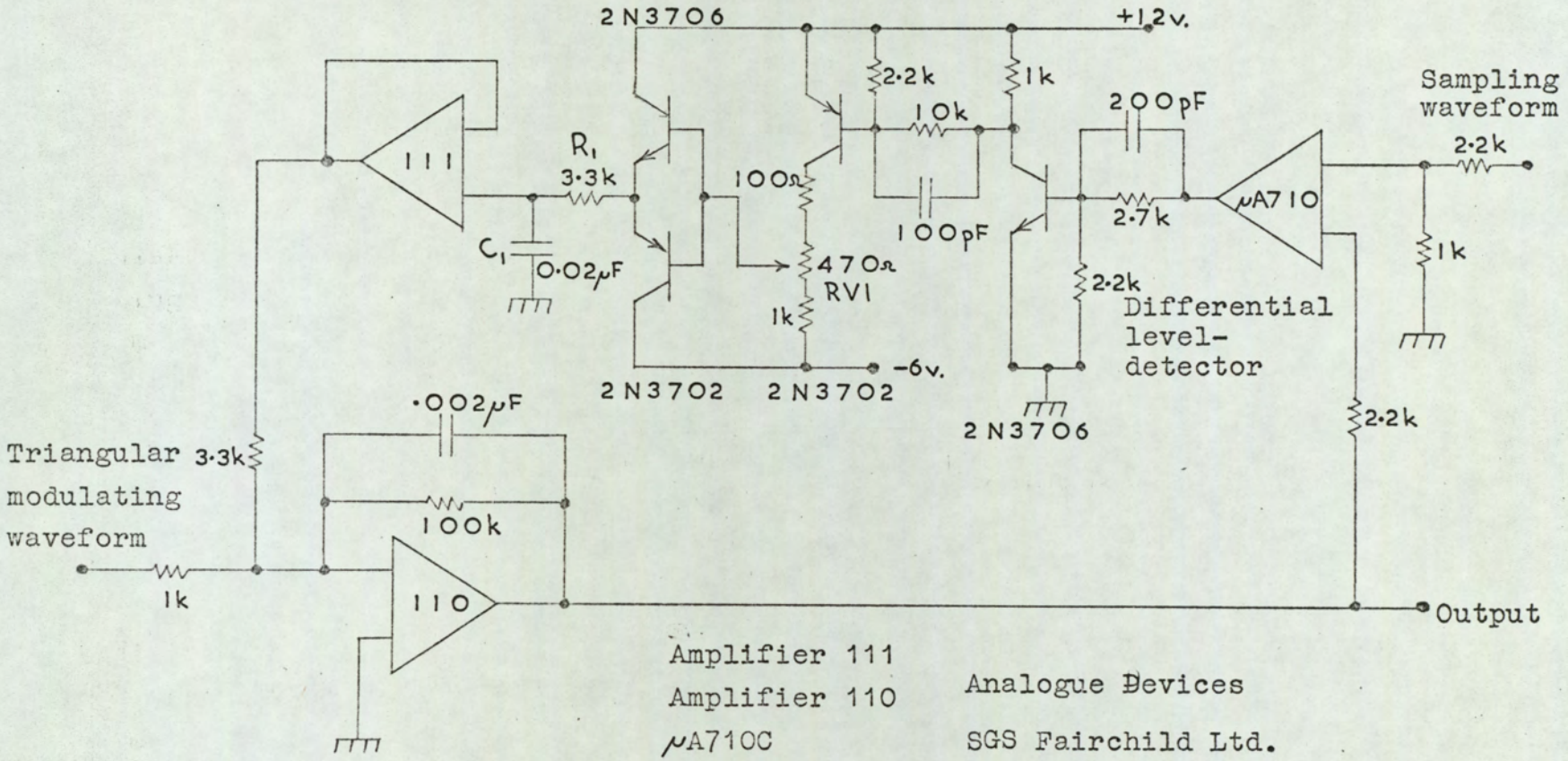

(391)

Fig.4.3. Circuit diagram of practical function generation system using pulse-length modulation.

loading of the R_1C_1 filter network. The symmetry, about Ov., of the pulse-length modulated wavetrain is adjusted by means of variable resistance RV1. Extensive tests were not carried out on the system as its purpose is merely to demonstrate the general principles of the technique. Fig. 4.4 shows the system input and output waveforms when the sampling waveform is a 100kHz. sine wave. The output waveform is seen to be a sine wave having the same frequency as the triangular modulating input waveform as predicted by the analytical work of section 3.

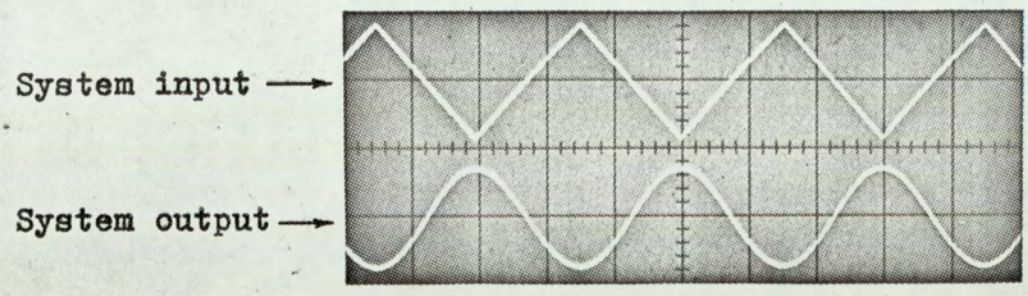

Amplitude = 10 v./ div.

Timebase = 5 msec. / div.

Fig.4.4. System input and output waveforms for the practical system with a 100 kHz. sampling waveform.

5. Discussion of results

A pulse-length modulation system has been described which may be used as a non-linear function generator or as a system having a non-linear transfer function. It is thought that the system could find extensive application as a means of generating functions such as sinusoids, exponential waveforms etc. in the very low frequency range where the capacitor and resistor values required by conventional techniques are impracticable. In order to produce a particular function the system requires a high frequency version of the required function and a triangular wave at the required frequency. Very low frequency triangular waves can be readily generated by digital techniques (e.g. By summing weighted outputs from a binary counter). In theory there is no lower limit to the frequency which can be generated since binary stages can be cascaded to give the required frequency, no matter how low.

Although the analytical work presented in the preceding sections establishes some of the theoretical foundations for the system, there are still a number of points which require investigation. The major one is that in the spectrum analysis it is assumed that the modulating input to the pulse-length modulation section is simply the required system output waveform. In practice however high frequency components also exist in this waveform due to components of the pulse waveform being fed through the operational amplifier. Since filtering of the pulse waveform is carried out within a negative feedback loop there is a limit to the rate at which the filter frequency response can fall off without producing high frequency instability in the system.

CHAPTER V

Conclusion

1. Summary and discussion of results

A survey of the literature relating to pulse-length modulation amplifiers has revealed the lack of information on the design of a practical system. Most of the published work either deals with ideal systems or else presents a complete amplifier circuit with very little indication of the methods used in the design. Since the work described in this thesis was started two papers have been published[44,45] which make some progress towards establishing a theoretical basis for the design of practical pulse-length modulation amplifiers, particularly with regard to output stage design.

From a study of the frequency spectra of pulse-length modulated wavetrains produced by both periodic and natural sampling it has been shown that the natural sampling process is inherently more suitable for use in pulse-length modulation amplifiers. Consequently all the analytical work is concentrated on systems using natural sampling. A study has been made of the static error in the demodulated output of both single-edge and double-edge modulation systems which have a number of practical imperfections. The results relate the system error to the system parameters thus enabling a practical system to be designed on an analytical basis rather than an empirical one. Analyses of the frequency spectra of the system outputs have been developed from the results of the static error analyses in order that harmonic and sideband distortion can be determined for a practical system. It has been shown that, in general, the error and distortion in systems using double-edge modulation are significantly less than in single-edge modulation systems. The results of the analytical work compare favourably with measurements made on an experimental system.

Analysis of power dissipation in the output stage of a pulse-length modulation amplifier has been carried out in two stages. Firstly expressions were obtained relating the dissipation in the output stage elements to the modulation index and the parameters of the low-pass filter. It has been shown that the input current to the low-pass filter may be approximated by a triangular wave superimposed on a constant term. Use of this approximation leads to some simplification of the analysis of output stage dissipation. The second stage of the analysis was to allow the modulation index to vary sinusoidally and then integrate the power dissipation expressions over one cycle of the modulation frequency. This is only an approximate method since the expressions relating the dissipation to the modulation index were derived under the assumption that the pulse-length modulated waveform applied to the output stage is an infinite wavetrain with a constant modulation index. The analytical results compare favourably with measurements made on an experimental output stage and low-pass filter. The efficiency of the output stage was shown to be greater than 90% for full modulation which is a considerable improvement on the maximum theoretical efficiency of 78.5% for a Class B output stage. In order to ensure efficient operation of the output stage, diodes were connected across the output transistors. It has been shown that these diodes introduce step discontinuities into the voltage waveform appearing at the filter input. Further work is required to determine the effect of these discontinuities on the system distortion.

Observations made from the analyses of error and distortion in practical systems led to a proposed scheme for producing non-linear transfer functions using pulse-length modulation techniques. A study of the relevant literature revealed that a description of an identical system had already been published[78]. However the description given in the paper was based largely on intuitive reasoning. Since the system appears to offer a convenient means of generating very low frequency functions, an analysis of the operation of the system has been presented and the results compared with those obtained from an experimental system. The analysis covers only a few of the more fundamental aspects of the operation and it is thought that the general technique of non-linear function generation by means of pulse-length modulation could provide a fruitful topic for further research.

Appendix 1

Numerical Evaluation of the Static Error in a Single-Edge Pulse-Length Modulation System with Finite Integrator Gain

Equations 3.1.18. and 3.1.19. of chapter II give the static error E_1 of a single-edge modulation system which utilises an operational integrator with finite gain to produce the sampling waveform. The expressions are rewritten below for convenience.

$$E_2 = 1 + \frac{2(1+\alpha)CR}{T_c}\left\{\log\frac{1}{2}\left[1+\exp\left(\frac{-T_c}{(1+\alpha)CR}\right)\right] + \log(1-MK) + MK\right\} \qquad (A1.1)$$

$$E_2 = 1 + \frac{2(1+\alpha)CR}{T_c}\left\{\log\frac{1}{2}\left[1+\exp\left(\frac{-T_c}{(1+\alpha)CR}\right)\right] - \sum_{n=2}^{\infty}\frac{1}{n}(M.K)^n\right\} \qquad (A1.2)$$

$$K = \frac{1-\exp\left(\frac{-T_c}{(1+\alpha)CR}\right)}{1+\exp\left(\frac{-T_c}{(1+\alpha)CR}\right)}$$

Care has to be taken in evaluating either of the above expressions when the normalised time constant $\frac{T_c}{(1+\alpha)CR}$ is small.

Consider the term $1 - \exp\frac{-T_c}{(1+\alpha)CR}$ which occurs in the factor K. As $\frac{T_c}{(1+\alpha)CR}$ tends to zero, calculation of the

numerical value for the term involves taking the difference of nearly equal numbers. This may be overcome by writing a Maclaurin expansion for the term $1 - \exp \frac{T_c}{(1+\alpha)CR}$. Thus,

$$K = \frac{1-\left[1-\left(\frac{T_c}{(1+\alpha)CR}\right)+\frac{1}{2!}\left(\frac{T_c}{(1+\alpha)CR}\right)^2-\frac{1}{3!}\left(\frac{T_c}{(1+\alpha)CR}\right)^3-\text{------}\right]}{1+\exp\left(\frac{-T_c}{(1+\alpha)CR}\right)}$$

$$\therefore \quad K = \frac{\sum_{p=1}^{\infty}\frac{(-1)^{p+1}}{p!}\left(\frac{T_c}{(1+\alpha)CR}\right)^p}{1+\exp\left(\frac{-T_c}{(1+\alpha)CR}\right)} \qquad (A1.3)$$

Sufficient terms may be taken in the series for K to give the required accuracy.

The second term, in the static error expressions, which presents problems of numerical evaluation, is the constant term:

$$C_e = 1+\frac{2(1+\alpha)CR}{T_c}\log\frac{1}{2}\left[1+\exp\left(\frac{-T_c}{(1+\alpha)CR}\right)\right] \qquad (A1.4)$$

Again, as the normalised time constant $\frac{T_c}{(1+\alpha)CR}$ tends to zero, the difference of nearly equal numbers is required. This is not very obvious at first sight. However, if the exponential term is approximated by $1 - \frac{T_c}{(1+\alpha)CR}$, then the constant term, equation A1.4., becomes:

$$C_e \triangleq 1+\frac{2(1+\alpha)CR}{T_c}\log\frac{1}{2}\left[1+1-\frac{T_c}{(1+\alpha)CR}\right]$$

Expanding the logarithmic term as a series gives:

$$C_e \simeq 1 + \frac{2(1+\alpha)CR}{T_c}\left[-\left(\frac{T_c}{2(1+\alpha)CR}\right) - \frac{1}{2}\left(\frac{T_c}{2(1+\alpha)CR}\right) - \frac{1}{3}\left(\frac{T_c}{2(1+\alpha)CR}\right) - \cdots\right] \qquad (A1.5)$$

It can now be seen that the numerical evaluation of C_e involves taking small differences. The approximate expression of equation A1.5. is inadequate, since only one term was taken in the series for the exponential. Extending the method by taking further terms in the exponential series would produce a very unwieldy expression for the constant C_e. A better way of carrying out the evaluation will now be described. For ease of writing the equations, let:

$$C_e = 1 + \frac{2}{x}\log\frac{1}{2}\left[1 + \exp(-x)\right]$$

where: $$x = \frac{T_c}{(1+\alpha)CR}$$

$$\therefore C_e = 1 + \frac{2}{x}\left\{\log\left[\exp\left(\frac{-x}{2}\right)\right] + \log\left[\cosh\left(\frac{x}{2}\right)\right]\right\} \qquad (A1.6)$$

Now $\cosh\left(\frac{x}{2}\right)$ may be expanded [57,58] as an infinite product:

$$\cosh\left(\frac{x}{2}\right) = \prod_{p=0}^{\infty}\left(1 + \frac{x^2}{(2p+1)^2\pi^2}\right) \qquad (A1.7)$$

Substituting equation A1.7. into equation A1.6. gives:

$$C_e = \frac{2}{x} \sum_{p=0}^{\infty} \log\left(1 + \frac{x^2}{(2p+1)^2 \pi^2}\right) \qquad (A1.8)$$

Expanding the logarithmic term in equation A1.8 as a Maclaurin series gives:

$$C_e = \frac{2}{x} \sum_{p=0}^{\infty} \sum_{n=1}^{\infty} \frac{1}{n} (-1)^{n+1} \left[\frac{x^2}{(2p+1)^2 \pi^2}\right]^n$$

Changing the order of summation gives:

$$C_e = \frac{2}{x} \sum_{n=1}^{\infty} \frac{1}{n} \left(\frac{x^2}{\pi^2}\right)^n (-1)^{n+1} \sum_{p=0}^{\infty} \frac{1}{(2p+1)^{2n}} \qquad (A1.9)$$

Thus, a series representation has been obtained for C_e and it is not necessary to take small differences when making a numerical evaluation.

Consider the term corresponding to n = 1 in equation A1.9

$$C_e\Big|_{n=1} = \frac{2}{x} \cdot \frac{x^2}{\pi^2} \sum_{p=0}^{\infty} \frac{1}{(2p+1)^2} \qquad (A1.10)$$

Now the numerical series in equation A1.10 does not converge very rapidly. To evaluate the series to an accuracy of eight significant figures, it is necessary to take approximately 10^4 terms. However, series of this type have a sum[57,59] which

can be expressed as:

$$\sum_{p=0}^{\infty} \frac{1}{(2p+1)^{2n}} = \sum_{p=1}^{\infty} \frac{1}{(2p-1)^{2n}} = \frac{(2^{2n}-1)\pi^{2n}}{2\,(2n)!} \left| B_{2n} \right| \qquad (A1.11)$$

where B_{2n} is the $2n^{th}$ Bernoulli number:

$$B_{2n} = (-1)^{n-1} \frac{2\,(2n)!}{(2\pi)^{2n}} \frac{1}{\prod_{m=1}^{\infty} \left(1 - \frac{1}{m^{2n}}\right)}$$

Bernoulli numbers are tabulated in the literature[60] and substituting their values in equation A1.11 gives the following expressions:

$$\sum_{p=1}^{\infty} \frac{1}{(2p-1)^2} = \frac{\pi^2}{8} \qquad (A1.12(a))$$

$$\sum_{p=1}^{\infty} \frac{1}{(2p-1)^4} = \frac{\pi^4}{96} \qquad (A1.12(b))$$

$$\sum_{p=1}^{\infty} \frac{1}{(2p-1)^6} = \frac{\pi^6 . 63}{60480} \qquad (A1.12(c))$$

$$\sum_{p=1}^{\infty} \frac{1}{(2p-1)^8} = \frac{\pi^8 . 255}{2419200} \qquad (A1.12(d))$$

$$\sum_{p=1}^{\infty} \frac{1}{(2p-1)^{10}} = \frac{\pi^{10} 31}{2903040} \qquad (A1.12(e))$$

$$\sum_{p=1}^{\infty} \frac{1}{(2p-1)^{12}} = \frac{\pi^{12} 8983}{31933440000} \qquad (A1.12(f))$$

Evaluation of the term $\sum_{p=1}^{\infty} \frac{1}{(2p-1)^{2n}}$, where $n \geqslant 7$, only requires a few terms in the series for an accuracy of eight significant figures. Thus, the expression for the constant term C_e becomes:

$$C_e = \frac{2}{x}\left\{\frac{x^2}{\pi^2}\cdot\frac{\pi^2}{8} - \frac{1}{2}\left(\frac{x^2}{\pi^2}\right)^2 \frac{\pi^4}{96} + \frac{1}{3}\left(\frac{x^2}{\pi^2}\right)^3 \frac{\pi^6 63}{60480} -\right.$$

$$\frac{1}{4}\left(\frac{x^2}{\pi^2}\right)^4 \frac{\pi^8 255}{2149200} + \frac{1}{5}\left(\frac{x^2}{\pi^2}\right)^5 \frac{\pi^{10} 31}{2903040} - \frac{1}{6}\left(\frac{x^2}{\pi^2}\right)^6 \frac{\pi^{12} 8983}{31933440000} +$$

$$\left.\sum_{n=7}^{\infty} \frac{1}{n}(-1)^{n+1}\left(\frac{x^2}{\pi^2}\right)^n \sum_{p=0}^{\infty} \frac{1}{(2p+1)^{2n}}\right\}$$

$$\therefore 1+\frac{2}{T_N}\log\frac{1}{2}\left[1+\exp\left(-T_N\right)\right]=2\left\{T_N\cdot\frac{1}{8}-T_N^3\cdot\frac{1}{198}+\right.$$

$$T_N^5\cdot\frac{21}{60480}-T_N^7\cdot\frac{85}{2865600}+T_N^9\cdot\frac{31}{14515200}-T_N^{11}\cdot\frac{8983}{51093504000}+$$

$$\left.\sum_{n=7}^{\infty}\frac{1}{n}(-1)^{n+1}\cdot T_N^{2n-1}\cdot\frac{1}{\pi^{2n}}\sum_{p=0}^{\infty}\frac{1}{(2p+1)^{2n}}\right\} \qquad (A1.13)$$

where $T_N = \dfrac{T_c}{(1+\alpha)CR}$

If terms up to T_N^{11} are taken in the above series, then the accuracy is approximately six significant figures for $T_N = 1$. As T_N is reduced, so the accuracy improves rapidly.

The system static error E_2 may now be written as:

$$E_2 = C_e - \frac{2}{T_N}\sum_{n=2}^{\infty}\frac{1}{n}(MK)^n \qquad (A1.14)$$

where

$$K = \frac{1-\exp\left(-T_N\right)}{1+\exp\left(-T_N\right)}$$

From equations 3.1.15. and 3.1.17. of part II section 2.1.:

$$E_1 = 1 + \frac{2}{T_N}\left\{\log \frac{1}{2}\left[1 - \exp(-T_N)\right] - \sum_{n=1}^{\infty} \frac{1}{n}(MK)^n\right\} + M$$

which may be rewritten as:

$$E_1 = E_2 + M\left(1 - \frac{2K}{T_N}\right) \qquad (A1.15)$$

$$\therefore E_1 = E_2 + M\left\{\frac{T_N\left[1 + \exp(-T_N)\right] - 2\left[1 - \exp(-T_N)\right]}{T_N \quad T_N\left[1 + \exp(-T_N)\right]}\right\}$$

Expanding the exponential terms as infinite series and rearranging the expression leads to the following result:

$$E_1 = E_2 + M.D \qquad (A1.16)$$

where

$$D = \frac{1}{1 + \exp(-T_N)} \sum_{p=2}^{\infty} (-1).(T_N)^p \ \frac{1}{p!}\left(1 - \frac{2}{p+1}\right) \qquad (A1.17)$$

By making use of the series methods outlined in this appendix, the system static errors, E_1 and E_2, may be evaluated for small values of normalised time constant T without large rounding errors due to subtracting nearly equal numbers. These rounding errors will still exist when (for a given value of T_N) the value of the modulation index M is

such that the error tends to zero. However, this is not important, since the maximum value of the error (for a given value of T_N) is evaluated accurately and the rounding errors only occur when the modulation index is such that the error is very much smaller than the maximum value. These methods were used in calculating the curves shown in figs. 3.1.4. and 3.1.5. of chapter 2, which show the system static error as a function of the normalised time constant and the modulation index. Fig. A1.1. is a flow chart of the method used for evaluating the system error on a digital computer.

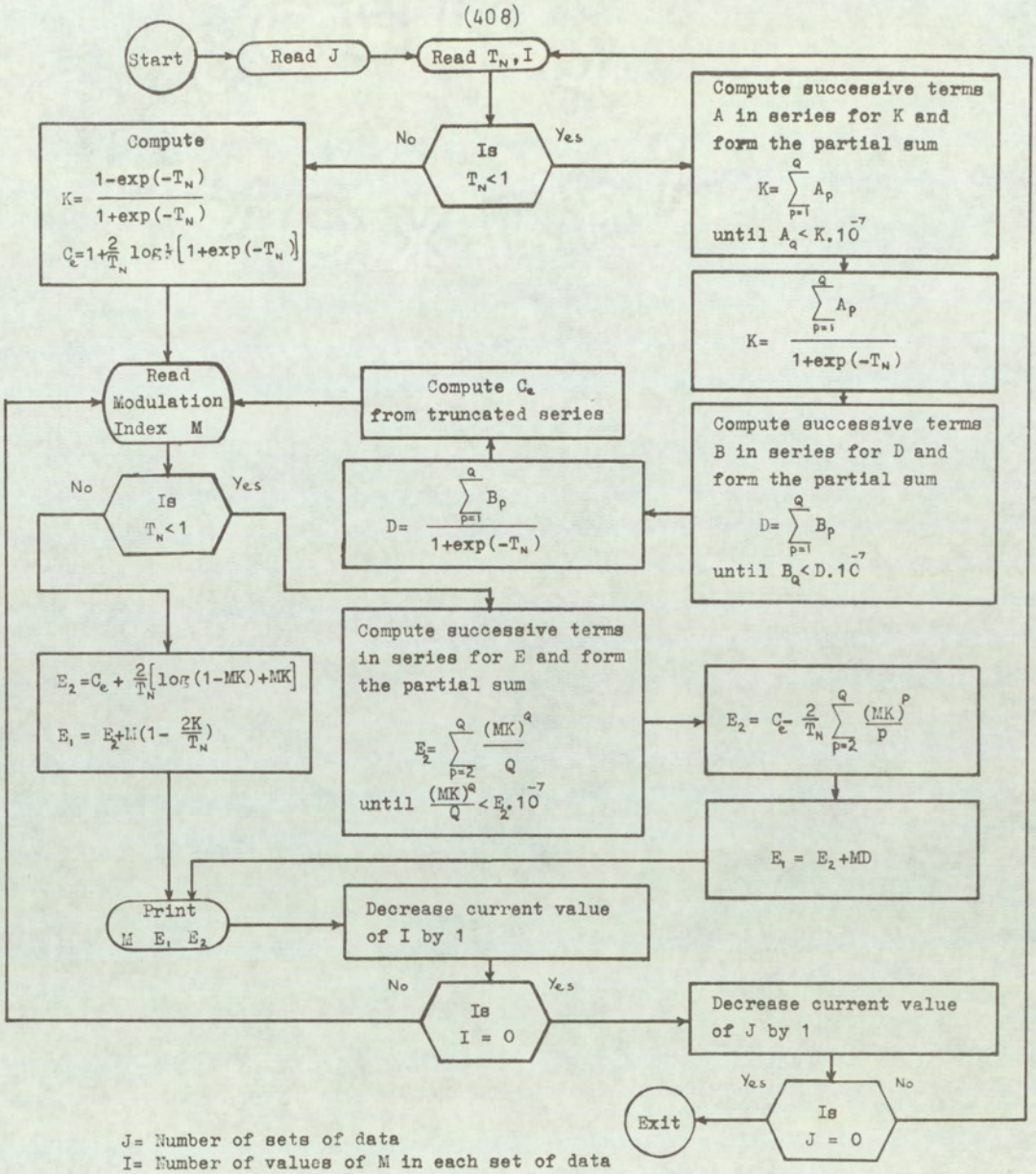

J= Number of sets of data
I= Number of values of M in each set of data

$$K = \frac{\sum_{p=1}^{\infty} A_p}{1+\exp(-T_N)} \qquad A = \frac{(-1)^{p+1}}{p!} T_N^{\,p} \qquad T_N = \frac{T_c}{(1+\alpha)CR}$$

$$D = \frac{\sum_{p=1}^{\infty} B_p}{1+\exp(-T_N)} \qquad B = (-1)^p (T_N)^p \left(\frac{1}{p!}\right)\left(1-\frac{2}{p+1}\right) \qquad T_N = \frac{T_c}{(1+\alpha)CR}$$

$$C = 2\left\{T_N\frac{1}{8} - T_N^3\frac{1}{198} + T_N^5\frac{21}{60480} - T_N^7\frac{85}{2865600} + T_N^9\frac{31}{14515200} - T_N^{11}\frac{8983}{5109350400}\right\}$$

Fig.A1.1. Flowchart for evaluating static error in single-edge modulation system with finite gain.

Appendix 2. Derivation of the expressions for the positions of the pulse-edges in a single-edge modulation system with finite amplifier bandwidth

The position t_1 of the leading edge of the pulses of a single-edge pulse-length modulation system with a bandwidth-limited integrator amplifier were shown (Chapter II, Section 2.3.1, equation 2.3.16) to be defined by:

$$\left\{1-\frac{1}{1-k_1/k_2}\exp(-k_1t_1)-\frac{1}{1-k_2/k_1}\exp(-k_2t_1)\right\}=$$

$$\frac{1}{2}(1+M)\left\{1-\frac{1}{1-k_1/k_2}\exp(-k_1T_c)-\frac{1}{1-k_2/k_1}\exp(-k_2T_c)\right\} \qquad (A2.1)$$

$$k_1=\frac{1}{2}\left\{\frac{T_a+(1+\alpha)CR}{T_a.CR}+\sqrt{\left[\left(\frac{T_a+(1+\alpha)CR}{T_a.CR}\right)^2-\frac{4}{T_a.CR}\right]}\right\} \qquad (A2.2)$$

$$k_2=\frac{1}{2}\left\{\frac{T_a+(1+\alpha)CR}{T_a.CR}-\sqrt{\left[\left(\frac{T_a+(1+\alpha)CR}{T_a.CR}\right)^2-\frac{4}{T_a.CR}\right]}\right\} \qquad (A2.3)$$

Since a direct expression for t_1 cannot be obtained from equation A2.1, it is required to represent t_1 as a power series in terms of the modulation index M.

$$\frac{t_1}{T_c}=\sum_{n=0}^{\infty}a_n.M^n \qquad (A2.4)$$

Before deriving expressions for the coefficients a_n, it is convenient to rearrange equations A2.2 and A2.3. With the above form of the expressions, the effect of allowing the amplifier time

constant T_a to approach zero is not readily deduced. Also, numerical evaluation of the coefficient k_2 will be subject to rounding errors when T_a is small, since the difference of nearly equal numbers is required. From equation A2.3

$$k_2 = \frac{1}{2}\left[\frac{T_a+(1+\alpha)CR}{T_a.CR}\right]\left\{1-\sqrt{\left[1-\frac{4}{T_a.CR}\left(\frac{T_a.CR}{T_a+(1+\alpha)CR}\right)^2\right]}\right\}$$

The square root term in the above equation may be expanded by the binomial theorem to give:

$$k_2 = \frac{1}{(1+\alpha)CR}\left[\frac{1}{1+\frac{T_a}{(1+\alpha)CR}}\right]A_2 \qquad (A2.5)$$

where

$$A_2 = 1+\frac{2.1}{2!}\left(\frac{1}{\Upsilon}\right)+\frac{2^2.1.3}{3!}\left(\frac{1}{\Upsilon}\right)^2+\frac{2^3.1.3.5}{4!}\left(\frac{1}{\Upsilon}\right)^3+\text{-----} \qquad (A2.6)$$

$$\Upsilon = \frac{CR}{T_a}\left[\frac{T_a}{CR}+1+\alpha\right]^2$$

From equations A2.2, A2.3 and A2.5:

$$k_1 = \frac{1}{(1+\alpha)CR}\left[\frac{1}{1+\frac{T_a}{(1+\alpha)CR}}\right](\Upsilon-A_2) \qquad (A2.7)$$

The effect on k_1 and k_2 of allowing the amplifier time constant T_a to approach zero is now readily seen.

For convenience of writing the equations in subsequent analytical work, equation A2.1 will be rewritten as:

$$1-(1+M)D = \frac{1}{1-k_1/k_2}\exp(-k_1 t_1) + \frac{1}{1-k_2/k_1}\exp(-k_2 t_1) \qquad (A2.8)$$

where:

$$D = \frac{1}{2}\left\{1 - \frac{1}{1-k_1/k_2}\exp(-k_1 T_c) - \frac{1}{1-k_2/k_1}\exp(-k_2 T_c)\right\} \qquad (A2.9)$$

There are a number of different approaches to the problem of obtaining a power-series representation of t_1 from equation A2.8. The first of these is to expand the exponential terms containing t_1 as infinite series, thus producing an expression for the modulation index M as a power series in terms of t_1. A series for t_1 in terms of M can then be obtained by reversion of the series for M in terms of t_1 [61]. However, as may be seen from equation A2.7, the term k_1 tends to infinity as T_a tends to zero, so the series for $\exp(-k_1 t_1)$ will converge very slowly. Evidently, the series reversion method is unsuitable. The second method involves solving equation A2.8 numerically for a range of values of modulation index M and then using a polynomial curve-fitting method [62,63] to obtain a polynomial for t_1 in terms of M. There are a number of difficulties entailed in applying this method, the major one being the numerical analysis problems involved. When the integrator gain α is large, the coefficients of terms involving powers of M greater than unity will be small; extreme care would thus be required in evaluating these coefficients by a curve fitting

technique. The third method makes use of Maclaurins theorem.

If the power series for t_1, equation A2.4, is a Maclaurin series, then the coefficients a_n may be written as:

$$a_o = \left.\frac{t_1}{T_c}\right|_{M=0} = \frac{\overset{\circ}{t}_1}{T_c} \qquad (A2.10)$$

where $\overset{\circ}{t}_1$ is the unmodulated position of the pulse leading edge.

$$a_n = \frac{1}{n!}\,\frac{1}{T_c}\,\left.\frac{d^n t_1}{dM^n}\right|_{M=0} \qquad (A2.11)$$

The power series for t_1 is, therefore:

$$\frac{t_1}{T_c} = \frac{1}{T_c}\sum_{n=0}^{\infty}\frac{1}{n!}\,\frac{1}{T_c}\,\left.\frac{d^n t_1}{dM^n}\right|_{M=0} M^n \qquad (A2.12)$$

Thus, the problem is that of obtaining successive differentials of t_1 with respect to M.

Differentiating both sides of equation A2.8 with respect to M gives:

$$-D = \left\{\frac{-k_1}{1-k_1/k_2}\exp(-k_1 t_1) + \frac{-k_2}{1-k_2/k_1}\exp(-k_2 t_1)\right\}\frac{dt_1}{dM}$$

$$\therefore \quad \frac{dt_1}{dM} = D\left(\frac{1}{k_2}-\frac{1}{k_1}\right)\left[\frac{1}{\exp(-k_2 t_1)-\exp(-k_1 t_1)}\right] \qquad (A2.13)$$

Equation A2.13 may be differentiated to give the following expression for the second differential:

$$\frac{d^2 t_1}{dM^2} = D\left(\frac{1}{k_2}-\frac{1}{k_1}\right)\left\{\frac{k_2\exp(-k_2 t_1)-k_1\exp(-k_1 t_1)}{\left[\exp(-k_2 t_1)-\exp(-k_1 t_1)\right]^2}\right\} \qquad (A2.14)$$

Substituting equation A2.13 in equation A2.14:

$$\frac{d^2t_1}{dM^2} = \left[D\left(\frac{1}{k_2} - \frac{1}{k_1}\right)\right]^2 \left\{\frac{k_2\exp(-k_2t_1) - k_1\exp(-k_1t_1)}{\left[\exp(-k_2t_1) - \exp(-k_1t_1)\right]^3}\right\} \qquad (A2.15)$$

It has not been found possible to obtain a general expression for the n^{th} differential of t_1 with respect to M, since equation A2.13 (for the first differential) is a function of a function. Expressions are available for the n^{th} differential of a composite function [57], but when applied to equation A2.13 they give expressions which are too complex to be of use.

Expressions for higher-order differentials are obtained by repeated differentiation of equation A2.15. Setting $t_1 = t_1$ in the expressions for the differentials, and substituting in equation A2.11, enables the coefficients a_n to be written as:

$$a_o = \frac{\overset{o}{t}_1}{T_c} \qquad (A2.16(a))$$

$$a_1 = \frac{1}{T_N}\left[D\left(\frac{1}{A_2} - \frac{1}{A_1}\right)\right]\left[\frac{1}{F_o}\right] \qquad (A2.16(b))$$

$$a_2 = \frac{1}{T_N 2!}\left[D\left(\frac{1}{A_2} - \frac{1}{A_1}\right)\right]^2\left[\frac{F}{F_o^3}\right] \qquad (A2.16(c))$$

$$a_3 = \frac{1}{T_N 3!}\left[D\left(\frac{1}{A_2} - \frac{1}{A_1}\right)\right]^3\left[\frac{3F_1^2 - F_oF_2}{F_o^5}\right] \qquad (A2.16(d))$$

$$a_4 = \frac{1}{T_N 4!}\left[D\left(\frac{1}{A_2} - \frac{1}{A_1}\right)\right]^4\left[\frac{-10F_oF_1F_2 + F_o^2F_3 + 15F_1^3}{F_o^7}\right] \qquad (A2.16(e))$$

$$a_5=\frac{1}{T_N 5!}\left[D\left(\frac{1}{A_2}-\frac{1}{A_1}\right)\right]\left[\frac{15F_o^2F_1F_3+10F_o^2F_2^2+105F_1^4-F_o^3F_4-105F_oF_1^2F_3}{F_o^9}\right] \qquad (A2.16(f))$$

$$a_6=\frac{1}{T_N 6!}\left[D\left(\frac{1}{A_2}-\frac{1}{A_1}\right)\right]\left[\frac{21F_o^3F_1F_4+35F_o^3F_2F_3+1260F_oF_1^3F_2-F_o^4F_5-}{F_o^{11}}\right.$$

$$\left.\frac{280F_o^2F_1F_2^2-945F_1^5-210F_o^2F_1^2F_3}{F_o^{11}}\right] \qquad (A2.16(g))$$

$$a_7=\frac{1}{T_N 7!}\left[D\left(\frac{1}{A_2}-\frac{1}{A_1}\right)\right]\left[\frac{28F_o^4F_1F_5+56F_o^4F_2F_4+35F_o^4F_3^2+3150F_o^2F_1^3F_3+}{F_o^{13}}\right.$$

$$\frac{6300F_o^2F_1^2F_2^2+10395F_1^6-F_o^5F_6-378F_o^3F_1^2F_4-}{F_o^{13}}$$

$$\left.\frac{1260F_o^3F_1F_2F_3-280F_o^3F_2^3-17325F_oF_1^4F_2}{F_o^{13}}\right] \qquad (A2.16(h))$$

where:

$$T_N=\frac{T_c}{(1+\alpha)CR}\left[\frac{1}{1+\frac{T_a}{(1+\alpha)CR}}\right] \qquad (A2.17(a))$$

$$A_2=\left\{1+\frac{2.1}{2!}\left(\frac{1}{\Psi}\right)+\frac{2^2.1.3}{3!}\left(\frac{1}{\Psi}\right)^2+\frac{2^2.1.3.5}{4!}\left(\frac{1}{\Psi}\right)^3+-----\right\} \qquad (A2.17(b))$$

$$A_1=\Psi-A_2 \qquad (A2.17(c))$$

$$F_n=A_2^n\exp\left(-A_2T_N\frac{t_1^o}{T_c}\right)-A_1^n\exp\left(-A_1T_N\frac{t_1^o}{T_c}\right) \qquad (A2.17(d))$$

Substituting equations A2.5 and A2.7 in equation A2.9 enables the term D to be rewritten as:

$$D = \frac{1}{2}\left\{1 - \frac{A_2}{A_2 - A_1}\exp\left(-A_1 T_N\right) - \frac{A_1}{A_1 - A_2}\exp\left(-A_2 T_N\right)\right\} \qquad (A2.18)$$

The unmodulated position t_1 of the leading edge of the pulse is obtained by numerical solution of equation A2.8 with M=0.

$$\therefore \frac{1}{1 - k_1/k_2}\exp\left(-k_1 \overset{\circ}{t}_1\right) - \frac{1}{1 - k_2/k_1}\exp\left(-k_2 \overset{\circ}{t}_1\right) = 1 - D \qquad (A2.19)$$

Substituting equations A2.5 and A2.7 in equation A2.19:

$$\frac{A_2}{A_2 - A_1}\exp\left(-A_1 T_N \frac{\overset{\circ}{t}_1}{T_c}\right) + \frac{A_1}{A_1 - A_2}\exp\left(-A_2 T_N \frac{\overset{\circ}{t}_1}{T_c}\right) = 1 - D \qquad (A2.20)$$

Thus, the coefficients a_n in the power series for $\frac{t_1}{T_c}$ have been expressed in terms of the two variables, T_N and Ψ.

In order to evaluate $\frac{\overset{\circ}{t}_1}{T_c}$ from equation A2.20, use is made of Newton's successive-approximation method [60].

$$\left(\frac{\overset{\circ}{t}_1}{T_c}\right)_{n+1} = \left(\frac{\overset{\circ}{t}_1}{T_c}\right)_n - \frac{f'\left(\frac{\overset{\circ}{t}_1}{T_c}\right)_n}{f\left(\frac{\overset{\circ}{t}_1}{T_c}\right)_n} \qquad (A2.21)$$

where:

$\left(\frac{\overset{\circ}{t}_1}{T_c}\right)_{n+1}$ is the $n+1^{th}$ approximation to $\frac{\overset{\circ}{t}_1}{T_c}$.

$f\left(\frac{t_1^\circ}{T_c}\right)_n$ is the equation defining $\frac{t_1^\circ}{T_c}$, evaluated with the n^{th} approximation to $\frac{t_1^\circ}{T_c}$.

$f'\left(\frac{t_1^\circ}{T_c}\right)_n$ is the first derivative of the equation defining $\frac{t_1^\circ}{T_c}$, evaluated with the n^{th} approximation to $\frac{t_1^\circ}{T_c}$.

From equation A2.20:

$$f\left(\frac{t_1^\circ}{T_c}\right)=\frac{A_2}{A_2-A_1}\exp\left(-A_1T_N\frac{t_1^\circ}{T_c}\right)+\frac{A_1}{A_1-A_2}\exp\left(-A_2T_N\frac{t_1^\circ}{T_c}\right)-1+D \qquad (A2.22(a))$$

$$f'\left(\frac{t_1^\circ}{T_c}\right)=\frac{-A_1A_2T_N}{A_2-A_1}\exp\left(-A_1T_N\frac{t_1^\circ}{T_c}\right)-\frac{A_1A_2T_N}{A_1-A_2}\exp\left(-A_2T_N\frac{t_1^\circ}{T_c}\right) \qquad (A2.22(b))$$

Substituting equation A2.18, for D, in equation A2.22 gives:

$$f\left(\frac{t_1^\circ}{T_c}\right)=\frac{A_2}{A_2-A_1}\left[\exp\left(-A_1T_N\frac{t_1^\circ}{T_c}\right)-\frac{1}{2}\exp\left(-A_1T_N\right)-\frac{1}{2}\right]+$$

$$\frac{A_1}{A_1-A_2}\left[\exp\left(-A_2T_N\frac{t_1^\circ}{T_c}\right)-\frac{1}{2}\exp\left(-A_2T_N\right)-\frac{1}{2}\right] \qquad (A2.23)$$

Considerable care has to be exercised when evaluating equation A2.23 for small values of T_N, since the second of the square brackets on the right hand side of the equation involves taking the difference of nearly equal numbers. Evaluation of the first of the square brackets does not present any difficulties since, for all practical values of the system parameters, the term $A_1 T_N$ is considerably greater than unity. Expanding the exponential terms in the second of the square brackets enables $f\left(\frac{t_1^\circ}{T_c}\right)$ to be written as:

$$f\left(\frac{t_1^\circ}{T_c}\right)=\frac{A_2}{A_2-A_1}\left[\exp\left(-A_1T_N\frac{t_1^\circ}{T_c}\right)-\frac{1}{2}\left(-A_1T_N\right)-\frac{1}{2}\right]+$$

$$\frac{A_1}{A_1-A_2}\sum_{n=1}^{\infty}\frac{1}{n!}\left(-A_2T_N\right)^n\left[\left(\frac{t_1^\circ}{T_c}\right)-\frac{1}{2}\right] \qquad (A2.24)$$

Rounding errors will still exist in the evaluation of $f(\frac{\mathring{t}_1}{T_c})$ from equation A2.24, but they will be very much smaller than the errors incurred by evaluating $f(\frac{\mathring{t}_1}{T_c})$ directly from equation A2.22. Evaluation of $f(\frac{\mathring{t}_1}{T_c})$ is straightforward, so that:

$$\frac{F(\frac{\mathring{t}_1}{T_c})}{F'(\frac{\mathring{t}_1}{T_c})} = \frac{A_2\left[\exp\left(-A_1T_N\frac{\mathring{t}_1}{T_c}\right)-\frac{1}{2}\exp\left(-A_1T_N\right)-\frac{1}{2}\right]-A_1\sum_{n=1}^{\infty}\frac{1}{n!}\left(-A_2T_N\right)^n\left[\left(\frac{\mathring{t}_1}{T_c}\right)-\frac{1}{2}\right]}{-A_1A_2\left\{\exp\left(-A_1T_N\frac{\mathring{t}_1}{T_c}\right)-\exp\left(-A_2T_N\frac{\mathring{t}_1}{T_c}\right)\right\}} \qquad (A2.25)$$

In order to make use of Newton's successive-approximation method, it is necessary to have an initial estimate of $\frac{\mathring{t}_1}{T_c}$. This could be taken as zero. However, a better approximation is 0.5, since the unmodulated position t_1 of the leading edge of the pulse in an ideal single-edge pulse-length modulation system is $\mathring{t}_1 = \frac{T_c}{2}$.

The terms A_1 and A_2 can be evaluated directly from equations A2.17(b) and A2.17(c).

The term $D(\frac{1}{A_2} - \frac{1}{A_1})$, which occurs in all the expressions for a_n, cannot be evaluated directly from equation A2.18 without incurring significant rounding error, since the term $1 - \frac{A_1}{A_1 - A_2}\exp(-A_2 T_N)$ approaches zero for small values of T_N.

From equation A2.18:

$$D\left(\frac{1}{A_2}-\frac{1}{A_1}\right)=\frac{1}{2}\left(\frac{1}{A_2}-\frac{1}{A_1}\right)\left\{1-\frac{A_2}{A_2-A_1}\exp\left(-A_1T_N\right)-\frac{A_1}{A_1-A_2}\exp\left(-A_2T_N\right)\right\} \qquad (A2.26)$$

Expanding the term $\exp(-A_2 T_N)$ as an infinite series leads to the following result:

$$D\left(\frac{1}{A_2}-\frac{1}{A_1}\right)=\frac{1}{2A_1A_2}\left\{A_1\sum_{n=1}^{\infty}\left[\frac{1}{n!}(-1)^{n+1}(A_2T_N)^n\right]-A_2\left[1-\exp\left(-A_1T_N\right)\right]\right\} \qquad (A2.27)$$

Although rounding errors will still exist when evaluating $D(\frac{1}{A_2} - \frac{1}{A_1})$ from equation A2.27, they will be considerably less than when evaluating $D(\frac{1}{A_2} - \frac{1}{A_1})$ directly from equation A2.18.

The numerical methods outlined probably do not represent the optimum methods of evaluating the equations, but are adequate for the purpose. Fig. A2.1 shows a flow chart of the method used for evaluating the expressions on a digital computer.

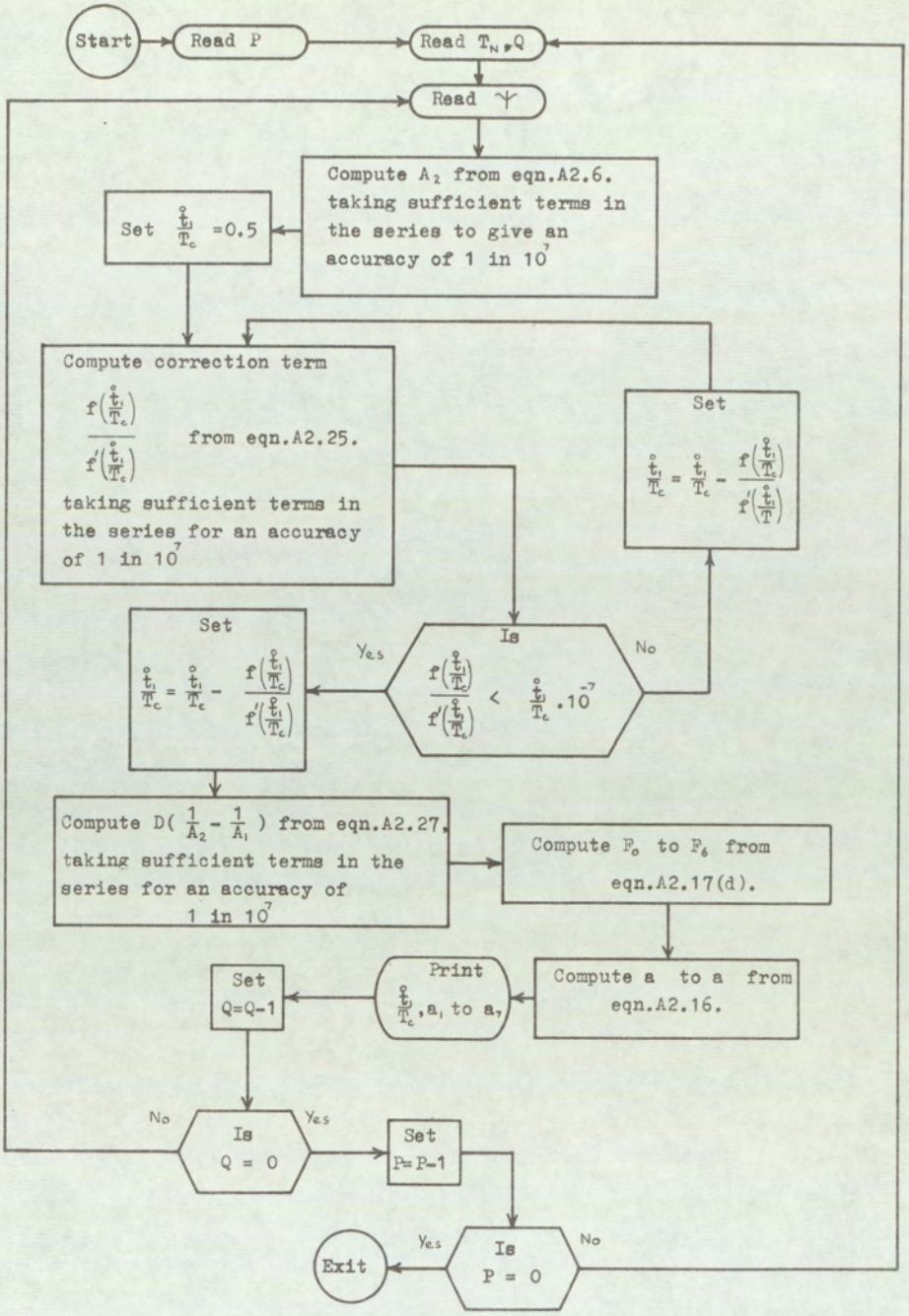

P = Number of values of T_N on data tape.
Q = Number of values of Ψ.

Fig.A2.1. Flowchart for computing the coefficients a_1 to a_7 .

Appendix 3. Derivation of the expressions for the positions of the pulse-edges in a double-edge modulation system with finite amplifier bandwidth

The positions of the leading and trailing edges of the pulses produced by a double-edge pulse-length modulation system utilising a bandwidth-limited integrator amplifier were shown (Chapter II, section 3.3.2, equations 3.3.40 and 3.3.41) to be defined by the equations:

$$\left\{1-\frac{2\left(\frac{k_2}{k_1-k_2}\right)}{1+\exp\left(\frac{-k_1T_c}{2}\right)}\exp(-k_1t_1)-\frac{2\left(\frac{k_1}{k_1-k_2}\right)}{1+\exp\left(\frac{-k_2T_c}{2}\right)}\exp(-k_2t_1)\right\}=$$

$$-M\left\{1-2\left[1+\exp\left(\frac{-k_1T_c}{2}\right)\right]^{\frac{k_2}{k_1-k_2}}\left[1+\exp\left(\frac{-k_2T_c}{2}\right)\right]^{\frac{-k_1}{k_1-k_2}}\right\} \qquad (A3.1)$$

$$\left\{-1+\frac{2\left(\frac{k_2}{k_2-k_1}\right)}{1+\exp\left(\frac{-k_1T_c}{2}\right)}\exp\left[-k_1\left(t_2-\frac{T_c}{2}\right)\right]+\frac{2\left(\frac{k_1}{k_1-k_2}\right)}{1+\exp\left(\frac{-k_2T_c}{2}\right)}\exp\left[-k_2\left(t_2-\frac{T_c}{2}\right)\right]\right\}=$$

$$-M\left\{1-2\left[1-\exp\left(\frac{-k_1T_c}{2}\right)\right]^{\frac{k_2}{k_1-k_2}}\left[1+\exp\left(\frac{-k_2T_c}{2}\right)\right]^{\frac{-k_1}{k_1-k_2}}\right\} \qquad (A3.2)$$

Since direct expressions for t_1 and t_2 cannot be obtained from equations A2.1 and A2.2, it is required to represent the switching points as power series in terms of the modulation index M.

$$\frac{t_1}{T_c}=\sum_{n=0}^{\infty}a_nM^n \qquad (A3.3)$$

$$\frac{t_2}{T_c}-\frac{1}{2}=\sum_{n=0}^{\infty}b_nM^n \qquad (A3.4)$$

It was shown in Appendix 1, in relation to the single-edge modulation system with a bandwidth-limited integrator amplifier, that the terms k_1 and k_2 can conveniently be expressed as:

$$k_2 = \frac{1}{(1+\alpha)CR}\left[\frac{1}{1+\frac{T_a}{(1+\alpha)CR}}\right]A_2 \qquad (A3.5)$$

$$k_1 = \frac{1}{(1+\alpha)CR}\left[\frac{1}{1+\frac{T_a}{(1+\alpha)CR}}\right](\Upsilon - A_2) \qquad (A3.6)$$

where $$A_2 = \left\{1+\frac{2.1}{2!}\left(\frac{1}{\Upsilon}\right)+\frac{2^2.1.3}{3!}\left(\frac{1}{\Upsilon}\right)^2+\frac{2^3.1.3.5}{4!}\left(\frac{1}{\Upsilon}\right)^3+---\right\} \qquad (A3.7)$$

and

$$\Upsilon = \frac{CR}{T_a}\left[\frac{T_a}{CR}+1+\alpha\right]^2$$

The various possible methods of obtaining expressions for the coefficients in the power series representation of the switching points t_1 and t_2 were discussed in Appendix 2 in relation to corresponding expressions for single-edge modulation. The method used is to represent t_1 and t_2 as Maclaurin series; the coefficients a_n in equation A3.3 may then be written as:

$$a_o = \frac{\overset{\circ}{t}_1}{T_c} = \frac{t_1}{T_c}\bigg|_{M=0} \qquad (A3.8)$$

where $\overset{\circ}{t}_1$ is the unmodulated position of the leading edge of the pulse.

$$a_n = \frac{1}{T_c}\,\frac{1}{n!}\,\frac{d^n t_1}{dM^n}\bigg|_{M=0} \qquad (A3.9)$$

Therefore t_1 may be expressed as:

$$\frac{t_1}{T_c} = \sum_{n=0}^{\infty}\frac{1}{T_c}\,\frac{1}{n!}\,\frac{d^n t_1}{dM^n}\bigg|_{M=0}.M^n \qquad (A3.10)$$

Thus, the problem is that of obtaining successive differentials of t_1 with respect to M.

Differentiating equation A3.1 with respect to M gives:

$$-D=\left\{\frac{2\left(\frac{k_2k_1}{k_1-k_2}\right)}{1+\exp\left(\frac{-k_2T_c}{2}\right)}\exp(-k_2t_1)+\frac{2\left(\frac{k_2k_1}{k_2-k_1}\right)}{1+\exp\left(\frac{-k_1T_c}{2}\right)}\exp(-k_1t_1)\right\}\frac{dt_1}{dM}$$

where: $$D=\left\{1-2\left[1+\exp\left(\frac{-k_1T_c}{2}\right)\right]^{\frac{k_2}{k_1-k_2}}\left[1+\exp\left(\frac{-k_2T_c}{2}\right)\right]^{\frac{-k_1}{k_1-k_2}}\right\} \qquad (A3.11)$$

$$\therefore \frac{dt_1}{dM}=-\frac{D}{2}\left(\frac{1}{k_2}-\frac{1}{k_1}\right)\left[\frac{1}{\frac{\exp(-k_2t_1)}{1+\exp\left(\frac{-k_2T_c}{2}\right)}-\frac{\exp(-k_1t_1)}{1+\exp\left(\frac{-k_1T_c}{2}\right)}}\right] \qquad (A3.12)$$

Equation A3.12 may be repeatedly differentiated to obtain expressions for the higher-order differentials. It has not been found possible to obtain a general expression for the n^{th} differential of t_1 with respect to M, since equation A3.12 is a function of a function. Expressions have been developed for the n^{th} differential of a composite function [57] but, when applied to equation A3.12, give results which are too complex to be of use.

Setting $t_1=\overset{\circ}{t}_1$ in the expressions for the differentials, and substituting in equation A3.9, gives the following expressions for the coefficients a_n.

$$a_o=\frac{\overset{\circ}{t}_1}{T_c} \qquad (A3.13(a))$$

$$a_1=\frac{1}{T_N}\left[\frac{-D}{2}\left(\frac{1}{A_2}-\frac{1}{A_1}\right)\right]\left[\frac{1}{F_o}\right] \qquad (A3.13(b))$$

$$a_2=\frac{1}{T_n\,2!}\left[\frac{-D}{2}\left(\frac{1}{A_2}-\frac{1}{A_1}\right)\right]^2\left[\frac{F_1}{F_o^3}\right] \qquad (A3.13(c))$$

$$a_3=\frac{1}{T_N 3!}\left[\frac{-D}{2}\left(\frac{1}{A_2}-\frac{1}{A_1}\right)\right]^3\left[\frac{3F_1^2-F_0F_2}{F_0^5}\right] \qquad (A3.13(d))$$

$$a_4=\frac{1}{T_N 4!}\left[\frac{-D}{2}\left(\frac{1}{A_2}-\frac{1}{A_1}\right)\right]^4\left[\frac{-10F_0F_1F_2+F_0^2F_3+15F_1^3}{F_0^7}\right] \qquad (A3.13(e))$$

$$a_5=\frac{1}{T_N 5!}\left[\frac{-D}{2}\left(\frac{1}{A_2}-\frac{1}{A_1}\right)\right]^5\left[\frac{15F_0^2F_1F_3+10F_0^2F_2^2+105F_1^4-F_0^2F_4-105F_0F_1^2F_3}{F_0^9}\right] \qquad (A3.13(f))$$

$$a_6=\frac{1}{T_N 6!}\left[\frac{-D}{2}\left(\frac{1}{A_2}-\frac{1}{A_1}\right)\right]^6\left[\frac{21F_0^3F_1F_4+35F_0^3F_2F_3+1260F_0F_1^3F_2-F_0^4F_5-}{F_0^{11}}\right.$$

$$\left.\frac{280F_0^2F_1F_2^2-945F_1^5-210F_0^2F_1^2F_3}{F_0^{11}}\right] \qquad (A3.13(g))$$

$$a_7=\frac{1}{T_N 7!}\left[\frac{-D}{2}\left(\frac{1}{A_2}-\frac{1}{A_1}\right)\right]^7\left[\frac{28F_0^4F_1F_5+56F_0^4F_2F_4+35F_0^4F_3^2+3150F_0^2F_1^3F_3+}{F_0^{13}}\right.$$

$$\frac{6300F_0^2F_1^2F_2^2+10395F_1^6-F_0^5F_6-378F_0^3F_1^2F_4-}{F_0^{13}}$$

$$\left.\frac{1260F_0^3F_1F_2F_3-280F_0^3F_2^3-17325F_0F_1^4F_2}{F_0^{13}}\right] \qquad (A3.13(h))$$

where: $$T_N=\frac{1}{(1+\alpha)CR}\left[\frac{1}{1+\frac{T_a}{(1+\alpha)CR}}\right] \qquad (A3.14(a))$$

$$A_2=\left\{1+\frac{2.1}{2!}\left(\frac{1}{\gamma}\right)+\frac{2^2.1.3}{3!}\left(\frac{1}{\gamma}\right)^2+\frac{2^3.1.3.5}{4!}\left(\frac{1}{\gamma}\right)^3+----\right\} \qquad (A3.14(b))$$

$$A_1=\gamma-A_2 \qquad (A3.14(c))$$

$$\gamma=\frac{CR}{T_a}\left[\frac{T_a}{CR}+1+\alpha\right]^2 \qquad (A3.14(d))$$

$$F_n=\frac{A_2^n\exp\left(-A_2T_N\frac{\overset{\circ}{t}_1}{T_c}\right)}{1+\exp\left(\frac{-A_2T_N}{2}\right)}-\frac{A_1^n\exp\left(-A_1T_N\frac{\overset{\circ}{t}_1}{T_c}\right)}{1+\exp\left(\frac{-A_1T_N}{2}\right)} \qquad (A3.14(e))$$

Substituting equations A3.4 and A3.6 in equation A3.11 enables the term D to be expressed as:

$$D=\left\{1-2\left[1+\exp\left(\frac{-A_1T_N}{2}\right)\right]^{\frac{A_2}{A_1-A_2}}\left[1+\exp\left(\frac{-A_2T_N}{2}\right)\right]^{\frac{-A_1}{A_1-A_2}}\right\} \qquad (A3.15)$$

The unmodulated position $\overset{\circ}{t}_1$ of the pulse leading edge is obtained by numerical solution of equation A3.1. with M set to zero. Therefore, substituting equations A3.5 and A3.6 in equation A3.1, and setting M=0 gives the following expression, which defines $\frac{\overset{\circ}{t}_1}{T_c}$.

$$1-\frac{2\left(\frac{A_2}{A_2-A_1}\right)}{1+\exp\left(\frac{-A_1T_N}{2}\right)}\exp\left(-A_1T_N\frac{\overset{\circ}{t}_1}{T_c}\right)-\frac{2\left(\frac{A_1}{A_1-A_2}\right)}{1+\exp\left(\frac{-A_2T_N}{2}\right)}\exp\left(-A_2T_N\frac{\overset{\circ}{t}_1}{T_c}\right)=0 \qquad (A3.16)$$

Thus, the coefficients a_n in the power series expression for the position of the pulse leading edge have been expressed in terms of the parameters T_N and Υ.

It is now necessary to carry out a similar procedure to determine the coefficients b_n in the power series for t_2. If M is set to zero in equations A3.1 and A3.2, then $t_1=\overset{\circ}{t}_1$ and $t_2=\overset{\circ}{t}_2$. Therefore, from equation A3.1:

$$1-\frac{2\left(\frac{k_2}{k_2-k_1}\right)}{1+\exp\left(\frac{-k_1T_c}{2}\right)}\exp\left(-k_1\overset{\circ}{t}_1\right)-\frac{2\left(\frac{k_1}{k_1-k_2}\right)}{1+\exp\left(\frac{-k_2T_c}{2}\right)}\exp\left(-k_2\overset{\circ}{t}_1\right)=0 \qquad (A3.17)$$

and from equation A3.2:

$$1-\frac{2\left(\frac{k_2}{k_2-k_1}\right)}{1+\exp\left(\frac{-k_1T_c}{2}\right)}\exp\left[-k_1\left(\overset{\circ}{t}_2-\frac{T_c}{2}\right)\right]-\frac{2\left(\frac{k_1}{k_1-k_2}\right)}{1+\exp\left(\frac{-k_2T_c}{2}\right)}\exp\left[-k_2\left(\overset{\circ}{t}_2-\frac{T_c}{2}\right)\right]=0 \qquad (A3.18)$$

Since equations A3.17 and A3.18 are identical in form, it may be deduced that:

$$\overset{\circ}{t}_1=\overset{\circ}{t}_2-\frac{T_c}{2} \qquad (A3.19)$$

By Maclaurins theroem, the coefficients b_n in equation A3.4 may be expressed as:

$$b_n=\frac{1}{T_c}\,\frac{1}{n!}\left[\frac{d}{dM^n}\left(t_2-\frac{T_c}{2}\right)\right]_{M=0} \qquad (A3.20)$$

Differentiating equation A3.2 with respect to M leads to the following expression for the first differential of $t_2 - \frac{T_c}{2}$ with respect to M:

$$\frac{d}{dM}\left(t_2-\frac{T_c}{2}\right)=\frac{D}{2}\left[\frac{1}{k_2}-\frac{1}{k_1}\right]\left[\frac{1}{\dfrac{\exp\left[-k_2\left(t_2-\frac{T_c}{2}\right)\right]}{1+\exp\left(\frac{-k_2T_c}{2}\right)}-\dfrac{\exp\left[-k_1\left(t_2-\frac{T_c}{2}\right)\right]}{1+\exp\left(\frac{-k_1T_c}{2}\right)}}\right] \qquad (A3.21)$$

where D is given by equation A3.11 or A3.15.

Comparing equation A3.21 with equation A3.12 shows that:

$$\left[\frac{d}{dM}\left(t_2-\frac{T_c}{2}\right)\right]_{M=0}=-\left[\frac{dt_1}{dM}\right]_{M=0} \qquad (A3.22)$$

since $\overset{\circ}{t}_2 - \frac{T_c}{2} = \overset{\circ}{t}_1$.

From the form of equations A3.12 and A3.21, it may be deduced that repeated differentiation of equation A3.21 will lead to the following result.

$$\left[\frac{d^n}{dM^n}\left(t_2-\frac{T_c}{2}\right)\right]_{M=0} = (-1)^n\left[\frac{d^n t_1}{dM^n}\right]_{M=0} \qquad (A3.23)$$

Therefore, from equations A3.20 and A3.10:

$$b_n = (-1)^n . a_n \qquad (A3.24)$$

Thus, the position t_2 of the trailing edges of the pulses is given by:

$$\frac{t_2}{T_c} - \frac{1}{2} = \sum_{n=0}^{\infty} (-1)^n a_n M^n \qquad (A3.25)$$

The unmodulated position $\overset{\circ}{t}_1$ of the pulse leading edge may be evaluated by applying Newton's successive-approximation method to equation A3.16:

$$\left(\frac{\overset{\circ}{t}_1}{T_c}\right)_{n+1} = \left(\frac{\overset{\circ}{t}_1}{T_c}\right)_n - \frac{f\left(\frac{\overset{\circ}{t}_1}{T_c}\right)_n}{f'\left(\frac{\overset{\circ}{t}_1}{T_c}\right)_n} \qquad (A3.26)$$

where: $(\frac{\overset{\circ}{t}_1}{T_c})_n$ is the n^{th} approximation to $\frac{\overset{\circ}{t}_1}{T_c}$

$$f\left(\frac{\overset{\circ}{t}_1}{T_c}\right) = 1 - \frac{2\left(\frac{A_2}{A_2-A_1}\right)}{1+\exp\left(\frac{-A_1T_N}{2}\right)}\exp\left(-A_1T_N\frac{\overset{\circ}{t}_1}{T_c}\right) - \frac{2\left(\frac{A_1}{A_1-A_2}\right)}{1+\exp\left(\frac{-A_2T_N}{2}\right)}\exp\left(-A_2T_N\frac{\overset{\circ}{t}_1}{T_c}\right) \qquad (A3.27)$$

$f'(\frac{\overset{\circ}{t}_1}{T_c})$ is the first derivative of $f(\frac{\overset{\circ}{t}_1}{T_c})$

$$f'\left(\frac{\overset{\circ}{t}_1}{T_c}\right) = \frac{2\left(\frac{A_1A_2T_N}{A_2-A_1}\right)}{1+\exp\left(\frac{-A_1T_N}{2}\right)}\exp\left(-A_1T_N\frac{\overset{\circ}{t}_1}{T_c}\right) + \frac{2\left(\frac{A_1A_2T_N}{A_1-A_2}\right)}{1+\exp\left(\frac{-A_2T_N}{2}\right)}\exp\left(-A_2T_N\frac{\overset{\circ}{t}_1}{T_c}\right) \qquad (A3.28)$$

Considerable care has to be taken when evaluating $f(\frac{\overset{\circ}{t}_1}{T_c})$ for small values of T_N, since rounding errors can be significant. By suitably rearranging equation A3.27, and expanding the terms $\exp(-A_2 T_N \frac{\overset{\circ}{t}_1}{T_c})$ and $\exp(\frac{-A_2 T_N}{2})$ as infinite series, the following expression is obtained for $f(\frac{\overset{\circ}{t}_1}{T_c})$:

$$f\left(\frac{\overset{\circ}{t}_1}{T_c}\right) \frac{A_2}{A_2-A_1}\left\{1-\frac{2\exp\left(-A_1T_N\frac{\overset{\circ}{t}_1}{T_c}\right)}{1+\exp\left(\frac{-A_1T_N}{2}\right)}-\frac{A_1}{A_2}\frac{\sum_{n=1}^{\infty}\frac{(-A_2T_N)^n}{n!}\left[\left(\frac{1}{2}\right)^n-2\left(\frac{\overset{\circ}{t}_1}{T_c}\right)^n\right]}{1+\exp\left(\frac{-A_2T_N}{2}\right)}\right\} \qquad (A3.29)$$

For practical values of the system parameters, $A_1 T_N$ is always considerably greater than unity. Consequently, direct evaluation of the first of the brackets on the right hand side of equation A3.29 presents no difficulties. Rounding errors will still exist in evaluating $f(\frac{\overset{\circ}{t}_1}{T_c})$ from equation A3.29, but the error will be very much less than direct evaluation from equation A3.27.

The ratio $\dfrac{f(\frac{\overset{\circ}{t}_1}{T_c})}{f'(\frac{\overset{\circ}{t}_1}{T_c})}$ can now be expressed as:

$$\frac{f\left(\frac{\overset{\circ}{t}_1}{T_c}\right)}{f'\left(\frac{\overset{\circ}{t}_1}{T_c}\right)} \frac{A_2\left\{1-\frac{2\exp\left(-A_1T_N\frac{\overset{\circ}{t}_1}{T_c}\right)}{1+\exp\left(\frac{-A_1T_N}{2}\right)}\right\}-A_1\frac{\sum_{n=1}^{\infty}\frac{(-A_2T_N)^n}{n!}\left[\left(\frac{1}{2}\right)^n-2\left(\frac{\overset{\circ}{t}_1}{T_c}\right)\right]}{1+\exp\left(\frac{-A_2T_N}{2}\right)}}{\left\{\frac{\exp\left(-A_1T_N\frac{\overset{\circ}{t}_1}{T_c}\right)}{1+\exp\left(\frac{-A_1T_N}{2}\right)}-\frac{\exp\left(-A_2T_N\frac{\overset{\circ}{t}_1}{T_c}\right)}{1+\exp\left(\frac{-A_2T_N}{2}\right)}\right\}2A_1A_2T_N} \qquad (A3.30)$$

In order to make use of Newton's successive-approximation method, it is necessary to have an initial estimate of $\frac{\overset{\circ}{t}_1}{T_c}$. This initial estimate could be zero. However, a better value is 0.25, since the unmodulated position of the leading edge of the pulse in an ideal double-edge pulse-length modulation system is $\overset{\circ}{t}_1 = \frac{T_c}{4}$.

Direct evaluation of the term D from equation A3.15 will give rise to errors since, for small values of T_N and the range of values of A_1 that arise from practical values of the system parameters, D is much less than unity.

From equation A3.15:

$$D = \frac{1}{1+\exp\left(\frac{-A_2T_N}{2}\right)}\left\{1+\exp\left(\frac{-A_2T_N}{2}\right)-2\left[\frac{1+\exp\left(\frac{-A_1T_N}{2}\right)}{1+\exp\left(\frac{-A_2T_N}{2}\right)}\right]^{\frac{A_2}{A_1-A_2}}\right\} \qquad (A3.31)$$

Making use of the expansion $x^a = \sum_{n=0}^{\infty}\frac{1}{n!}(a.\log x)^n$, and the usual expansion for e^{-x}, equation A3.31 may be written as:

$$D = \frac{1}{1+\exp\left(\frac{-A_2T_N}{2}\right)}\left\{1+\sum_{n=0}^{\infty}\frac{1}{n!}\left(\frac{-A_2T_N}{2}\right)^n-2\sum_{n=0}^{\infty}\frac{1}{n!}\left[\frac{A_2}{A_1-A_2}\log\left(\frac{1+\exp\left(\frac{-A_1T_N}{2}\right)}{1+\exp\left(\frac{-A_2T_N}{2}\right)}\right)\right]^n\right\}$$

$$D = \frac{1}{1+\exp\left(\frac{-A_2T_N}{2}\right)}\sum_{n=1}^{\infty}\frac{1}{n!}\left\{\left(\frac{-A_2T_N}{2}\right)^n-2\left[\frac{A_2}{A_1-A_2}\log\left(\frac{1+\exp\left(\frac{-A_1T_N}{2}\right)}{1+\exp\left(\frac{-A_2T_N}{2}\right)}\right)\right]^n\right\} \qquad (A3.32)$$

Evaluation of D from equation A3.32 gives considerably greater accuracy than evaluating D directly from equation A3.15.

The numerical methods developed for evaluating the equations probably do not represent the optimum techniques but have been found adequate for evaluating the expressions on a digital computer which has an accuracy of approximately eight significant figures. Fig. A3.1 shows a flow chart of the method used for evaluating the equations on a digital computer.

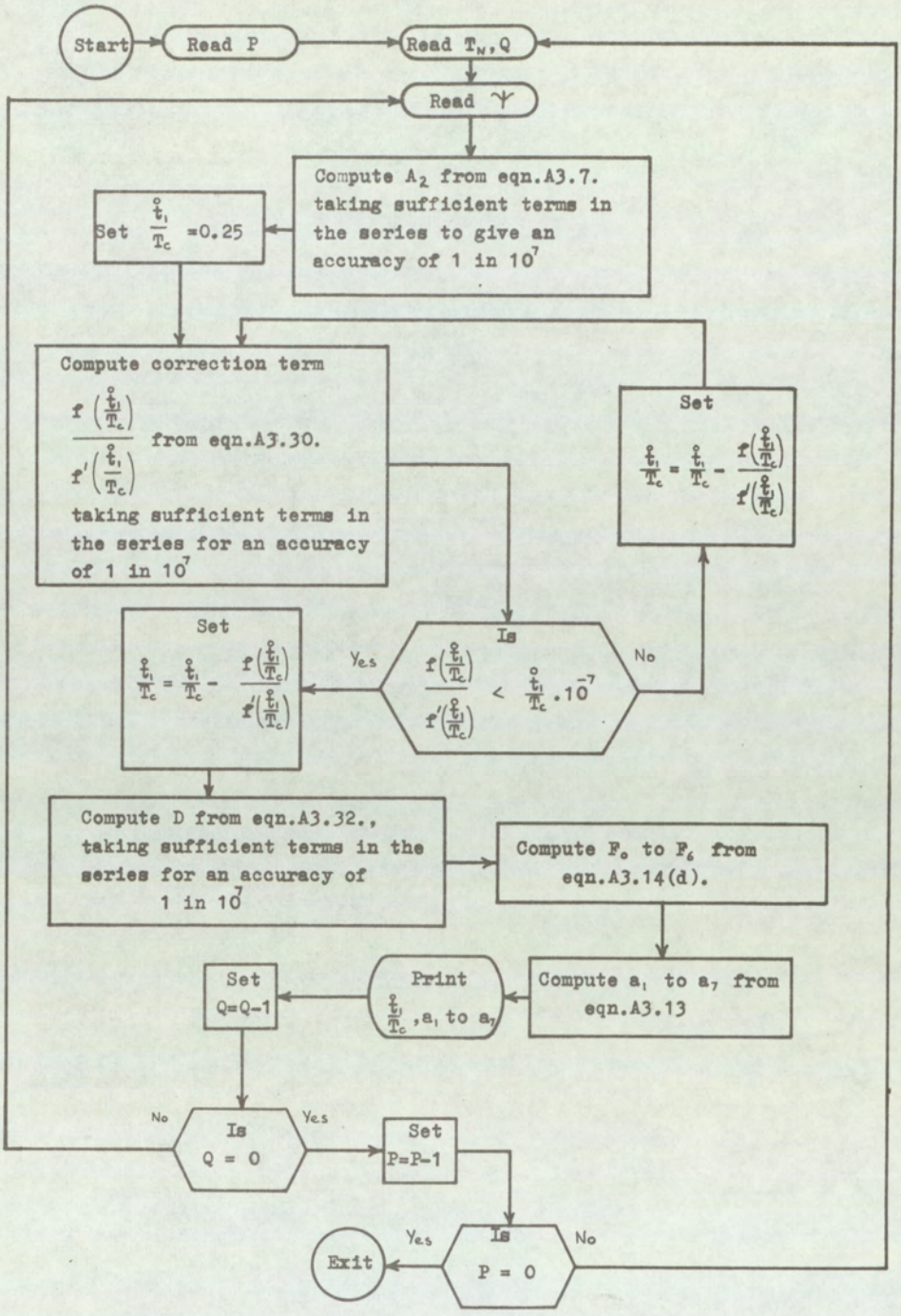

P = Number of values of T_N on data tape.
Q = Number of values of γ.

Fig.A3.1. Flowchart for computing the coefficients a_1 to a_7 .

Appendix 4 Derivation of the Frequency Spectrum for a Single-edge Modulation System with Finite Integrator Gain

The spectrum of a single-edge pulse-length modulated wavetrain, produced by a system having finite integrator gain, is given by the following expression (chapter II, section 4.2.1. equation 4.2.9.):

$$F(t)=\frac{1}{2\pi j}\sum_{p=-\infty}^{\infty}\frac{1}{p}\left\{\exp\left[jp\omega_c\left(t+\frac{T_o}{2}-\sum_{n=0}^{\infty}k_n.\cos(n\omega_m t)\right)\right]-\exp\left[jp\omega_c\left(t-\frac{T_o}{2}\right)\right]\right\} \qquad (A4.1)$$

The terms $\exp\left[-j.p.\omega_c k_n . \cos(n\omega_m t)\right]$ may be expanded as Bessel function series of the form:

$$\exp\left[-jp\omega_c k_n\cos(n\omega_m t)\right]=\sum(-j)^q J_q(p\omega_c k_n)\exp(jqn\omega_m t)$$

$$\therefore F(t)=\frac{1}{2\pi j}\sum_{p=-\infty}^{\infty}\frac{1}{p}\left\{\exp\left[jp\omega_c\left(t+\frac{T_o}{2}-k_o\right)\right]\times \prod_{n=1}^{\infty}\left[\sum_{q=-\infty}^{\infty}(-j)^q J_q(p\omega_c k_n)\exp(jqn\omega_m t)\right]-\exp\left[jp\omega_c\left(t-\frac{T_o}{2}\right)\right]\right\} \qquad (A4.2)$$

Manipulation of the above expression is obviously rather

difficult and the results are likely to be too complex to be of use. In order to ease the problem it is assumed that the first three harmonic terms of ω_m will give an adequate representation. Equation A4.2. now becomes:

$$F(t) \triangleq \frac{1}{2\pi j} \sum_{p=-\infty}^{\infty} \frac{1}{p} \left\{ \exp\left[jp\omega_c\left(t+\frac{T_o}{2}-k_o\right)\right] \times \right.$$

$$\sum_{\substack{e,f,g \\ =-\infty}}^{\infty} J_e(p\omega_c k_1) J_f(p\omega_c k_2) J_g(p\omega_c k_3) \times \exp\left[j(e+2f+3g)\omega_m t\right] -$$

$$\left. \exp\left[jp\omega_c\left(t-\frac{T_o}{2}\right)\right]\right\} \qquad (A4.3)$$

Rewriting equation A4.3. in terms of only positive values of p, and temporarily disregarding the term corresponding to p = 0, gives:

$$F(t) \triangleq \frac{1}{2\pi j} \sum_{p=1}^{\infty} \frac{1}{p} \left\{ -2j \sin\left[p\omega_c\left(t-\frac{T_o}{2}\right)\right] + \right.$$

$$+ \sum_{\substack{e,f,g \\ =-\infty}}^{\infty} J_e(p\omega_c k_1) J_f(p\omega_c k_1) J_g(p\omega_c k_2) \times$$

$$\left[(-1)^{e+f+g} \exp\left(j\left[p\omega_c\left(t+\frac{T_o}{2}-k_o\right)+(e+2f+3g)\omega_m t\right]\right)-\right.$$

$$\left.\exp\left(-j\left[p\omega_c\left(t+\frac{T_o}{2}-k_o\right)-(e+2f+3g)\omega_m t\right]\right)\right]\Bigg\} \qquad (A4.4)$$

Since the second of the summations in the above expression is over all positive and negative combinations of e, f and g, the second of the exponential terms within the summation can be written in terms of the negative combination of e, f and g.

$$F(t) \triangleq \frac{1}{2\pi j}\sum_{p=1}^{\infty}\frac{1}{p}\Bigg\{-2j\sin\left[p\omega_c\left(t-\frac{T_o}{2}\right)\right]+$$

$$\sum_{\substack{e,f,g\\=-\infty}}^{\infty}\Bigg[(j)^{e+f+g}\,J_e(p\omega_c k_1)\,J_f(p\omega_c k_2)\,J_g(p\omega_c k_3)\times$$

$$(-1)^{e+f+g}\exp\left(j\left[p\omega_c\left(t+\frac{T_o}{2}-k_o\right)+(e+2f+3g)\omega_m t\right]\right)-$$

$$(j)^{-e-f-g}\,J_{-e}(p\omega_c k_1)\,J_{-f}(p\omega_c k_2)\,J_{-g}(p\omega_c k_3)\times$$

$$\left.\exp\left(-j\left[p\omega_c\left(t+\frac{T_o}{2}-k_o\right)-(-e-2f-3g)\omega_m t\right]\right)\right]\Bigg\} \qquad (A4.5)$$

$$\therefore F(t) = \frac{1}{\pi} \sum_{p=1}^{\infty} \frac{1}{p} \left\{ -\sin\left[p\omega_c \left(t - \frac{T_o}{2} \right) \right] + \right.$$

$$\sum_{\substack{e,f,g \\ =-\infty}}^{\infty} J_e(p\omega_c k_1)\, J_f(p\omega_c k_2)\, J_g(p\omega_c k_3) \times$$

$$\left. \sin\left[\left(p\omega_c + \left[e+2f+3g \right] \omega_m \right) t + p\omega_c \left(\frac{T_o}{2} - k_o \right) - \left(e+f+g \right) \frac{\pi}{2} \right] \right\} \qquad (A4.6)$$

It is now necessary to determine the expression for F(t) when p = 0 since this term has been disregarded from equation A4.4. onwards. From equation A4.1., the expression for F(t) is indeterminate when p = 0 so that L'Hopital'srule for the limit of a quotient must be applied. This gives:

$$F(t)\Big|_{p=0} = \frac{1}{T_c} \left[T_o - \sum_{n=1}^{\infty} k_n . \cos(n\omega_m t) \right]$$

Taking the first three harmonic terms in the above expression, the complete frequency spectrum becomes:

$$F(t) \triangleq \frac{1}{T_c} \left[T_o - k_o . \cos(\omega_m t) - k_2 . \cos(2\omega_m t) - k_3 . \cos(3\omega_m t) \right] +$$

$$\frac{1}{\pi} \sum_{p=1}^{\infty} \frac{1}{p} \left\{ -\sin\left[p\omega_c \left(t - \frac{T_o}{2} \right) \right] + \right.$$

$$\sum_{\substack{e,f,g \\ =-\infty}}^{\infty} J_e(p\omega_c k_1)\ J_f(p\omega_c k_2)\ J_g(p\omega_c k_3) \times$$

$$\sin\left[\left(p\omega_c+\left[e+2f+3g\right]\omega_m\right)t+p\omega_c\left(\frac{T_o}{2}-k_o\right)-\left(e+f+g\right)\frac{\pi}{2}\right]\Bigg\} \qquad (A4.7)$$

Numerical Methods

Care is required in evaluating the constants, k_o, k_1, k_2 and k_3 in equation A4.7. when the normalised time constant $\frac{T_c}{(1+\alpha)CR}$ is small, since considerable rounding errors can occur. The expressions for the constants are given by equations 3.1.10(a). and (b) of section 3.2.1. (chapter II). The constant K which occurs in the expressions is given by equation 3.2.1(b). The equations are rewritten below for convenience:

$$k_o = -(1+\alpha)CR.\log\left\{\frac{\frac{1}{2}(MK)^2}{1-\sqrt{\left[1-(M.K)^2\right]}}\right\} \qquad (A4.8)$$

$$k_n=(1+\alpha)CR\,\frac{2}{n}\left\{\frac{1}{MK}-\left[\left(\frac{1}{MK}\right)^2-1\right]\right\}^n \qquad (4.9)$$

$$K=\frac{1-\exp\left[\frac{-T_c}{(1+\alpha)CR}\right]}{1+\exp\left[\frac{-T_c}{(1+\alpha)CR}\right]} \qquad (4.10)$$

For small values of $\frac{T_c}{(1+\ )CR}$, evaluation of K involves taking the difference of nearly equal numbers which leads to rounding errors. These errors may be avoided by expanding the exponential term in the numerator of equation A4.10. as an infinite series. Thus:

$$K=\frac{1}{1+\left(\frac{-T_c}{(1+\alpha)CR}\right)}\sum_{n=1}^{\infty}(-1)^{n+1}\frac{1}{n!}\left(\frac{T_c}{(1+\alpha)CR}\right)^n \qquad (4.11)$$

Since K is small when $\frac{T_c}{(1+\alpha)CR}$ is small, it can be seen that evaluation of the denominator of equation A4.8. will be susceptible to errors. This problem may be overcome by expanding the square root term by the bonomial theorem. This gives:

$$k_o = (1+\alpha)CR \log\left\{1+\frac{1}{2.2!}(MK)^2+\frac{1.3}{2^2.3!}(MK)^4+\frac{1.3.5}{2^3.4!}(MK)^6+\text{---}\right\} \quad (A4.12)$$

Rounding errors will also occur if k_n is evaluated directly from equation A4.9. for small values of $\frac{T_c}{(1+\alpha)CR}$. These errors are avoided by expanding the square root as a binomial series:

$$k_n = (1+\alpha)CR \frac{2}{n}\left\{\frac{MK}{2}\left[1+\frac{1}{2.2!}(MK)^2+\frac{1.3}{2^2.3!}(MK)^4+\frac{1.3.5}{2^3.4!}(MK)^6+\text{---}\right]\right\}^n \quad (A4.13)$$

The normalised unmodulated pulse-length $\frac{T_o}{T_c}$ is given by equation 3.2.4. of section 3.2.1. (chapter II) and is rewritten below:

$$\frac{T_o}{T_c} = 1+\frac{(1+\alpha)CR}{T_c} \log\frac{1}{2}\left[1+\exp\left(\frac{-T_c}{(1+\alpha)CR}\right)\right] \quad (A4.14)$$

The problems of evaluating the term $1 + \frac{2(1+\alpha)}{T_c} \times \log \frac{1}{2}\left[1 + \exp \frac{-T_c}{(1+\alpha)CR}\right]$ for small values of $\frac{T_c}{(1+\alpha)CR}$

are discussed in detail in appendix 1, and a series is derived for the term. Equation A4.14. may be rewritten as:

$$\frac{T_o}{T_c} = \frac{1}{2} + \frac{1}{2}\left\{1 + \frac{2(1+\alpha)CR}{T_c}\log\frac{1}{2}\left[1+\exp\left(\frac{-T_c}{(1+\alpha)CR}\right)\right]\right\} \qquad (A4.15)$$

Therefore, from equation A1.13. of appendix 1:

$$\frac{T_o}{T_c} \triangleq \frac{1}{2} + \frac{T_c}{(1+\alpha)CR}\cdot\frac{1}{8} - \left[\frac{T_c}{(1+\alpha)CR}\right]^3\frac{1}{198} + \left[\frac{T_c}{(1+\alpha)CR}\right]^5\frac{21}{60480} \qquad (A4.16)$$

The above expression is accurate to five decimal places for values of $\frac{T_c}{(1+\alpha)CR} < 0.1$. For larger values of normalised time constant $\frac{T_c}{(1+\alpha)CR}$, the normalised unmodulated pulse length may be evaluated directly from equation A4.14.

The Bessel function terms in equation A4.7. for the frequency spectrum are evaluated from the standard series:

$$J_n(x) = \sum_{q=0}^{\infty} \frac{(-1)^q}{q!\,(q+n)!}\left(\frac{x}{2}\right)^{n+2q} \qquad (A4.17)$$

Computational Methods

The first problem is to decide what limits must be set on the integer variables, e, f and g. Approximate calculations

show that no significant components will be neglected if the following limits are used:

$$-8 \leqslant e \leqslant 8$$

$$-6 \leqslant f \leqslant 6$$

$$-4 \leqslant g \leqslant 4$$

Having defined these limits, a computer programme can be written to determine which combinations of the integers give a particular sideband component $(\omega_c - N.\omega_m)$, where $N = e + 2f + 3g$. The maximum value chosen for N is 8. It is obviously undesirable to calculate these combinations for every set of values of system parameters so that it is necessary to store the combinations of e, f and g which give rise to a particular sideband component. It is also necessary to know how many combinations (I_N) there are for each sideband, in order to be able to read out the stored combinations.

Now the part of equation A4.7 which defines the sideband components is the summation containing the Bessel function terms, and this may be rewritten as:

$$\sum_{\substack{e,f,g \\ =-\infty}}^{\infty} J_{|e|}(p\omega_c k_1).J_{|f|}(p\omega_c k_2).J_{|g|}(p\omega_c k_3)\left(\frac{e}{|e|}\right)^{|e|}\left(\frac{f}{|f|}\right)^{|f|}\left(\frac{g}{|g|}\right)^{|g|}(-1)^{\frac{e+f+g}{2}} \times$$

$$\sin\left[\left(p\omega_c+\left[e+2f+3g\right]\omega_m\right)t+p\omega_c\left(\frac{T_o}{2}-k_o\right)\right] \qquad (A4.18)$$

for $e + f + g =$ even

and

$$\sum_{\substack{e,f,g \\ =-\infty}}^{\infty} J_{|e|}(p\omega_c k_1)\, J_{|f|}(p\omega_c k_2)\, J_{|g|}(p\omega_c k_3) \left(\frac{e}{|e|}\right)^{|e|} \left(\frac{f}{|f|}\right)^{|f|} \left(\frac{g}{|g|}\right)^{|g|} (-1)(-1)^{\frac{e+f+g+1}{2}} \times$$

$$\cos\left[\left(p\omega_c + [e+2f+3g]\,\omega_m\right)t + p\omega_c\left(\frac{T_o}{2} + k_o\right)\right] \qquad \text{(A4.19)}$$

for $e+f+g$ = odd

Two integer functions may therefore be defined for each combination. Namely:

$$SI = \left(\frac{e}{|e|}\right)^{|e|} \left(\frac{f}{|f|}\right)^{|f|} \left(\frac{g}{|g|}\right)^{|g|} (-1)^{\frac{e+f+g}{2}}$$

$$\text{Func} = 0$$

for $e+f+g$ = even (A4.20)

$$SI = \left(\frac{e}{|e|}\right)^{|e|} \left(\frac{f}{|f|}\right)^{|f|} \left(\frac{g}{|g|}\right)^{|g|} (-1)(-1)^{\frac{e+f+g+1}{2}}$$

$$\text{Func} = 1$$

for $e+f+g$ = odd (A4.21)

The factor (Func) indicates whether the contribution to the sideband is a sine wave or a cosine wave (i.e. Func = 0 for a sine wave, and Func = 1 for a cosine wave). Fig. A4.1. shows the flow chart for computing and storing the following information. The values of the integers e, f and g which give

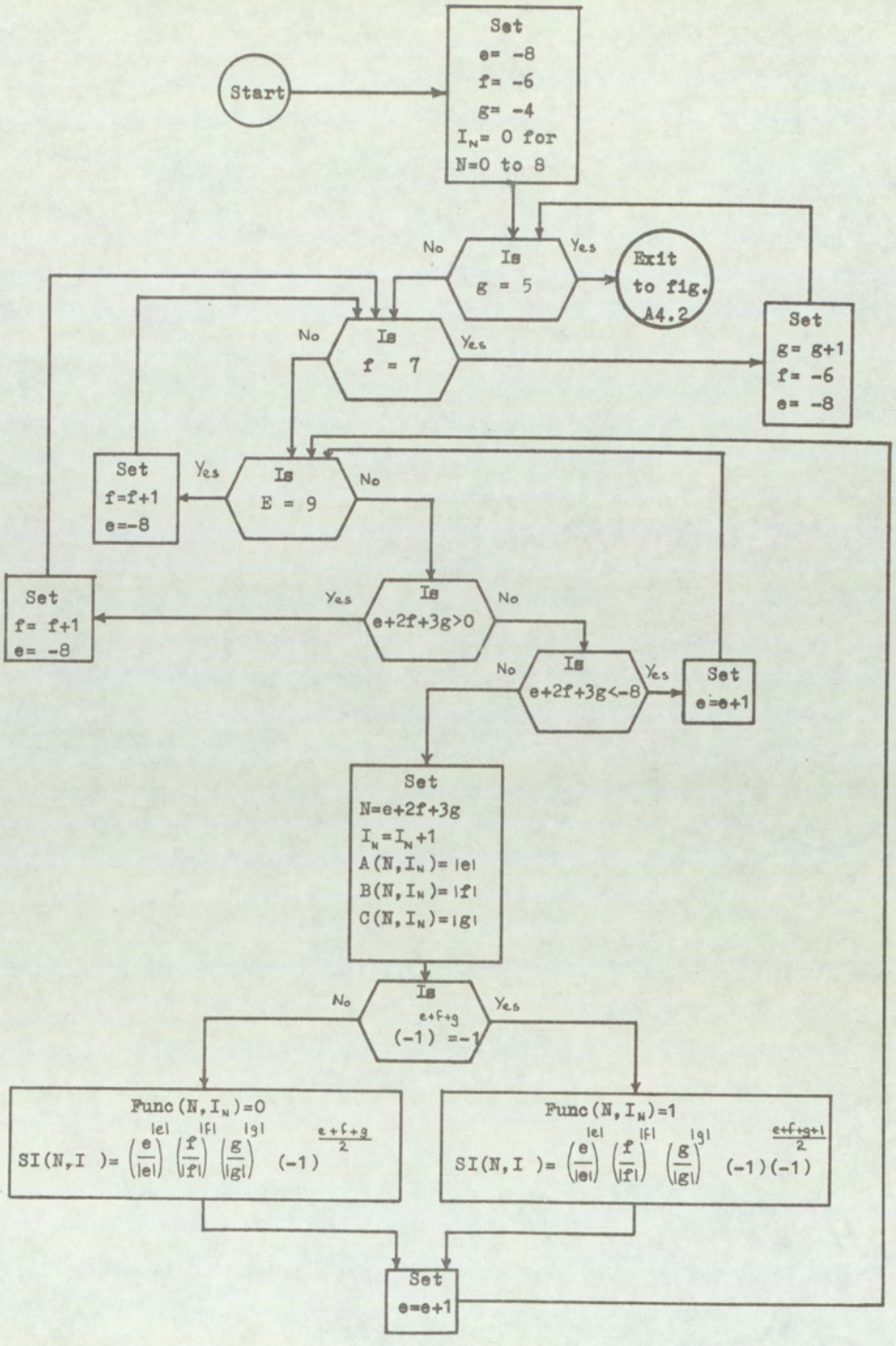

Fig.A4.1. Flowchart for computing sideband combinations.

rise to a particular sideband component $(\omega_c + N\omega_m)$, (where $-8 \leqslant N \leqslant 0$), the number of combinations (I_N) there are for each sideband, and two functions SI and Func for each combination. All the variables, except I_N, have a two-dimensional subscript in order to identify which sideband $(\omega_c - N\omega_m)$ the variable is associated with, and also the particular combination it is associated with. Thus the first subscript is N and the second subscript lies within the range 1 to I_N.

The flow chart for evaluating the amplitudes of the spectral components is shown in fig. A4.2. The method used is to calculate the amplitude of all the contributions to a particular sideband component and sum the components for which Func = 0, and also sum the components for which Func = 1. This gives an expression of the form:

$$\text{Sum1}.\sin\left[(p\omega_c + N\omega_m)t + p\omega_c\left(\frac{T_o}{2} - k_o\right)\right] +$$

$$\text{Sum2}.\cos\left[(p\omega_c + N\omega_m)t + p\omega_c\left(\frac{T_o}{2} - k_o\right)\right] \qquad (A4.22)$$

The expressions are evaluated only for the lower sidebands of the pulse repetition frequency (i.e. p = 1) since these are the most important sideband components. From equation A4.22 the amplitude of the sideband component is, therefore:

$$\text{Sideband amplitude} = \frac{1}{\pi}\sqrt{\left[(\text{Sum1})^2 + (\text{Sum2})^2\right]} \qquad (A4.23)$$

The amplitude of the repetition frequency component has an additional term, as may be seen from equation A4.7.

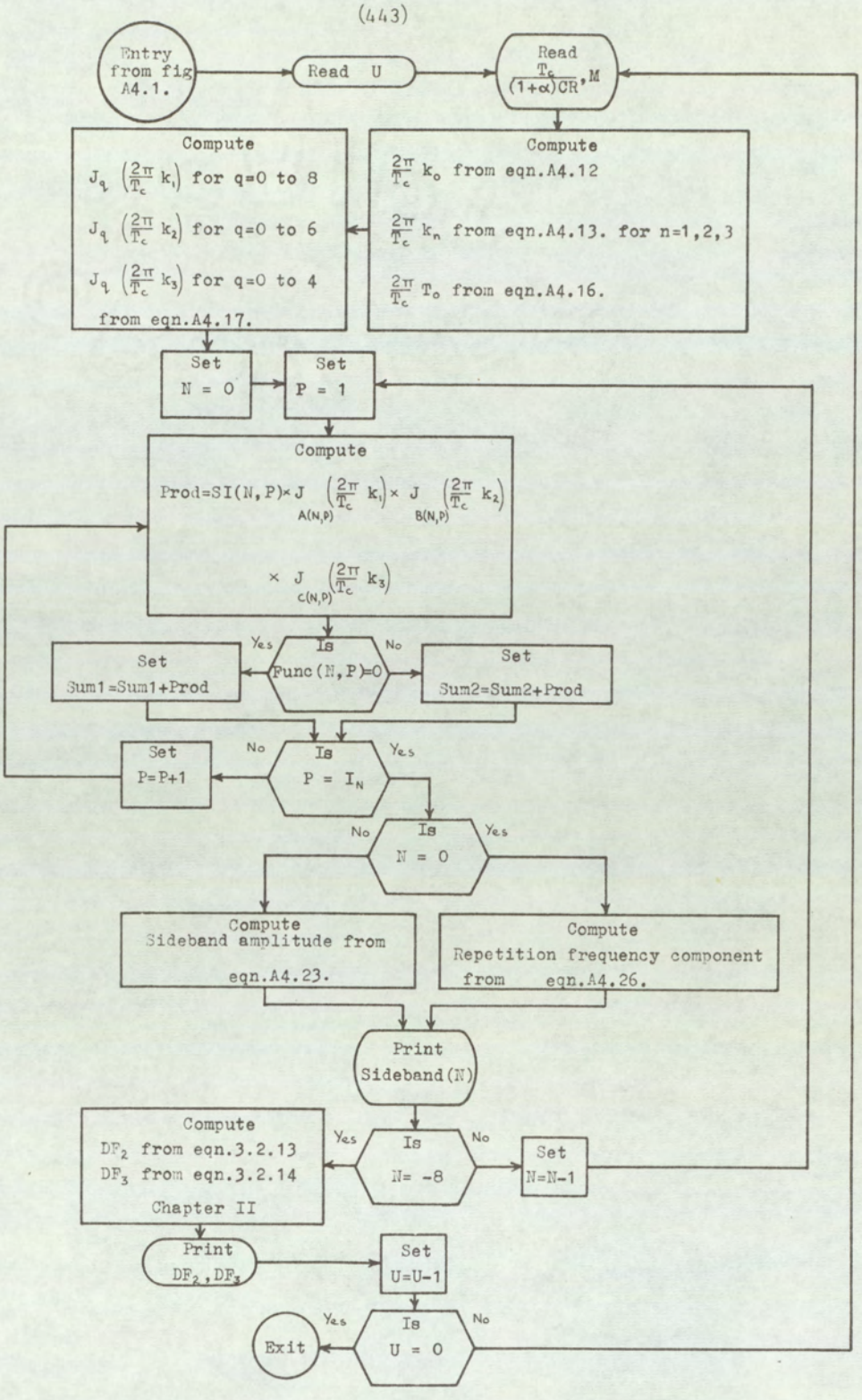

Fig.A4.2. Flowchart for computing amplitude of spectral components for single-edge modulation system with finite integrator gain.

Repetition frequency component =

$$\frac{1}{\pi}\left\{-\sin\left[\omega_c\left(t-\frac{T_o}{2}\right)\right]+\text{Sum1}.\sin\left[\omega_c t+\omega_c\left(\frac{T_o}{2}-k_o\right)\right]\right.$$

$$\left.+\text{Sum2}.\cos\left[\omega_c t+\omega_c\left(\frac{T_o}{2}-k_o\right)\right]\right\} \qquad \text{(A4.24)}$$

The above expression may be rewritten as:

$$\frac{1}{\pi}\left\{-\sin\left[\omega_c t+\omega_c\left(\frac{T_o}{2}-k_o\right)+\omega_c\left(k_o-T_o\right)\right]+\right.$$

$$\text{Sum1}.\sin\left[\omega_c t+\omega_c\left(\frac{T_o}{2}-k_o\right)\right]+$$

$$\left.\text{Sum2}.\cos\left[\omega_c t+\omega_c\left(\frac{T_o}{2}-k_o\right)\right]\right\} \qquad \text{(A4.25)}$$

Expanding the trigonometric terms in equation A4.25. gives the following expression for the amplitude of the repetition frequency component:

$$\frac{1}{\pi}\sqrt{\left\{\left[\text{Sum1}-\cos\left(2\pi\left(\frac{k_o}{T_o}-\frac{T_o}{T_c}\right)\right)\right]^2+\right.}$$

$$\left.\left[\text{Sum2}-\sin\left(2\pi\left(\frac{k_o}{T_o}-\frac{T_o}{T_c}\right)\right)\right]^2\right\} \qquad \text{(A4.26)}$$

Appendix 5. Derivation of the Frequency Spectrum for a Double-Edge Modulation System with Finite Integrator Gain

The spectrum of a double-edge pulse-length modulated wavetrain, produced by a system having finite integrator gain, is given by equation 4.2.28. of section 4.2.2. , chapter II.

$$F(t)=\frac{1}{2\pi j}\sum_{p=-\infty}^{\infty}\frac{1}{p}\left\{\exp\left[jp\omega_c\left(t+\frac{T_c}{4}-\sum_{n=0}^{\infty}k_n.\cos(n\omega_m t)\right)\right]-\right.$$

$$\left.\exp\left[jp\omega_c\left(t-\frac{T_c}{4}-\sum_{n=0}^{\infty}(-1)^n k_n.\cos(n\omega_m t)\right)\right]\right\} \qquad (A5.1)$$

The terms $\exp\left[-jp\omega_c k_n \cos(n\omega_m t)\right]$ may be expanded as Bessel function series of the form:

$$\exp\left[-jp\omega_c k_n\cos(n\omega_m t)\right]\sum_{q=-\infty}^{\infty}(-j)^q J_q(p\omega_c k_n)\exp(jqn\omega_m t)$$

$$\therefore F(t)=\frac{1}{2\pi j}\sum_{p=-\infty}^{\infty}\frac{1}{p}\left\{\exp\left[jp\omega_c\left(t+\frac{T_c}{4}-k_o\right)\right]\times\right.$$

$$\prod_{n=1}^{\infty}\left[\sum_{q=-\infty}^{\infty}(-j)^q J_q(p\omega_c k_n)\exp(jqn\omega_m t)\right]-$$

$$\exp\left[jp\omega_c\left(t-\frac{T_c}{4}-k_o\right)\right]\times$$

$$\left.\prod_{n=1}^{\infty}\left[\sum_{q=-\infty}^{\infty}(-1)^n(-j)^q J_q(p\omega_c k_n)\exp(jqn\omega_m t)\right]\right\} \qquad (A5.2)$$

Manipulation of equation A5. 2. is extremely difficult and the results are likely to be too complex to be of use. In order to ease the problem, the assumption is made that the first three terms containing harmonics of ω_m will give an adequate representation. Equation A5. 2. now becomes:

$$F(t) \triangleq \frac{1}{2\pi j} \sum_{p=-\infty}^{\infty} \frac{1}{p} \Bigg\{ \sum_{\substack{e,f,g \\ =-\infty}}^{\infty} J_e(p\omega_c k_1) J_f(p\omega_c k_2) J_g(p\omega_c k_3) \times$$

$$\exp\left[j(e+2f+3g)\omega_m t\right] \Big[(-j)^{e+f+g} \exp\left[jp\omega_c\left(t+\frac{T_c}{4}-k_o\right)\right] -$$

$$(-1)^{e+g} (-j)^{e+f+g} \exp\left[jp\omega_c\left(t-\frac{T_c}{4}-k_o\right)\right] \Big] \Bigg\} \qquad (A5.3)$$

Rewriting equation A5. 2. in terms of only positive values of p, and temporarily disregarding the term corresponding to p = 0, gives

$$F(t) \triangleq \frac{1}{2\pi j} \sum_{p=1}^{\infty} \frac{1}{p} \Bigg\{ \sum_{\substack{e,f,g=-\infty \\ e+g=\text{even}}}^{\infty} J_e(p\omega_c k_1) J_f(p\omega_c k_2) J_g(p\omega_c k_3) \times$$

$$\exp\left[j(e+2f+3g)\omega_m t\right] (-j)^{e+f+g} 2j \sin\left(\frac{p\omega_c T_c}{4}\right) \times$$

$$\left[\exp\left[jp\omega_c(t-k_o)\right] + (-1)^{e+f+g} \exp\left[-jp\omega_c(t-k_o)\right] \right] +$$

$$\sum_{\substack{e,f,g=-\infty \\ e+g=\text{odd}}}^{\infty} J_e(p\omega_c k_1)\, J_f(p\omega_c k_2)\, J_g(p\omega_c k_3) \times$$

$$\exp\left[j(e+2f+3g)\omega_m t\right](-j)^{e+f+g}\, 2.\cos\left(\frac{p\omega_c T_c}{4}\right) \times$$

$$\left[\exp\left[jp\omega_c(t-k_o)\right]-(-1)^{e+f+g}\exp\left[-jp\omega_c(t-k_o)\right]\right]\Bigg\} \qquad \text{(A5.4)}$$

Since the summations involving e, f and g are over all positive and negative combinations of e, f and g, equation A5.4. may be expressed as:

$$F(t)\triangleq\frac{1}{2\pi j}\sum_{p=1}^{\infty}\frac{1}{P}\Bigg\{\sum_{\substack{e,f,g=-\infty \\ e+g=\text{even}}}^{\infty} J_e(p\omega_c k_1)\, J_f(p\omega_c k_2)\, J_g(p\omega_c k_3)(-j)^{e+f+g}\, 2j\sin\left(\frac{p\omega_c T_c}{4}\right) \times$$

$$\exp\left[j\left(p\omega_c(t-k_o)+(e+2f+3g)\omega_m t\right)\right] +$$

$$\sum_{\substack{e,f,g=-\infty \\ e+g=\text{even}}}^{\infty} J_{-e}(p\omega_c k_1)\, J_{-f}(p\omega_c k_2)\, J_{-g}(p\omega_c k_3)(-j)^{-e-f-g}\, 2j\sin\left(\frac{p\omega_c T_c}{4}\right) \times$$

$$(-1)^{e+f+g} \exp\left[-j\left(p\omega_c(t-k_o)-(-e-2f-3g)\omega_m t\right)\right] +$$

$$\sum_{\substack{e,f,g=-\infty \\ e+g=\text{odd}}}^{\infty} J_e(p\omega_c k_1)\, J_f(p\omega_c k_2)\, J_g(p\omega_c k_3)\,(-j)^{e+f+g}\, 2.\cos\left(\frac{p\omega_c T_c}{4}\right) \times$$

$$\exp\left[j\left(p\omega_c(t-k_o)+(e+2f+3g)\omega_m t\right)\right] -$$

$$\sum_{\substack{e,f,g=-\infty \\ e+g=\text{odd}}}^{\infty} J_{-e}(p\omega_c k_1)\, J_{-f}(p\omega_c k_2)\, J_{-g}(p\omega_c k_3)\,(-j)^{-e-f-g}\, 2.\cos\left(\frac{p\omega_c T_c}{4}\right) \times$$

$$(-1)^{-e-f-g} \exp\left[-j\left(p\omega_c(t-k_o)-(-e-2f-3g)\right)\right]\Bigg\} \qquad \text{(A5.5)}$$

The above expression may be simplified to give:

$$F(t) \triangleq \frac{2}{\pi}\sum_{p=1}^{\infty}\frac{1}{p}\left\{\sum_{e,f,g=-\infty}^{\infty} J_e(p\omega_c k_1)\, J_f(p\omega_c k_2)\, J_g(p\omega_c k_2) \times \right.$$

$$\sin\left(\frac{p\omega_c T_c}{4} - (e+g)\frac{\pi}{2}\right) \times$$

$$\left.\cos\left[\left(p\omega_c + (e+2f+3g)\omega_m\right)t - p\omega_c k_o - f\frac{\pi}{2}\right]\right\} \qquad (5.6)$$

It is now necessary to determine the expression for F(t) when = 0 since this term has been disregarded from equation A5.4 onwards. From equation A5.1., the expression for F(t) is indeterminate when p = 0 so that L'Hopital's rule for the limit of a quotient must be applied. This gives:

$$F(t)\Big|_{p=0} = \frac{1}{T_c}\left\{\frac{T_c}{2} - \sum_{n=0}^{\infty}\left(1-(-1)^n\right)k_n \cdot \cos(n\omega_m t)\right\} \qquad (5.7)$$

Taking the first three harmonic terms in the above expression (i.e. n = 0 to 3), the complete expression for the frequency spectrum becomes:

$$F(t) \triangleq \frac{1}{2} - \frac{k_1}{T_c}\cos(n\omega_m t) - \frac{k_3}{T_c}\cos(3\omega_m t) +$$

$$\frac{2}{\pi}\sum_{p=1}^{\infty}\frac{1}{p}\left\{\sum_{e,f,g=-\infty}^{\infty} J_e(p\omega_c k_1)\, J_f(p\omega_c k_2)\, J_g(p\omega_c k_3) \times \right.$$

$$\left.\sin\left(\frac{\pi}{2}(p-e-g)\right)\cos\left[\left(p\omega_c + (e+2f+3g)\omega_m t\right) - p\omega_c k_o - f\frac{\pi}{2}\right]\right\} \qquad (5.8)$$

Numerical Methods

When evaluating the constants k_1, k_2 and k_3 in equation A5.8, care must be exercised since appreciable rounding errors can occur for small values of $\frac{T_c}{(1+\alpha)CR}$. The expressions for the constants are given by equation 3.2.29(b). The constant K which occurs in the expressions is given by equation 3.2.19. (section 3.2.2., chapter II). The equations are rewritten below for convenience:

$$k_n = (1+\alpha)CR\frac{2}{n}\left\{\frac{1}{MK} - \sqrt{\left[\left(\frac{1}{MK}\right)^2 - 1\right]}\right\}^n \qquad (A5.9)$$

$$K = \frac{1-\exp\left(\frac{-T_c}{2(1+\alpha)CR}\right)}{1+\exp\left(\frac{-T_c}{2(1+\alpha)CR}\right)} \qquad (A5.10)$$

For small values of $\frac{T_c}{(1+\alpha)CR}$, evaluation of K involves taking the difference of nearly equal numbers, which may lead to errors. These errors may be avoided by expanding the exponential term in the numerator of equation A5.10. as an infinite series. Thus:

$$K = \frac{1}{1+\exp\left(\frac{-T_c}{2(1+\alpha)CR}\right)} \sum_{n=1}^{\infty} (-1)^{n+1} \frac{1}{n!}\left(\frac{T_c}{2(1+\alpha)CR}\right)^n \qquad (A5.11)$$

Since K is small when $\frac{T_c}{(1+\alpha)CR}$ is small it can be seen

that evaluation of equation A5.9. for k_n will be susceptible to errors. These errors are avoided by expanding the square root term as a binomial series. Therefore:

$$k_n=(1+\alpha)CR\,\frac{2}{n}\left\{\frac{MK}{2}\left[1+\frac{1}{2.2!}(MK)^2+\frac{1.3}{2.3!}(MK)^4+\frac{1.3.5}{2^3.4!}(MK)^6+\cdots\right]\right\} \qquad (A5.12)$$

The Bessel function terms in the expression for the frequency spectrum (equation A5.7.) are evaluated from the standard series:

$$J_n(x)=\sum_{q=0}^{\infty}\frac{(-1)^q}{q!\,(q+n)!}\left(\frac{x}{2}\right)^{n+2q} \qquad (A5.13)$$

Computational Methods

The general method of computing the amplitude of the spectral components is very similar to that discussed in appendix A4. in relation to the single-edge modulation system, so only a brief description will be given here. The sidebands of interest are the lower order sidebands of the pulse repetition frequency (i.e. p = 1 in equation A5.8.). The term which defines the sidebands, in equation A5.8. is the summation containing the Bessel function terms. Setting p = 1, the summation may be rewritten as:

$$\sum_{e,f,g=-\infty}^{\infty} J_{|e|}(\omega_c k_1)\, J_{|f|}(\omega_c k_2)\, J_{|g|}(\omega_c k_3) \left(\frac{e}{|e|}\right)^{|e|} \left(\frac{f}{|f|}\right)^{|f|} \left(\frac{g}{|g|}\right)^{|g|} (-1)^{\frac{e+g}{2}} (-1)^{\frac{f}{2}} \times$$

$$\sin\left\{\left[\omega_c + (e+2f+3g)\omega_m\right]t - \omega_c k_o\right\} \qquad \text{(A5.14)}$$

for $e+g$ = even , f = even

$$\sum_{e,f,g=-\infty}^{\infty} J_{|e|}(\omega_c k_1)\, J_{|f|}(\omega_c k_2)\, J_{|g|}(\omega_c k_3) \left(\frac{e}{|e|}\right)^{|e|} \left(\frac{f}{|f|}\right)^{|f|} \left(\frac{g}{|g|}\right)^{|g|} (-1)^{\frac{e+g}{2}} (-1)^{\frac{f+1}{2}} \times$$

$$\cos\left\{\left[\omega_c + (e+2f+3g)\omega_m\right]t - \omega_c k_o\right\} \qquad \text{(A5.15)}$$

for $e+g$ = even , f = odd

The sideband components are zero when $e + g$ is odd.

Thus for each combination of the integers e, f and g which gives a particular sideband component, two integer variables can be defined:

$$SI = \left(\frac{e}{|e|}\right)^{|e|} \left(\frac{f}{|f|}\right)^{|f|} \left(\frac{g}{|g|}\right)^{|g|} (-1)^{\frac{e+f+g}{2}}$$

$$\text{Func} = 0$$

for $e+g$ = even , f = even (A5.16)

$$SI = \left(\frac{e}{|e|}\right)^{|e|} \left(\frac{f}{|f|}\right)^{|f|} \left(\frac{g}{|g|}\right)^{|g|} (-1)^{\frac{e+f+g+1}{2}}$$

$$\text{Func} = 1$$

for $e+g$ = even , f = odd (A5.17)

Since no sideband components exist for e + g = odd, it is not necessary to specify values for the integer variables under these conditions. The variable (Func) is to indicate whether the contribution to the sideband component is a sine wave or a cosine wave (i.e. Func = 0 for sine wave, Func = 1 for cosine wave). Fig. A5.1. shows the flow chart for computing and storing the values of the integers e, f and g which give rise to a particular sideband frequency. The integer variables, SI and Func, are also computed and stored for each combination of e, f and g.

The flow chart used for calculating the amplitudes of the sideband components is shown in fig. A5.2. The method used is to form sums of all the contributions to a particular sideband. One sum (Sum 1) consists of the components for which the sideband is a sine wave (i.e. Func = 0), the second sum (Sum 2) consists of the components for which the sideband is a cosine wave. The sideband then has the form:

$$\frac{2}{\pi}\left\{\mathrm{Sum1}.\sin\left[(\omega_c - N\omega_m)t - \omega_c k_o\right] + \mathrm{Sum2}.\cos\left[(\omega_c - N\omega_m)t - \omega_c k_o\right]\right\} \qquad (A5.18)$$

Therefore the sideband amplitude is:

$$\mathrm{Sideband}(N) = \frac{2}{\pi}\sqrt{\left[(\mathrm{Sum1})^2 + (\mathrm{Sum2})^2\right]} \qquad (A5.19)$$

The above expression is also valid for the repetition frequency component (i.e. N = 0).

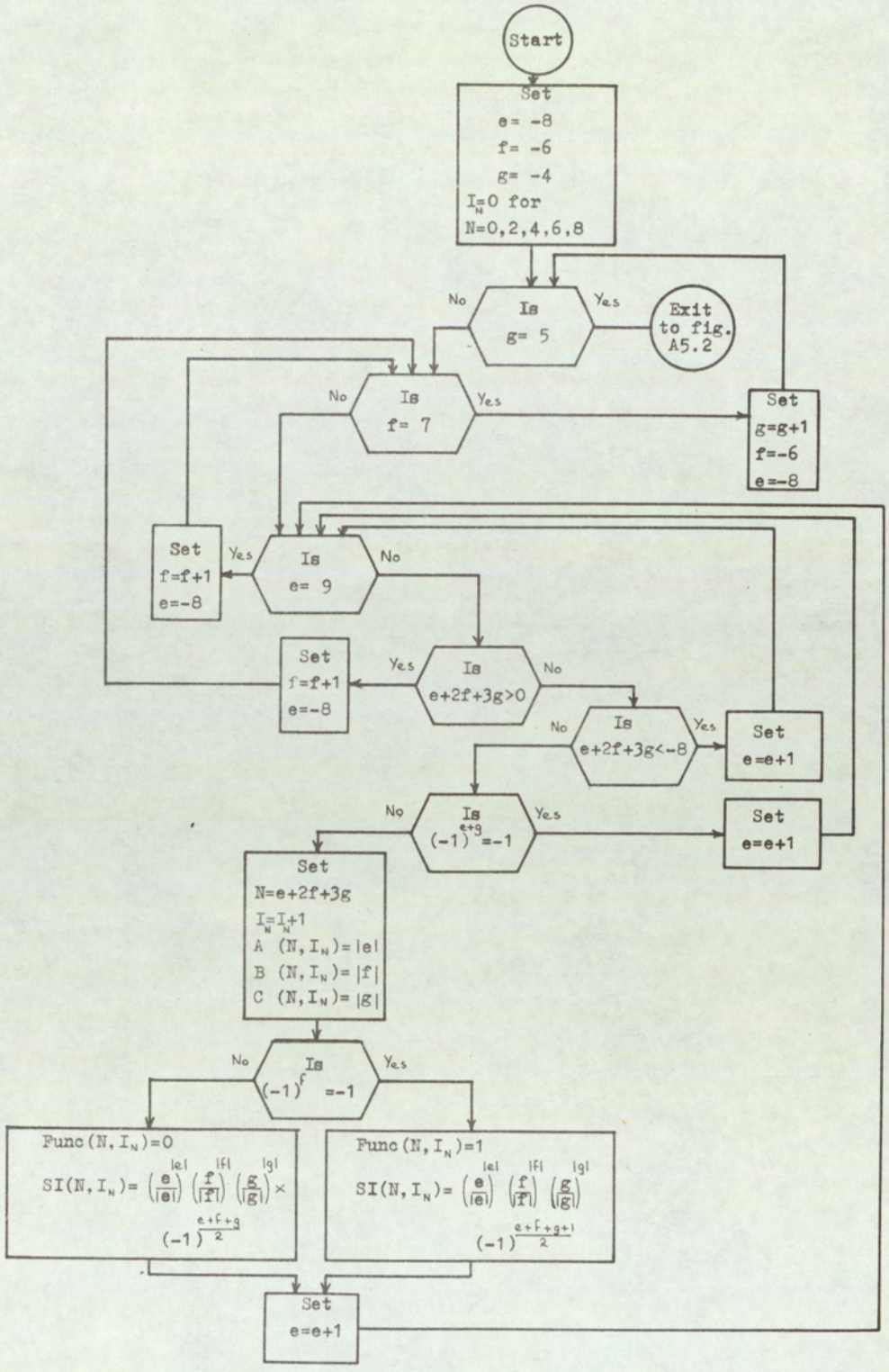

Fig.A5.1. Flowchart for computing sideband combinations.

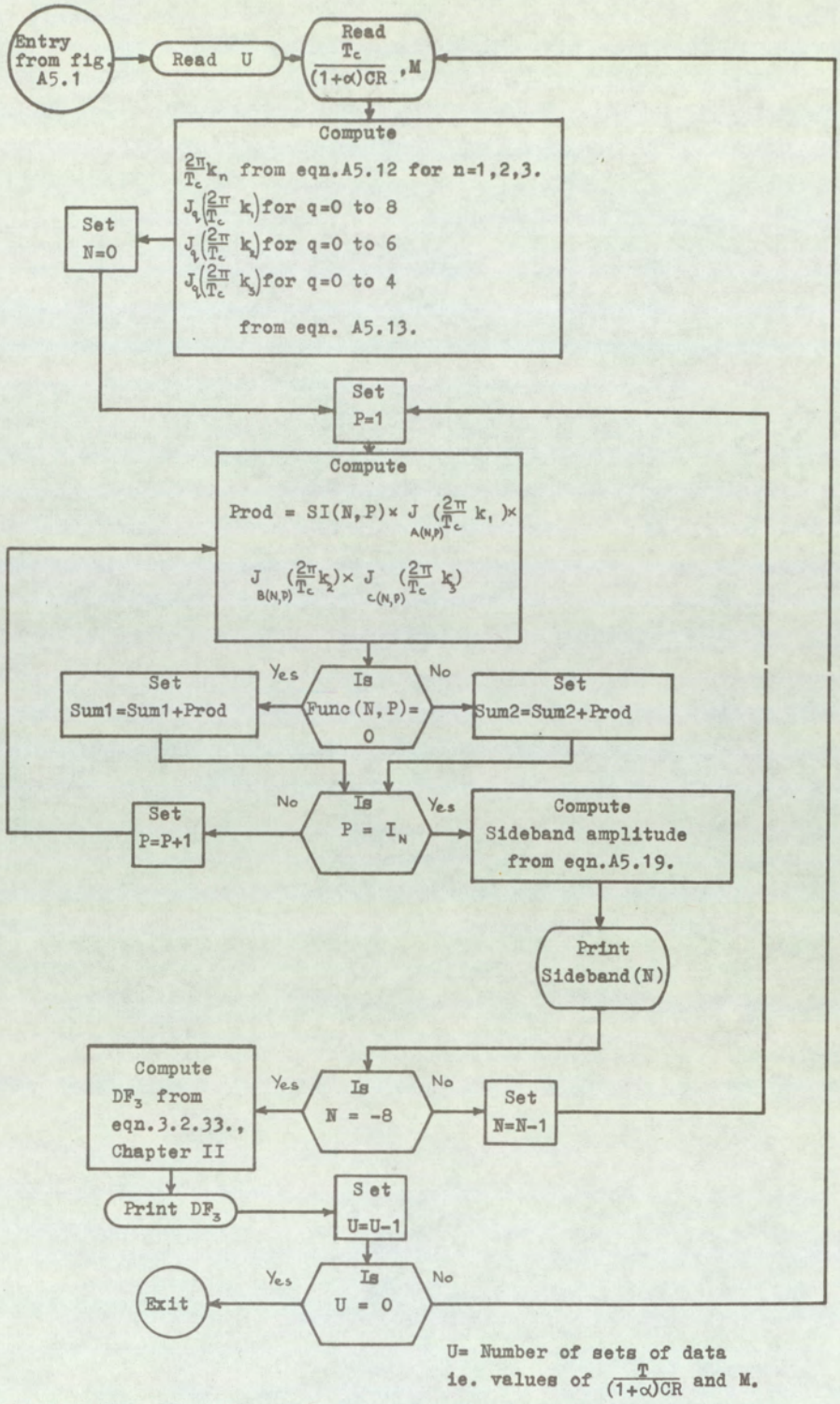

Fig.A5.2. Flowchart for computing amplitude of spectral components for double-edge modulation system with finite integrator gain.

Appendix 6. Derivation of the Coefficients involved in the Generalised Spectrum Analysis of Non-linear Pulse-length Modulation Systems

It is required to obtain expressions for the coefficients A_k, B_k, C_k and D_k in equations 3.1.13(a). (b), (c) and (d) of section 3.4. (chapter II). The equations are rewritten below for convenience:

$$\cos\left[p2\pi\sum_{n=1}^{\infty}\alpha_n M^n \cos^n(\omega_m t)\right] = \sum_{k=0}^{\infty} A_k \cos^k(\omega_m t) \qquad (A6.1(a))$$

$$\cos\left[p2\pi\sum_{n=1}^{\infty}\beta_n M^n \cos^n(\omega_m t)\right] = \sum_{k=0}^{\infty} B_k \cos^k(\omega_m t) \qquad (A6.1(b))$$

$$\sin\left[p2\pi\sum_{n=1}^{\infty}\alpha_n M^n \cos^n(\omega_m t)\right] = \sum_{k=0}^{\infty} C_k \cos^k(\omega_m t) \qquad (A6.1(c))$$

$$\sin\left[p2\pi\sum_{n=1}^{\infty}\beta_n M^n \cos^n(\omega_m t)\right] = \sum_{k=0}^{\infty} D_k \cos^k(\omega_m t) \qquad (A6.1(d))$$

As a result of the similarity of the above equations, it is necessary to consider only one set (e.g. equations A6.1(a). and A6.1(c).). Applying Maclaurin's theorem to the expressions enables the coefficients to be written as:

$$A_o = \left| \cos\left[p2\pi\sum_{n=1}^{\infty}\alpha_n M^n . \cos^n(\omega_m t)\right]\right|_{\cos(\omega_m t)=0} \qquad (A6.2(a))$$

$$A_k = \frac{1}{k!}\left|D^k\left[\cos\left(p2\pi\sum_{n=1}^{\infty}\alpha_n M^n \cos^n(\omega_m t)\right)\right]\right|_{\cos(\omega_m t)=0} \qquad (A6.2(b))$$

$$C_o = \left|\sin\left[p2\pi\sum_{n=1}^{\infty}\alpha_n M^n \cos^n(\omega_m t)\right]\right|_{\cos(\omega_m t)=0} \qquad (A6.3(a))$$

$$C_k = \frac{1}{k!}\left|D^k\left[\sin\left(p2\pi\sum_{n=1}^{\infty}\alpha_n M^n \cos^n(\omega_m t)\right)\right]\right|_{\cos(\omega_m t)=0} \qquad (A6.3(b))$$

where D^k ( ) is the differential operator $\frac{d^k(\quad)}{d\cos(\omega_m t)^k}$. Thus the problem is that of finding the kth differential of the expressions $\cos\left[p2\pi\sum_{n=1}^{\infty}\alpha_n M^n.\cos^n(\omega_m t)\right]$ and $\sin\left[p2\pi\sum_{n=1}^{\infty}\alpha_n M^n.\cos^n(\omega_m t)\right]$ with respect to $\cos(\omega_m t)$.

Let

$$z = p2\pi\sum_{n=1}^{\infty}\alpha_n . M^n \cos^n(\omega_m t) \qquad (A6.4)$$

$$f_1 = \cos(z) \qquad (A6.5)$$

$$f_2 = \sin(z) \qquad (A6.6)$$

It is now required to find the kth differential of f_1 and f_2 with respect to $\cos(\omega_m t)$. Since f_1 and f_2 are 'functions of a function', repeated differentiation is difficult if carried out directly. However, differentiating f_1 with respect to $\cos(\omega_m t)$ gives:

$$Df_1 = -\sin(z).Dz \qquad (A6.7)$$

Substituting equation A6.6. in equation A6.7

$$Df_1 = -f_2.Dz \qquad (A6.8)$$

Equation A6.8. may be repeatedly differentiated by application of the Liebnitz theorem. Therefore:

$$D^2f_1 = -\left(D^2z.f_2 + Dz.Df_2\right) \qquad (A6.9(a))$$

$$D^3f_1 = -\left(D^3z.f_2 + 2\,D^2z.Df_2 + Dz.D^2f_2\right) \qquad (A6.9(b))$$

$$D^kf_1 = -\left(D^kz.f_2 + \frac{(k-1)}{1!}D^{k-1}z.Df_2 + \frac{(k-1)(k-2)}{2!}D^{k-2}.D^2f_2 + \ldots + Dz.D^{k-1}f_2\right) \qquad (A6.9(c))$$

Differentiate equation A6.6. with respect to $\cos(\omega_m t)$:

$$Df_2 = \cos(z).Dz \qquad (A6.10)$$

Substituting equation A6.5. in equation A6.10. gives:

$$Df_1 = f_1.Dz \qquad (A6.11)$$

The kth differential of f_2 is calculated by applying the

Liebnitz theorem to equation A6.11.:

$$D^2 f_2 = \left(D^2 z . f_1 + Dz . f_1 \right) \qquad \text{(A6.12(a))}$$

$$D^3 f_2 = \left(D^3 z . f_1 + 2 . D^2 z . Df_1 + Dz . D^2 f_1 \right) \qquad \text{(A6.12(b))}$$

$$D^k f_2 = \left(D^k z . f_1 + \frac{(k-1)}{1!} D^{k-1} z . Df_1 + \frac{(k-1)(k-2)}{2!} D^{k-2} z . D^2 f_1 + \ldots + Dz . D^{k-1} f_1 \right) \qquad \text{(A6.12(c))}$$

Equations A6.11., A6.12(a)., (b) and (c) may be substituted in equation A6.9(c). If the terms containing $D^{k-2} f_1$, $D^{k-3} f_1$, ... f_1 are grouped together, then the following result is obtained:

$$D^k f_1 = -\left\{ D^k z . f_2 + f_1 \left[\frac{(k-1)}{1!} D^{k-1} z . Dz + \frac{(k-1)(k-2)}{2!} D^{k-2} z . D^2 z + \ldots \right. \right.$$

$$\left. \ldots + Dz . D^{k-1} z \right] +$$

$$Df_1 \left[\frac{(k-1)(k-2)}{2!} D^{k-2} z . Dz + \frac{(k-1)(k-2)(k-3)}{3!} D^{k-3} z . 2 . D^2 z + \right.$$

$$\left. \frac{(k-1)(k-2)(k-3)(k-4)}{4!} D^{k-4} z . 3 . D^3 z + \ldots + Dz\,(k-2) . D^{k-2} z \right] +$$

$$D^2 f_1\left[\frac{(k-1)(k-2)(k-3)}{3!} D_z^{k-3}.D_z + \frac{(k-1)(k-2)(k-3)(k-4)}{4!} D_z^{k-4} \frac{3.2}{2!} D_z^2 +\right.$$

$$\left.\frac{(k-1)(k-2)(k-3)(k-4)(k-5)}{5!} D_z^{k-5} \frac{4.3}{2!} D_z^3 + \ldots + D_z \frac{(k-2)(k-3)}{2!} D_z^{k-3}\right] +$$

$$D^3 f_1\left[\frac{(k-1)(k-2)(k-3)(k-4)}{4!} D_z^{k-4}.D_z +\right.$$

$$\frac{(k-1)(k-2)(k-3)(k-4)(k-5)}{5!} D_z^{k-5} \frac{4.3.2}{3!} D_z^2 +$$

$$\frac{(k-1)(k-2)(k-3)(k-4)(k-5)(k-6)}{6!} D_z^{k-6} \frac{5.4.3}{3!} D_z^3 + \ldots\ldots$$

$$\left.\ldots + D_z \frac{(k-2)(k-3)(k-4)}{3!} D_z^{k-4}\right] + \ldots + D^{k-2} f_1\left[D_z.D_z\right]\Bigg\} \qquad (A6.13)$$

It is required to evaluate the above expression when $\cos(\omega_m t) = 0$ in order that the coefficients A_k may be evaluated from equation A6.2(b).

From equation A6.4.

$$Z\Big|_{\cos(\omega_m t)=0} = 0 \qquad \text{(A6.14(a))}$$

$$DZ\Big|_{\cos(\omega_m t)=0} = p2\pi(\alpha_1 M) \qquad \text{(A6.14(b))}$$

$$D^2Z\Big|_{\cos(\omega_m t)=0} = p2\pi(2!\alpha_2 M^2) \qquad \text{(A6.14(c))}$$

$$D^kZ\Big|_{\cos(\omega_m t)=0} = p2\pi(k!\alpha_k M^k) \qquad \text{(A6.14(d))}$$

Substituting equation A6.14(a). in equations A6.5. and A6.6. gives:

$$f_1\Big|_{\cos(\omega_m t)=0} = 1 \qquad \text{(A6.15(a))}$$

$$f_2\Big|_{\cos(\omega_m t)=0} = 0 \qquad \text{(A6.15(b))}$$

Substituting equations A6.14(d). and A6.15(b). in equation A6.13 enables the kth differential of f_1 to be written as:

$$D^k F_1 \Big|_{\cos(\omega_m t)=0} = -(2\pi p)^2 \left[(k-1)!\right] \sum_{q=0}^{k-2} \left\{ M^{k-q} \left. \frac{D^q F_1}{q!} \right|_{\cos(\omega_m t)=0} \times \right.$$

$$\left. \sum_{r=q+1}^{k-1} \frac{(r-q)(k-r)}{r} \alpha_{k-r} \cdot \alpha_{r-q} \right\} \qquad \text{(A6.16)}$$

where $f_1 \Big| \cos(\omega_m t) = 0 = 1$

and $Df_1 \Big| \cos(\omega_m t) = 0 = 0$ (from equation A6.7.)

Noting that $f_1 = \cos z = \cos\left[p2\pi \sum_{n=1}^{\infty} \alpha_n . M^n . \cos^n(\omega_m t)\right]$,

equation A6.16. may be substituted in equations A6.2(a) and (b) to give the following recurrence relationship for the coefficient A_k:

$$A_k = -\frac{(2\pi p)^2}{k} \sum_{q=0}^{k-2} \left\{ M^{k-q} A_q \sum_{r=q+1}^{k-1} \frac{(r-q)(k-r)}{r} \alpha_{k-r} \cdot \alpha_{r-q} \right\} \qquad \text{(A6.17(a))}$$

$$A_o = 1 \qquad \text{(A6.17(b))}$$

$$A_1 = 0 \qquad \text{(A6.17(c))}$$

A similar process may be carried out to determine a recurrence relationship for C_k. Substituting equations

A6.8., A6.9(a), (b), (c) and (d) in equation A6.12(b) leads to the following expression for C_k:

$$C_k = M^k p 2\pi \alpha_k - \frac{(p2\pi)^2}{k} \sum_{q=0}^{k-2} \left\{ M^{k-q} C_q \sum_{r=q+1}^{k-1} \frac{(r-q)(k-r)}{r} \alpha_{k-r} \alpha_{r-q} \right\} \qquad \text{(A6.18(a))}$$

$$C_0 = 0 \qquad \text{(A6.18(b))}$$

$$C_1 = M p 2\pi \alpha_1 \qquad \text{(A6.18(b))}$$

Since equations A6.1(b). and (d) have the same form as equations A6.1(a) and (c) respectively, the recurrence relationships for B_k and D_k may be written down by inspection of equations A6.17. and A6.18.

$$B_k = -\frac{(p2\pi)^2}{k} \sum_{q=0}^{k-2} \left\{ M^{k-q} B_q \sum_{r=q+1}^{k-1} \frac{(r-q)(k-r)}{r} \beta_{k-r} \beta_{r-q} \right\} \qquad \text{(A6.19(a))}$$

$$B_0 = 1 \qquad \text{(A6.19(b))}$$

$$B_1 = 0 \qquad \text{(A6.19(c))}$$

$$D_k = M^k p2\pi\beta_k - \frac{(p2\pi)^2}{k}\sum_{q=0}^{k-2}\left\{M^{k-q} D_q \sum_{r=q+1}^{k-1}\frac{(r-q)(k-r)}{r}\beta_{k-r}.\beta_{r-q}\right\} \qquad (A6.20(a))$$

$$D_o = 0 \qquad (A6.20(b))$$

$$D_1 = M p2\pi\beta_1 \qquad (A6.20(c))$$

The power series on the right hand sides of equations A6.(a)., (b), (c) and (d) may be expressed as Fourier series in terms of harmonics of the modulation frequency ω_m. Therefore

$$\cos\left[p2\pi\sum_{n=1}^{\infty}\alpha_n M^n \cos^n(\omega_m t)\right] = \sum_{k=0}^{\infty} A_k.\cos^k(\omega_m t)$$

$$= \frac{E_o}{2} + \sum_{n=1}^{\infty} E_n.\cos(n\omega_m t). \qquad (A6.21(a))$$

$$\cos\left[p2\pi\sum_{n=1}^{\infty}\beta_n M^n \cos^n(\omega_m t)\right] = \sum_{k=0}^{\infty} B_k.\cos^k(\omega_m t)$$

$$= \frac{F_o}{2} + \sum_{n=1}^{\infty} F_n.\cos(n\omega_m t) \qquad (A6.21(b))$$

$$\sin\left[p2\pi\sum_{n=1}^{\infty}\alpha_n M^n\cos^n(\omega_m t)\right]=\sum_{k=0}^{\infty}C_k.\cos^k(\omega_m t)$$

$$=\frac{G_o}{2}+\sum_{n=1}^{\infty}G_n.\cos(n\omega_m t) \qquad (A6.21(c))$$

$$\sin\left[p2\pi\sum_{n=1}^{\infty}\beta_n M^n\cos^n(\omega_m t)\right]=\sum_{k=0}^{\infty}D_k\cos^k(\omega_m t)$$

$$=\frac{H_o}{2}+\sum_{n=1}^{\infty}H_n.\cos(n\omega_m t) \qquad (A6.21(d))$$

The constant terms E_o, F_o, G_o and H_o are defined in the manner shown for the sake of convenience in later equations. Since equations A6.21(a)., (b), (c) and (d) have the same form, it is sufficient to derive expressions for the Fourier series coefficients for only one of the equations (e.g. A6.21(a).). The terms $\cos^k(\omega_m t)$ may be expanded as Fourier series by means of the trigonometric identities[57]:

$$\cos^{2k}(\omega_m t)=\frac{1}{2^{2k}}\left\{\sum_{q=0}^{k-1}2\binom{2k}{q}\cos\left[2(k-q)\omega_m t\right]+\binom{2k}{k}\right\} \qquad (A6.22(a))$$

$$\cos^{2k-1}(\omega_m t) = \frac{1}{2^{2k-2}}\left\{\sum_{q=0}^{k-1}\binom{2k-1}{q}\cos(2k-2q-1)\omega_m t\right\} \qquad (A6.22(b))$$

Therefore, from equation A6.21(a).:

$$\frac{E_o}{2} + \sum_{n=1}^{\infty} E_n \cdot \cos(n\omega_m t) \equiv \left\{A_o + A_1\cos(\omega_m t) + A_2\frac{1}{2}\left[1+\cos(2\omega_m t)\right] +\right.$$

$$A_3\frac{1}{4}\left[\cos(3\omega_m t)+3\cos(\omega_m t)\right] + A_4\frac{1}{8}\left[\cos(4\omega_m t)+4\cos(2\omega_m t)+3\right] +$$

$$A_{2u-1}\frac{1}{2^{2u-2}}\left[\sum_{v=0}^{u-1}\binom{2u-1}{v}\cos(2u-2v-1)\omega_m t\right] +$$

$$\left. A_{2u}\frac{1}{2^{2u}}\left[\sum_{v=0}^{u-1} 2\binom{2u}{v}\cos\left[2(u-v)\omega_m t\right] + \binom{2u}{u}\right] + ----\right\} \qquad (A6.23)$$

Equating like terms in the above identity results in the following expressions for the coefficients E_n:

$$E_o = \sum_{u=0}^{\infty} A_{2u}\frac{1}{2^{2u-1}}\binom{2u}{u} \qquad (A6.24(a))$$

$$E_{2n-1} = \sum_{u=n}^{\infty} A_{2u-1} \frac{1}{2^{2u-2}} \binom{2u-1}{u-n} \qquad (A6.24(b))$$

$$E_{2n} = \sum_{u=n}^{\infty} A_{2u} \frac{1}{2^{2u-1}} \binom{2u}{u-n} \qquad (A6.24(c))$$

The expressions for the coefficients F_n, G_n and H_n may be written down by inspection of equations A6.24(a)., (b) and (c)

$$F_o = \sum_{u=o}^{\infty} B_{2u} \frac{1}{2^{2u-1}} \binom{2u}{u} \qquad A6.25(a)$$

$$F_{2n-1} = \sum_{u=n}^{\infty} B_{2u-1} \frac{1}{2^{2u-2}} \binom{2u-1}{u-n} \qquad (A6.25(b))$$

$$F_{2n} = \sum_{u=n}^{\infty} B_{2u} \frac{1}{2^{2u-1}} \binom{2u}{u-n} \qquad (A6.25(c))$$

$$G_o = \sum_{u=o}^{\infty} C_{2u} \frac{1}{2^{2u-1}} \binom{2u}{u} \qquad (A6.26(a))$$

$$G_{2n-1} = \sum_{u=n}^{\infty} C_{2u-1} \frac{1}{2^{2u-2}} \binom{2u-1}{u-n} \qquad (A6.26(b))$$

$$G_{2n} = \sum_{u=n}^{\infty} C_{2u} \frac{1}{2^{2u-1}} \binom{2u}{u-n} \qquad (A6.26(c))$$

$$H_o = \sum_{u=0}^{\infty} D_{2u} \frac{1}{2^{2u-1}} \binom{2u}{u} \qquad (A6.27(a))$$

$$H_{2n-1} = \sum_{u=n}^{\infty} D_{2u-1} \frac{1}{2^{2u-2}} \binom{2u-1}{u-n} \qquad (A6.27(b))$$

$$H_{2n} = \sum_{u=n}^{\infty} D_{2u} \frac{1}{2^{2u-1}} \binom{2u}{u-n} \qquad (A6.27(c))$$

The frequency spectrum given by equation 3.4.11, section 3.4. (chapter II) can now be expressed in terms of the Fourier coefficients by substituting equations A6.21(a)., (b), (c) and (d) in equation 3.4.11.:

$$F(t) = \frac{1}{\pi} \sum_{p=1}^{\infty} \frac{1}{p} \left\{ \sin\left[p\omega_c\left(t+\frac{T_o}{2}\right)\right]\left[\frac{E_o}{2} + \sum_{n=1}^{\infty} E_n \cdot \cos(n\omega_m t)\right] + \right.$$

$$\cos\left[p\omega_c\left(t+\frac{T_o}{2}\right)\right]\left[\frac{G_o}{2} + \sum_{n=1}^{\infty} G_n \cdot \cos(n\omega_m t)\right] -$$

$$\sin\left[p\omega_c\left(t-\frac{T_o}{2}\right)\right]\left[\frac{F_o}{2} + \sum_{n=1}^{\infty} F_n \cdot \cos(n\omega_m t)\right] +$$

$$\left. \cos\left[p\omega_c\left(t-\frac{T_o}{2}\right)\right]\left[\frac{H_o}{2} + \sum_{n=1}^{\infty} H_n \cdot \cos(n\omega_m t)\right]\right\} \qquad (A6.28)$$

Equation A6.28. may be rearranged to give:

$$F(t)=\frac{1}{2\pi}\sum_{p=1}^{\infty}\frac{1}{P}\sum_{n=-\infty}^{\infty}\left\{\sqrt{(\gamma_n^2+\delta_n^2)}\times\right.$$

$$\left.\sin\left[(p\omega_c+n\omega_m)t+\phi_n\right]\right\} \qquad (A6.29)$$

where:

$$\gamma_n=(E_n-F_n)\cos\left(\frac{p\omega_c T_o}{2}\right)+(H_n-G_n)\sin\left(\frac{p\omega_c T_o}{2}\right) \qquad (A6.30(a))$$

$$\delta_n=(H_n+G_n)\cos\left(\frac{p\omega_c T_o}{2}\right)+(E_n+F_n)\sin\left(\frac{p\omega_c T_o}{2}\right) \qquad (A6.30(b))$$

$$\phi_n=\tan^{-1}\left(\frac{\delta_n}{\gamma_n}\right) \qquad (A6.30(c))$$

$$E_{-n}=E_n\,,\ F_{-n}=F_n\,,\ G_{-n}=G_n\,,\ H_{-n}=H_n \qquad (A6.30(d))$$

It is shown in equation 3.4.17. (section 3.4., chapter II) that the modulation frequency and harmonic components of the frequency spectrum are given by the expression:

$$\sum_{n=1}^{\infty}(\alpha_n+\beta_n)M^n\cos^n(\omega_m t) \qquad (A6.31)$$

Now the form of equation A6.31. is very similar to equations A6.21(a)., (b), (c) and (d) so that the following expression may be written down by inspection of equations A6.24:

$$\sum_{n=1}^{\infty}(\alpha_n+\beta_n)M^n.\cos^n(\omega_m t)=\frac{K_o}{2}+\sum_{v=1}^{\infty}K_v.\cos(v.\omega_m t) \qquad (A6.32)$$

where

$$K_o \quad \sum_{w=1}^{\infty}(\alpha_{2w}+\beta_{2w})M^{2w}\frac{1}{2^{2w-1}}\binom{2w}{w} \qquad (A6.33(a))$$

$$K_{2v-1} \quad \sum_{w=v}^{\infty}(\alpha_{2w-1}+\beta_{2w-1})M^{2w-1}\frac{1}{2^{2w-2}}\binom{2w-1}{w-v} \qquad (A6.33(b))$$

$$K_{2v} \quad \sum_{w=v}^{\infty}(\alpha_{2w}+\beta_{2w})M^{2w}\frac{1}{2^{2w-1}}\binom{2w}{w-v} \qquad (A6.33(c))$$

Computational Methods

It will be noted that equations A6.17., A6.18., A6.19. and A6.20., for the coefficients A_k, B_k, C_k and D_k have the same form. From the point of view of computing the numerical values of these terms, it is convenient if they can be expressed in a general form. It is also convenient if the variables are identified by a subscripted letter rather than by different letters. Therefore let:

$$A_k = Y_k(1) \qquad (A6.34(a))$$

$$C_k = Y_k(2) \qquad (A6.34(b))$$

$$B_k = Y_k(3) \qquad (A6.34(c))$$

$$D_k = Y_k(4) \qquad (A6.34(d))$$

The general expression for $Y_k(N)$ is obtained by inspection of equations A6.17., A6.18., A6.19. and A6.20. The sidebands of most interest are the lower order sidebands of the pulse-repetition frequency so that the expression for $Y_k(N)$ is written for $p = 1$.

$$Y_k(N) = \frac{1}{2}\left(1+(-1)^N\right) M^k . 2\pi x_k - \frac{(2\pi)^2}{k} \sum_{q=0}^{k-2} \left\{ M^{k-q}\, Y_q(N) \sum_{r=q+1}^{k-1} \frac{(r-q)(k-r)}{r}\, x_{k-r} . x_{r-q} \right\} \qquad (A6.35)$$

where

$$x_k = \alpha_k \quad \text{for } N=1 \text{ and } 2 \qquad (6.36(a))$$

$$x_k = \beta_k \quad \text{for } N=3 \text{ and } 4 \qquad (6.36(b))$$

The coefficients E_n, F_n, G_n and H_n, given by equations A6.24., A6.25., A6.26. and A6.27., can also be identified by subscripted letters, and expressed in general form. Let:

$$E_n = Z_n(1) \qquad (6.37(a))$$

$$G_n = Z_n(2) \qquad (6.37(b))$$

$$F_n = Z_n(3) \qquad (A6.37(c))$$

$$H_n = Z_n(4) \qquad (A6.37(d))$$

By inspection of equations A6.24., A6.25., A6.26. and A6.27., the general expression for $Z_n(N)$ is:

$$Z_n(N) = \sum_{\substack{u=n \\ u=\text{even}}}^{\infty} Y_u(N) \frac{1}{2^{u-1}} \binom{u}{\frac{u-n}{2}} \quad \text{for } n=\text{even} \qquad (A6.38(a))$$

$$Z_n(N) = \sum_{\substack{u=n \\ u=\text{odd}}}^{\infty} Y_u(N) \frac{1}{2^{u-1}} \binom{u}{\frac{u-n}{2}} \quad \text{for } n=\text{odd} \qquad (A6.38(b))$$

The flow chart for evaluating the coefficients Z_N is shown in fig. A6.1. It is necessary to specify the following parameters for the flow chart: the highest order sideband of interest (i.e. $\omega_c - J.\omega_m$), the order (U) of the power series defining the positions of the pulse leading and trailing edges, and the highest modulation frequency harmonic $(R\omega_m)$ of interest. The values of the power series coefficients α_p and β_p are also required, together with the modulation index M. The method used is to evaluate the terms $Z_o(N)$ to $Z_J(N)$ for successive values of N of 1, 2, 3 and 4.

The values of the coefficients $Z_J(N)$ are then used to

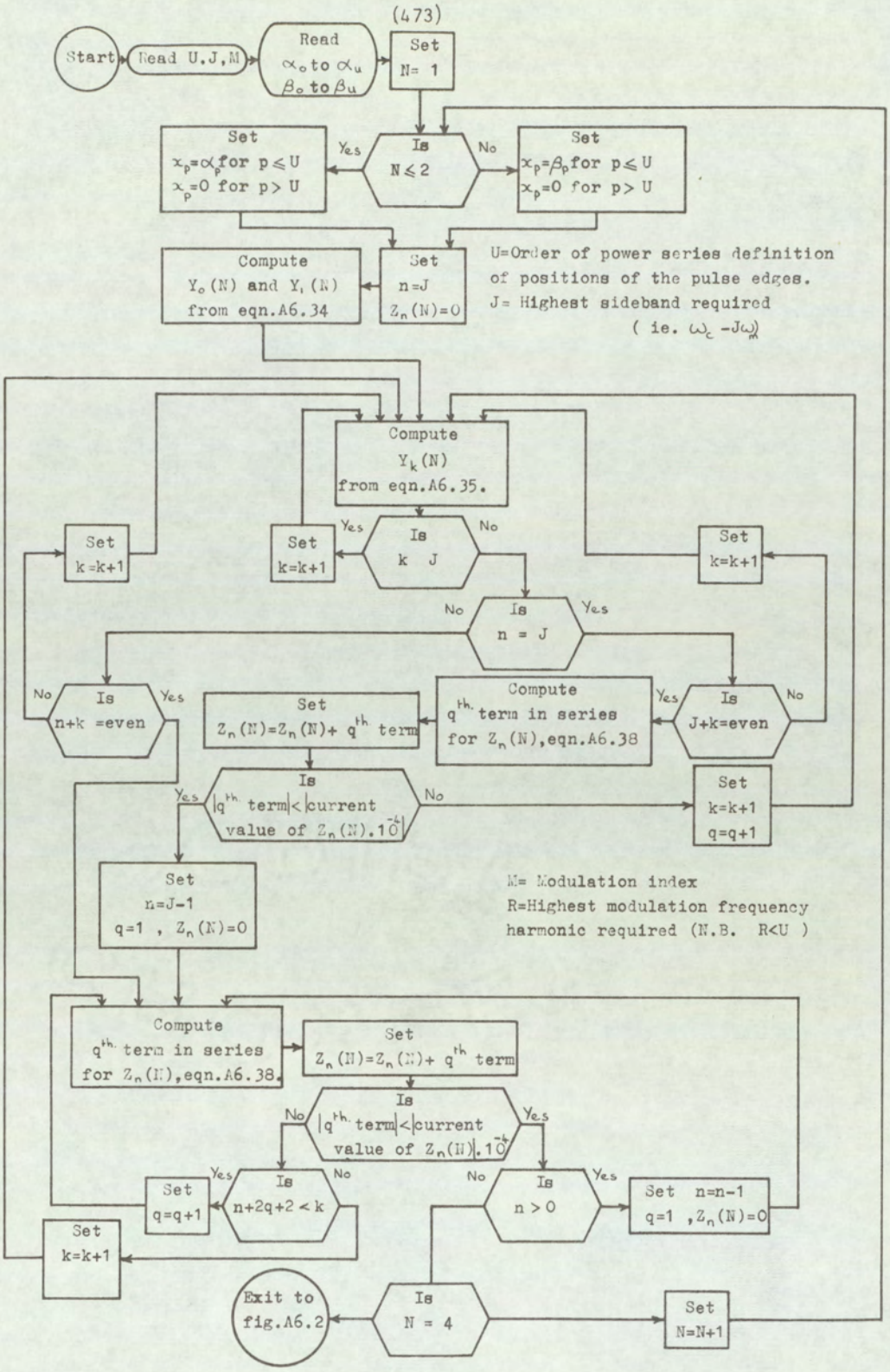

Fig.A6.1. Flowchart for computing coefficients in the generalised spectrum analysis.

evaluate the amplitudes of the repetition frequency component and the sideband frequency components as shown in fig. A6.2. From equations A6.29., A6.30. and A6.37., the amplitude of the sideband $(\omega_c - n\omega_m)$ may be written as:

$$\text{Sideband amplitude} = \frac{1}{2\pi}\sqrt{\left(\gamma_n^2 + \delta_n^2\right)} \qquad \text{(A6.39(a))}$$

where:

$$\gamma_n = \left(Z_n(1) - Z_n(3)\right)\cos\left(\pi\frac{T_o}{T_c}\right) + \left(Z_n(4) - Z_n(2)\right)\sin\left(\pi\frac{T_o}{T_c}\right) \qquad \text{(A6.39(b))}$$

$$\delta_n = \left(Z_n(4) + Z_n(2)\right)\cos\left(\pi\frac{T_o}{T_c}\right) + \left(Z_n(1) + Z_n(3)\right)\sin\left(\pi\frac{T_o}{T_c}\right) \qquad \text{(A6.39(c))}$$

$\frac{T_o}{T_c}$ is given by equation 4.4.5(b). of section 4.4. (chapter II)

$$\frac{T_o}{T_c} = \beta_o - \alpha_o \qquad \text{(A6.39(d))}$$

The amplitude of the modulation frequency and harmonic components are given by equations A6.32. and A6.33. For ease of computing the coefficients K_r may be written in general form:

$$K_r = \sum_{\substack{w=r \\ w=\text{odd}}}^{\infty}\left(\alpha_w + \beta_w\right)M^w \frac{1}{2^{w-1}}\binom{w}{\frac{w-r}{2}} \qquad \text{(A6.40(a))}$$

for r = odd

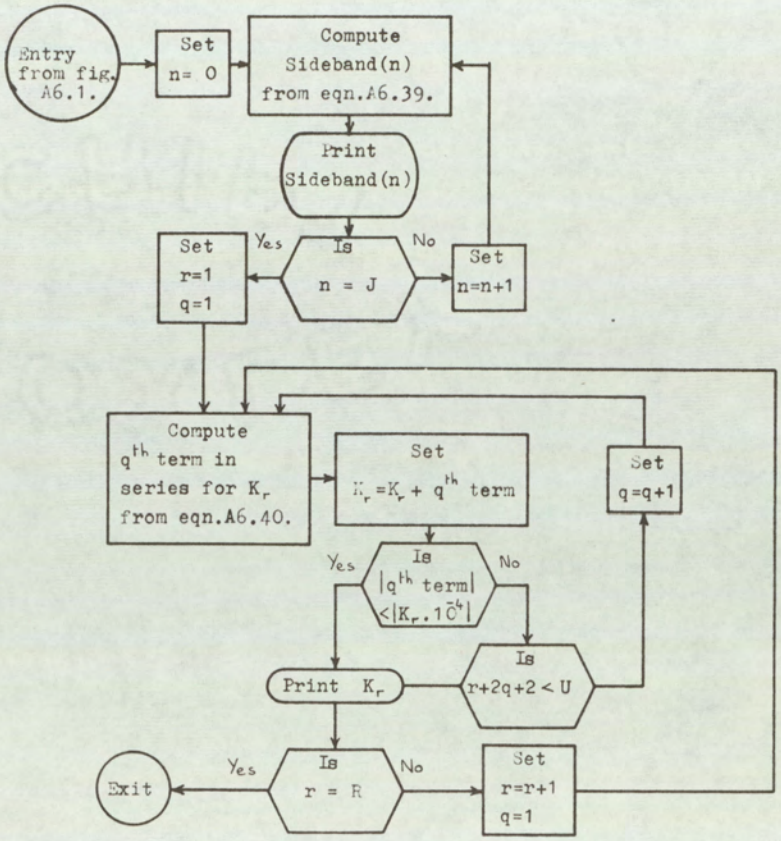

Fig.A6.2. Computation of sideband frequency components and modulation frequency harmonic components.

$$K_r = \sum_{\substack{w=r \\ w=\text{even}}}^{\infty} (\alpha_w + \beta_w) M^w \frac{1}{2^{w-1}} \binom{w}{\frac{w-r}{2}} \qquad \text{(A6.40(b))}$$

for $r = \text{even}$

From equations A6.40(a). and (b), it can be seen that the highest modulation frequency harmonic required ($r = R$) must be less than, or equal to, the order U of the power series defining the positions of the pulse edges.

Appendix 7 Evaluation of the expressions for the static power dissipation in the output stage elements

The power dissipation in transistor VT1 of the output stage is given by eqn. 4.24, section 4, Chapter III. The expression is rewritten below for convenience:

$$\bar{P}_{VT1} = \frac{1}{T_c}\int_{T'}^{T_1} i(t)\left[i(t)\,R_{E1} + \frac{kT}{q}\log\left(1+\frac{i(t)}{I_{ES1}}\right) + V_{CB1}\right]dt \qquad (A7.1)$$

The filter input current i(t) is given by the approximate expressions developed in Chapter III section 3.2 (eqns. 3.2.22(a) and (b)).

$$\frac{R_L}{V_1}\,i(t) = M + \Delta\left(\frac{4}{M+1}\cdot\frac{t_1}{T_c} - 1\right) \quad \text{for } 0 \leqslant \frac{t}{T_c} \leqslant \left(\frac{T_1}{T_c} = \frac{M+1}{2}\right) \qquad (A7.2)$$

$$\frac{R_L}{V_1}\,i(t) = M + \Delta\left(\frac{3+M}{1-M} - \frac{4}{1-M}\cdot\frac{t}{T_c}\right) \quad \text{for } \left(\frac{M+1}{2} = \frac{T_1}{T_c}\right) \leqslant \frac{t}{T_c} \leqslant 1 \qquad (A7.3)$$

Substituting eqn. A7.2 in A7.1 gives the following expression for the power dissipation in VT1.

$$\bar{P}_{VT1} = \frac{1}{T_c}\int_{T'}^{T_1} I\left\{M+\Delta\left[\frac{4}{M+1}\,\frac{t}{T_c}-1\right]\right\}\frac{kT}{q}\log\left\{1+\frac{I}{I_{ES1}}\left[M+\Delta\left(\frac{4}{M+1}\,\frac{t}{T_c}-1\right)\right]\right\}dt +$$

$$\frac{1}{T_c}\int_{T'}^{T_1} I^2\left\{M+\Delta\left[\frac{4}{M+1}\cdot\frac{t}{T_c}-1\right]\right\}^2 R_{E1}\,.\,dt +$$

$$\frac{1}{T_c}\int_{T'}^{T_1} I\left\{M+\Delta\left[\frac{4}{M+1}\,\frac{t}{T_c}-1\right]\right\}V_{CB1}\,.\,dt \qquad (A7.4)$$

where $I = V_1/R_L$

Evaluation of the first of the three integrals in the above expression is the only one that is not straightforward.

If the substitutions $b = 1 + \frac{I}{I_{ES1}}\left[M+\Delta\left(\frac{4}{M+1}\,\frac{t}{T_c}-1\right)\right]$

and $dt = \frac{I_{ES1}(M+1)T_c}{4I\Delta}.db$

are made in the first of the integrals then eqn. A7.4 becomes:

$$\bar{P}_{VT1} = \frac{kT}{q}\,\frac{I_{ES1}^2(M+1)}{4I\Delta}\int_{b_1}^{b_2}\left[(b-1)\log b\right]db + \frac{I^2R_{E1}}{T_c}\int_{T'}^{T_1}\left\{M-\Delta\left(\frac{4}{M+1}\cdot\frac{t}{T_c}-1\right)\right\}^2 dt +$$

$$\frac{I.V_{CB1}}{T_c}\int_{T'}^{T_1}\left\{M+\Delta\left(\frac{4}{M+1}\cdot\frac{t}{T_c}-1\right)\right\}dt \qquad (A7.5)$$

Integrating the first of the integrals by parts gives the following expression for the power dissipation.

$$\bar{P}_{VT1} = \frac{kT}{q}\,\frac{I_{ES1}^2(M+1)}{4I\Delta}\left\{b_2\left(\frac{b_2}{2}-1\right)\log b_2 - b_1\left(\frac{b_1}{2}-1\right)\log b_1 - b_2\left(\frac{b_2}{4}-1\right)+b_1\left(\frac{b_1}{4}-1\right)\right\} +$$

$$I^2R_{E1}\left\{(M-\Delta)^2\left(\frac{T_1}{T_c}-\frac{T'}{T_c}\right)+(M-\Delta)\Delta\,\frac{4}{M+1}\left[\left(\frac{T_1}{T_c}\right)^2-\left(\frac{T'}{T_c}\right)^2\right]+\frac{1}{3}\left(\frac{4\Delta}{M+1}\right)^2\left[\left(\frac{T_1}{T_c}\right)^3-\left(\frac{T'}{T_c}\right)^3\right]\right\} +$$

$$IV_{CB1}\left\{M\left(\frac{T_1}{T_c}-\frac{T'}{T_c}\right)+\Delta\left[\frac{2}{M+1}\left(\left(\frac{T_1}{T_c}\right)^2-\left(\frac{T'}{T_c}\right)^2\right)-\left(\frac{T_1}{T_c}-\frac{T'}{T_c}\right)\right]\right\} \qquad (A7.6(a))$$

where $b_1 = 1+\frac{I}{I_{ES1}}\left[M+\Delta\left(\frac{4}{M+1}\,\frac{T'}{T_c}-1\right)\right]$ $\qquad$ $b_2 = 1+\frac{I}{I_{ES1}}\left[M+\Delta\left(\frac{4}{M+1}\,\frac{T_1}{T_c}-1\right)\right]$

Eqns. 4.25, 4.26 and 4.27 (Chapter III, Section 4) may be integrated in the same manner to give expressions for the power dissipation in diodes D_1 and D_2, and transistor VT2.

$$\bar{P}_{D1} = -\frac{kT}{q}\,\frac{I_{S1}^2(M+1)}{4I\Delta}\left\{a_2\left(\frac{a_2}{2}-1\right)\log a_2 - a_1\left(\frac{a_1}{2}-1\right)\log a_1 - a_2\left(\frac{a_2}{4}-1\right)+a_1\left(\frac{a_1}{4}-1\right)\right\} +$$

$$I^2 R_{D1}\left\{(M-\Delta)^2\frac{T'}{T_c}+(M-\Delta)\Delta\frac{4}{M+1}\left(\frac{T'}{T_c}\right)^2+\frac{1}{3}\left(\frac{4\Delta}{M+1}\right)^2\left(\frac{T'}{T_c}\right)^3\right\} \qquad (A7.6(b))$$

where $a_1=1-\frac{I}{I_{S1}}(M-\Delta)$ $\qquad$ $a_2=1-\frac{I}{I_{S1}}\left[M+\Delta\left(\frac{4}{M+1}\frac{T'}{T_c}-1\right)\right]$

$$\bar{P}_{VT2}=\frac{kT}{q}\frac{I_{ES2}^2(1-M)}{4I\Delta}\left\{d_2\left(\frac{d_2}{2}-1\right)\log d_2-d_1\left(\frac{d_1}{2}-1\right)\log d_1-d_2\left(\frac{d_2}{4}-1\right)+d_1\left(\frac{d_1}{4}-1\right)\right\}+$$

$$I^2R_{E2}\left\{\left[M+\Delta\frac{3+M}{1-M}\right]^2\left[1-\frac{T'}{T_c}\right]-\left[M+\Delta\frac{3+M}{1-M}\right]\left[\frac{4\Delta}{1-M}\right]\left[1-\left(\frac{T''}{T_c}\right)^2\right]+\frac{1}{3}\left[\frac{4\Delta}{1-M}\right]^2\left[1-\left(\frac{T''}{T_c}\right)^3\right]\right\}-$$

$$V_{CB2}I\left\{M\left[1-\frac{T''}{T_c}\right]+\Delta\left[\frac{3+M}{1-M}\left(1-\frac{T''}{T_c}\right)-\frac{2}{1-M}\left(1-\left(\frac{T''}{T_c}\right)^2\right)\right]\right\} \qquad (A7.6(c))$$

where $d_1=1-\frac{I}{I_{ES2}}\left[M+\Delta\left(\frac{3+M}{1-M}-\frac{4}{1-M}\frac{T''}{T_c}\right)\right]$ $\qquad$ $d_2=1-\frac{I}{I_{ES2}}\left[M+\Delta\left(\frac{3+M}{1-M}-\frac{4}{1-M}\right)\right]$

$$\bar{P}_{D2}=-\frac{kT}{q}\frac{I_{S2}^2(1-M)}{4I\Delta}\left\{c_2\left(\frac{c_2}{2}-1\right)\log c_2-c_1\left(\frac{c_1}{2}-1\right)\log c_1-c_2\left(\frac{c_2}{4}-1\right)+c_1\left(\frac{c_1}{4}-1\right)\right\}$$

$$I^2R_{D2}\left\{\left[M+\Delta\frac{3+M}{1-M}\right]^2\left[\frac{T''}{T_c}-\frac{T_1}{T_c}\right]-\left[M+\Delta\frac{3+M}{1-M}\right]\left[\frac{4\Delta}{1-M}\right]\left[\left(\frac{T''}{T_c}\right)^2-\left(\frac{T_1}{T_c}\right)^2\right]+\frac{1}{3}\left[\frac{4\Delta}{1-M}\right]^2\left[\left(\frac{T''}{T_c}\right)^3-\left(\frac{T_1}{T_c}\right)^3\right]\right\} \qquad (A7.6(d))$$

where $c_1=1+\frac{I}{I_{S2}}\left[M+\Delta\left(\frac{3+M}{1-M}-\frac{4}{1-M}\cdot\frac{T_1}{T_c}\right)\right]$ $\qquad$ $c_2=1+\frac{I}{I_{S2}}\left[M+\Delta\left(\frac{3+M}{1-M}-\frac{4}{1-M}\cdot\frac{T''}{T_c}\right)\right]$

Now the normalised times T'/T_c and T''/T_c are given by eqns. 4.1, 4.4, 4.7 and 4.8 of section 4, Chapter III. Substituting these expressions in eqns. A7.6(a), (b), (c) and (d), and substituting for T_1/T_c from $M=2T_1/T_c-1$, gives the following expressions for the power dissipation in the output stage elements.

For $M \gg \Delta$

$$\bar{P}_{VT1}=\frac{kT}{q}\frac{I_{ES1}^2(M+1)}{4I\Delta}\left\{b_2\left(\frac{b_2}{2}-1\right)\log b_2-b_1\left(\frac{b_1}{2}-1\right)\log b_1-b_2\left(\frac{b_2}{4}-1\right)+b_1\left(\frac{b_1}{4}-1\right)\right\}+$$

$$\frac{I V_{CB1} M(M+1)}{2} + I^2 R_{E1} \Delta^2 \frac{M+1}{2}\left[\left(\frac{M}{\Delta}\right)^2 + \frac{1}{3}\right] \qquad (A7.7(a))$$

where: $b_1 = 1 + \frac{I}{I_{ES1}}(M-\Delta) \qquad b_2 = 1 + \frac{I}{I_{ES1}}(M+\Delta)$

$$\bar{P}_{D1} = 0 \qquad (A7.7(b))$$

$$\bar{P}_{VT2} = 0 \qquad (A7.7(c))$$

$$\bar{P}_{D2} = \frac{kT}{q}\frac{I_{S2}^2(1-M)}{4I\Delta}\left\{c_1\left(\frac{c_1}{2}-1\right)\log c_1 - c_2\left(\frac{c_2}{2}-1\right)\log c_2 - c_1\left(\frac{c_1}{4}-1\right) + c_2\left(\frac{c_2}{4}-1\right)\right\} +$$

$$I^2 R_{D2} \Delta^2 \frac{1-M}{2}\left[\left(\frac{M}{\Delta}\right)^2 + \frac{1}{3}\right] \qquad (A7.7(d))$$

where: $c_1 = 1 + \frac{I}{I_{S2}}(M+\Delta) \qquad c_2 = 1 + \frac{I}{I_{S2}}(M-\Delta)$

For $-\Delta \leqslant M \leqslant \Delta$

$$\bar{P}_{VT1} = \frac{kT}{q}\frac{I_{ES1}^2(M+1)}{4I\Delta}\left\{b_2\left(\frac{b_2}{2}-1\right)\log b_2 - b_2\left(\frac{b_2}{4}-1\right) - \frac{3}{4}\right\} +$$

$$I V_{CB1}\left[\frac{(M+1)(M+\Delta)^2}{8\Delta}\right] + \frac{I^2 R_{E1} \Delta^2 (M+1)}{12}\left(1+\frac{M}{\Delta}\right)^3 \qquad (A7.8(a))$$

where: $b_2 = 1 + \frac{I}{I_{ES1}}(M+\Delta)$

$$\bar{P}_{D1} = \frac{kT}{q}\frac{I_{S1}^2(M+1)}{4I\Delta}\left\{a_1\left(\frac{a_1}{2}-1\right)\log a_1 - a_1\left(\frac{a_1}{4}-1\right) - \frac{3}{4}\right\} +$$

$$\frac{I^2 R_{D1} \Delta^2 (M+1)}{12}\left(1-\frac{M}{\Delta}\right)^2 \qquad (A7.8(b))$$

where: $a_1 = 1 - \frac{I}{I_{S1}}(M-\Delta)$

$$\bar{P}_{VT2} = \frac{kT}{q}\frac{I_{ES2}^2(1-M)}{4I\Delta}\left\{d_2\left(\frac{d_2}{2}-1\right)\log d_2 - d_2\left(\frac{d_2}{4}-1\right) - \frac{3}{4}\right\} +$$

$$IV_{CB2}\left[\frac{(1-M)(M-\Delta)^2}{8\Delta}\right] + \frac{I^2R_{E1}\Delta^2(1-M)}{12}\left(1-\frac{M}{4}\right)^3 \qquad (A7.8(c))$$

where $d_2 = 1 - \frac{I}{I_{ES1}}(M-\Delta)$

$$\bar{P}_{D2} = \frac{kT}{q}\frac{I_{S2}^2(1-M)}{4I\Delta}\left\{c_1\left(\frac{c_1}{2}-1\right)\log c_1 - c_1\left(\frac{c_1}{4}-1\right) - \frac{3}{4}\right\} +$$

$$\frac{I^2R_{D2}\Delta^2(1-M)}{12}\left(1+\frac{M}{\Delta}\right)^3 \qquad (A7.8(d))$$

where $c_1 = 1 + \frac{I}{I_{S2}}(M+\Delta)$

For $M \ll \Delta$

$$\bar{P}_{VT1} = 0 \qquad (A7.9(a))$$

$$\bar{P}_{D1} = \frac{kT}{q}\frac{I_{S1}^2(1-M)}{4I\Delta}\left\{a_1\left(\frac{a_1}{2}-1\right)\log a_1 - a_2\left(\frac{a_2}{2}-1\right)\log a_2 - a_1\left(\frac{a_1}{4}-1\right) + a_2\left(\frac{a_2}{4}-1\right)\right\} +$$

$$\frac{I^2R_{D1}\Delta^2(M+1)}{2}\left[\left(\frac{M}{\Delta}\right)^2 + \frac{1}{3}\right] \qquad (A7.9(b))$$

where $a_1 = 1 - \frac{I}{I_{S1}}(M-\Delta)$ $\qquad$ $a_2 = 1 - \frac{I}{I_{S1}}(M-\Delta)$

$$\bar{P}_{VT2} = \frac{kT}{q}\frac{I_{ES2}(1-M)}{4I\Delta}\left\{d_2\left(\frac{d_2}{2}-1\right)\log d_2 - d_1\left(\frac{d_1}{2}-1\right)\log d_1 - d_2\left(\frac{d_2}{4}-1\right)+d_1\left(\frac{d_1}{4}-1\right)\right\} -$$

$$\frac{V_{cB2}IM(1-M)}{2} + \frac{I^2R_{E2}\Delta^2(1-M)}{2}\left[\left(\frac{M}{\Delta}\right)^2+\frac{1}{3}\right] \qquad \text{(A7.9(c))}$$

where $d_1 = 1 - \frac{I}{I_{ES2}}(M+\Delta)$ $\qquad$ $d_2 = 1 - \frac{I}{I_{ES2}}(M-\Delta)$

$$\bar{P}_{D2} = 0 \qquad \text{(A7.9(d))}$$

Appendix 8 Application of the mean square error criterion to the measured data for a junction diode

In chapter III (Section 6 , eqn. 6.2) an expression is given relating the forward voltage (V_D) of a junction diode to the forward current (I_D).

$$V_D \doteq I_D R_D + \frac{kT}{q} \log\left(\frac{I_D}{I_s}\right) \qquad (A8.1)$$

It is required to evaluate the constant I_s and R_D, in the above expression, from a set of measured values of forward current and voltage for a junction diode. It is unlikely that values of I_s and R_D can be calculated which will make eqn. A8.1 exactly fit the measured data. The difference between the measured values of diode voltage and the values calculated from eqn. A8.1 may be defined as the error

$$\varepsilon_n = \frac{kT}{q}\left[\log(I_n) - \log(I_s)\right] + I_n R_D - V_n \qquad (A8.2)$$

where V_n and I_n are the n^{th} pair of measured values of diode voltage and current.

The total squared error (E) for N sets of measured values is:

$$E = \sum_{n=1}^{N} \varepsilon_n^2 \qquad (A8.3)$$

In order to minimise the squared error E, the partial derivatives of E are set to zero and the resulting equations solved for I_s and R_D. Substituting eqn. A8.2 in eqn. A8.3, and differentiating with respect to I_s and R_D gives:

$$\frac{\partial E}{\partial I_s} = \sum_{n=1}^{N} -2\left\{\frac{kT}{q}\left[\log(I_n)-\log(I_s)\right]+I_n R_D - V_n\right\}\frac{kT}{q}\cdot\frac{1}{I_s} \qquad (A8.4)$$

$$\frac{\partial E}{\partial R_D} = \sum_{n=1}^{N} 2\left\{\frac{kT}{q}\left[\log(I_n)-\log(I_s)\right]+I_n R_D - V_n\right\} I_n \qquad (A8.5)$$

For minimum squared error $\frac{\partial E}{\partial I_s} = \frac{\partial E}{\partial R_D} = 0$. Therefore, from eqns. A8.4 and A8.5:

$$\sum_{n=1}^{N}\left\{\frac{kT}{q}\left[\log(I_n)-\log(I_s)\right]+I_n R_D - V_n\right\} = 0 \qquad (A8.6)$$

$$\sum_{n=1}^{N}\left\{\frac{kT}{q}\left[\log(I_n)-\log(I_s)\right]+I_n R_D - V_n\right\} I_n = 0 \qquad (A8.7)$$

Eqns. A8.6 and A8.7 may be rewritten as:

$$\sum_{n=1}^{N}\left[\frac{kT}{q}\log(I_n)-V_n\right]-\frac{kT}{q}N\log(I_s)+R_D\sum_{n=1}^{N} I_n = 0 \qquad (A8.8)$$

$$\sum_{n=1}^{N} I_n\left[\frac{kT}{q}\log(I_n)-V_n\right]-\frac{kT}{q}\log(I_s)\sum_{n=1}^{N} I_n + R_D\sum_{n=1}^{N} I_n^2 = 0 \qquad (A8.9)$$

Solving these two simultaneous equations for $\log(I_s)$ and R_D gives:

$$\log(I_s) = \frac{\begin{vmatrix} \sum_{n=1}^{N}\left[\frac{kT}{q}\log(I_n) - V_n\right] & -\sum_{n=1}^{N} I_n \\ \sum_{n=1}^{N} I_n\left[\frac{kT}{q}\log(I_n) - V_n\right] & -\sum_{n=1}^{N} I_n^2 \end{vmatrix}}{\begin{vmatrix} \frac{kT}{q}N & -\sum_{n=1}^{N} I_n \\ \frac{kT}{q}\sum_{n=1}^{N} I_n & \sum_{n=1}^{N} I_n^2 \end{vmatrix}} \qquad (A8.10)$$

$$R_D = \frac{\begin{vmatrix} \frac{kT}{q}N & \sum_{n=1}^{N}\left[\frac{kT}{q}\log(I_n) - V_n\right] \\ \frac{kT}{q}\sum_{n=1}^{N} I_n & \sum_{n=1}^{N} I_n\left[\frac{kT}{q}\log(I_n) - V_n\right] \end{vmatrix}}{\begin{vmatrix} \frac{kT}{q}N & -\sum_{n=1}^{N} I_n \\ \frac{kT}{q}\sum_{n=1}^{N} I_n & -\sum_{n=1}^{N} I_n^2 \end{vmatrix}} \qquad (A8.11)$$

The flowchart used as a basis for a computer program to evaluate I_s and R_D is shown in fig. A8.1

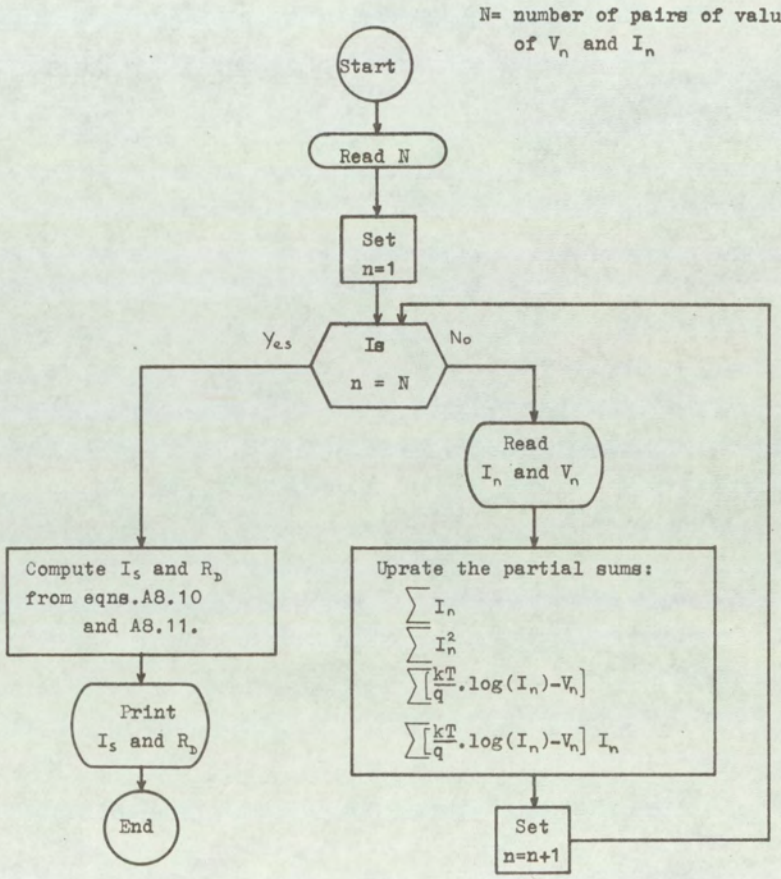

Fig.A8.1. Flowchart for determining diode parameters from measured data.

Appendix 9 Evaluation of the frequency spectrum for the pulse-length modulation section of the function generation system.

The frequency spectrum for the pulse-length modulation section of the system described in Chapter IV is given by eqn. 3.18 of section 3.1 (Chapter IV) and is rewritten below for convenience:

$$F(t)=\frac{1}{2\pi j}\sum\frac{1}{n}\left\{\exp\left[jn\omega_c\left(t+\frac{T_c}{4}+t_{dl}\right)\right]-\right.$$

$$\left.\exp\left[jn\omega_c\left(t-\frac{T_c}{4}-t_{dt}\right)\right]\right\} \qquad (A9.1)$$

where $$t_{dl}=t_{dt}=\frac{M}{4}\left(1-4\frac{t}{T_m}\right) \qquad (A9.2)$$

for $0 \leqslant t \leqslant \frac{T_m}{2}$

and $$t_{dl}=t_{dt}=\frac{M}{4}\left(-3+4\frac{t}{T_m}\right) \qquad (A9.3)$$

for $\frac{T_m}{2} \leqslant t \leqslant T_m$

The expression for F(t) when n=0 may be evaluated by applying L'Hopital's rule to eqn. A9.1. Therefore:

$$F(t)=\frac{1}{2}+\frac{t_{dl}}{T_c}+\frac{t_{dt}}{T_c}+$$

$$\frac{1}{2\pi j}\sum_{n=\pm 1}^{\pm\infty}\frac{1}{n}\left\{\exp\left[jn\omega_c\left(t+\frac{T_c}{4}+t_{dl}\right)\right]-\right.$$

$$\exp\left[jn\omega_c\left(t-\frac{T_c}{4}-t_{dt}\right)\right]\Bigg\} \qquad (A9.4)$$

Rewriting eqn. A9.4 in terms of only positive values of n, and making the substitution $t_{dt}=t_{dl}$, gives:

$$F(t)=\frac{1}{2}+\frac{t_{dl}}{T_c}+\frac{t_{dt}}{T_c}+\frac{1}{\pi}\sum_{n=1}^{\infty}\frac{1}{n}2\cos(n\omega_c t).\sin\left[n\omega_c\left(\frac{T_c}{4}+t_{dl}\right)\right] \qquad (A9.5)$$

Substitution of eqns. A9.1 and A9.2 in the above equation shows that the term $\sin\left[n\omega_c\left(\frac{T_c}{4}+t_{dl}\right)\right]$ is a periodic function and may be expressed as a Fourier series of the form:

$$\sin\left[n\omega_c\left(\frac{T_c}{4}+t_{dl}\right)\right]=\sum_{p=-\infty}^{\infty}c_p.\exp(jp\omega_m t) \qquad (A9.6)$$

where

$$c_p=\frac{1}{T_m}\int_0^{T_m}\sin\left[n\omega_c\left(\frac{T_c}{4}+t_{dl}\right)\right]\exp(-jp\omega_m t).dt \qquad (A9.7)$$

Substituting eqns. A9.2 and A9.3 in eqn. A9.7 gives:

$$c_p=\frac{1}{T_m}\Bigg\{\int_0^{T_m/2}\sin\left[n\omega_c\left(\frac{T_c}{4}+\frac{M}{4}\left[1-4\frac{t}{T_m}\right]\right)\right]\left[\exp\left(-jp\omega_m t\right)\right]dt+$$

$$\int_{T_m/2}^{T_m}\sin\left[n\omega_c\left(\frac{T_c}{4}+\frac{M}{4}\left[-3+4\frac{t}{T_m}\right]\right)\right]\left[\exp(-jp\omega_m t)\right]dt\Bigg\} \qquad (A9.8)$$

The integrals in the above expression are evaluated by integrating by parts twice. Applying the limits to the resulting equation gives:

$$c_p=\frac{1}{n\pi M\left[\left(\frac{p}{nM}\right)^2-1\right]}\left\{-\cos(p\pi).\cos\left[\frac{n\pi}{2}(1-M)\right]+\cos\left[\frac{n\pi}{2}(1+M)\right]\right\} \qquad (A9.9)$$

Substituting eqns. A9.6 and A9.9 in eqn. A9.5 gives:

$$F(t)=\frac{1}{2}+\frac{t_{dl}}{T_c}+\frac{t_{dt}}{T_c}+\sum_{n=1}^{\infty}\sum_{p=-\infty}^{\infty}\frac{2}{(n\pi)^2 M\left[\left(\frac{P}{nM}\right)^2-1\right]}\times$$

$$\left\{-\cos(p\pi).\cos\left[\frac{n\pi}{2}(1-M)\right]+\cos\left[\frac{n\pi}{2}(1+M)\right]\right\}\exp(jp\omega_m t).\cos(n\omega_c t) \qquad \text{(A9.10)}$$

As a result of the positive and negative values of the integer p, the term $\exp(jp\omega_m t)$ in the above expression reduces to $\cos(p\omega_m t)$. Eqn. A9.10 may therefore be rewritten as:

$$F(t)=\frac{1}{2}+\frac{t_{dl}}{T_c}+\frac{t_{dt}}{T_c}-$$

$$\sum_{n=1}^{\infty}\frac{4}{(n\pi)^2 M}\sin\left(\frac{n\pi}{2}\right).\sin\left(\frac{n\pi}{2}M\right).\cos(n\omega_c t)+$$

$$\sum_{n=1}^{\infty}\sum_{p=\pm1}^{\pm\infty}\frac{2}{(n\pi)^2 M\left[\left(\frac{P}{nM}\right)^2-1\right]}\left\{\left[1-\cos(p\pi)\right]\cos\left(\frac{n\pi}{2}\right).\cos\left(\frac{n\pi}{2}M\right)-\right.$$

$$\left.\left[1+\cos(p\pi)\right]\sin\left(\frac{n\pi}{2}\right)\sin\left(\frac{n\pi}{2}M\right)\right\}\cos(p\omega_m t).\cos(n\omega_c t) \qquad \text{(A9.11)}$$

Consider the term $\sum_{p=\pm1}^{\pm\infty}\cos(p\omega_m t).\cos(n\omega_c t)$ in the above expression. Since the coefficient of this term does not change sign for negative values of p, the term may be expanded in the following manner:

$$\sum_{p=\pm1}^{\pm\infty}\cos(p\omega_m t).\cos(n\omega_c t)=\sum_{p=\pm1}^{\pm\infty}\frac{1}{2}\left[\cos(n\omega_c+p\omega_m)t+\cos(n\omega_c-p\omega_m)t\right]=\sum_{p=\pm1}^{\pm\infty}\cos(n\omega_c+p\omega_m)t$$

(A9.12)

Substituting eqn. A9.12 in eqn. A9.11 gives the frequency spectrum as:

$$F(t) = \frac{1}{2} + \frac{t_{dl}}{T_c} + \frac{t_{dt}}{T_c} -$$

$$\sum_{n=1}^{\infty} \frac{4}{(n\pi)^2 M} \sin\left(\frac{n\pi}{2}\right).\sin\left(\frac{n\pi}{2}M\right).\cos(n\omega_c t) +$$

$$\sum_{n=1}^{\infty} \sum_{p=\pm 1}^{\pm\infty} \frac{2}{(n\pi)^2 M\left[\left(\frac{p}{nM}\right)^2 - 1\right]} \left\{\left[1-\cos(p\pi)\right].\cos\left(\frac{n\pi}{2}\right).\cos\left(\frac{n\pi}{2}M\right) -\right.$$

$$\left.\left[1+\cos(p\pi)\right]\sin\left(\frac{n\pi}{2}\right).\sin\left(\frac{n\pi}{2}M\right)\right\}\cos(n\omega_c + p\omega_m)t \qquad \text{(A9.13)}$$

The frequency spectrum given by the above equation is for a pulse-train of unit positive amplitude. The spectrum for a pulse train of amplitude $\pm h$ is obtained by adding a constant of $-\frac{1}{2}$ to eqn. A9.13 and multiplying the complete expression by 2h.

3. References.

1) Gouy, M., "On a constant temperature oven", Journal Physique, vol.6, ser.3, pp.497-483, 1897.
2) Bedford, B.D. British Patent No.389,855: 25/9/31.
3) Zworykin, British Patent No.434,890: 1933.
4) Roosenstein, H.A., U.S. Patent No.2,270,108:1936.
5) Kharbanda, S.R., British Patent No.564,511.
6) Lawson, D.I., Lord, A.V. and Kharbanda, S.R.,"A method of transmitting sound on the vision carrier of a television system", Journal I.E.E.,1946, Vol.93,Pt.III, pp.251-274.
7) Fredendall, G.L., Schlesinger, K. and Schroeder, A.C., "Transmission of television sound on the picture carrier", Proc.I.R.E., 1946, Vol.34,No.2,pp.49P-61P.
8) Parks, G.H. and Moss, S.H.,"A new method of wide-band modulation of pulses", Journal I.E.E.,1947, Vol.94, Part IIIA, No.13, pp.511-516.
9) James, E.G., Dix, J.C., Cope, J.E., Ellis, C.F. and Anderson, E.W.,"The development of the wireless set No.10: An early application of pulse-length modulation", ibid, 1947, Vol.94, Part IIIA, No.13, pp.517-527.
10) Gouriet, G.G.,"Random noise characteristics of a pulse-length modulated system of communication", ibid, 1947, Vol.94, Part IIIA, No.13, pp.551-555.
11) Fitch, E.,"The spectrum of modulated pulses", ibid, 1947, Vol.94, Part IIIA, No.13, pp.556-564.
12) Levy, M.M.,"Some theoretical and practical considerations of pulse modulation", ibid, 1947, Vol.94, Part IIIA, No.13, pp.565-572.

13) Roberts, F.F. and Simmonds, J.C.,"Multichannel communication systems", Wireless Engineer, 1945, Vol. XXII, No.266, pp.538-548.

14) Kretzmer, E.R.,"Distortion in pulse-duration modulation", Proc.I.R.E., 1947, Vol.35,No.11, pp.1230-1235.

15) Lozier, J.C.,"Spectrum analysis of pulse modulated waves", Bell System Technical Journal, 1947, Vol.26, pp.360-387.

16) Krauss, H.L. and Ordung, P.F.,"Distortion and bandwidth characteristics of pulse modulation", A.I.E.E. Transactions, 1947, Vol.66, pp.984-988.

17) Moss, S.H.,"Frequency analysis of modulated pulses", Philosophical Magazine, 1948, Series7, Vol.39, No.296, pp.663-691.

18) Bright, R.L.,"Junction transistors used as switches", A.I.E.E. Transactions, 1955, Vol.74,Part I,pp.111-121.

19) Milnes, A.G.,"Transistor power amplifiers with switched mode of operation", A.I.E.E. Transactions, 1956, Vol.75, Part I, pp.368-372.

20) Collins, H.W."Magnetic amplifier control of switching transistors", A.I.E.E. Transactions, 1956, Vol.75, Part I, pp.585-589.

21) Van Scoyoc, J.N. and Bull, R.W.,"Pulse-width control of transistors", Transactions I.R.E., 1958, Vol. PGIE-6, pp.95-100.

22) Ageev, D.V., Malanov, V.V. and Polov, K.P.,"A new highly efficient audio-frequency pulse power amplifier", Radiotekhnika, 1958, Vol.13, Part 6, pp.47-51.

23) Flesher, G.T.,"Transistor pulse width control amplifier", Proc. National Electronics Conference, 1958, Vol.14, pp.454-463.

24) Ettinger, G.M.,"Some methods of measuring power loss in switching transistors", ibid, Vol.14, pp.464-477.

25) Ettinger, G.M. and Cooper, B.J.,"The design of high-power switched transistor amplifiers", Proc. I.E.E.,1959, Vol.106B, Suppl.15-18, pp.1285-1288.

26) Vackar, J.,"Audio-frequency recuperation amplifier", S.N.T.L. Technical Digest,1960, Vol.11, No.4, pp.71-72.

27) Wright, M.J.,"A transistor switching circuit for power regulation purposes", Electronic Engineering, 1960, Vol.32, pp.484-487.

28) Bacon, K.F.,"Transistorized regulation and control of aircraft electrical power systems", Proc. I.E.E., 1960, Vol.107A, No.34, pp.343-352.

29) Cudahy, M.J.,"An audio amplifier without tubes or transistors", Proc. National Electronics Conference, 1961, Vol.17, pp.258-262.

30) Ohno, E.,"All transistorized high efficiency servo amplifiers using pulse width modulation", Mitsubushi Denki Lab. Report, 1962, Vol.3, No.1,pp.39-52.

31) Chase, R.F.,"Design aspects of transistor power amplifiers", Jour. Audio Engng. Society, 1962, Vol. 10, Part III, pp.232-235.

32) Birt, D.R.,"Modulated pulse A.F. amplifiers", Wireless World, 1963, Vol.69, No.2,pp.76-83.

33) Miller, C.H.,"High efficiency amplification using width modulated pulses", Proceedings I.R.E.E. (Australia),1964, Vol.25, Part 5, pp.314-323.

34) Bell, E.C. and Sergent, T.,"Distortion and power output of pulse duration modulated amplifiers", Electronic Engineering,1965, Vol.37, pp.540-542.

35) Turnbull, G.F., and Townsend, J.M.,"A feedback pulse-width modulated amplifier", Wireless World, 1965, Vol.71, No.4, pp.160-168.

36) Turnbull, G.F., Atherton, D.P. and Townsend, J.M., "A method for the theoretical analysis of relay amplifiers", Proc.I.E.E.

37) Schaefer, R.A.,"A new pulse modulator for accurate d.c. amplification with linear or nonlinear devices", I.R.E. Transactions, 1962, Vol,I-11, No.2,pp.34-47.

38) Rosenthal, J.A.,"A pulse modulator that can be used as an amplifier, a multiplier, or a divider", ibid, 1963, Vol.IM-12, No.3, pp.125-134.

39) Sorensen, A.A.,"Linear control using on-off controllers", Electrotechnology, 1963, Vol.74, No.4, pp.99-101

40) Bose, A.G."A two-state modulation system", ibid, 1964, Vol.74, No.2, pp.42-47.

41) Johnson, K.C., Correspondence to the editor, ibid, 1963, Vol.69, No.3, pp.135-136.

42) Salmain, M.D.,Correspondence to the edtior, Wireless World, 1965, Vol.71, No.6, pp.287-288.

43) Josephson, B.D., Correspondence to the editor, ibid, 1965, Vol.71, No.7, pp.335-336.

44) Turnbull, G.F.,and Townsend, G.M.,"Efficiency considerations in a class D amplifier Part 1", ibid,1967, Vol.73, No.4, pp.154-158.

45) Turnbull, G.F. and Townsend, G.M.,"Efficiency considerations in a class D amplifier, Part II", ibid, 1967, Vol.73, No.6, pp.214-217.

46) Johnson, K.C.,"1. Class D principles analysed", ibid, 1967, Vol.73, No.12, pp.576-580.

47) Johnson, K.C.,"2. The design of a circuit", ibid, 1968, Vol.73, No.13, pp.645-649.

48) Johnson, K.C.,"3. Distortions inherent in P.W.M.", ibid, 1968, Vol.73, No.14, pp.672-676.

49) Stuart,R.D.,"An introduction to fourier analysis", Methuen's Monographs on physical subjects, 1961, Methuen and Co. Ltd.

50) Bennett, W.R.,"New results in the calculation of modulation products", The Bell System Technical Journal, New York, Vol.12, April 1933, pp.228-243.

51) Black, H.S.,"Modulation Theory", D. Van Nostrand Company, Inc., 1953

52) Bloch, A.,"Discussion on pulse communication", I.E.E. Radiocommunication Convention, 1947, I.E.E. Journal, Vol.94, Part IIIA, No.13, pp.586.

53) Narayna Rao, V.,"A mehtod of generating width modulated pulses", Electrotechnics, 1951, March, No.23, pp.85-92.

54) Roehr, W.D.(editor) "Switching transistor handbook", Motorola Semiconductor Products Inc. 1963.

55) Van Valkenburg, M.E.,"Network Analysis", Prentice Hall, Inc.,1955.

56) Whittaker, E.T. and Watson, G.N.,"Modern analysis", (Cambridge University Press, 1952), Chapter IX.

57) Gradshteyn, I.S. and Ryzhik, I.M.,"Table of integrals, series and products", Academic Press,1965.

58) Lyusternik, L.A., Chervonenkis, O.A. and Yanpol'skii, A.R.,"Handbook for computing elementary functions", International series of monographs on pure and applied mathematics, Vol.76, Pergammon Press, 1965.

59) Dwight,H.B.,"Tables of integrals and other mathematical data", The Macmillan Company, 1964.

60) Abramowitz, M. and Stegun, I.A.,"Handbook of mathematical functions", Dover Publications Inc., New York, 1965.

61) Scarborough, J.B.,"Numerical mathematical analysis", The John Hopkins Press, 6th edition, 1966,pp.96-97.

62) Milne, W.E.,"Numerical Calculus", Princetown University Press, 1949, Chapter IX.

63) Wylie Jr.,C.R.,"Advanced Engineering Mathematics", McGraw-Hill, Second Edition, 1960, pp.175-191.

64) "Micrologic Handbook", SGS Fairchild Ltd., May 1965, Chapter 2, Section 2.1, Circuit No.2.1.3.

65) "The application of linear microcircuits", SGS Fairchild Ltd., August 1967.

66) Beaufoy, R. and Sparkes, J.J.,"The junction transistor as a charge-controlled device", A.T.E. Journal,1957, Vol.13, pp.310-327.

67) Beaufoy, R.,"Transistor switching circuit design using the charge-control parameters", Proc. I.E.E., 1959, Vol.106B, Suppl.17, pp.1085-1091.

68) Cleary, J.F.(editor)."G.E. Transistor Manual", Semiconductor Products Dept., General Electric Company, New York, 1964, pp.171-173.

69) Ebers, J.H., and Moll, J.L.,"Large-signal behaviour of junction transistors", Proc.I.R.E.,1954, Vol.42, No.12, pp.1761-1772.

70) Searl, C.L.,Boothroyd, A.R.,Angelo Jr., E.J., Gray, P.E., and Pederson, D.O.,"Elementary circuit properties of transistors", Semiconductor Electronics Education committee (Wiley,1964).

71) Gray, P.E.,DeWitt, D.,Boothroyd, A.R. and Gibbons, J.F.,"Physical electronics and circuit models of transistors", Semiconductor Electronics Education Committee (Wiley 1964).

72) Molloy, E. and Pannett, W.E.(Editors) "Radio and television engineers reference book" (G.Newnes Ltd. 1956), Chapter 30.

73) Kendall, D.N.,Dixon, W.P.,Schulte, E.H."Semiconductor surface thermocouples for determining heat transfer rates", I.E.E.E. Trans.,Aerospace and Electronic Systems, 1967, Vol.AES-3, No.4. pp.596-603,

74) Loeffler, R.F.,"Thermocouples, resistance temperature detectors, thermistors - which? ", Instruments and Control Systems, 1967, Vol.40, pp.89-93.

75) Flood, J.E. and Rayner, P.J.W.,"Transient power dissipation in a transistor switch with capacitive load", Proc. I.E.E.,1967, Vol.114,No.12,pp.1852-1858.

76) Schmid, H.,"A transistorised, all electronic cosine-sine function generator", I.R.E. WESCON Convention Record, 1958, Vol.2,Pt,4,pp.89-107.

77) Schmid, H.,"A repetitive analog pulse time computing technique", I.E.E.E. Trans. on Aerospace, 1964, Vol.2, No.2, pp.211-226.

78) Klein, G. and den Hertog, J.M."A sine-wave generator with a period of hours", Electronic Engineering, 1959, Vol.31, pp.320-325.

4. Published work

The following papers were published during the course of the research work described in the thesis.

(1) Flood,J.E. and Rayner,P.J.W. " Transient power dissipation in a transistor switch with capacitive load ", Proc.I.E.E.,1967,Vol.114,No.12,pp.1852-1858.

(2) Harry,J.E. and Rayner,P.J.W. "A high current mains-frequency synchronous switch",Journal of Scientific Instruments (Journal of Physics E),1968,Series 2, Vol.1,pp.570-572.

5. ACKNOWLEDGEMENTS

The author of this thesis wishes to thank Professor J.E. Flood for his counsel and encouragement during the course of this work, and also acknowledge the financial support given by the Science Research Council.